Modelling Ozonation Processes for Disinfection By-Product Control in Potable Water Treatment: From Laboratory to Industrial Units

Pierre Mandel

N° d'ordre : 4189 **ANNÉE 2010**

UNIVERSITÉ DE RENNES 1

THÈSE / UNIVERSITÉ DE RENNES 1
sous le sceau de l'Université Européenne de Bretagne

pour le grade de

DOCTEUR DE L'UNIVERSITÉ DE RENNES 1

Mention : Chimie

Ecole doctorale : Sciences de la matière

présentée par

Pierre MANDEL

préparée à l'Unité Mixte de Recherche CNRS 6226
Laboratoire Sciences Chimiques de Rennes
Equipe Chimie et Ingénierie des Procédés
Ecole Nationale Supérieure de Chimie de Rennes

Modelling Ozonation Processes for Disinfection By-Product Control in Potable Water Treatment: From Laboratory to Industrial Units

Thèse soutenue à l'ENSCR le 8 septembre 2010

devant le jury composé de :

Hervé GALLARD
Professeur à l'ESIP (Poitiers) / *Rapporteur*

Luuk C. RIETVELD
Professeur à la Delft University of Technology (Pays-Bas) / *Rapporteur*

Nigel J. D. GRAHAM
Professeur à l'Imperial College London (Royaume-Uni) / *Président*

Aziz BELMILOUDI
Maître de Conférences à l'INSA Rennes/ *Examinateur*

Cyrille LEMOINE
Responsable de pôle à Veolia Environnement Recherche & Innovation/ *Examinateur*

Dominique WOLBERT
Professeur à l'Ecole Nationale Supérieure de Chimie de Rennes / *Directeur de thèse*

to Dr. Ferdinand Jelly Roll Morton
and to his Red Hot Peppers

Acknowledgements

Remerciements

Je remercie grandement tous ceux qui m'ont permis de mener à bien ce long projet de recherche. Ils ont été nombreux et leur implication, si minime fût-elle, a été à chaque fois un enrichissement et un encouragement supplémentaires.

Ce mémoire est le fruit d'une collaboration entre mondes académique et industriel et je tiens à saluer tous les partenaires du projet : Veolia Environnement, l'ENSCR, l'ANRT et la Commission Européenne. Être à la croisée des chemins m'a beaucoup appris.

In particular, I would like to acknowledge the financial support from the European Techneau Project (European Contract Number: 018320). This doctoral research was imbedded in the Work Package 2.4 on Oxidation Processes and I thank all the members of the Work Package, and further all the people met during Techneau workshops.

Mes premiers remerciements vont au professeur Dominique Wolbert qui a accepté de diriger cette thèse. Qu'il trouve ici l'expression de mon profond respect et de ma gratitude. Sa rigueur et son honnêteté intellectuelle ont constitué un exemple que j'ai tâché de suivre. Sa disponibilité et son indéfectible gentillesse m'ont toujours permis de confronter, de préciser, d'affiner mes idées (mais le plus souvent aussi de les enterrer…)

I was deeply honoured to present the results of this research work to a high class examining board. I am very grateful to Professor Nigel Graham, who accepted to chair the board and to Professors Luuk Rietveld and Hervé Gallard, who reviewed this manuscript. Je remercie également très chaleureusement M. Aziz Belmiloudi pour sa participation au jury et pour avoir su m'éclairer patiemment sur un certain nombre de points mathématiques.

J'ai eu le plaisir de bénéficier des conseils avisés de deux experts de Veolia Environnement avec lesquels l'échange a été aussi plaisant qu'enrichissant. Pascal Roche a été à l'origine de ce travail, l'a suivi et l'a grandement facilité, du labo jusqu'à l'usine de potabilisation. Cyrille Lemoine m'a fait bénéficier de sa vision scientifique et m'a permis d'intégrer une équipe de spécialistes tout en me laissant une grande liberté d'initiative. Qu'ils soient tous deux remerciés.

Un grand nombre de personnes s'est finalement trouvé mêlé à cette histoire, de près ou de loin. Je voudrais remercier Mme Balannec-Léon de l'IUT de Rennes, pour son

attention constante. A Veolia, j'ai eu le privilège de travailler avec Marie Maurel pour la création de SimOx et avec Delphine Bourdin pour toutes les manips de labo ; qu'elles soient remerciées. Par ailleurs, de nombreux soutiens spécifiques m'ont été apportés : Benoît (optimisation), Arnaud (statistiques), Olivier et Daniel (Matlab), Florencio (M. Ozone) et Jacques (logistique). De manière générale, je remercie tous les membres de l'équipe MCP ainsi que tous ceux avec qui j'ai partagé un bout de paillasse ou de bureau. L'étude de cas sur l'usine d'Annet-sur-Marne n'a été possible qu'avec l'appui de MM. Cablan, Pujol et Dano. Qu'ils soient remerciés, ainsi que tout le personnel de l'usine : Raphaël, Claude et tous les autres. Je n'oublie pas non plus les experts de la direction technique Yves Jaeger, Magali Guitard, Christophe Piet, Hélène Habarou, Anne Gicquel, Jean-Paul Courcier. Enfin je remercie Anne Bonneau, Sophie Vaudran et Nadine Mailfait pour leur précieuse aide.

L'ambiance chaleureuse du labo de l'ENSCR a été souvent d'un grand réconfort. Je voudrais remercier le jovial fantaisiste/pantomime/conteur… Azziz, Pierre-François, pour ses camemberts de Lourdes, et les très chères Aurélie et Souhila. Je remercie aussi Minh Duc, Gaël, Benoît, Pascal, Guillaume, Hayat, Derradji, Abdellah et Nolwenn, sans oublier les chenus Ludo et Ronan, ainsi que tous les étrangers de passage au labo. Merci aussi aux organiciens Alicia, Thomas et Bastien. Merci à Valérie pour sa bonne humeur et son dynamisme ainsi qu'à tous les permanents du laboratoire. J'adresse un grand remerciement à Isabelle Soutrel, Emilie Renault et Marguerite Lemasle pour leur expertise analytique. Merci également à Dominique Allaire et Lionel Leforestier pour tous leurs coups de pouce.
Enfin un très grand merci à mes deux stagiaires avec lesquels il a été très agréable et fructueux de travailler : Adela Cantero-García et Huy-Hoang Pham, qui m'a enduré pendant un an - un record qui tient toujours.

Merci à mes amis qui ont supporté mon embarras et mes explications un peu embrouillées quand ils me posaient des questions sur l'avancement de ma thèse. Merci à ma famille qui m'a toujours soutenu et à mon père qui m'a filé quelques bons tuyaux. Je vous remercie d'avoir lu jusqu'ici, vous pouvez maintenant refermer cette thèse ;).

List of Abbreviations

ADM	Axial Diffusion Model
AOC	Assimilable Organic Carbon
BFCM	Back-Flow Cell Model
CAE	Computer-Aided Engineering
CAE-SM	Veolia Environnement Centre for Environmental Analysis, Saint-Maurice (Centre d'Analyse de l'Environnement, Saint-Maurice)
CFD	Computational Fluid Dynamics
CSTR	Continuous Stirred-Tank Reactor
DAE	Differential-Algebraic Equation
DBP	Disinfection By-Product
DOC	Dissolved Organic Carbon
EDC	Endocrine Disrupting Chemical
FAST	Fourier Amplitude Sensitivity Test
*e*FAST	*Extended* Fourier Amplitude Sensitivity Test
ENSCR	School of Chemistry, Rennes (Ecole Nationale de Chimie de Rennes)
GA	Genetic Algorithm
GUI	Graphical User Interface
HPLC	High Pressure Liquid Chromatography
IDDF	Integrated Disinfection Design Framework
IOD	Instantaneous Ozone Demand
LA	Linear Algebraic
LHS	Latin Hypercube Sampling
ND	No Data
NLA	Non-Linear Algebraic
NLP	Non-Linear Programming
NOM	Natural Organic Matter
NOM^d	O_3 Consuming fraction of NOM
NOM^i	$^{\bullet}OH$ Initiating fraction of NOM
NOM^p	$^{\bullet}OH$ Promoting fraction of NOM
NOM^s	$^{\bullet}OH$ Scavenging fraction of NOM
NSGA	Non-Dominant Sorting Genetic Algorithm
ODE	Ordinary Differential Equation
*p*CBA	*para* Chlorobenzoic Acid
PDE	Partial Differential Equation
PFR	Plug-Flow Reactor
RTD	Residence Time Distribution
SBH	Staehelin, Bühler and Hoigné
SUVA	Specific Ultra-Violet A
TFG	Tomiyasu, Fukutomi and Gordon
TOC	Total Organic Carbon

UPLC	Ultra Performance Liquid Chromatography
UPW	Ultra Pure Water
USEPA	U.S. Environmental Protection Agency
UV	Ultra-Violet

List of Symbols

Latin alphabet

Symbol	Name
a	Volumetric interfacial aera
A	UV Absorbance
A_T	Alkalinity
C	Disinfectant concentration
C_0	Initial disinfectant concentration
C_1, C_2, …	Constants
dV	Elementary volume
D^A	Molecular diffusivity of compound A
E	E function for RTD
E_A	Energy of activation
H_c	Henry's dimensionless constant for ozone
$H_c{}^A$	Henry's dimensionless constant for compound A
J	Jacobian matrix
k	Lethality coefficient of microorganisms
k'	First order decay rate of disinfectant
k_0	Frequency factor
K_A	Acidity constant
k_{BrO3}	Kinetic rate constant for empirical bromate formation
k_{inst}	Kinetic rate constant for empirical instantaneous ozone demand
k_L	gas transfer coefficient
k_{UV}	UV (254 nm) decay rate
k_{pro}	Kinetic rate constant for protonation in acid/base equilibrium
k_{depro}	Kinetic rate constant for deprotonation in acid/base equilibrium
l	Number of experimental reference data for parameter identification
L	Length of a reactor
m	Number of parameters to be determined
M_σ	Observational error variance matrix
N	Microorganism concentration
n	Disinfectant's reaction order
N_0	Microorganism initial concentration
o_H	Empirical constant for Hom's model
O	Objective function ($O(\theta)$)
O_f	Final value of the objective function
$Or(A)$	Relative order to compound A in kinetics constant rate expression
p	Pressure
Q	Volumetric flowrate
r	Reaction speed, reaction rate

r_P	Pearson's correlation
R	Universal gas constant
r^A	Reaction rate relative to species A
$\mathcal{R}^A$	Collection of reactions in which species A is involved
S	Cross section of the reactor
S^p	First order sensitivity with respect to parameter p
$S_T{}^p$	Total order sensitivity with respect to parameter p
t	Time
T	Temperature
u_{SG}	Superficial gas velocity
UV	UV absorbance (254 nm)
V	Volume of the reactor
w	Pseudo first-order constant for ozone decomposition
w_2	Pseudo second-order constant for ozone decomposition
x	Space coordinates
y	
z	
X	Model dependant variable
Y_{exp}	Experimental output used as reference for parameter identification
Y_{sim}	Model output
Y_{sim}^A	Model output for species A

Greek alphabet

Symbol	Name
α	Hydraulic efficiency
β_i	collection of reagents for reaction i.
η	Fractional stoichiometric coefficient
κ	Correction factor (P,T)
ν	Integer stoichiometric coefficient
ν_i^A	Stoichiometric coefficient for compound A in reaction i
ρ	Volumic mass
$\sigma_{\exp,i}^A$	Experimental standard deviation for the i^{th} point of species A
σ_{hydr}^2	Hydraulic variance
$\Phi^{[A]}$	Molar flow rate for compound A
θ	Model parameter(s)

Subscripts

Subscripts	Reference
0	Initial
a	Acidic
abs	Absolute
b	Basic
end	Final
g	Gazeous
H	Related to Hom's model for disinfection
in	Inlet
inf	Inferior
l	Aqueous, liquid
out	Outlet
rel	Relative
exp	Experimental
sim	Simulated
sup	Superior
$\overline{X}$	Mean value of X

Superscripts

Exponents	Reference
*	Saturated, at the equilibrium (in gas-liquid transfer)
A	For compound A
0	Set (given)
i	Initiating fraction
d	Direct consumers
p	Promoting fraction
s	Scavenging fraction

Table of Contents

INTRODUCTION

A changing context requiring new modelling tools

In the last decades, the legal, environmental and technological contexts of industrial ozonation have evolved dramatically. Consequently, the interest for new techniques related to information technology has grown in ozonation management.

With increasing suspicion on the carcinogen effect of one of the ozonation by-products, namely bromate, regulations have become more and more restrictive. In the European Community, maximum contaminant level for bromate was successively set at 50 $\mu g.L^{-1}$, 25 $\mu g.L^{-1}$ (December 2003) and finally 10 $\mu g.L^{-1}$ (December 2008). Moreover, it is likely that the maximum contaminant level may drop even further to 5 $\mu g.L^{-1}$ [Bonacquisti, 2006].

With increasing concerns about occurrence and fate of micropollutants in the environment, management of water works has to take new elements into account. Recognised as an important class of organic pollutants, micropollutants are repeatedly detected in surface and ground waters at concentration ranging from $\mu g.L^{-1}$ to $ng.L^{-1}$ (see *e.g.* [Serensen *et al.*, 1998]). For example, a large variety of pharmaceutical residues can be found in the environment: antibiotics, anti-epileptics, analgesics, antineoplastics, pharmaceuticals acting as endocrine disruptors, contraceptives… [von Gunten *et al.*, 2005].

With increasing computational power, fundamental studies on chemical kinetics can now be applied to accurately model ozonation. In the last years, different approaches were tested and sometimes applied to industrial ozonation units. Nowadays, facing new challenges, operators of water services are seeking for insight into very processes included in water works. Therefore, management of ozonation processes shall increasingly rely on modelling.

Adaptive models are required

Models for industrial ozonation units have to be adaptive. On one hand, the amounts and the types of organic species found in water bodies may dramatically evolve, either from one resource to another or from one season to another: as a consequence, natural water may react in very different manners with ozone. On the other hand, hydraulic flow conditions are specific to each ozonation unit since the geometry of tanks is case-dependent: as a consequence, contact times with ozone (and hence ozone doses) may be very different.

Natural Organic Matter (NOM) is generally described as a poorly defined mix of organic substances with variable properties in terms of acidity, molecular weight and molecular structure [Goslan *et al.*, 2002]. NOM concentration, composition, and chemistry are thus highly variable and depend on the sources of organic matter (allochthonous versus autochthonous); on the temperature, ionic strength, pH, major cation composition of the water; and on the presence of photolytic and microbiological degradation processes. Moreover, NOM not only depends on the nature of the watershed, but is also influenced by seasonal variations and particulate organic carbon inputs such as runoff or algae bloom [Leenheer and Croué, 2003]. The difficulty in quantifying the concentration of the various ozone-consuming sites in the constituents of NOM explains for a large part the dearth of related reaction kinetics data [Bezbarua, 1997].

Flow conditions impact for a large part on disinfection efficiency and bromate formation levels by affecting the overall conversion of inactivation and chemical reactions [Roustan *et*

al., 1996]. Consequently, residence time distributions are significant factors when considering the effectiveness of disinfection and chemical reactions.
Considering that industrial modelling can rely only on a limited amount of available operational data, many researchers have used statistical methods (multiple linear regressions, Artificial Neural Networks…). However, as these methods are based on an experimental exploration of limited domains for process conditions, they lack from their poor ability to extrapolate outside the calibration, or learning, domain. Moreover, physical interpretations are difficult to draw.

Objectives and Constraints
The main objective of this work is to develop and evaluate an integrated modelling procedure for industrial ozonation processes, which will enable users to predict concentration profiles for: ozone (in particular to calculate disinfection), bromate and various micropollutants. This objective can be divided into following sub-objectives:

- Select or develop models for the various chemical phenomena involved in ozonation;
- Define a modelling framework in order to consider both chemistry and hydraulics;
- Select numerical methods to calibrate and validate models;
- Determine the domain of validity of the models under perfectly known experimental conditions (model validation);
- Propose a strategy to best calibrate parameterised models, *i.e.* adapt to site-specific conditions;
- Test and discuss up-scaling possibilities;
- Propose a modelling procedure for industrial ozonation units.

In regards to these objectives, the following constraints have to be taken into account:

- The calibration procedure must be as simple and as rapid as possible;
- The model has to adapt to the majority of the water works;
- The predictions of bromate concentrations have to be accurate enough to be used in a prediction tool;
- Low computational time and eventually ease-of-use for end-users are required.

Approach
Reviewing the chemical phenomena occurring during ozonation, we considered two types of models: semi-empirical models with adjustable kinetics (for the role of NOM) and mechanistic models with predetermined kinetics (for other phenomena related to ozonation). The modelling of hydraulic flow conditions by *systematic networks* (patterns of ideal reactors) was preferred to a thorough solving of Navier-Stockes equations by Computational Fluid Dynamics (CFD) codes. Throughout the study, three numerical issues related to parameter identification have been dealt with: identifiability, estimation, and optimisation. Eventually, techniques for model validation have also been selected.

Thesis layout
Chapter 1 reviews the chemical models that have been developed by various authors for the decomposition of ozone, the inactivation of microorganisms and the formation of bromate ions. Empirical models are rapidly presented, before focusing on fundamental models. According to fundamental models, ozone decomposition can be divided into several phenomena: ozone self-decomposition, influence of organic carbon and reactions with

inorganic carbon. Fundamental kinetic models related to these phenomena are presented and discussed.

Chapter 2 reviews the modelling approaches for considering simultaneously chemical kinetics and hydraulic flow conditions. On one hand, researchers seeking an in-depth knowledge of hydraulics used CFD coupled to simplified chemical mechanisms. On the other hand, classical systematic networks composed of ideal reactors cannot achieve a completely detailed description of the flow conditions, but can be used in combination with refined chemical kinetic models. Finally, an overview of available simulator handling ozonation processes is given.

Chapter 3 reviews some of the numerical techniques for parameter identification. Parameter identification techniques are required for calibrating the model parameters. A generic methodology for modelling, leading from the understanding of an industrial process to its modelling, is presented. This section introduces more generally the concepts of *system characterisation*, *model analysis*, *calibration* and *validation*. Focus is then put on model analysis, reviewing classical parameter identification techniques. Addressing the issue of parameter *identifiability*, theoretical and practical methods are presented and their respective relevancy discussed. The choices for parameter identifiability, parameter estimation, optimisation and model validation are given.

Chapter 4 presents modelling results of lab-scale experiments investigating the decomposition of ozone in natural waters under various conditions. The experimental apparatus developed is presented. 11 water samples were studied under changing experimental conditions: contact time with ozone, pH, temperature, ozone dose, NOM concentration and NOM content. The model used is presented and the calibration of its parameters is discussed. A variance-based sensitivity analysis is used for practical identifiability of the model parameters. Further, the optimisation procedure is compared to a traditional genetic algorithm. Two calibration procedures are proposed and their results are compared. The results are presented and discussed with regards to water qualities (alkalinity, TOC) and experimental conditions.

Chapter 5 presents modelling results of lab-scale experiments investigating the formation of bromate ions in natural waters under various conditions. Experimental methods and conditions are comparable to those used in Chapter 4. Three water samples were collected at different periods of the year. The model for bromate formation is presented and its reaction kinetics are discussed. The ability of the model to best reproduce the experimental results obtained under varying conditions is discussed. Seasonal variations of the model parameters are discussed.

Chapter 6 presents modelling results of a case-study done on an industrial ozonation unit. Concentration profiles were followed for both ozone and bromate. During the field study, process conditions varied significantly: three values for the residual ozone setpoint were tested and the liquid flow was varied. Water entering the unit was characterised at lab-scale and the models for the influence of NOM on ozone decomposition and bromate formation were calibrated. Additionally, the development of a systematic network representing the hydraulics of the unit is presented. The direct implementation of the chemical models calibrated at lab-scale is then discussed.

Bibliography

- **Bezbarua B. K.,** (1997). Modeling Reactions of Ozone with NOM, Ph.D. thesis, University of Massachusetts Amherst, USA.
- **Bonacquisti T. P**., (2006). A drinking water utility's perspective on bromide, bromate, and ozonation, *Toxicology*, Vol. **221**, pp. 145-148.
- **Goslan E. H., Fearing D. A., Banks J., Wilson D., Hills P., Campbell A. T., Parsons S. A.,** (2002). Seasonal variations in the disinfection by-product precursor profile of a reservoir water, *Journal of Water Supply: Research and Technology – AQUA*, Vol. **51**, pp. 475– 482.
- **Leenheer J. A.** and **Croué J.-P.**, (2003). Characterizing Aquatic Dissolved Organic Matter, *Environmental Science and Technology*, Vol. **37**, pp. 19A-26A.
- **Roustan M., Duguet J.-P., Laine J.-M., Do-Quang Z., Mallevialle J.,** (1996). Bromate ion formation: impact of ozone contactor hydraulics and operating conditions, *Ozone: Science and Engineering*, Vol. **18**, pp. 87-97.
- **Serensen B. H., Nielsen S. N., Lanzky P. F., Ingerslev F., Holten Lutzhoft H. C., Jorgensen S. E.,** (1998). Occurrence, Fate and Effects of Pharmaceutical Substances in the Environment, A Review, *Chemosphere*, Vol. **36**, pp. 357-393.
- **von Gunten U., Huber M. M., Göbel A., Joss A., Hermann N., Löffler D., McArdell C. S., Ried A., Siegrist H., Ternes T. A.,** (2005). Oxidation of Pharmaceuticals during Ozonation of municipal Wastewater Effluents: A pilot Study, *Proceedings of the IOA 17th World Ozone Congress,* Strasbourg.

1. OZONE CHEMISTRY

Abstract

Given the stringent regulations on Disinfection By-Product (DBP) formation levels (10 $\mu g.L^{-1}$ in the case of bromate ions), process modellers are seeking an in-depth understanding of all chemical phenomena occurring during ozonation. This remains an uneasy task since ozone may, directly *via* molecular reactions involving ozone or indirectly *via* reactions involving radicals formed during ozone decomposition, interact with a variety of species naturally present in water.

Facing this complexity, two approaches were considered. On one hand, numerous authors have proposed integrated approaches, for which the main influent experimental factors were characterised and reduced to empirical laws with one or more adjustable parameter(s). The results of empirical laws are restricted to the calibration domain of the model, which tends to be very narrow for natural waters. On the other hand, the possibilities offered by modern experimental techniques, such as pulse radiolysis, fostered the advances in fundamental kinetics for all reactions in which ozone may be involved. Hence, several mechanistic models are available in literature for the following phenomena: ozone self-decomposition, reactions with alkaline species, reactions for the formation of bromate ions, reactions with micropollutants.

Despite the fact that many phenomena have been understood and modelled, ozone chemistry remains for a large part unknown when dealing with natural waters. The fractionation techniques used to individually study the interactions of ozone – and the main radical species – with classes of natural substances (humic, fulvic, tanic acids…) gave interesting results with artificially recreated waters. However, no conclusive evidence of a possibility to extrapolate such results to natural waters could be given. Moreover, fractionation techniques remain difficult to systematically carry out in order to characterise water samples. Authors have therefore proposed empirical or semi-empirical models for the role of Natural Organic Matter (NOM) based on rough chemical considerations (division of the NOM into several fractions with distinct roles).

As a consequence, mechanistic models available in the literature can be chosen for the following phenomena:

- ozone self-decomposition: a Staehelin, Bühler and Hoigné-based (SBH-based) mechanism shall be chosen;
- reactions with inorganic carbon: a classical pathway combining reactions widely used in different studies will be considered;
- reactions for bromate formation: all the reactions present in the literature shall not be considered, but a selection shall be done based on kinetics.

Considering the influence of NOM, a semi-empirical model shall be proposed for modelling needs. The model shall be based on the classical categorisation: *consumers*, *initiators*, *promoters* and *inhibitors*. The number of adjustable parameters may vary.

Contents

1.1. Introduction

Ozone is a gas of limited solubility that must first be dissolved into water to be effective against microorganisms. Once dissolved, aqueous ozone engages in complex chemistry, reacting in two manners: direct reactions by molecular ozone; indirect reactions involving radical species formed when ozone decomposes in water. Depending on modelling goals, either pathway may be relevant. If one is concerned with disinfection, only the direct, slow and selective reactions of molecular ozone with microorganisms will have to be taken into account. Now, if one wants to focus on Disinfection By-Product (DBP) formation, rapid radical reactions (particularly those involving hydroxyl radicals) with many types of dissolved species shall also be relevant and added to the previous reaction pathway for disinfection [Doré, 1989].
Due to its high reactivity, ozone is an unstable compound when dissolved in synthetic and natural waters. At neutral pH, typical half-lives are under 60 minutes. The kinetics regulating ozone decomposition are complex. For simplification's sake, it has often been reduced into two main phases: an initial phase with half-lives less than twenty seconds for raw water and a second phase with a half-life between thirty seconds and sixty minutes (figure **1**).

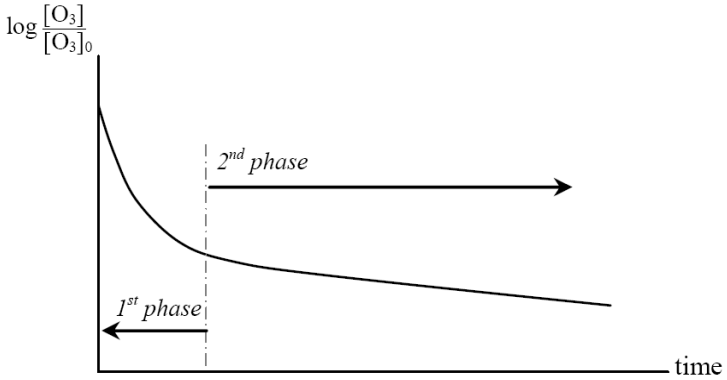

Figure 1 **Typical ozone decomposition profile in natural water**

The modelling of ozone decomposition in water has therefore often separated the two phases. In the following, we shall speak of Instantaneous Ozone Demand (IOD) for the first phase of figure **1** and of "long-term ozone demand", or simply "ozone decomposition" for the second phase. IOD corresponds thus to the difference between the applied dose and the ozone remaining in the first sample, which can be withdrawn.
The objective of this chapter is to select the modelling framework for all chemical phenomena occurring during ozonation of natural waters. Consequently, a critical review of the main reactions related to ozonation is given in this chapter. In the first section, examples of integrated approaches for ozone decomposition, bromate formation and disinfection efficiency assessment are presented (section **1.2.**, paragraphs **3** to **5**). The main experimental factors of influence, the analysis of which has led to the development of such integrated approaches are presented beforehand (paragraph **1.2.2.**). In the following sections, different mechanistic chemical models are presented for the phenomena: ozone self-decomposition (section **1.3.**); reactions with inorganic and organic carbon (sections **1.4.** and **1.5.**, respectively). A section is devoted to the successive oxidation steps leading from bromide to bromate (section **1.6.**). Finally, other reactions of interest (phosphate, micropollutants) are presented in section **1.7.**

1.2. Integrated Approaches

1.2.1. Introduction

Integrated approaches aim at giving simple tools to evaluate key phenomena, which occur during ozonation: ozone decomposition, disinfection and bromate formation. As the term suggests, *integrated* approaches integrate different parameters, at various scales: hydrodynamics and process conditions (batch, bubble column, ozone contactor, temperature…), chemistry (pH, alkalinity, NOM, bromide concentration…).
Integrated approaches are therefore generally based on empirical relations, though they may partly rely on fundamental results. Widely used, multiple linear regression models give a mathematical analytical relationship between a dependent variable and independent variables. The output dependent variable is what the scientist is seeking to evaluate, and the independent variables are experimental parameters that can easily be measured. Integrated approaches are simple to use, however they require extensive experimental harvesting for model-fitting. Experiment planning techniques may reduce the number of experimental measurements, but data harvesting remains a major task when developing an integrated model.
Predictions of integrated model are of two types: interpolation and extrapolation. Interpolation is a prediction within the range of values in the dataset used for model-fitting, while a prediction outside this range is called extrapolation. Generally, interpolation gives good modelling results (*i.e.* model output is close to experimental value measured *a posteriori*). Extrapolation results are less accurate than interpolation ones. Depending on the type of model and on the physical nature of the phenomena, the error between model predictions and experimental measurements may increase very fast when moving outside the fitting domain. Therefore, some researchers recommend not using integrated models for extrapolation [Chiang, 2003].

1.2.2. Most Influent Experimental Factors on Ozone Decomposition, Bromate Formation, Disinfection Efficiency

1.2.2.1. pH

Hydroxide ions are initiators of the chain reaction for ozone decomposition. An increase in pH therefore favours ozone decomposition and influences the oxidation reactions of ozone with other species, according to their pK_A values [Krasner *et al.*, 1995]. It was notably reported that dissolved ozone at pH levels below 7 does not react with water but dissociates into dioxygen and molecular oxygen [Sehested *et al.*, 1991]. With increasing pH, self-decomposition of ozone occurs to eventually yield a variety of very reactive free radials, such as the hydroxyl radical, •OH [Staehelin *et al.*, 1984].
pH greatly influences bromate formation as well. Decreasing pH changes the bromate formation in two ways:

i. Shift of $BrOH/BrO^-$ equilibrium to BrOH (pK_A = 8.8) to reduce further oxidation by ozone;
ii. Decrease of the rate of hydroxyl radical formation from ozone decomposition, which drops the oxidation rate of BrOH. This explains why bromate formation is often controlled by pH depression (see *e.g.* [Pinkernell and von Gunten, 2001]).

1.2.2.2. Temperature

Numerous physicochemical factors evolve with temperature: reaction rate constants, equilibrium constants, Henry's law coefficients… When temperature is raised, less ozone is dissolved in water and ozone decomposition rates increase. As a consequence, ozone doses applied in industrial units are generally higher in summer than in winter, when the same residual – final – ozone concentration is targeted. Bromate formation is also enhanced at higher temperatures, though some authors agree that temperature has a relatively small effect on bromate formation relative to pH and ammonia concentration [von Gunten and Pinkernell, 2000]. Disinfection kinetics are relatively insensitive to temperature changes.

1.2.2.3. Initial Bromide Concentration

Bromate is an oxidised form of bromide, consequently an increase in bromide concentration directly reflects on bromate concentration. Moreover, by consuming hydroxyl radicals rather than molecular ozone, the oxidised forms of bromide diminish the ratio $[^{\bullet}OH]/[O_3]$ [Westerhoff, 2002]. It is however difficult to assess the effect on global ozone decomposition, as it depends on both concentrations of ozone and hydroxyl radicals.

1.2.2.4. Alkalinity

Carbonate and hydrogenoarbonate ions can scavenge hydroxyl radicals formed during ozone decomposition. As a result, alkaline species may reduce the decomposition rate of the dissolved ozone and inhibit the radical pathway of bromate formation. However, above pH 8.5, the effect of alkalinity becomes pH dependent because carbonate ions scavenge hydroxyl radicals with a larger rate constant than that of hydrogenocarbonate ion [Hoigné and Bader, 1979]. Finally, an increase in alkalinity favours bromate formation only under high pH conditions as:

i. The equilibrium HCO_3^-/ CO_3^{2-} is shifted (pK_A = 10.3), advantaging carbonate ions that are more reactive than hydrogenocarbonate ions towards hydroxyl radicals;
ii. Both hydroxyl radicals and hypobromite (BrO^-) ions concentrations increase with pH. The carbonates and hydrogenocarbonates may react first with hydroxyl radicals to form the carbonate radical ($^{\bullet}CO_3^-$), which in turn may react with hypobromite, leading to bromate formation [von Gunten and Hoigné, 1993].

1.2.2.5. Natural Organic Matter (NOM)

The stability of ozone largely depends on the type and content of NOM. Generally, the presence of the NOM in water will lower the stability of ozone through direct reaction with molecular ozone and consumption of hydroxyl radicals. The presence of NOM generally inhibits the formation of bromate especially at the initial period of ozonation [Song *et al.*, 1996].

Different measures can be used to characterise NOM. The most used are Total Organic Carbon (TOC) and Dissolved Organic Carbon (DOC). As organic carbon is either dissolved or particulate, one has DOC ≤ TOC. Focusing on aqueous chemistry, particulate carbon is seldom considered. For a given type of water, UV absorbance can serve as surrogate for the DOC value [Hoigné, 1994]. Specific UVA (SUVA = UV absorbance per gram of TOC), which is related to the humic content of NOM, is generally not considered as an indicator for the organic content and used as such in predictive models (*e.g.* [Legube *et al.*, 2004]).

1.2.2.6. Ammonia

Despite limited reactivity with ozone, ammonia, in the presence of bromide ions, can temporarily divert the hypobromite ions formed during ozonation and thereby delay the

formation of bromate, as well as bromoform and further bromo-organic compounds [Langlais *et al.*, 1991]. As a result, the formation of bromate can be inhibited in ammonia-containing water. Addition of ammonia may thus be used as a bromate control method. However, bromate removal by ammonia addition is not efficient for waters that have a low pH and/or already contain high ammonia levels [Westerhoff, 2002].

1.2.2.7. Summary

Table **1** gives an overview of the consequences of a change in the over-listed factors upon disinfection efficiency, decomposition rate of ozone and bromate formation. It appears that all the factors play a role. As a result, these experimental factors are generally present in the empirical laws for disinfection, ozone decomposition or bromate formation (see examples in the next paragraph).

Table 1 Summary of the effects of water factors, adapted from [Westerhoff, 2002]

Factor increasing	Disinfection efficiency	Ozone decomposition rate	Bromate formation rate
pH	**-**	**+**	**+**
Temperature	**+**	**+**	**+**
Bromide	*unchanged*	*unchanged*	**+**
Alkalinity	**+**	**-**	**+***for high pH*, **-***else*
NOM	**-**	**+**	**-**
Ammonia	*unchanged*	*unchanged*	**-**

1.2.3. Integrated Approaches for Ozone Decomposition

Before experimental investigation of complex radical chemistry could be achieved, researchers have tried to model empirically ozone decomposition. One of the first studies in this field has been carried out by [Rothmund and Burgstaller, 1913]. Since then, various authors have postulated reaction rate laws with different kinetic order. The general form of such rate equations is given in equation **1**. A good review of these early works is to be found in [Gurol and Singer, 1982].

$$r^{O_3} = -w_2[HO^-]^{Or(HO^-)}[O_3]^{Or(O_3)} \quad \textbf{(1)}$$

The difficulty to mechanistically model ozone self-decomposition, and more generally ozone decay in natural waters has led researchers to continue developing such laws. We refer interested readers to [Savary, 2002] for a summary of common empirical relations for ozone decomposition. For our part, we shall concentrate on two models proposing pseudo first-order kinetics (reaction **2**).

$$r^{O_3} = -w[O_3] \quad \textbf{(2)}$$

A clear definition setting standardized guidelines for the application of equation **2** was given by [Hoigné and Bader, 1994] (another procedure for two-phase systems has been proposed by [Roche *et al.*, 1994]). Hoigné and Bader introduced a convenient parameter called the "second half-life", defined as the ozone decomposition rate in the timeframe where the residual concentration decreases from 50 to 25% of its initial value. The authors suggested a simple method to characterise the raw-water quality by analysing the IOD (see **1.5.5.**) and the second half-life of ozone. Similar approaches have been adopted in other studies (*e.g.* [Roustan *et al.*, 1998]).

In the following, we solely present the results of two studies, where equation **2** has been implemented. Purpose is here to illustrate the sensibility of the aggregated constant w to experimental conditions. Working with aliquots from a stock humic solution diluted in distilled water, [Yurteri and Gurol, 1988] proposed relation **3**.

$$\log(w) = -3.98 + 0.66.pH + 0.61.\log(TOC) - 0.42.\log\frac{A_T}{10} \quad \textbf{(3)}$$

with the following requirements
- w in h^{-1}
- 6.8 < pH < 9
- T = 20 ± 1 °C
- 10 g $CaCO_3.m^{-3}$ < A_T < 500 g $CaCO_3.m^{-3}$
- 0.3 $g.m^{-3}$ < TOC < 5 $g.m^{-3}$
- synthetic waters
- magnetically agitated discontinuous reactor

Working with potable water from the distribution network, [Wang, 1995] found w to obey relation **4**.

$$\log(w) = -4 + 0.29.pH + 1.19.\log(TOC) + 0.41.\log(A_T) \quad \textbf{(4)}$$

under the subsequent conditions
- w in min^{-1}
- 7.5 < pH < 8.1
- T = 15 °C
- 84 g $CaCO_3.m^{-3}$ < A_T < 150 g $CaCO_3.m^{-3}$
- 2 $g.m^{-3}$ < TOC < 6 $g.m^{-3}$

Although having similar forms, such relations are difficult to generalise. For example, alkalinity seems to play opposite roles when considering the relationships **3** or **4**. Such laws tend to be very dependent on experimental conditions (organic and inorganic nature of the water, buffer used, humic/fulvic substances added, temperature…) and should therefore be adapted. Consequently, their use remains restricted.

1.2.4. Integrated Approaches for the Formation of Bromate Ions

Similarly, empirical relations predicting the formation of bromate during ozonation have been developing for the past twenty years. As previously, we shall only review two fully empirical models and a semi-empirical model in this paragraph. Reviews on integrated approaches for the prediction of bromate formation can extensively be found in the literature (see *e.g.* [Sadiq and Rodriguez, 2004]; [Jarvis *et al.*, 2007]).

1.2.4.1. Two Empirical Models

[Song *et al.*, 1996] developed an empirical model based on a set of experimental points obtained on NOM isolates in a closed reactor. Data was collected according to an experimental design built to cover a wide range of conditions. The evolution of bromate concentration could be evaluated according to equation **5**.

$$[BrO_3^-] = 10^{-6.11}[Br^-]^{0.88}[DOC]^{-1.18}[N-NH_3]^{-0.18}[O_3]^{1.42}\,pH^{5.11}[A_T]^{0.18}\,t^{0.27} \quad \textbf{(5)}$$

under the subsequent conditions
- [BrO_3^-] in $\mu g.L^{-1}$
- 6.5 < pH < 8.5
- 100 $\mu g.L^{-1}$ < [Br-] < 1000 $\mu g.L^{-1}$
- 1 mg $CaCO_3.L^{-1}$ < A_T < 216 mg $CaCO_3.L^{-1}$
- 1.5 $mg.L^{-1}$ < [DOC] < 6.0 $mg.L^{-1}$
- 0.005 $mg.L^{-1}$ < [$N-NH_3$] < 0.70 $mg.L^{-1}$
- 1.5 $mg.L^{-1}$ < [O_3] < 6.0 $mg.L^{-1}$
- 1 min < t < 30 min
- batch reactor or ideal Plug Flow Reactor (PFR)

Since its formulation, this model has been used by different researchers and can be seen as a rapid way to roughly estimate the level of bromate that may be formed during ozonation [Savary, 2002]. However, it strictly remains devoted to lab-scale experiments.

[Ozekin and Amy, 1997] have designed an empirical model from an experimental design done on waters originating from seven different drinking water sources. Waters containing ammonia where treated separately. The correlations (**6**) and (**7**) are valid for a temperature of 20 °C only.

Model without ammonia: **(6)**

$$\log[BrO_3^-] = -3.361 + 0.006.t + 0.249.pH + 1.575.\log[O_3] + 1.136.\log[Br^-] - 1.267.\log[DOC]$$

Model with ammonia: **(7)**

$$\log[BrO_3^-] = -3.561 + 0.006.t + 0.253.pH + 1.598.\log[O_3] + 1.137.\log.[Br^-] - 1.186.\log.[DOC] - 0.086.\log.[NH_3]$$

under following conditions

- $[BrO_3^-]$ in µg.L^{-1}
- 6.5 < pH < 8.5
- 69 µg.L^{-1} < [Br$^-$] < 440 µg.L^{-1}
- 1.9 mg.L^{-1} < [DOC] < 8.4 mg.L^{-1}
- 0 mg.L^{-1} < [N-NH_3] < 3 mg.L^{-1}
- 1.05 mg.L^{-1} < [O_3] < 10 mg.L^{-1}
- 1 min < t < 60 min
- batch reactor or ideal PFR

Equation **8** was proposed afterwards to account for the temperature effect on bromate formation [Sohn *et al.*, 2004].

$$[BrO_3^-]_T = [BrO_3^-]_{20°C}.1.035^{T-20} \qquad \textbf{(8)}$$

The relation **8** is valid in the temperature range: 2°C < T < 24°C.

1.2.4.2. A Semi-Empirical Model

[Mizuno *et al.*, 2007a] have developed a semi-empirical predictive model for bromate formation. It is namely based on a simplified mechanism of bromate formation (figure **2**), for which a reaction is supposed rate-limiting step of the overall formation mechanism (reaction R1 in figure **2**). The kinetics of this particular reaction is then assessed statistically using multiple linear regression analysis.

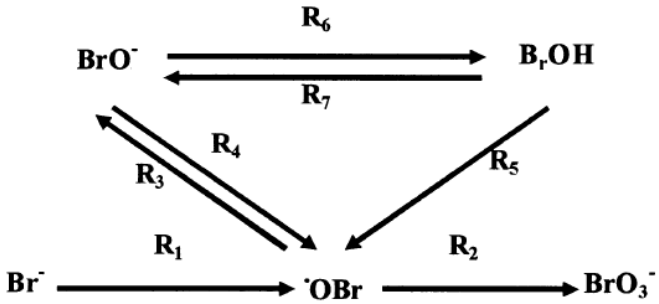

Figure 2 Simplified reaction pathway for the formation of bromate (adapted from [Mizuno *et al.*, 2007a])

The proposed model was calibrated and validated on experimental data obtained with a lab reactor column considered as a PFR, for which different sampling points were installed. The experiments were performed on ultra-pure water spiked with various concentration levels of bromine stock solution. pH was adjusted using phosphate buffer.
The presented results show a good agreement of the model to experimental data. However, they should be confirmed on NOM-containing water. Moreover, phosphate buffer is known to act as scavenger of ozone self-decomposition in NOM-free water [Staehelin and Hoigné, 1985], what could therefore influence the experimental results.

1.2.5. Integrated Approach for the Determination of Disinfection Efficiency

In order to compare the biocidal effectiveness of disinfectants, the U.S. Environment Protection Agency (USEPA) defined and imposed in 1991 the Ct concept as measurement for disinfection [USEPA, 1991]. Major considerations are the disinfectant concentration and the time needed to attain inactivation of a certain microbial population exposed under specific conditions.
The Ct concept originates from the disinfection model of Chick and Watson (based on the works by [Chick, 1908]), more extensively presented in Appendix **A**. The Chick and Watson model is presented in equation **9**.

$$r^N = -kC^n N \qquad \textbf{(9)}$$

n : disinfectant's reaction order
C : disinfectant concentration
N : microorganism concentration
k : apparent constant rate, sometimes called lethality coefficient

Modelling the considered tank by a perfectly mixed discontinuous reactor and assuming a constant disinfectant concentration, one obtains equation **10**.

$$\ln\left(\frac{N}{N_0}\right) = -kC^n \cdot t \qquad \textbf{(10)}$$

For a disinfectant's reaction order n = 1, the log-inactivation is then directly linked to the product Ct. This led to the introduction of the Ct concept in potable water treatment.

t is a contact time, which is usually prescribed as t_{10}, the residence time of the earliest ten percent of water (and microorganisms) to travel from the contactor inlet to outlet, as determined from a tracer Residence Time Distribution (RTD) study [USEPA, 1991]. The USEPA uses this conservative t_{10} value to ensure minimum exposure time to disinfectants for ninety percent of the water (and microorganisms). C is defined as average disinfectant (*i.e.* ozone) residual concentration at the outlet of each contact chamber, which again is a conservative estimation of the oxidant level within the chamber. This value is directly measured through sampling ports or estimated from table **2**. Thus, inactivation credits may be given to each chamber, the Ct of the ozonation unit being defined as the sum of chamber inactivation credits.

Table 2 Concentration values used in the Ct calculation [USEPA, 1991]

Type of chamber	C value for the Ct calculation
First dissolution	*Not applicable because of the IOD for* Cryptosporidium, *but certain inactivation credit can be granted for* Giardia *and viruses, provided that the ozone residual at the outlet of the first contact chamber meets minimum concentration levels*
Reactive	C_{out}
Co-current dissolution	$\max(C_{out}, \frac{C_{in} + C_{out}}{2})$
Counter-current dissolution	$\frac{C_{out}}{2}$
Turbine diffuser	C_{out}

Ct values have been developed for inactivation of various microorganisms for the major disinfectants. Examples of these values are shown in table **3** [Adams and Clark, 2001]. Considering only one disinfectant, Ct table are usually expressed as function of both temperature and inactivation log credit.

Values gathered in table **3** show that ozone has the highest disinfection efficiency, inactivating 99% of most types of microorganisms at very low Ct values. Chloramine shows the lowest efficiency. For these data, the disinfectant's reaction order n varies between 0.7 and 1.3; therefore, a value of n = 1 was chosen for the referenced analysis. Preformed chloramine was used because of its conservative character with respect to Ct values.

Table 3 Summary of Ct value ranges for inactivation of various microorganisms by disinfectants (mg.L^{-1}.min^{-1}), adapted from [Adams and Clark, 2001]

Microorganism	Free chlorine 6 < pH < 7	Preformed chloramine 8 < pH < 9	Chlorine dioxide 6 < pH < 7	Ozone 6 < pH < 7
E. coli	0.34 - 0.05	95 - 180	0.4 - 0.75	0.02
Polio virus	1.1 – 2.5	768 – 3740	0.2 – 6.7	0.1 – 0.2
Rotavirus	0.01 – 0.05	3806 – 6476	0.2 – 2.1	0.006 – 0.06
Phage f_2	0.08 – 0.18	ND	ND	ND
G. lamblia cysts	47 – 150	2200[a]	26[a]	0.5 – 0.6
G. muris cysts	30 – 630	1400	7.2 – 18.5	1.8 – 2.0
Cryptosporidium parvum	7200[b]	7200[c]	78[c]	5 – 10[b]

Note: all Ct values are for 99% inactivation at 5°C except for *Giardia lamblia* and *Cryptosporidium parvum*.
[a]Values for 99.9% inactivation at pH 6 – 9
[b]99% inactivation at pH 7 and 25°C
[c]90% inactivation at pH 7 and 25°C

Simple in its formulation and use, the Ct approach suffers from important drawbacks:

- Many chemical phenomena such as ozone mass transfer, competitive consumption of ozone by other components (and notably by NOM), self-decomposition of ozone, diversity of organisms present… are not taken into account by the Ct approach [Masschelein, 2000]. Case-studies and reports on application of the Ct approach to industrial tanks have consequently shown important decreases in ozone concentration from chamber to chamber (*e.g.* [Hunter and Rakness, 1997]). Using different residual concentrations for the calculation of the Ct (table **2**) gives only a partial answer to this issue.

- Describing ozone contactor hydraulics by a single parameter, t_{10}, appears questionable. Firstly, because the choice of t_{10} is considered as arbitrary [Roustan *et al.*, 1991]. Secondly, because this single parameter can obviously not render an account of the hydrodynamic complexity of industrial ozonation units [Haas and Betz, 2009].
- The conservative approach for inactivation credit allocation, *i.e.* considering always the lowest oxidant concentration and the shortest contact time, maximises the inactivation but does hide, and thus jeopardize, a secondary health goal : the DBP formation (bromate being just the critical one for ozone). The best case scenario for inactivation may indeed also be the worst case scenario for DBP formation.

Other models for the microbial inactivation and other approaches for evaluating disinfection efficiency are presented in Appendix **A**.

1.3. Ozone Self-Decomposition

1.3.1. SBH and SBH-Based Mechanisms

Using pulse radiolysis experiments, Staehelin, Bühler and Hoigné (SBH) have established a mechanism for ozone self-decomposition in water, under acidic to weak alkaline conditions ([Staehelin and Hoigné, 1982]; [Bühler *et al.*, 1984]; [Staehelin *et al.*, 1984]). Since then, this mechanism has been widely used and adapted by several authors. Table **4** summarises the main reactions comprised in the original model and the subsequent adaptations by [Westerhoff *et al.*, 1997] and [Beltrán *et al.*, 2000]. An alternative initiation step was proposed by the authors, but the reaction engaging hydroxide ions is generally preferred.

Additionally, termination reactions may be incorporated to the model. They were proposed by [Staehelin *et al.*, 1984] and are presented in table **5**, completed by the recombination of two $^{\bullet}HO_2$ radicals ($2^{\bullet}HO_2 \rightarrow H_2O_2 + O_2$, [Bielski and Allen, 1977]). The recent paper of [Mizuno *et al.*, 2007c] suggests taking also these reactions into account when modelling ozone self-decomposition in ultra-pure water. Although not present in table **4**, the model proposed by [Mizuno *et al.*, 2007c] is a variant of SBH mechanism, for which reactions involving radical $^{\bullet}HO_4$ were removed. Reactions **11** and **12** were thus replaced by reaction **13**, taken from the TFG model (presented in the next paragraph). Using kinetics values taken from the literature, the authors found that the model strongly overpredicted ozone decomposition. The reaction rate constant value was therefore optimised and lowered from 3.10^9 $M^{-1}.s^{-1}$ to 9.10^5 $M^{-1}.s^{-1}$ (see table **6**).

$$^{\bullet}OH + O_3 \rightarrow {}^{\bullet}HO_4 \quad \textbf{(11)}$$

$$^{\bullet}HO_4 \rightarrow {}^{\bullet}HO_2 + O_2 \quad \textbf{(12)}$$

$$^{\bullet}OH + O_3 \rightarrow {}^{\bullet}HO_2 + O_2 \quad \textbf{(13)}$$

Table 4 SBH self-decomposition mechanism

Type	Reaction	Kinetic constant value (T=293 K)		Reference
Initiation	$O_3 + HO^- \rightarrow {}^\bullet O_2^- + {}^\bullet HO_2$	70 $M^{-1}.s^{-1}$		[Staehelin and Hoigné, 1982]
		$1.8.10^2$ $M^{-1}.s^{-1}$		[Bezbarua and Reckhow, 2003]
Alternative initiation	$HO_2^- + O_3 \rightarrow {}^\bullet OH + {}^\bullet O_2^- + O_2$	$2.8.10^6$ $M^{-1}.s^{-1}$		[Staehelin and Hoigné, 1982]
		$2.2.10^6$ $M^{-1}.s^{-1}$		[Westerhoff *et al.*, 1997]
Propagation	${}^\bullet O_2^- + O_3 \rightarrow {}^\bullet O_3^- + O_2$	$1.6.10^9$ $M^{-1}.s^{-1}$		[Taube and Bray, 1940]
	${}^\bullet HO_3 \rightarrow {}^\bullet OH + O_2$	$1.1.10^5$ s^{-1}		[Bühler *et al.*, 1984]
		$1.4.10^5$ s^{-1}		[Beltrán *et al.*, 2000]
	${}^\bullet OH + O_3 \rightarrow {}^\bullet HO_4$	2.10^9 $M^{-1}.s^{-1}$		[Staehelin *et al.*, 1984]
		2.10^8 $M^{-1}.s^{-1}$		[Bezbarua and Reckhow, 2003]
	${}^\bullet HO_4 \rightarrow {}^\bullet HO_2 + O_2$	$2.8.10^4$ s^{-1}		[Staehelin *et al.*, 1984]
Termination	${}^\bullet HO_4 + {}^\bullet HO_4 \rightarrow H_2O_2 + 2O_3$	5.10^9 $M^{-1}.s^{-1}$		[Staehelin *et al.*, 1984]
	${}^\bullet HO_4 + {}^\bullet HO_3 \rightarrow H_2O_2 + O_2 + O_3$	5.10^9 $M^{-1}.s^{-1}$		[Staehelin *et al.*, 1984]
Acid-base equilibria		**Direct**	**Indirect**	
pK_A = 8.2	${}^\bullet O_3^- + H^+ \leftrightarrow {}^\bullet HO_3$	$5.2.10^{10}$ $M^{-1}.s^{-1}$	$3.3.10^2$ s^{-1}	[Bühler *et al.*, 1984]
		$3.15.10^{10}$ $M^{-1}.s^{-1}$	$2.5.10^2$ s^{-1}	[Westerhoff *et al.*, 1997]
pK_A = 4.8	${}^\bullet O_2^- + H^+ \leftrightarrow {}^\bullet HO_2$	5.10^{10} $M^{-1}.s^{-1}$	$7.9.10^5$ s^{-1}	[Westerhoff *et al.*, 1997]
pK_A = 11.6	$HO_2^- + H^+ \leftrightarrow H_2O_2$	5.10^{10} $M^{-1}.s^{-1}$	$1.25.10^{-1}$ s^{-1}	[Westerhoff *et al.*, 1997]
		2.10^{10} $M^{-1}.s^{-1}$	$4.5.10^{-2}$ s^{-1}	[Chelkowska *et al.*, 1992]

Table 5 Additional termination reactions for SBH mechanism

Reaction	Kinetic constant value (293 K)	Reference
$2{}^\bullet HO_4 \rightarrow H_2O_2 + 2O_3$	5.10^9 $M^{-1}.s^{-1}$	[Staehelin *et al.*, 1984]
$2{}^\bullet HO \rightarrow H_2O_2$	5.10^9 $M^{-1}.s^{-1}$	[Farhataziz and Ross, 1977]
${}^\bullet HO + {}^\bullet O_2^- \rightarrow HO^- + O_2$	10^{10} $M^{-1}.s^{-1}$	[Farhataziz and Ross, 1977]
${}^\bullet HO + {}^\bullet HO_3 \rightarrow H_2O_2 + O_2$	5.10^9 $M^{-1}.s^{-1}$	[Staehelin *et al.*, 1984]
$2{}^\bullet HO_3 \rightarrow H_2O_2 + 2O_2$	5.10^9 $M^{-1}.s^{-1}$	[Staehelin *et al.*, 1984]
${}^\bullet HO_3 + {}^\bullet O_2^- \rightarrow HO^- + 2O_2$	10^{10} $M^{-1}.s^{-1}$	[Staehelin *et al.*, 1984]
${}^\bullet HO + {}^\bullet HO_4 \rightarrow H_2O_2 + O_3$	5.10^9 $M^{-1}.s^{-1}$	[Staehelin *et al.*, 1984]
${}^\bullet O_2^- + {}^\bullet HO_4 \rightarrow HO^- + O_3 + O_2$	10^{10} $M^{-1}.s^{-1}$	[Staehelin *et al.*, 1984]
${}^\bullet HO_4 + {}^\bullet HO_3 \rightarrow H_2O_2 + O_2 + O_3$	5.10^9 $M^{-1}.s^{-1}$	[Staehelin *et al.*, 1984]
$2{}^\bullet HO_2 \rightarrow H_2O_2 + O_2$	$8.3.10^5$ $M^{-1}.s^{-1}$	[Bielski and Allen, 1977]

1.3.2. TFG and TFG-Based Mechanisms

The second well-known self-decomposition mechanism for aqueous ozone has been proposed by Tomiyasu, Fukutomi and Gordon (TFG) [Tomiyasu *et al.*, 1985]. The authors have studied the kinetics of the decomposition of ozone in aqueous alkaline solutions (pH ~ 12) by means of an accumulated stopped-flow method. It has also been widely used and very frequently adapted. The model and subsequent modifications by selected authors is presented in table **6**.

Table 6 TFG self-decomposition mechanism

Type	Reaction	Kinetic constant value (293 K)	Reference
Initiation	$O_3 + HO^- \rightarrow HO_2^- + O_2$	4.10^1 $M^{-1}.s^{-1}$	[Tomiyasu *et al.*, 1985]
		$1.2.10^2$ $M^{-1}.s^{-1}$	[Chelkowska *et al.*, 1992] ; [Gordon, 1995] ; [Hassan *et al.*, 2003]
	$HO_2^- + O_3 \rightarrow {}^\bullet O_3^- + {}^\bullet HO_2$	$2.2.10^6$ $M^{-1}.s^{-1}$	[Tomiyasu *et al.*, 1985]
		$1.5.10^6$ $M^{-1}.s^{-1}$	[Chelkowska *et al.*, 1992]
		$1.8.10^6$ $M^{-1}.s^{-1}$	[Gordon, 1995]
Propagation	${}^\bullet O_2^- + O_3 \rightarrow {}^\bullet O_3^- + O_2$	$1.6.10^9$ $M^{-1}.s^{-1}$	[Taube and Bray, 1940]
	${}^\bullet O_3^- + H_2O \rightarrow {}^\bullet OH + O_2 + HO^-$	2.10^1-3.10^1 $M^{-1}.s^{-1}$	[Tomiyasu *et al.*, 1985]
		$1.5.10^1$ $M^{-1}.s^{-1}$	[Chelkowska *et al.*, 1992]; [Gordon, 1995]
	${}^\bullet OH + {}^\bullet O_3^- \rightarrow {}^\bullet O_2^- + {}^\bullet HO_2$	6.10^9 $M^{-1}.s^{-1}$	[Tomiyasu *et al.*, 1985]
		3.10^9 $M^{-1}.s^{-1}$	[Chelkowska *et al.*, 1992] ; [Gordon, 1995]
	${}^\bullet OH + O_3 \rightarrow {}^\bullet HO_2 + O_2$	3.10^9 $M^{-1}.s^{-1}$	[Bahnemann and Hart, 1982] ; [Tomiyasu *et al.*, 1985]
		2.10^9 $M^{-1}.s^{-1}$	[Acero and von Gunten, 2000]; [Elovitz and von Gunten, 1999]
		5.10^8 $M^{-1}.s^{-1}$	[Chelkowska *et al.*, 1992] ; [Gordon, 1995]
		$2.7.10^7$ $M^{-1}.s^{-1}$	[Nemes *et al.*, 2000]
		9.10^5 $M^{-1}.s^{-1}$	[Mizuno *et al.*, 2007c]
Termination	${}^\bullet OH + {}^\bullet O_3^- \rightarrow O_3 + HO^-$	$2.5.10^9$ $M^{-1}.s^{-1}$	[Tomiyasu *et al.*, 1985]
		10^{10} $M^{-1}.s^{-1}$	[Chelkowska *et al.*, 1992] ; [Gordon, 1995]
Acid-base equilibria		**Direct**	**Indirect**
pK_A = 4.8	${}^\bullet O_2^- + H^+ \leftrightarrow {}^\bullet HO_2$	5.10^{10} $M^{-1}.s^{-1}$	$7.9.10^5$ s^{-1} [Westerhoff *et al.*, 1997]
pK_A = 11.6	$HO_2^- + H^+ \leftrightarrow H_2O_2$	5.10^{10} $M^{-1}.s^{-1}$	$1.25.10^{-1}$ s^{-1} [Westerhoff *et al.*, 1997]

1.3.3. Elements of Appreciation and Comparison

SBH and TFG self-decomposition mechanisms have been used in ozonation modelling studies for over twenty years. A summary of both models, discussing many mechanistic aspects is given in [Langlais *et al.*, 1991]. However, changes in their kinetic rate constant values can be found in numerous papers, more particularly when using the TFG model. This fact underlines the hypothetical character of ozone self-decomposition modelling. Sub listed are the main points of divergence between SHB and TFG modelling approaches.

- Initiation steps: SBH states an oxygen-atom transfer from ozone to a hydroxide ion, followed by a reverse one-electron transfer. In contrast, TFG only states an oxygen-atom transfer. However, the fundamental reaction in both mechanisms is the initial step, where ozone reacts with HO^-.
- pH conditions for model development: TFG model was developed working under basic conditions (pH ~ 12), whereas the SBH model is indicated for waters at near neutral or low pH levels (6.3 to 7.9).
- Intermediate radical species: $^{\bullet}HO_3$ and $^{\bullet}HO_4$ radicals appearing in the SBH model were never detected and still are hypothetical.
- Concentration profiles: significant differences were pointed out in terms of concentration range, especially for the couple H_2O_2/HO_2^-, and to a smaller extend for superoxide radical, $^{\bullet}O_2^-$ [Gordon, 1995].
- Reported weaknesses: studies highlighted discrepancies between SBH model predictions and experimental data at neutral-alkaline pH (the predicted decay was more rapid than what was observed ([Chelkowska *et al.*, 1992]; [Hassan *et al.*, 2003]).
- Modification of the models: fitting to experimental data has often been achieved through optimisation of the kinetics of a propagation reaction. It has often be reaction **11** for SBH ([Bezbarua and Reckhow, 2003]) and reaction **13** for TFG ([Chelkowska *et al.*, 1992]; [Elovitz and von Gunten, 1999]; [Mizuno *et al.*, 2007c]).
  Other authors have modified initiation steps, whether it be for SBH ([Bezbarua and Reckhow, 2003]) or TFG ([Chelkowska *et al.*, 1992]; [Gordon, 1995]; [Hassan *et al.*, 2003]) models. Using the two SBH initiation reactions, [Kim *et al.*, 2004] have modified the kinetic constant rate value of reaction **14** (from 70 $M^{-1}.s^{-1}$ to 38 $M^{-1}.s^{-1}$).

$$O_3 + HO^- \rightarrow {}^{\bullet}O_2^- + {}^{\bullet}HO_2 \qquad \textbf{(14)}$$

  It should be mentioned that kinetic rate constants for all propagation reactions of the SBH model involving ozonide radical or its protonated form, $^{\bullet}HO_3$, including the acid-base equilibrium were determined simultaneously. Therefore, it is preferable to consider these reactions together, without any modification of the kinetics.

1.4. Reactions with Inorganic Carbon

1.4.1. Generalities

The role played by inorganic carbon (*i.e.* carbonate species) in ozone decomposition in natural waters has been discussed in various studies ([Hoigné and Bader, 1976]; [Yurteri and Gurol, 1988]; [Morioka *et al.*, 1993]; [von Gunten and Hoigné, 1994]; [Acero and von Gunten, 2000] ; [Mizuno *et al.*, 2007b]).
The major finding that was reported is the possibility for carbonate species to react with hydroxyl radicals forming carbonate radicals, less active in ozone decomposition. Often, carbonate and hydrogenocarbonate ions are therefore seen as scavengers of ozone decomposition. As a consequence, a rise in alkalinity is generally accompanied by a stabilisation of aqueous ozone. The works of [von Gunten and Hoigné, 1994] also consider the role played by carbonate radicals in the bromate formation pathway. Details shall be presented in paragraph **1.6.2.2**.

1.4.2. Mechanism and Variants

Several authors have used mechanistic descriptions for the influence of inorganic carbon over ozone decomposition in natural water. Comparing with models for ozone self-decomposition, it appears that there is relative consensus about kinetic constant rate values

for the reactions involved in this mechanism. However, depending on the authors, particular reactions may be added or removed. The mechanism gathered in table **7** sums up the reactions presented in [Mizuno *et al.*, 2007b] and [Westerhoff *et al.*, 1997] with addition of an alternative initiation reaction, and a possible termination reaction.

Table 7 Mechanism for the influence of inorganic carbon

Type	Reaction	Kinetic constant value (293 K)	Reference
Initiation	$CO_3^{2-} + {}^{\bullet}OH \rightarrow {}^{\bullet}CO_3^- + HO^-$	$3.9.10^8$ $M^{-1}.s^{-1}$	[Buxton *et al.*, 1988]
	$HCO_3^- + {}^{\bullet}OH \rightarrow {}^{\bullet}CO_3^- + H_2O$	5.10^7 $M^{-1}.s^{-1}$	[Farhataziz and Ross, 1977]
Alternative initiation	$HCO_3^- + {}^{\bullet}OH \rightarrow {}^{\bullet}HCO_3 + HO^-$	$8.5.\ 10^6$ $M^{-1}.s^{-1}$	[Buxton and Elliot, 1986]
Propagation	${}^{\bullet}CO_3^- + HO_2^- \rightarrow CO_3^{2-} + {}^{\bullet}HO_2$	$5.6.10^7$ $M^{-1}.s^{-1}$	[Westerhoff *et al.*, 1997]
	${}^{\bullet}CO_3^- + H_2O_2 \rightarrow HCO_3^- + {}^{\bullet}HO_2$	8.10^5 $M^{-1}.s^{-1}$	[Farhataziz and Ross, 1977]
	${}^{\bullet}CO_3^- + O_3 \rightarrow CO_2 + {}^{\bullet}O_2^- + O_2$	-	[Mizuno *et al.*, 2007b]
Termination	${}^{\bullet}CO_3^- + {}^{\bullet}O_2^- \rightarrow CO_3^{2-} + O_2$	4.10^8 $M^{-1}.s^{-1}$	[Westerhoff *et al.*, 1997]
	${}^{\bullet}CO_3^- + {}^{\bullet}O_3^- \rightarrow CO_3^{2-} + O_3$	6.10^7 $M^{-1}.s^{-1}$	[Chelkowska *et al.*, 1990]
	${}^{\bullet}CO_3^- + {}^{\bullet}HO \rightarrow CO_2 + HO_2^-$	3.10^9 $M^{-1}.s^{-1}$	[Westerhoff *et al.*, 1997]
	$2\,{}^{\bullet}CO_3^- \rightarrow CO_2 + CO_4^{2-}$	2.10^7 $M^{-1}.s^{-1}$	[Song, 1996]
Acid-base equilibria			
pK_A = 10.3	$CO_3^{2-} + H^+ \rightarrow HCO_3^-$	5.10^{10} $M^{-1}.s^{-1}$	[Westerhoff *et al.*, 1997]
	$HCO_3^- \rightarrow CO_3^{2-} + H^+$	2.5 s^{-1}	Calculated
pK_A = 9.6	${}^{\bullet}CO_3^- + H^+ \rightarrow {}^{\bullet}HCO_3$	5.10^{10} $M^{-1}.s^{-1}$	[Chen *et al.*, 1973]
	${}^{\bullet}HCO_3 \rightarrow {}^{\bullet}CO_3^- + H^+$	$1.26.10^1$ s^{-1}	Calculated
pK_A = 6.4	$HCO_3^- + H^+ \rightarrow H_2CO_3$ [1]	5.10^{10} $M^{-1}.s^{-1}$	[Westerhoff *et al.*, 1997]
	$H_2CO_3 \rightarrow HCO_3^- + H^+$	2.10^4 s^{-1}	Calculated

For the three greyed rows of table **7**, the following remarks shall be made:

- The alternative initiation reaction is generally neglected, given that the hydrogenocarbonate radicals are only loosely involved in hydroxyl radical scavenging reactions. Most modelling studies, although using a high value for the pK_A of carbonate radicals (9.6), neglect the reactions involving hydrogenocarbonate radicals (*e.g.* [Westerhoff *et al.*, 1997]; [Mizuno *et al.*, 2007b]).
- Different values for the kinetic constant rate for the propagation reaction proposed by Mizuno were tested [Mizuno *et al.*, 2007b]. It appeared that, assuming a value of zero, calculated results did match experimental data over a wide range of operating conditions.

[1] The H_2CO_3 formulation is here used for convenience.

- The termination reaction proposed by Song in his Ph. D. thesis has been reported by [Westerhoff *et al.*, 1997].

Classically, the kinetic constants of the deprotonation reactions (acid-base equilibria) were calculated based on the values of pK_A and protonation kinetic constants. A typical acid-base equilibrium decomposes into two reactions, with distinct kinetics, as presented in equation **15**.

$$AH \leftrightarrow A^- + H^+ \begin{cases} AH \xrightarrow{k_{depro}} A^- + H^+ \\ A^- + H^+ \xrightarrow{k_{pro}} AH \end{cases} \quad \textbf{(15)}$$

The thermodynamic equilibrium is generally reached rapidly, and the concentrations do not evolve sensibly. Thus, one can write equation **16.**

$$k_{depro}.[AH] = k_{pro}.[A^-].[H^+] \quad \textbf{(16)}$$

According to the definition of the acidity constant K_A, the relation **17** is obtained.

$$K_A = \frac{[A^-].[H^+]}{[AH]} = \frac{k_{depro}}{k_{pro}} \quad \textbf{(17)}$$

Contrary to the results presented in [Chen *et al.*, 1973] and in following studies ([Eriksen *et al.*, 1985]; [Zuo *et al.*, 1999]), some researchers reported much lower values for the pK_A of hydrogenocarbonate radical/carbonate radical: whereas [Czapski *et al.*, 1999] have shown that carbonate radical may be very acidic with pK_A lower than zero, [Bisby *et al.*, 1998] indicated a pK_A lower than 8. In this study however, the original value of 9.6 has been selected in order to be consistent with the other parts of the mechanism, mainly taken from [Westerhoff *et al.*, 1997].

1.5. Reactions with Organic Carbon

1.5.1. What is NOM?

Natural waters contain varying concentrations of organic and inorganic natural compounds, either in suspended or dissolved forms. NOM found in water results from elutriation of the soil and also from biological, chemical and photochemical reactions in the water that occur when algae or (animal or vegetal) by-products are present [Langlais *et al.*, 1991].

NOM is primarily derived from plant and/or microbial residues. On land, dead plants leave roots within the upper soil layers and "litter" on the soil surface. Within the soil, microorganisms represent a very large biomass. The residues of organic matter produced on land are then transferred from the soil into the hydrosphere. Transport usually occurs due to rainfall that runs off, or percolates through the soil column carrying soluble and particulate NOM to streams, lakes, and oceans, or into groundwater. The organic matter that originates from terrestrial sources makes up an important fraction of the total NOM, especially in small continental water bodies [vanLoon and Duffy, 2005].

Organic matter is also produced within water bodies, for example in wetlands. There, the luxuriant growth of vegetation produces a thick mat of aerial material and roots that, upon death, are deposited in the water. Besides the natural sources, human inputs may contribute to the organic matter in water. These include large volumes of poorly defined wastes, such as domestic sewage or pulp mill effluent, that are sometimes discharged directly or after treatment into rivers, lakes, and oceans [vanLoon and Duffy, 2005].

Fractionation techniques are often used when characterising NOM. Fractionation generally decomposes into microfiltration of the water and adsorption on XAD resins, at a specific pH. Elution and separation are performed afterwards. The most common protocol was proposed by [Thurman and Malcolm, 1981]. The main organic constituents in natural waters are a collection of polymerised organic acids called humic substances. Other types of carboxylic acids, amino acids and carbohydrates can also be added to this group [Langlais *et al.*, 1991].

1.5.2. Models without pH-Dependence

In natural water, the stability of ozone is strongly dependent on species found in NOM. Observing various molecules (acids, alcohols…) or groups (alkyl, aryl…) found in NOM, [Staehelin and Hoigné, 1985] proposed to distinguish four fractions of NOM interfering in ozone self-decomposition mechanism: *direct consumers*, *initiators*, *promoters* and *scavengers*.
This convenient classification has been adapted by various authors. It has been summarised in [Langlais *et al.*, 1991] and extensively used by [Bezbarua, 1997]:

- The initiators may react with ozone and induce the formation of hydroxyl radicals (•OH), which in turn initiate the ozone chain reaction;
- The promoters may react with hydroxyl radicals (•OH) and regenerate superoxide radicals ($^{\bullet}O_2^-$ or $^{\bullet}HO_2^-$);
- The scavengers are capable of consuming hydroxyl radicals without generating new radicals.

Although most authors adopt the previous mechanism, different reactions involving NOM were presented and tested. An overview is given in table **8**, where four different sets of reactions (corresponding to different row colours) are gathered.

Table 8 Reactions proposed for the influence of NOM

Type	Reaction	Reference
Direct consumption	$O_3 + NOM^{\,d} \rightarrow products$	[Langlais *et al.*, 1991] ; [Bezbarua, 1997]
	$O_3 + NOM_1 \rightarrow NOM_{1,ox}$	[von Gunten, 2003a]
Initiation	$O_3 + NOM^{\,i} \rightarrow {}^{\bullet}OH + products$	[Langlais *et al.*, 1991] ; [Bezbarua, 1997]
	$O_3 \rightarrow \eta_{W,1}\,{}^{\bullet}OH$	[Westerhoff *et al.*, 1997]
	$O_3 + NOM_2 \rightarrow {}^{\bullet}NOM_2^+ + {}^{\bullet}O_3^-$	[von Gunten, 2003a]
	$O_3 + NOM^{\,i} \rightarrow NOM^{\,i,ox} + \eta_{K,1}\,{}^{\bullet}O_3^- + \eta_{K,2} H_2O_2$	[Kim, 2004]
Propagation	${}^{\bullet}OH + NOM^{\,p} \rightarrow {}^{\bullet}O_2^- + products$	[Langlais *et al.*, 1991] ; [Bezbarua, 1997]
	${}^{\bullet}OH + NOM^{\,p} \rightarrow \eta_{W,2}\,{}^{\bullet}O_2^- + NOM^{\,p,ox} + products$	[Westerhoff *et al.*, 1997]
	${}^{\bullet}OH + NOM_3 \rightarrow \begin{cases} {}^{\bullet}NOM_3 + H_2O \\ {}^{\bullet}NOM_3 + HO^- \end{cases}$ ${}^{\bullet}NOM_3 + O_2 \rightarrow NOM_3^+ + {}^{\bullet}O_2^-$	[von Gunten, 2003a]
	${}^{\bullet}OH + NOM^{\,p} \rightarrow \eta_{K,3}\,{}^{\bullet}O_2^- + NOM^{\,p,ox}$	[Kim, 2004]
Scavenging	${}^{\bullet}OH + NOM^{\,s} \rightarrow products$	[Langlais *et al.*, 1991] ; [Bezbarua, 1997]
	${}^{\bullet}OH + NOM_4 \rightarrow {}^{\bullet}NOM_4 + H_2O$ ${}^{\bullet}NOM_4 + O_2 \rightarrow no\ {}^{\bullet}O_2^-\ formation$	[von Gunten, 2003a]

The model proposed by [Westerhoff *et al.*, 1997] can be seen as a simplification of the model by [Langlais *et al.*, 1991]. The two other presented models are more different. Both postulate the formation of ozonide radical ($^{\bullet}O_3^-$) instead of hydroxyl radical during initiation. It is difficult to assess the impact of such dissimilarity; however it can be noted that the role played by ozonide radicals is slightly different in the TFG model. According to TFG, ozonide radicals are namely formed "earlier" than hydroxyl radicals during ozone self-decomposition.
Regeneration of peroxide hydrogen during initiation [Kim, 2004] should be avoided, since hydrogen peroxide has a major impact on ozone decomposition kinetics ([Mizuno *et al.*, 2007c]; [Vandersmissen *et al.*, 2008]; [Lovato *et al.*, 2009]).
Being formulated differently, the reaction pathways of [von Gunten, 2003a] and [Langlais *et al.*, 1991] are nevertheless comparable, the first one letting appear intermediate species (radicals) engaged in intermediate reactions with dioxygen. Given that radicals are extremely reactive species present in very small quantities, such distinction between pathways should neither significantly change kinetics, nor dioxygen concentration. The following equivalences may thus be established:

$NOM_1 \equiv NOM^d$ $\quad$ $NOM_2 \equiv NOM^i$
$NOM_3 \equiv NOM^p$ $\quad$ $NOM_4 \equiv NOM^s$

1.5.3. A Model with pH-Dependence

Even if some constants presented in [Kim, 2004] may be adjusted as functions of the pH, all models presented in table **8** have no direct pH dependence. However, NOM generally contains an important fraction composed by acids (humic, fulvic, tannic…). This observation has motivated [Savary, 2002] to propose an innovative model for the role of NOM in ozone decomposition.
Simplifying the classification formulated by [Staehelin and Hoigné, 1985], [Savary, 2002] distinguishes three fractions in NOM:

- initiators and promoters (no difference is made between them), noted NOM_1 (reactions **18** and **19**);
- scavengers, noted NOM_2 (reaction **20**);
- final NOM not reacting anymore, noted NOM_f.

A reaction for direct ozone consumption by NOM is also proposed (reaction **22**), the reaction rate of which is generally adjusted with an empirical correlation such as those presented in paragraph **1.2.3.** (the entire NOM is regarded as direct ozone consumer). pH dependence is modelled through the definition of a pK_A for the initiators and promoters. Thus, a distinction is made between $NOM_{1,a}$ (acid) and $NOM_{1,b}$ (base); the two fractions are in equilibrium (equation **21**).

$$NOM_{1,a} + O_3 \rightarrow NOM_2 + HO\cdot \quad \textbf{(18)}$$

$$NOM_{1,b} + O_3 \rightarrow NOM_2 + HO\cdot \quad \textbf{(19)}$$

$$NOM_2 + {}^{\bullet}OH \rightarrow NOM_f \quad \textbf{(20)}$$

$$NOM_{1,a} \leftrightarrow NOM_{1,b} + H^+ \quad \textbf{(21)}$$

$$NOM + O_3 \rightarrow products \quad \textbf{(22)}$$

A singularity of this model is also to propose a transformation of NOM, from initiators to scavengers and inert species. Working with NOM-containing water from Neuilly-sur-Marne (pH = 7.5, A_T = 4 meq.L^{-1}), the effects of the scavenging fraction were found to be negligible

when compared to those of carbonate/hydrogenocarbonate. Hence, the model essentially consisted of equations **18**, **19**, **21** and **22**.

1.5.4. Elements of Appreciation and Comparison

All reviewed models share a common basis: their integration in the ozone self-decomposition mechanism. Thus, the models of [von Gunten, 2003a] and [Westerhoff *et al.*, 1997] can be seen respectively as advanced and simplified models of [Langlais *et al.*, 1991]. The model proposed by [Savary, 2002] differs more from the others, due to the transformation of the reactive fractions of NOM.

The results obtained with kinetic models for NOM remain nevertheless difficult to compare. Three main reasons explain this situation:

- The models used in the literature are very rarely similar. Changes are often found in the set of reactions considered or in the values of kinetic constant rates.
- Few data is available for NOM models. It is always difficult to get two pieces of information: initial concentrations and reaction rate constants of the NOM fractions.
- NOM characteristics and reactivity towards ozone change considerably from water to water. For instance, [Cho *et al.*, 2003] and [Park *et al.*, 2001] have characterised the NOM fractions causing Instantaneous Ozone Demand (IOD, see paragraph **1.5.5.**) in raw water using the classical distinction between *direct consumers*, *initiators*, *promoters* and *scavengers*. Their conclusions were opposite: [Cho *et al.*, 2003] have found direct consumers to be the major contributor to IOD, whereas [Park *et al.*, 2001] have stated that initiators should be regarded as the fraction achieving the greatest part in IOD.

More generally, linking model characteristics to observable physical data remains difficult, not to say impossible. While the rate constants for the reactions of main inorganic species of interest (including carbonates) are known, it is difficult to assess the stability of ozone in natural waters due to the unknown effect of NOM. In particular, it is extremely difficult to estimate the fraction of the NOM, which promotes or inhibits ozone decay [von Gunten, 2003a]. Direct consumption and initiation by NOM are slightly better characterised and generally attributed to double bonds, activated aromatic systems, amines and sulfides. Using their simplified model [Westerhoff *et al.*, 1997] reported a correlation between the {initiation and direct consumption} kinetic constant rate and the value of SUVA.

There have been various attempts to deduce the kinetics of both the direct ozone-NOM reaction and the promoting and inhibiting NOM fractions from spectroscopic and structural investigation of the NOM. The rate constant for direct reaction of ozone with NOM showed the best correlation with the UV absorbance or the SUVA at 254 nm. It is more difficult to estimate the fraction of promotion and inhibition of NOM [von Gunten, 2003a].

1.5.5. Instantaneous Ozone Demand

IOD has not received yet a clear definition. It is often referred to as the amount of ozone consumed by water within a few seconds after ozone addition. However, practical experimental reasons have often conducted authors to define different durations for the initial phase: 30 seconds for [Hoigné and Bader, 1994]; 20 seconds for [Buffle, 2005]. IOD often cannot be taken in account when modelling, because of its difficult measurement and characterisation. Nevertheless, many authors remarked that this demand could be possibly linearly linked to the UV absorbance.

In her Ph. D., [Muñoz Ramirez, 1997] determined apparent kinetics for IOD, applying a method based on competition towards ozone between NOM and a specific compound, the reaction rate constant of which was already known. Assuming reactions in parallel, the

average reaction speed is given by equation **23** (S_i representing the i^{th} species contributing to IOD).

$$r = \sum_i k_{0,i}[S_i]_0 \cdot [O_3] \quad \textbf{(23)}$$

Studying water samples from Neuilly-sur-Marne and Choisy-le-Roi (in the Parisian surroundings), she showed that the parameter $\sum_i k_{0,i}[S_i]_0$ - representing the reaction speed for very rapid consumers of ozone - could reasonably be correlated to 254nm UV absorbance, except when mineral species such as NO_2^-, Fe^{2+}, Mn^{2+} were present, and notably participated to IOD. The relation is given in equation **24**.

$$\sum_i k_{0,i}[S_{0,i}] = 11 \cdot UV_{254} - 0.44 \quad \textbf{(24)}$$

Nevertheless, this correlation remains weak and relatively difficult to exploit. Furthermore, instantaneous reactions involving ozone and inorganic species have to be taken into account in the set of reactions as well.

More recently, in his Ph. D. thesis, [Buffle, 2005] focused on IOD characterisation, based on an original experimental apparatus, that makes it possible to start measuring ozone decomposition in water (potable or wastewater) only 350 ms after ozone addition. Without getting in the details of a full explanation, the measurements can be performed 100 times faster with the continuous quench-flow system developed than with a discontinuous reactor system. The measurement system was used to evaluate ozone decomposition and hydroxyl radical generation in surface water and wastewater.
Though the relation between UV absorbance and ozone concentration is not the main topic of this work, it is several times mentioned as a linear relation. We shall therefore present here some results obtained by Buffle, even if the UV measurements were done at 285 nm. Investigating a wastewater from Zürich at pH 8, Buffle found a linear relationship between ozone exposure $\int_{u=0}^{u=t}[O_3]du$ and UV absorbance. The result of the experiment is presented in figure **3**: Buffle followed the temporal depletion of ozone after addition of 2.1 mg.L^{-1} representing 44 µM ozone.

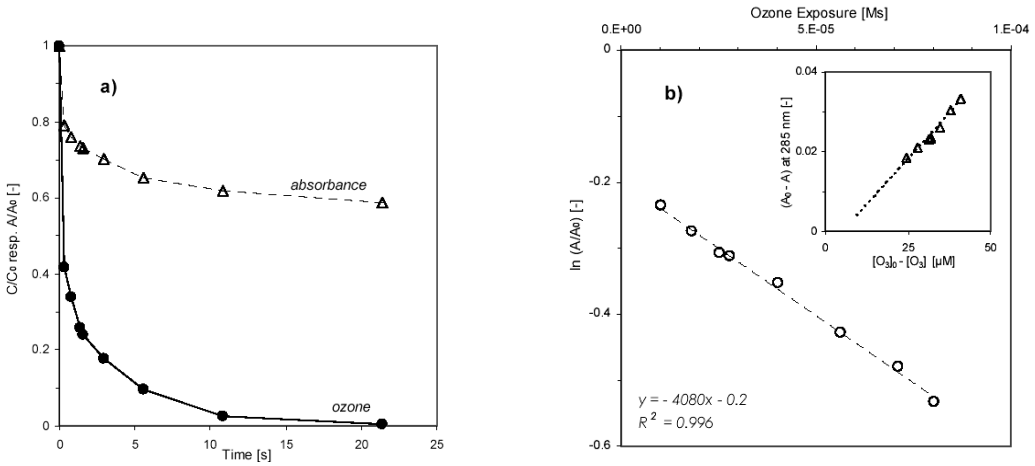

Figure 3 Absorbance (285 nm) and dissolved ozone concentration profiles. (a) linear time scale; (b) ozone exposure $\int_{u=0}^{u=t}[O_3]du$ semi-log scale [Buffle, 2005].

The empirical correlation obtained by Buffle, reported on figure **3 (b)**, is given in equation **25**.

$$\ln\left(\frac{A(t)}{A_0}\right) = -4080 \cdot \int_{u=0}^{u=t} [O_3]du - 0.2 \qquad \textbf{(25)}$$

Obviously, this relation cannot simply be extended to any water sample. It deeply depends on specific characteristics varying from site to site, from water to water. In fact, the absorbance drop varies considerably according to the type of water: it can represent only 10-20% for potable waters, and over 90% for wastewaters.
Buffle tackled the problem introducing a kinetic model based on distributions of NOM moieties. According to his results, the radical chain reaction does not appear to control ozone decomposition in wastewater. He therefore hypothesised ozone decomposition to be controlled by direct reactions between ozone and some highly reactive moieties of the dissolved organic matter. Using a fitted distribution, changes in ozone dose could be well predicted by the model, thereby supporting the above hypothesis.
Although seducing, this approach remains case dependent and cannot be extrapolated without a preliminary calibration procedure, which is fairly complicated because of the long calibration time and the heavy experimental equipment it requires.

1.6. Formation of Bromate Ions in NOM-free Water

1.6.1. Generalities

Bromide ions occur in natural waters in highly variable quantities, typically ranging from 10 $\mu g.L^{-1}$ to 1000 $\mu g.L^{-1}$. Originally due to natural processes (*e.g.* salt water intrusion, spindrift, geological specificities…), their presence is increased by anthropogenic activities such as potassium mining, coal mining etc. Generally, waters containing less than 20 $\mu g.L^{-1}$ bromide are unproblematic regarding bromine-derived by-products. The situation tends to be more difficult to handle for levels in the range 50-100 $\mu g.L^{-1}$ and becomes a serious problem above 100 $\mu g.L^{-1}$ [von Gunten, 2003b].
Indeed, as soon as ozone is being dissolved in natural water containing bromide ions, bromate may be formed. There are two main pathways[2] to oxidise bromide

- Direct molecular oxidation through ozone;
- Indirect radical reactions involving species preliminary formed during ozone degradation (mainly hydroxyl and carbonate radicals).

Figure **4** gives an overview of the reaction pathway leading from bromide to bromate (oxidation states appear in brackets).

[2] Some authors distinguish three pathways conducting to bromate: direct, direct-indirect and indirect-direct ozonations [Song *et al.*, 1997].

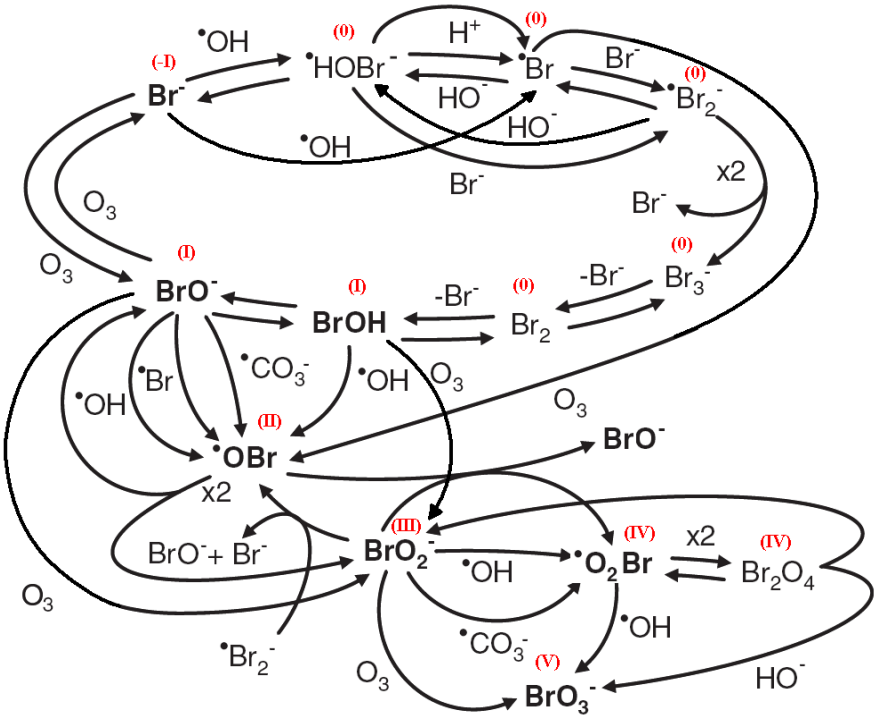

Figure 4 **Bromate formation pathways (adapted from [Kim *et al.*, 2007])**

1.6.2. Most Important Reactions

1.6.2.1. Molecular Reactions

Molecular reactions only represent a small part of the whole reaction set involved during the formation of bromate ions. Yet, they are particularly important achieving the first oxidation step, from bromide to hypobromite, thus allowing the second and third oxidation steps leading to bromate. The final oxidation leading to bromate (III→V) is also essentially due to a molecular reaction. As depicted in figure **4**, the first molecular oxidation step is reversible (table **9**). Besides, the couple BrOH/BrO^- plays a central role. However, its reactivity is highly pH-dependent since hypobromite is much more reactive than hypobromous acid (under both molecular and radical pathways). Other reactions commonly found in literature are gathered in table **10**. Their importance remains still secondary, involving minor species. The kinetics for acid-base equilibrium reactions are presented in table **11**.

Table 9 **Successive molecular oxidation from bromide to bromate**

Type	Reaction	Kinetic constant value (293K)	Reference
Oxidation (-I) → (I)	$Br^- + O_3 \rightarrow BrO^- + O_2$	$1.6.10^2$ $M^{-1}.s^{-1}$	[Haag and Hoigné, 1983]
	$BrO^- + O_3 \rightarrow Br^- + 2O_2$	$3.3.10^2$ $M^{-1}.s^{-1}$	[Haag and Hoigné, 1983]
Oxidation (I) → (III)	$BrOH + O_3 \rightarrow BrO_2^- + O_2 + H^+$	10^{-2} $M^{-1}.s^{-1}$	[Haag and Hoigné, 1983]
	$BrO^- + O_3 \rightarrow BrO_2^- + O_2$	10^2 $M^{-1}.s^{-1}$	[Haag and Hoigné, 1983]
Oxidation (III) → (V)	$BrO_2^- + O_3 \rightarrow BrO_3^- + O_2$	$> 10^5$ $M^{-1}.s^{-1}$	[von Gunten and Hoigné, 1994]
		10^5 $M^{-1}.s^{-1}$	[Pinkernell and von Gunten, 2001]

Table 10 Secondary molecular reactions

Reaction	Kinetic constant value (293K)	Reference
$Br_2O_2 + H_2O \rightarrow BrO_2H + BrOH$	10 $M^{-1}.s^{-1}$	[Buxton and Dainton, 1968]
$BrOH + HO_2^- \rightarrow Br^- + O_2 + H_2O$	$7.6.10^9$ $M^{-1}.s^{-1}$	[Buxton and Dainton, 1968]
$Br_2OH^- + H^+ \rightarrow Br_2 + H_2O$	2.10^{10} $M^{-1}.s^{-1}$	[Eigen and Kustin, 1962]
$Br_2OH^- \rightarrow BrOH + Br^-$	5.10^9 s^{-1}	[Eigen and Kustin, 1962]

Table 11 Acid-base equilibria within bromate formation pathway

Type	Reaction	Kinetic constant value (293K)	Reference
pK_A = 9.3	$NH_3 + H^+ \rightarrow NH_4^+$	5.10^{10} $M^{-1}.s^{-1}$	Calculated according to equation **17**
	$NH_4^+ \rightarrow NH_3 + H^+$	$2.5.10^1$ s^{-1}	
pK_A = 8.8	$BrO^- + H^+ \rightarrow BrOH$	5.10^{10} $M^{-1}.s^{-1}$	[Westerhoff, 1995]
	$BrOH \rightarrow BrO^- + H^+$	$7.9.10^1$ s^{-1}	Calculated according to equation **17**
pK_A = 3	$BrO_3^- + H^+ \rightarrow BrO_3H$	5.10^{10} $M^{-1}.s^{-1}$	[Buxton and Dainton, 1968]
	$BrO_3H \rightarrow BrO_3^- + H^+$	5.10^7 s^{-1}	Calculated according to equation **17**
pK_A = 4.9	$BrO_2^- + H^+ \rightarrow BrO_2H$	5.10^{10} $M^{-1}.s^{-1}$	[Faria *et al.*, 1994]
	$BrO_2H \rightarrow BrO_2^- + H^+$	$6.3.10^5$ s^{-1}	Calculated according to equation **17**

1.6.2.2. Radical Reactions

Accounting usually for approximately 40 % to 80% of the bromate formation ([Laplanche *et al.*, 1998]; [Westerhoff *et al.*, 1998]; [von Gunten, 2003b]), radical reactions are extremely important in bromate formation, mostly because of the high reactivity of $^{\bullet}OBr$.

For clarity reasons, the most widely used radical reactions presented in this paragraph have been classified according to radical species. Certain reactions less susceptible to occur, or less frequently considered in literature are classified as "secondary". Complementary reactions can be found in [Gélinet, 1999]. The terms "initiation", "propagation", "termination" refer to the formation, transformation or destruction of the radical species considered in the table.

Table 12 Formation and reactivity of $^{\bullet}OBr$, $^{\bullet}O_2Br$ within bromate formation pathway

Type	Reaction	Kinetic constant value (293K)	Reference
Main initiation	$BrO^- + {}^{\bullet}OH \rightarrow {}^{\bullet}OBr + HO^-$	$4.5.10^9$ $M^{-1}.s^{-1}$	[Buxton and Dainton, 1968]
	$BrOH + {}^{\bullet}OH \rightarrow {}^{\bullet}OBr + H_2O$	2.10^9 $M^{-1}.s^{-1}$	[Buxton and Dainton, 1968]
	$BrO_2^- + {}^{\bullet}OH \rightarrow {}^{\bullet}O_2Br + HO^-$	2.10^9 $M^{-1}.s^{-1}$	[Buxton and Dainton, 1968]
Secondary initiation	$^{\bullet}OH + BrO_3^- \rightarrow {}^{\bullet}OBr + HO^- + O_2$	3.10^6 $M^{-1}.s^{-1}$	[Amichai *et al.*, 1969]
Propagation	$^{\bullet}OBr + BrO_2^- \rightarrow BrO^- + {}^{\bullet}O_2Br$	$3.4.10^8$ $M^{-1}.s^{-1}$	[Buxton and Dainton, 1968]
	$2\,{}^{\bullet}OBr + H_2O \rightarrow BrO_2^- + BrO^- + 2H^+$	5.10^9 $M^{-1}.s^{-1}$	[Buxton and Dainton, 1968]
Termination	$^{\bullet}O_2Br + {}^{\bullet}OH \rightarrow BrO_3^- + H^+$	2.10^9 $M^{-1}.s^{-1}$	[Buxton *et al.*, 1988]
	$2\,{}^{\bullet}OBr \rightarrow Br_2O_2$	$2.5.10^9$ $M^{-1}.s^{-1}$	[Buxton and Dainton, 1968]

Table 13 Formation and reactivity of $^{\bullet}Br$ within bromate formation pathway

Type	Reaction	Kinetic constant value (293K)	Reference
Initiation	$Br^- + {}^{\bullet}OH \rightarrow {}^{\bullet}Br + HO^-$	$1.1.10^9$ $M^{-1}.s^{-1}$	[von Gunten and Hoigné, 1996]
Initiation 2.1	$Br^- + {}^{\bullet}OH \rightarrow {}^{\bullet}HOBr^-$	10^{10} $M^{-1}.s^{-1}$	[Zehavi and Rabani, 1972]
	${}^{\bullet}HOBr^- \rightarrow Br^- + {}^{\bullet}OH$	$3.3.10^7$ s^{-1}	[Zehavi and Rabani, 1972]
Initiation 2.2	${}^{\bullet}HOBr^- \rightarrow {}^{\bullet}Br + HO^-$	$4.2.10^6$ s^{-1}	[Zehavi and Rabani, 1972]
	${}^{\bullet}HOBr^- + H^+ \rightarrow {}^{\bullet}Br + H_2O$	$4.4.10^{10}$ $M^{-1}.s^{-1}$	[Zehavi and Rabani, 1972]
Secondary initiation	$BrOH + {}^{\bullet}O_2^- \rightarrow {}^{\bullet}Br + O_2 + HO^-$	$3.5.10^9$ $M^{-1}.s^{-1}$	[Schwarz and Bielski, 1986]
Principal reactions	${}^{\bullet}Br + O_3 \rightarrow {}^{\bullet}OBr + O_2$	$1.5.10^8$ $M^{-1}.s^{-1}$	[von Gunten and Hoigné, 1994]
	${}^{\bullet}Br + HO^- \rightarrow {}^{\bullet}HOBr^-$	$1.3.10^{10}$ $M^{-1}.s^{-1}$	[Kläning and Wolff, 1985]
	${}^{\bullet}Br + BrO^- \rightarrow {}^{\bullet}OBr + Br^-$	$4.1.10^9$ $M^{-1}.s^{-1}$	[Kläning and Wolff, 1985]
Secondary reactions	${}^{\bullet}Br + {}^{\bullet}OBr \rightarrow 2BrOH$	10^9 $M^{-1}.s^{-1}$	[Kläning and Wolff, 1985]
	$2{}^{\bullet}Br \rightarrow Br_2$	10^9 $M^{-1}.s^{-1}$	[Kläning and Wolff, 1985]

Table 14 Formation and reactivity of $^{\bullet}Br_2^-$ within bromate formation pathway

Type	Reaction	Kinetic constant value (293K)	Reference
Initiation	${}^{\bullet}HOBr^- + Br^- \rightarrow {}^{\bullet}Br_2^- + HO^-$	$1.9.10^8$ $M^{-1}.s^{-1}$	[Zehavi and Rabani, 1972]
	${}^{\bullet}Br + Br^- \rightarrow {}^{\bullet}Br_2^-$	10^{10} $M^{-1}.s^{-1}$	[Zehavi and Rabani, 1972]
Principal reactions	${}^{\bullet}Br_2^- \rightarrow {}^{\bullet}Br + Br^-$	5.10^4 s^{-1}	[Behar, 1972]
	${}^{\bullet}Br_2^- + BrO^- \rightarrow {}^{\bullet}OBr + 2Br^-$	8.10^7 $M^{-1}.s^{-1}$	[Buxton and Dainton, 1968]
	${}^{\bullet}Br_2^- + BrO_2^- \rightarrow Br^- + {}^{\bullet}OBr + BrO^-$	8.10^7 $M^{-1}.s^{-1}$	[Buxton and Dainton, 1968]
	${}^{\bullet}Br_2^- + HO^- \rightarrow {}^{\bullet}HOBr^- + Br^-$	$2.7.10^6$ $M^{-1}.s^{-1}$	[Mamou *et al.*, 1977]
Secondary reactions	$2{}^{\bullet}Br_2^- \rightarrow 3Br^- + BrOH$	2.10^9 $M^{-1}.s^{-1}$	[Sutton *et al.*, 1965]
	$2{}^{\bullet}Br_2^- \rightarrow Br_3^- + Br^-$	2.10^9 $M^{-1}.s^{-1}$	[Sutton *et al.*, 1965]

Table 15 Reactions engaging ammonia within bromate formation pathway

Reaction	Kinetic constant value (293K)	Reference
$BrOH + NH_3 \rightarrow NH_2Br + H_2O$	$7.5.10^7$ $M^{-1}.s^{-1}$	[Wajon and Morris, 1982]
$NH_2Br + HO^- \rightarrow BrO^- + NH_3$	*fitted value :* $7.5.10^6$ $M^{-1}.s^{-1}$	[Pinkernell and von Gunten, 2001]
$NH_2Br + O_3 \rightarrow Br^- + NO_3^- + 2H^+$	40 $M^{-1}.s^{-1}$	[Hofmann and Andrews, 2001]
$2NH_2Br \rightarrow NHBr_2 + NH_3$	*fitted value :* $2.5.10^2$ $M^{-1}.s^{-1}$	[Pinkernell and von Gunten, 2001]
$NHBr_2 + NH_3 \rightarrow 2NH_2Br$	*fitted value :* 10^2 $M^{-1}.s^{-1}$	[Pinkernell and von Gunten, 2001]
$NHBr_2 + O_3 \rightarrow 2Br^- + NO_3^- + H^+$	10 $M^{-1}.s^{-1}$	[Hofmann and Andrews, 2001]

Table 16 Reactions with carbonate species within bromate formation pathway

Reaction	Kinetic constant value (293K)	Reference
$^{\bullet}CO_3^- + BrO^- \rightarrow CO_3^{2-} + {}^{\bullet}OBr$	4.3.10^7 M^{-1}.s^{-1}	[Kläning and Wolff, 1985]
$^{\bullet}HCO_3 + BrO^- \rightarrow HCO_3^- + {}^{\bullet}OBr$	4.3.10^7 M^{-1}.s^{-1}	[Buxton and Dainton, 1968]
$^{\bullet}CO_3^- + BrO_2^- \rightarrow CO_3^{2-} + {}^{\bullet}O_2Br$	1.1.10^8 M^{-1}.s^{-1}	[Buxton and Dainton, 1968]

1.6.3. Secondary Reactions

The reactions presented in this paragraph are often not considered in literature or can be regarded as unlikely to happen, due to their kinetics or the unstable character of the species involved.

Table 17 Reactions with Br_2 within bromate formation pathway

Reaction	Kinetic constant value (293K)	Reference
$Br_2 + Br^- \rightarrow Br_3^-$	10^{10} M^{-1}.s^{-1}	[Mamou *et al.*, 1977]
$Br_3^- \rightarrow Br_2 + Br^-$	8.3.10^8 s^{-1}	[Mamou *et al.*, 1977]
$Br_2 + H_2O \rightarrow Br_2OH^- + H^+$	2 M^{-1}.s^{-1}	[Eigen and Kustin, 1962]

Table 18 Reactions with Br_2O_4 within bromate formation pathway

Reaction	Kinetic constant value (293K)	Reference
$2{}^{\bullet}O_2Br \rightarrow Br_2O_4$	1.4.10^9 M^{-1}.s^{-1}	[Buxton and Dainton, 1968]
$Br_2O_4 \rightarrow 2{}^{\bullet}O_2Br$	7.10^7 s^{-1}	[Buxton and Dainton, 1968]
$Br_2O_4 + HO^- \rightarrow BrO_2^- + BrO_3^- + H^+$	7.10^8 M^{-1}.s^{-1}	[Buxton and Dainton, 1968]
$Br_2O_4 + H_2O \rightarrow BrO_2H + BrO_3H$	2.10^1 M^{-1}.s^{-1}	[Buxton and Dainton, 1968]

Table 19 Reactions with $^{\bullet}O^-$ within bromate formation pathway

Reaction	Kinetic constant value (293K)	Reference
$^{\bullet}O^- + Br^- \rightarrow products$	2.2.10^8 M^{-1}.s^{-1}	[Buxton *et al.*, 1988]
$^{\bullet}O^- + BrO^- \rightarrow {}^{\bullet}OBr + HO^-$	3.5.10^9 M^{-1}.s^{-1}	[Buxton *et al.*, 1988]
$^{\bullet}O^- + BrO_2^- \rightarrow {}^{\bullet}O_2Br + HO^-$	1,7.10^9 M^{-1}.s^{-1}	[Buxton *et al.*, 1988]
$^{\bullet}O^- + BrO_3^- \rightarrow {}^{\bullet}O_3Br + HO^-$	1.6.10^6 M^{-1}.s^{-1}	[Buxton *et al.*, 1988]

Table 20 Other reaction within bromate formation pathway

Reaction	Kinetic constant value (293K)	Reference
$BrO_3^- + {}^{\bullet}OH \rightarrow {}^{\bullet}O_3Br + HO^-$	5.10^6 M^{-1}.s^{-1}	[Buxton *et al.*, 1988]

1.6.4. Elements of Appreciation

Although relative consensus on the reaction pathway leading to bromate formation in NOM-free water [von Gunten, 2003b], various differences may be found when comparing mechanistic models. Based on three examples ([Westerhoff *et al.*, 1998]; [Savary, 2002] and

[Kim *et al.*, 2004]), we shall analyse differences done in the choice of the reactions and of their kinetics (frequency factor and energy of activation in Arrhenius' theory).

- Acid-base equilibria: All the species exhibiting an acidic character have been taken into account in the three studies. The values for kinetics are close to each other.
- Reactions involving two or more radical species: these reactions were not taken into account by Savary. Although potential high reactivity, a reaction that involves two species with very low concentrations cannot actually account significantly in the overall chemical mechanisms. Westerhoff also reduced the number of such reactions.
- Energies of activation: not available, except in the work of Savary. They were mostly assumed according to table **21**.

Table 21 **Assumptions made concerning values missing in the literature [Savary, 2002]**

Reaction type	Activation energy
Radical reaction involving mineral species	7.5 kJ.mol^{-1}
Radical reaction involving organic species	15 kJ.mol^{-1}
Molecular reaction	42 kJ.mol^{-1}
Reaction between radical species	*Not considered*

- Molecular oxidation (III) → (V): While Westerhoff and Kim give similar values for the kinetic constant rate (10^5 and $5.7.10^4$ M^{-1}.s^{-1}, respectively), Savary gives a value superior to 10^6 M^{-1}.s^{-1}. Comparing with other modelling studies, it appears that the kinetic constant rate values for the molecular pathway are often fitted.
- Molecular oxidation (-I) → (I): Westerhoff fitted the value of the kinetic constant rate for this reaction. Values reported in the literature range from 90 M^{-1}s^{-1} to 270 M^{-1}s^{-1}; the final value of 50 M^{-1}s^{-1} was finally selected by Westerhoff and co-workers.
- Carbonate mechanism: The mechanism proposed by Westerhoff contains only few reactions involving carbonate radicals: two reactions are considered for carbonate radical formation (reactions **26** and **27**) and only the carbonate radical takes part in the bromate formation pathway (reaction **28**).

$$CO_3^{2-} + {}^{\bullet}OH \rightarrow {}^{\bullet}CO_3^{-} + HO^{-} \quad \textbf{(26)}$$

$$HCO_3^{-} + {}^{\bullet}OH \rightarrow {}^{\bullet}HCO_3 + HO^{-} \quad \textbf{(27)}$$

$${}^{\bullet}CO_3^{-} + BrO^{-} \rightarrow CO_3^{2-} + {}^{\bullet}OBr \quad \textbf{(28)}$$

1.7. Other Reactions of Interest

1.7.1. Reactions Involving Phosphate

The role played by phosphate species during ozonation is relatively intricate and remains for a large part undocumented. In NOM-free waters, phosphate is generally known to be a radical scavenger [Staehelin and Hoigne, 1985]. Equations and kinetics have been established for this type of reactions (see table **22**). In natural water with organic content however, phosphate is usually regarded as promoter agent [Langlais *et al.*, 1991]. It has been shown for instance, that low concentrations of phosphate may indeed accelerate the ozone decay in the presence of organic matter [Vandersmissen *et al.*, 2008]. Dihydrogen phosphate radical, ${}^{\bullet}H_2PO_4$, is indeed able to abstract hydrogen atoms from organic compounds; for example, a hydrogen atom standing in α position to an alcoholic group (see table **22**). Additionally,

phosphate radicals abstract hydrogen from saturated organic compounds, add to olefins, and oxidise many organic and inorganic compounds. For example, $^{\bullet}PO_4^{2-}$ oxidises I^- rapidly, $^{\bullet}HPO_4^-$ can oxidise also Br^-, and $^{\bullet}H_2PO_4$ oxidises even Cl^-. The phosphate radicals oxidise phenoxide ions, phenols, and anilines with moderate or high rate constants, the acidic form oxidises also benzoic acid fairly rapidly [Neta *et al.*, 1988]. Thus, phosphate can interfere with the radical-type chain reaction and even act as a secondary promoter accelerating the ozone decay [Staehelin and Hoigné, 1985]. Obviously, when modelling ozonation of natural waters, one cannot list all the reactions susceptible to occur with species present in NOM. Experimentally investigating the ozonation of natural water, one should therefore avoid phosphate pH-buffer. The use of nitric acid is often preferred, organic content already exhibiting natural pH-buffer capability.

Despite these observations, few kinetics data is available for the phenomena involving phosphate. Reactions (with radicals involved in the ozone self-decomposition) reported in literature can be found in table **22**. Three examples of α abstraction on 2-propanol by the different forms of phosphate radicals are given as well.

Table 22 Reactions involving phosphate species

Type	Reaction	Kinetic constant value (293K)	Reference
Radical generation	$^{\bullet}OH + H_2PO_4^- \rightarrow HO^- + {}^{\bullet}H_2PO_4$	2.10^4 $M^{-1}.s^{-1}$	[Maruthamutuh and Neta, 1978]
	$^{\bullet}OH + HPO_4^{2-} \rightarrow HO^- + {}^{\bullet}HPO_4^-$	$1.5.10^5$ $M^{-1}.s^{-1}$	[Maruthamutuh and Neta, 1978]
Acid-base reaction	$^{\bullet}O_3^- + H_2PO_4^- \rightarrow {}^{\bullet}HO_3 + HPO_4^{2-}$	$2.1.10^8$ $M^{-1}.s^{-1}$	[Bühler *et al.*, 1984]
	$^{\bullet}HO_3 + HPO_4^{2-} \rightarrow {}^{\bullet}O_3^- + H_2PO_4^-$	2.10^7 $M^{-1}.s^{-1}$	[Bühler *et al.*, 1984]
Alpha-H abstraction	$CH_3 - CHOH - CH_3 + {}^{\bullet}PO_4^{2-} \rightarrow CH_3 - \dot{C}OH - CH_3 + HPO_4^{2-}$	$1.8.10^7$ $M^{-1}.s^{-1}$	[Neta *et al.*, 1988]
	$CH_3 - CHOH - CH_3 + {}^{\bullet}HPO_4^- \rightarrow CH_3 - \dot{C}OH - CH_3 + H_2PO_4^-$	$2.5.10^7$ $M^{-1}.s^{-1}$	[Neta *et al.*, 1988]
	$CH_3 - CHOH - CH_3 + {}^{\bullet}H_2PO_4 \rightarrow CH_3 - \dot{C}OH - CH_3 + H_3PO_4$	$1.4.10^8$ $M^{-1}.s^{-1}$	[Neta *et al.*, 1988]
Acid-base equilibria			
pK_A = 2.3	$H_2PO_4^- + H^+ \rightarrow H_3PO_4$	5.10^{10} $M^{-1}.s^{-1}$	Calculated according to equation **17**
	$H_3PO_4 \rightarrow H_2PO_4^- + H^+$	$2.51.10^8$ s^{-1}	
pK_A = 7.2	$HPO_4^{2-} + H^+ \rightarrow H_2PO_4^-$	5.10^{10} $M^{-1}.s^{-1}$	
	$H_2PO_4^- \rightarrow HPO_4^{2-} + H^+$	$3.2.10^3$ s^{-1}	
pK_A = 12.3	$PO_4^{3-} + H^+ \rightarrow HPO_4^{2-}$	5.10^{10} $M^{-1}.s^{-1}$	
	$HPO_4^{2-} \rightarrow PO_4^{3-} + H^+$	$2.51.10^{-2}$ s^{-1}	

1.7.2. Micropollutants and Specific Molecules

Specific compounds will be used in this study. *para*-chlorobenzoic acid (*p*CBA) and *tert*-butanol are molecules that react very fast with hydroxyl radicals and very slowly with ozone. As such, they can either be used to "trace" radical concentrations (*p*CBA) or as radical scavengers (*tert*-butanol). We give in table **23** their kinetics.

Table 23 Reactions with specific micropollutants or molecules

Type	Reaction	Kinetic constant value (293K)	Reference
pCBA	Direct oxidation	$1.5.10^{-1}$ $M^{-1}.s^{-1}$	[Cho *et al.*, 2003]
	Indirect oxidation	5.10^{9} $M^{-1}.s^{-1}$	[Neta and Dorfman, 1968]
***tert*-BuOH**	Direct oxidation	3.10^{-2} $M^{-1}.s^{-1}$	[Hoigné and Bader, 1983]
		10^{-3} $M^{-1}.s^{-1}$	[Yao and Haag, 1991]
	Indirect oxidation	6.10^{8} $M^{-1}.s^{-1}$	[Buxton *et al.*, 1988]; [Dong *et al.*, 2008]
		5.10^{8} $M^{-1}.s^{-1}$	[Langlais *et al.*, 1991]
		$7.3.10^{8}$ $M^{-1}.s^{-1}$	[Sutherland and Adams, 2007]

1.8. Conclusion

Very unstable in water, ozone reacts with a large variety of organic and inorganic compounds. Since its discovery by Schönbein in 1840, the interactions with its environment have been studied.

Many phenomena have been understood and modelled. Ozone self-decomposition, reactions with inorganic carbon are well-documented topics, still arousing the interest of many authors of the scientific community. However, due to its ability to indirectly generate radical species when decomposing, ozone is involved in very intricate chemistry, which cannot be considered exhaustively yet. This is particularly the case when ozone is brought in natural water and reacts with present organic fractions.

As a consequence, mechanistic models available in the literature can be chosen for the following phenomena:

- ozone self-decomposition: a SBH-based mechanism will be chosen;
- reactions with inorganic carbon: a classical pathway combining reactions widely used in different studies will be considered;
- reactions for bromate formation: all the reactions present in the literature will not be considered, but a selection will be done based on kinetics.

Considering the influence of NOM, a semi-empirical model shall be proposed for modelling needs. The model shall be based on the classical categorisation: *consumers*, *initiators*, *promoters* and *inhibitors*. Based on the reviewed models including NOM fractions, the number of model parameters, the value of which may have to be optimised or identified may vary; roughly there will be around five to fifteen parameters to be fitted to experimental data.

1.9. Bibliography

Articles and books

- **Acero J. L.** and **von Gunten U.**, (2000). Influence of Carbonate on the Ozone/Hydrogen Peroxide Based Advanced Oxidation Process for Drinking Water Treatment, *Ozone: Science and Engineering*, Vol. **22**, pp. 305-328.
- **Adams J. Q.** and **Clark R. M.**, (1991). Controlling Disinfection By-Products and Microbial Contaminants in Drinking Water, Chapter **14**: Control of microbial contaminants and Disinfection By-Products (DBPs): Cost and Performance, USEPA.
- **Amichai A., Czapski G., Treinin A.**, (1969). Flash Photolysis of the Oxybromine. Anions, *Israeli Journal of Chemistry*, Vol. **7**, pp. 351-359.
- **Bahnemann D.** and **Hart E.J.,** (1982). Rate constants of the reaction of the hydrated electron and hydroxyl radical with ozone in Aqueous Solution, *Journal of Physical Chemistry*, Vol. **86**, pp. 252-255.
- **Behar D.**, **(**1972). Pulse Radiolysis Studies on Br^- in Aqueous Solution: the Mechanism of Br_2^- Formation, *Journal of Physical Chemistry*, Vol. **76**, pp. 1815-1818.
- **Beltrán F.J., González M., Acedo B.**, **Rivas F. J.,** (2000). Kinetic Modelling of Aqueous Atrazine Ozonation Processes in a Continuous Flow Bubble Contactor, *Journal of Hazardous Materials B80*, Vol. **80**, pp. 189-206.
- **Bezbarua B. K.** and **Reckhow D. A.,** (2003). Modification of the Standard Neutral Ozone decomposition Model, *Ozone: Science and Engineering*, Vol. **26**, pp. 345-357.
- **Bezbarua B. K.,** (1997). Modeling Reactions of Ozone with NOM, Ph.D. thesis, University of Massachusetts Amherst, USA.
- **Bielski B.H.J.** and **Allen A.O.**, (1977). Mechanisms of disproportionation of superoxide radicals, *Journal of Physical Chemistry*, Vol. **81**, pp. 1048-1050.
- **Bisby R. H., Johnson S. A., Parker A. W., Tavender S. M.,** (1998). Time-resolved resonance Raman spectroscopy of the carbonate radical, *Journal of the Chemistry Society*, *Faraday Transactions*, Vol. **94**, pp. 2069-2072.
- **Buffle M.-O.**, (2005). Mechanistic Investigation of the Initial Phase of Ozone Decomposition in Drinking Water and Wastewater, Ph.D. thesis, Swiss Federal Institute of Technology Zürich, Switzerland.
- **Bühler R.E., Staehelin J., Hoigné J.**, (1984). Ozone Decomposition in Water Studied by Pulse Radiolysis. 1. HO_2 / O_2^- and HO_3 / O_3^- as Intermediates, *Journal of Physical Chemistry*, Vol. **88**, pp. 2560-2564.
- **Buxton G. V.** and **Dainton F. S.**, (1968). The Radiolysis of Aqueous Solutions of Oxybromine Compounds; the Spectra and Reactions of BrO and BrO_2, *Proceedings of the Royal Society A.*, Vol. **304**, pp. 427-439.
- **Buxton G. V.** and **Elliot A. J.,** (1986). Rate Constants for Reaction of Hydroxyl Radicals with Bicarbonate Ions, *Radiation Physical Chemistry*, Vol. **27**, pp. 241-243.
- **Buxton G. V., Greenstock C. L., Helman W.P., Ross A. B.,** (1988). Critical Review of Reactions of Hydrated Electrons, *Journal of Physical Chemistry Ref. Data*, Vol. **17**, pp. 513-886.
- **Chelkowska K., Grasso D., Fábián I., Gordon G.,** (1990). Mechanistic Comparison of Residual Ozone Decomposition, *Proceedings of the IOA Conference*, Shreveport, pp. 427-437.
- **Chelkowska K., Grasso D., Fabian I., Gordon G.,** (1992). Numerical Simulations of Aqueous Ozone Decomposition, *Ozone: Science and Technology*, Vol. **14**, pp. 33-49.
- **Chen S.-N., Cope V. W., Hoffman M. Z.,** (1973). Behavior of carbon trioxide (-) radicals generated in the flash photolysis of carbonatoamine complexes of cobalt (III) in aqueous solution, *Journal of Physical Chemistry*, Vol. **77**, pp. 1111-1116.
- **Chiang C. L.,** (2003). Statistical Methods of Analysis, *World Scientific Editors*, Singapore, section 9.7.4, p. 274.
- **Chick H.,** (1908). An investigation of the laws of disinfection, *Journal of Hygiene*, Vol. **8**, pp. 92-158.
- **Cho M., Kim H., Cho S. H., Yoon J.**, (2003). Investigation of Ozone Reaction in River Waters causing Instantaneous Ozone Demand, *Ozone: Science and Engineering*, Vol. **25**, pp. 251-259.

- **Czapski G., Lymar S. V., Schwartz H. A.,** (1999). Acidity of Carbonate Radical, *Journal of Physical Chemistry*, Vol. **102**, pp. 3447-3450.
- **Dong Y., Yang H., He K., Wu X., Zhang A**., (2008). Catalytic activity and stability of Y zeolite for phenol degradation in the presence of ozone, *Applied Catalysis B: Environmental*, Vol. **82**, pp. 163–168.
- **Doré M.**, (1989). Chimie des oxydants et traitement des eaux, Tec et Doc Lavoisier, Paris.
- **Eigen M.** and **Kustin K.**, (1962). The Kinetics of Halogen Hydrolysis, *Journal of the American Chemical Society*, Vol. **84**, pp. 1355-1361.
- **Elovitz M. S.** and **von Gunten U.**, (1999). Hydroxyl Radical/Ozone Ratios during Ozonation Processes. I. The R_{ct} Concept, *Ozone: Science and Engineering*, Vol. **21**, pp. 239-260.
- **Eriksen T. E., Lind J., Merényi G.,** (1985). On the acid-base equilibrium of the carbonate radical, *Radiation Physics and Chemistry*, Vol. **26**, pp. 197-199.
- **Farhataziz** and **Ross, A. B.,** (1977). Selective Specific Rates of Reactions of Transients from Water in Aqueous Solutions, National Bureau of Standards: Washington, DC, Natl. Stand. Ref. Data Ser. (U.S., Natl. Bur. Stand.) No. **59**.
- **Faria R. B., Epstein I. R., Kustin K.**, (1994). Kinetics of Disprotonation and pKa of Bromous Acid, *Journal of Physical Chemistry*, Vol. **98**, pp. 1363-1367.
- **Gélinet K.**, (1999). Importance des caractéristiques physico-chimiques des eaux naturelles sur la formation des ions bromates lors de l'ozonation, Ph.D. thesis, ESIP, France.
- **Gordon G.**, (1995). The Chemical Aspects of Bromate Control in Ozonated Drinking Water Containing Bromide Ion, *Water Supply*, Vol. **13**, pp. 35-43.
- **Gurol M. D.** and **Singer P. C.,** (1982). Kinetics of Ozone decomposition: A Dynamic Approach, *Environmental Science and Technology*, Vol. **16**, pp. 377-383.
- **Haag W. R.** and **Hoigné J.**, (1983). Ozonation of bromide-containing waters: kinetics of formation of hypobromous acid and bromate, *Environmental Science and Technology*, Vol. **17**, 261-267.
- **Haas C. N.** and **Betz L. D.,** (2009). Future Design Techniques for Chemical Disinfection, *Proceedings of the 5th Japan - U.S. Joint Conference on Drinking Water Quality Management and Wastewater Control*, Las Vegas, March 2-5.
- **Hassan K. Z. A., Bower K. C., Miller C M.,** (2003). Numerical Simulation of Bromate Formation during Ozonation of Bromide, *Journal of Environmental Engineering*, Vol. **129**, pp. 991-998.
- **Hofmann R.** and **Andrews R. C.**, (2001). Ammoniacal Bromamines: A Review of Their Influence on Bromate Formation During Ozonation, *Water Research*, Vol. **35**, pp. 599-604.
- **Hoigné J.** and **Bader H.,** (1976). The Role of Hydroxyl Radical Reactions in Ozonation Processes in Aqueous Solutions, *Water Research*, Vol. **10**, pp. 377-386.
- **Hoigné J.** and **Bader H.,** (1979). Ozonation of Water: "Oxidation-Competition Values" of Different Types of Waters Used in Switzerland, *Ozone: Science and Engineering*, Vol. **1**, pp. 357-372.
- **Hoigné J.** and **Bader H.,** (1983). Rate constants of reactions of ozone with organic and inorganic compounds in water: II dissociating organic compounds, *Water Research.*, Vol. **17**, pp. 185-194.
- **Hoigné J.** and **Bader H.,** (1994). Characterization of water quality criteria for ozonation processes. Part II: Lifetime of added ozone, *Ozone: Science and Engineering,* Vol. **16**, pp. 121-134.
- **Hoigné J.**, (1994). Characterization of water-quality criteria for ozonation processes. Part I: Minimal set of analytical data, *Ozone: Science and Engineering*, Vol. **16**, pp. 113-120.
- **Hunter G. F.** and **Rakness K. L.,** (1997). Start-Up and Optimization of the Ozone Disinfection Process at the Sebago Lake Water Treatment Facility, *Ozone: Science and Engineering*, Vol. **19**, pp. 255-272.
- **Jarvis P., Parsons S. A., Smith R.,** (2007). Modeling Bromate Formation During Ozonation, *Ozone: Science and Engineering*, Vol. **29**, pp. 429-442.
- **Kim J.-H,** (2004).Integrated optimization of Cryptosporidium inactivation and bromate formation control in ozonation contactors, *Presentation at the Gwangju Institute of Technology*, May 27.
- **Kim J.-H., Elovitz M. S., von Gunten U., Shukairy H. M., Mariñas B. J.,** (2007). Modeling Cryptosporidium parvum oocyst inactivation and bromate in a flow-through ozone contactor treating natural water, *Water Research*, Vol. **41**, pp. 467-475.
- **Kim J.-H., von Gunten U., Mariñas B. J.**, (2004). Simultaneous predicion of *Cryptosporidium parvum Oocyst* inactivation and bromate formation during ozonation of synthetic waters, *Environmental Science and Technology*, Vol. **38**, pp. 2232-2241.

- **Kläning U.K.** and **Wolff T.**, (1985). Laser Flash Photolysis of HClO, ClO^-, HBrO, and BrO^- in Aqueous Solution, *Ber. Bunsenges. Physik. Chem.*, Vol. **89**, pp. 243–245.
- **Krasner S. W., Gramith J. T., Coffey B. M., Yates R.S.**, (1995). Impact of water quality and operational parameters on the formation and control of bromate during ozonation, *Water Supply*, Vol. **13**, pp. 145-156.
- **Langlais B., Reckhow D. A., Brink D.R.,** (1991). Ozone in Water Treatment: Application and Engineering, *LEWIS Publishers*, Washington D.C., U.S.A.
- **Laplanche A., Lemasle M., Wolbert D., Galey C., Cavard J.**, (1998). Contribution of molecular and radical mechanisms in bromate formation during ozonation processes, *International Regional Conference I.O.A. Poitiers, September 23-25*, 29-1-29-10.
- **Legube B., Parinet B., Gélinet K., Berne F., Croué J.-P.,** (2004). Modeling of bromate formation by ozonation of surface waters, *Water Research*, Vol. **38**, pp. 2185-2195.
- **Lovato M. E., Martín C., Cassano A. E.,** (2009). A reaction kinetic model for ozone decomposition in aqueous media valid for neutral and acidic pH, *Chemical Engineering Journal*, Vol. **146**, pp. 486-497.
- **Mamou A., Rabani J., Behar D.**, (1977). Oxidation of aqueous bromide (1-) by hydroxyl radicals, studies by pulse radiolysis, *Journal of Physical Chemistry*, Vol. **81**, pp. 1447-1448.
- **Maruthamutuh P.** and **Neta P.**, (1978). Phosphate Radicals. Spectra, acid-base equilibria, and reactions with inorganic compounds, *Journal of Physical Chemistry*, Vol. **82**, pp. 710-713.
- **Masschelein W. J.,** (2000). Considerations on the chick-Watson Law Applied to the Ozonation of Drinking Water, *Ozone: Science and engineering*, Vol. **22**, pp. 227-239.
- **Mizuno T., Tsuno H., Yamada H.,** (2007a). A Simple Model to Predict Formation of Bromate Ion and Hypobromous Acid/Hypobromite Ion through Hydroxyl Radical Pathway during Ozonation, *Ozone: Science and Engineering*, Vol. **29**, pp. 3-11.
- **Mizuno T., Tsuno H., Yamada H.,** (2007b). Effect of Inorganic Carbon on Ozone Self-Decomposition, *Ozone: Science and Engineering*, Vol. **29**, pp. 31-40.
- **Mizuno T., Tsuno H., Yamada H.,** (2007c). Development of Ozone Self-Decomposition Model for Engineering Design, *Ozone: Science and Engineering*, Vol. **29**, pp. 55-63.
- **Morioka T., Motoyama B., Hoshikawa H., Murakami A., Okada M. Moniwa T.,** (1993). Kinetic Analysis on the Effects of Dissolved Inorganic and Organic Substances in Raw Water on the Ozonation of Geosmin and 2-MIB, *Ozone: Science and Engineering*, Vol. **15**, pp. 1-18.
- **Muñoz Ramirez G.**, (1997). Approche cinétique de la demande immédiate en ozone, Ph.D. thesis, ENSC-R, France.
- **Nemes A., Fábián I., Gordon G.**, (2000). Experimental Aspects of Mechanistic Studies on Aqueous Ozone Decomposition in Alkaline Solution, *Ozone: Science and Engineering*, Vol. **22**, pp. 287-304.
- **Neta P.** and **Dorfman L. M.,** (1968). Pulse radiolysis studies. XIII: rate constants for the reaction of hydroxyl radicals with aromatic compounds in aqueous solutions, in *Radiation Chemistry*, Chapter **15**, pp. 222–230.
- **Neta P., Huie R. E., Ross A. B.**, (1988). Rate Constants for Reactions of Inorganic Radicals in Aqueous Solutions, *Journal of Physical Chemistry, Reference Data* **17**, pp. 1027-1284.
- **Ozekin K.** and **Amy G.,** (1997). Threshold levels of bromate formation in drinking water, *Ozone: Science and Engineering*, Vol. **19**, pp. 323-337.
- **Park H.-S., Hwang T.-M., Kang J. W., Choi H., Oh H.-J.,** (2001).Characterization of raw water for the ozone application measuring ozone consumption rate, *Water Research*, Vol. **35**, pp. 2607-2614.
- **Pinkernell U.** and **von Gunten U.**, (2001). Bromate Minimization during Ozonation: Mechanistic Considerations, *Environmental Science and Technology*, Vol. **35**, pp. 2525-2531.
- **Roche P., Volk C., Charbonnier F., Paillard H.**, (1994). Water Oxidation by Ozone or Ozone/Hydrogen Peroxide Using the « Ozotest » or « Peroxotest » Methods, *Ozone: Science and Engineering*, Vol. **16**, pp. 135-155.
- **Rothmund V** and **Burgstaller A.**, (1913). Über die Geschwindigkeit der Zersetzung des Ozons in wässeriger Lösung, *Monatshefte für Chemie*, Vol. **34**, pp. 665-692.
- **Roustan M., Debellefontaine H., Do-Quang Z., Duguet J.-P.,** (1998). Development of a Method for the Determination of Ozone Demand of a Water, *Ozone: Science and Engineering*, Vol. **20**, pp. 513-520.
- **Roustan M., Stambolieva Z., Duguet J. P., Wable O., Mallevialle J.,** (1991). Influence of Hydrodynamics on *Giardia* Cyst Inactivation by Ozone, Study by Kinetics and by "CT" Approach, *Ozone: Science and Engineering*, Vol. **13**, pp. 451-462.

- **Sadiq R.** and **Rodriguez M. J.,** (2004). Disinfection by-products (DBPs) in drinking water and predictive models for their occurence: a review, *Science of the Total Environment*, Vol. **321**, pp. 21-46.
- **Savary B.**, (2002). Influence des caractéristiques d'une eau naturelle sur la formation des ions bromates au cours de l'ozonation: Observations-Prévisions-Simulations dans un réacteur diphasique du type colonne à bulles, Ph.D. thesis ENSC-R, France.
- **Schwartz H. A.** and **Bielski B. H. J.**, (1986). Reactions of hydroperoxo- and superoxide with iodine and bromine and the iodide (I_2^-) and iodine atom reduction potentials, *Journal of Physical Chemistry*, Vol. **90**, pp. 1445-1448.
- **Sehested K.**, **Corfitzen H., Holcman J., Fischer C. H**., **Hart E. J**., (1991). The primary reaction in the decomposition of ozone in acidic aqueous solutions, *Environmental Science and Technology*, Vol. **25**, pp. 1589-1596.
- **Sohn J., Amy G., Cho J., Lee Y., Yoon Y.,** (2004). Disinfectant decay and disinfection by-products formation model development: chlorination and ozonation by-products, *Water Research*, Vol. **38**, pp. 2461-2478.
- **Song R.** (1996). Ozone-Bromide-NOM Interactions in Water Treatment, Ph.D. thesis, University of Illinois at Urbana-Champaign, USA.
- **Song R., Donohoe C., Minear R., Wetserhoff P., Ozekin K., Amy G.,** (1996). Empirical Modelling of Bromate Formation During Ozonation of Bromide-Containing Waters, *Water Research*, Vol. **30**, pp. 1161-1168.
- **Song R., Minear R., Westerhoff R., Amy G.,** (1996). Bromate formation and control during water ozonation, *Environmental Technology*, Vol. **17**, pp. 861-868.
- **Song R., Westerhoff R., Minear R.**, **Amy G.**, (1997). Bromate minimization during ozonation, *Journal A.W.W.A.,* Vol. **89**, pp. 69-78.
- **Staehelin J.** and **Hoigné J.**, (1982). Decomposition of ozone in water: Rate of Initiation by Hydroxide Ions and Hydrogen Peroxide, *Environmental Science and Technology*, Vol. **16**, pp. 676-681.
- **Staehelin J., Bühler R.E., Hoigné J.**, (1984). Ozone Decomposition in Water Studied by Pulse Radiolysis. 2. OH and HO_4 as Chain Intermediates, *Journal of Physical Chemistry*, Vol. **88**, pp. 5999-6004.
- **Staehelin, J.** and **Hoigné, J.,** (1985). Decomposition of Ozone in Water in the Presence of Organic Solutes Acting as Promoters and Inhibitors of Radical Chain Reactions, *Environmental Science and Technology*, Vol. **19**, pp. 1206-1213.
- **Sutherland J.** and **Adams C., (**2007). Determination of Hydroxyl Radical Rate Constants for Fuel Oxygenates, *Environmental Engineering Science*, Vol. **24**, pp. 998-1005.
- **Sutton H. C., Adams G. E., Boag J. W., Michael B. D.**, (1965), in *Pulse Radiolysis*, Edited by Ebert M., Keene J. P., Swallow A. J., Baxendale J. H., Academic Press, London.
- **Taube, H.** and **Bray, W. C.,** (1940). Chain Reactions in Aqueous Solutions Containing Ozone, Hydrogen Peroxide and Acid, *Journal of the American Chemistry Society*, Vol. **62**, pp. 3357-3373.
- **Thurman E. M.** and **Malcolm R. L.,** (1981). Preparative Isolation of Aquatic Humic Substances, *Environmental Science and Technology*, Vol. **15**, pp. 463-466.
- **Tomiyasu H., Fukutomi H., Gordon G.,** (1985). Kinetics and Mechanism of Ozone Decomposition in Basic Aqueous Solution, *Inorganic Chemistry*, Vol. **24**, pp. 2962-2966.
- **USEPA**, (1991). Guidance manual for compliance with the filtration and disinfection requirements for public water systems using surface water sources. EPA 68-01-6989, U.S. Environmental Protection Agency, Washington D.C, U.S.A.
- **Vandersmissen K., de Smedt F., Vinckier C.,** (2008). The Impact of Traces of Hydrogen Peroxide and Phosphate on the Ozone Decomposition Rate in "Pure Water", *Ozone: Science and Engineering*, Vol. **30**, pp. 300-309.
- **vanLoon G. W.** and **Duffy S. J.**, (2005). Environmental Chemistry – A global Perspective, New York, Chapter **12**, pp. 254-264, Oxford University Press, Second Edition.
- **von Gunten U.** and **Hoigné J,** (1993). Bromate formation during ozonation of bromide containing waters, *Proceedings of the 11th Ozone world congress, San Francisco*, Vol. **1**, S-9-42, S-9-45.
- **von Gunten U.** and **Hoigné J.,** (1994). Bromate Formation during Ozonation of Bromide-Containing Waters: Interaction of Ozone and Hydroxyl Radical Reactions, *Environmental Science and Technology*, Vol. **28**, pp. 1234-1242.

- **von Gunten U.** and **Hoigné J., (**1996), in *Disinfection By-Products in Water Treatment: The Chemistry of Their Formation and Control*, Edited by Minear R. A., Amy G. L.**,** Chapter **8**, pp. 187-206, CRC Press Inc.: Boca Raton.
- **von Gunten U.** and **Pinkernell U.**, (2000). Ozonation of bromide-containing drinking waters: a delicate balance between disinfection and bromate formation. *Water Science and Technology*, Vol. **41**, pp. 53-59.
- **von Gunten U.**, (2003a). Ozonation of drinking water: Part I. Oxidation kinetics and product formation-Review, *Water Research*, Vol. **37**, pp. 1443-1467.
- **von Gunten U.,** (2003b). Ozonation of drinking water: Part II. Disinfection and by-product formation in presence of bromide, iodide or chlorine, *Water Research*, Vol. **37**, pp. 1469-1487.
- **Wajon J.E.** and **Morris J.C.**, (1982). Rates of formation of N-bromo amines in aqueous solution, *Inorganic Chemistry*, Vol. **21**, pp. 4258–4263.
- **Wang R. Y.**, (1995). Etude de l'hydrodynamique et du transfert de l'ozone dans une colonne à bulles en ascension libre, Ph.D. thesis, Université de Toulouse, France.
- **Westerhoff P.**, (1995). Ozone Oxidation of Bromide and Natural Organic Matter, Ph.D. thesis, University of Boulder, USA.
- **Westerhoff P.**, (2002). Kinetic-based models for bromate formation in natural waters, EPA final report.
- **Westerhoff P., Song R., Amy G.**, **Minear R.**, (1997). Application of Ozone Decomposition Models, *Ozone: Science and Engineering*, Vol. **19**, pp. 55-73.
- **Westerhoff P.**, **Song R.**, **Amy G., Minear R.**, (1998). Numerical kinetic models for bromide oxidation to bromine and bromate, *Water Research*, Vol. **32**, pp. 1687-1699.
- **Yao C. C. D.** and **Haag W. R.**, (1991). Rate Constants for Direct Reactions of Ozone with several Drinking Water Contaminants, *Water Research*, Vol. **25**, pp. 761-773.
- **Yurteri C.** and **Gurol M. D.**, (1988). Ozone consumption in natural waters: effects of background organic matter, pH and carbonate species. *Ozone: Science and Engineering*, Vol. **10**, pp. 277-290.
- **Zehavi D.** and **Rabani J.**, (1972). The Oxidation of Aqueous Bromide Ions by Hydroxyl Radicals. A Pulse Radiolytic Investigation, *Journal of Physical Chemistry*, Vol. **76**, pp. 312-319.
- **Zuo Z., Cai Z., Katsumura Y., Chitose N., Muroya Y.,** (1999). Reinvestigation of the acid–base equilibrium of the (bi)carbonate radical and pH dependence of its reactivity with inorganic reactants, *Radiation Physics and Chemistry*, Vol. **55**, pp. 15-23.

2. INTEGRATING HYDRAULIC FLOW CONDITIONS

Abstract

The first concerns about the modelling of the hydraulics for ozonation units emerged with the application of the Ct concept (in which the unit is compared to an ideal Plug Flow Reactor, PFR, with assumed constant ozone concentration). Critics claimed that industrial ozonation units usually exhibit strong non-ideal characteristics, for instance backmixing zones or bypass flows. The Ct calculation method was therefore modified and other approaches proposed. Nowadays, with increasing concerns about micropollutants and Disinfection By-Products, *i.e.* bromate, it appears that global approximations on both chemistry and hydraulics can no longer be used. More refined models are required, which have to take into account radical chemistry and real hydraulic behaviours that had been previously neglected, when focusing on disinfection.

Taking this complexity into account, two generic approaches can be proposed to model ozonation processes:

On one hand, the use of Computational Fluid Dynamics (CFD) allows a very precise description of the flow conditions. Combining it with complex chemical kinetics (approximately 50 reactions on 30 chemical species or so) is possible, still numerically difficult, mainly because of the *stiffness* of the problem (coexistence of phenomena with very different characteristic times). The authors who have applied CFD tools to the simulation of ozonation units have therefore always opted for simplified models with 4 to 6 reactions. Even if the simulations gave interesting results (especially regarding the disinfection efficiency), the robustness of the models proposed with CFD has very rarely been assessed. Finally, the use of CFD can only be achieved with a long CPU time, what hinders an on-site use.

On the other hand, a classical representation by a pattern of ideal reactors called "systematic network" can globally represent the hydrodynamics of an ozonation installation as suggested by comparing the generated and experimental Residence Time Distributions (RTDs). Moreover, such networks may well be used in conjunction with advanced chemical kinetics models, thus generating precise information on the chemistry of the process. The use of systematic networks appears therefore as the best *a priori* compromise for simulating ozonation units.

The mass balances which have to be solved when using a systematic network are presented. Due to the formulation of the kinetics laws, these are highly non-linear systems of equations. The difficulty of solving depends on both chemical and systematic models chosen. In the case of recycling loops, the size of the problem can be high (up to 500 variables for a relatively complex problem). Moreover, the equations may exhibit a relatively *stiff* character. The review of currently available simulators, generic Computer Aided Engineering (CAE) and water treatment software products, indicates that a tailored simulator would be preferable, due to the high complexity of the systems to be solved. An adjustable solver previously developed at the ENSCR is therefore chosen.

Contents

2.1. Introduction

In the first decades of the twentieth century, experimental evidence of the pathogenic character of bacteria was given. Further investigations carried out during the 1930-1970 period, during which various rate expressions for disinfection were developed [Gélinet, 1999], enlightened that the disinfectant residual combined with the contact time (also as functions of pH and temperature) were crucial predictors of disinfection efficiency. Accordingly, the Ct parameter (residual disinfectant concentration multiplied by exposure time) was formulated and used.
Increasing concerns about the non-ideal nature of the hydraulics of industrial disinfection tanks led to the empirical use of the conservative t_{10} (time for most rapid 10% of water to pass through a system) for describing disadvantageous hydraulic flow conditions. Despite additional refinements, many have recognised that the Ct_{10} approach has severe limitations, as opposed to a fuller consideration of the overall Residence Time Distribution (RTD) [Trussel and Chao, 1977]. Other approaches were proposed using the full RTD, but they suffer from oversimplification of mixing conditions [Haas and Betz, 2009].
At the beginning of the nineties, with the emergence of micropollutants in the aquatic environment and the suspicion on Disinfection By-Product (DBP) toxicity, new challenges appeared in disinfection management. Approximately at the same period, two strides were made in water treatment science. On one hand, detailed hydrodynamic modelling with Computational Fluid Dynamics (CFD) tools was achievable ([Do-Quang 1993]; [Murrer *et al.*, 1995]; [Dumeau de Traversay, 2000]). On the other hand, the chemical reaction mechanisms and their kinetics for hydroxyl radical and bromate formation were described in controlled laboratory conditions (see chapter **1, 1.3.** to **1.6.**). Both improvements encouraged researchers to explore new modelling approaches, coupling refined hydraulic models with advanced chemical models.
Different software products can be used for the simulation of ozonation units: classical Computer Aided Engineering (CAE) software products, generally used for CFD computations are available; simulators for water treatment can also be found on the market. Their use for solving a problem similar to ours shall be assessed.
The objective of this chapter is to specify the modelling framework for the simultaneous prediction of hydraulic and chemical phenomena occurring during ozonation. Therefore, we shall first review the use of CFD in management of ozonation units (section **2.2.**). Then, we shall present an approach focusing on precise chemical description using mechanistic reaction pathways (section **2.3.**). These two approaches will be discussed and their respective relevancy in regards to the modelling of ozonation units (especially based on the specificities of the mathematical equations for the mass balances to be solved) will be compared. Finally, a brief presentation of common modelling platforms used for comparable problems will be given (section **2.4.**).

2.2. Focusing on Hydraulics: CFD Approach

2.2.1. Generalities

Computational Fluid Dynamics (CFD) is the science of predicting fluid flow, possibly combined with heat transfer, mass transfer, chemical reactions and related phenomena by solving the mathematic equations governing these processes using numerical algorithms [Versteeg and Malalasekera, 1995]. The fluid hydrodynamics governing equations are known as the Navier-Stokes equations. These are partial differential equations established in the

early nineteenth century. No general analytical solution can be given, so the equations are discretised and solved numerically.
As most fields in simulation science, CFD has increased in popularity during recent years due to the development of advanced commercial CFD codes and to the rising power of computational resources. Key advantage of the CFD approach is its efficiency to simulate equally well small scale (laboratory pilots) and large scale (full-scale) facilities without the use of particular scale-up laws [Zhang, 2006]. Thus, CFD can be used to obtain more accurate information about the performance of water treatment processes and find design solutions for improvement [Do-Quang *et al.*, 1999]. Main fields of CFD application are the automotive industry, the aerospace industry, and the medical/biological/chemical research sector. CFD as been less used in the drinking water industry, but its potential has clearly been recognised.
The first works using CFD to model oxidation units were issued in the nineties ([Do-Quang, 1993]; [Murrer *et al.*, 1995]; [Do-Quang *et al.*, 1996]; [Cockx *et al.*, 1999]), first for chlorination units, then for ozonation units. Hence, the application of CFD methods to simulate ozonation process is relatively new, and represents a very lively research field.

2.2.2. Predicting Disinfection Efficiency

2.2.2.1. Using CFD as Improvement for Ct Approach

One of the shortcomings of the Ct concept (see chapter **1**, **1.2.5.**) is the assumption that the unit is liken to a plug flow reactor, meaning that neither geometry nor hydraulic characteristics are taken into account. However, a survey by [Jaeger *et al.*, 2009] of existing ozonation tanks has shown that in many contactors, recycling loops, dead zones and bypass flows exist, what can highly decrease the disinfection efficiency. The authors proposed hence to improve the Ct approach using CFD to better characterise the hydraulic efficiency of the unit, α, defined in equation **1** as the ratio of t_{10} to hydraulic retention time τ (geometrical volume to inlet flowrate ratio). α is indeed needed when calculating inactivation credits by the Ct approach (definitions and properties for RTDs can be found in Appendix **B**).

$$\alpha = \frac{t_{10}}{\tau} \quad \textbf{(1)}$$

Purpose of the study was to determine which geometrical characteristics influence the most hydraulic efficiency. This approach was supported by two designs of experiments (CFD simulations), thus performing simulations for 59 ozonation units. The results highlighted the influence of three main parameters on the hydraulic efficiency (see figure **1**): length L (negative influence), water height at the inlet $h_{w,in}$ (positive influence) and total water height h_w (positive influence). Results showed that width W had no major impact on hydraulic efficiency.

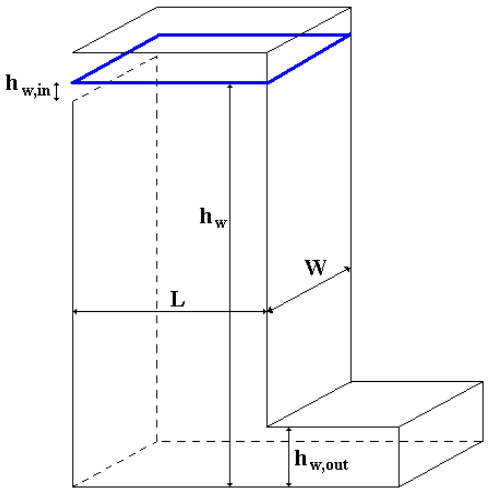

Figure 1 Schematic representation of the geometrical characteristics investigated in [Jaeger *et al.*, 2009]

Although giving interesting results, this study remains of limited use because it was restricted to a single chamber. Besides, it was found that the model could not easily extrapolate to geometries exhibiting different characteristics than those used within the work. Prospects are to study connected chambers and to give an analytical expression for the hydraulic efficiency as function of geometrical characteristics.

In a recent paper, [Wols *et al.*, 2010] have used CFD combined with a particle tracking technique to get information on residence and contact times in chemical reactors (using the COMSOL® simulation package). Objective of this study was to propose a comparison of different methods for disinfection evaluation.
Approaching the movements of individual microorganisms in the system more closely, the particle tracking method was used as reference for calculations of microbial inactivation. Using this technique, it was possible to calculate the ozone exposure for every particle in the flow-domain by integrating the ozone concentration over the particle's trajectory. Then a comparison with classical methods was carried out: Ct (using t_{10}), CSTR method, segregated flow analysis, micro-mixing analysis. Modelling concentration profiles for ozone and microbial organisms was achieved implementing classical Chick-Watson kinetics coupled to first order decomposition law for ozone decomposition.
It was reported that small residence times caused by short-circuit flows lead to low ozone exposures and hence to poor disinfection performances. Methods for prediction of disinfection performance that do not incorporate short-circuit flows in a correct manner, like the segregated flow analysis, therefore tend to overestimate disinfection capacity. Considerations on tank design were also discussed. The authors did not propose any comparison to experimental concentration measurements. However, in a previous paper from the same research team ([Hofman *et al.*, 2007]), it was shown that the combination of CFD with particle tracking technique give valid simulation results when compared to experimental data. These results are nevertheless to be considered with caution given that: (i) chemical parameters as ozone decay rate constant are fitted; (ii) results are given only under specific operational conditions.

2.2.2.2. Simulating Systems with CFD

The first studies using CFD approach for simulating disinfection units have focused on the modelling of tank hydraulics, especially for chlorination processes ([Do-Quang, 1993]; [Stambolieva *et al.*, 1993]). Later, improvements were achieved setting up more

comprehensive models with simplified kinetics model for chlorine decay and microbial inactivation [Greene *et al.*, 2004].
Involving two-phase mass transfer and more intricate kinetics, modelling ozonation means much larger systems to be solved, and accordingly new techniques to be developed. Some authors tried to get round the problem by developing single-phase CFD models ([Murrer *et al.*, 1995]; [Huang *et al.*, 2002]). However, neglecting the effects of the gas phase on contactor hydraulics, these models cannot simulate changes in gas flow, gas concentration or gas location, and remain thus of limited use. Moreover, these studies focused on hydraulics and did not take chemical phenomena into account.
[Gong *et al.*, 2007] have studied the mass transfer process of ozone dissolution in a bubble plume inside a rectangular water tank. The authors mainly investigated the effect of bubble diameter and plume structure on mass transfer efficiency of ozone in bubble plumes. Besides, a first order model for ozone decomposition was integrated, but no comparison with experimental concentration measurements was given. Studying a circulating fluidised bed, [Dong *et al.*, 2007] also focused on mass transfer modelling, comparing three approaches, which differ in their drag coefficient closure and mass transfer equations. The CFD simulation integrated ozone decomposition through first order decomposition rate. Comparisons to measured ozone concentrations were performed for two operational sets of conditions. The calculated ozone concentration showed a relatively good agreement with experimental measurements.
[Bolaños *et al.*, 2008] studied an ozonation bubble column with CFD modelling and also considered ozone decomposition and microbial inactivation. These chemical phenomena were classically modelled by first order kinetic rate and Chick-Watson law. The kinetic constant for ozone decomposition was optimised in order to fit simulation results to experimental concentration measurements. Having integrated chemical kinetics, [Do-Quang *et al.*, 1999] formulated an ozone disinfection model for a two-phase ozone disinfection system. Once water velocity and ozone gas hold-up fields numerically estimated, ozone concentrations in the aqueous phase were predicted solving coupled mass transfer and first-order ozone decay expressions. It was reported that predicted ozone concentrations for the reactor correlated well with experimental results.
Many reviewed papers have represented improvements in modelling ozonation processes, proposing original approaches and comparing them to existing techniques. All the reviewed papers in this paragraph have also demonstrated how CFD can be helpful in order to improve the design of existing water treatment plants and the process efficiency. In some papers, the influence of process conditions has also been assessed. In this scope, CFD may enable more reliable designs and cost effective water treatment processes.

2.2.3. Predicting Ozone Decomposition and Bromate Formation

Main difficulty when modelling the chemistry of ozonation processes is the simultaneous presence of molecular and radical species, reacting in extremely different fashions: some phenomena occur within nanoseconds as the acid-base equilibrium for superoxide radical [Bühler *et al.*, 1984], whereas other may have characteristic times of an hour or so. This discrepancy in characteristic times is particularly difficult to take into account for numerical approaches based on space and time "discretisations". Complex strategies for meshing have to be developed in order to optimise calculation and avoid too long computational times. Some attempts to model ozone decomposition and bromate formation in ozonation reactors are presented hereafter.
Two recent studies have proposed CFD modelling for ozonation reactors coupled with more complex chemistry ([Zhang, 2006]; [Bartrand, 2007]). With different CFD modelling approaches - Zhang used particle tracking technique, whereas Bartrand used a classical Eulerian-Eulerian approach – the authors simulated the same chemical phenomena.

Moreover, the modelling assumptions were very similar; they are summarised in table **1**. Zhang and Bartrand have used the same chemical models except for microbial inactivation: Bartrand implanted Chick-Watson kinetics, whereas Zhang opted for the Hom model (the "H" index referring to Hom's model, see Appendix **A**).
Focusing on CFD modelling approaches and reactor design, the authors did not fully determine the validity of their chemical models and considered experimental measurements only for ozone. [Zhang, 2006] validated the chemical description performing concentration measurements on an industrial water treatment works. The measurements were performed only for given operational conditions and were not repeated. Microbial inactivation mechanism was not supported by any specific experimental measurement. Bromate formation mechanism was not experimentally validated. Some scenarios were tested to assess if design improvements could be achieved. [Bartrand, 2007] used the decolourisation of a solution of Indigo Dye in order to determine the aqueous ozone concentration using spectrophotometry (same principle as exposed in [Bader and Hoigné, 1981]). Measurements of ozone concentration were performed on a laboratory bubble column reactor operating tap water. The validation was done for three operational conditions where gas and liquid flow rates varied; all other conditions were kept constant. The model predicted experimental data adequately for two of the three experiments.
In terms of chemical predictions, these studies remain limited and cannot be directly applied to realistic cases. However, a major outcome consists in demonstrating that a simplified chemical modelling can be coupled with advanced hydraulics description done with CFD tools. Further research shall continue developing chemical models.

Table 1 Comparison of the chemical modelling in [Zhang, 2006] and in [Bartrand, 2007]

Chemical phenomenon	Rate expression	Kinetic constant value	Used by	Reference or origin
IOD	$r^{O_3} = -k_{inst}.[O_3].[NOM]$	3.2 L.mg^{-1}.s^{-1}	[Bartand, 2007]	Determined to occur faster than other phenomena
			[Zhang, 2006]	[Hunt and Mariñas, 1999]
Ozone decomposition	$r^{O_3} = -w.[O_3]$	0.011 s^{-1}	[Bartand, 2007]	Batch experiments
		No data	[Zhang, 2006]	
Microbial inactivation (*Cryptosporidium* oocysts)	$r^{N} = -k[O_3]N$	0.0917*1.097^{T} L.mg$(O_3)^{-1}$.min^{-1}	[Bartand, 2007]	Ct tables
	$r^{N} = -ko_H[O_3]^{n_H} N.t^{o_H-1}$	See [Gyurek *et al.*, 1999]	[Zhang, 2006]	[Gyurek *et al.*, 1999]
Bromate formation	$r^{BrO_3^-} = k_{BrO_3}.[O_3]$	9.5.10^{-5} s^{-1}	[Bartand, 2007]	Batch experiments
		No data	[Zhang, 2006]	

2.2.4. CFD Simulations for an Ozone/UV Reactor

Chemical processes are increasingly investigated by CFD studies coupling hydraulics with chemical kinetics. However, as for ozonation processes, the chemical pathways implemented remain simple and their validity and robustness are rarely discussed.

However, [Kamimura *et al.*, 2002] developed a single-phase CFD approach for extensively modelling the chemical kinetics of an ozone/UV reactor. A complex radical reaction pathway was combined with the single-phase fluid dynamics model. Comparing experimental results for TOC, hydrogen peroxide and aqueous ozone with simulated concentrations, the chemical model was evaluated. This was done at bench scale with a batch reactor. Then CFD simulations were run to obtain spatial distributions of NOM, ozone and other compounds within the Ozone/UV reactor. CFD calculations were launched in order to test various scenarios and to get more insight into configuration design.
Although considering complex kinetics, the results of this study are difficult to evaluate, since the model only includes one (liquid) phase. Additionally, no validation was carried out at reactor scale.

2.2.5. Conclusion

Important strides were made since the first application of CFD to disinfection tanks: reliable modelling procedures have been proposed and evaluated; benefits from CFD have been proven, for design and operation. These improvements were successfully applied to chlorination and ozonation processes.
Although achievable, the coupling of CFD hydraulics representation with accurate chemical models remains unpublished yet. Reviewing the studies on ozonation modelling through CFD, it appears that chemical modelling is seldom considered. The rare chemical models are basic and their validity is not discussed in articles. The presented simulation results match experimental data because parameter fitting led them to. There are very few studies considering the effects of water quality on CFD models for example and there is limited information on applying CFD model to optimise the operation of ozone contactors for different operational conditions [Zhang, 2006].
CFD represents a promising tool with huge possibilities, combining hydraulics and chemical kinetics. Nevertheless, with current systems, simulation of a complete description of an ozonation unit would be overly resource consuming, - computational time and memory. In all research fields where complex chemistry is observed, CFD studies tend to simplify chemical models (*e.g.* [Bittker, 1993]). The need for a tool able to solve an approximate but realistic model emerged, from the chemical and hydraulic points of view.

2.3. Focusing on Chemistry: Systematic Approach

2.3.1. Introduction

A commonly used approach in chemical engineering consists in subdividing complex flow systems into networks of smaller ideal reactors, for which mass and energy balances have analytical forms (algebraic or differential functions) [Missen *et al.*, 1999]. This approach is called *systematic approach*. Contrary to CFD approaches, where a full description of the phenomena occurring in reactors is sought, systematic networks only consider inputs and outputs of each and every ideal reactor in the network. It can therefore be qualified as mesoscopic, while CFD is a microscopic approach.
Ideal reactors considered in this study are Plug Flow Reactors (PFRs) and Continuous Stirred Tank Reactors (CSTRs). A systematic network may comprise bypass flows, recycling loops or parallel streams. Characteristic concentration profiles for single-phase PFRs and CSTRs are summarised in figures **2** and **3**, respectively.

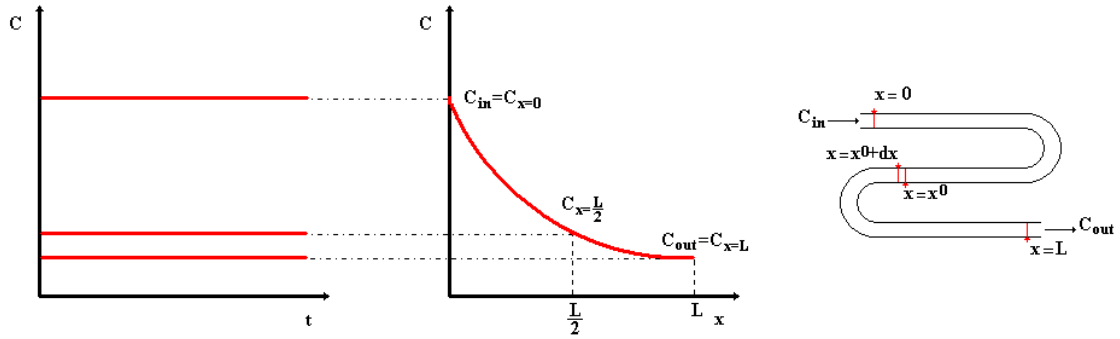

Figure 2 **Characteristic concentration profiles for a PFR; schematic of a PFR**

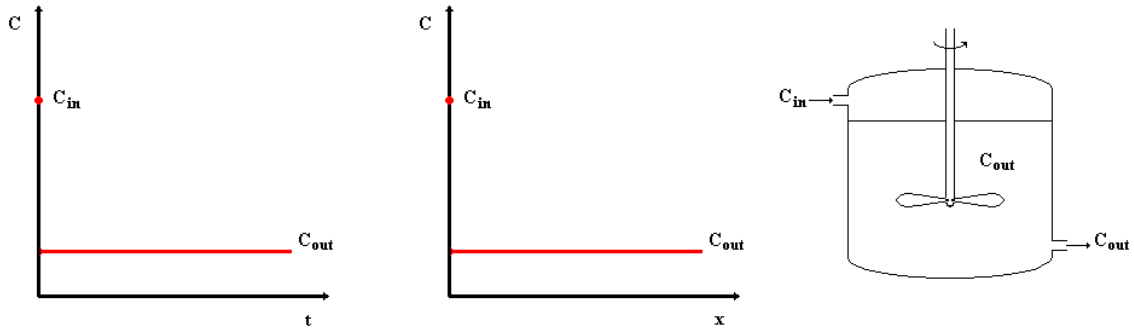

Figure 3 **Characteristic concentration profiles for a CSTR; schematic of a CSTR**

Reactors operate under steady-state conditions. PFRs show spatial dependency, whereas concentration is assumed to be uniform and equal to the outlet concentration over the whole reactor in a CSTR (see figure **3**). Mass balances are achieved over an element of volume for the PFR (for example, between x^0 and x^0+dx, see figure **2**) and over the whole reactor for a CSTR (see paragraph **2.3.2.3.**).

Systematic networks are widely used when modelling industrial processes. In the research field of ozonation, they may be used in a very simple fashion as in [Roustan *et al.*, 1998] – simple CSTR, or may be arranged to form new models, as the Back-Flow Cell Model, sometimes used for modelling bubble columns [Smith and Zhou, 1994].

Although reproducing satisfactorily the flow dispersion inside the contactor, a systematic network provides less information than CFD regarding the flow pattern. Considering hydraulics, [Dumeau de Traversay, 2000] proposed a procedure to build up systematic networks from results obtained by CFD analysis. Recently, [Mizuno *et al.*, 2004] used such an approach to model an industrial ozonation unit. In comparison to CFD, calculations (mass balances) require much less computational time and memory with a systematic approach.

2.3.2. Modelling Ideal Reactors

2.3.2.1. Chemical Kinetics

Simple Reaction Rate

For a given chemical species *X*, the reaction rate r^X is defined as the number of mole of *X* consumed or produced per unit volume and unit time. Reaction rates can thus either be positive or negative: a positive rate means the concentration is increasing with time, *i.e.* for a product; a negative rate means the concentration is falling with time, *i.e.* for a reagent. Defining an overall reaction rate, one should avoid such discrepancies considering one or another species engaged in a reaction. Therefore, the overall rate of a reaction includes the stoichiometric coefficients ν (positive for products, negative for reagents) in its definition. Given the following example, say (equation **2**):

$$\left|\nu^{R_1}\right|R_1 + \left|\nu^{R_2}\right|R_2 \rightarrow \left|\nu^{P}\right|P \quad \textbf{(2)}$$

The reaction rate becomes actually independent of the species considered when defined as in equation **3**.

$$r = \frac{1}{\nu^{R_1}} \cdot r^{R_1} = \frac{1}{\nu^{R_2}} \cdot r^{R_2} = \frac{1}{\nu^{P}} \cdot r^{P} \quad \textbf{(3)}$$

Rate Laws

In simple cases such as those considered herein, reactions are often found to have explicit rate laws of the form (equation **4**)

$$r = k.[R_1]^{Or(R_1)}.[R_2]^{Or(R_2)} \quad \textbf{(4)}$$

For an elementary process, the coefficients in equation **4** are substituted by the stoichiometric coefficients, *i.e.* $Or(R_1) = \left|\nu^{R_1}\right|$ and $Or(R_2) = \left|\nu^{R_2}\right|$. Moreover, temperature dependence is generally expressed by the Arrhenius law (equation **5**).

$$k = k_0.\exp\left(\frac{-E_A}{RT}\right) \quad \textbf{(5)}$$

where k_0 : frequency factor (same unit as k)
E_A : energy of activation of the considered reaction (J.mol^{-1})
R : universal gas constant (J.K^{-1}.mol^{-1})
T : temperature (K)

Multiple Reaction Systems

There are usually multiple reactions proceeding simultaneously in any natural reaction system. Since mass balances are performed on specific elements involved in more than one reaction, the definitions for chemical kinetics given above should be completed. Considering the chemical species A, two collections are defined:

- $\mathcal{R}^A$ collection of reactions in which A is involved (either as reagent or as product);
- $\mathbf{ß_i}$ collection of reagents for reaction i.

Moreover, the subsequent parameters must also be introduced:

- ν_i^A stoichiometric coefficients of A for reaction i;
- $\boldsymbol{k_i}$ kinetic constant rate for reaction i.

With the previous notations, the reaction rate relative to A can be expressed as follows (equation **6**). For a CSTR, concentrations considered in this equation are those found within the reactor, also equal to outlet concentrations, due to the assumption of homogeneity. The reactions were considered as elementary processes.

$$r^A = \sum_{i \in \mathcal{R}^A} \nu_i^A k_i \prod_{j \in ß_i} [j]^{\left|\nu_i^j\right|} \quad \textbf{(6)}$$

2.3.2.2. Mass Transfer

Various theories have been asserted in order to model mass transfer: Lewis and Whitman, Higbie, Danckwerts, Torr and Marchello etc… [Kraume, 2004]. We shall solely present here the equation for the two-film theory of Lewis and Whitman [Whitman, 1923]. Although it does not closely reproduce the conditions in most practical equipment, the theory gives

expressions which can be applied to experimental data which are generally available, and for that reason it is still extensively used [Coulson and Richardson, 1999].
The two-film model considers two stagnant layers between the interface and the bulk of each phase, where mass transfer occurs, according to a stationary diffusion process [Whitman, 1923]. In the bulk of each phase, assumed turbulent regime conditions ensure homogeneous concentrations. Besides, thermodynamical equilibrium is reached at the interface. More complex descriptions have been developed by Higbie (1935) and later by Danckwerts (1951) assuming that, at the interface, small stagnant elements of liquid are constantly replaced, leading to a non-stationary diffusional mass transfer process. After contact time, these elements are withdrawn from the interface, mixed within the liquid bulk and replaced by fresh elements (surface renewal). While Higbie considers an equal renewal rate for each element, Danckwerts suggests an equal probability for each element to be replaced at any instant of time, independent of its age. More accurate descriptions of the mass transfer phenomena exist, yet they introduce additional parameters, which require being determined. Since ozone is sparingly soluble in water, the gas phase resistance is usually considered negligible and the concentration gradient within the liquid phase film controls the ozone mass transfer rate towards the bulk fluid [Langlais *et al.*, 1991]. Thus, the interfacial transfer of ozone between gas and water can be modelled following equation **7**.

$$\Phi^{[O_3]} = k_L \cdot a\left([O_3]_l^* - [O_3]_l\right) \cdot dV \qquad \textbf{(7)}$$

where
$\Phi^{[O_3]}$: volumetric molar flow rate of ozone at the interface (mol.s^{-1}.m^{-3})
k_L : liquid phase mass transfer coefficient (m.s^{-1})
a : volumetric interfacial area (m^2.m^{-3} =m^{-1})
$[O_3]_l$: liquid phase ozone concentration in the bulk (mol.m^{-3})
$[O_3]_l^*$: liquid phase ozone equilibrium concentration (mol.m^{-3}) related to the local gas phase ozone concentration
dV : elemental volume considered (m^3)

Very fast reactions may accelerate the mass transfer by affecting the concentration profile within the laminar stagnant liquid layer. An enhancement factor E is then introduced, yielding the equation **8**. This type of modelling is frequently used; especially in catalytic systems such as advanced oxidation processes (see *e.g.* [Biard *et al.*, 2009]).

$$\Phi^{[O_3]} = E.k_L \cdot a\left([O_3]_l^* - [O_3]_l\right) \cdot dV \qquad \textbf{(8)}$$

More detailed information about the enhancement factor can be found in [Coulson and Richardson, 1999].

■ The liquid phase mass transfer coefficient of ozone k_L can be determined by batch-scale experiments or estimated using some empirical equations proposed by Higbie (1935), Van Hughmark (1967), or Calderbank (1959). The value of volumetric interfacial area a can be evaluated under the assumption that ozone is dispersed in the gaseous phase in form of identical spherical bubbles. Usually, this assumption does not hold, so the specific interfacial area a is not very accurately determined. Large differences are thus often observed when comparing correlations developed for bubble columns and those suggested for single bubbles [Biń and Roustan, 2000]. To tackle such discrepancies, most authors suggest evaluating directly the product k_La, which does not involve the representative bubble diameter and/or bubble rise velocity. This type of correlation is valid for particular types of

reactors (generally for bubble columns) and requires knowledge of the column diameter, gas superficial velocity and some fluid parameters. Gas disperser manufacturers may also provide similar correlations. [Hikita *et al.*, 1981] proposed a rather intricate relationship to evaluate k_La, but we shall present a simpler approach, valid for bubble columns, which consists in linking k_La directly to the superficial gas velocity according to equation **9**.

$$k_L a = C_1 . u_{SG}^{\ C_2} \tag{9}$$

With k_La : transfer coefficient (s^{-1})
u_{SG} : superficial gas velocity ($m.s^{-1}$)
C_1, C_2 : dimensionless constants (-)

V_{SG} has prior to be calculated as follows (equation **10**):

$$u_{SG} = \frac{Q_g}{S} \tag{10}$$

With S : cross section of the reactor (m^2)
Q_g : gaseous ozone flow ($m^3.s^{-1}$)

Reviewing previous works, [Langlais *et al.*, 1991] give following values for parameters C_1 and C_2 at three different temperatures (table **2**). The values for C_1 have been recalculated to be compatible with the units given in equation **9**.

Table 2 **Values for C_1 and C_2 at different temperatures, adapted from [Langlais *et al.*, 1991]**

	5°C	12°C	20°C
C_1	0.191	0.779	0.066
C_2	0.82	0.95	0.54

Numerous studies have been carried out to assess the values of C_1 and C_2 (*e.g.* [Tsuno *et al.*, 1985]; [Roustan *et al.*, 1987]; [Le Sauze, 1990]; [Roustan *et al.*, 1996]). A much more pronounced dependence upon the flow conditions has notably been reported for C_1 than for C_2. Other relations for mechanically stirred reactors and packed towers are also available in the literature.

■ The aqueous concentration of ozone at the equilibrium, $[O_3]_l^*$, can be estimated using the modified Henry's law (equation **11**).

$$[O_3]_l^* = \frac{[O_3]_g}{H_C} \tag{11}$$

With $[O_3]_g$: concentration in the gas bulk
H_C : dimensionless Henry's constant

■ Empirical relations for modified Henry's constant have been developed by various researchers. A review of these relations is given in [Sander, 1999].Two relations widely used when modelling ozone mass transfer are presented below.

i. [Mariñas *et al.*, 1993] proposed, for the data reported by [Perry *et al.*, 1973] a set of two equations for H_C (equations **12** and **13**). These are quite often used when modelling ozone transfer (*e.g.* [Kim *et al.*, 2002]; [Zhang, 2006]).

$$\log(H_C) = \begin{cases} 3.25 - \dfrac{840}{T} & \text{for } 278\ \text{K} \le T \le 288\ \text{K} \quad \textbf{(12)} \\ 6.20 - \dfrac{1687}{T} & \text{for } 288\ \text{K} < T \le 303\ \text{K} \quad \textbf{(13)} \end{cases}$$

ii. Other authors use instead the relation **14**, available in [Langlais *et al.*, 1991] (in this equation, *He* has another unit: atm/ozone molar fraction).

$$\ln(He) = 22.3 - \frac{4030}{T} \quad \textbf{(14)}$$

Based on the relations reported in [Sander, 1999] with addition of the two previously presented expressions for H_c (after conversion of *He*), a graphical comparison of the different temperature dependencies proposed by several authors is given in figure **4**.

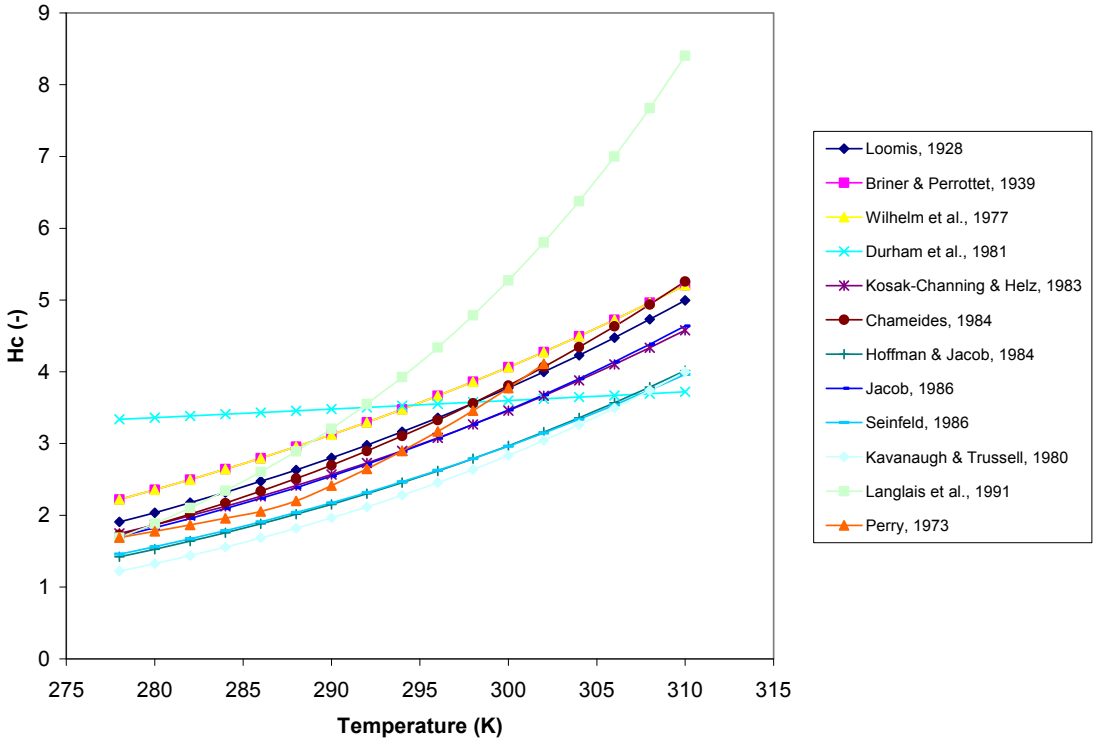

Figure 4 **Temperature dependency for Henry's dimensionless constant**

One can see a global agreement between authors, even for relatively old studies. However, the relation reported in [Langlais *et al.*, 1991] gives very high values for temperatures above 295 K which tend to underestimate ozone solubility in water. It is also worth considering the gap between the values reported: the ratio of the largest to the smallest value is always greater than 1.5. This difference underlines the experimental difficulty for the determination of Henry's constants.

2.3.2.3. Mass Balances

The mass that enters a system must (conservation of mass principle) either leave the system or accumulate within the system (equation **15**).

$$\text{IN} = \text{OUT} + \text{ACC} \quad \textbf{(15)}$$

where IN denotes what enters the system, OUT denotes what leaves the system and ACC denotes accumulation within the system (which may be negative or positive). Mass balances are often developed for total mass crossing the boundaries of a system, but they can also focus on one element (*e.g.* carbon) or chemical compound (*e.g.* water) as in our case. When mass balances are written for specific compounds, a production term (PROD) is introduced such that equation **15** becomes equation **16**. The term PROD describes the production or consumption due to chemical reactions and/or, when considering a given phase, mass transfer (see **2.3.2.1.** and following). It can either be positive or negative, depending on the type of species (*i.e.* product or reagent) and/or on the concentration gradients.

$$\text{IN} + \text{PROD} = \text{OUT} + \text{ACC} \qquad \textbf{(16)}$$

Analytical expressions for mass balance can only be written for isotropic volumes, *i.e.* where all quantities (concentrations, temperature, pressure …) are constant. Mass balances can thus either be integral, if the whole reactor volume is isotropic like for CSTRs, or differential if only elemental volume fractions of the reactor obey isotropy like for PFRs.

CSTR model

Main property of CSTRs is the chemical isotropy of the whole reactor, which implies constant concentrations. Figure **5** depicts a two-phase CSTR with its parameters, considering a single chemical species termed *A*.

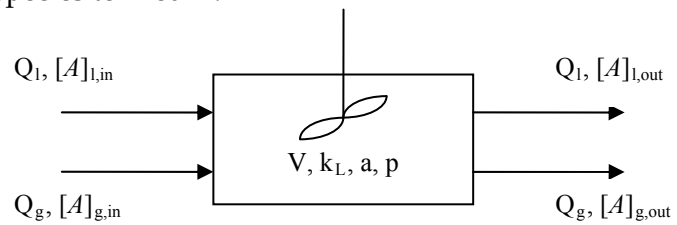

Legend: Respectively,
Q stands for volumetric flowrate
The indexes g and l stand for gaseous and liquid phases
in and out stand for inlet and outlet
p stands for the pressure within the reactor
V stands for the volume of the reactor

Figure 5 Schematic of a two-phase CSTR with its parameters

Consequently, the mass balances for the reactor are expressed in equations **17** and **18**, for liquid and gas phases respectively (no reaction occurs in the gas phase). For single-phase CSTRs, the transfer term simply drops out.

$$Q_l\left([A]_{l,in} - [A]_{l,out}\right) + Vk_L a \cdot \left(\frac{[A]_{g,out}}{H_c^A} - [A]_{l,out}\right) + Vr^A = 0 \qquad \textbf{(17)}$$

$$Q_g\left([A]_{g,in} - [A]_{g,out}\right) - Vk_L a \cdot \left(\frac{[A]_{g,out}}{H_c^A} - [A]_{l,out}\right) = 0 \qquad \textbf{(18)}$$

where $H_c{}^A$: Henry's constant for the compound *A*

Single-phase PFR model

A schematic of a PFR is given in figure **6**. Here, isotropy is guaranteed only on elemental volumes, as in the fraction of the reactor comprised between x_0 and x_0+dx. Mass balance is

performed on elemental volumes, yielding the Ordinary Differential Equation system (ODE) equations **19** and **20** for the species *A*.

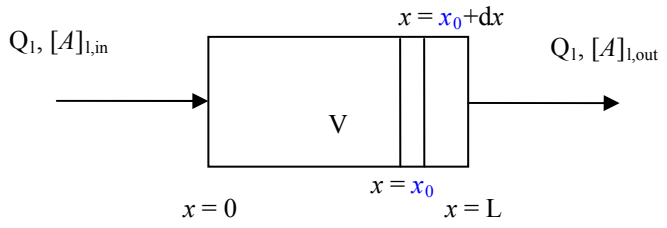

Legend: Respectively,
Q stands for volumetric flowrate
The indexes g and l stand for gaseous and liquid phases
in and out stand for inlet and outlet
L stands for the length of the PFR
V stands for the volume of the reactor

Figure 6 **Schematic of a single-phase PFR with its parameters**

$$\frac{\partial [A]_l}{\partial x} = r^A \qquad \text{for } 0 < x \leq L \qquad \textbf{(19)}$$

$$[A]_l = [A]_{l,in} \qquad \text{for } x = 0 \qquad \textbf{(20)}$$

Two-phase PFR mass balances can be setup as well, however it requires a perfectly co-current flow of both phases in the modelled reactor. This situation is not often encountered experimentally, except in some static mixer contact units. When needed, the PFR models, single or two-phase, can be approximated by CSTRs: an infinite number of infinitively small CSTRs operating in series is equivalent to a PFR. In practice, one takes a sufficiently high number of sufficiently small CSTRs (see *e.g.* [Smeets *et al.*, 2006]).
Solving the mass balances presented in this paragraph can be achieved by available algorithms. However, the solving method should be chosen paying attention to three main difficulties:

- Non-linearity: kinetic rates are expressed as power laws, and subsequently, reaction terms are highly non-linear.
- Large systems: usually, the size of the systems is moderate (30 variables to solve), but it can turn to an intricate problem when a large CSTR is to be solved (troubles for initialising the solution) or when the size of the system increases. This is the case when the CSTRs placed in a counter-current cascade, have to be solved simultaneously or when considering a recycling loop; the number of variables is then multiplied by the number of reactors.
- *Stiff* problems: variables may have very different evolutions in terms of characteristic times. This discrepancy can cause the problem to exhibit a *stiff* character.

2.3.3. Constructing A Systematic Network

Commonly used in chemical engineering, systematic representations should be regarded as integrated forms of the flow field. Besides, local turbulent areas should be modelled as such and placed accordingly in the systematic network.
Given that an adjustment method based only on RTD results cannot guarantee uniqueness of the calibration, additional information has to be introduced to reduce the degree of freedom.

This can be achieved through the use of CFD, which gives a better insight of the hydraulic behaviours. With an analysis of the velocity fields, turbulence zones are better located, and CSTRs are placed accordingly. Taking an example, the velocity field for the first chambers of an industrial ozonation tank is reproduced in figure **7**. Arrows are underlining the main streams in the water flow. They clearly show how water particles actually may have very different residence times: a major part of the stream follows the baffles, while another is stagnating in dead zones or in recycling loops. Such piece of information is important to design systematic networks: typically, recycling zones correspond to large CSTRs, while laminar direct flows may be accurately represented by PFRs.

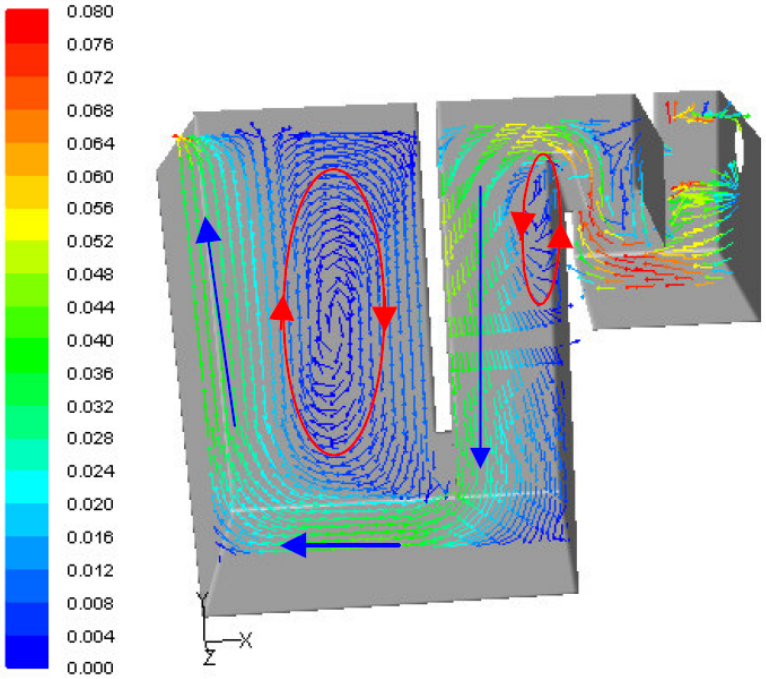

Figure 7 **Velocity field for the first chambers of an industrial ozonation tank**

Additionally, the placement of ideal reactors can be determined by analysing the turbulent kinetic energy distribution [Dumeau de Traversay *et al.*, 2001a] in order to better locate the back-mixing zones and to estimate the direct flow and recycling flow volumes with respect to the incoming flow rate. In simple cases, this calibration step is skipped.

As illustration, we give in the following some results of a study on the hydraulics of an ozone contactor of Neuilly-sur-Marne water works [Dumeau de Traversay *et al.*, 2001b]. The contactor consisted of three main chambers (circa 400 m^3 each) and was operated at a flowrate of approximately 8300 $m^3.h^{-1}$. Hydraulic retention time was approximately 8 minutes.
CFD study was performed using the commercial FLUENT™ package. 3D calculations yielded three main pieces of information: RTDs, velocity fields and turbulent kinetic energy distributions. Characteristic times of the numerical RTDs were compared to experimental values obtained beforehand with on-site tracer tests. These results, local flowrates and turbulent areas, were then used to build the 2D systematic network.
We give in figure **8** the flow pattern (turbulent kinetic energy distribution) obtained numerically with FLUENT™. The ideal reactors forming the systematic network are placed accordingly on the pattern. One can note the presence of recycling loops and the modification of the nature of the reactors according to the velocity field of water. High

turbulent kinetic energy zones, corresponding to CSTRs, are located at the inlet of the narrow baffles, while PFRs correspond to less turbulent flows (typically within the baffles). Figure **9** shows the RTD functions (see definition in Appendix **B**) obtained with CFD and systematic approach for the contactor considered by [Dumeau de Traversay *et al.*, 2001b]. The different RTDs corresponding to successive sampling points are compared (see figure **8** for location in the unit). A good agreement is observed between the two models. RTD curves calculated at different locations are used to define more precisely the systematic scheme by calibrating each volume fraction comprised between two sampling points individually.

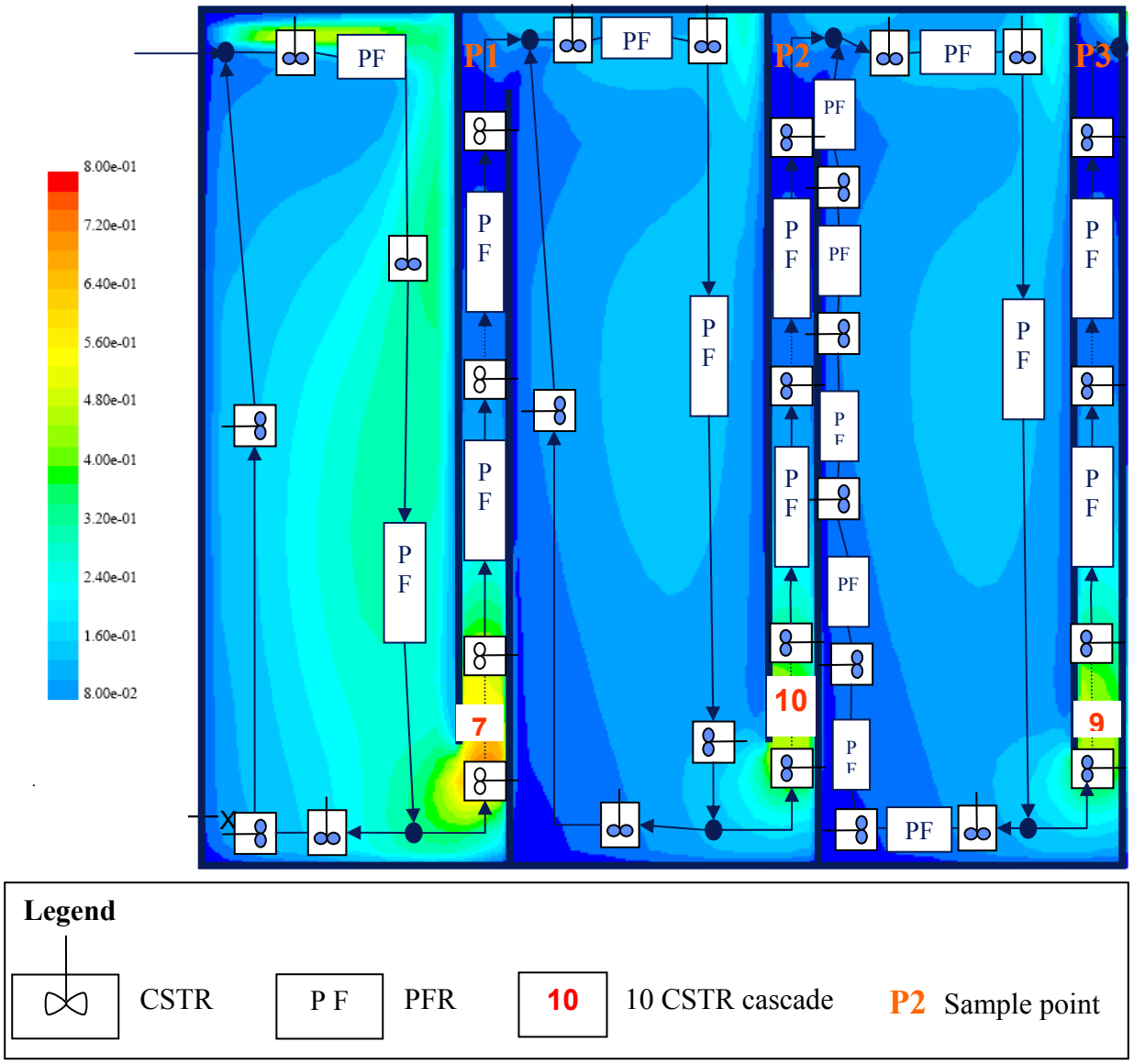

Figure 8 CFD flow pattern (turbulent kinetic energy distribution) and systematic network associated

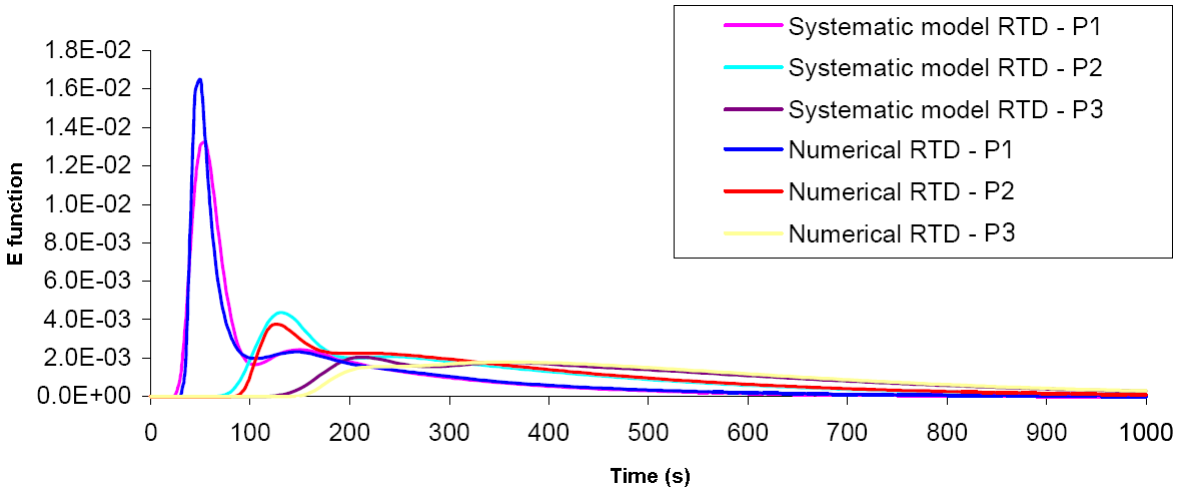

Figure 9 RTD functions obtained with Fluent simulation and the corresponding systematic network, adapted from [Dumeau de Traversay *et al.*, 2001b]

2.3.4. Defining A Chemical Description

Chemical transformations are represented by several sets of chemical equations associated with mixed order kinetic rate models and Arrhenius-type temperature dependences. Each set corresponds to a consistent group of reactions forming a part of the chemical description: for example one set for the ozone self-decomposition mechanism, one for the reactions implying carbone-containing mineral entities (ions, radicals …), one for the reactions of bromate formation, one per identified micropollutant, etc… One special set handles the inactivation of bacteria or *oocysts* with reaction-like equations. The selection of reactions is based on the conclusions of chapter **1**.

Figure 10 Example of a reaction set for a consistent chemical description [Mandel *et al.*, 2008]

In figure **10**, we present an example of a consistent chemical description with 3 identified groups: the core reactions, the interactions with the NOM (instantaneous ozone demand, ozone consumption, promotion and scavenging of radicals), and the targets (*i.e.* bromate, micropollutant, inactivation).

2.4. Already existing software products

2.4.1. Generalities

In this section, we review some of the tools available for simulation of similar problems arising in the Chemical Engineering field. From one section to another, we shall progressively focus on a simulation system specifically adapted to our calculation needs.
In a first section, a selection of Computer-Aided Engineering (CAE) software products will be presented. CAE systems have increasingly been used in numerous scientific and research fields, but we will concentrate on tools used in Chemical Engineering. We shall give details for three products, different in their design, before giving a summary of the CAE software solutions reviewed. In a second section, potable water treatment simulators will be reviewed. Again, details will be given for two specified products, before establishing a more general summary of the simulators that can be found on the market. In a last section, the chosen simulation engine, SimOx, with which all subsequent simulation work has been carried out, will be presented.

2.4.2. CAE software Systems

2.4.2.1. ASCEND

ASCEND is a free, open source, mathematical modelling system developed at Carnegie Mellon University since the late 1980s. ASCEND is a system for solving systems of equations, aimed at engineers and scientists. It allows the user to build up complex models as systems constructed from simpler sub-models. This product has been interfaced, but some issues are still under development (implementation of the derivatives in equations) [ASCEND's Wiki].
The program can solve sets of linear and non-linear equations. The Livermore Solver for Ordinary Differential Equations (LSODE) package has been attached to ASCEND and, hence, the program supports the solution of various initial value problem types. Lastly, the developer group from Carnegie Mellon University has also developed collocation methods allowing one to solve two points boundary value problems [K. K. Chittur's homepage].
Developing the environment proposed by [Piela *et al.*, 1991], the different types of solver available in ASCEND include:

- **LA,** linear algebraic solvers:
$$Ax - b = 0 \quad \textbf{(21)}$$
- **NLA,** non-linear algebraic solvers:
$$\begin{cases} f(x) = 0 \\ a \le x \le b \end{cases} \quad \textbf{(22)}$$
- **ODE,** ordinary differential equation solvers:
$$\frac{\partial x}{\partial t} = f(x,t) \quad \textbf{(23)}$$
- **DAE,** differential-algebraic equation solvers:
$$f(x,x',t) = 0 \quad \textbf{(24)}$$
- **NLP,** non-linear programming solvers (optimisation).

ASCEND is currently being used by numerous researchers [ASCEND developers collaboration project]. Its versatile and evolutionary features are often cited as its main advantages. Using ASCEND to model a two-phase physicochemical system (as ozonation

units) is possible since a toolbox handling mass transfer problems has been added by Krishnan Chittur [K. K. Chittur's homepage].
As described in **2.3.2.3.**, the systems of equations to be solved in the case of ozonation processes can exhibit a *stiff* character. Using the LSODE package, which contains the Gear method, ASCEND is able to handle this type of problem. It is likely that the integration code DOPRI5, which is currently being connected with ASCEND, will therefore not represent an improvement.

2.4.2.2. COMSOL Multiphysics®

COMSOL Multiphysics® is a commercial finite element analysis, solver and simulation software package for various physics and engineering applications, especially coupled phenomena, or multiphysics. It has therefore been extensively used in CFD studies, where fluid flow, transport of mass and energy, and chemical reactions are coupled.
Classical reactors, filtration and separation units, heat exchangers, and other equipment common in the chemical industry are available in the software's library. The development environment therefore proposes complementary add-ons for the following topics [COMSOL's Website]: Chemical Reaction Engineering, Fluid Mechanics (CFD), Mass Transfer, Process Modelling… For Chemical Reaction Engineering and Process Modelling, a *Reaction Engineering Lab* is available. This tool allows one to create models of reacting systems. It solves the material and energy balances, including reaction kinetics, where the composition and temperature only vary with time. As a result, ozonation units can be modelled under the COMSOL Multiphysics® environment (see **2.2.2.1.**).
Numerous research papers in related chemical engineering fields done with COMSOL can be found in the literature. We shall only present the work of [Shao, 2007]. Studying the treatment of specific Endocrine Disrupting Chemicals (EDCs) with UV/H_2O_2 technology on Shanghai water, Shao has followed a two-step approach: experimental kinetic analysis; modelling with COMSOL.
The first phase showed that the target EDC degradation process fits with pseudo first order equation for UV-dose and H_2O_2-dose. The second phase consisted in modelling a UV reactor through CFD in order to improve the reactor design. A 2D flow model incorporating the phenomena related to UV physics (UV irradiation, UV dose) was implemented to simulate UV distribution dose.
Combining the results obtained by CFD for UV measurements and the pseudo first order degradation mechanism for the target EDC, it was possible to link both steps and to assess the reactor efficiency in regards to micropollutant removal. However, a complete degradation modelling through the adding of a specific chemical pathway has not been done. This study is proposed as prospect but will remain an uneasy task, especially due to the time-consuming calculation.
As explained in **2.2.5.**, it still remains difficult to add chemical reaction kinetics to a CFD approach (see *e.g.* [Hofman *et al.*, 2007]). This difficulty explains why finite elements software strategies, particularly efficient for fluid dynamics calculation are avoided when modelling complex chemical problems with multiple pathways.

2.4.2.3. ChemCAD

ChemCAD is an other popular process simulation software product with highlights on designing and rating chemical processes. ChemCAD has been conceived as a suite with special applications for steady-state and dynamical processes. Focus has been put on three particular processes: batch distillation column, heat exchangers and piping networks.
As illustrated by the study of [Gál & Lakatos, 2008], ChemCAD is able to handle complex chemical processes where a large amount of chemical reactions are considered, the kinetic constant rates of which are extremely different. ChemCAD was thus used by the authors to

simulate hydrocarbon pyrolysis, a process where most reactions involve radical species, while some of them are purely molecular. Dealing with this type of problem, ChemCAD has proven its capability to treat chemical problems where phenomena have extremely different time scales. The systematic network considered by [Gál & Lakatos, 2008] remained nevertheless rather simple: a single PFR was considered. The question whether ChemCAD can easily handle the simulation complexity of an ozonation process remains open.

2.4.2.4. Summary

Incorporating other reviewed process simulation software systems, the comparison of their capabilities is summarised in table **3**. The comparison criteria were selected in regards to the specificity of ozonation unit modelling. It was not possible to find information matching the grey cells.

Table 3 Main characteristics of the process simulators reviewed

CAE system	Can handle: stiff problems	Can handle: 2-phase mass transfer	Can handle: large chemical problems	Suitable for commercial use	Interfaced	License (€)	Highlight	Drawback
Ansys products	N	Y	N	Y	+	12000	CFD	Not adapted
Ascend	N	Y	Y	N	-		Dynamical problems	No commercial use
Aspen Hysys	Y	Y	Y	Y		15000		expensive
ChemCAD	Y	Y	Y	Y	+	13000		expensive
COMSOL	N	Y	N	Y	++	15000 + 3000/yr	CFD	Expensive-Not adapted
ProSimPlus2		Y	Y	Y	+	3500/yr	Design, troubleshooting	Not customable enough

2.4.3. Water Treatment Software Systems

2.4.3.1. OTTER

OTTER is a commercial process tool developed by WRc PLC (Swindon, UK), designed to dynamically simulate the performances of potable water treatment works. The OTTER software contains models of most common potable water treatment processes that can be linked together via a Graphical User Interface (GUI) to form a model of the whole treatment works. Hence, the user may simulate individual treatment processes or a complete treatment plant.

Typical uses of the software include operational decision support, works optimisation, plant design and operator training. The GUI enables the user to rapidly design a plant flowsheet, to capture the initial values for the variables and to run simulations, generating results for each stream and process. Version 2 of the OTTER package includes [Dudley and Dillon, 2005]:

- Chemical floc formation and pH adjustment
- Clarification (floc blanket clarifiers, dissolved air flotation, sedimentation tanks, lamella settlers)
- Rapid gravity filtration
- Granular activated carbon adsorption
- Ozonation

- Disinfection
- Sludge treatment

Concerning ozonation, the software was designed to determine by-products concentrations (bromate ions) and to model pesticide oxidation. Each compartment is modelled by a PFR reactor for the water and a series of CSTRs for the gas co-current or counter-current (no backmixing). Ozone decomposition is modelled by a pseudo-first order kinetic law, the kinetic constant value being determined by an empirical law, as those presented in chapter **1** (equation **3** or **4**). Bromate formation is also empirically determined by empirical laws (similar to equation **5** in chapter **1**). Chemical species A – and especially micropollutants – which are degraded by ozone are modelled according to equation **25** [WRc plc, 2002].

$$r^A = -C_1^A.[A]^{C_2^A}.[O_3] \quad \textbf{(25)}$$

Since a range of different disinfectants is modelled in OTTER – including chlorine, chloramine, chlorine dioxide and ozone – the software could also be used to assess strategies for the reduction of by-products (*e.g.* using alternative disinfectants, performing enhanced precursor removal…).

2.4.3.2. Stimela

As OTTER, **Stimela** is a PC-based simulation package that enables the user to model at different scales: from the individual unit to the whole treatment works. Besides, the simulator is available on the web: http://www.stimela.com.

Its application field is very close to OTTER's: management and design of water treatment works, analysis and research, operator and students training [van der Helm and Rietveld, 2002]. The user has also the possibility to build the installation he/she wishes to simulate on a flowsheet (see figure **11**). Fields in dialog boxes have then to be filled with the values of the physicochemical parameters (including all the initial state concentrations).

Considering a whole treatment train, Stimela can predict concentration profiles for dissolved compounds such as gases (CH_4, CO_2, O_2, O_3), inorganic compounds (HCO_3^-, NH_4^+, CO_3^{2-}, Ca^{2+}) and organic compounds (DOC, organic micropollutants, AOC) and other indicators (UV_{254}…). In addition, floc removal is modelled by filtration [Dudley and Dillon, 2005].

The Stimela-package models several processes:

- Aeration (cascades, towers, plates, sprayers)
- Filtration (single layer, double layer, continuous, biological)
- Granular activated carbon filtration
- Softening and conditioning
- Ozonation (bubble column and contact chambers)
- Flocculation

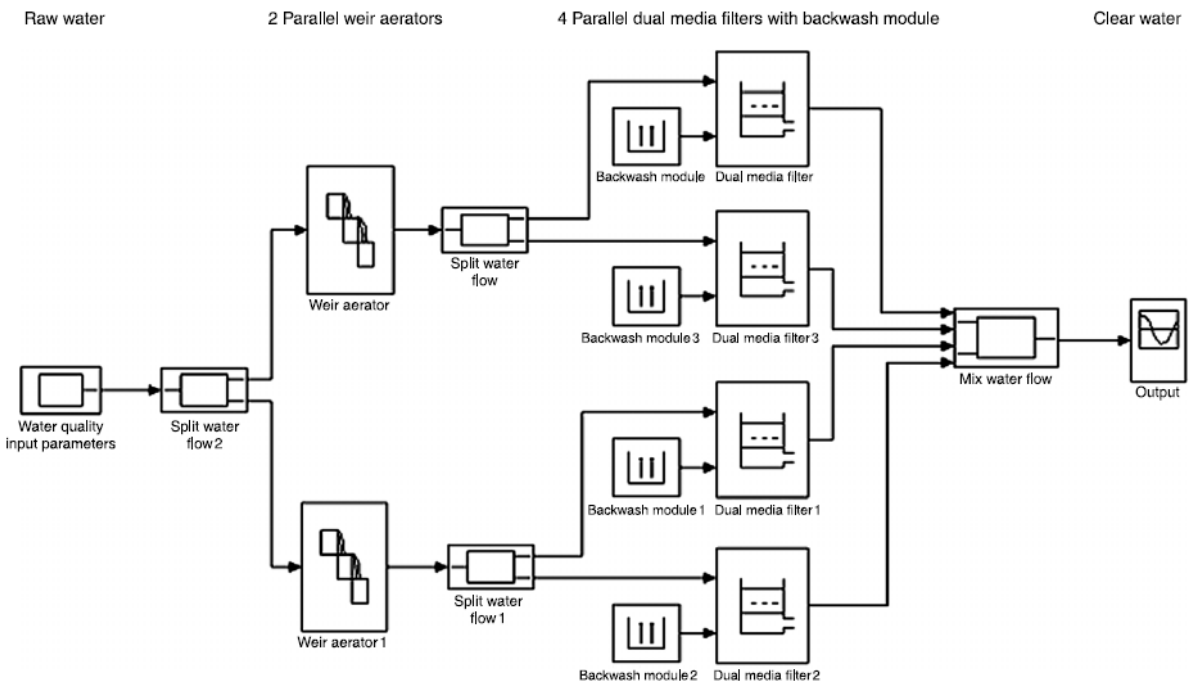

Figure 11 Example of a treatment train visualised in the Stimela environment [Dudley *et al.*, 2008]

The modelling of ozonation units lays on an empirical description of the phenomena occurring during the process. For ozone decomposition, a classical two-step approach is implemented as in [Rietveld, 2005]: the instantaneous ozone demand being correlated to the UV (254 nm) measurement; the slow ozone decay being modelled by a pseudo-first order kinetics law. This implies to feed the model with on-line measurements of UV absorbance. The equations can be found in [Rietveld *et al.*, 2009] for the ozone decomposition, and in [van der Helm, 2007] for the formation of bromate ions. More details are given in Appendix **C**.

2.4.3.3. Summary

Existing water treatment plant simulators, whether it be for potable water or wastewater propose similar functionalities: design, process optimisation, operator training, educational purposes, automation. Some of them, such as GPS-X (wastewater treatment simulator developed by Hydromantis), include additionally cost savings investigation modes.

Furthermore, the simulators are similar in their use. The interface allows ones to build up his/her own model and to run the simulation, having specified certain characteristics (regarding the water, the processes etc…). Table **4** gives an overview of the most common simulators currently available.

Contrary to SimOx, all the simulators present in the table **4** are not process-specific. They all aim at simulating a whole water treatment works, for potable water or wastewater. This is why, even though focusing on disinfection, secondary objectives (DBPs for instance) are handled by correlations and simplified reaction models. In particular, these simulators do not consider radical species. Their use has consequently given evidence of the lack of precision in their predictions for oxidation processes [Dudley and Dillon, 2005].

As it appears in table **4**, the main drawback of common simulators lies in their poor adaptability to specific on-site conditions. When adaptable, the simulators require a very long calibration period. This is mainly imputable to the choice of basing the models on correlations or empirical relations, the role of which is not to be physically valid but to fit simulation results to experimental data. Obviously, one cannot simply eliminate such

correlations (for instance, see chapter **1, 1.5.** (NOM)), but our efforts will have to be directed towards reducing their number.

Table 4 Comparison of water treatment works simulators

Name	Developed by	Use	Highlights/ Strenghts	Drawbacks/ Weaknesses	Chemical models
OTTER	WRc	Potable water	Readily extensible by users familiar with FORTRAN/C/C++	Excessive data needs	Semi-empirical relations
Stimela	TU Delft	Potable water	Online access	Basic oxidation models	Semi-empirical relations
Metrex	University of Duisburg	Potable water	Particle removal	Not tested on site	Mechanistic + correlations
Watpro	Hydromantis	Potable water	Disinfection-DBPs	Long calibration time: 1 year of data	USEPA correlations
WTPmodel	USEPA	Potable water	Removal of NOM-DBPs	Limited validity domain	Empirical relations
BioWin	Envirosim	Wastewater	Activated sludge	No oxidation module	ASM (IWA)
WEST	Hemmis	Wastewater	Editing model mode	Simplistic oxidation models	ASM (IWA)

Additionally, the over-mentioned simulators only offer limited possibilities regarding hydrodynamic modelling. In fact, the single way to tailor an already designed reactor to represent more adequately a real process is often to change the number of CSTRs. Such representation appears at first sight to be insufficient, however, this shall be under discussion and we should investigate the impact of the hydraulic representation (as a systematic model) so as to assess how refined hydraulic models should be.

2.4.4. SimOx

2.4.4.1. Generalities

Used as prototype on a study on chlorination by-products [Mahé *et al.*, 2000], this software was originally proposed by [Savary, 2002] in her thesis. Inspired directly by the works of [Dumeau de Traversay, 2000] regarding the hydrodynamic modelling through systematic approach, she developed a new chemical pathway of reactions for the role of NOM during ozonation and implemented it in a simulator: $SimO_3$. The name was changed to **SimOx** when the development of the GUI was launched.

Its inner structure makes it easy to adapt to various situations. Indeed, the chemical reactions can be entered (without any restriction concerning reactants or the reaction number), as well as the hydrodynamics, that can be coded in form of a systematic network. SimOx was developed using the FORTRAN 77 programming language. A more detailed presentation of the history and the principles of SimOx is given in [Mandel *et al.*, 2008].

2.4.4.2. Hydraulic Aspects

Preliminary to its use on a specific site, a systematic network has to be set up. This is done calibrating the network in comparison to RTD curves and/or numerical experiments done with CFD (using Fluent for instance; see **2.3.3.**). The systematic representation may include by-passes or recycling flows and is composed of single-phase CSTRs, two-phase CSTRs (co-current and counter-current) and single-phase PFRs (two-phase PFRs can be represented by cascades of CSTRs).

2.4.4.3. Kinetic Aspects

SimOx is neither specific to a particular reaction mechanism, nor to ozonation. It was designed to simulate single-phase and two-phase reactors with reactions occurring in the liquid phase and can therefore be used as well to model chlorination for instance. The chemical transformations are thus represented by several sets of chemical equations with mixed order kinetic rates and Arrhenius-type temperature dependences.

2.4.4.4. Solver Environment and Capabilities

Presented in **2.3.2.3.**, the mass balances equations for the different reactors considered for hydraulic representation are solved using classical methods gathered in table **5**. The Gear method is taken from the LSODI solver library (variant of the LSODE package). More details can be found in [Savary, 2002].

Table 5 Solving capabilities of SimOx

Reactor	Type of equation	Solving method
CSTR	NLA	Newton-Raphson, analytical Jacobian matrix
CSTR cascade	NLA	Newton-Raphson, analytical Jacobian matrix
Recycling loop	NLA	Broyden quasi-Newton, numerical initial Jacobian matrix
PFR	ODE	Gear

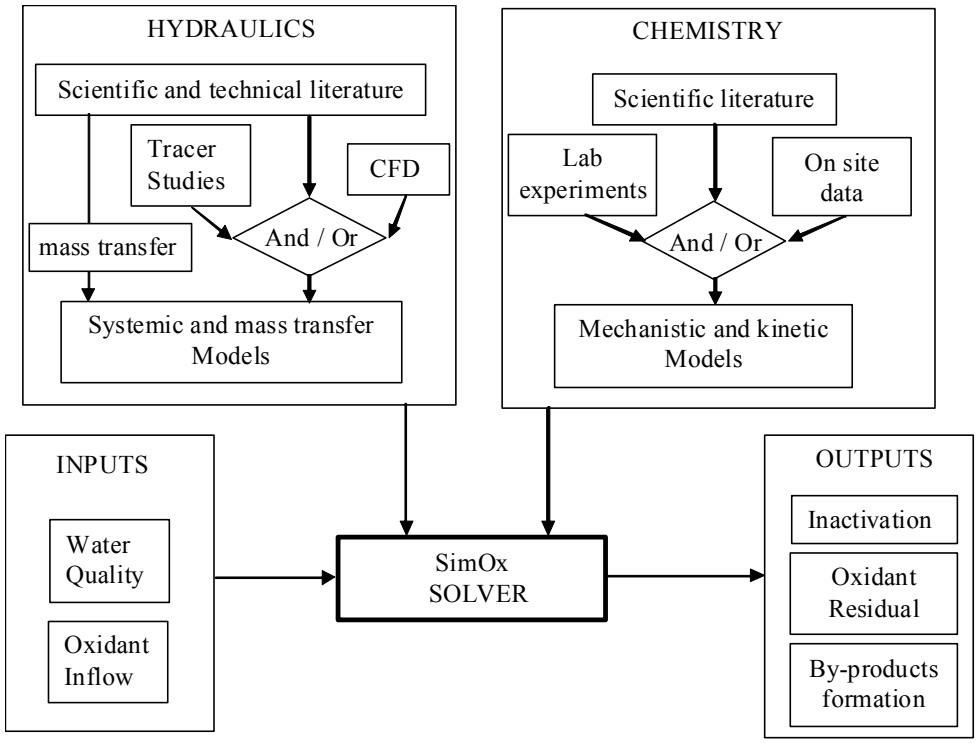

Figure 12 Solver environment

Figure **12** summarises the information flow for the definition and the solution of a problem. Numerous pieces of information can be gathered from the literature, especially concerning

the chemistry and mass transfer data; the remainder can be obtained through experiments, calculations (CFD), and possibly by exploiting existing on-site historical data collections.

2.5. Conclusion

Two major approaches in modelling have been discussed in this chapter. They derive from the main concerns of the researchers when modelling ozonation: hydraulics and chemical kinetics.
On one hand, authors focusing on hydraulics have applied very ambitious techniques based on CFD to accurately take into account the characteristics of ozonation units. Despite interesting results for assessing disinfection efficiency, the chemical models used remain basic. On the other hand, authors focusing on chemistry have either studied extensively chemical kinetics in batch reactors, or have used simplified hydraulics description when considering industrial ozonation units.

Reviewing already published studies on ozonation modelling, it appears that:

- even appealing, the use of CFD is not realistic when combined with accurate chemical models (for example for predicting ozone decomposition or bromate formation);
- systematic hydraulics representation, commonly used in many chemical engineering fields, may represent a good alternative where the global behaviour of ozonation tank is taken into account. This approach should however be tested with real industrial data.

The mass balances which shall be solved when using a systematic representation have been presented. Due to the formulation of the kinetics laws, these are highly non-linear systems of equations. In the case of recycling loops or CSTR cascades, the size can dramatically increase (up to 500 variables for a relatively complex problem). There is therefore a strong influence of the systematic network chosen over the easiness to solve the problem. Moreover, the equations may exhibit a relatively *stiff* character (coexistence of reactions with very different characteristic times). The review of currently available simulators, both generic CAE and water treatment software products, indicates that a tailored simulator would be preferable, due to the high complexity of the systems to be solved. An adjustable solver previously developed at the ENSCR is therefore chosen.

2.6. Bibliography

Articles and books

- **Bader H.** and **Hoigné J.,** (1981). Determination of Ozone in Water by the Indigo Method, *Water Research*, Vol. **15**, pp. 449-456.
- **Bartrand T. A.,** (2007). High resolution experimental studies and numerical analysis of fine bubble ozone disinfection contactors, Ph.D. thesis, Drexel University, U.S.A.
- **Biard P.-F., Couvert A., Renner C., Levasseur J.-P.,** (2009). Assessment and optimisation of VOC mass transfer enhancement by advanced oxidation process in a compact wet scrubber, *Chemosphere*, Vol. **77**, pp. 182-187.
- **Biń A. K.** and **Roustan M.,** (2000). Mass transfer in ozone reactors, *Proceedings of the IOA international specialised symposium on Fundamental and engineering concepts for ozone reactor design*, Toulouse, March 1-3, pp. 99-131.
- **Bittker D. A.,** (1993). Mathematical description of complex chemical kinetics and application to CFD, *Computing Systems in Engineering*, Vol. **4**, pp. 1-12.
- **Bolaños E. Q., Ocampo J. T., Rodríguez L. C.,** (2008). Applicability of computational fluid dynamics to simulate ozonation processes, *Ingeniería y Desarrollo*, Vol. **24**, pp. 97-116.
- **Buffle M.-O.**, (2005). Mechanistic Investigation of the Initial Phase of Ozone Decomposition in Drinking Water and Wastewater, Ph. D. thesis, Swiss Federal Institute of Technology Zürich, Switzerland.
- **Bühler R.E., Staehelin J., Hoigné J.**, (1984). Ozone Decomposition in Water Studied by Pulse Radiolysis. 1. HO_2 / O_2^- and HO_3 / O_3^- as Intermediates, *Journal of Physical Chemistry*, Vol. **88**, pp. 2560-2564.
- **Chick H.,** (1908). An investigation of the laws of disinfection, *Journal of Hygiene*, Vol. **8**, pp. 92-158.
- **Cockx A., Do-Quang Z., Liné A., Roustan M.,** (1999). Use of Computational Fluid Dynamics for Simulating Hydrodynamics and Mass Transfer in Industrial Ozonation Towers, *Chemical Engineering Science*, Vol. **54**, pp. 5085-5090.
- **Coulson J. M., Richardson J. F., Backhurst J. R., Harker J. H.,** (1999). Coulson and Richardson's Chemical Engineering, Volume **1** – Sixth Edition, *Butterworth-Heinemann,* Oxford.
- **Dong W., Wang W., Li J.,** (2007). A multiscale mass transfer model for gas–solid riser flows: Part II—Sub-grid simulation of ozone decomposition, *Chemical Engineering Science*, Vol. **63**, pp. 2811-2823.
- **Do-Quang Z.**, (1993). Etudes expérimentale et numérique des performances des contacteurs de désinfection de l'eau par le chlore, Ph.D. thesis INSA Toulouse, France.
- **Do-Quang Z., Duguet J-P., Roustan M., Lainé J-M,** (1996). Study of full scale reactor performance for drinking water advanced oxidation treatment, *Proceedings of the IOA Regional Conference*, Amsterdam, 24-26 September, pp. 237-250.
- **Do-Quang, Z., Cockx, A., Liné, A., Roustan, M.,** (1999). Computational fluid dynamics applied to water and wastewater treatment facility modeling, *Environmental Engineering and policy*, Vol. **1**, pp. 137-147.
- **Dudley J.** and **Dillon G.**, (2005). Water treatment simulators: state-of-the-art review, *Techneau internal note*.
- **Dudley J., Dillon G, Rietveld L.,** (2008). Water treatment simulators, *Journal of Water Supply: Research and Technology – AQUA*, Vol. **57**, pp. 13-21.
- **Dumeau de Traversay C.**, (2000). De la mécanique des fluides numérique à l'approche systémique: application aux réacteurs d'oxydation en potabilisation, Ph.D. thesis ENSC-R, France.
- **Dumeau de Traversay C.**, **Luck F.**, **Wolbert D.**, **Laplanche A.**, (2001a). Hydrodynamics of ozonation tanks: definition of systemic models from CFD, Vivendi internal note.
- **Dumeau de Traversay C., Luck F., Wolbert D., Laplanche A.,** (2001b). RTD: A useful step to define systemic models from CFD information – Application to industrial ozonation tanks for drinking water treatment, *Récents progrès en genie des procédés,* Vol. **79**, pp. 121-128.
- **Gál T.** and **Lakatos B. G.,** (2008). Re-pyrolysis of recycled hydrocarbon gas-mixtures: A simulation study, *Chemical Engineering and Processing: Process Intensification*, Vol. **47**, pp. 603-612.

- **Gélinet K.**, (1999). Importance des caractéristiques physico-chimiques des eaux naturelles sur la formation des ions bromates lors de l'ozonation, Ph.D. thesis, ESIP, France.
- **Gong X., Takagi S., Huang H., Matsumoto Y.,** (2007). A numerical study of mass transfer of ozone dissolution in bubble plumes with an Euler–Lagrange method, *Chemical Engineering Science*, Vol. **62**, pp. 1081-1093.
- **Greene D. J., Farouk B., Haas C. N.,** (2004). CFD design approach for chlorine disinfection processes, *Journal of the American Water Works Association*, Vol. **96**, pp. 138-150.
- **Gyurek L.L., Li H., Belosevic M., Finch G. R.,** (1999). Ozone inactivation kinetics of cryptosporidium in phosphate buffer, *Journal of Environmental Engineering*, Vol. **125**, pp. 913-924.
- **Haas C. N.** and **Betz L. D.,** (2009). Future Design Techniques for Chemical Disinfection, *Proceedings of the 5th Japan - U.S. Joint Conference on Drinking Water Quality Management and Wastewater Control*, Las Vegas, March 2-5.
- **Hikita H., Asai S., Tanigawa K., Segawa K., Kitao M**., (1981). The volumetric liquid-phase mass transfer coefficient in bubble columns, *Chemical Engineering Journal*, Vol. **22**, pp. 61-69.
- **Hofman J., Wind D., Wols B., UIjttewaal W., van Dijk H., Stelling G.,** (2007). The use of CFD Modeling to determine the influence of residence time distribution on the disinfection of drinking water in ozone contactors, *Proceedings of the Comsol Users Conference*, Grenoble.
- **Hoigné J.** and **Bader H.,** (1983). Rate constants of reactions of ozone with organic and inorganic compounds in water: II dissociating organic compounds, *Water Research.*, Vol. **17**, pp. 185-194.
- **Hoigné J.** and **Bader H.,** (1994). Characterization of water quality criteria for ozonation processes. Part II: Lifetime of added ozone, *Ozone: Science and Engineering,* Vol. **16**, pp. 121-134.
- **Huang T.** and **Brouckaert C.J.,** (2002). A CFD and experimental study of an ozone contactor, *Water Science and Technology*, Vol. **46**, pp. 87-93.
- **Hunt N. K.** and **Mariñas B.J.,** (1999). Inactivation of *Escherichia coli* with ozone: chemical and inactivation kinetics, *Water Research*, Vol. **33**, pp. 2633-2641.
- **Jaeger Y., Lénès D., Le Bihan M., Ponthieux A., Génin A.,** (2009). Disinfection optimization by a better control of ozonation process, *Water Science and Technology: Water Supply*, Vol. **9**, pp. 699–706.
- **Kamimura M., Furukawa S., Hirotsuji J.,** (2002). Development of a simulator for ozone/UV reactor based on CFD analysis, *Water Science and Technology*, Vol. **46**, pp. 13-19.
- **Kim J. H., Tomiak R. B., Mariñas B. J.**, (2002). Inactivation of Cryptosporidium oocysts in a pilot-scale ozone bubble-diffuser contactor. I: Model development. *Journal of Environmental Engineering-Asce*, Vol. **128**, pp. 514-521.
- **Kraume M.,** (2004). Verfahrenstechnik II, Skript zur Vorlesung, Berlin University of Technology, Germany.
- **Langlais B., Reckhow D. A., Brink D.R.,** (1991). Ozone in Water Treatment: Application and Engineering, *LEWIS Publishers*, Washington D.C., U.S.A.
- **Le Sauze N.**, (1990). Etude du transfert de l'ozone dans les colonnes à bulles. Modélisation, application au traitement des eaux potables et à la déodorisation de gaz soufrés, Ph.D. thesis, ENSC-R, France.
- **Mahé E., Wolbert D., Laplanche A.,** (2000). Simulation of disinfection and by-product formation in real reactors using the systemic approach, *Proceedings of the 1st World Water Congress of the I.W.A.*, Paris, 3-7 July.
- **Mandel P., Roche P., Bréant P., Wolbert D.**, **Balannec-Léon B.,** (2008). Modeling Ozonation and Chlorination in potable Water Treatment, *Proceedings of the IOA International Conference*, Brussels, May 15-16.
- **Mariñas B. J., Liang S., Aieta E. M.,** (1993). Modeling Hydrodynamics and Ozone Residual Distribution in a Pilot-Scale Ozone Bubble-Diffuser Contactor, *Journal of the American Water Works Association*, Vol. **85**, pp. 90-99.
- **Missen R. W., Mims C. A., Saville B. A.,** (1999). Introduction to Chemical Reaction Engineering and Kinetics, Chapter **19**, *John Wiley and Sons*, New York.
- **Mizuno T., Park N.-S., Tsuno H., Hidaka T.,** (2004). Development of the Simulation Model to Predict Dissolved Ozone Concentration for a Real Water Treatment Plant, *Environmental Engineering Research*, Vol. **41**, pp. 237-246.
- **Mizuno T., Tsuno H., Yamada H.,** (2007b). Effect of Inorganic Carbon on Ozone Self-Decomposition, *Ozone: Science and Engineering*, Vol. **29**, pp. 31-40.

- **Muñoz Ramirez G.**, (1997). Approche cinétique de la demande immédiate en ozone, Ph.D. thesis, ENSC-R, France.
- **Murrer J., Gunstaed J., Lo S.,** (1995). The development of an ozone contact tank simulation model, *Ozone: Science and Engineering*, Vol. **17**, pp. 607-617.
- **Orta de Velasquez M.T.,** (1992). Elimination des micropolluants dans les filières d'ozonation du traitement de l'eau potable, Ph.D. thesis, ENSC-R, France.
- **Perry R. H., Green D. W., Maloney J.O.**, (1973). Chemical Engineers handbook. New York, McGraw-Hill Professional, U.S.A.
- **Piela, P. C., Epperly, T. G., Westerberg, K. M., Westerberg, A. W.**, (1991). ASCEND: An Object Oriented Computer Environment for Modeling and Analysis. 1 - the Modeling Language, *Computers and Chemical Engineering*, Vol. **15**, pp. 53-72.
- **Rietveld L. C.,** (2005). Improving operation of drinking water treatment through modelling, Ph.D. thesis, Delft University of Technology, The Netherlands.
- **Rietveld L. C., van der Helm A. W. C., van Schagen K. M., van der Aa L. T. J.,** (2009). Good modelling practice in drinking water treatment, applied to Weesperkarspel plant of Waternet, *Environmental Modelling & Software , in press*, doi:10.1016/j.envsoft.2009.05.015.
- **Roustan M., Debellefontaine H., Do-Quang Z., Duguet J.-P.,** (1998). Development of a Method for the Determination of Ozone Demand of a Water, *Ozone: Science and Engineering*, Vol. **20**, pp. 513-520.
- **Roustan M., Duguet J. P., Laine J. M., Do-Quang Z., Mallevialle J.**, (1996). Bromate ion formation: impact of ozone contactor hydraulics and operating conditions, *Ozone: Science and Engineering*, Vol. **18**, pp. 87-97.
- **Roustan M., Duguet J.-P., Brette B., Brodard E., Mallevialle J.,** (1987). Mass Balance Analysis of Ozone in Conventional Bubble Contactors, *Ozone: Science and Engineering*, Vol. **9**, pp. 289-297.
- **Sander R.,** (1999). Compilation of Henry's Law Constants for Inorganic and Organic Species of Potential Importance in Environmental Chemistry, 3rd Version. Available at: http://www.mpch-mainz.mpg.de/~sander/res/henry.html
- **Savary B.**, (2002). Influence des caractéristiques d'une eau naturelle sur la formation des ions bromates au cours de l'ozonation: Observations-Prévisions-Simulations dans un réacteur diphasique du type colonne à bulles, Ph.D. thesis ENSC-R.
- **Shao L.,** (2007). Degradation of 4TBP by Advanced Oxidation Process, CFD Modeling and Validation for UV Reactor, *Master's degree thesis*, Delft University of Technology, The Netherlands.
- **Smeets P. W. M. H., van der Helm A. W. C., Dullemont Y. J., Rietveld L. C., van Dijk J. C., Medema G. J.,** (2006). Inactivation of *Escherichia coli* by ozone under bench-scale plug flow and full-scale hydraulic conditions, *Water Research*, Vol. **40**, pp. 3239-3248.
- **Smith D. W.** and **Zhou H.,** (1994). Theoretical Analysis Of Ozone Disinfection Performance In A Bubble Column, *Ozone: Science and Engineering*, Vol. **16**, pp. 429-441.
- **Stambolieva Z., Roustan M., Wable O., Duguet J. P., Mallevialle J.,** (1993). Methods for design of chlorine contactors for drinking water treatment. Kinetic and hydraulic considerations for disinfection efficiency estimation, *Proceedings of the American Water Works Association Conference*, Denver, U.S.A.
- **Trussell R. R.** and **J.-L. Chao,** (1977). Rational Design of Chlorine Contact Facilities, *Journal of the Water Pollution Control Federation*, Vol. **49**, pp. 659-667.
- **Tsuno H., Somiya I., Kume M.,** (1985). Absorption of Ozone into Water in Gas-Liquid Countercurrent Column, *Proceedings of the 7th IOA World Congress*, Tokyo, pp. 181-186.
- **van der Helm A.W.C.** and **Rietveld L.C.**, (2002).Modelling of drinking water treatment processes within the Stimela environment, *Water Science and Technology: Water supply*, Vol. **2**, pp. 87-93.
- **van der Helm A.W.C., Rietveld L.C., Baars E.T., van Dijk J.C.,** (2008). Modeling disinfection and by-product formation during the initial and the second phase of natural water ozonation in a pilot-scale plug flow reactor, *Journal of Water Supply: Research and Technology – AQUA*, Vol. **57**, pp. 435-449.
- **van der Helm, A. W. C.,** (2007). Integrated modeling of ozonation for optimization of drinking water treatment, Ph.D. thesis, Delft University of Technology, The Netherlands.
- **Versteeg H. K.** and **Malalasekera W.,** (1995). An Introduction to Computational Fluid Dynamics, The Finite Volume Method, Addison-Wesley.
- **von Gunten U.** and **Oliveras Y.,** (1998). Advanced oxidation of bromide-containing waters: bromates formation mechanisms, *Environmental Science and Technology*, Vol. **32**, pp. 63-70.

- **Whitman W.G.,** (1923), A preliminary experimental confirmation of the two-film theory of gas absorption, *Chemical and Metallurgical Engineering,* Vol. **29, pp.** 146-148.
- **Wols B. A., Hofman J. A. M. H., UIjttewaal W.S. J., Rietveld L. C., van Dijk J. C.,** (2010). Evaluation of different disinfection calculation methods using CFD, *Environmental Modelling and Software*, Vol. **25**, pp. 573-582.
- **WRC plc,** (2002). WRC OTTER 2.1.3 Process Model Descriptions, Swindon, U.K.
- **Zhang J.,** (2006). An integrated design approach for improving drinking water ozone disinfection treatment based on computational fluid dynamics, Ph.D. thesis, University of Waterloo, Canada.

Internet resources

CAE software systems

ASCEND (Last access: January 2010)

- The ASCEND project at Carnegie Mellon university: http://ascend.cheme.cmu.edu/
- ASCEND's Wiki: http://ascendwiki.cheme.cmu.edu
- ASCEND developers collaboration project: https://pse.cheme.cmu.edu/wiki/view/Ascend/AscendProject
- Krishnan K. Chittur's homepage: http://www.eng.uah.edu/~kchittur/
- ASCEND's applications for Chemical Engineering: http://www.che.uah.edu/courseware/toolbox/ascend/

COMSOL Multiphysics® (Last access: January 2010)

- COMSOL® webpage: http://www.comsol.com
- Chemical Engineering with COMSOL®: http://www.comsol.com/industry/application/chem/

ChemCAD (Last access: January 2010)

- ChemCAD webpage: http://www.chemstations.com/

Water Treatment Simulators (Last access: October 2009)

- The most comprehensive software catalogue on the web: http://www.mpassociates.gr
- WRc Website: http://www.wrcplc.co.uk
- Stimela homepage: http://www.stimela.nl
- WEST's Homepage: http://www.hemmis.com/products/west/default_west.htm
- About BioWin: http://www.envirosim.com/products/bw32/bw32intro.php
- About Watpro: http://www.hydromantis.com/software08.html

3. MODELLING APPROACH

Abstract

The previous chapters have already brought different elements of answer for the modelling approach: (i) systematic networks have been chosen in combination with accurate chemical mechanisms; (ii) the equations to be solved have been presented and characterised. Besides, two main tasks have been identified as modelling issues to deal with: (i) the solving of simulation runs; (ii) the parameter identification process, the latter comprising iterative simulations.

Presenting a generic methodology for modelling, we show how the already performed choices are included in a larger approach leading from the understanding of an industrial process to its modelling. This section introduces more generally the concepts of *system characterisation*, *model analysis*, *calibration* and *validation*. Focus is then put on model analysis, reviewing classical parameter identification techniques. Addressing the issue of parameter *identifiability*, theoretical and practical methods are presented and their respective relevancy discussed.

Additionally, several techniques (sensitivity analysis, covariance analysis) associated to the identification procedure are presented. Local and sampling-based methods for sensitivity analyses are distinguished and practical examples are given in order to elaborate an *ad-hoc* parameter identification procedure. Moreover, numerous optimisation techniques can be applied to similar identification problems. In this chapter, two choices were made, the first concerning the parameter estimation (definition of an objective function); the second concerning the optimisation algorithm used. Basic strategies for the determination of global minima are given as well, presented as complementary or preliminary steps to classical optimisation.

Having reviewed the techniques for parameter identification relevant to our needs, the main conclusions can be summarised as follows:

- theoretical identifiability will not be carried out; instead, practical identifiability techniques shall be used;
- sampling-based methods for exploring the sensitivities of the system shall be preferred. Accordingly, it appears doubtful if a covariance analysis step is needed;
- weighted least squares estimation will be considered for parameter estimation instead of Bayesian estimation techniques or maximum likelihood functions;
- classical reparametrisations will be performed on the problem to better achieve parameter identification;
- prior to optimisation using the Nelder-Mead method, a Monte-Carlo search implementing Latin Hypercube Sampling (LHS) strategy will be used for exploration.

Contents

3.1. Introduction

The previous chapters **1** and **2** have set the framework of the study and specified the modelling needs: (i) given the current understanding of chemical phenomena, chemical kinetics shall be partly calibrated (chapter **1**); (ii) given the modelling framework chosen (systematic), series of mass balances will have to be solved (chapter **2**).
These two items correspond to two different numerical problems, one being incorporated in another. The first shall be named parameter identification or, by extension, optimisation problem. The second corresponds to simulation runs, the iterative solving of which is performed as parameter estimation progresses.
The work presented herein focuses on parameter identification for chemical models, but some comments are also given on the simulation solving. Actually, both hydraulic and chemical models have to be calibrated, respectively building up a systematic scheme (chapter **2**) and determining the kinetics of specific reactions (chapter **1**). Considering a given industrial ozonation unit, only the chemical phenomena may evolve since seasonal changes are known to impact on the chemistry of water resources. As a consequence, calibration of systematic schemes was considered not relevant when focusing on a given ozonation unit and is beyond the scope of this work.

The review of the first chapters also characterises the main modelling constraints:

- Two factors may affect the solving of the mass balances: on one hand, the choice of the model describing the chemical kinetics, directly modifying the expressions for reaction rates, can increase or decrease the complexity of the equations to be solved. On the other hand, the choice of the systematic network describing the hydraulic flow conditions, modifying the number, the volumes and the connections of ideal reactors, can increase or decrease the size of the problem;
- As we shall focus in the following on chemical models, only the calibration procedure for such models shall be discussed. Therefore, only the choice of the chemical model shall influence the difficulty to identify parameters. A relevant criterion for the difficulty of the identification process will be the number of parameters to be determined, which may vary.

The objective of this chapter is to select numerical tools or strategies adapted to our modelling needs and to the parameter identification problem. Therefore, in a first section (**3.2.**), we show how the choice for the modelling frame is included in a more generic methodology leading from the understanding of an industrial process to its modelling. This section introduces more generally the concepts of *system characterisation*, *model analysis*, *calibration* and *validation*. The previous concepts are illustrated by the example of ozonation units modelling.
Focus will then be put on model analysis reviewing classical ways parameters from a chemical model may be identified. Three aspects will be discussed: (i) the feasibility of the parameter identification called parameter *identifiability* (section **3.3.**), with emphasis on practical identifiability which empirically addresses the question; (ii) the procedure for identification, detailing the steps that can be taken (also presented in section **3.3.**); (iii) and the techniques used for optimisation (in both sections **3.4.** and **3.5.**), treated as the last step in parameter identification.

3.2. Generic Modelling Methodology and Special Needs

3.2.1. Generalities

Given the very characteristics of industrial ozonation processes (physical phenomena, water chemical nature, design and operational process conditions), no unique model can be formulated yet.
When modelling, there is hence a necessary model calibration step in order to best adapt simulation outputs to measured experimental data. Following the conclusions of various research works for developing unified modelling approaches (*e.g.* [Murthy *et al.*, 1990], [Pascual *et al.*, 2003]), a generic modelling methodology is presented in figure **1**. Main steps in model building methodology are outlined below.

3.2.2. Proposing a Model: Modelling Objectives, Model Type and System Characterisation

This general task corresponds to the two first stages represented in figure **1**. The modelling objectives were expressed by operators of water treatment works and essentially motivated by an increasingly stringent legal context. They were presented in introduction of this work and are summarised in figure **1**.
Characterising the process involves a comprehensive study of the relationships between the different elements, which compose the process. In our case, aqueous ozone chemistry, reactions with organic and inorganic elements (chapter **1**), hydrodynamics and industrial operational conditions (chapter **2**) are the most relevant elements. This step is often supported by a state of the art in related fields, and in particular in modelling. This work has been presented in the two first chapters.
Once the process has been characterised, axioms are formulated which describe, idealising or approximating, the process behaviour. Modelling ozonation, this has led us to consider the use of systematic networks, linked with detailed mechanistic chemical models as the most suitable approach (chapter **2**).

3.2.3. Building up a Model: Mathematical Model Formulation

Refining the axioms formulated previously into mathematical expressions leads to the formulation of the model itself. This step necessitates a good knowledge of the already proposed modelling procedures and of the physicochemical nature of the phenomena involved. Within this stage, parameters to be identified during calibration are defined. Considering ozonation, the model can be seen as a series of conservation laws (mass balances) applied to constitutive relations (mechanistic or semi-empirical models): calibration should hence regard only selected constitutive relations.
In a completely different direction, an arbitrary structure for the model can be chosen. Model parameters are then varied to achieve agreement between the process and the model. This type of model originates from the field of system identification and is only suitable for model realisation from observed process data [Jeppsson, 1996].
We shall now focus on system identification, which corresponds to the next stage in figure **1**.

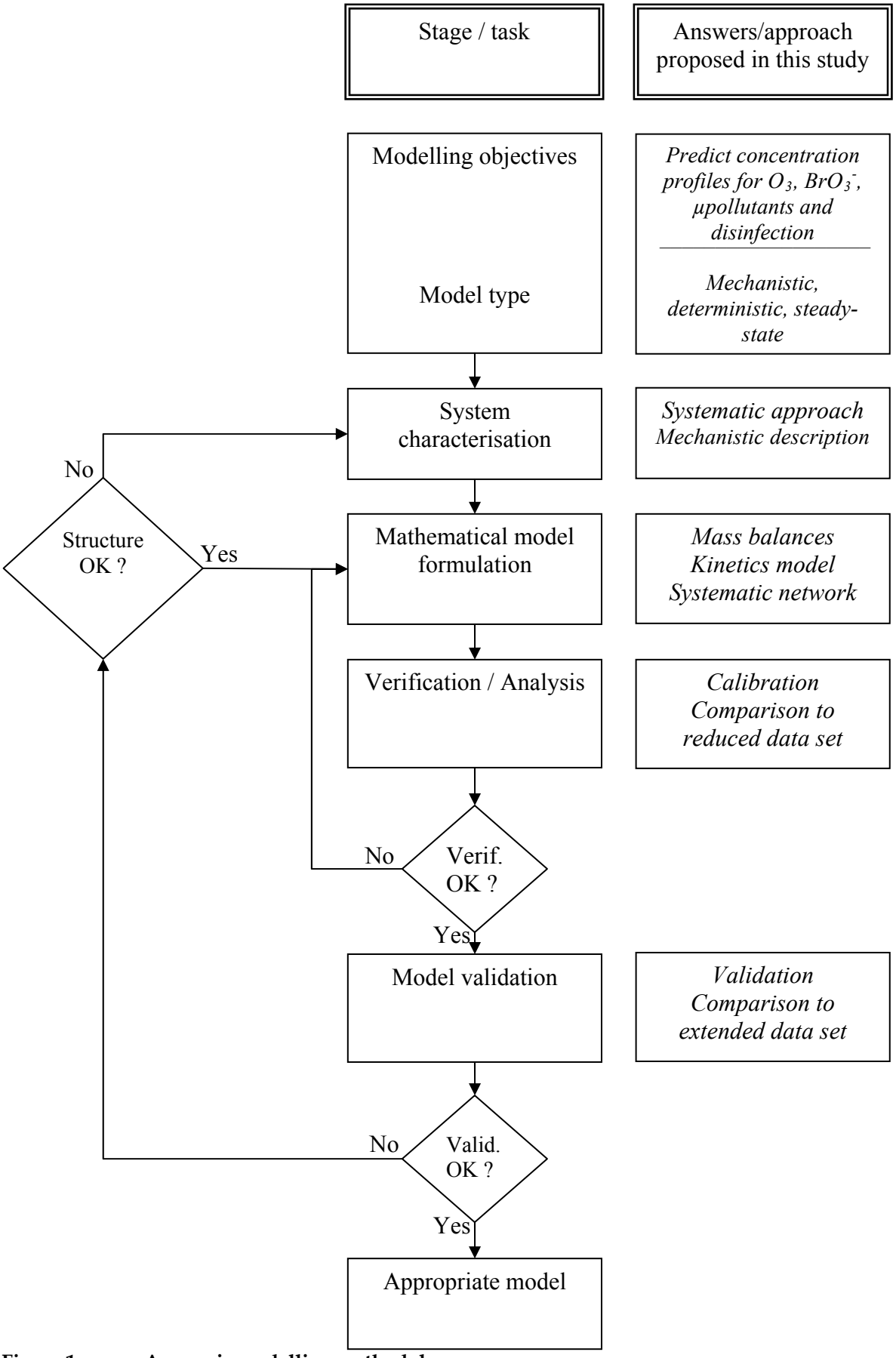

Figure 1 **A generic modelling methodology**

3.2.4. System Identification: Verification and Analysis

System identification is the art and science of building mathematical models of systems from observed input-output data. It can be seen as the interface between the real world of applications and the mathematical world of model abstractions [Ljung, 2008]. It encompasses various steps in modelling, from the evaluation of the model structure to the final model validation.

System identification techniques have been used in this work to identify parameter values, *i.e.* to calibrate models. In figure **2**, a schematic of the iterative parameter estimation procedure used in this study is given; it comprises:

- static blocks: experimental data (input corresponding to experimental conditions and output to measured data);
- Semi-dynamic blocks: the model is fixed during its evaluation but can be changed if not validated (*i.e.* modelling results are not meeting the modelling objectives). Another evaluation begins with each new model;
- Dynamic blocks: model parameters, which are constantly being changed during process, and simulated output which varies accordingly;
- Tasks: comparison and decision about the new values of the parameters. Comparison relies on an evaluation criterion (see **3.4.**). This criterion is then used by an identification algorithm to proceed to next step, *i.e.* to set new parameter values and evaluate in turn their validity by comparing simulated and experimental outputs.

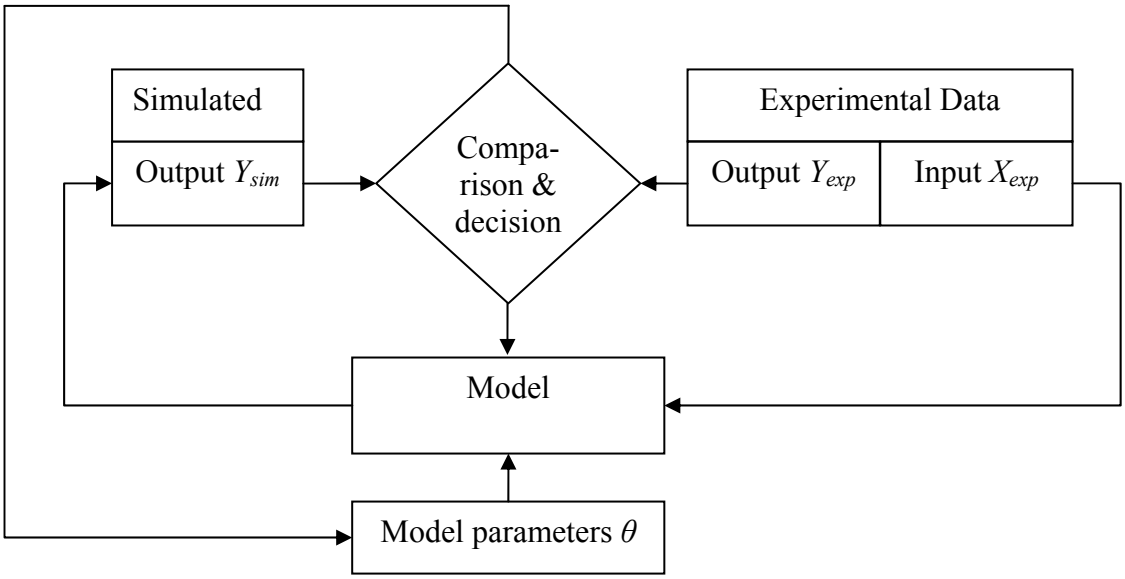

Figure 2 Schematic of the parameter identification process

We shall in the next section present the main topics relevant to our needs. Model structure evaluation, also part of system identification science, will therefore not be presented. As we try to best estimate model parameter values for simulated output to fit with experimental data, we shall discuss model identifiability issues and parameter estimation techniques.

3.2.5. Model Validation

3.2.5.1. Generalities

Once calibrated, the model shall ultimately be validated. This is done with "fresh" experimental data, *i.e.* with data sets which have not been used during model calibration. Goal of the validation is to set the boundaries of the model's validity domain. Data sets used

for validation should therefore be sufficiently large, in order to contain indications on the success and on the failure of the model. This fact explains why some authors consider validation rather as an attempt to refute a model (*e.g.* [Jeppsson, 1996]; [Tedeschi, 2006]), and others as a confirmation of the model's abilities (*e.g.* [Rykiel, 1996]). This distinction can also be formulated as in [Vanrolleghem and Dochain, 1998] between *models for prediction* and *models for understanding*. Models for prediction should predict the behaviour of the studied process as accurately as possible, so authors may preferentially focus on the domain of validity of the model. Models for understanding should capture most or at least the most important mechanisms that determine the behaviour of the process. These models hold until significant deviations from reality are observed and are *de facto* characterised by their limitations.

In order to assess the quality of the validation, the results of the model will be analysed in a two-step approach: (i) qualitative analysis (with different scatterplots and "common sense"); (ii) statistical analysis based on the prediction errors. These two analyses shall always be confronted to the underlying model assumptions.
Statistical validation can also be performed on the basis of the residual difference between simulated and experimental data. Various criteria were introduced by researchers ([Akaike, 1974]; [Craven and Wahba, 1979]), but many authors consider that, for an appropriate model, the residual differences should verify four criteria [Söderström and Stoica, 1989]:

- white noise with zero mean;
- symmetric distribution;
- independent of past inputs;
- independent of all inputs.

3.2.5.2. Evaluating the Badness-of-Fit

To test the significance of the linear relationship between calculated and observed concentration values, the Pearson test can be used. The Pearson product-moment correlation (in the following called Pearson's correlation, r_P) is simply the covariance of Y_{exp} and Y_{sim} transformed into centred and reduced variables (equation **1**). It is widely used as measure of strength of linear dependence between two variables.
For a sample distribution of size n, it can be shown that the t parameter as defined in equation **2** obeys a Student's law if variables Y_{exp} and Y_{sim} are not linearly correlated. The value of t is hence compared to t(p,n-2), where p is the risk associated to the statistical test [Legendre, 2009]. Additionally, confidence intervals for the linear regression parameters found with the data set can be calculated.

$$r_P = \frac{\sum_i \left(Y_{\exp,i} - \overline{Y}_{\exp}\right)\left(Y_{sim,i} - \overline{Y}_{sim}\right)}{\sqrt{\sum_i \left(Y_{\exp,i} - \overline{Y}_{\exp}\right)^2 . \sum_i \left(Y_{sim,i} - \overline{Y}_{sim}\right)^2}} \quad \textbf{(1)}$$

$$t = \frac{r_P \sqrt{n-2}}{\sqrt{1-r^2}} \quad \textbf{(2)}$$

In order to verify the criteria of [Söderström and Stoica, 1989] on the residuals (see precedent paragraph), the residual distribution can be compared to normal distribution. Various tests exist, but the most used is the univariate Student's t-test verifying the normal character of the distribution and the mean of the distribution. Different populations can be studied in order

to investigate the effects of different inputs as experimental factors, or values of the independent variable. However, such techniques will not be applied to our results, given the relatively small size of the samples.

3.2.5.3. Evaluating the Goodness-of-Fit

Statistical tests are generally performed as measures of badness-of-fit, evaluating the possibility of rejecting a specific hypothesis. Fewer measures concern the assessment of goodness-of-fit. Whereas several evaluations of goodness-of-fit including model complexity have been proposed (*e.g.* [Akaike, 1973]; [Schwartz, 1978]), we have focused on measures of goodness-of-fit *per se*.

Following the conclusions of [Schunn and Wallach, 2005], it was decided to use a combination of the value of the objective function (see section **3.4.1.**) and the classical coefficient of determination R^2. Considering experimental data with very different orders of magnitude, a preliminary change of variable was performed. Thus, values for *p*CBA concentrations were weighted according to equation **3**, where y stands for the original concentration values and Y the weighted ones. Definition of the coefficient of determination is then applied to the new defined concentrations (equation **4**).

$$Y_{\exp,sim}^{pCBA} = y_{\exp,sim}^{pCBA} \cdot \frac{\overline{Y}_{\exp}^{O_3}}{\overline{y}_{\exp}^{pCBA}} \quad \textbf{(3)}$$

$$R^2 = 1 - \frac{\sum_i \left(Y_{\exp,i} - Y_{sim,i}\right)^2}{\sum_i \left(Y_{\exp,i} - \overline{Y}_{\exp}\right)} \quad \textbf{(4)}$$

3.3. Practical Parameter Identifiability

3.3.1. Theoretical and Practical Identifiabilities

Before using parameter estimation techniques, investigation on uniqueness of the model parameter identification shall be undertaken. This can be done with theoretical identifiability analysis. It also gives indication on the theoretical soundness of the model. A parameter is called:

- *uniquely* or *globally identifiable*, if the solution for the parameter is unique;
- *locally identifiable*, if a finite number of parameter values can be found;
- *unidentifiable*, if there is an infinite number of parameter values, for which the model reproduces (exactly) the measurements.

In the case of unidentifiable parameters, different sets of parameter values will lead to (exactly) the same results. It is then important to investigate which combinations of parameters are identifiable (*e.g.*, if only the product of two parameters is used in a model, the parameters are not separately identifiable but the product may very well be identifiable).

Whereas several methods are available for theoretical identifiability analysis of linear models, there is only one universal technique applicable to nonlinear systems [van den Bos, 2007]. This technique is based on Taylor series expansion for the measured variables with respect to time [Pohjanpalo, 1978]. The decision whether the parameters can be identified is then reduced to an algebraic problem involving the parameters and the Taylor series coefficients. Finally, the parameters are identifiable if there is a set of parameters which is a

solution of the algebraic equation. However, practical limitations make this method troublesome to apply for more complex models. For nonlinear systems, there is indeed no theoretical upper limit to the number of model differentiations which may provide new information. The use of computer algebra programs can partially improve the situation, but the fundamental problem still remains (see *e.g.* [Davidescu and Jørgensen, 2008]).
Linearising the model around an operating point in order to apply one of the various methods for identifiability analysis of linear systems is a feasible approach. However, non-identifiability of a linearised system does not necessary indicate that the original nonlinear model is unidentifiable [Jeppsson, 1996]. Investigation of *local* identifiability is quite simple to conduct. This can be done by examining the rank of the Jacobian of the model [Godfrey and DiStefano, 1985].

Handling experimental measurements, often exhibiting a partial and noisy character, theoretical identifiability cannot be carried out. Instead, methods for practical identifiability analysis should be used.
Being fundamentally related to parameter uncertainty, practical identifiability cannot strictly give rules and state on the parameter identifiability of a model. Instead, results of practical identifiability depend on the values of the measured data and on the desired accuracy of the parameters. For example, practical identifiability methods may fail when similar experimental conditions (experimental data input in figure **2**) have led to major discrepancies in experimental measurements (experimental data output in figure **2**). Therefore, a critical analysis of experimental results should be done prior to any identifiability analysis. Parameter estimation results where the identified parameter values vary depending on the initial values is also an indication to proceed with care. Altogether, it is often easy to obtain sets of parameters which provide a good model fit, but since these parameters may be far from the true ones, situations where they are given an exact physicochemical interpretation should be avoided. Practical identifiability problems often arise as a result of the following factors [Jeppsson, 1996]:

- unsuitable model structure;
- poor sampling strategies, lack of reliable sensors and troublesome noise conditions;
- poor system "excitement" during the identification experiment;
- unsuitable identification algorithms.

Improvement of the practical identifiability may be obtained by:

- changing the model structure (use reduced order models);
- improving the experimental design, available information and noise characteristics;
- model reparametrisation (use combinations of model parameters).

Several procedures for practical identifiability are briefly reviewed below:
Using an optimisation–based approach, [Asprey and Macchietto, 2000] have given a criterion for the evaluation of the maximal distance between two parameter vectors that essentially give the same model output: the model is judged identifiable if this distance is smaller than some threshold. Alternately, [Brun *et al.*, 2002] proposed a local or global (multilocal) sensitivity analysis approach for practical identifiability. This technique is now commonly used for large models.
In order to identify complex reaction networks, [Brendel *et al.*, 2006] developed step-wise identifiability analysis. Each step corresponds to a part of the model: stoichiometry, reaction

rates, reaction kinetics and kinetic parameters. All possible model candidates are first considered: inadequate models are eliminated *a posteriori*. Potential drawback is that each individual reaction rate is considered independently, thus interaction effects between reactions are neglected ([Davidescu and Jørgensen, 2008]).

We shall focus here on two general techniques that are often used for practical identifiability analysis: sensitivity analysis and parameter covariance estimation. Depending on the problem and on the techniques used, these steps may be performed successively:

- sensitivity analysis gives good indications on the possibility to identify parameters and on the relative importance of parameters in regards to simulated outputs;
- parameter covariance estimation allows one to estimate interrelationship (that is, correlation) of parameters in order to determine which parameters can be determined independently.

3.3.2. Using Sensitivity Analysis to Gain Information on the Model

Many classes of methods can be distinguished in sensitivity analysis. Two of them are commonly used for practical identifiability: local and sampling-based methods.

3.3.2.1. Local and Sampling-Based Methods

The simplest local method analysis consists in calculating a linear approximation of the partial derivative of a model variable relatively to parameter(s). In order to facilitate the comparison of one model output with another, or of one parameter with another, different absolute or relative measures may be distinguished (equations **5** to **8**).

$$S^{\theta}_{abs,abs} = \left(\frac{\partial Y_{sim}}{\partial \theta}\right)_{Y_{sim}=Y^0_{sim}} \quad \textbf{(5)} \qquad S^{\theta}_{rel,abs} = \frac{1}{Y^0_{sim}}\left(\frac{\partial Y_{sim}}{\partial \theta}\right)_{Y_{sim}=Y^0_{sim}} \quad \textbf{(6)}$$

$$S^{\theta}_{abs,rel} = \theta\left(\frac{\partial Y_{sim}}{\partial \theta}\right)_{Y_{sim}=Y^0_{sim}} \quad \textbf{(7)} \qquad S^{\theta}_{rel,rel} = \frac{\theta}{Y^0_{sim}}\left(\frac{\partial Y_{sim}}{\partial \theta}\right)_{Y_{sim}=Y^0_{sim}} \quad \textbf{(8)}$$

Relative sensitivity coefficients are often preferred (see *e.g.* [Cruz and Perkins, 1973]): expression for the absolute change in Y_{sim} for a 100% change in θ (equation **7**) or for the relative change in Y_{sim} for a 100% change in Y_{sim} (equation **8**). Another technique consists in using centred and reduced variables with the following change of variable, for both parameters and simulation outputs (equation **9**). Equation **5** can then be used with the new variables.

$$Y_{new} = \frac{Y_{old} - \overline{Y_{old}}}{\sigma^{Y}_{old}} \quad \textbf{(9)}$$

Where $\overline{Y_{old}}$: mean value of Y_{old}

σ^{Y}_{old} : standard deviation of Y_{old}

Generally, the larger the value of the sensitivity coefficient, the higher is the likelihood for a parameter to be identified [Ascher *et al.*, 1995]. Dealing with several parameters, the sensitivity functions of the parameters as functions of the independent variable of the

measurements (*e.g.* time) have to be linearly independent. Otherwise, the parameters are not individually identifiable because a change in one parameter can be compensated by changes in other parameters. The more different the patterns of the sensitivity functions are, the better the parameters can be identified [Jeppsson, 1996]. Other techniques relative to local sensitivity analysis as adjoint modelling and automated differentiation may be applied as well (see *e.g.* [Navon, 1998]).

Sampling-based methods evaluate repeatedly the model's output for combinations sampled from the parameter distribution (using methods such as Monte-Carlo). Analyses of this type involve the generation and exploration of a mapping from uncertain analysis inputs to uncertain analysis results [Helton *et al.*, 2006]. Sampling-based methods hence require more insight into the system characteristics, since (at least) approximate knowledge of the probability distributions of the parameter is needed. Covering a wider value spectrum for the parameters, sampling-based sensitivity analyses necessitate much larger computational effort compared to local methods. Sampling-based methods however take much better account of nonlinear behaviours and consequently bear more information.
Accordingly, the general procedure to ascertain sensitivity measures for sampling-based sensitivity analysis methods is given in the following (see *e.g.* [Saltelli *et al.*, 2000] and [Helton *et al.*, 2006]):

1. Definition of probability distribution functions for the input parameters;
2. Generation of samples according to the defined probability distributions;
3. Evaluation of the model outputs using the generated samples;
4. Graphical analysis of the propagation of the input variations over the outputs;
5. Calculation of the sensitivity analysis results, linking input to output variations.

Despite the existence of various techniques to best approximate probability distributions, steps one to three remain for a large part problem-dependent. The graphical analysis presented in step four is often performed using scatterplots or distribution plots, associated with statistical measures such as correlation analysis, regression analysis, partial correlation analysis etc… Numerous techniques can be applied to conduct step five; they include: nonparametric regression analysis, squared rank differences/rank correlation coefficient test, two-dimensional Kolmogorov–Smirnov test, tests for patterns based on distance measures, top down coefficient of concordance, variance decomposition… See [Helton *et al.*, 2006] for more details.

3.3.2.2. Particular Sampling-Based Analyses: Variance-Based Methods

In this study, a specific variance-based sensitivity analysis technique has been employed. The main measures for variance-based sensitivity shall be presented before focusing on the technique used.
Using the statistical notion of variance, variance-based sensitivity analyses aim at estimating the variances of the conditional expectation variables $s^2_{E(Y_{sim}|\theta_i)}$ for an output Y_{sim}. This quantity is calculated by holding θ_i to its optimal value $\widetilde{\theta}_i$. $\widetilde{\theta}_i$ remaining by essence unknown, variance-based sensitivity analysis implement sampling strategies to perform multi-dimensional averaging. However, a relative measure is often preferred to the term $s^2_{E(Y_{sim}|\theta_i)}$. Therefore, the first order sensitivity is defined as the ratio of the variance of the conditional expectation to the total variance for output Y_{sim} (equation **10**).

$$S^i = \frac{s^2_{E(Y_{sim}|\theta_i)}}{s^2_{Y_{sim}}} \quad \textbf{(10)}$$

The index S^i represents the fraction of model output variance explained by the input variation of a given parameter θ_i. The second major sensitivity indicator for parameter θ_i is the total order sensitivity index $S_T{}^i$. It is expressed as the variance of the conditional expectation variable resulting from the variation of all input parameters *except* θ_i. With definition of the variance for the data set complementary to θ_i (equation **11**), the expression for $S_T{}^i$ becomes equation **12**.

$$s^2_{E(Y_{sim}|\theta_i^C)} = s^2_{E(Y_{sim}|\theta_1,\theta_2,\ldots,\theta_{i-1},\theta_{i+1},\ldots,\theta_m)} \quad \textbf{(11)}$$

$$S_T^i = 1 - \frac{s^2_{E(Y_{sim}|\theta_i^C)}}{s^2_{Y_{sim}}} \quad \textbf{(12)}$$

For additive models (*i.e.* with no interaction among parameters), the following equivalence holds: $S^i = S_T{}^i$. In particular, the subsequent relationships (equations **13** and **14**) are observed [Schwieger, 2006]:

$$\begin{cases} \sum_{i=1}^{m} S_T^i = 1 & \text{for additive models} \quad \textbf{(13)} \\ \sum_{i=1}^{m} S_T^i > 1 & \text{for non-additive models} \quad \textbf{(14)} \end{cases}$$

3.3.2.3. FAST and *e*FAST Methods

Based on the original Fourier Amplitude Sensitivity Test (FAST) method developed by [Cukier *et al.*, 1973], *e*FAST is a variance-based method, proposed by [Saltelli *et al.*, 1999]. Since its formulation, this technique has become very popular in many research areas.

The main idea governing the FAST method is to convert a *m*-dimensional problem into a one dimensional problem using Fourier decomposition (*m* represents the number of parameters). After Fourier transform, it is namely possible to separate parameter influences by encoding the identity of parameters in the frequency of their variation. Each input parameter θ_i is assigned to a frequency ω_i and transformed according to equation **15**.

$$\theta_i = G_i\left(\sin\left(\omega_i s\right)\right) \quad \textbf{(15)}$$

Where G_i is a suitably defined parametric equation, making it possible to vary each parameter in its range $[a;b]$ as s is varied between $-\pi$ and π. In practice, [Saltelli *et al.*, 1999] recommend the following parametric transformation (equation **16**):

$$\theta_i = G_i\left(\sin\left(\omega_i s\right)\right) = \frac{a+b}{2} + \frac{b-a}{2\pi\omega_i}\arcsin(\sin(\omega_i s)) \quad \textbf{(16)}$$

The frequencies are chosen so that the set $\{\omega_1,\ldots,\omega_m\}$ has a rank equal to m, ensuring independency of the frequencies and of their higher harmonics. A_j and B_j, the Fourier coefficients are defined in equations **17** and **18**, with f the model function defined as $f(s) = f(G_1(\sin(\omega_1 s)),G_2(\sin(\omega_2 s)),\ldots,G_m(\sin(\omega_m s)))$. They are evaluated using the procedure proposed by [McRae *et al.*, 1982].

$$A_j = \frac{1}{2\pi}\int_{-\pi}^{\pi} f(s)\cos(js)ds \quad \textbf{(17)}$$

$$B_j = \frac{1}{2\pi}\int_{-\pi}^{\pi} f(s)\sin(js)ds \quad \textbf{(18)}$$

The variance of the conditional expectation variable can then be expressed as (equation **19**):

$$s^2_{E(Y_{sim}|\theta_i)} = 2\sum_{p=1}^{M}(A^2_{p\omega_i} + B^2_{p\omega_i}) \quad \textbf{(19)}$$

Where M is the maximum harmonic considered.

The major improvement of the *extended* FAST is to propose a way to calculate the total order sensitivity indexes by estimating the variance of the complementary set (equation **12**).This is done by assigning a particular frequency ω_i for the parameter θ_i (usually high) and almost identical frequencies to the remaining frequencies ω_i^C [Ekström, 2005]. The partial variance of the complementary set is computed according to equation **20**.

$$s^2_{E(Y_{sim}|\theta_i^C)} = 2\sum_{p=1}^{M}(A^2_{p\omega_i^C} + B^2_{p\omega_i^C}) \quad \textbf{(20)}$$

The parametric transformation **16** is also slightly modified in the *extended* FAST version in order to produce more flexible sampling schemes. Due to the symmetry properties of trigonometric functions, the sinusoidal function induces eventually a repetition of the same samples. Therefore, a *resampling* strategy is implemented to avoid this inefficiency [Saltelli *et al.*, 1999]: *e*FAST algorithm is repeated N_r (resampling size) times with different search curves specified by introducing a random phase shift φ_i into each sinusoidal function (equation **21**).

$$\theta_i = G_i(\sin(\omega_i s)) = \frac{a+b}{2} + \frac{b-a}{2\pi\omega_i + \varphi_i}\arcsin(\sin(\omega_i s + \varphi_i)) \quad \textbf{(21)}$$

Consequently, the computational cost to obtain all first and total order sensitivity indexes is: $m.(2M\omega_{max}+1).N_r$. According to the recommendation of [Saltelli *et al.*, 1999], a minimum value of 65 should be chosen for the expression $2M\omega_{max}+1$; *resampling* should at least performed once ($N_r \geq 2$). Similar values for the *e*FAST parameters can be found in literature (see *e.g.* [Marino *et al.*, 2008]). The *e*FAST algorithm used in this work is that developed by [Ekström, 2005]. More details on the method itself can be found in [Saltelli *et al.*, 2000].
Other techniques for practical identifiability analysis are mostly correlated to entropy theory, evaluating the quality of information enclosed in the parameters to be identified. Among others, methods use the mathematical properties of the mode shape correlation matrix (*e.g.* [Wage *et al.*, 2005]), covariance matrix of the estimated parameters, observability matrix or Fisher information matrix (*e.g.* [Cherng, 1999]; [Banga *et al.*, 2000]). Such analyses have better chance to detect unidentifiable parameters. Moreover, they are frequently considered when formulating strategies for experimental design aiming at improving the parameter identification [Buzzi-Ferraris and Manenti, 2009].

3.3.3. Refining the Knowledge on the Model with Covariance Analysis

Interrelationship of parameters can easily be evaluated by means of the Jacobian matrix J (also called sensitivity matrix), the components of the latter being defined in equation **22**.

$$J_{i,j} = \left[\frac{\partial Y_{sim}^{i}}{\partial \theta_j} \right]_{i=1\ldots l; j=1\ldots m} \quad \textbf{(22)}$$

where l : number of experimental reference data (for example concentration measurements);
m : number of parameters to be determined.

An estimation of the covariance matrix of the model parameters is given in equation **23** (*e.g.* [Sun, 1994]).

$$Cov(\theta) \approx M_{\sigma}^{2} (J^{T} J)^{-1} \quad \textbf{(23)}$$

where M_{σ}^{2} : observation error variance matrix;
J and J^{T} : Jacobian and its transpose, respectively.

The resulting covariance matrix is also called correlation matrix since it gives indications on the way parameters are correlated. $Cov(\theta)$ is symmetric; the diagonal elements are the variances of the parameters, the elements outside the diagonal are the covariances among parameters. Working with centred and reduced variables yields thus ones in the diagonal and coefficients ranging from -1 to +1 outside the diagonal. A covariance coefficient $Cov(\theta)_{i,j,i\neq j}$ with value close or equal to 0 indicates that parameters i and j are not correlated, and, in the case of centred and reduced variables, a value close to -1 or +1 indicates extreme correlation. Due to its format, the covariance matrix is not able to give indications on correlations where more than two parameters would be involved.

Correspondingly, the Fisher information matrix (not presented herein) also encapsulates information about the sensitivity of the system (Jacobian matrix) and about the experimental error (inverse of the experimental error covariance matrix). It is alternately used to investigate parameter correlations.
Despite the variety of techniques available for performing the calculations needed to evaluate the covariance matrix (computation of the Jacobian matrix, inversion techniques), a simple estimation of its coefficients often only provides limited information. Two major drawbacks are listed below:

- Similarly to sensitivity analysis methods, local strategies for covariance analysis often fail when dealing with nonlinear problems (this explains why, sampling-based sensitivity analyses are preferred in such cases). Values for parameter correlation coefficients (covariance matrix coefficients) can therefore be found very different, depending on the value of the parameter set considered. For example, [Poeter and Hill, 1997] showed that the parameter correlation coefficients for a simple ground water flow problem could vary between 0.05 and 0.998 depending on the parameter values for which the calculation was done. This difficulty is shared, to a smaller extent though, by other local techniques such as singular value decomposition [Hill and Osterby, 2003].
- Difficulties also arise when considering correlation coefficients with absolute values close to one. For example, [Hill and Osterby, 2003] reported that parameters *a priori* highly correlated with correlation coefficient of -0.996 could be determined uniquely. On the other hand, values of 0.7 can sometimes be regarded as high [Hill and Osterby, 2003]. This situation is all the more problematic as errors originating from numerical approximations (especially when the matrices are badly scaled) may

corrupt correlation coefficients, such as values of -1 and +1 can no longer be achieved to sufficient precision to be identified. Limited precision of sensitivities and correlation coefficients is especially problematic when sensitivities are calculated by perturbation methods.

3.3.4. Determining Practical Identifiability: The Example of Least Squares Estimation

Practical identifiability not only depends on uniqueness and stability of the parameter identification, but also relies on the quantity and quality of the experimental output data. Correlated to the use of least squares estimation (see next **3.4.1.**), a definition of parameter identifiability has been proposed by [Chavent, 1987]. This definition is often used because it considers the effect of measurement error [Sun *et al.*, 2001]. A parameter is said to be identifiable if the least squares estimation has a unique minimum in a given region and if the minimisation is continuously dependent on the measurement errors. To directly verify sufficient conditions for this identifiability criterion is a difficult task. Therefore, [Sun *et al.*, 2001] have proposed a practical method to test identifiability conducting additional parameter identifications:

- Uniqueness of the minimum can be assessed by analysing the stability of the identified parameters with regards to initial guesses;
- Verification of the continuous dependence can be achieved by analysing the stability of the identified parameters with regards to experimental data. First, parameter identification is carried out with the original experimental data. Then, various experimental data sets are generated, altered with increasing artificial errors. Parameter identifications are carried out for each set, and the convergence of the identified parameter when artificial errors tend to zero is studied.

3.3.5. Improving Identifiability through Reparameterisation

Classical formulation of kinetics models may be a critical factor for parameter identification. Kinetics parameters may indeed exhibit strong correlations among them and moreover be strongly unbalanced.

Major drawbacks are associated with these characters: respective influences of correlated parameters are intricate to determine; unbalanced parameters may narrow valleys when using optimisation methods. Consequently, a parameter identification problem may be ill-conditioned if not reparameterised. For instance, the condition number of the Jacobian matrix obtained by linearising the model in the neighbourhood of the minimum can easily be improved by 10^6 to 10^{10} with adequate reparameterisation [Buzzi-Ferraris and Manenti, 2009]. Following the historical examples proposed by [Kittrell *et al.*, 1966] and [Hawthorn, 1974], classical forms for model reparameterisation have been adopted. However, it is important to note that the dependent variable r (*i.e.* the reaction rate) must not be modified. For example, if the parameters to be determined are the frequency factor k_0 and the energy of activation E_A in an Arrhenius-like form (equation **24**).

$$k = k_0 e^{\frac{-E_A}{RT}} \quad \textbf{(24)}$$

It is suitable to rewrite it according to equation **25**. The new parameters to identify are θ_1 and θ_2; C_1 and C_2 are constants; $\overline{T}$ is the mean temperature (equations **26** and **27**).

$$k = \exp\left[\theta_1 + C_1\theta_2\left(\frac{1}{T} + C_2\right)\right] \quad \textbf{(25)}$$

$$C_1 = \frac{1}{\left|\frac{1}{T} + C_2\right|} \quad \textbf{(26)} \qquad C_2 = -\frac{1}{\overline{T}} \quad \textbf{(27)}$$

Integrating k_0 in the exponential and using the two constants C_1 and C_2 considerably improves the balance between the two parameters. Correlation is also lowered since the parameters to identify do not appear as product anymore. If experiments were conducted for two temperatures, such as $T_1 < \overline{T} < T_2$, the original parameters k_0 and E_A have the following expressions (equations **28** and **29**, respectively):

$$k_0 = \exp\left[\theta_1 + \theta_2 . \frac{T_1 + T_2}{T_1 - T_2}\right] \quad \textbf{(28)} \qquad E_A = 2R\theta_2 . \frac{T_1 T_2}{T_1 - T_2} \quad \textbf{(29)}$$

The reparameterisation presented in equation **25** is however impossible to apply when more than two experimental temperatures have been investigated. Moreover, experiment temperatures are forced to be constant. Therefore, a simplified reparameterisation is often preferred (equation **30**), where new parameters θ_1' and θ_2' are respectively defined in equations **31** and **32**. The new parameters remain reasonably well-balanced, given that temperatures are quite stable in practice (generally varying between 278 K and 298 K).

$$k = \exp\left[\theta_1' - \frac{1}{T} . \theta_2'\right] \quad \textbf{(30)}$$

$$\theta_1' = \ln(k_0) \quad \textbf{(31)} \qquad \theta_2' = \frac{E_A}{R} \quad \textbf{(32)}$$

3.4. Parameter Estimations

3.4.1. Conventional Methods

Parameter estimation procedure is schematised in figure **2**: its goal is to determine the best parameter values θ for a specified model and a specified set of experimental data Y_{exp}, used as reference. After having proposed methods to check for the possibility of success of such procedure, we shall focus on parameter estimation, *i.e.* the way a parameter set is evaluated (corresponding to the "comparison" task of figure **2**).

Although used for a specified model structure, this procedure is not completely independent of model structure evaluation, because the model may degenerate to a simpler structure for particular values of some parameters [Jeppsson, 1996]. However, this will not be considered in the following since the values given for the parameters should prevent model simplification (for example, conditions of non-nullity for concentrations and bounds for the kinetic constant rates). Four conventional techniques can be used for parameter estimation:

- Bayesian estimation;
- maximum likelihood estimation;
- weighted least squares estimation;
- least squares estimation.

These four methods are listed in decreasing order of the amount of information that has to be provided by the user of the method, or, equivalently, in increasing order of the number of *a priori* assumptions already included in the method: while Bayesian estimation requires the parametrisation of some probability distributions (for the parameters and the measurements), least squares estimation can be conducted without any extrinsic information. In Bayesian estimation, both measurements and model parameters are considered as random variables. According to Bayes' rule, the probability density of the parameters for given values of the measurements can be expressed as in equation **33**.

$$p(\theta|Y_{\exp}) = \frac{p(Y_{\exp}|\theta)\,p(\theta)}{p(Y_{\exp})} \tag{33}$$

Where $p(\theta)$: *a priori* probability density for the occurrence of the parameter (or set of parameters) θ

$p(Y_{\exp}|\theta)$: conditional probability density of the model for measuring the values $Y_{\exp}$ conditionally to given parameter θ

Though equation **33** does not directly specify estimates of the parameters, it yields a complete description of the distribution of parameter values for given measurements. The estimation of the parameters then requires additional assumptions, in particular on the set of experimental values $Y_{\exp}$. In particular, small data sets may frequently lead to estimation errors [Chi, 2008].

Under maximum likelihood estimation assumptions, the parameters are not considered anymore as random variables, but as constant parameters of the distributions of the measurements. Goal of maximum likelihood estimation is then to maximise the L function – which is the probability $p(Y_{\exp}|\theta)$ of equation **33** – named likelihood function. It represents the probability density of a model for the occurrence of the measurements Y_{exp} conditionally to given parameters θ. The general form of L function is intricate, but can be reduced to equations **34-35** when the probability distributions of the measurements are uncorrelated and normal. For given measurements $Y_{\exp}$, the maximum likelihood estimates $\theta(Y_{\exp})$ of the parameters are those values of θ for which the likelihood function has its maximum.

$$L(Y_{\exp}|\theta) = \frac{1}{\sqrt[n]{2\pi}} \prod_{i=1}^{l} \frac{1}{\sigma_{\varepsilon_i}} \exp\left[-\frac{1}{2} \sum_{i=1}^{n} \left(\frac{\varepsilon_i(\theta)}{\sigma_{\varepsilon_i}} \right)^2 \right] \tag{34}$$

$$\varepsilon_i(\theta) = Y_{\exp,i} - Y_{sim,i}(\theta) \tag{35}$$

where $Y_{sim,i}(\theta)$:calculated value of the model corresponding to $Y_{\exp,i}$ using the parameters θ

σ_{ε_i} : standard deviation of the error of the model (relatively to experimental measurements)

l : number of experimental measurements

A step further is taken when the model is considered as perfect, *i.e.* as not generating errors. As most modellers propose a model, test it and accept it until they find a better one, this assumption generally holds, at least temporarily. Under this assumption, the standard

deviation of the model σ_{ε_i} is replaced by the standard deviation of $Y_{\exp,i}$. Maximising equation **34** becomes then equivalent to minimising the equation **36**. Assuming uncorrelated measurements normally distributed, the maximum likelihood estimation thus reduces to weighted least squares method. In equation **36** is introduced the objective function O, that shall be minimised during parameter identification.

$$O(\theta) = \sum_{i=1}^{l} \left(\frac{Y_{\exp,i} - Y_{sim,i}(\theta)}{\sigma_{\exp,i}} \right)^2 \quad \textbf{(36)}$$

Where $\sigma_{exp,i}$: estimated or observed standard deviation of $Y_{\exp,i}$

If the measurements Y_{exp} are distributed over a large range of values, a relative measure of weighted least squares is generally preferred. The objective function to minimise during optimisation becomes equation **37**. By means of an analysis of the experimental covariance matrix, the uncertainty of the estimates may in turn be estimated.

$$O(\theta) = \sum_{i=1}^{l} \left(\frac{Y_{\exp,i} - Y_{sim,i}(\theta)}{Y_{\exp,i}.\sigma_{\exp,i}} \right)^2 \quad \textbf{(37)}$$

Finally, assuming a uniform experimental deviation, further simplification can be carried out and the estimation becomes that of the well-known least squares (equation **38**):

$$O(\theta) = \sum_{i=1}^{l} \left(Y_{\exp,i} - Y_{sim,i}(\theta) \right)^2 \quad \textbf{(38)}$$

Practical experience has however shown that the methods above may not always suffice, since distributions of real data are never known exactly. This has led to the development of methods for robust estimation [Fieller, 2004].

3.4.2. Dealing with Experimental Distribution: Robust Estimation

Treating real experimental data sets, it is sometimes necessary to find and reconcile possible outliers. Even for large experimental sets of data, outliers may induce large inaccuracy in parameter identification. Main possible sources for these are listed below:

- experimental error;
- inability for the model to explain the entire experimental domain.

In order to make parameter estimation less dependent on non-existing points or outliers, it is possible to consider not the sum of least squares as in equations **36** or **38**, but their arithmetic mean. However, [Rousseeuw and Leroy, 1987] reported, illustrated by several examples, the following problems:

- outliers are often not detected;
- some experiments are frequently pointed out as outliers, although they are acceptable or even good points;
- models can be wrongly discarded as inadequate.

One of the simplest ways to overcome such shortcomings is to replace the arithmetic mean by the median, much less sensitive to outliers. More efficiently, the sum of least square may

be modified to include only the smaller half of the squares of the residuals [Rousseeuw and Leroy, 1987]. Applying such strategies to nonlinear problems increases however computational time ([Fieller, 2004]; [Buzzi-Ferraris and Manenti, 2009]). Moreover, outliers can be detected when manually analysing simulation results (for relatively small sets of data).

3.5. Optimisation techniques

3.5.1. Choice of the Methods Used

In this section, we present the optimisation techniques used in this work. Very different techniques are available to determine optimal values for the parameters. Therefore, we have chosen a technique adapted to our needs and to the type of problem to be solved.
The main characteristics of the optimisation problem of this study are:

- high nonlinearity due to the expression of the mass balances, and in particular of the reaction kinetics (see chapter **2**);
- difficulty, when not impossibility, to assess if a unique solution exists. It is generally admitted, that parameter values for models of chemical/biochemical phenomena should not support conclusions on the nature of the phenomena themselves [Jeppsson, 1996]. In other words, very different combinations of parameter values may lead to similarly acceptable results in terms of model predictions;
- extremely vast domains of search for the optimal values of the parameters, because: (i) a large amount of parameters has to be determined (generally 12, see chapter **4**); (ii) *a priori* optimal values are difficult to guess, given the very few data available in literature (see chapter **1** and chapter **4**).

Optimisation techniques can be classified according to various criteria: local versus global methods, order of the method, convergence speed, single-objective versus multi-objective, derivative versus derivative-free, etc. In regards to the above-listed characteristics, the following constraints can be expressed, that will govern the choice of an optimisation method:

- robustness towards parameter values, given that nonlinear behaviours may induce very intricate response surfaces of the model;
- robustness towards experimental values;
- ability to determine solutions as global as possible;
- relatively limited number of function evaluation.

Considering robustness, we have chosen derivative-free methods. Sometimes, the computation of derivatives and the inversion of the Jacobian matrix might cause the algorithm to diverge, especially for highly nonlinear problems. Divergence is all the more frequent as initial guesses of the unknown parameters are far from their optimal values. Derivative-free methods generally necessitate reduced numbers of function evaluations, although this may vary according to the characteristics of each optimisation problem. However, convergence rate is quite low with derivative-free methods, especially in the neighbourhood of a solution.
An additional objective was to try to get solutions as global as possible, considering a very large parameter space where local minima may be found. Various global search algorithms (simulated annealing, genetic algorithms, hill climbing, ant colony optimisation…) exist, and

several tests were performed with Genetic Algorithms (GAs). Despite their ability to find good solutions relatively rapidly, GAs may suffer from early convergence, *i.e.* may be entrapped in local minima. Another way to achieve global search is to combine global exploration with local optimisation. During the first step, a constrained Monte-Carlo search is performed in order to select candidates that are optimised in a second time, with a traditional optimisation method.
In this study, an exploratory phase using Latin Hypercube Sampling (LHS) technique was used to find good global candidates for optimisation. Then, Nelder-Mead optimisation method was used to locally optimise the values found by LHS. Nelder-Mead is a derivative-free method, well-known for its stability.
A review of the most common numerical methods used for optimisation, especially when maximising the loglikelihood function or minimising the least squares criterion, can be found in reference books, such as [van den Bos, 2007]. The methods presented by van den Bos are generally based on the estimation of the Jacobian matrix (sometimes with the Hessian); for derivative-free methods, see *e.g.* [Weise, 2009].

3.5.2. The Nelder-Mead Method

3.5.2.1. Principle

The Nelder-Mead method ([Nelder and Mead, 1965]) is based on parameter space mapping by special geometrical figures called simplexes. A simplex is a m dimensional polytope with $m + 1$ vertices (for example, a triangle in a plane, a tetrahedron in tri-dimensional space etc.). Nelder-Mead method finds local optima for m dimensional regular functions. No gradient, numerical nor analytical, is used. This method is very popular among the methods, which merely compare function values, in terms of robustness and efficiency.
Nelder-Mead is an improved version of the simplex search method presented on figure **3**. Contrary to simplex method, Nelder-Mead algorithm allows for irregular simplexes: automatic distortions are performed by the solver in order to account for the very geometry of the objective function. Illustrated by the example of figure **3** considering a minimum search in a two-dimensional space, the simplex method is explained in the following. Simplex method progressively explores the parameter space by defining successive simplexes converging to a local minimum. Below are described the steps taken (refer to figure **3**).

First iterations
The algorithm first creates a simplex around the initial guess θ_0 by adding a given percentage (5% for the method used) of each component $\theta_0(i)$ to θ_0, and using these m vertices as elements of the simplex in addition to θ_0. The vertex for which the objective function value is the highest is determined (vertex #1). The vertex is then reflected in the centroid of the other m vertices (#2 and #3), thus forming a new simplex {#2, #3 and #4, reflection point}. The objective function is computed for the new vertex and the process repeated (#5, reflection of #2; #6, reflection of #3; #7, reflection of #5).
If the newest vertex has the highest value,
the new vertex is not defined as reflection in the centroid of the m other vertices. This would indeed cause the new vertex to coincide with a precedent one and would generate oscillations. Hence, the largest objective function value other than that at the newest vertex is subsequently used to decide which vertex to reflect.
In figure **3**, the simplex {4,6,7} is such as: $O(\#7) > O(\#4) > O(\#6)$ (O is the objective function). Vertex #7 has already been defined as reflection, therefore vertex #4 is chosen for reflection, leading to vertex #8.

Vertex #9 is constructed with the same method as the first iterations, vertex #10 as reflection of the second highest vertex.

If all new simplexes would coincide with already existing ones,

it is expected that smaller values are to be found inside the last simplex. Consequently, the new simplex is defined as contraction of the last simplex. The centre of similitude is the lowest point of the last simplex (#11 and #12 are defined during contraction).

In higher dimensions, this rule is also applied when a given vertex #*i* has been in the current simplex for more than a fixed number of iterations.

The algorithm continues to reflect and contract the simplex until the required tolerance has been achieved.

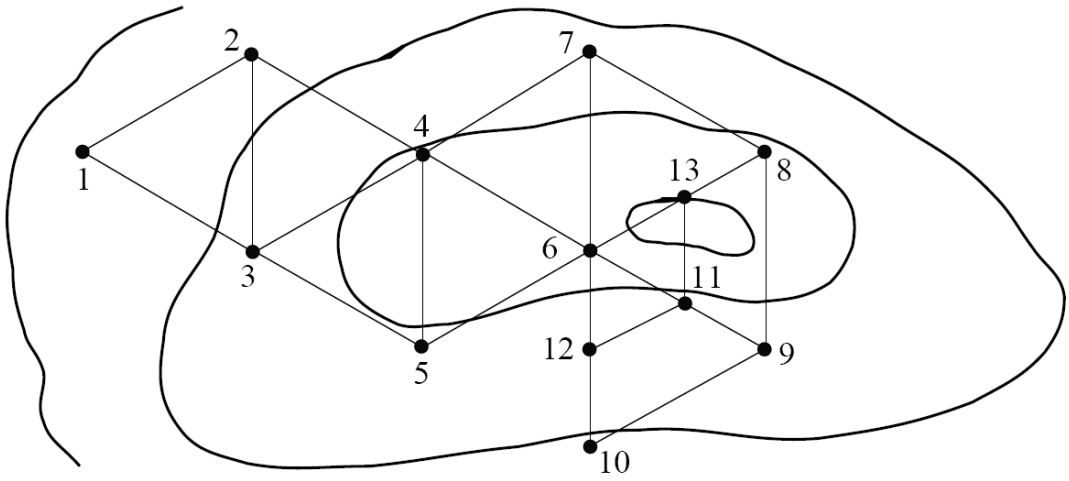

Figure 3 **Schematic of the simplex algorithm for a two-dimensional problem.**

Convergence rate is slow but the algorithm is very robust and quite insensitive to noise. Often the method can be used in combination with more sophisticated ones. The simplex method is then applied in an early stage of the optimization in order to get the convergence going in the right direction and thereby producing suitable initial values for methods that converge faster. Such faster algorithms are usually less robust and might diverge if the initial estimates are far from the true ones (for example, the Gauss-Newton algorithm).

3.5.2.2. *Fminsearch* and *Fminsearchbnd*

In this study, the *fminsearch* algorithm from Matlab™ has been used, which implements an improved version of Nelder-Mead proposed by [Lagarias *et al.*, 1998]. The algorithm was chosen because of its robustness and the relatively small amount of function evaluations needed to achieve satisfactorily results with moderate accuracy.

Trying to avoid unphysical values for the parameter to be identified (negative concentrations for instance), changes of variables were performed in order to add inequality constraints to the optimisation problem. Given that *fminsearch* does not naturally accept constrained optimisation problems, this has been achieved introducing the changes of variables as suggested for the *fminsearchbnd* function proposed by John d'Errico (Matlab™ Central, see bibliography).

For example, for a parameter to be superior to a certain lower bound, one defines a new variable X as in equation **39**.

$$x = B_{\inf} + X^2 \qquad \textbf{(39)}$$

Where x *stands for the original parameter to be determined and* X *for the new unconstrained parameter;* B_{inf} *is the inferior bound.*
Similarly, for an upper bound, one gets equation **40**, where B_{sup} is a superior bound.

$$x = B_{\sup} - X^2 \tag{40}$$

For bounded parameters, a bounded function as *sin* is used (equation **41**).

$$x = B_{\inf} + \frac{B_{\sup} - B_{\inf}}{2} \cdot (\sin(X) + 1) \tag{41}$$

When using these changes of variables, attention should however be paid to the following points:

- Bounds should not be defined as strict constraints, since round-off errors might cause these to be subtly exceeded.
- The introduced functions are not bijective ones. As a result, there is no uniqueness for the determination of parameter *X*. This has however no consequence on the determination of *x*.

Other changes of variables are possible: sin^2 is a good alternative, even if its slightly more nonlinear character might induce round-off errors. *Atan* may also be a good choice for strict bounds, as it is when used in artificial neural networks.

3.5.3. Genetic Algorithms (GAs)

GAs are based on the evolution of a population of candidates for the solution of an optimisation problem. The algorithm proposes successive generations of candidates that progressively converge to a solution, thus iteratively improving. The principles leading to the formulation of GAs were derived from considerations on natural species evolution [Holland, 1975].
Two key principles are used for the generation of new candidate solutions: mutation and recombination (also called *crossover*). Mutation consists in altering the current solution to see what could be achieved in its neighbourhood. It is a pretty old technique and can be seen as a simple modification of traditional hill-climbing techniques [Béraud *et al.*, 2009]. Recombination consists in taking two good solutions and exchanging some of their characteristics. This strategy was directly inspired by considerations on the evolution of species, and on the genetic interbreeding techniques aiming at producing the best fitted individuals. The recombination is assumed to provide fast convergence to the optimum (compared to mutation) and to avoid the entrapment in local extrema by early convergence. Early convergence is encountered when a very fit member of the population appears early. Due to its high fitness, it is more likely to reproduce and propagate its characteristics through the generations, eliminating the options that may have eventually led a global optimum. Practically, early convergence can be prevented by high mutation rates, but this strategy remains case-dependent [Yadgari *et al.*, 1998]. The main drawback is that only near optimal solutions are found with GAs [Béraud *et al.*, 2009].

3.5.4. Enhancing Optimisation/Identification Possibilities by Exploration

3.5.4.1. Generalities

Traditional optimisation techniques may suffer severe limitations when:

- limited amounts of experimental data are available, or when using semi-quantitative information on system behaviour;
- objective functions exhibit intricate response surfaces towards parameter values, and especially many secondary minima.

In those cases, global search methods may be good alternatives. The simplest global search method is the exhaustive search. A systematic exploration of the (discretised) parameter space is performed, and all parameter values within the considered space are visited. Although this method may be ideal for problems with low dimensionality (*i.e.* with few parameters), the task is computationally unfeasible when problems with many parameters are considered.
When identifying many parameters for highly nonlinear problems, it is therefore necessary to severely restrict the number of calculations for the objective function, as compared to an exhaustive search. One way to do this is to use a Monte Carlo search, which consists of a (possibly guided) random walk in the model space. A Monte Carlo search extensively samples the model space, avoids entrapment in local likelihood maxima, and therefore provides a useful way to attack such highly nonlinear inverse problems [Mosegaard and Tarantola, 1995]. If probability densities for parameters are specified to the Monte Carlo method, all local likelihood maxima shall be sampled, provided that a sufficient number of iterations is performed. Consequently, this method often does not lead to a unique set of acceptable parameter values. Explanations on the use of Monte Carlo methods for parameter identification can be found in [Tarantola, 2005].
If *a priori* density functions are not known, Monte Carlo search is often used as a first stage for pre-selection of candidates (*e.g.* [Drews *et al.*, 2004]). In those cases, a simple uniform density function is generally chosen. The best promising candidates are then treated separately using other techniques (local optimisation codes, for instance). Similarly, probabilistic metaheuristic techniques such as genetic algorithms or simulated annealing can be used as first stages, before using classical optimisation codes (*e.g.* the SIMPSA code proposed by [Cardoso *et al.*, 1997] or the method of [Luersen and Le Riche, 2004]). Very large domains of research can indeed be mapped using Monte Carlo techniques. However, to improve the screening, several algorithms were developed. We shall only present the most used: Latin Hypercube Sampling (LHS).

3.5.4.2. Latin Hypercube Sampling (LHS)

Originally proposed by [McCay *et al.*, 1979], LHS is a random design of experiments that relies on a subdivision of the space to be explored. For a two-dimensional problem, a latin square is a square grid containing only one sample in each row and each column. Generalising this concept to an arbitrary number of dimensions, each sample of a latin hypercube is the only one in its axis-aligned hyperplane. This sampling strategy is then applied to the space of parameter values to select sets of parameters. A more detailed explanation of the principles of LHS can be found in [Wyss and Jorgensen, 1998].
The main advantage of LHS is that it ensures uniformity of the marginal distributions of the input variables, in other words LHS ensures that the ensemble of random combinations is representative of the real variability. LHS can also be optimised using several criteria; for instance, the maximum minimum distance between sampling points. Other space-filling strategies include maximum-entropy designs, low-discrepancy sequences, etc. [Niederreiter, 1992]. LHS design is very popular in various fields; it is for example used for sampling-based sensitivity analyses [Helton *et al.*, 2006], or in conjunction to kriging techniques (*e.g.* [Park *et al.*, 2006]).

3.6. Conclusion

A general methodology for modelling has been presented in this chapter. Focus was put on system identification, which shall represent a central task in ozonation modelling since ozonation processes have not completely been characterised and their modelling cannot overpass the use of semi-empirical relationships (that have to be calibrated).
Therefore, techniques for parameter estimation have been reviewed. The main conclusions are gathered below:

- due to the great complexity of the model, theoretical identifiability will not be carried out; instead, practical identifiability techniques shall be used;
- given the highly nonlinear character of the problem to be solved, sampling-based methods for exploring the sensitivities of the system shall be preferred. Accordingly, it appears doubtful if a covariance analysis step is needed, due to the limitations of such methods: computational inaccuracy and possible entrapment in local behaviours.
- given the very scarce information available on semi-empirical models used for ozonation modelling, the distribution probabilities of the parameters cannot be known *a priori*. Bayesian estimation techniques and maximum likelihood functions will therefore not be used as estimation techniques and we will consider weighted least squares estimation. Moreover, handling experimental concentrations with different ranges, a relative measure will be preferred;
- classical reparametrisations will be performed on the problem to better achieve parameter identification;
- in order to avoid too many objective function evaluations and to maximise the chances of determining global minima, the robust Nelder-Mead method will be combined to a Monte-Carlo search implementing LHS strategy.

3.7. Bibliography

Articles and books

- **Akaike H., (**1973). Information Theory and an Extension of the Maximum Likelihood Principle, in Petrov and Csaki (Ed.). Second International Symposium on Information Theory. Budapest: Akademiai Kiado, pp. 267–281.
- **Akaike H.,** (1974). A new look at the statistical model identification. *IEEE Transactions on Automatic Control*, Vol. **AC-19**, pp. 716–723.
- **Ascher U. M.**, **Mattheij R. M. M., Russel R. D.**, (1995). Numerical Solution of Boundary Value Problems for Ordinary Differential Equations, *SIAM Classics in Applied Mathematics*, Philadelphia, U.S.A.
- **Asprey S.** and **Macchietto S.,** (2000). Statistical tools for optimal dynamic model building, *Computers and Chemical Engineering*, Vol. **24**, pp. 1261–1267.
- **Banga J. R., Versyck K. J., van Impe J. F.,** (2000). Numerical Strategies for Optimal Experimental Design for Parameter Identification of Nonlinear Dynamic (Bio-) Chemical Processes, *Proceedings of ESCAPE-10,* 8-10 May, Florence, Italy.
- **Béraud B., Lemoine C., Steyer J.-P.,** (2009). Multiobjective Genetic Algorithms for the Optimisation of Wastewater Treatment Processes, *in Computational Intelligent Techniques for Bioprocess Modelling, Supervision and Control*, Springer Verlag, Berlin-Heidelberg, pp. 163-195.
- **Brendel M., Bonvin D., Marquardt W.,** (2006). Incremental identification of kinetic models for homogeneous reactions systems, *Chemical Engineering Science*, Vol. **61**, pp. 5404–5420.
- **Brun R., Kühni M., Siegrist H., Gujer W., Reichert P.,** (2002). Practical identifiability of ASM2d parameters—systematic selection and tuning of parameter subsets, *Water Research*, Vol. **36**, pp. 4113–4127.
- **Buzzi-Ferraris G.** and **Manenti F.,** (2009). Kinetic models analysis, *Chemical Engineering Science*, Vol. **64**, pp. 1061-1074.
- **Cardoso M. F., Salcedo R. L., Feyo de Azevedo S., Barbosa D.,** (1997). A simulated annealing approach to the solution of minlp problems, *Computers and Chemical Engineering*, Vol. **21**, pp. 1349-1364.
- **Chavent G.,** (1987). Identifiability of parameters in the output least square formulation, in *Identifiability of Parametric Models*, edited by E. Walter, Pergamon, Tarrytown, N.Y.
- **Cherng A.-P.,** (1999). Optimal sensor placement for modal parameter identification using signal subspace correlation techniques, *Proceedings of the 17th international modal analysis conference*, 8-11 February, Kissimmee, U.S.A.
- **Craven P.** and **Wahba G.,** (1979). Smoothing noisy data with spline functions: estimating the correct degree of smoothing by the method of generalized cross- validation, *Numerische Mathematik.*, Vol. **31**, pp. 377–403.
- **Cruz J. B.** and **Perkins W. R.,** (1973). A new approach to the sensitivity problem in multivariable feedback system design, in *System Sensitivity Analysis*, edited by J. B. Cruz Jr., pp. 125-132, Van Nostrand Reinhold, New-York.
- **Cukier R. I., Fortuin C. M., Shuler K. E., Petschek A. G., Schaibly J. H.,** (1973). Study of the sensitivity of coupled reaction systems to uncertainties in rate coefficients. Part I: theory, *Journal of Chemical Physics*, Vol. **59**, pp. 3873–3878.
- **Davidescu F. P.** and **Jørgensen S. B.,** (2008). Structural parameter identifiability analysis for dynamic reaction networks, *Chemical engineering Science*, Vol. **63**, pp. 4754-4762.
- **Drews T. O., Webb E. G., Ma D. L., Alameda J., Braatz R. D., Alkire R. C.,** (2004). Coupled mesoscale-continuum simulations of copper electrodeposition in a trench, AIChE Journal, Vol. **50**, pp. 226–240.
- **Ekström P.-A.,** (2005). Eikos – A Simulation Toolbox for Sensitivity Analysis, *Master of Science thesis*, Uppsala University, Faculty of Science and Technology.
- **Godfrey K. R.** and **DiStefano J. J.,** (1985). Identifiability of Model Parameters, Identification and System Parameter Estimation 1985, (H.A. Barker, P.C. Young eds.), *Proceedings of the 7th IFAC/IFORS Symposium*, Vol. **1**, pp. 89-114.

- **Hawthorn R. D.,** (1974). Afterburner Catalysts-effects of Heat and Mass Transfer Between Gas and Catalytic Surface, *AIChE Symposium Series*, Vol. **70**, pp. 428-438.
- **Helton J. C., Johnson J. D., Sallaberry C. J., Storlie C. B.,** (2006). Survey of sampling-based methods for uncertainty and sensitivity analysis, *Reliability Engineering and System Safety*, Vol. **91**, pp. 1175-1209.
- **Hill M. C.** and **Osterby O.,** (2003). Determining extreme parameter correlation in ground water models, *Ground Water*, Vol. **41**, pp. 420-430.
- **Holland J. H.,** (1975). Adaptation in Natural and Artifical Systems, *University of Michigan Press*, Ann Arbor, Michigan.
- **Jeppsson U.,** (1996). Modelling Aspects of Wastewater Treatment Processes, Ph.D. thesis, Lund University, Sweden. Available at: http://www.iea.lth.se/~ielulf/publications/phd-thesis/PhD-thesis.pdf
- **Kittrell J. R., Hunter W. G., Watson C. C.,** (1966). Obtaining precise Parameter Estimates for nonlinear catalytic rate models, AIChE Journal, Vol. **12**, pp. 5-10.
- **Lagarias J. C., Reeds J. A., Wright M. H., Wright P. E.**, (1998). Convergence Properties of the Nelder-Mead Simplex Method in Low Dimensions, *SIAM Journal of Optimization*, Vol. **9**, pp. 112-147.
- **Ljung L.,** (2008). Perspectives on System Identification, *Plenary at IFAC Congress*, July, Seoul. Available at: http://www.control.isy.liu.se/~ljung/seoul2dvinew/plenary2.pdf
- **Luersen M. A.** and **Le Riche R.,** (2004). Globalized Nelder–Mead method for engineering optimization, *Computers and Structures*, Vol. **82**, pp. 2251-2260.
- **Marino S., Hogue I. B., Ray C. J., Kirschner D. E.,** (2008). A Methodology For Performing Global Uncertainty And Sensitivity Analysis In Systems Biology, *Journal of Theoretical Biology*, Vol. **7**, pp. 178-196.
- **McCay M. D., Beckman R. J., Conover W. J.,** (1979). A Comparison of Three Methods for Selecting Values of Input Variables in the Analysis of Output from a Computer Code, *Technometrics*, Vol. **21**, pp. 239-245.
- **McRae G. J., Tilden J. W., Seinfeld J. H.,** (1982). Global sensitivity analysis - a computational implementation of the Fourier amplitude sensitivity test (FAST), *Computers and Chemical Engineering*, Vol. **6**, pp. 15–25.
- **Mosegaard K.** and **Tarantola A.,** (1995). Monte Carlo sampling of solutions to inverse problems, *Journal of Geophysical Research*, Vol. **100**, pp. 431–447.
- **Murthy D. N. P., Page N. W., Rodin E.Y.,** (1990). Mathematical Modelling, *Pergamon Press*, New York, U.S.A.
- **Navon I. M.,** (1998). Practical and theoretical aspects of adjoint parameter estimation and identifiability in meteorology and oceanography, *Dynamics of atmospheres and Oceans*, Vol. **27**, pp. 55-79.
- **Nelder J. A.** and **Mead R.,** (1965). A Simplex Method for Function Minimization, *The Computer Journal*, Vol. **7**, pp. 308-313.
- **Niederreiter H.,** (1992). Random number generators and quasi-Monte Carlo methods, *SIAM*.
- **Park K., Oh P.-K., Lim H.-J.,** (2006). The application of the CFD and Kriging method to an optimization of heat sink, *International Journal of Heat and Mass Transfer*, Vol. **49**, pp. 3439-3447.
- **Poeter E. P.** and **Hill M. C.,** (1997). Inverse Models: A Necessary Next Step in Groundwater Modeling, *Ground Water*, Vol. **35**, pp. 250-260.
- **Pohjanpalo H.,** (1978). System Identifiability Based on Power Series Expansion of the Solution, *Mathematical Biosciences*, Vol. **41**, pp. 21-33.
- **Rousseeuw P. J.** and **Leroy A. M.,** (1987). Robust Regression and Outlier Detection, John Wiley and Sons, New York, U.S.A.
- **Rykiel E. J. J.,** (1996). Testing ecological models: the meaning of validation. *Ecological modeling*, Vol. **90**, pp. 229-244.
- **Saltelli A., Chan K., Scott E. M.** (Ed.), (2000). Sensitivity Analysis, John Wiley and Sons, Chichester.
- **Saltelli A., Tarantola S., Chan K. P. S.,** (1999). A quantitative Model-independent method for global sensitivity analysis of model output, *Technometrics*, Vol. **41**, pp. 39-56.
- **Schunn C. D.** and **Wallach D.,** (2005). Evaluating goodness-of-fit in comparison of models to data, in W. Tack (Ed.), *Psychologie der Kognition: Reden and Vorträge anlässlich der Emeritierung von Werner Tack*. Saarbrüken, Germany: University of Saarland Press, pp. 115-154.

- **Schwarz G.,** (1978). Estimating the Dimension of a Model, *The Annals of Statistics*, Vol. **6**, pp. 461–464.
- **Schwieger V.,** (2006). Sensitivity Analysis as A General Tool for Model Optimisation – Examples for Trajectory Estimation, *Proceedings from the 3rd IAG / 12th FIG Symposium,* Baden, May 22-24.
- **Söderström T.** and **Stoica P.** (1989). System Identification, Prentice Hall, Inc., Englewood Cliffs, New Jersey, USA.
- **Sun N., Sun N.-Z., Elimelech M., Ryan J. N.,** (2001). Sensitivity analysis and parameter identifiability for colloid transport in geochemically heterogeneous porous media, *Water Resources Research*, Vol. **37**, pp. 209-222.
- **Sun N.-Z.,** (1994). Inverse Problems in Groundwater Modeling, Kluwer Academic Press, Norwell, U.S.A.
- **Tarantola A.,** (2005). Inverse Problem Theory and Methods for Model Parameter Estimation, *SIAM.*
- **Tedeschi L. O.,** (2006). Assessment of the adequacy of mathematical models, *Agricultural Systems*, Vol. **89**, pp. 225-247.
- **van den Bos, A.,** (2007). Parameter Estimation for Scientists and Engineers, *Wiley-Interscience*, Hoboken, U.S.A.
- **Vanrolleghem P. A.** and **Dochain D.,** (1998). Bioprocess model identification, in Van Impe J. F., Vanrolleghem P. A., Iserentant D. M. editors, *Advanced Instrumentation, Data Interpretation, and Control of Biotechnological Processes*, pp. 251-318. Kluwer Academic Publishers.
- **Wage K. E., Dzieciuch M. A., Worcester P. F., Howe B. M., Mercer J. A.,** (2005). Mode coherence at megameter ranges in the North Pacific Ocean, *Journal of the Acoustical Society of America*, Vol. **117**, pp. 1565-1581.
- **Weise T.,** (2009). Global Optimization Algorithms – Theory and Application, eBook available at: http://www.it-weise.de/projects/book.pdf
- **Wyss G. D.** and **Jorgensen K. H.,** (1998). A user's guide to LHS: Sandia's latin hypercube sampling software, *Sandia National Laboratories Technical Report SAND98-0210*, Albuquerque, USA.
- **Yadgari J., Amir A., Unger R.,** (1998). Genetic Algorithms for Protein Threading, *Proceedings of the 6th International Conference on Intelligent Systems for Molecular Biology*, Vol. **6**, pp. 193-202.

Reports, manuals and courses

- **Fieller N.**, (2004). Statistical Modelling and Computing, *Course of the University of Sheffield, Department of Probability and Statistics*, Available at: http://www.nickfieller.staff.shef.ac.uk/sheff-only/StatModall05.pdf
- **Pascual P.** ***et al.***, (2003). Draft Guidance on the Development, Evaluation and Application of Regulatory Environmental Models, *Background Document of the Transatlantic Uncertainty Colloquim*, 10-11 October, Washington D. C., U.S.A. Available at: http://www.modeling.uga.edu/tauc/other_papers/CREM%20Guidance%20Draft%2012_03.pdf

Internet resources

Courses (last access: February 2010)

- **Legendre P.,** (2009). Cours de Biostatistique I, Université de Montréal, available at: http://www.bio.umontreal.ca/legendre/BIO2041/index.html.
- **Chi M.,** (2008). Maximum-Likelihood & Bayesian Parameter Estimation (Sections 3.1-3.5), CSE Fudan University, Shanghai, available at: http://homepage.fudan.edu.cn/~mingmin/course/PatternRecogntion/08PR/Chap3-1.pdf

Programs and algorithms

Matlab™ Central

- *fminsearchbnd* download (last access : January 2009) http://www.mathworks.com/matlabcentral/fileexchange/8277

4. MODELLING THE INFLUENCE OF NOM ON OZONE DECOMPOSITION

Abstract

The semi-empirical model proposed for the role of NOM on ozone decomposition is able to adequately reproduce changes in contact time with ozone, pH, temperature, ozone dose, NOM nature and NOM concentration. However, specific water characteristics or specific experimental conditions are less satisfactorily taken into account.

Numerical tests have shown that the numerical strategies for parameter identification are sound. A sampling-based sensitivity analysis gave interesting insights on practical identifiability: among the parameters whose values should be determined during calibration, a group of parameters to be determined first was isolated. Accordingly, two calibration procedures were proposed and evaluated by comparing their results to results obtained with a genetic algorithm. It appears that the three calibrations give good results in terms of prediction, but that parameter values may be far from the optimal ones.

At lab-scale, an apparatus was especially developed to collect the experimental data used to calibrate and/or validate the model for the role of NOM. Under various experimental conditions (pH, temperature, ozone dose, NOM nature and NOM concentration) ozone and *p*CBA (*para* chorobenzoic acid, used as hydroxyl radical probe compound) concentrations were followed. For each water sample, 14 to 32 experiments were performed. 11 water samples originating from seven different locations were collected at different period of the year, so that two types of comparisons could be established: seasonal variations considering samples originating from the same location, and general variations among all water samples.

A good agreement of modelling results with experimental data was found for about 75 % of the experiments. Generally, ozone concentrations were better modelled than *p*CBA concentrations. Ozone decomposition rates at high ozone doses were however underestimated by the model and experiments for which pH and NOM concentration were simultaneously lowered could not be adequately predicted. The analysis of the experiments performed at lab scale showed that water with high organic content (TOC > 2.4 $mg.L^{-1}$) and simultaneous low inorganic content (A_T < 0.3 $meq.L^{-1}$) could not be modelled adequately. Seasonally, NOM reacted differently with ozone and hydroxyl radicals and accordingly, the values of the parameters varied.

Using only 6 experiments to calibrate the model for the role of NOM, an alternate modelling procedure also gave good results: considering a group of five water samples, 70 % of the experiments were modelled satisfactorily; when using all the experiments for calibration, 80 % of the experiments were modelled satisfactorily. Quality of the results was found weaker than with the calibration set comprising all the experiments, especially for experiments performed at low NOM concentration. A procedure to systematically minimise the number of experiments to consider for calibration purposes shall be developed.

Contents

4.1. Introduction

The previous chapters have set the framework of the study in terms of chemical modelling (chapter **1**), hydrodynamic modelling (chapter **2**) and numerical methods (chapters **3**). The conclusions of these earlier chapters are applied in this chapter for the predictions of ozone and hydroxyl radical concentrations.
Precise predictions for ozone and hydroxyl radical concentrations are crucial when modelling ozonation. Adequately simulated concentration profiles for the main oxidative species indeed represent the first and major step for accurately calculating disinfection or simulating the removal of micropollutants (pharmaceuticals, pesticides, additives…). Therefore, numerous studies on ozonation (*e.g.* [Bezbarua, 1997], [Westerhoff *et al.*, 1997], [Kim *et al.*, 2007]) have first focused on the models involving NOM in the ozone decomposition and the generation of radicals. As stated in chapter **1**, NOM remains the major unknown parameter involved in the chemistry of the ozonation process.
The need for precise simulation results is all the more important, as NOM interactions with ozone may vary seasonally, considering the same water throughout the year; and/or locally, comparing water samples from different locations. Considering the literature, very few studies have, to our knowledge, dealt with seasonal variations (except [Wei *et al.*, 2008]). It is even more difficult to find modelling studies, which deal with the seasonal variations of the NOM interaction with ozone. Furthermore, the issues of calibrating models and assessing the robustness of these models have, to our knowledge, not been addressed in literature.
The main objective of the chapter is to determine how ozone decomposition, and in particular the influence of NOM on ozone decomposition, can be modelled in natural water. Accordingly, the following issues shall be addressed: apparatus developed for characterising the chemistry of the water sample, accuracy of the predictions, domain of validities (both considering the type of water and the experimental conditions), calibration procedure and seasonal variations of the water chemistry.
In this chapter, all the experiments performed in order to characterise and model the influence of NOM are single-phase experiments which served to abstract from transfer phenomenon. The apparatus and the models used are presented in sections **4.2** and **4.3**. Techniques for parameter identification will be defined and/or tested in section **4.4**. The quality of the modelling for the chemical phenomena experimentally observed will be discussed in section **4.5**. Particular attention will be paid on the ability to model at different period of the year, for different types of water and under different experimental conditions. The last section **4.6.** presents a normalised calibration procedure for engineering purpose. Special care has been taken to reduce the amount of experimental data necessary for calibration. Prospects are given to generalise the process of reduction of the number of experiments.

4.2. Materials and Methods

4.2.1. Protocols

4.2.1.1. Aqueous Ozone Production

Aqueous ozone was produced letting an ozone flow bubbling in a specially conceived vessel filled with Ultra Pure Water (UPW). Most of the ozone dissolutions were carried out at room temperature, others at low temperature (typically, T=2°C), since low temperatures favour the dissolution of ozone into water. In figure **1**, both set-ups are presented: ozone comes in the

reactor via a glass tube (a), bubbles into UPW through a sintered glass diffuser (b) and goes to the ozone destructor via an exhaust glass tube (c).

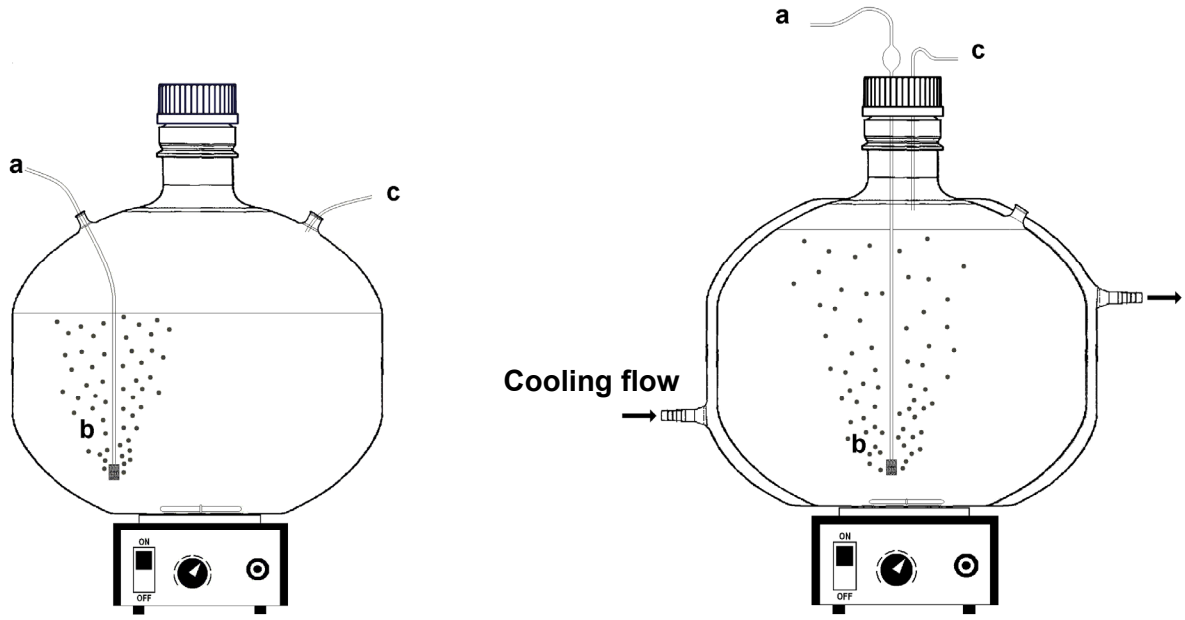

Figure 1 Set-ups for ozone dissolution into UPW, at room temperature (left hand-side) and at low temperature (right hand-side)

Different ozone generators and analysers were used throughout the study:

- Trailigaz ozone generator fed with pure oxygen coupled to UVOzon 200.125 and UVOzon 200.200 analysers;
- BMT 802 X ozone generator fed with pure oxygen coupled to a BMT 964 analyser;
- Astex Sorbios ozone generator fed with pure oxygen coupled to a BMT 964 analyser.

Despite the use of different ozone generators, the same amount of ozone was approximately dissolved in UPW, working with gaseous concentrations for ozone always kept around 100±20 $g.Nm^{-3}$.

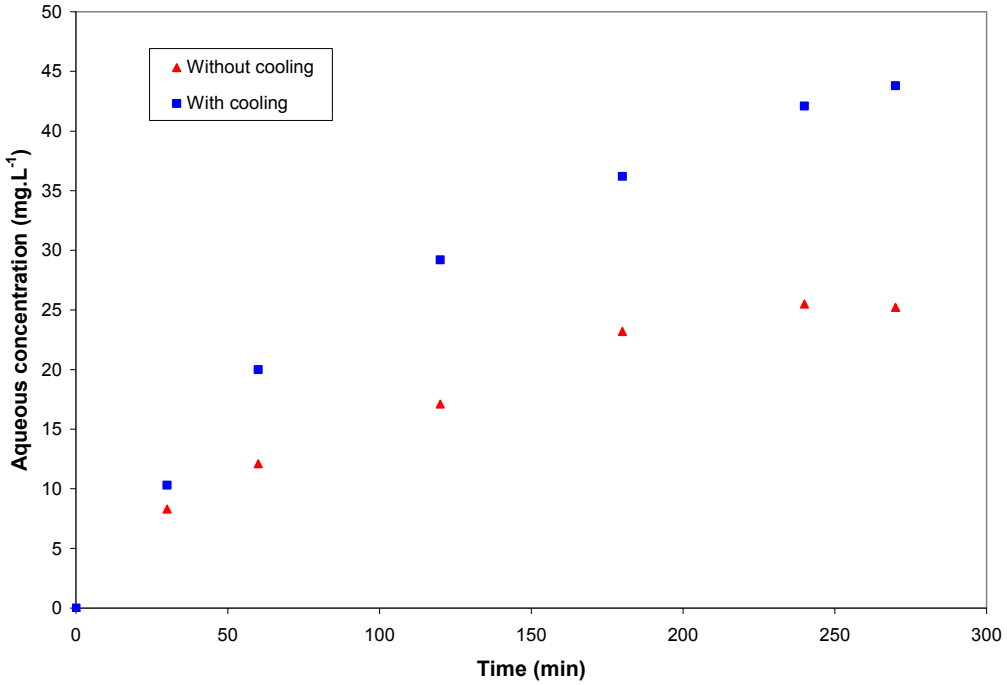

Figure 2 **Typical concentration profiles in the ozonation vessels**

A significant change could be noted when using the vessel with cooling system for the ozone dissolution. Typical concentration profiles are given for both set-ups in figure **2**. As expected, dissolved ozone concentrations were always higher using the refrigerated vessel. Although stabilised, the concentrations did not reach saturation: according to Henry's law (chapter **2**, figure **4**), at room temperature, aqueous concentration should nearly reach a third of gaseous concentration (half of gaseous concentration at T=2°C).

4.2.1.2. Description of the Gas-Tight Syringe Set-Up

Focusing on chemical phenomena related to natural water ozonation, a single-phase experimental set-up was developed. Contrary to traditional set-ups, for which different reactors correspond to different contact times with ozone, a unique reactor was used in this study. In doing so, preparation time was saved and better homogeneity among sampling points was achieved. The major difficulty was to take several samples without generating a gaseous head space where ozone could have desorbed. This was mastered using a gas-tight syringe, allowing thus to modify the reactor volume during sample withdrawal.

As presented in figure **3**, ozone dissolution was mainly conducted at room temperature. 10 mL gas-tight syringes are used to withdraw predetermined quantities of ozonated water (d) and to inject them in the 100 mL gas-tight syringe (e) or to take samples from the 100 mL gas-tight syringe, which is held horizontally in a thermostatic water bath (right hand side of figure **3**). The total volume of water (after aqueous ozone injection) was always 100 mL. Septa allowed one to rapidly withdraw and inject. Initial ozone concentrations were systematically dosed twice from samples taken from the dissolution vessel. If a major discrepancy was observed in concentration between both measurements, the experiment was postponed (analytical problem, unstable aqueous ozone concentration…)

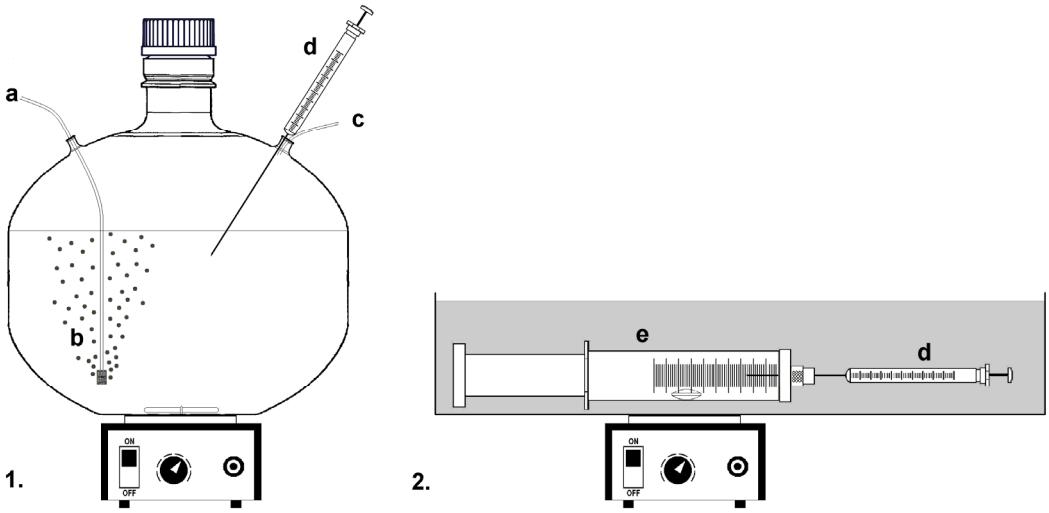

Figure 3 **Schematic of the gas-tight experimental set-up**

Samples were used to determine concentrations of ozone and *p*CBA (*para* ChloroBenzoic Acid, used here as hydroxyl radical probe compound, due to its reactivity ([Elovitz and von Gunten, 1999]; [Beltrán, 2004]). After having measured ozone concentration, remaining ozone in samples was quenched using fresh concentrated sodium thiosulfate. Generally, seven samples were analysed corresponding to seven contact times with ozone: 30''; 1'; 2'30''; 5'; 15'; 35' and 60'. Similar protocols have already been used by several researchers; see *e.g.* [Kim *et al.*, 2004]. The same effort was devoted in this study to avoid any ozone stripping and to ensure reproducible experimental conditions [Mandel, 2008]. All materials in contact with ozone were especially selected according to their chemical compatibility: glass, PTFE, stainless steel.

Given the very characteristic of the gas-tight syringe, special care was taken to define perfectly adequate stirring conditions. Tests were performed with Indigo used as coloured tracer to qualitatively assess if stirring was effective. These investigations were recorded on a camera; a sequence of images extracted from the film is given in figure **4**.

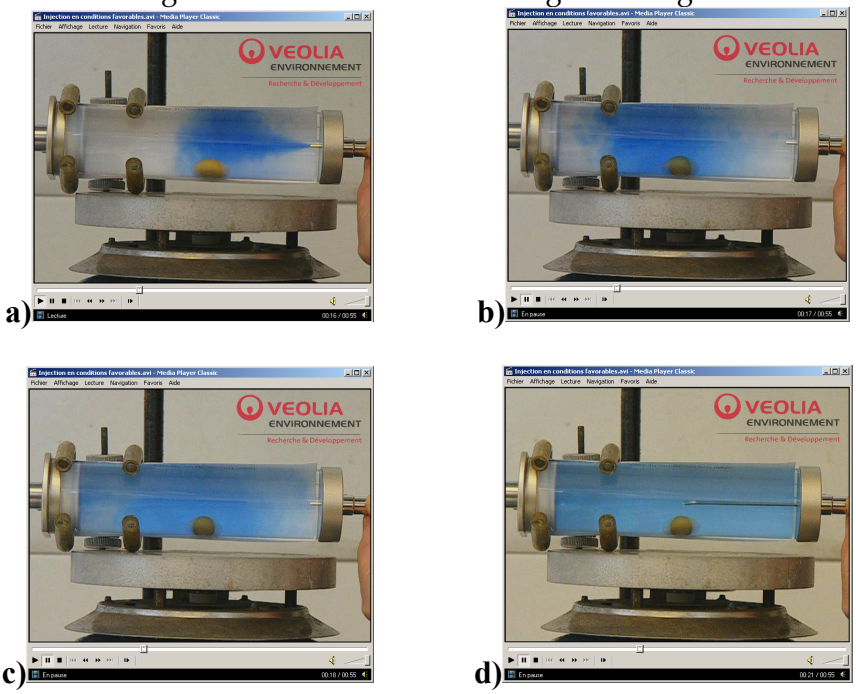

Figure 4 **Four moments following tracer injection. a) injection; b) after 1 second; c) after 2 seconds; d) after 5 seconds**

Mixing conditions were found to be optimal using an oval stirring bar, the dimensions of which are determined by the syringe geometry. With appropriate material, homogenisation occurs in less than five seconds.

4.2.1.3. Experimental Uncertainty of the Gas-Tight Syringe Set-Up

In order to best characterise the developed protocol and to assess the reliability of experimental results, experiments and analyses were replicated. Various experimental conditions were tested with changes in pH, ozone doses, temperature, NOM content and NOM concentration. Three replicate experiments performed on Méry-sur-Oise water and 109 analysis replicates (Méry-sur-Oise and Maisons-Laffitte waters) showed that:

- the experiments were reproducible, for both ozone and *p*CBA species;
- the standard deviation was not uniform when considering the experimental points: the smaller the contact time, the higher the experimental standard deviation (the example of ozone is given in figure **5**).

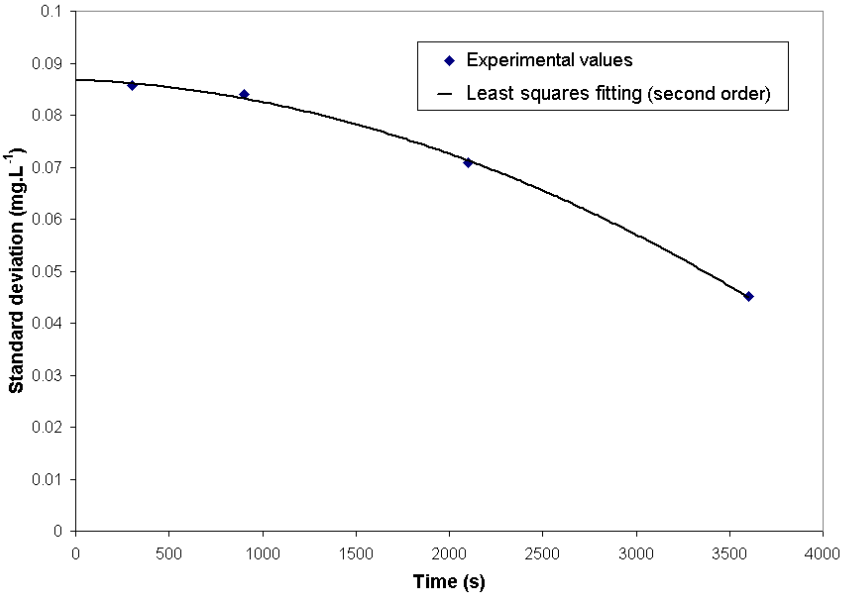

Figure 5 Standard deviations for the ozone concentration measurements

The standard deviation for *p*CBA analysis was found to exhibit the same behaviour with regards to the experimental (contact) time. We concluded that the protocol itself and the sampling schedule may explain the higher standard deviations obtained for short times: as a matter of fact, it is more difficult to achieve great reproducibility when having less time to collect a sample.

4.2.2. Reactants And Water Characteristics

4.2.2.1. Reactants

All reactants used in this part are summarised in table **1**. It comprises radical scavengers or "tracer" (*tert*-butanol and *p*CBA, respectively), quenching agents, analytical compounds... All other reactants used in this study were reagent grade or analytical grade.

Table 1 Overview of all reactants used during ozonation experiments

Reactant	Purity	Supplier/Origin
Tert-butanol	99.5 %	Acros Organic (Geel, Belgium)
*p*CBA	99.9 %	Supelco (USA)
Potassium bromide	99%	Labosi, France
Sodium thiosulfate	99.5 %	Grosseron S.A. (Nantes, France)
Ultra Pure Water (UPW)	18.2 MΩ.cm^{-1}	Elga Labwaters
Sodium Hydrogenocarbonate	99.5 %	Merck (Darmstadt, Germany)
Nitric Acid	65 %	Merck (Darmstadt, Germany)

Solutions were always prepared diluting the non-aqueous reactants in Ultra Pure Water (UPW). Concentrations were high enough to guarantee minimal dilution (<3%), in order not to alter too strongly NOM.

4.2.2.2. Water Characteristics

Various types of natural water were investigated, taken from wells (Maisons-Laffitte), from three different rivers (River Oise: Méry-sur-Oise; bank-filtered Seine River: Meulan; Marne River: Annet-sur-Marne) and from dams or lakes (Vitré dam: Vitré, Beaufort dam: Beaufort, Jonsvatnet lake: Trondheim). Moreover, specific waters were collected at different periods of the year to estimate the effect of seasonal changes (Annet-sur-Marne, Meulan and Vitré). For these waters, a number indicates the experimental session in table **2**. The main physicochemical data and the dates of sampling are also specified for each water sample in table **2**. The three designs of experiments (see in the following **4.2.4.**) are also separated by the double horizontal lines.

Table 2 Main characteristics of the waters investigated

Water origin	pH	A_T meq.L^{-1}	Bromide µg.L^{-1}	TOC mg C.L^{-1}	UV 254 nm 5 cm
Méry-sur-Oise (November 2008) Sand filtered surface water	7.85	4.55	51	3.1	0.164
Maisons-Laffitte (December 2008) Artesian well	8.15	2.4	34	<0.5	0.119
Vitré (February 2009) Sand filtered dam water	7.4	1.02	155.6	2	0.130
Annet-sur-Marne (February 2009) Sand filtered surface water	7.4	2.82	29	1.3	0.093
Meulan (March 2009) Sand filtered surface water	7.25	6.24	88.4	0.9	0.091
Beaufort (March 2009) Sand filtered dam water	6.05	0.12	111	2.4	0.142
Trondheim (March 2009) Jontsvatnet Lake water	7.35	0.32	140.5[1]	3.1	0.102
Annet-sur-Marne 2 (July 2009)	8.05	4.24	48	1.6	0.082
Annet-sur-Marne 3 (October 2009)	7.7	3.08	30	1.6	0.098
Meulan 3 (November 2009)	7.3	6.02	94[2]	1.3	0.088
Vitré 3 (November 2009)	7.1	1.24	200[2]	2.3	0.118

[1] Trondheim water was doped with potassium bromide. The original concentration is 20.5 µg.L^{-1}

[2] Vitré 3 and Meulan 3 waters have been doped with potassium bromide. The original concentrations are 180 and 74 µg.L^{-1}, respectively.

4.2.3. Analyses

4.2.3.1. Aqueous Ozone Measurement

Aqueous ozone concentrations were measured using the method proposed by [Bader and Hoigné, 1981]. Two indigo solutions were used, for high concentrations (within dissolution vessel) and for low concentrations (within the syringe). The volumes of aqueous ozone withdrawn ranged from 2 mL to 5 mL. A Thermo Spectronic Helios Gamma spectrophotometer was used to determine aqueous ozone concentrations with Indigo method [Bader and Hoigné, 1981]. Special attention was paid to avoid ozone stripping by injecting the aqueous ozone directly into the Indigo and by submerging the tip of the needle into the Indigo solution.

4.2.3.2. UPLC Analyses

*p*CBA was analysed at the Laboratory of Chemistry and Chemical Engineering of the ENSCR (Rennes). The samples were filtrated through 0.2 µm GHP Waters© filters before analysis by UPLC coupled to mass detection. A Waters© Acquity – Bridged Ethyl Hybrid C_{18} Reverse Phase column was used. Table **3** summarises the method and transitions for *p*CBA. The composition of the eluant was: UPW 9:1Acetonitril (ACN). Quantification limit was inferior to 1 µg.L^{-1}. No preconcentration step was needed.

Table 3 Analysis of *p*CBA by UPLC: main parameters

Compound	Method type	Main mass transition	Cone energy (V)
*p*CBA	Isocratic	155 > 111	20

4.2.3.3. Other Analyses

TOC was measured on each matrix before ozonation. The measurements were performed at Centre for Environmental Analysis – Saint-Maurice (CAE-SM), and confirmed by additional analyses carried out in the lab at ENSCR. Quantification limit was 0.5 mg.L^{-1}. UV_{254} was measured with the Thermo Spectronic Helios Gamma spectrophotometer. pH was measured with Knick Portamess pH meter, model 751.

4.2.4. Experiments Performed

4.2.4.1. Experimental Factors

Experimental factors were chosen according to their influence on ozone and hydroxyl radical concentration profiles. Reported in the literature, the main influences are attributed to: radical scavenger concentration, pH, temperature, ozone dose, NOM concentration. Accordingly, representative levels for these factors were set (table **4**), on which subsequent designs of experiments were based.

Table 4 Values for the experimental factors of the designs of experiments

Experimental Factor	Means/Method	Level 1	Level 2
Radical scavenging	*Tert*-butanol adding	No adding	10 mM adding (excess)
pH	Nitric acid adding	Natural pH	Natural pH - 1
Temperature	Thermostatic bath	20 °C / 19 °C	5 °C / 13.5 °C
Ozone Dose	Volume of aqueous ozone injected	~1.7 mg.L^{-1}	~2.4 mg.L^{-1}
NOM concentration	Water dilution with ozonated and deozonated UPW	No dilution	1:2 dilution

In the following, details on the experimental methods used are given:

- *tert*-butanol is a classical radical scavenger widely used in the literature (see *e.g.* [Staehelin and Hoigné, 1985]) when authors are willing to assess the relative importance of molecular phenomena. Concentrations ranging from 0.1 to 10 mM are generally used ([von Gunten and Hoigné, 1994]; [Xiong and Legube, 1991]). A high concentration (10 mM) was selected in this study in order to guarantee total scavenging of radicals for all waters, even for waters with low alkalinity where "natural" scavenging by carbonate species is weak;
- pH was adjusted adding nitric acid, due to its relatively inert character towards ozone and hydroxyl radicals (sulphuric acid can also be used, even when potentially forming sulphate radicals; phosphoric acid should be avoided, according to chapter **1**, **1.7.1.**);
- the volumes of injected ozone varied between 7 mL and 10 mL when having dissolved ozone at room temperature, and between 3 mL and 5 mL when having dissolved ozone at low temperature;
- the temperature of the cooling bath depicted in figure **3** was maintained using a RE 106 Lauda Ecoline Cryostat. The temperatures of 19°C and 13.5°C were used only in the first design of experiments; the values were set respectively at 20°C and 5°C afterwards.
- water samples were generally prepared the day preceding the experiments and stored in a fridge at 2°C. For experiments at room temperature, the samples were taken from the fridge three hours before being distributed in the gas-tight syringes. For experiments at low temperature, water samples from the fridge were directly distributed in the syringes. Then, the syringe were disposed on the stirring plates and, if necessary, in the thermostatic bath. After one hour stirring, the experiments were launched. Temperatures were closely followed during testing phases and temperatures inside the syringe appeared to be exactly those of the thermostatic bath, or of the room.
- dilution of natural water was done with UPW, ozonated and deozonated (under N_2 bubbling) beforehand, thus having an ozone demand as low as possible. The alkalinity was readjusted adding a calculated amount of hydrogenocarbonate ions (carbonate ions were added only when pH was above 8);
- results of the first design of experiments indicated that it was irrelevant to add *p*CBA to experiments where *tert*-butanol had been already injected. Therefore, *p*CBA was only added to experiments for which radicals were not scavenged; concentrations ranged from 50 $\mu g.L^{-1}$ to 90 $\mu g.L^{-1}$, representing $3.2.10^{-1}$ µM to $5.7.10^{-1}$ µM.

The levels of the experimental parameters were chosen in accordance with engineering issues, so that experimental conditions were likely to be encountered on-site. Several designs of experiments were built on the base of these experimental parameters; they are presented in the next paragraphs.

4.2.4.2. First Design of Experiments

First experiments were done with Méry-sur-Oise and Maisons-Laffitte waters. Main goal was to investigate all possible combinations of physicochemical effects, thus adopting a full factorial experimental design approach. The overview of the experiments done for natural NOM concentration is presented in table **5**. Likewise, the same experiments as those presented in table **5** were done with NOM diluted water. Using a full factorial design of

experiments with five parameters and two levels represents $2^5 = 32$ experiments, performed within two weeks. Seven contact times were considered for each experiment.

Table 5 Overview of the first design of experiments for natural NOM concentration

Experiment #	1	2	3	4	5	6	7	8	9	10	11	12	13	14	15	16
Scavenger adding		X		X		X		X		X		X		X		X
pH drop			X	X			X	X			X	X			X	X
Large O_3 dose					X	X	X	X					X	X	X	X
Temperature drop									X	X	X	X	X	X	X	X

4.2.4.3. Second Design of Experiments

Based on initial modelling results obtained with the first design of experiments, it was decided to simplify the full factorial design by suppressing experiments, which were modelled very satisfactorily. This led to the definition of a second design of experiments comprising 14 experiments (table **6**), which was applied to the following waters: Vitré, Annet-sur-Marne, Meulan, Beaufort, Trondheim. Moreover, temperature level # 2 was set at 5°C to better bring out temperature dependence (valid for each subsequent design of experiments). Again, seven contact times per experiments were considered.

Table 6 Overview of the second design of experiments

Experiment #	1	2	3	4	5	6	7	8	9	10	11	12	13	14
Scavenger adding		X		X				X		X		X		X
pH drop			X	X					X	X	X	X	X	X
Large O_3 dose					X	X							X	X
Temperature drop						X	X	X	X	X				
NOM dilution											X	X	X	X

4.2.4.4. Third Design of Experiments

Simplifying in turn the second design of experiments, and reintroducing two experiments of the first design of experiments, a third one was proposed with ten experiments (table **7**). It was applied to: Annet-sur-Marne 2, Annet-sur-Marne 3, Meulan 3, Vitré 3. Seven contact times were also considered for these experiments.

Table 7 Overview of the third design of experiments

Experiment #	1	2	3	4	5	6	7	8	9	10
Scavenger adding		X					X	X		
pH drop			X		X			X		X
Large O_3 dose				X	X					X
Temperature drop						X	X		X	
NOM dilution								X	X	X

4.3. Chemical Kinetics Models

4.3.1. Introduction

Following the conclusions of the review presented in chapter **1**, a SBH-based mechanism was considered for the self decomposition of ozone and classical reactions were gathered to model the reaction of ozone with inorganic carbon. A semi-empirical model for the role of NOM during ozonation was developed. In this section, all the chemical phenomena considered for the modelling of natural water ozonation are presented. Additionally, all the reactions are presented in Appendix **D**, with their respective kinetics.

4.3.2. Ozone Self-Decomposition

The mechanism used for ozone self-decomposition derives from the one proposed by [Mizuno *et al.*, 2007c], which can be seen as the latest of the SBH-based models. Two minor modifications were however performed:

- [Mizuno *et al.*, 2007c] have proposed equations **1** and **2** as initiation steps for ozone self decomposition, thus combining two different hypotheses emitted by [Staehelin and Hoigné, 1982] for initiation. This combination is not frequently used, as reaction **2** is likely never to happen when associated to reaction **1**: $^{\bullet}HO_2$ readily transforms into $^{\bullet}O_2^-$ (pK_A=4.8) and further in $^{\bullet}O_3^-$, which finally leads to $^{\bullet}OH$ (according to the self decomposition pathway). HO_2^- can only be formed *via* acid-base equilibrium with hydrogen peroxide, but in very small quantities given the high value of the pK_A=11.6.

$$O_3 + HO^- \rightarrow {}^{\bullet}O_2^- + {}^{\bullet}HO_2 \quad \textbf{(1)}$$

$$HO_2^- + O_3 \rightarrow {}^{\bullet}OH + {}^{\bullet}O_2^- + O_2 \quad \textbf{(2)}$$

  Now, recent studies on ozone self-decomposition ([Hassan *et al.*, 2003]; [Mizuno *et al.*, 2007c]; [Vandersmissen *et al.*, 2008]; [Lovato *et al.*, 2009]) have insisted on the importance of hydrogen peroxide (under protonated and ionic forms) in ozone self-decomposition. We therefore proposed to keep equation **2** as initiation and to combine it with TFG initiation, yielding the following two-stage initiation (equations **3** and **4**). Despite the very high pK_A of hydrogen peroxide, equation **4** is kinetically possible due to the large concentration of ozone.

$$O_3 + HO^- \rightarrow HO_2^- + O_2 \quad \textbf{(3)}$$

$$HO_2^- + O_3 \rightarrow {}^{\bullet}OH + {}^{\bullet}O_2^- + O_2 \quad \textbf{(4)}$$

- The reaction **5** was removed because it is unlikely to occur, due to its low reactivity ($k(293\ K) = 6.5.10^{-3}\ M^{-1}.s^{-1}$).

$$O_3 + H_2O_2 \rightarrow H_2O + O_2 \quad \textbf{(5)}$$

The complete mechanism, with the kinetics of the reactions, is given in Appendix **D**.

4.3.3. Reactions With Inorganic Carbon

Most reactions found in literature have been considered in this study. However, reactions including hydrogenocarbonate radical were removed, due to its minor role (see chapter **1**, **1.4.2.**). The acid-base equilibrium **6** was considered. The values of the kinetic constant rates for acid-base equilibria were partially recalculated, classically based on the reported values for pK_A and protonation constants (see chapter **1**, equation **17**). The complete mechanism, with the kinetics of the reactions, is given in Appendix **D**.

$$^{\bullet}CO_3^- + H^+ \leftrightarrow {}^{\bullet}HCO_3 \quad \textbf{(6)}$$

4.3.4. Reactions With NOM

On one hand, it is well known that a large part of NOM found in natural waters is composed by organic acids (humic, fulvic, tannic acids etc.). On the other hand, NOM can play different roles reacting with molecular ozone as consumer or radical initiator, but also reacting with radicals as chain-promoter or chain-scavenger. The model used in this study is based on these observations and can be seen as a new version of the model for NOM presented in [Savary 2002]. Consequently, NOM was divided into three fractions (consumers, initiators, promoters) and six species (two for each fraction). The reactivities of the species ($NOM^d{}_a$, $NOM^d{}_b$, $NOM^i{}_a$, $NOM^i{}_b$, $NOM^p{}_a$ and $NOM^p{}_b$) had to be calibrated. The scavenging effect of NOM was considered negligible compared to that of carbonate/hydrogenocarbonate in the

waters investigated following the conclusions of [Savary, 2002]. The reactions of NOM are summarised in table **8**.

Table 8 Reactions with organic matter

Type (NOM fraction)	Reaction
Direct consumption (consumers)	$NOM^{d} + O_3 \rightarrow products$
Chain initiation (initiators)	$NOM^{i} + O_3 \rightarrow {}^{\bullet}OH + products$
Chain promotion (promoters)	$NOM^{p} + {}^{\bullet}OH \rightarrow {}^{\bullet}O_2^{-} + products$
Acid-base equilibrium	$NOM_a^{d,i,p} \xleftrightarrow{K_A^{d,i,p}} NOM_b^{d,i,p} + H^+$

In order to describe the acid character of the NOM fractions presented in table **8**, a pK_A was defined for each fraction. Each fraction was thus distributed over two species (acid or base). Because many organic compounds have pH-dependent kinetics in their reactions with ozone, one of the species was considered having a negligible reactivity. For example, formic and glycoxylic acids have pH-dependent kinetics [Staehelin and Hoigné, 1985]. Similarly, [Poznyak and Araiza, 2005] showed that phenol degradation is pH-dependent.

The reactive species of each NOM fraction was determined by preliminary optimisations such as those presented in section **4.6**. For a given fraction, only one species was considered and the initial concentration was determined for two different pHs. If the concentration was found to increase with pH, the basic species was selected; otherwise, so was the acid species. The reactive species were assumed to be the same among water samples (collected at different times) from the same water resource.

Moreover, temperature effects were modelled through the adjustment of three energies of activation. In the end, 12 model parameters have to be adjusted to fit simulations to experimental data: 3 kinetic constants, 3 initial concentrations, 3 pK_A and 3 energies of activation. More precisely, pK_A are not directly determined, but the frequency factor $k_{0,depro}$ of the deprotonation; a value of 10^6 $M^{-1}.s^{-1}$ being assumed for the protonation kinetic constant. Initial concentrations are determined for pH=7.

4.3.5. Other Reactions

Kinetics for *p*CBA and *tert*-butanol are given in table **9**. Considering the experimental uncertainty for the determination of the kinetics of *p*CBA's reaction with hydroxyl radical, it was decided to slightly alter the value of 5.10^9 $M^{-1}.s^{-1}$ proposed by [Neta and Dorfman, 1968]. Based on the experimental results gathered all along this study, the value was optimised and set at $7.9.10^9$ $M^{-1}.s^{-1}$.

The reaction rate constants determined by [Neta and Dorfman, 1968] may vary with pH and *p*CBA concentration. The authors reported for benzoate ion a slight increase of the indirect oxidation constant with pH and/or when benzoate concentration decreased. For example, at pH=6, the rate constant increased from $4.8.10^9$ $M^{-1}.s^{-1}$ to $7.2.10^9$ $M^{-1}.s^{-1}$ when benzoate concentration decreased from 60.5 $mg.L^{-1}$ to 24.2 $mg.L^{-1}$. The authors studied *p*CBA degradation at comparable concentrations (~10^{-4} M). In this study however, initial *p*CBA concentrations were kept below 120 $\mu g.L^{-1}$. Under this experimental conditions, a slight increase from 5. 10^9 $M^{-1}.s^{-1}$ to 7.9. 10^9 $M^{-1}.s^{-1}$ of the kinetic constant of *p*CBA is reasonable.

Table 9 Kinetic data for the hydroxyl radical scavengers

Type	Reaction	Kinetic constant value (293K)	Reference
***p*CBA**	Direct oxidation	$1.5.10^{-1}$ $M^{-1}.s^{-1}$	[Hoigné and Bader, 1983a]
	Indirect oxidation	$7.9.10^9$ $M^{-1}.s^{-1}$	This study
***tert*-BuOH**	Direct oxidation	3.10^{-2} $M^{-1}.s^{-1}$	[Hoigné and Bader, 1983b]
	Indirect oxidation	6.10^8 $M^{-1}.s^{-1}$	[Buxton *et al.*, 1988]

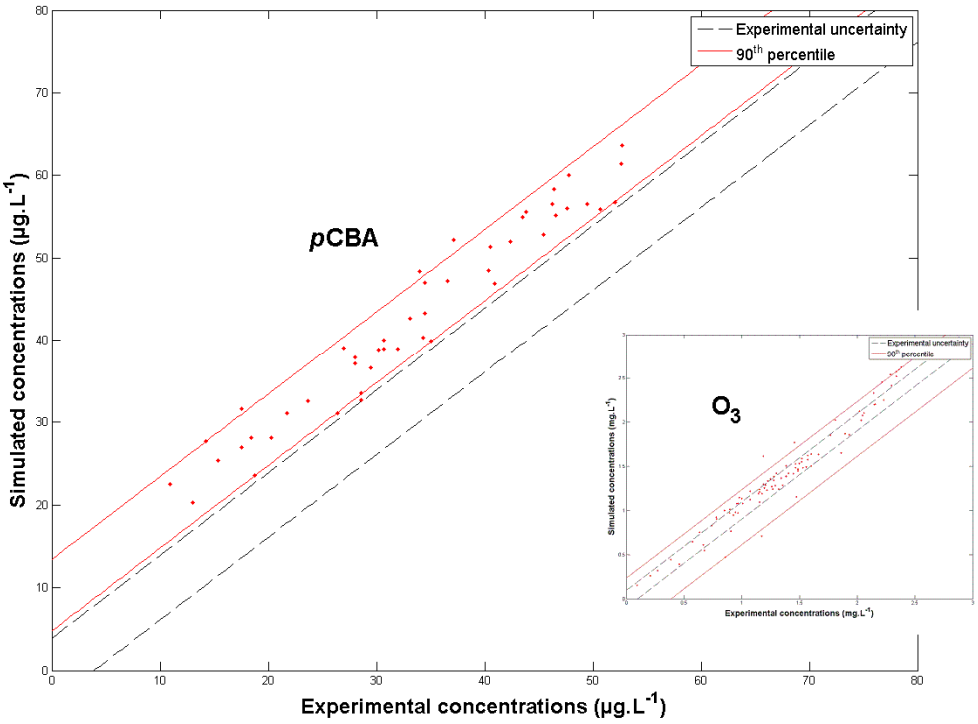

Figure 6 Compared simulation and experimental results for Annet-sur-Marne water for *p*CBA and ozone (insert graph); literature value for indirect oxidation of *p*CBA (5.10^9 $M^{-1}.s^{-1}$)

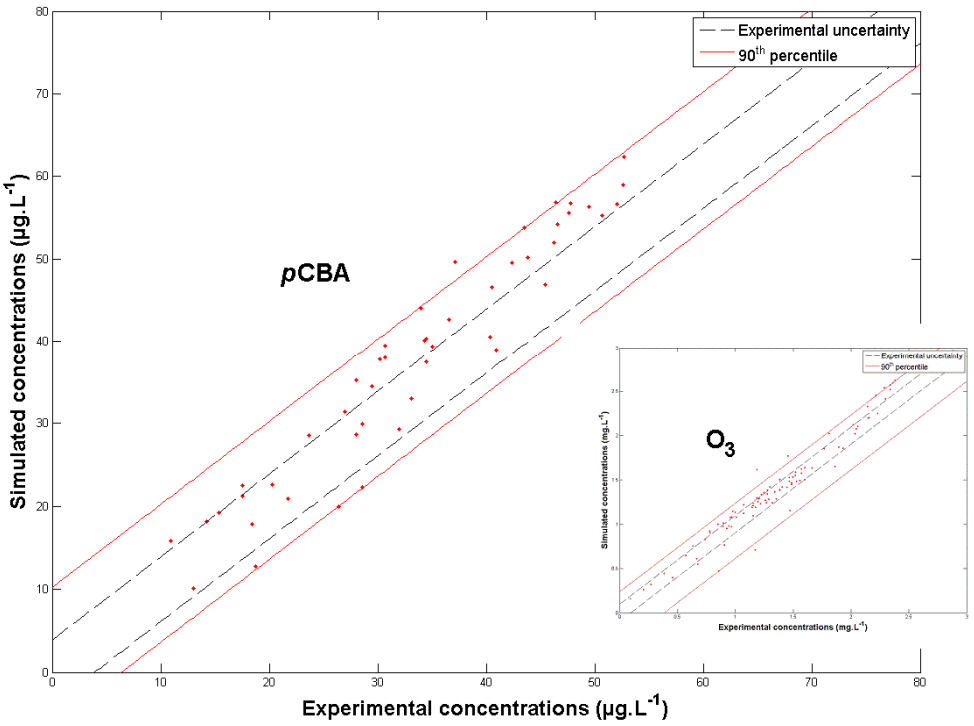

Figure 7 Compared simulation and experimental results for Annet-sur-Marne water for *p*CBA and ozone (insert graph); optimised value for indirect oxidation of *p*CBA ($7.9.10^9$ $M^{-1}.s^{-1}$)

The slight increase in the kinetic constant value for *p*CBA was moreover supported by modelling results. An example is given in figures **6** and **7** for Annet-sur-Marne water sample, for which the simulations have been done with the literature value and the optimised value, respectively. Modelling results show that this kinetic modification has major impact on *p*CBA, while modelling results for ozone remain unchanged.

4.3.6. Energies Of Activation

Energies of activation were given to all reactions taken from the literature for which the values were missing. Reactions were classified and values were assumed, according to table **10**. The assumptions are the same as those of [Savary, 2002], except for acid-base equilibria.

Table 10 **Energies of activation for the reactions taken from the literature**

Reaction type	Energy of activation
Molecular reaction	42 kJ.mol^{-1}
Radical reaction involving organic species	15 kJ.mol^{-1}
Radical reaction involving mineral species	7.5 kJ.mol^{-1}
Reaction between radical species	0 kJ.mol^{-1}
Acid-base equilibria	0 kJ.mol^{-1}

Considering the acid/base equilibrium presented in equation **7**, Savary linked thermodynamic (ΔH) and kinetic (E_A) parameters according to equation **8**. The energy of activation of the protonation reaction was assumed equal to zero and the energy of activation of the deprotonation calculated. Calculated values for energies of activation were always lower than 16 kJ.mol^{-1}, which is quite low compared to other molecular reactions. An energy of activation of 16 kJ.mol^{-1} lowers the kinetic constant value by 30% when passing from 20°C to 5°C. The same effect is obtained by a change of 0.15 in pH (experimental uncertainty of 0.1 on pH measures). Temperature dependence was therefore neglected in this study.

$$AH \leftrightarrow A^- + H^+ \begin{cases} AH \xrightarrow{k_{depro}} A^- + H^+ \\ A^- + H^+ \xrightarrow{k_{pro}} AH \end{cases} \quad \textbf{(7)}$$

$$K_A = K_{A,0}.e^{\frac{-\Delta H}{RT}} = \frac{k_{depro}}{k_{pro}} = \frac{k_{0,depro}}{k_{0,pro}} e^{\frac{E_{A,pro}-E_{A,depro}}{RT}} \quad \textbf{(8)}$$

4.3.7. Initial Concentrations for the Simulations

Most initial concentrations being unknown, they were set to default values according to table **11**. The initial concentration of hydroxyl radicals was set according to classical values for the R_{ct} [Elovitz and von Gunten, 1999].

Table 11 **Energies of activation for the reactions taken from the literature**

Species or type of species	Initial concentration (µM), $[O_3]$ in µM
Neutral radicals	10^{-10}
Basic radicals	10^{-10}
Acid radicals	At equilibrium with basic radicals
Hydroxyl radicals, •OH	$[O_3].10^{-8}$
Hydrogen peroxide	Dilution factor.4.exp($[O_3]$.0.03)

Hydrogen peroxide may be formed during the preparation of aqueous ozone, when ozone bubbles into UPW and decomposes. Therefore, an estimate of the initial hydrogen peroxide concentration was yielded by simulating the decomposition of ozone into UPW at pH=7. An exponential relation was found between ozone and hydrogen peroxide concentrations and then applied to all subsequent simulation for the ozonation of natural waters. The dilution factor (cf. table **11**) equals the ratio of the volume of injected aqueous ozone to the total volume of the reactor (100 mL).

4.4. Defining and Testing the Identification Procedure

4.4.1. Definition of the Identification Procedure and Methods Used

Following the conclusions of chapter **3**, techniques were selected for the parameter identification. Details on the solving procedures are given in the following paragraphs.

4.4.1.1. Reparameterisation

Parameters were classically redefined in order to minimise correlations. Working with two experimental temperatures, the parameters were reparameterised according to equations **25** to **27** from chapter **3**.

4.4.1.2. Parameter Estimation and Objective Function

Weighted least squares estimation was used in this study. Given that modelling results had to be compared to experimental measurements with different scales (ozone and *p*CBA), a relative measure was selected. The objective function is given in equation **9**.

$$O(\theta) = \sum_{i=1}^{l} \left(\frac{Y_{\exp,i} - Y_{sim,i}(\theta)}{Y_{\exp,i}.\sigma_{\exp,i}} \right)^2 \qquad \textbf{(9)}$$

4.4.1.3. Explorations with Latin Hypercube Sampling (LHS)

LHS was performed with the Matlab™ built-in function *lhsdesign*. Uniform distributions were always assumed for the parameters and the sampling scheme was generated in order to maximise the distance between points. In a first time, 2^m points – that is, 4096 points for 12 parameters – were systematically explored. The boundaries for the first exploration were set according to table **12**. Then, the distribution of the best points of the first exploration was graphically analysed and subsequent explorations on reduced parameter spaces were launched.

Table 12 Ranges for the parameter values, LHS first exploration

Parameter type	Initial guess	Lower bound	Upper bound
Frequency factor	k_0	$k_0/10$	$10.k_0$
Energy of activation	E_A	E_A-3000	E_A+3000
Initial concentration	$[]_0$	$[]_0/5$	$5.[]_0$

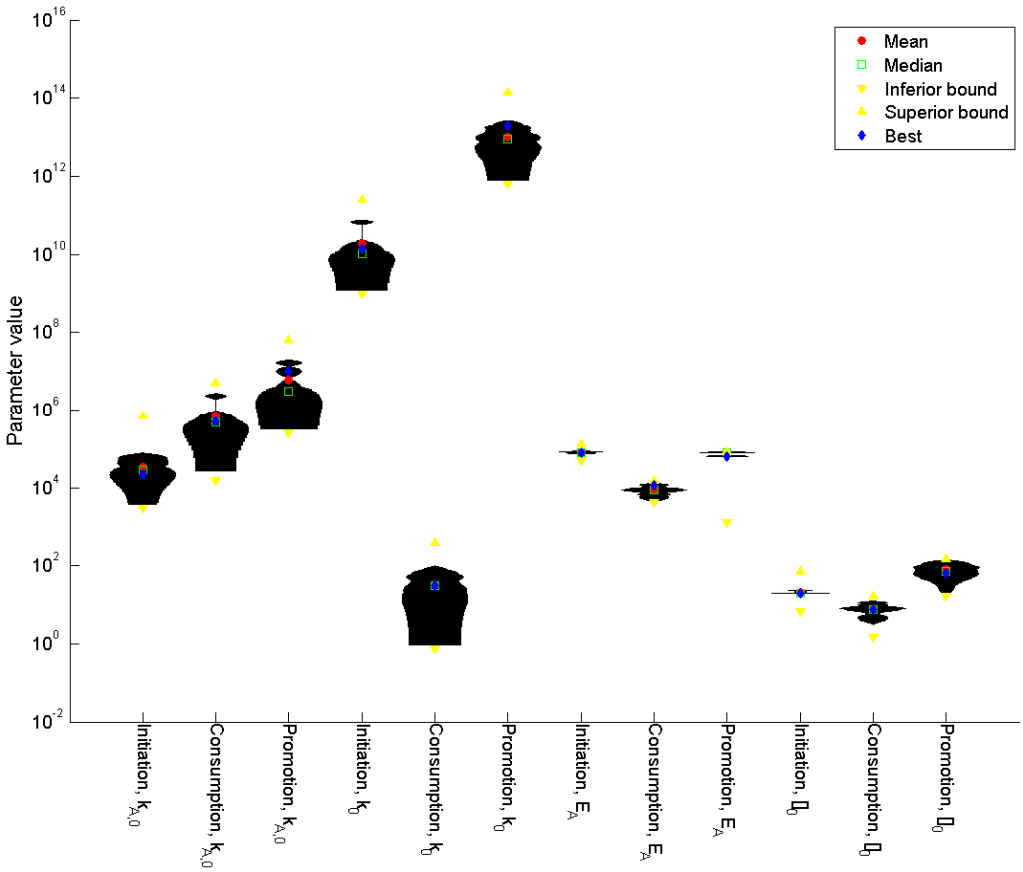

Figure 8 Example of distribution plot of the parameter values for the best points after first exploration, Annet-sur-Marne 2 water

An example of distribution plot for graphical analysis of the exploration by LHS is given in figure **8**. The points, for which the objective function does not exceed by more than 10% the lowest value of the objective function (best point), are represented. In the case of figure **8**, 14 points were considered. For each parameter, a patch represents the distribution of values taken for that parameter (for each patch, 14 points were thus considered). Considering a single patch, the density of the values of the points is proportional to the width of the patch. The best point is also represented and its position within the distribution is analysed. For example, on figure **8**, the value of the initial concentration for the initiating fraction (10th parameter) appears to be critical since no other value than the value for the best point has led to satisfactorily results. On the contrary, the initial concentration for the promoting fraction (12th parameter) appears to be quite arbitrary. Considering the energy of activation for the promoting fraction, the best point has a value comparable to the lower bound. Accordingly, a subsequent exploration can be performed on a reduced parameter space (lowering the upper bound of the first 6 parameters and fixing the initiation energy of activation and initial concentration; initial concentration for the promoting fraction will also be fixed).

4.4.1.4. Optimisation with Nelder-Mead Method

The best promising point determined by LHS exploration is optimised. Details on the Nelder-Mead method used in this study can be found in chapter **3**, **3.5.2.** and in [Lagarias *et al.*, 1998]. Termination tolerance on the objective function value was manually set at 0.01. The other solving criteria were set at their default values:

- maximum number of function evaluations and maximum number of iterations were set at 200.m ;
- tolerance on the values of the parameters was set at 0.0001.

4.4.1.5. Genetic Algorithm (GA)

The Non-Dominated Sorting Genetic Algorithm-II (NSGA-II), originally proposed by [Deb *et al.*, 2000] was used in this study. A population size of 100, which varied over 600 generations, was considered. In total, the objective function was evaluated 6000 times. The other solving criteria are very robust and provide solid performance on most problems [Béraud *et al.*, 2009]. They were consequently set to their default value for all optimisations:

- probability of crossover was set at 0.9;
- probability of mutation was set at 0.1;
- index for the distribution of real values during crossover was set at 10;
- index for the distribution of real values during mutation was set at 20.

4.4.2. Practical Identifiability

4.4.2.1. Aim and Techniques Used

The *e*FAST variance-based technique for sensitivity analysis was applied (see chapter **3**, **3.3.2.3.**) to determine if the parameters of the NOM model may be identifiable and if some parameters could be determined independently from the others. Such a sequential calibration is possible if the objective function is particularly sensitive to the values of a reduced group of parameters. The *e*FAST code used in this study originates from the work of [Ekström, 2005]. It has been slightly modified in order to be compatible with already coded features and it calculated the sensitivity of the objective function relatively to the parameters of the model.

Correlations among parameters were roughly determined based on the physical reality of the model. Thus, parameters appearing as product in the model formulation or parameters acting on the same part of the system can be considered as correlated. For example, parameters referring to the same NOM fraction are considered as correlated and have therefore to be determined simultaneously. Consequently, the original set of parameters, without reparameterisation was considered.

Overtaking the notations of the chapter **3** (paragraph **3.3.2.3.**), a minimum value of 65 was chosen for the expression $2M\omega_{max}+1$; *resampling* was performed once ($N_r=2$). Consequently, the computational cost to obtain all first and total order sensitivity indexes corresponded to 1560 iterations ($m.(2M\omega_{max}+1).N_r$). This is in agreement with the recommendations of [Saltelli *et al.*, 1999] (details can be found in chapter **3** paragraph **3.3.2.3.**).

The chemical and hydraulic models used for this study are those used when calibrating the model for the role of NOM (corresponding to the experiments done in the gas-tight syringe).

4.4.2.2. Sensitivity Analysis Results

Two types of problems were analysed: pseudo-theoretical problems and real problems, for which the solution of the parameters is respectively known and unknown. Knowing exactly the solution is useful in order to concentrate on the behaviour of the objective function around its minimum. Real problems give a general overview on a realistic parameter space. Each parameter i to be identified is characterised by the sensitivity of first order S^i and the total order sensitivity index $S_T{}^i$.

Pseudo-theoretical Problems: Focusing on the Optimum

Pseudo-theoretical problems are problems for which an exact solution for the parameter set θ exists. Actually, the experimental concentrations used as references in the identification

process were recreated, based on the knowledge of *a priori* values for the parameters to be identified. Pseudo-theoretical problems were thus generated based on altered experimental results for the experiments done with Maisons-Laffitte water and Annet-sur-Marne water. The same experimental conditions were considered, so that 32 and 14 sets of concentrations for both *p*CBA and ozone were respectively created for Maisons-Laffitte and Annet-sur-Marne waters. Additionally, the range of the parameter space explored during sensitivity analysis was varied: for Annet-sur-Marne water, the parameter values were kept at ± 5% and ± 10% of their optimal values; for Maisons-Laffitte water, parameter values were kept at ± 10% of their optimal values. These ranges were chosen to focus on the optimum zone. As illustration, we give in figure **9** the results obtained with Annet-sur-Marne water for parameters kept at ± 5% of their optimal values. On the figure, both sensitivities S^i and $S_T{}^i$ have been reproduced. Similar distributions were observed at ± 10% and for Maisons-Laffitte water.

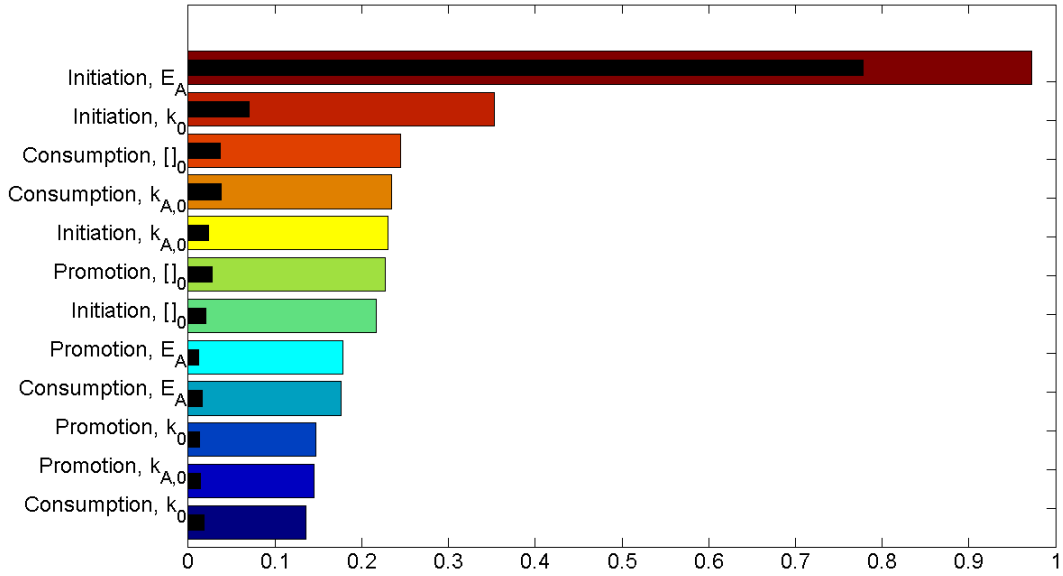

Figure 9 Total order sensitivity indexes $S_T{}^i$ (coloured bar) and first order sensitivity indexes S^i for a pseudo-theoretical problem, Annet-sur-Marne altered results, parameters at ± 5% of their optimal values

Real Problems: Determining the Importance of Parameters

The sensitivities of the model parameters were assessed with three experimental data sets, obtained with water samples originating from Meulan, Beaufort and Vitré. The parameter values varied in much larger parameter spaces than those previously explored. The ranges were chosen according to the spaces explored by the LHS technique (see table **12**). We give in figure **10** the results of the *e*FAST applied to Vitré water. The corresponding ranges for parameter values are gathered in table **13**. Similar distributions were observed for Meulan and Beaufort waters.

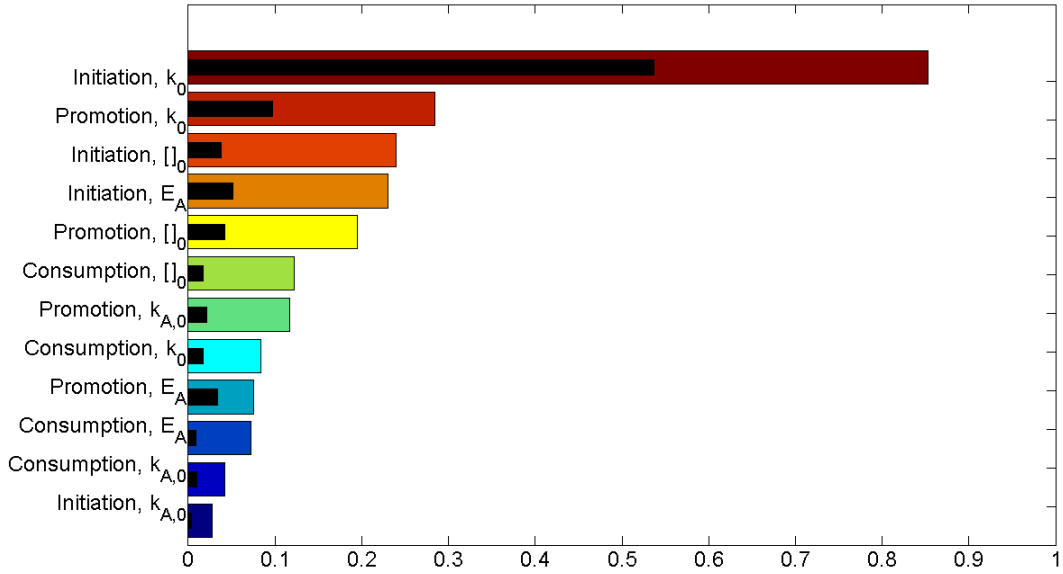

Figure 10 Total order sensitivity indexes S_T^i (coloured bar) and first order sensitivity indexes S^i for a real problem, Vitré water, large domain for parameter values

Table 13 Ranges for parameter values for *e*FAST, Vitré water

Minimum	Maximum	Type of parameter	Fraction
$1.11.10^2$	$1.11.10^4$	Frequency factor for: $NOM_a \rightarrow NOM_b + H^+$	Initiation
$1.39.10^2$	$1.39.10^4$		Consumption
$3.11.10^4$	$3.11.10^6$		Promotion
$1.35.10^3$	$1.35.10^5$	Frequency factor for initiation, consumption or promotion by NOM.	Initiation
$9.36.10^{28}$	$9.36.10^{30}$		Consumption
$7.44.10^6$	$7.44.10^8$		Promotion
$5.05.10^4$	$5.45.10^4$	Energy of activation for initiation, consumption or promotion by NOM.	Initiation
$1.75.10^5$	$1.79.10^5$		Consumption
$1.80.10^4$	$2.20.10^4$		Promotion
$2.84.10^1$	$1.14.10^2$	Initial concentration for the considered fraction at pH=7.	Initiation
2.19	8.75		Consumption
9.17	36.7		Promotion

Summary

The results obtained with pseudo-theoretical and real problems were averaged and are summarised in figure **11** and **12**, respectively. The two types of problem bring similar conclusions, to a different extent though:

- NOM fractions which contribute mainly in the modification of the concentration profiles for ozone and *p*CBA, are the initiating and consuming fractions. Promoting fraction plays a smaller role: given its low sensitivity indexes, determination of its parameters may not be accurate;
- The acidity of the NOM fractions may only play a minor role, refining the value of the initial concentration at pH=7.

The parameter space explored in the case of the pseudo-theoretical problems favours the energy of activation of the initiating fraction. In the case of real problems, parameter sensitivities are more balanced.

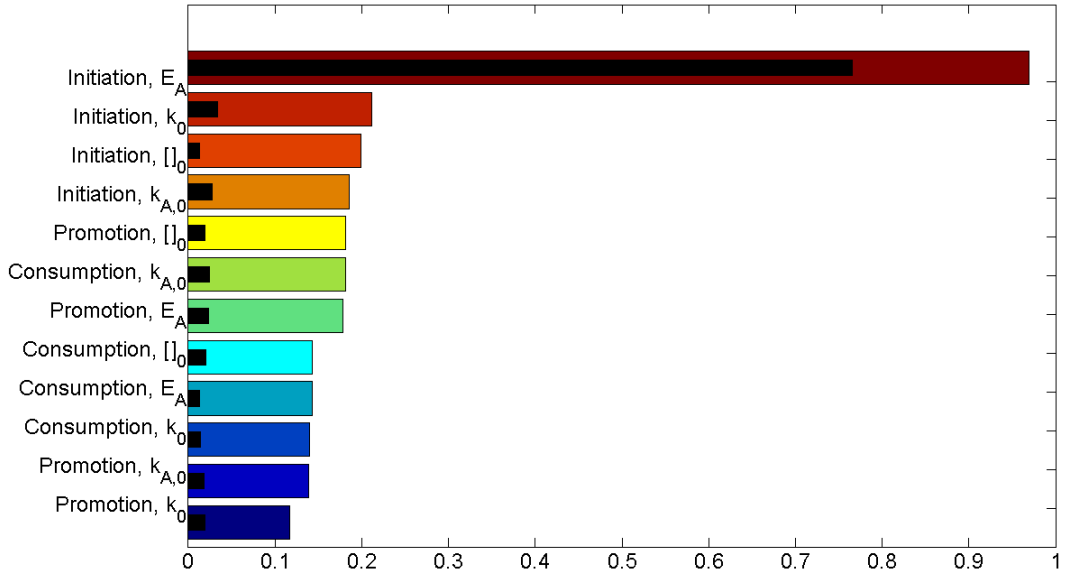

Figure 11 Average total order sensitivity indexes S_T^i (coloured bar) and first order sensitivity indexes S^i for the pseudo-theoretical problems tested

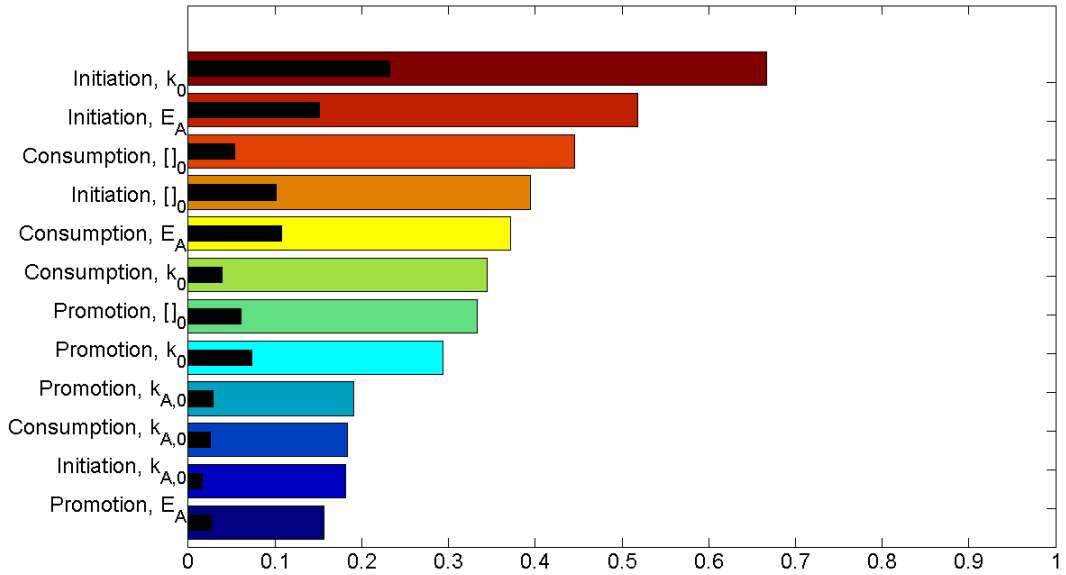

Figure 12 Average total order sensitivity indexes S_T^i (coloured bar) and first order sensitivity indexes S^i for the real problems tested

4.4.2.3. Conclusion

Sensitivity tests showed that (i) the initiation and consumption reactions are likely to have major influence on the concentrations of ozone and *p*CBA; (ii) the promoting fraction is likely to have minor influence on the same concentrations. Furthermore, the acidities of the NOM fractions may play minor roles compared to concentration values valid at pH=7.

As a consequence, a sequential determination of the parameters may be applied to the identification of the parameters of the model. The following steps shall be taken:

1. Exploration(s) for the parameters related to the initiating and consuming fractions;
2. Exploration(s) for the parameters related to the promoting fraction;
3. Optimisation for all the parameters.

Given the medium-low values for the sensitivity indexes of the consuming and promoting fractions, the identification of their parameters could be inaccurate. This sequential strategy shall be tested and compared to an unsequential determination in paragraph **4.6**.

4.4.3. Testing the Identification Procedure

4.4.3.1. Aim and Techniques Used

In order to evaluate the efficiency of the parameter identification procedure, a it was compared to two other procedures. The procedures involved are:

- Procedure #1: exploration(s) and optimisation (as presented in **4.4.1.** to **4.4.1.4.**);
- Procedure #2: sequential explorations and optimisation (as presented in **4.4.2.3.**);
- Procedure #3: genetic algorithms (as presented in **4.4.1.5.**).

These three identification procedures are applied to the same pseudo-theoretical problem, that is, the determination of the parameters of the model for the role of NOM (same chemical and hydraulic pathways).

4.4.3.2. Problem Statement

Similarly to paragraph **4.4.2.2.**, a pseudo-theoretical problem was considered and solved with the three techniques. The results were evaluated based on the agreement of simulated with experimental data and on the deviation from the exact solution. The ranges within which the parameters varied were the same as those used for the first exploration by LHS (presented in table **12**).

4.4.3.3. Results

Table **14** gathers the results for the three identification procedures. The values of the parameters for the exact solution are given; the values of the parameters determined by the three procedures are expressed as deviations (in percents) from the exact solution.

Table 14 Comparing the results of three parameter identification procedures

Deviation from the exact solution (%)					
Procedure #1	**Procedure #2**	**Procedure #3**	**Exact solution**	**Type of parameter**	**Fraction**
2.14	57.88	-3.62	$4.62.10^4$	Frequency factor for: $NOM_a \rightarrow NOM_b + H^+$	Initiation
-44.68	72.70	34.85	$3.29.10^5$		Consumption
-555.51	99.91	2280	$4.15.10^6$		Promotion
50.04	-3440.83	35	$1.73.10^{10}$	Frequency factor for initiation, consumption or promotion by NOM.	Initiation
82.52	38.77	-36.62	23.8		Consumption
-165.12	98.19	-45.91	$9.33.10^{12}$		Promotion
1.95	-8.27	0.81	$8.36.10^4$	Energy of activation for initiation, consumption or promotion by NOM.	Initiation
12.42	20.36	-24.09	$8.80.10^3$		Consumption
-1.45	15.19	-2.20	$5.72.10^4$		Promotion
-0.49	54.34	-0.95	30.0	Initial concentration for the considered fraction.	Initiation
-1.12	1.77	0.77	7.95		Consumption
45.48	26.44	7.77	66.6		Promotion
5759	1558	6000		Number of iterations (LHS+Nelder-Mead or NSGA-II)	
0.24	3.21	0.13		Final value of the objective function	

Although satisfactorily minimising the objective function, all the procedures have determined solutions, which, for some parameters, largely differ from those of the exact

solution. The deviation from the exact solution is generally higher when considering the promoting fraction. For the procedures #1 and #3, the values for the parameters of the initiating fraction are generally close to those of the exact solution. Both observations are in agreement with the results of the sensitivity analyses (**4.4.2.2.**). However, the parameter values determined by the procedure #2 for the initiating fraction are far from the optimal ones.

With a reduced number of iterations (1558 instead of 5759 and 6000, for the procedures #1 and #3, respectively), the procedure #2 has led to a sensibly higher value of the final objective function. This value appears high enough to induce small errors in the predictions of the model, especially for ozone (figure **13**); *p*CBA concentrations could be modelled satisfactorily (figure **14**).

Despite large variations from the exact solution for the values of the parameters, the procedure #2 gives reliable results: 94 % and 100 % of the simulated points are located within the experimental error bars, for ozone and *p*CBA respectively. This result confirms that physicochemical interpretations based on the values of the parameters should be avoided [Jeppsson, 1996].

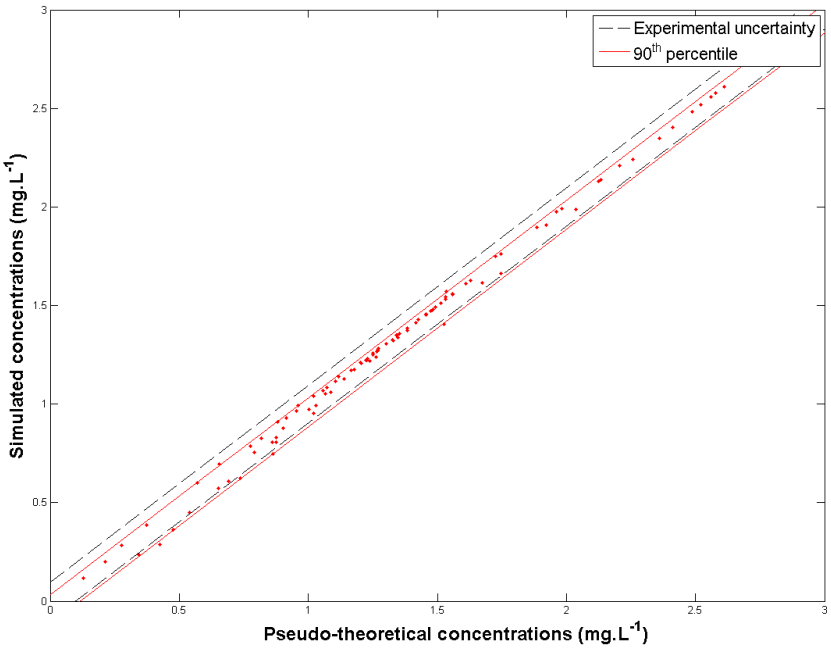

Figure 13 **Comparison of simulated and pseudo-theoretical ozone concentrations, procedure #2**

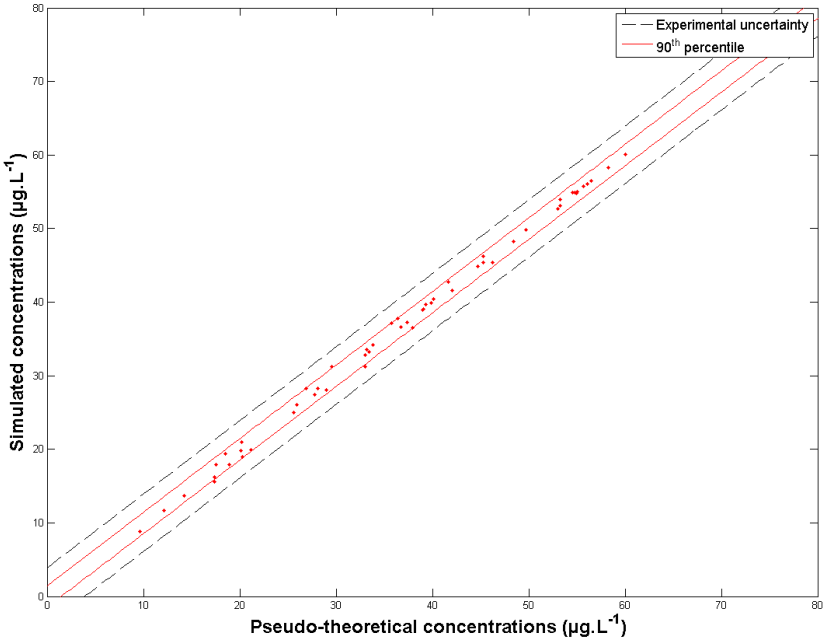

Figure 14 Comparison of simulated and pseudo-theoretical *p*CBA concentration, procedure #2

4.4.3.4. Conclusion

The procedure for determining the values of the parameters, which combines sampling and optimisation, appears to be reliable and comparable to another optimisation technique, genetic algorithms. However, the parameter values determined can be far from their optimal values.

With partially sequenced parameter identification, calibration is faster (average time per iteration is about 20 seconds) and results are of sufficient quality. Therefore, such calibration technique may be appropriate when one has an idea of the values of the parameters that shall be found. For example, sequenced calibration may be used for readjusting the model when dealing with the same water at different periods of the year. However, this has not been tested numerically.

4.5. Testing the Model

4.5.1. Qualitative Analysis of the Experimental Results

Qualitative analysis of the experimental results was performed while experiments were being done, in order to detect possible outliers. Experiments exhibiting abnormal characteristics were systematically done a second time, and the results compared with those obtained previously. Three experiments, out of the 134 comprised in the first and second designs of experiments, were thus done a second time. The results of the replicate experiments were always found consistent with the remaining set of experiments and were considered in lieu of the previous experiments.

Qualitative analysis showed that the global experimental data set (on all water samples) was consistent with already observed phenomena:

- if pH or temperature increases, so will the ozone decomposition rate;
- if tert-butanol is added or NOM is diluted, the ozone depletion will occur more slowly;
- large ozone doses generally enhanced the initial decomposition rates for both ozone and pCBA.

An example of such experimental influences is given in figure **15**, where different relative ozone concentration profiles for different experimental conditions have been drawn (Vitré water). Comparing the curves, temperature and radical scavenger adding effects are clearly to be seen; NOM dilution influence is also illustrated (TOC/2).

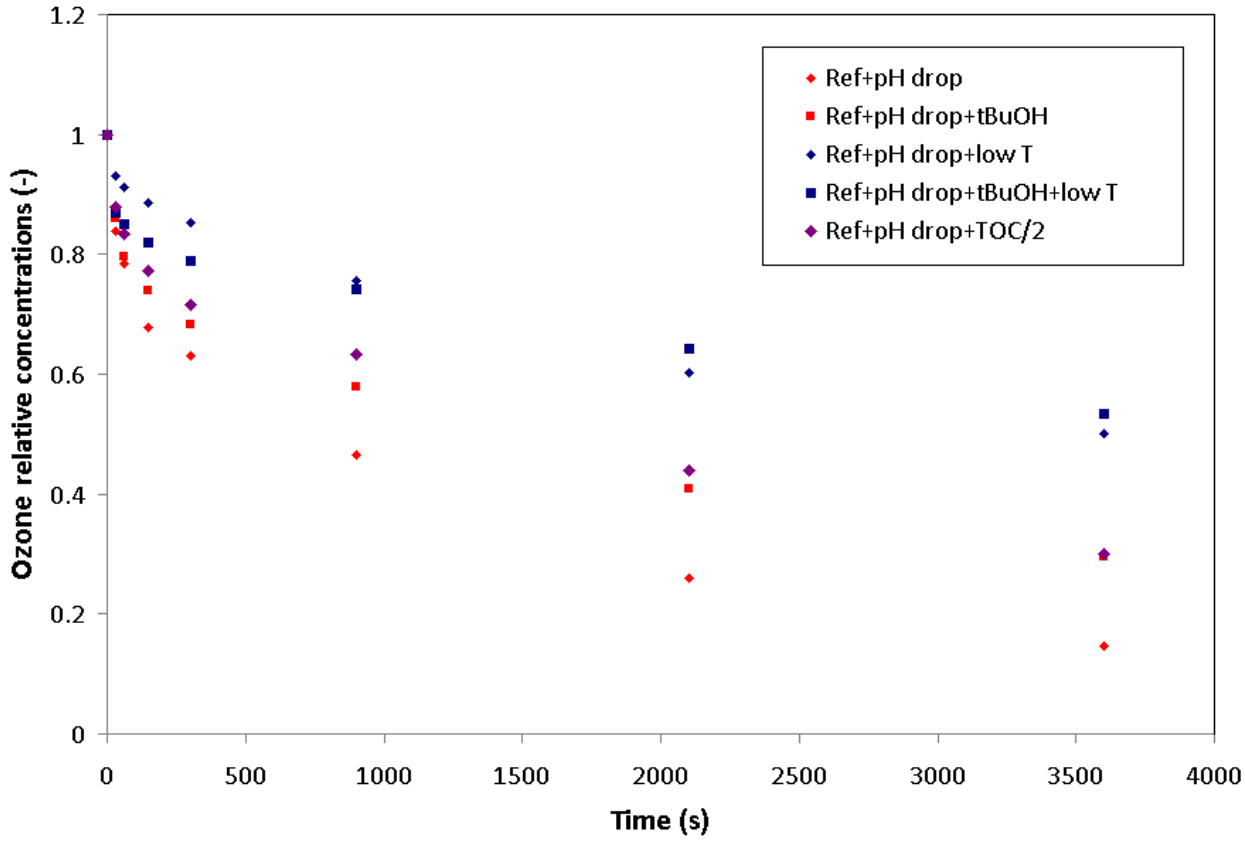

Figure 15 Typical depletion profiles for ozone, obtained under various experimental conditions for Vitré water

The initial decrease in *p*CBA concentration was generally more dramatic than the decrease for ozone concentration; however, this observation was reversed for water samples with a large inorganic/organic ratio. Studying instantaneous ozone demand (see chapter **1**, **1.5.5.**), authors have already reported similar trends: [Park *et al.*, 2001] and [Buffle *et al.*, 2006] concluded that initial ozone demand is mainly due to initiation reactions. Based on opposite observations, [Cho *et al.*, 2003] concluded that initial ozone demand is mainly due to direct consumption of ozone by NOM. Based on our experimental results, 10 of 11 water samples showed a sharper initial decrease for *p*CBA, thus supporting the conclusions of Park and Buffle. Sharper initial decreases for ozone were obtained only with Meulan water, for small ozone doses: for example, compare the profiles for ozone and *p*CBA in figure **24**. Moreover, on Meulan water, the addition of a scavenger as *tert*-butanol does not have major impact on the concentration of ozone: compare figure **24** and **25**. Such behaviour can be explained by the fact that inorganic content (6.24 meq.L^{-1}) is extremely high compared with organic content (0.9 mgC.L^{-1}). Under such conditions, hydrogenocarbonate and carbonate ions are likely to play a major role inhibiting the hydroxyl radical formed and therefore competing with *tert*-butanol.

4.5.2. Main Results

4.5.2.1. Examples of Results

We show in this paragraph how the model is able to take into account experimental changes. A selection of simulated experiments illustrates the possibilities of the model to simulate changes in: contact time with ozone, ozone dose, temperature, pH, NOM content and NOM nature. The references of the experiments can be found in tables **5** and **6**. The experimental uncertainties, determined with experiment replicates performed during the first design of experiments are following: ±0.1 $mg.L^{-1}$ for ozone and ±4$\mu g.L^{-1}$ for *p*CBA.

■ Change in ozone dose

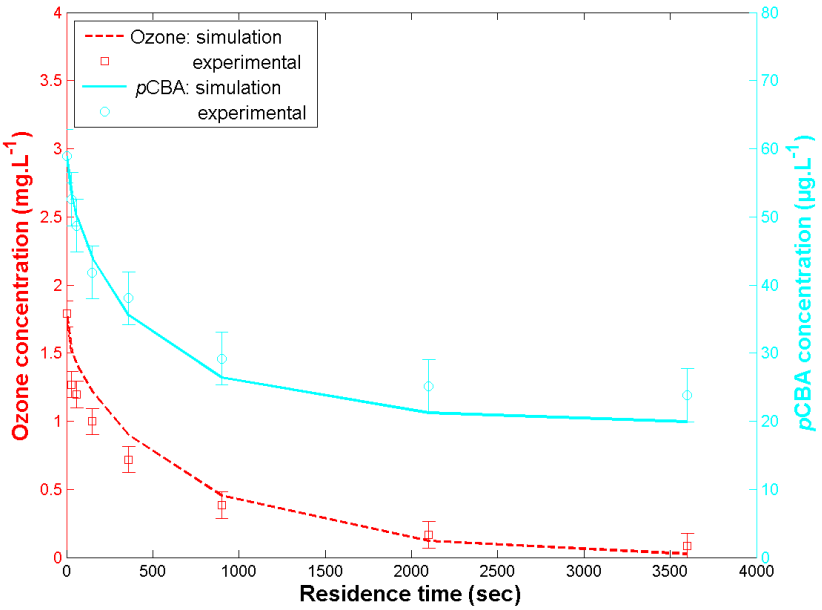

Figure 16 Experimental and simulated concentration profiles, Méry-sur-Oise water, experiment #9: no *tert*-butanol adding; natural pH=7.85; small ozone dose; T=13.5°C; A_T=4.55 meq.L^{-1}; TOC = 3.1 mgC.L^{-1}

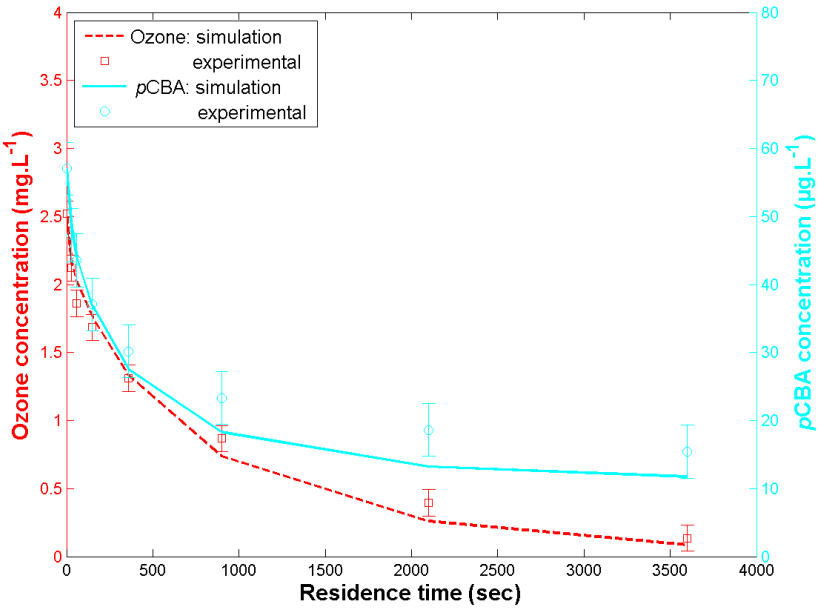

Figure 17 Experimental and simulated concentration profiles, Méry-sur-Oise water, experiment #13: no *tert*-butanol adding; natural pH=7.85; large ozone dose; T=13.5°C; A_T=4.55 meq.L^{-1}; TOC = 3.1 mgC.L^{-1}

■ Change in temperature

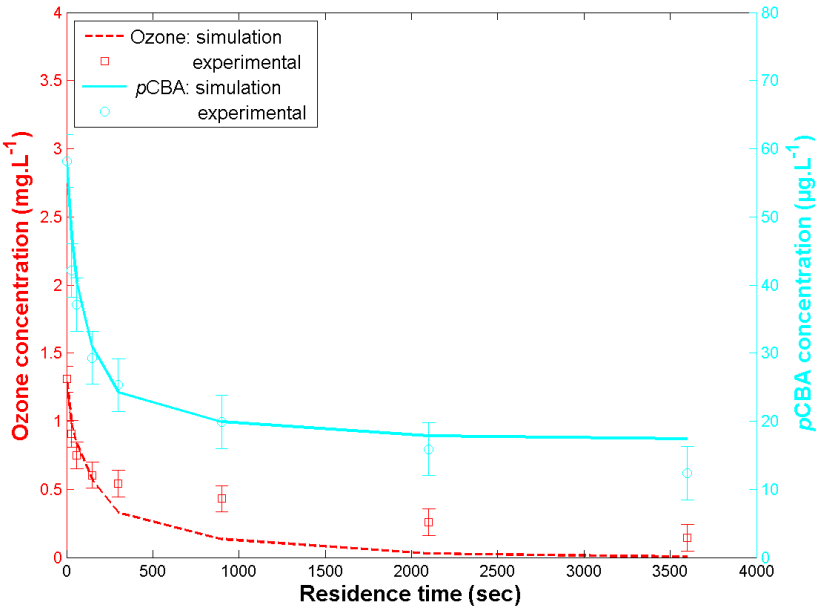

Figure 18 Experimental and simulated concentration profiles, Annet-sur-Marne 3 water, experiment #1: no *tert*-butanol adding; natural pH=7.7; small ozone dose; T=23°C; A_T=3.08 meq.L^{-1}; TOC = 1.6 mgC.L^{-1}

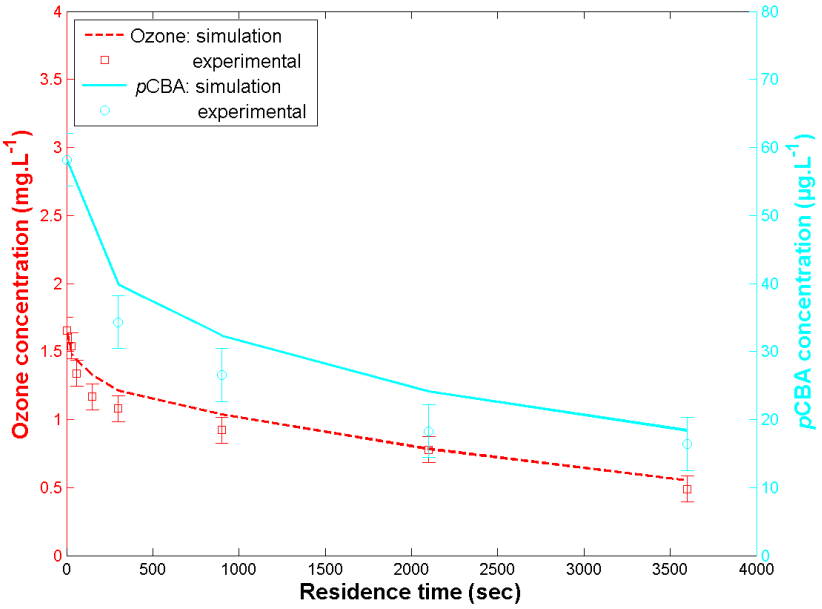

Figure 19 Experimental and simulated concentration profiles, Annet-sur-Marne 3 water, experiment #6: no *tert*-butanol adding; natural pH=7.7; small ozone dose; T=5°C; A_T=3.08 meq.L^{-1}; TOC = 1.6 mgC.L^{-1}

■ Change in pH

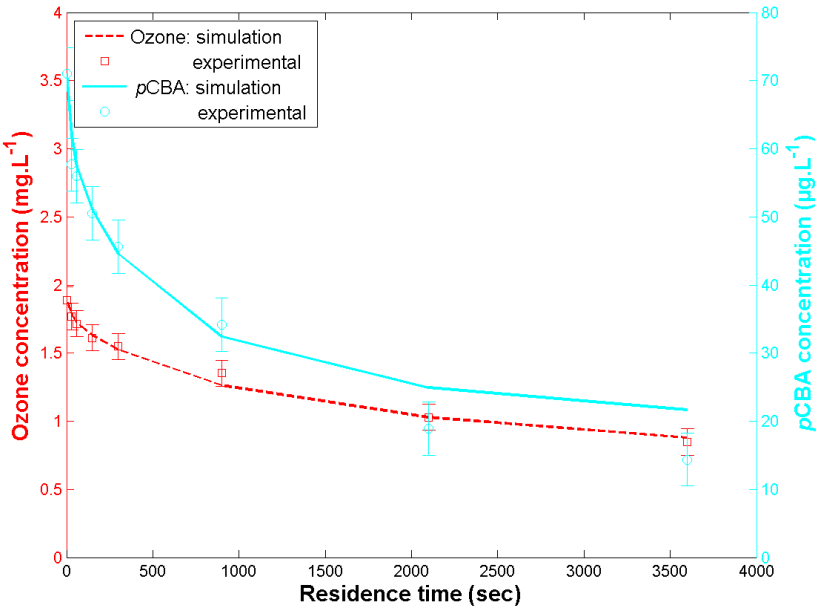

Figure 20 Experimental and simulated concentration profiles, Maisons-Laffitte water, experiment #9: no *tert*-butanol adding; natural pH=8.15; small ozone dose; T=13.5°C; A_T=2.4 meq.L^{-1}; TOC < 0.5 mgC.L^{-1}

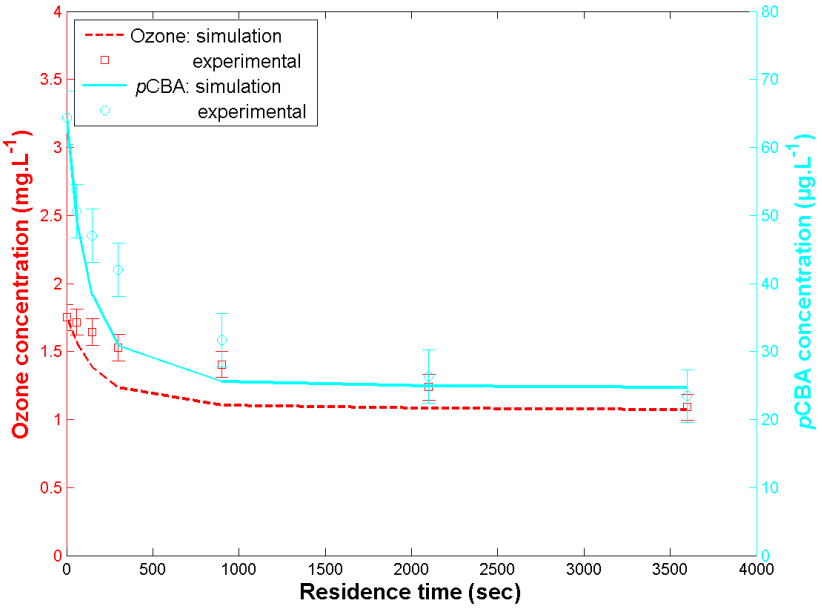

Figure 21 Experimental and simulated concentration profiles, Maisons-Laffitte water, experiment #11: no *tert*-butanol adding; lowered pH=7.15; small ozone dose; T=13.5°C; A_T=2.4 meq.L^{-1}; TOC < 0.5 mgC.L^{-1}

■ Change in NOM content

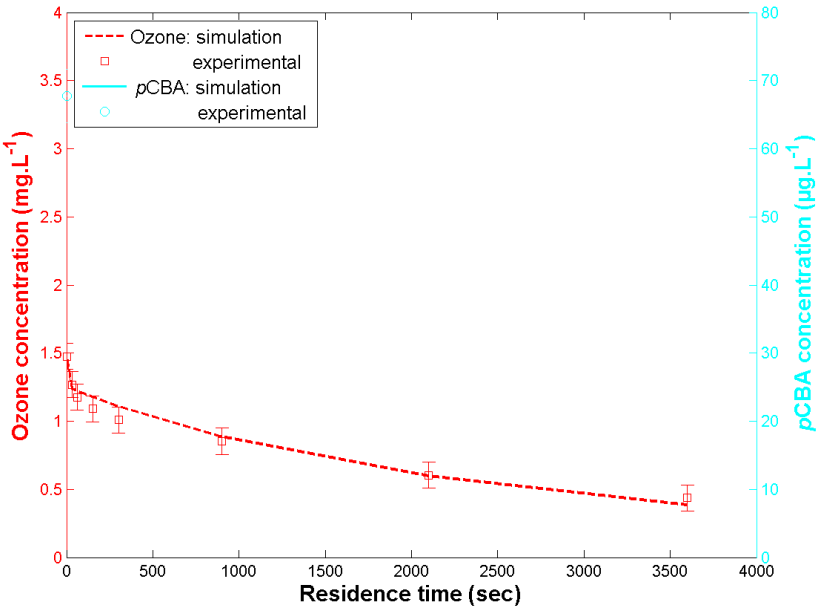

Figure 22 Experimental and simulated concentration profiles, Vitré water, experiment #4: 10 mM *tert*-butanol adding; lowered pH=6.4; small ozone dose; T=20°C; A_T=1.02 meq.L^{-1}; TOC=2 mgC.L^{-1}

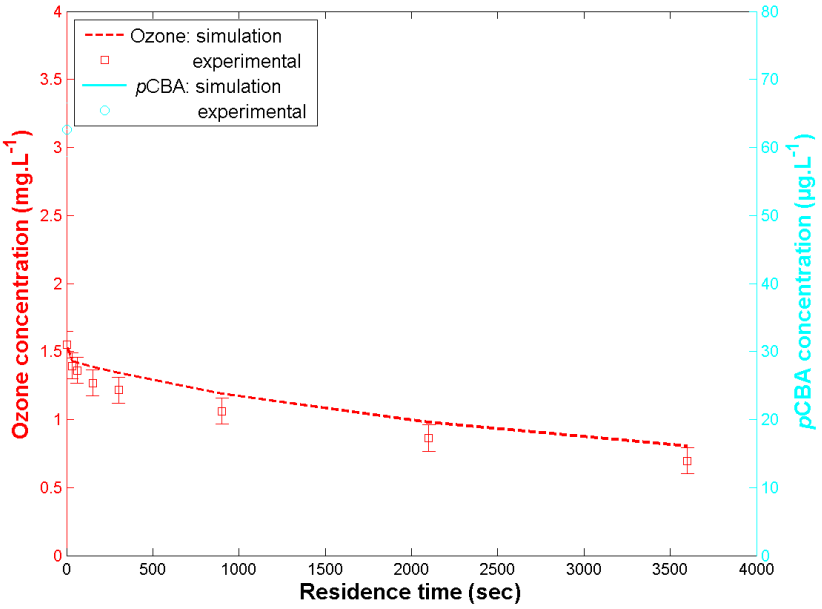

Figure 23 Experimental and simulated concentration profiles, Vitré water, experiment #12: 10 mM *tert*-butanol adding; lowered pH=6.4; small ozone dose; T=20°C; A_T=1.02 meq.L^{-1}; TOC=1 mgC.L^{-1}

■ **Change in NOM nature (radical scavenger adding)**

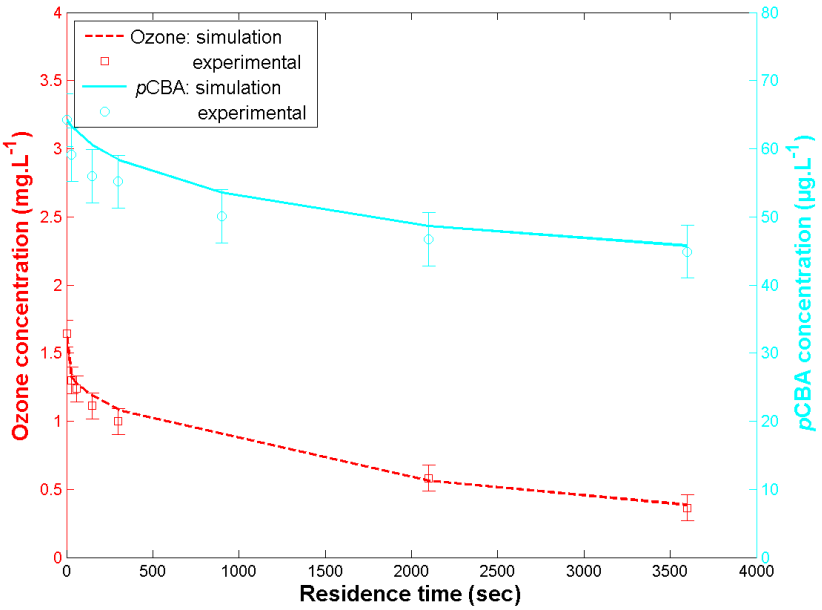

Figure 24 Experimental and simulated concentration profiles, Meulan water, experiment #1: no *tert*-butanol adding; natural pH=7.25; small ozone dose; T=20°C; A_T=6.24 meq.L^{-1}; TOC=0.9 mgC.L^{-1}

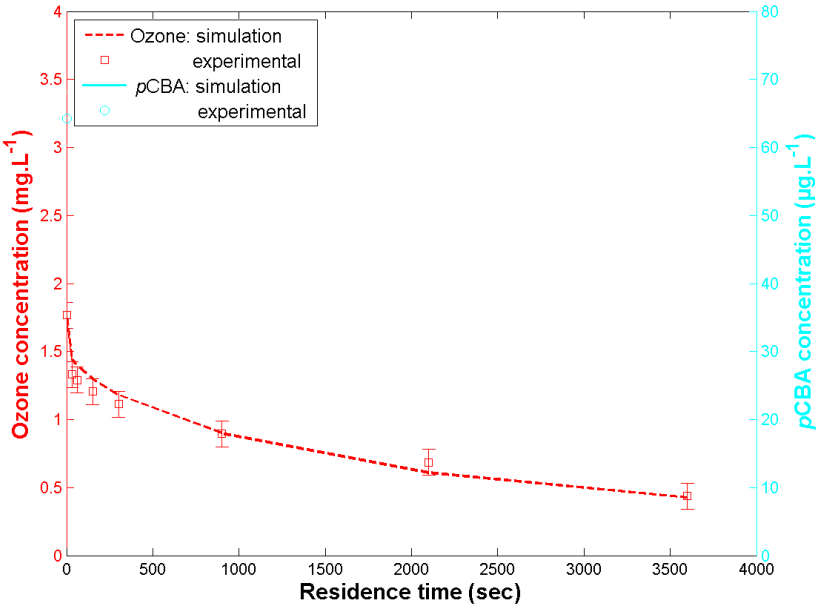

Figure 25 Experimental and simulated concentration profiles, Meulan water, experiment #2: 10 mM *tert*-butanol adding (→no *p*CBA); natural pH=7.25; small ozone dose; T=20°C; A_T=6.24 meq.L^{-1}; TOC=0.9 mgC.L^{-1}

4.5.2.2. Focusing on Three Different Waters

Results are presented for three specific waters with different physicochemical characteristics: Annet-sur-Marne, Méry-sur-Oise and Beaufort samples. Results for the remaining water samples will be summarised in the paragraph **4.5.2.3.** and can be extensively found in Appendix **E**.

The results are presented as scatterplots and analysed using the Pearson's test (with a 5% risk) and the 95% interval of confidence for the estimates of the offset and slope (linear regression analysis). The confidence intervals are compared to the intervals for experimental uncertainty and if the estimate for the offset or the slope is found outside the uncertainty interval, the test is failed. Both tests evaluate the badness-of-fit. Therefore, those tests may only bring conclusive evidence of the inadequate character of the model.
A measure of the goodness-of-fit is given by the percentage of simulated points located within the domain of experimental uncertainty (between the dashed lines in the figures). Other measures will be given in the summary (**4.5.2.3.**).

Méry-sur-Oise water

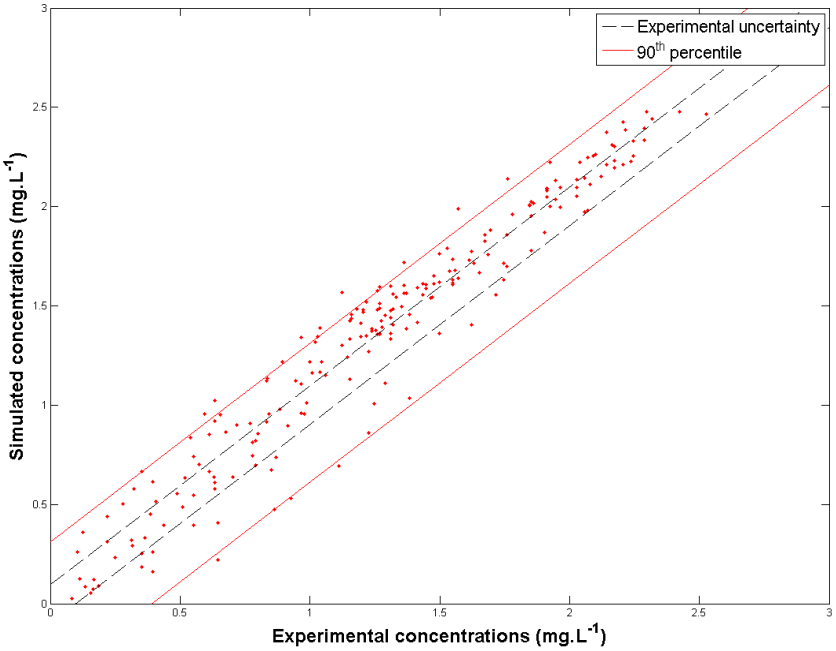

Figure 26 Comparison of simulated and experimental ozone concentrations, Méry-sur-Oise water

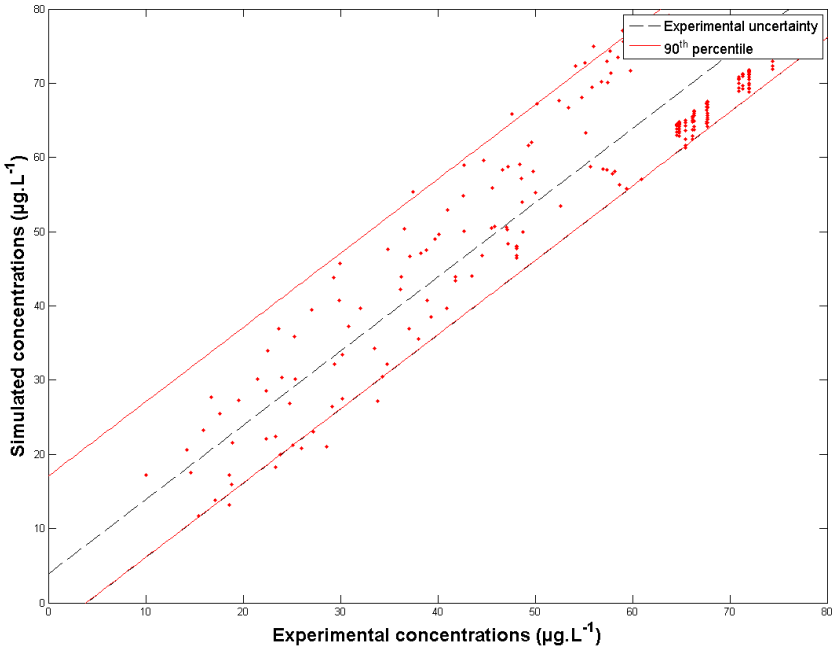

Figure 27 Comparison of simulated and experimental *p*CBA concentrations, Méry-sur-Oise water

Table 15 Statistical results, Méry-sur-Oise water

Compound	r_P	Pearson test	Offset (mg.L^{-1} or µg.L^{-1})	Test	Slope	Test	% points within error
Ozone	0.97	Passed	0.06±0.06	Passed	1.03±0.04	Passed	34.4
*p*CBA	0.93	Passed	8.28±3.06	Failed	0.90±0.06	Passed	64.4

Globally, a good agreement of simulated with experimental data is observed, despite a tendency to overpredict *p*CBA concentrations (figure **27** and table **15**). The clusters of high concentrations in figure **27** correspond to experiments with *tert*-butanol adding.

Annet-sur-Marne water

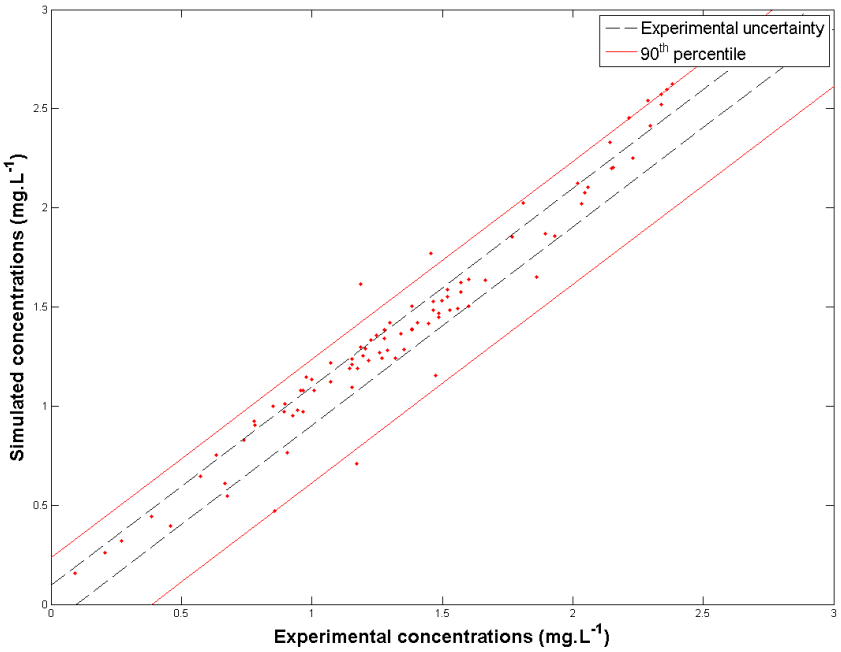

Figure 28 Comparison of simulated and experimental ozone concentrations, Annet-sur-Marne water

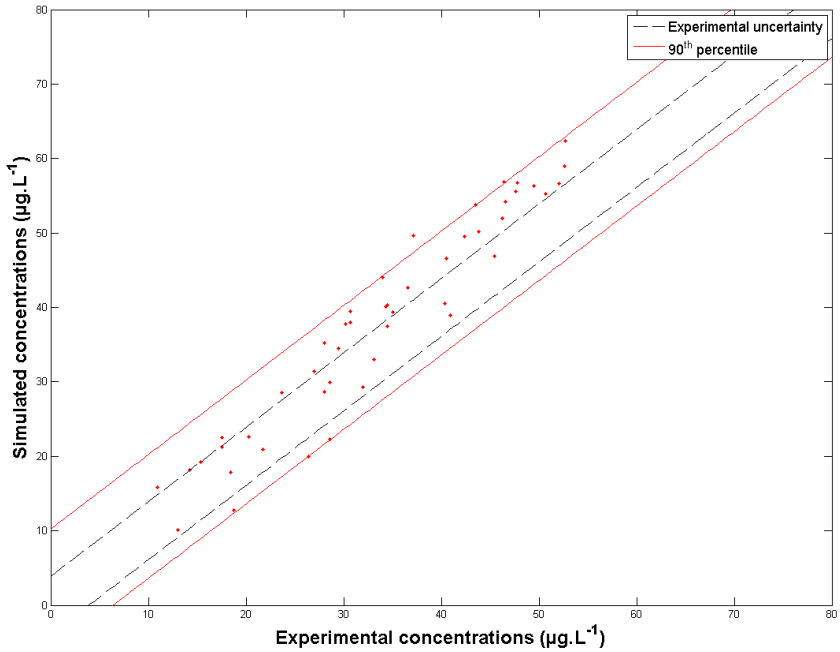

Figure 29 Comparison of simulated and experimental *p*CBA concentrations, Annet-sur-Marne water

Table 16 Statistical results, Annet-sur-Marne water

Compound	r_P	Pearson test	Offset (mg.L^{-1} or µg.L^{-1})	Test	Slope	Test	% points within error
Ozone	0.97	Passed	-0.01±0.08	Passed	1.04±0.06	Passed	60.4
*p*CBA	0.96	Passed	-0.56±5.25	Passed	1.14±0.15	Passed	29.2

Again, simulated data match experimental data, particularly for ozone concentrations (figure **28**). Although a relatively small amount of simulation points for *p*CBA concentration is located within the experimental uncertainty, the results of the model remain good (slight overprediction of *p*CBA concentration, see figure **29**).

Beaufort water

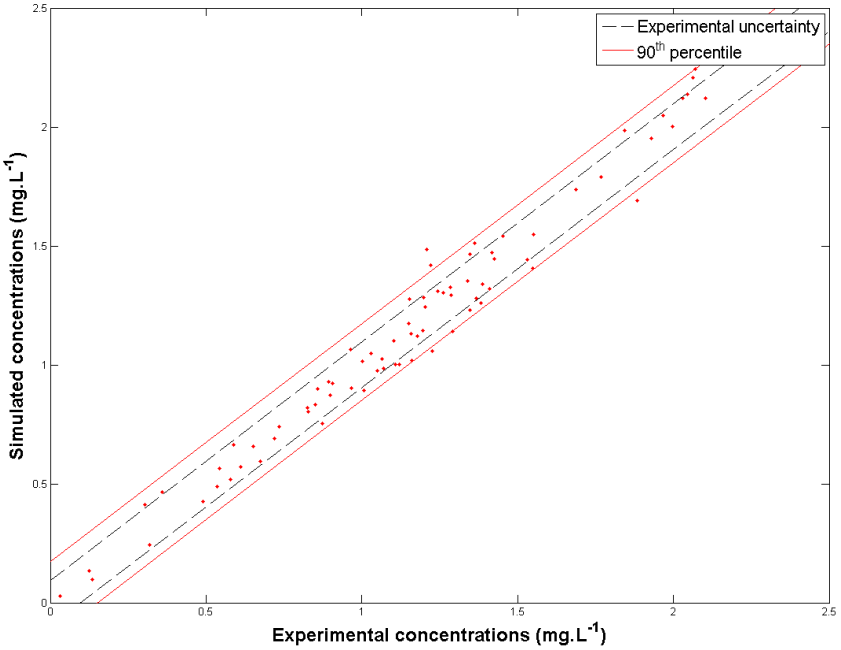

Figure 30 Comparison of simulated and experimental ozone concentrations, Beaufort water

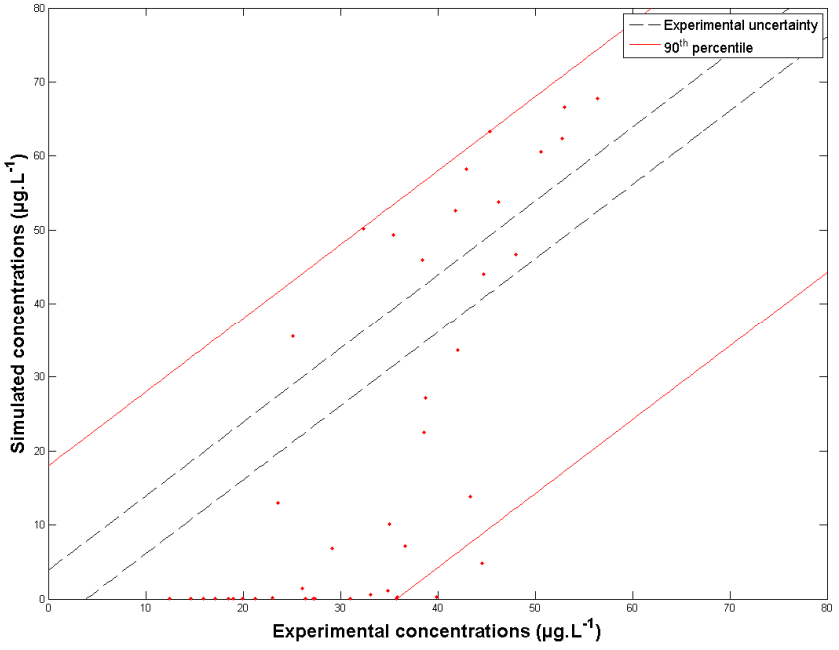

Figure 31 Comparison of simulated and experimental *p*CBA concentrations, Beaufort water

Table 17 Statistical results, Beaufort water

Compound	r_P	Pearson test	Offset (mg.L^{-1} or µg.L^{-1})	Test	Slope	Test	% points within error
Ozone	0.99	Passed	-0.05±0.05	Passed	1.05±0.04	Passed	68.8
*p*CBA	0.75	Passed	-32.10±20.74	Failed	1.59±0.59	Passed	4.7

Whereas the model gave excellent predictions for the ozone concentrations (see figure **30**), simulated *p*CBA concentrations were found to be inaccurate (figure **31**). This discrepancy is also to be seen in table **17**: almost 70 % of the ozone predicted concentrations are located within the experimental uncertainty; less than 5 % of the predicted concentrations for *p*CBA.

4.5.2.3. Summary

The goodness-of-fit of the simulated data has been estimated by two measures: the final value of the objective function, O_f, and the coefficient of determination, R^2. Three groups of experiments were defined:

- *very good* experiments, for which $R^2 \geq 0.7$ and $O_f \leq 1.5$;
- *good* experiments, for which {$R^2 \geq 0.7$ and $O_f \geq 1.5$} or {$R^2 \leq 0.7$ and $O_f \leq 1.5$};
- *mediocre or bad* experiments, in any other cases.

The boundary of 0.7 for the coefficient of determination was determined qualitatively. The value of 1.5 for the objective function has been determined statistically. 1.5 is the approximate median value of an empirical cumulative distribution function built with 5000 acceptable data sets of simulated concentrations created randomly. Two typical temporal profiles, for ozone and *p*CBA were considered as experimental reference data, and simulated profiles were randomly generated adding to or subtracting from each experimental point a fraction of the experimental error smaller than one. Thus, all randomly simulated profiles were comprised within the experimental error (±0.1 mg.L^{-1} for ozone and ±4 µg.L^{-1} for *p*CBA).

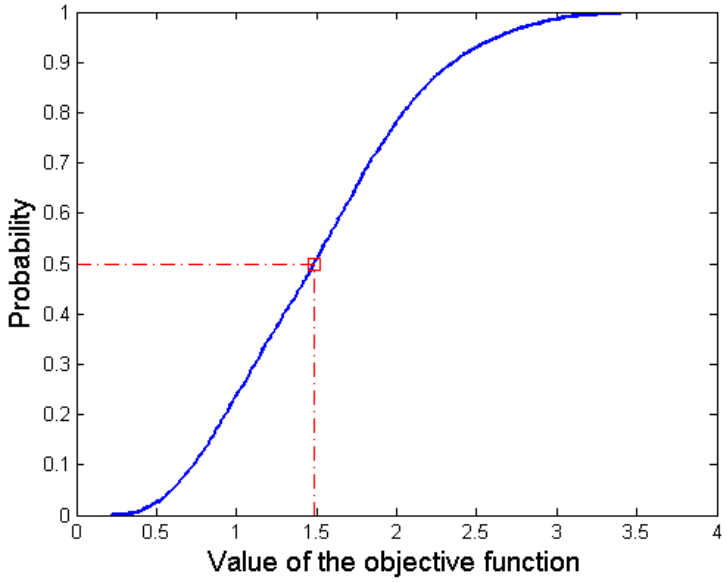

Figure 32 Empirical cumulative distribution function considering 5000 simulations, for which simulated points are located within experimental uncertainty

The distribution of the groups of experiments over the water samples investigated is represented in figure **33** (the model is optimised individually for each water sample).

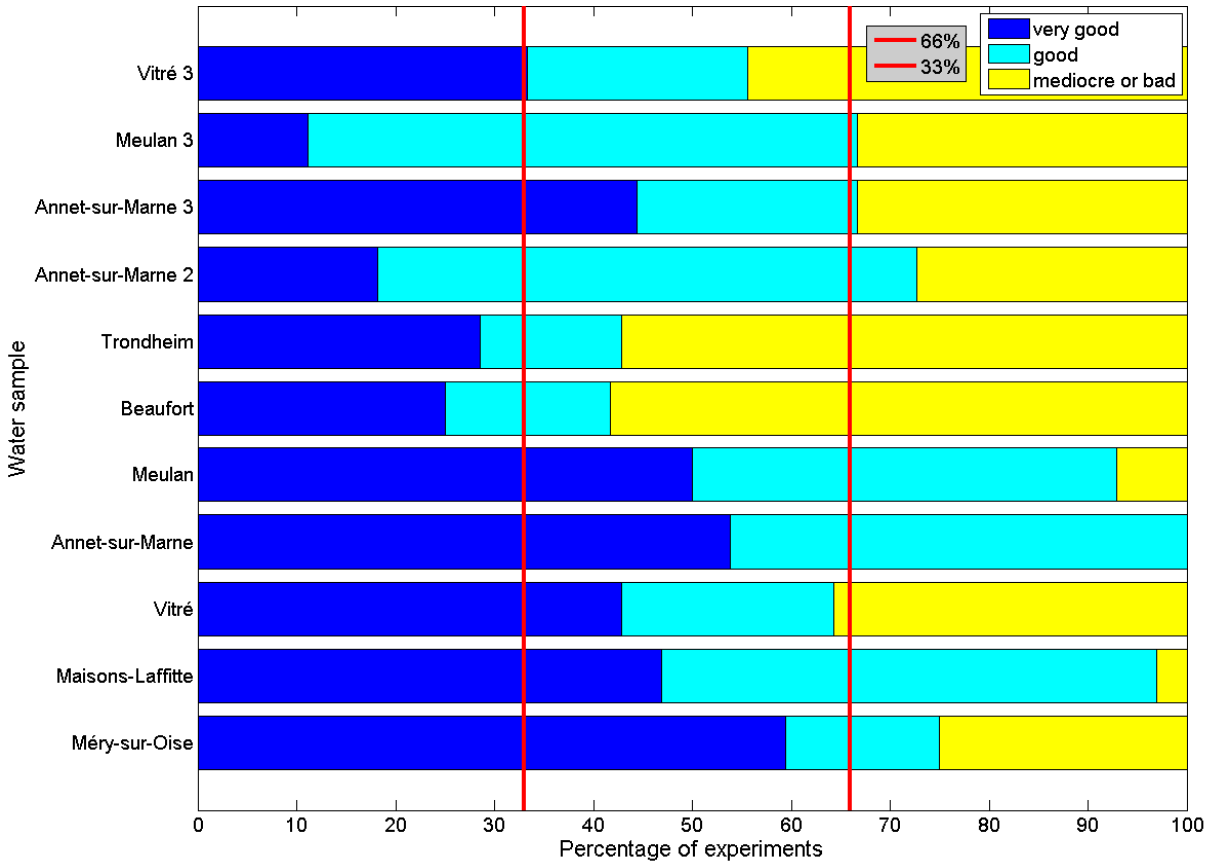

Figure 33 Distribution of the quality of the simulations, all water samples

Both water samples from Beaufort and Trondheim could not be satisfactorily modelled: in each case, more than 50% of the experiments were classified as *mediocre* or *bad*. In each case, the concentration profiles for ozone were nevertheless adequately modelled: almost all experiments performed with *tert*-butanol adding were thus classified as *very good* (see figure **33**). As exemplified in figure **34**, the model tends to rapidly underpredict *p*CBA concentrations. An explanation is given in **4.5.4.1**.

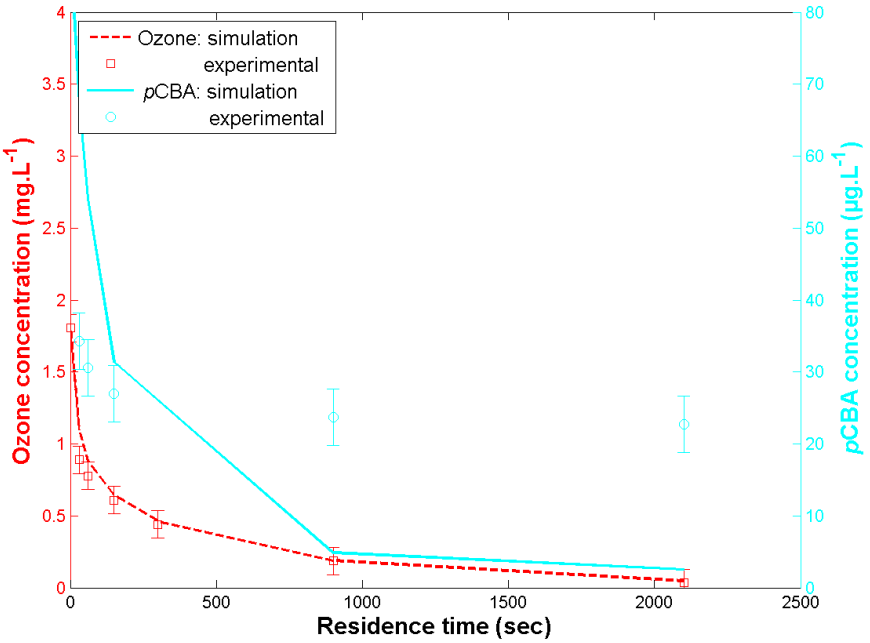

Figure 34 Experimental and simulated concentration profiles for Trondheim water, Experiment #6: no *tert*-butanol adding; natural pH=7.35; large ozone dose; T=5°C; A_T=0.32 meq.L^{-1}; TOC= 3.1 mgC.L^{-1}

Considering the other water samples, the results of which are presented in figure **33**, the model is able to adequately simulate different types of water, under varying experimental conditions. With exception of the results obtained with Beaufort and Trondheim water samples:

- for 78% of the water samples studied (7 out of 9), simulations of very good quality represent more than a third of the experiments;
- for 78% of the water samples studied, simulations of mediocre or bad quality represent less than a third of the experiments.

Generally, *p*CBA was found more difficult to model than ozone: in total, 55% of the simulated points for ozone and 45% of the simulated points for *p*CBA are located within experimental uncertainty (see Appendix **E**). A discussion on the experimental conditions, for which experiments could not be adequately simulated, is given in the paragraph **4.5.4.2**.

4.5.3. Values of the Parameters and Comparison with Other Studies

The minimum, median and maximum values for the parameters of the model are gathered in table **18**. As physicochemical discussions should not be based on such results, we shall only discuss the orders of magnitude and the ranges of variation with regards to what can be found in the literature. The distribution of the values for the parameters of the model is presented as boxplots in figure **35**.

Table 18 Ranges for the values of the parameters, all water samples

25th percentile	Median	75th percentile	Type of parameter	Fraction
5.19	6.35	6.95	pK_A for: $NOM_a \rightarrow NOM_b + H^+$	Initiation
4.72	5.76	7.86		Consumption
4.05	5.51	7.39		Promotion
$1.78.10^1$	$2.31.10^1$	$9.28.10^1$	Kinetic constant rate at T=293K ($M^{-1}.s^{-1}$)	Initiation
$2.75.10^3$	$7.31.10^3$	$2.07.10^6$		Consumption
$1.26.10^6$	$5.56.10^7$	8.10^8		Promotion
$4.93.10^4$	$7.00.10^4$	$8.35.10^4$	Energy of activation for initiation, consumption or promotion ($J.mol^{-1}$).	Initiation
$7.96.10^3$	$1.07.10^4$	$8.77.10^4$		Consumption
$2.00.10^4$	$5.56.10^4$	$9.56.10^4$		Promotion
0.1	0.4	0.75	Initial concentration for the considered fraction ($mg\ C.L^{-1}$).	Initiation
0.0	0.1	0.2		Consumption
0.5	0.8	1.25		Promotion

pK_A values are stable around 6, although, as already reported in [Savary, 2002], they may be smaller. A value close to the pH of the experiments indicates that the concentrations of the reactive fractions of NOM considered in this study may significantly evolve when altering the natural pH. This justifies *a posteriori* the acid-base speciation of the model.
The values of the kinetic constant rates are globally consistent with values already reported in the literature. Studying the ozonation of NOM fractions, under varying *tert*-butanol concentration (49 to 497 µM), [Bezbarua, 1997] also found kinetic constant rates such that $k^i < k^d < k^p$. However, the reactivities determined in this study for the initiating and consuming fractions were generally higher than those determined by Bezbarua (see table **19**). The presence of *tert*-butanol during the ozonation experiments can be given as explanation. Considering initiating and consuming fractions, the results presented in table **18** are in agreement with those obtained by [Kim, 2004], see table **19**. Previous studies investigating

the kinetics of NOM isolates, typically obtained by filtration on ion exchanging resins, have estimated the promoting kinetics of NOM fractions around 10^8-10^{10} $M^{-1}.s^{-1}$ ([Xiong *et al.*, 1992]; [Westerhoff *et al.*, 2007]). Comparison with other studies remains nevertheless an uneasy task given the very differences in chemical composition of the investigated waters and in the apparatus used. As values for frequency factors are rather different from a study to another, it is not surprising to see that the values determined with different water samples are spread over several decades (figure **35**).

Table 19 Average kinetic values found in previous studies

[Bezbarua, 1997]	[Kim, 2004]	Type of parameter	Fraction
$7.6.10^0$	5.10^1	Kinetic constant rate at T=293K ($M^{-1}.s^{-1}$)	Initiation
$2.36.10^1$	$1.31.10^2$		Consumption
$4.1.10^8$	3.10^8		Promotion
0.2	0.2-2	Initial concentration for the considered fraction (mg $C.L^{-1}$).	Initiation
0.4	0.9		Consumption
0.3	0.4-0.8		Promotion

Energies of activation below 10^4 $J.mol^{-1}$ were rather rare, and most of the values are comprised in the range 10^4-10^5 $J.mol^{-1}$ (see figure **35**). Such values are comparable to molecular reactions or with reactions involving a molecule and a radical. To our knowledge, no comparison with models can be found in the literature, except in [Savary, 2002], where similar values have been determined. The initial concentrations for the reactive fractions of NOM are expressed in mg $C.L^{-1}$ in table **18**. The sum of the initial concentrations for the three fractions was in most cases comparable with, or inferior to the TOC (see Appendix **G**).

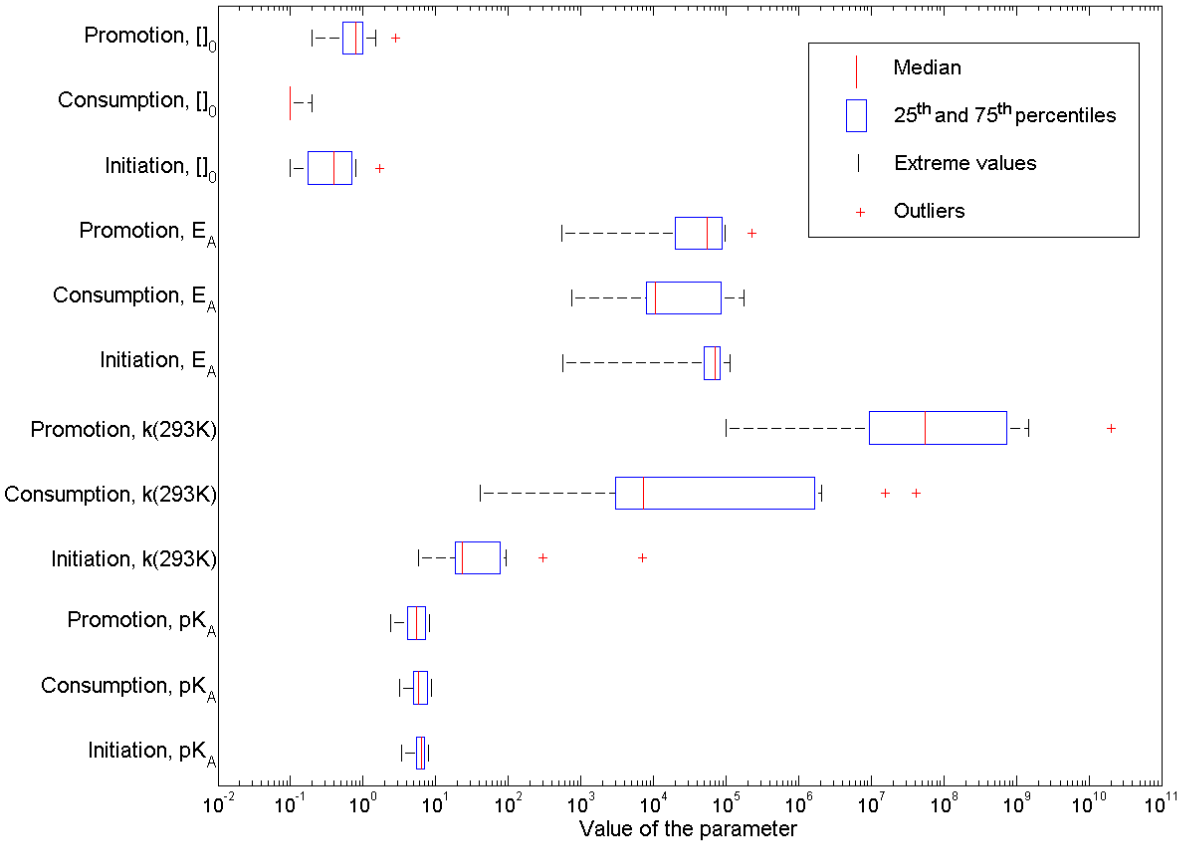

Figure 35 Boxplot distribution for the values of the parameter, all eleven water samples

4.5.4. Domain of Validity of the Model

4.5.4.1. Water Characteristics

The quality of the model predictions is poor for two water samples out of eleven: Beaufort and Trondheim. Both samples have high organic content, and at the same time, low inorganic content. The water from Vitré, for which more than a third of the experiments were classified as mediocre or bad in figure **33,** has also a large organic/inorganic ratio, to a smaller extent however.

One possible explanation for the limitation of the model is that NOM scavenging is not anymore negligible compared to carbonate/hydrogenocarbonate scavenging. Consequently, test simulations were run with a model including a radical-scavenging fraction of NOM. The model was tested with Trondheim water, but the results were only slightly improved. Given the gap observed between the experimental and simulated points at the end of the ozonation experiments (see the example of figure **34**), it is likely that the stoichiometry of the scavenging reaction has to be changed.

A wide range of water characteristics has been experimentally studied and modelled. If we consider three global indicators for water quality: pH, A_T and TOC, experiments have been performed at low, medium and high values for the three indicators. Practical boundaries defining low, medium and high levels for the indicators are given in table **20**.

Table 20 Boundaries for the three indicators pH, A_T and TOC

Indicator	Low level	Medium level	High level
pH	pH < 6.5	6.5 < pH < 7.5	pH > 7.5
A_T (meq.L^{-1})	A_T < 1	1 < A_T < 2.5	A_T > 2.5
TOC (mg C.L^{-1})	TOC < 1	1 < TOC <2.5	TOC > 2.5

Theoretically, 3^3=27 combinations for the values of the indicators are possible. Considering the water characteristics (presented in table **2**) and the experiments performed (see the tables **5** to **7** corresponding to the designs of experiments), 16 combinations were explored, many of them twice. Although satisfactorily covering a wide spectrum of possibilities, some experimental conditions were not tested:

- 1: medium A_T; high TOC;
- 2: medium or high pH; low A_T; low TOC.

The first experimental conditions should not be problematic since numerous experiments were done with medium TOC and A_T values. An increase in TOC concentration should to the contrary stabilise the system by reinforcing the role of NOM. The second experimental conditions may certainly be more problematic, since low alkalinity means more importance given to the NOM, despite its low level. Experiments at low alkalinity and low TOC were only done with Vitré water, and gave satisfactorily results (pH=6.4; A_T=1.02; TOC=1 mg.L^{-1}).

4.5.4.2. Experimental Conditions

By reviewing the results obtained with the first and the second designs of experiments (discarding the results from Beaufort and Trondheim waters), a ranking of the best simulated experiments could be established. It was found that some experiments were systematically well predicted while others were less accurately predicted.

The worse predictions were obtained for the experiments #5, #9 and #11 using the reference of the second design of experiments. They respectively correspond to:

- large ozone dose;
- simultaneous temperature and pH drop;
- NOM dilution with simultaneous pH drop.

4.5.5. Seasonal Variations

Three water samples were collected at different periods of the year 2009. Water from Annet-sur-Marne was collected in February, July and October; water from Meulan was collected in March and November; water from Vitré was collected in February and November.
In order to roughly estimate the reactivity of ozone, the apparent one hour relative ozone demand Δ_{Ozone} was calculated for experiments done at two different periods of the year. The definition for Δ_X is given in equation **10** for the species X ($[X]_0$ and $[X]_f$ are initial and final concentrations of species X, respectively).

$$\Delta_X = \frac{[X]_0 - [X]_f}{[X]_0} \quad \textbf{(10)}$$

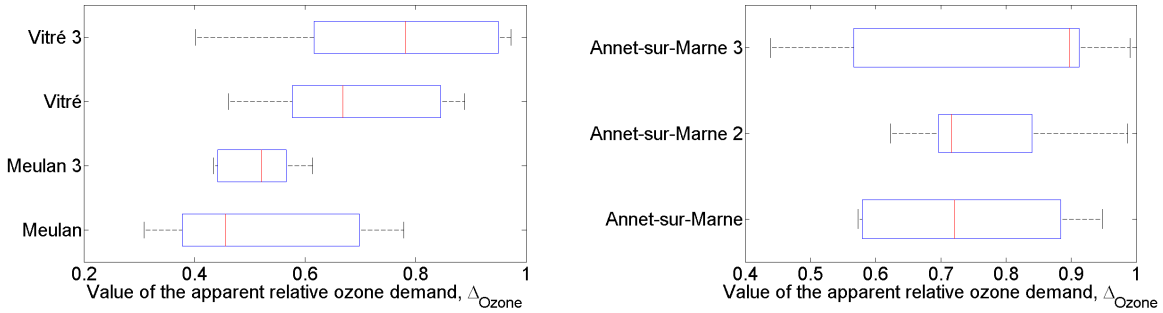

Figure 36 Values of the apparent one hour relative ozone demand for water samples from the same water resource and collected at different periods of the year. 8 experiments done at two different periods of the year were considered for Meulan and Vitré waters (left hand-side); 6 experiments done at three different periods of the year were considered for Annet-sur-Marne water (right hand-side)

As depicted in figure **36**, apparent one hour relative ozone demands may change throughout the year. Although water samples collected in October (Annet-sur-Marne 3) and November (Meulan 3, Vitré 3) tend to exhibit larger values for Δ_{Ozone} than those obtained earlier in the year, it remains difficult to draw conclusions on seasonal trends. In the literature, seasonal effects are rarely discussed, except when considering the evolution of NOM isolates (*e.g.* [Sharp *et al.*, 2006]). Consequently, we shall not discuss in detail the seasonal variations of the values for the parameters of the model.
The values of the parameters are presented in Appendix **G**. In most cases, the sum of the initial NOM concentrations could be kept lower than the TOC value. However, for 5 water samples the following inequality is observed: $[NOM^i]_0+[NOM^d]_0+[NOM^P]_0 > TOC$. The most important difference is observed with Annet-sur-Marne 2 (TOC = 1.6 mgC.L^{-1} and $\Sigma[NOM]_0$ = 3.6 mgC.L^{-1}). These differences underline the hypothetical character of the proposed model, which considers a one-to-one stoichiometry for every reaction with NOM. In reality, discrepancies can be observed as molecules present in natural waters may have a varying number of reactive sites (carboxylic, alcohol, alkyl or aryl groups…)

4.6. Simplifying the Calibration Procedure: a First Approach

4.6.1. Aim and Scope of the Study

In this section, we propose a simplified approach in using a complete chemical description for natural water ozonation. This procedure was elaborated as engineering tool for practical application, in order to rapidly characterise investigated waters. Rapid calibration and

acceptable model predictions for the most common experimental conditions encountered on-site were targeted.
The objective is to use only a limited number of experiments in order to calibrate a model for the role of NOM. An empirical approach is proposed, selecting the experiments, which lead to the most significant changes for ozone and *p*CBA decomposition rates.
This modelling procedure has been tested on the following water samples: Méry-sur-Oise, Maisons-Laffitte, Vitré, Annet-sur-Marne, Meulan and Trondheim. The physicochemical characteristics of these water samples are available in table **2**. Performed experiments are summarised in table **5** for Méry-sur-Oise and Maisons-Laffitte waters and in table **6** for the remaining ones. The chemical reaction set comprises reactions for ozone self-decomposition, reactions with alkaline species, reactions with NOM and specific reactions with *p*CBA and *tert*-butanol (see Appendix **D** and the previous paragraphs).

4.6.2. Determining the Most Influent Experimental Parameters

4.6.2.1. First Design of Experiments

The most influent experimental factors over the apparent one hour demand of both ozone and *p*CBA were determined by a multiple linear regression analysis. Given that the concentrations of these species can only decrease, a convenient way to quantify the influence of experimental factors is to calculate the apparent one hour demand Δ_X, as defined in equation **10**. Δ_X is calculated for each experiment (32 in the case of the first design of experiments). The results are then interpreted in terms of linear dependence of Δ_X towards experimental factors $F_1 \ldots F_n$ (equation **11**). In order to avoid size effects, the decomposition rate and the experimental factors are centred and reduced (see chapter **3**, equation **9**).

$$\Delta_X = Offset + C_1.F_1 + \ldots + C_n.F_n \qquad \textbf{(11)}$$

C_i is a constant, the absolute value of which reflects the influence of factor i over the apparent one hour ozone demand. A positive value means that the factor enhances the decomposition of species X. The values for C_i are gathered in table **21**. Values below 0.1 are not considered as relevant since they approach the standard error of the estimation. The coefficient of determination R^2 is also given.

Table 21 Results of the multiple linear regression, first design of experiments (the most relevant influences are written in bold characters)

Experimental factor	Méry-sur-Oise		Maisons-Laffitte	
	Ozone	*p*CBA	Ozone	*p*CBA
Scavenger adding	$-3.35.10^{-1}$	**$-9.88.10^{-1}$**	*Not signif.*	**$-9.57.10^{-1}$**
pH drop	**$-6.03.10^{-1}$**	*Not signif.*	**$-6.87.10^{-1}$**	$-1.56.10^{-1}$
Temperature drop	$3.03.10^{-1}$	*Not signif.*	$5.53.10^{-1}$	$1.10.10^{-1}$
Large O_3 dose	$-3.76.10^{-1}$	*Not signif.*	$-1.55.10^{-1}$	*Not signif.*
NOM dilution	$-4.49.10^{-1}$	*Not signif.*	$1.61.10^{-1}$	*Not signif.*
Offset	0	0	0	0
Coefficient of determination	$9.11.10^{-1}$	$9.87.10^{-1}$	$8.46.10^{-1}$	$9.81.10^{-1}$

Results from table **21** show that the pH and the addition of radical scavenger have great impact over decomposition rate of ozone and *p*CBA, respectively. Paradoxically, temperature was found not to play an important role over the overall decomposition of ozone and *p*CBA. This is explained by the small temperature gap observed between high (19°C) and low (13.5°C) experiment temperatures. Therefore, experiment temperatures were set at 20°C and

5°C, respectively for high and low levels in all subsequent experiments. NOM concentration plays a more significant role for Méry-sur-Oise than for Maisons-Laffitte water because of its high TOC (3.1 $mg.L^{-1}$).

4.6.2.2. Second Design of Experiments

The same approach has been adopted for the second design of experiments. However, a distinction was made among water samples. Beaufort and Trondheim waters were treated separately as they appeared to react differently with ozone. In terms of water characteristics, both water exhibit high organic content (2.4 $mg.L^{-1}$ and 3.1 $mg.L^{-1}$, for Beaufort and Trondheim respectively) coupled to low alkalinity (0.12 $meq.L^{-1}$ and 0.32 $meq.L^{-1}$ respectively). Results for Beaufort and Trondheim are presented in table **23**; other waters are gathered in table **22**.

Table 22 Results of the multiple linear regression, second design of experiments, Annet-Meulan-Vitré (the most relevant influences are written in bold characters)

Experimental factor	Annet-sur-Marne		Meulan		Vitré	
	Ozone	*p*CBA	Ozone	*p*CBA	Ozone	*p*CBA
Scavenger adding	$-1.31.10^{-1}$	**$-9.59.10^{-1}$**	*Not signif.*	**$-8.96.10^{-1}$**	$-5.60.10^{-1}$	**$-9.47.10^{-1}$**
pH drop	$-3.16.10^{-1}$	*Not signif.*	$-1.58.10^{-1}$	$1.33.10^{-1}$	*Not signif.*	*Not signif.*
Temperature drop	**$-8.24.10^{-1}$**	$-2.31.10^{-1}$	**$-9.87.10^{-1}$**	$-2.87.10^{-1}$	**$-9.05.10^{-1}$**	$-2.07.10^{-1}$
Large O_3 dose	$-2.43.10^{-1}$	*Not signif.*	$-1.72.10^{-1}$	*Not signif.*	$-3.19.10^{-1}$	*Not signif.*
NOM dilution	$-5.57.10^{-1}$	*Not signif.*	$-5.89.10^{-1}$	*Not signif.*	$-5.39.10^{-1}$	*Not signif.*
Offset	$-4.80.10^{-1}$	$-1.95.10^{-1}$	$-5.30.10^{-1}$	$-2.17.10^{-1}$	$-6.66.10^{-1}$	$-1.35.10^{-1}$
Coefficient of determination	$8.35.10^{-1}$	$9.47.10^{-1}$	$8.63.10^{-1}$	$9.38.10^{-1}$	$9.85.10^{-1}$	$9.48.10^{-1}$

Again, considering the decomposition of *p*CBA, the influence of adding a radical scavenger species is to be seen in table **22** and **23**. In both tables, the effect of temperature is also clearly enlightened: a temperature drop leads to smaller apparent one hour relative decomposition rates. The dilution of NOM and the change in pH have comparable influence over the decomposition rate, while an increase in the ozone dose is less significant.

Waters appearing in table **23** (Beaufort and Trondheim)present homogeneous characteristics towards ozonation: NOM is the major experimental factor explaining ozone decomposition rates. The effects of temperature and pH are not as significant as for other water samples.

Table 23 Results of the multiple linear regression, second design of experiments, Beaufort-Trondheim (the most relevant influences are written in bold characters)

Experimental factor	Beaufort		Trondheim	
	Ozone	*p*CBA	Ozone	*p*CBA
Scavenger adding	$-3.65.10^{-1}$	**$-9.94.10^{-1}$**	$-2.86.10^{-1}$	**-1.02**
pH drop	$3.65.10^{-1}$	*Not signif.*	$-1.71.10^{-1}$	$-1.06.10^{-1}$
Temperature drop	$-5.20.10^{-1}$	$-1.69.10^{-1}$	$-1.86.10^{-1}$	*Not signif.*
Large O_3 dose	$-1.98.10^{-1}$	*Not signif.*	*Not signif.*	*Not signif.*
NOM dilution	**-1.22**	*Not signif.*	**$-7.83.10^{-1}$**	*Not signif.*
Offset	$-8.26.10^{-1}$	$-1.57.10^{-1}$	$-1.42.10^{-1}$	$4.05.10^{-2}$
Coefficient of determination	$9.59.10^{-1}$	$9.70.10^{-1}$	$9.82.10^{-1}$	$9.93.10^{-1}$

4.6.3. Calibration Procedure

4.6.3.1. Defining Calibration Group

Based on the results obtained with the first design of experiments, a practical calibration procedure is proposed. In order to be rapid and effective, calibration should only require a

limited number of experiments, enabling the model to account for the main experimental influences determined in the previous paragraph.
First, a reference experiment is chosen as the most likely to happen in real conditions encountered on-site. The experimental conditions for this experiment are:

- no addition of radical scavenger;
- natural pH;
- temperature = 19°C or 20°C;
- small ozone dose (between 1.6 $mg.L^{-1}$ and 1.85 $mg.L^{-1}$);
- no dilution of NOM.

Secondly, three other experiments are considered to calibrate the model at the temperature of the reference experiment. Following the conclusions of the analysis of the experimental factors' influences, these experiments are:

- Reference experiment with additional [*tert*-butanol] = 10 mM;
- Reference experiment at $pH_{natural}$ – 1;
- Reference experiment with additional [*tert*-butanol] = 10 mM at $pH_{natural}$ – 1.

Two other experiments are incorporated if temperature effect is sought to be modelled: Reference experiment with [*tert*-butanol] and Reference experiment, both at low temperature (13.5 or 5 °C). All other experiments not included in the calibration set are used for validation. The same strategy was used in [Mandel *et al.*, 2009].

4.6.3.2. Building Up the Calibration Procedure

Given the role in the model of the parameters to be determined and their correlation to experimental factors, it was decided not to optimise all model parameters simultaneously. For example, energies of activation and frequency factors were determined by comparing the values obtained for the kinetic constant rates for two temperatures. This is equivalent to a reparameterisation strategy, as presented in chapter **3**, paragraph **3.3.5**. Similarly, the pK_A of a NOM fraction is calculated once initial concentrations for that fraction have been optimised for different pH values. Experiments conducted with *tert*-butanol, where radical promotion is blocked, allow neglecting the promoting fraction of NOM, thus reducing the size of the optimisation problem. The calibration procedure is summarised in table **24**, where all steps are detailed for the determination of specific parameters.

Table 24 Calibration procedure overview

Procedure step and experiment description	Parameter determined	Comments
1 - Ref. + *tert*-butanol	$k^d(T=T_{ref})$, $k^i(T=T_{ref})$ $[NOM^d]_0(pH=pH_{ref})$, $[NOM^i]_0(pH=pH_{ref})$	*1. Alternately determined* *2. Commonly determined*
2 - Ref.	$k^p(T=T_{ref})$, $[NOM^p]_0(pH=pH_{ref})$	*Same as first optimisation*
3 - Ref + *tert*-butanol + pH drop	$[NOM^d]_0(pH=pH_{low})$, $[NOM^i]_0(pH=pH_{low})$ $\rightarrow pK_A{}^d$, $pK_A{}^i$	*Comparison of initial NOM concentrations for different pH yields the pK_A value*
4 - Ref. + pH drop	$[NOM^p]_0(pH=pH_{low})$ $\rightarrow pK_A{}^p$	
5 - Ref. + *tert*-butanol at low T	$k^d(T=T_{low})$, $k^i(T=T_{low})$ $\rightarrow E_A{}^d$, $E_A{}^i$, $k_0{}^d$, $k_0{}^i$	*Comparison of kinetic constant rates for different temperatures yields the activation energies and frequency factors*
6 - Ref. at low T	$k^p(T=T_{low})$ $\rightarrow E_A{}^p$, $k_0{}^p$	

The calibration procedure design is sequential and considered as orthogonal, so that a determined parameter is fixed after its optimisation. This kind of determination is easy to implement but can induce errors because the value of a fixed parameter may influence the next optimisation: each piece of information relies on only one experiment and affects the following, while during the global approach the experiments contributed almost equally to all parameter values. A small bias on one experiment, especially during the first stages, may have dramatic consequences. This has been limited as possible, (i) setting boundaries of physical relevance for the parameters to be optimised (non-negative concentrations, use of the *fminsearch* function) and (ii) separating optimisation for the kinetic constant values and the initial concentrations in a first time (see table **24**) before proceeding to global optimisation on all variables.

4.6.4. Focusing on Two Different Waters

We shall only present the results obtained with two water samples: Annet-sur-Marne and Méry-sur-Oise. Given the poor quality of the results obtained previously with Beaufort water, it was indeed decided not to recalibrate the model. The parameters obtained on the selected 6 experiments using the sequential procedure, are injected in the model to simulate all the other experimental conditions. This procedure is repeated for each water sample. The same objective function could be determined, and the same statistical tools used on the same sample sizes.

4.6.4.1. Méry-sur-Oise

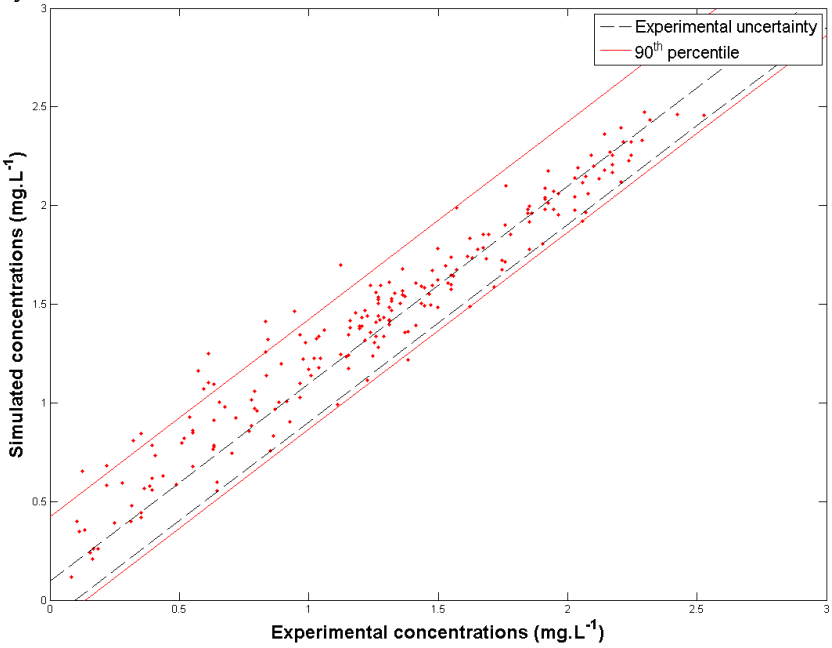

Figure 37 Comparison of simulated and experimental ozone concentrations, Méry-sur-Oise water, sequential reduced calibration

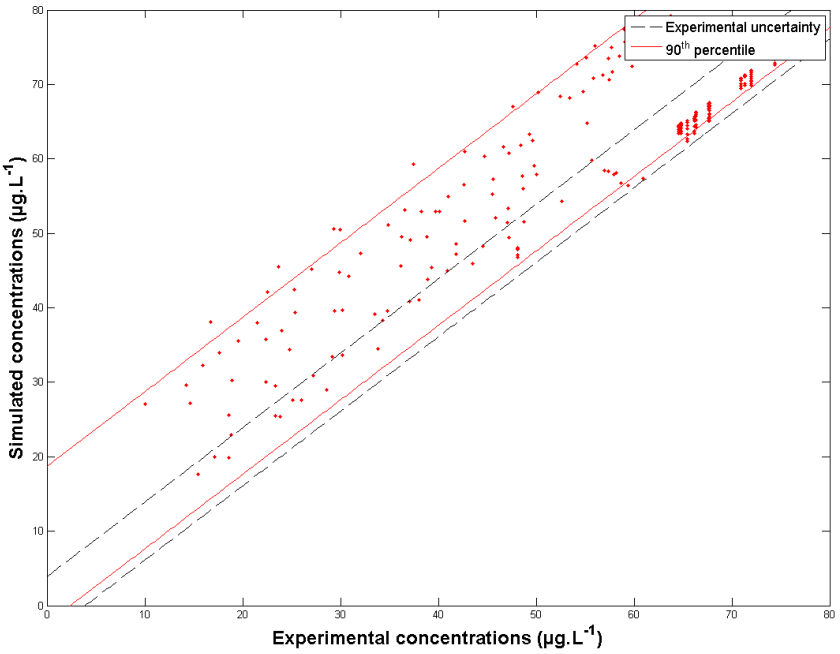

Figure 38 Comparison of simulated and experimental *p*CBA concentrations, Méry-sur-Oise water, sequential reduced calibration

Table 25 Statistical results – validation of the model, Méry-sur-Oise water, sequential reduced calibration

Compound	r_P	Pearson test	Offset	Test	Slope	Test	% points within error
Ozone	0.97	Passed	0.30±0.07	Failed	0.89±0.05	Passed	31.6
*p*CBA	0.91	Passed	18.38±3.85	Failed	0.75±0.07	Failed	57.9

4.6.4.2. Annet-sur-Marne

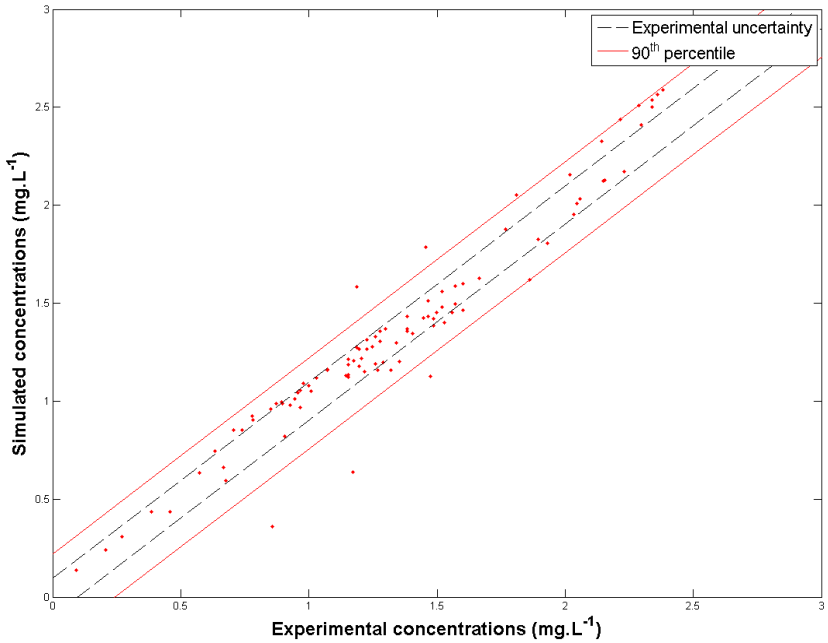

Figure 39 Comparison of simulated and experimental ozone concentrations, Annet-sur-Marne water, sequential reduced calibration

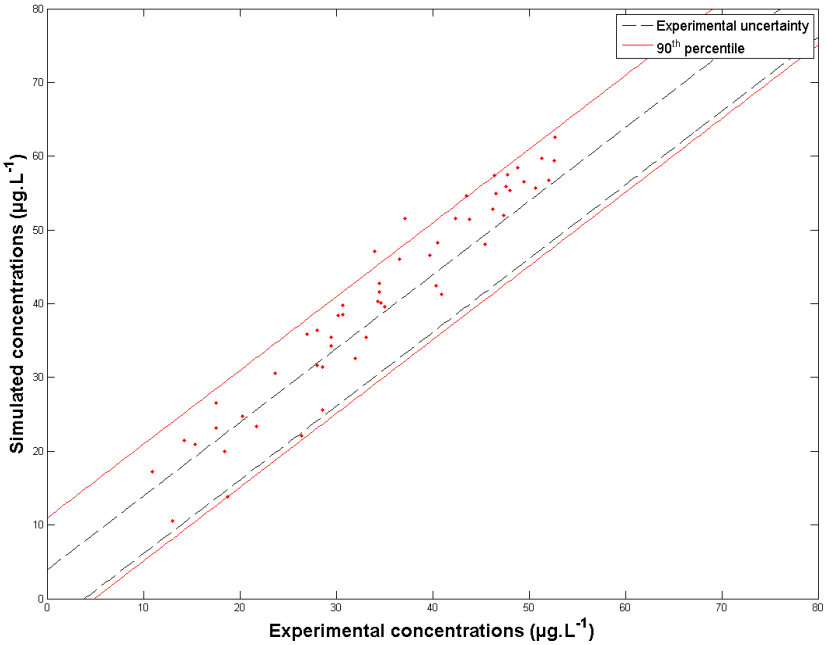

Figure 40 Comparison of simulated and experimental *p*CBA concentrations, Annet-sur-Marne water, sequential reduced calibration

Table 26 Statistical results – validation of the model, Annet water, sequential reduced calibration

Compound	r_P	Pearson test	Offset	Test	Slope	Test	% points within error
Ozone	0.97	Passed	0±0.08	Passed	1.02±0.06	Passed	64.3
*p*CBA	0.96	Passed	2.17±5.91	Passed	1.11±0.16	Passed	20

4.6.5. Summary

The main results of the simplified calibration procedure are gathered in table **27** and represented in figure **41**. Globally, the predictions are almost as good as when using all experiments for calibrating the model (significant loss of accuracy for Annet-sur-Marne and Meulan).

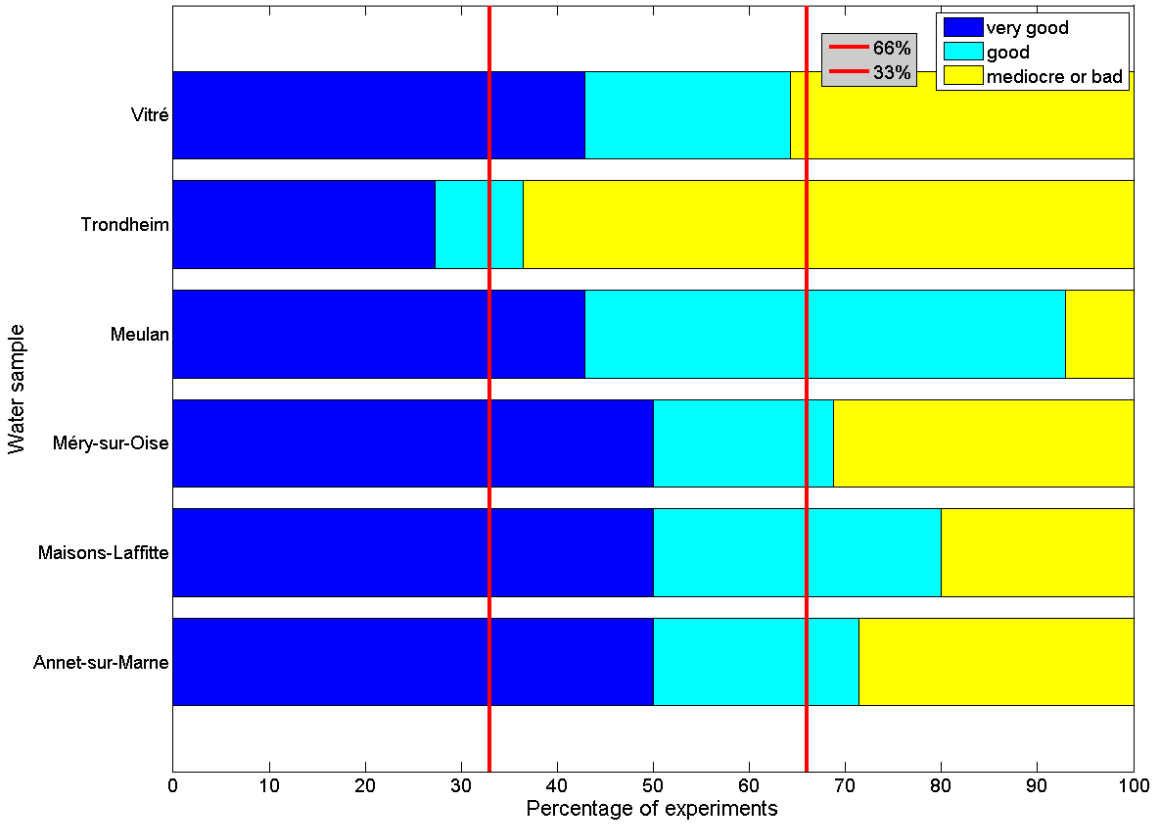

Figure 41 **Distribution of the quality of the simulations, sequential reduced calibration**

Table **27** shows that the number of experiments can be reduced without significant losses in the quality of the model predictions. The results obtained with this calibration also show that the model is able to extrapolate results since the vast majority of the experiments were not used for calibrating the model: only 36 experiments (6 per water) were used for calibration out of 120, that is, 30%. The values of the parameters are presented in Appendix **H**.

Table 27 **Statistical results: percentage of simulated points within experimental uncertainty**

Water sample	Calibration with all experiments	Sequential reduced calibration
Méry-sur-Oise	49.6	48.4
Maisons-Laffitte	63	64.4
Vitré	49.4	44.8
Annet-sur-Marne	51.4	41.5
Meulan	35	20.0
Trondheim	40.9	37.0

4.6.6. Conclusion

Simple to implement, the simplified calibration procedure presented in this section gives modelling results almost as good as with a calibration comprising much more experimental data. The following conclusions can be drawn:

- There is a possibility to reduce the number of experiments to do at laboratory to calibrate the proposed model for the role of NOM;
- The model was validated *a posteriori*, given that 70% of the experiments could be predicted by extrapolation.

However, special care has to be taken to obtain high quality experimental results, since experimental errors can dramatically impact on the quality of the calibration. Therefore, some of the experiments may be done twice in order to compensate possible experimental weaknesses.

4.7. Conclusion

To investigate and model the influence of NOM on ozone decomposition, a single-phase apparatus was especially developed. Various experimental conditions could easily be tested: contact time with ozone, pH, temperature, ozone dose, NOM nature and NOM concentration. 11 water samples originating from seven different locations were collected at different period of the year and experimentally studied.
Once proposed, the model was studied: numerical tests have shown that the strategies for parameter identification are sound. Sensitivity analysis gave evidence of the major role played by the initiating and consuming fractions of NOM. It appears that the calibration gives good results in terms of prediction, but that parameter values may be far from the optimal ones.
The semi-empirical model proposed for the role of NOM is able to adequately reproduce changes in contact time with ozone, pH, temperature, ozone dose, NOM nature and NOM concentration (75% of the experiments were modelled satisfactorily). Generally, ozone concentrations were better modelled than *p*CBA concentrations. Seasonally, NOM reacted slightly differently with ozone and hydroxyl radicals and accordingly, the values of the parameters varied. However, specific water characteristics or specific experimental conditions are less satisfactorily taken into account:

- Ozone decomposition rates at high ozone doses were underestimated by the model and experiments for which pH and NOM concentration were simultaneously lowered could not be adequately predicted;
- Waters with high organic content (TOC > 2.4 $mg.L^{-1}$) and simultaneous low inorganic content (A_T < 0.3 $meq.L^{-1}$) could not be modelled adequately;

Using only 6 experiments to calibrate the model for the role of NOM, an alternate modelling procedure also gave good results: considering a group of five water samples, 70 % of the experiments were modelled satisfactorily; when using all the experiments for calibration, 80 % of the experiments were modelled satisfactorily. Quality of the results was found weaker than with the calibration set comprising all the experiments, especially for experiments performed at low NOM concentration.

In order to broaden the results of this study, following modelling and experimental prospects can be formulated:

- It was not possible to adequately simulate waters with high TOC/A_T ratios, most likely because of the necessity for such matrices to consider a model for radical scavenging by NOM. First tries have been unsuccessful in incorporating NOM scavenging. Future work shall deal with this issue;
- A procedure to systematically minimise the number of experiments to be considered for calibration purposes shall be developed. So far, six experiments have been chosen for a simplified calibration. Was this choice optimal? Could the number of experiments considered for calibration be further reduced?

Bibliography

Articles and books

- **Bader H.** and **Hoigné J.**, (1981). Determination of Ozone in Water by the Indigo Method, *Water Research*, Vol. **15**, pp. 449-456.
- **Beltrán F. J.,** (2004). Ozone Reaction Kinetics for Water and Wastewater Systems, *LEWIS Publishers*, Washington D.C., U.S.A.
- **Béraud B., Lemoine C., Steyer J.-P.,** (2009). Multiobjective Genetic Algorithms for the Optimisation of Wastewater Treatment Processes, *in Computational Intelligent Techniques for Bioprocess Modelling, Supervision and Control*, Springer Verlag, Berlin-Heidelberg, pp. 163-195.
- **Bezbarua B. K.,** (1997). Modeling Reactions of Ozone with NOM, Ph.D. thesis, University of Massachusetts Amherst, USA.
- **Buffle M. O., Schumacher J., Meylan S., Jekel M., von Gunten U.,** (2006). Ozonation and Advanced Oxidation of Wastewater: Effect of O_3 Dose, pH, DOM and HO•-scavengers on Ozone Decomposition and HO• Genration, *Ozone: Science and Engineering*, Vol. **28**, pp. 247-259.
- **Buxton G. V., Greenstock C. L., Helman W.P., Ross A. B.,** (1988). Critical Review of Reactions of Hydrated Electrons, *Journal of Physical Chemistry Ref. Data*, Vol. **17**, pp. 513-886.
- **Cho M., Kim H., Cho S. H., Yoon J.**, (2003). Investigation of Ozone Reaction in River Waters causing Instantaneous Ozone Demand, *Ozone: Science and Engineering*, Vol. **25**, pp. 251-259.
- **Deb K., Agrawal S., Pratap A., Meyarivan T.,** (2000). A Fast Elitist Non-Dominated Sorting Genetic Algorithm for Multi-Objective Optimization: NSGA-II, *Proceedings of 6th International Conference on Parallel Problem Solving from Nature,* 16th-20th September, Paris, France, pp. 849-858.
- **Ekström P.-A.,** (2005). Eikos – A Simulation Toolbox for Sensitivity Analysis, *Master of Science thesis*, Uppsala University, Faculty of Science and Technology, Sweden.
- **Elovitz M. S.** and **von Gunten U.**, (1999). Hydroxyl Radical/Ozone Ratios during Ozonation Processes. I. The R_{ct} Concept, *Ozone: Science and Engineering*, Vol. **21**, pp. 239-260.
- **Hassan K. Z. A., Bower K. C., Miller C. M.,** (2003). Numerical Simulation of Bromate Formation during Ozonation of Bromide, *Journal of Environmental Engineering*, Vol. **129**, pp. 991-998.
- **Hoigné J.** and **Bader H.,** (1983b). Rate constants of reactions of ozone with organic and inorganic compounds in water: II non-dissociating organic compounds, *Water Research.*, Vol. **17**, pp. 173-183.
- **Hoigné J.** and **Bader H.,** (1983a). Rate constants of reactions of ozone with organic and inorganic compounds in water: II dissociating organic compounds, *Water Research.*, Vol. **17**, pp. 185-194.
- **Jeppsson U.,** (1996). Modelling Aspects of Wastewater Treatment Processes, Ph.D. thesis, Lund University, Sweden. Available at: http://www.iea.lth.se/~ielulf/publications/phd-thesis/PhD-thesis.pdf
- **Kim J.-H., von Gunten U., Mariñas B. J.**, (2004). Simultaneous Predicion of *Cryptosporidium Parvum Oocyst* Inactivation and bromate Formation during Ozonation of Synthetic Waters, *Environmental Science and Technology*, Vol. **38**, pp. 2232-2241.
- **Kim J.-H,** (2004).Integrated optimization of Cryptosporidium inactivation and bromate formation control in ozonation contactors, *Presentation at the Gwangju Institute of Technology*, May 27.
- **Kim J.-H., Elovitz M. S., von Gunten U., Shukairy H. M., Mariñas B. J.,** (2007). Modeling Cryptosporidium parvum oocyst inactivation and bromate in a flow-through ozone contactor treating natural water, *Water Research*, Vol. **41**, pp. 467-475.
- **Lagarias J. C., Reeds J. A., Wright M. H., Wright P. E.**, (1998). Convergence Properties of the Nelder-Mead Simplex Method in Low Dimensions, *SIAM Journal of Optimization*, Vol. **9**, pp. 112-147.
- **Lovato M. E., Martín C., Cassano A. E.,** (2009). A reaction kinetic model for ozone decomposition in aqueous media valid for neutral and acidic pH, *Chemical Engineering Journal*, Vol. **146**, pp. 486-497.
- **Mandel P.,** (2008). Modelling Micropollutant Removal by Ozonation and Chlorination in potable Water Treatment—Experimental Report, *TECHNEAU Technical Deliverable D.2.4.2.5.*
- **Mandel P., Wolbert D., Roche P., Pham H.-H., Bréant P.,** (2009). A modelling procedure for on-site ozonation steps in potable water treatment, *Water Science and Technology: Water Supply*, Vol. **9**, pp. 459-467.

- **Mizuno T., Tsuno H., Yamada H.,** (2007c). Development of Ozone Self-Decomposition Model for Engineering Design, *Ozone: Science and Engineering*, Vol. **29**, pp. 55-63.
- **Neta P.** and **Dorfman L. M.,** (1968). Pulse radiolysis studies. XIII: rate constants for the reaction of hydroxyl radicals with aromatic compounds in aqueous solutions, in *Radiation Chemistry*, Chapter **15**, pp. 222–230.
- **Park H.-S., Hwang T.-M., Kang J. W., Choi H., Oh H.-J.,** (2001).Characterization of raw water for the ozone application measuring ozone consumption rate, *Water Research*, Vol. **35**, pp. 2607-2614.
- **Poznyak T.** and **Araiza B.,** (2005). Ozonation of Non-Biodegradable Mixtures of Phenol and Naphtalene Derivatives in Tanning Wastewaters, *Ozone: Science and Engineering*, Vol. **27**, pp. 351-357.
- **Saltelli A., Tarantola S., Chan K. P. S.,** (1999). A quantitative Model-independent method for global sensitivity analysis of model output, *Technometrics*, Vol. **41**, pp. 39-56.
- **Savary B.**, (2002). Influence des caractéristiques d'une eau naturelle sur la formation des ions bromates au cours de l'ozonation: Observations-Prévisions-Simulations dans un réacteur diphasique du type colonne à bulles, Ph.D. thesis ENSC-R, France.
- **Sharp E. L., Parsons S., Jefferson B.,** (2006). Seasonal variations in natural organic matter and its impact on coagulation in water treatment, *Science of the Total Environment*, Vol. **363**, pp. 183-194.
- **Staehelin J.** and **Hoigné J.**, (1982). Decomposition of ozone in water: Rate of Initiation by Hydroxide Ions and Hydrogen Peroxide, *Environmental Science and Technology*, Vol. **16**, pp. 676-681.
- **Staehelin, J.** and **Hoigné, J.,** (1985). Decomposition of Ozone in Water in the Presence of Organic Solutes Acting as Promoters and Inhibitors of Radical Chain Reactions, *Environmental Science and Technology*, Vol. **19**, pp. 1206-1213.
- **Vandersmissen K., de Smedt F., Vinckier C.,** (2008). The Impact of Traces of Hydrogen Peroxide and Phosphate on the Ozone Decomposition Rate in "Pure Water", *Ozone: Science and Engineering*, Vol. **30**, pp. 300-309.
- **von Gunten U.** and **Hoigné J.,** (1994). Bromate Formation during Ozonation of Bromide-Containing Waters: Interaction of Ozone and Hydroxyl Radical Reactions, *Environmental Science and Technology*, Vol. **28**, pp. 1234-1242.
- **Wei Q.-S., Feng C.-H., Wang D.-S., Shi B.-Y., Zhang L.-T., Wei Q., Tang H.-X.,** (2008). Seasonal variations of chemical and physical characteristics of dissolved organic matter and trihalomethane precursors in a reservoir: a case study, *Journal of Hazardous Materials*, Vol. **150**, pp. 257-264.
- **Westerhoff P., Song R., Amy G.**, **Minear R.**, (1997). Application of Ozone Decomposition Models, *Ozone: Science and Engineering*, Vol. **19**, pp. 55-73.
- **Westerhoff P., Mezyk S. P., Cooper W. J., Minakata D.,** (2007). Electron Pulse Radiolysis Determination of Hydroxyl Radical Rate Constants with Suwannee River Fulvic Acid and Other Dissolved Organic Matter Isolates, *Environmental Science and Technology*, Vol. **41**, pp. 4640-4646.
- **Xiong F.** and **Legube B.,** (1991). Enhancement of Radical Chain Reactions of Ozone in Water in the Presence of an Aquatic Fulvic Acid, *Ozone: Science and Engineering*, Vol. **13**, pp. 349-362.
- **Xiong F., Croué J.-P., Legube B.,** (1992). Long-Term Ozone Consumption by Aquatic Fulvic Acids Acting as Precursors of Radical Chain Reactions, *Environmental Science and Technology*, Vol. **26**, pp. 1059-1064.

5. MODELLING THE FORMATION OF BROMATE IONS IN NATURAL WATERS

Abstract

Experiments on the formation of bromate in natural waters brought into light the importance of NOM: Models for the simulation of bromate formation have to be calibrated when dealing with natural water.

A mechanistic model for bromate formation was first proposed, based on a critical analysis of the reaction sets found in the literature. Several reactions and species were neglected, respectively based on their relative low kinetics or on their weak probability of being formed; finally a consistent set of 18 reactions was kept. Considering three water samples for which ozone and *p*CBA concentrations were correctly modelled, the bromate concentrations were modelled.

Using the values for kinetic rates from the literature resulted in a large overprediction of the modelled concentrations. Therefore, a reaction was selected for which the kinetic rate constant was calibrated. Further, modelling results showed that the kinetics of the considered reaction could not be commonly determined for the three water samples, but should instead be determined for each water sample. However, with the same kinetics for the three waters, a good linearity was observed, for each water sample, between experimental and simulated concentrations. Consequently, calibration was performed separately for each water sample. Results showed that, relatively to the experimental error, precise predictions for bromate concentrations could be obtained. Moreover, the best results were obtained at low concentration ranges (typically below 15-20 $\mu g.L^{-1}$): for the crucial concentrations below 20 $\mu g.L^{-1}$, 68% of the simulated concentrations were located within experimental uncertainty.

Comparing natural water samples, the value of the kinetic rate constant was found to vary by an order of magnitude. Seasonal variations were also observed and were found to be considerable, supporting the hypothesis of a major role played by NOM during bromate formation.

Contents

5.1. Introduction

Ozone and hydroxyl radical are the main oxidative species involved during ozonation; as such, their concentrations have to be accurately modelled when seeking to predict the formation of bromate ions. We have therefore first proposed and validated a model representing the ozone decomposition and the generation of hydroxyl radicals in natural waters (chapter **4**). In the current chapter, we discuss modelling possibilities for bromate formation in natural waters.

Modelling bromate formation remains no easy task since many reactions may occur, with very different kinetics as both molecular and radical reactions are involved. As a consequence, fundamental studies on the kinetics of elementary reactions have focused on particular parts of the pathway leading to bromate. The first studies, which have proposed models for the formation of bromate have thus merged results obtained by different authors, often under different experimental conditions (pH, temperature, alkalinity etc.) Having determined models valid in NOM-free waters, researchers have then tried to model bromate formation in natural waters. The influence of NOM in the formation of bromate is often modelled by on one or two additional reactions added to the models developed in NOM-free waters. Whether it be for NOM-free or natural waters, there is no unified model that has been adopted by the scientific community.

Moreover, very few studies have dealt with the impact of seasonal changes in NOM characteristics on the levels of bromate formation. However, it has been reported that seasonal changes in NOM may induce changes in the formation of ozonation by-products such as trihalomethane [Wei *et al.*, 2008] or brominated organics [Huang *et al.*, 2004].

The main objective of this chapter is to propose and validate a model for the formation of bromate in natural waters. As many individual chemical reactions can be found in literature, we shall develop a model by selecting a consistent set of specific reactions. The validity of the model shall be determined for three types of waters. Additionally, the impact of seasonal variations in NOM characteristics will be studied with water samples collected at different periods of the year.

The two single-phase protocols used to study the formation of bromate are presented in section **5.2**. Different modelling procedures are presented in sections **5.3** and **5.4**: in the section **5.3**, a unified model for the different water samples is tested; in the section **5.4**, the kinetics of a specific reaction of the model is adjusted, for each water sample. Comparisons among water samples reveal the inability of a model developed in NOM-free water to represent the formation of bromate in natural waters. This conclusion is underlined by the seasonal variations observed in the levels of bromate formed.

5.2. Materials and Methods

5.2.1. Protocols

5.2.1.1. Aqueous Ozone Production

Aqueous ozone was prepared dissolving gaseous ozone into UPW (Ultra Pure Water) as explained in chapter **4**, **4.2.1.1**. The vessel used for dissolution was cooled for the water samples: Vitré 3 and Meulan 3 (see the specifications of the samples in chapter **4**, **4.2.2.2.**). For the other water samples, the dissolution occurred at room temperature.

5.2.1.2. Gas-Tight Syringe Set-Up

Water samples Annet-sur-Marne, Vitré and Meulan were experimentally investigated using the gas-tight syringe set-up described in chapter **4**, **4.2.1.2**.

5.2.1.3. Erlenmeyers Set-Up

Water samples Annet-sur-Marne 2, Vitré 3 and Meulan 3 were experimentally investigated using another single-phase set-up for ozonation. This set-up is schematically depicted in figure **1**. This set-up was used in order to withdraw larger quantities of water for bromate concentration measurements, as required by the CAE-SM.

Ozone is first dissolved in a specially conceived 2L reactor: ozone goes in the reactor via a glass tube (see figure **1**, a), bubbles into UPW through a sintered glass diffuser (b) and goes to the ozone destructor via an exhaust glass tube (c). Once dissolved, aqueous ozone is introduced into all reactors using a 10-60 mL headless Ceramus dispenser (Hirschmann Laborgeräte, Heilbronn, Germany) screwed on the dissolution vessel (figure **1**, d). The volumes introduced varied from 10 mL to 40 mL, corresponding to dilution factors of 1/30 to 4/30, respectively (erlenmeyers contained 300 mL liquid, thus minimising gas phase). Ozonation takes place in a series of 250 mL screw cap erlenmeyer flasks placed on a magnetic multistirrer (figure **1**, e). Each reactor corresponds thus to a contact time with aqueous ozone; performing several measurements with the same reactor would have indeed generated a gaseous headspace, hence favouring ozone stripping.

Special care was taken to ensure repeatable injection, stirring, sample withdraws and sample analysis steps. These items were closely followed during the protocol test phase (not presented here). All materials in contact with ozone were especially chosen according to their chemical compatibility.

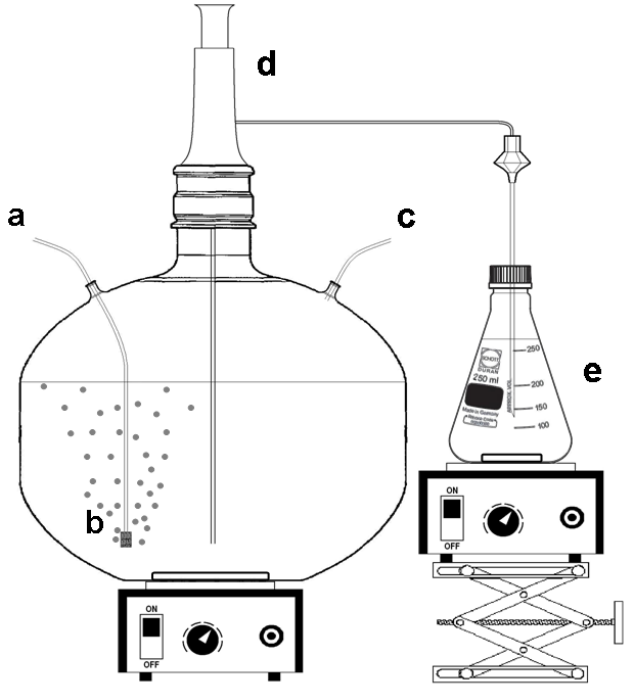

Figure 1 **Schematic of the erlenmeyer experimental set-up**

Such protocols have been widely used over the past years; see *e.g.* [Pinkernell and von Gunten, 2001]. Contact times were generally 30'', 1', 2'30'', 5', 15', 35' and 60'. Samples were withdrawn with a Kloehn gas-tight syringe and then analysed for assessments of: aqueous ozone concentration, bromide and bromate ion concentrations (for aqueous ozone, see

chapter **4**, **4.2.3.**). For all analyses, except aqueous ozone concentration, the samples were quenched using fresh sodium thiosulfate.

5.2.1.4. Comparison of the Set-Ups

The results obtained with both set-ups were compared. Results showed a good agreement of experimental procedures. An example of an ozonation experiment performed with both set-ups is given in figures **2** and **3**. Experiments were conducted under the same experimental conditions (Ozone dose = 1.65 ± 0.05 mg.L^{-1}; natural pH = 7.85; T = 18°C; $[p\text{CBA}]_0$ = 95.2 µg.L^{-1}), the same day, on the same water (sand-filtered water from Méry-sur-Oise water works).

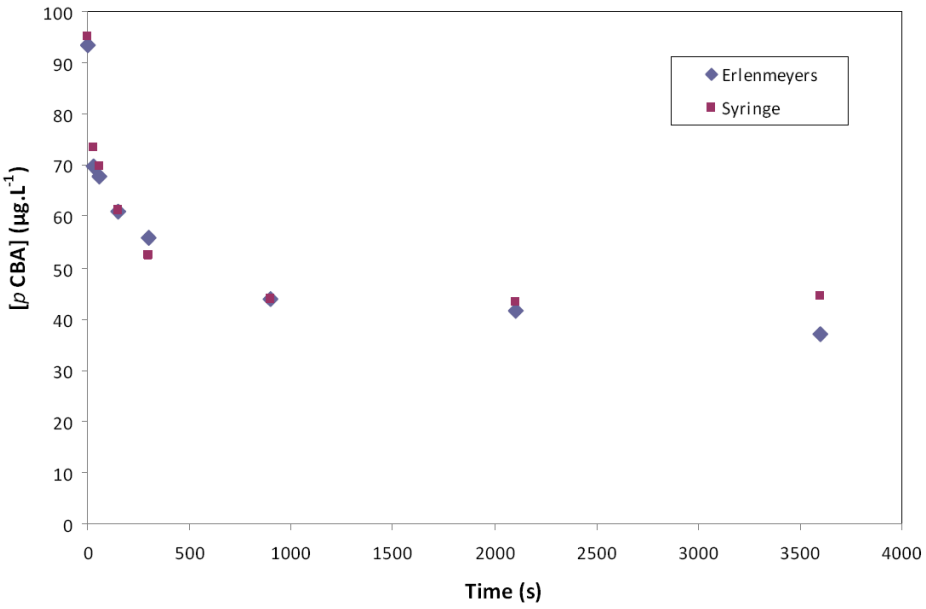

Figure 2 **Compared *p*CBA concentration profiles for Erlenmeyer and Syringe set-ups**

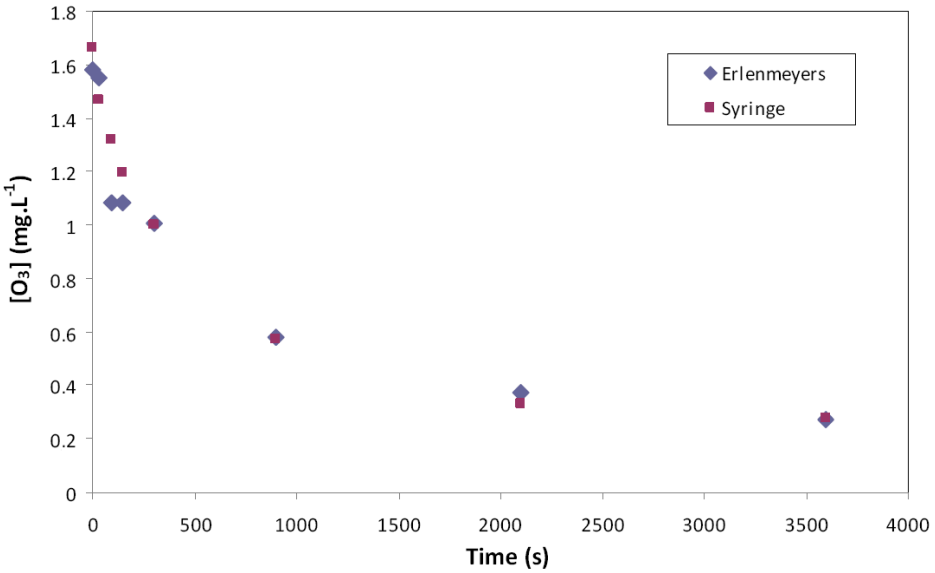

Figure 3 **Compared ozone concentration profiles for Erlenmeyer and Syringe set-ups**

5.2.2. Reactants and Water Characteristics

The reactants and water characteristics have been presented in chapter **4**, **4.2.2.2**.

5.2.3. Analyses

5.2.3.1. Bromide/Bromate Concentrations

ENSCR

At ENSCR, bromide and bromate ion concentrations were measured with a DX-120 Dionex (Sunnyvale, USA) ionic chromatography using an AS 50 autosampler, a IONPAC AS19 column and a EGC II KOH EluGen cartridge. The potassium hydroxide concentration gradient decomposed into following steps: constant (=10 mM) during 10 minutes, linear increase to 45 mM within 15 minutes, linear decrease to 10 mM within 10 minutes; total duration = 35 minutes. Quantification limits for bromide and bromates were 15 $\mu g.L^{-1}$ and 2 $\mu g.L^{-1}$, respectively.

CAE-SM

At CAE-SM, bromide and bromate concentrations were measured with a Dionex (Sunnyvale, USA) ionic chromatography system using a IONPAC AS19 column with a EGC KOH EluGen Potassium Hydroxide Cartridge. The elutant was composed of water and potassium hydroxide (058900 Dionex). Quantification limit for bromate was 2 $\mu g.L^{-1}$.

5.2.3.2. Other Analyses

All other analyses were done according to chapter **4**, **4.2.3.**

5.2.4. Experiments Performed

5.2.4.1. First design of Experiments

The formation of bromate for the water samples Annet-sur-Marne, Vitré and Meulan was studied under the same experimental conditions as those, which served to characterise the influence of NOM over ozone decomposition and hydroxyl radical generation (see table **1** and **2**). Nevertheless, the very short contact times with ozone were not considered; for each experiment, 4 contact times were tested: 5', 15', 35' and 60'. Bromate concentrations for the experiments where NOM was diluted were not measured with Vitré water due to analytical troubleshooting.

Table 1 Overview of the first design of experiments

Experiment #	**1**	**2**	**3**	**4**	**5**	**6**	**7**	**8**	**9**	**10**	**11**	**12**	**13**	**14**
Scavenger adding (10mM *tert*-BuOH)		X		X				X		X		X		X
pH drop (pH natural-1)			X	X					X	X	X	X	X	X
Large O_3 dose (1.4 $mg.L^{-1}$→2.3 $mg.L^{-1}$)					X	X							X	X
Temperature drop (20°C→5°C)						X	X	X	X	X				
NOM dilution (with UPW)											X	X	X	X

5.2.4.2. Second Design of Experiments

Annet-sur-Marne 2 water sample was investigated with a second design of experiments. Focus was put on two experimental factors: initial bromide concentration and ozone dose.:

- Five levels were defined for initial bromide concentration: natural concentration; natural concentration increased by 20 $\mu g.L^{-1}$; 40 $\mu g.L^{-1}$; 60 $\mu g.L^{-1}$ and 80 $\mu g.L^{-1}$.
- Three levels were defined for ozone dose: 0.9 $mg.L^{-1}$; 1.6 $mg.L^{-1}$; 2.3 $mg.L^{-1}$.

A full-factorial approach was chosen, thus resulting in 15 experiments. All other experimental parameters were kept constant at their natural value (pH, alkalinity, TOC). The

experiments were done at room temperature and contact time with ozone was kept constant at 10 minutes.

5.2.4.3. Third Design of Experiments

Vitré 3 and Meulan 3 water samples were investigated with a third design of experiments. The overview of the experiments performed is given in table **2**. Based on the analysis of the experimental results obtained with the first two designs, the experiments of the third design were chosen in order to produce low, medium and high amounts of bromate. Two contact times with ozone were tested: 10 minutes and 35 minutes.

Table 2 Overview of the third design of experiments

Experiment #	**1**	**2**	**3**	**4**	**5**	**6**	**7**	**8**	**9**
Scavenger adding (10mM *tert*-BuOH)		X	X			X			
pH drop (pH natural-1)			X					X	X
Large O_3 dose (1.4 $mg.L^{-1}$→2.3 $mg.L^{-1}$)				X			X		X
Temperature drop (20°C→5°C)					X	X	X		
NOM dilution (with UPW)								X	X

5.2.4.4. Summary

The experimental conditions for the above presented series of experiments are summarised in table **3**. More details on the materials used can be found in chapter **4**, **4.2.4**.

Table 3 Summary of the experiments done in this chapter

	1st DoE[1]	**2nd DoE**	**3rd DoE**
Ozone generator	Trailigaz	BMT	Astex Sorbios
Ozonation vessel	Not thermostated	Not thermostated	Thermostated
Protocol	Gas-tight syringe	Erlenmeyers	Erlenmeyers
Water	Annet-sur-Marne, Vitré, Meulan	Annet-sur-Marne 2	Vitré 3, Meulan 3
Bromate analyses	ENSCR	CAE-SM	CAE-SM

5.3. Towards a Unified Model for the Prediction of Bromate Formation in Natural Waters

5.3.1. Scope and Objective

The influence of NOM on bromate formation is unclear, so that its modelling essentially remains case-dependent. Halogens are known to react with NOM, principally by oxidation or substitution. Studies investigating the effects of halogens on the formation of DBPs have generally focused on chlorinated species (*e.g.* [Reckhow *et al.*, 1990]; [Gallard and von Gunten, 2002]). Considering brominated species, experimental studies have shown that NOM generally lowers the levels of bromate formed (*e.g.* [Westerhoff *et al.*, 1998b]; [Pinkernell and von Gunten, 2001]). Additionally, studies using fractionation technique have also shown that NOM nature may influence the formation of bromate [Westerhoff *et al.*, 1998b]. Studies underlined the role of hypobromous acid (and hypobromite, BrO^-), however, the kinetics and the action of NOM into bromate formation remains for a large part unknown.

Moreover, the influence of NOM on ozone and hydroxyl radical concentrations has already been taken into account in the model. Results of the previous chapter showed that variations in contact time with ozone, pH, temperature, ozone dose, NOM content and NOM concentration can be represented by the proposed model.

[1] DoE: Design of Experiments

The objective of this section is to evaluate the possibility of using the same kinetics to describe the formation of bromate in different natural waters. We will first apply a model valid in NOM-free water and compare its results to experimental measurements. Then, the model will be slightly readjusted for all water types considered together, in order to assess if a unified model can be considered for the prediction of bromate formation in natural waters. Only the experiments done with the following water samples are considered in this section: Annet-sur-Marne, Vitré and Meulan. The reader is referred to chapter **4** for details on the protocol, the analyses etc.

5.3.2. Chemical Model Selected

The chemical pathway developed for modelling bromate formation comprises the most important reactions that may occur. Out of the 51 most important reactions presented in chapter **1** (section **1.6.**), only 18 have been eventually selected. A schematic overview of the chemical pathway leading to bromate is presented in figure **4**. The complete model, with its kinetics (frequency factors and energies of activation) can be found in Appendix **D**.

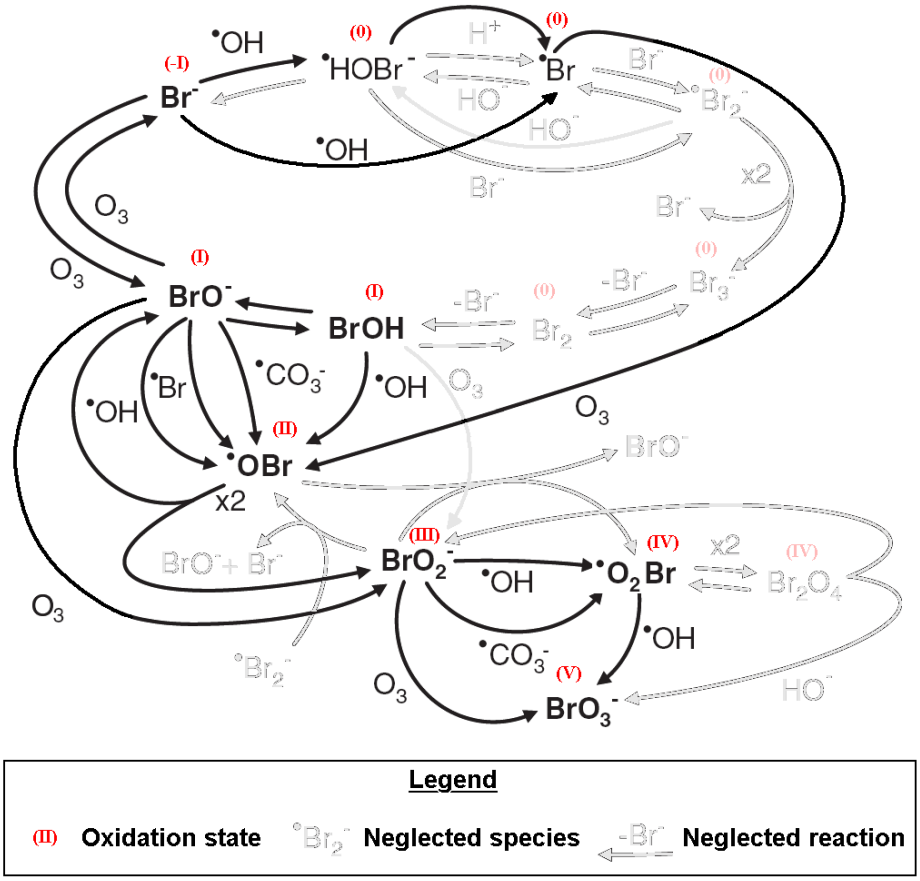

Figure 4 **Schematic overview of the chemical pathway for the formation of bromate ions**

Some species have been considered as negligible within the bromate formation mechanism. All reactions producing or consuming a neglected species were removed. The neglected species are:

- Br_2O_2, formed by a termination step: $2^{\bullet}OBr \rightarrow Br_2O_2$ is generally neglected (*e.g.* [Westerhoff *et al.*, 1998a]; [Pinkernell and von Gunten, 2001]; [Kim *et al.*, 2004]);
- Br_2O_4, only formed by a termination step ($2^{\bullet}O_2Br \rightarrow Br_2O_4$) and rapidly dismutated;

- $^{\bullet}HCO_3$ compared to $^{\bullet}CO_3^-$. Despite the predominance of hydrogenocarbonate radicals at the pHs investigated (pK_A=9.6), it has been neglected as in previous studies (*e.g.* [von Gunten and Hoigné, 1994]; [Westerhoff *et al.*, 1998a]; [Kim *et al.*, 2004]);
- $^{\bullet}Br_2^-$, Br_3^-, Br_2, Br_2OH^- since these compounds are not directly involved in bromate generation, but may act as "sinks" for bromide. The removal of these compounds is discussed and justified on the basis of modelling results in Appendix **I**.

Reactions have been considered as negligible:

- $BrOH + O_3 \rightarrow BrO_2^- + O_2 + H^+ << BrO^- + O_3 \rightarrow BrO_2^- + O_2$: even if hypobromous acid is predominantly found at pHs of natural waters (pK_A =8.8), the ratio (10^4) of the kinetic rate constants supports this assumption;
- $^{\bullet}OH + BrO_3^- \rightarrow {}^{\bullet}OBr + HO^- + O_2 << BrO_2^- + {}^{\bullet}OH \rightarrow {}^{\bullet}O_2Br + HO^-$ given the ratio (660) of the kinetic rate constants.

Besides, reactions involving key concentrations controlling ozone decomposition, as superoxide radicals or hydrogen peroxide (protonated or not), were not considered in the bromate formation mechanism.

5.3.3. Results With a NOM-free Model

The model, with all the kinetics taken from the literature, is evaluated by comparing the simulated and experimental results obtained with the water samples: Annet-sur-Marne, Vitré and Meulan. The results are presented in figure **5**.

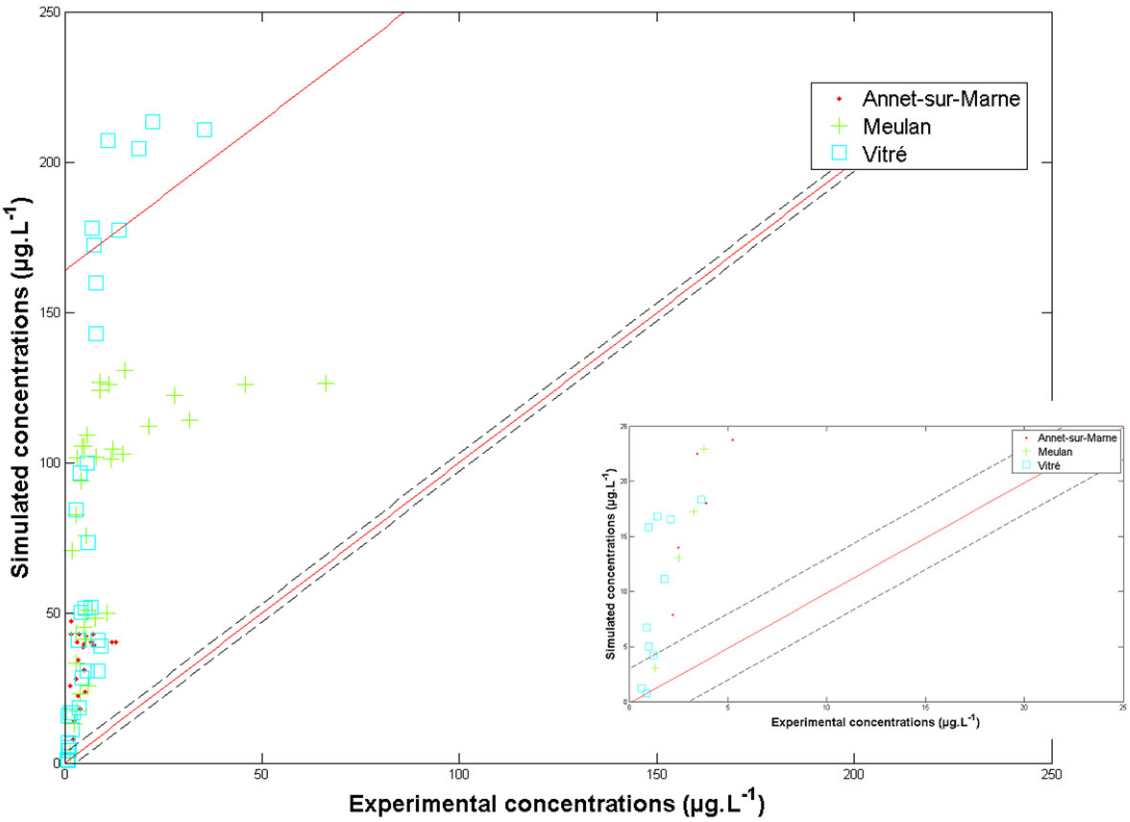

Figure 5 Comparison of simulated and experimental bromate concentrations with a unified model, kinetic values from the literature (the dashed bars represent the experimental uncertainty, the solid red lines the 90th percentiles); insert: blow-up for concentrations below 25 µg.L-1

The model considered in this study, with kinetics valid in NOM-free water, massively overpredicts bromate formation, when dealing with natural water. This observation is in agreement with already reported observations (*e.g.* [Westerhoff *et al.*, 1998b]; [Pinkernell and von Gunten, 2001]). The ratio of simulated to experimental concentration varies between 3 (Meulan water sample) and 10 (Vitré water sample). These values are comparable to what was obtained by [Westerhoff *et al.*, 1998a]: with a model already validated in NOM-free water, Westerhoff overpredicted the concentrations of bromate in the presence of an organic fraction by a factor of approximately 3. [Kim *et al.*, 2007] experimentally studied the ozonation of sand-filtered water from the Ohio River in an ozone contactor comprising a bubble column and a reactive column connected in series. Kim and co-workers found that their model overpredicted bromate concentrations 5 to 6.5-fold when neglecting the influence of NOM (into the bromate formation pathway). Note also in figure **5** the scattering of the points for higher experimental concentration values.
Although NOM's role is already considered in the model for ozone decomposition and hydroxyl radical generation, the results showed that its influence over bromate formation has to be specifically taken into account.

5.3.4. Taking into Account the Role of NOM

5.3.4.1. Previous Approaches

Previous studies also reported the dramatic decrease of bromate formation when experimentally studying natural waters and applying NOM-free models. Some authors have proposed models for the role of NOM into bromate formation.
By analogy with the formation of THMs during chlorination, hypobromous/hypobromite is often considered as a key species prone to react with NOM. Therefore, chemists and modellers have proposed different strategies, presented in table **4**:

- The reaction of hypobromous acid and hypobromite with NOM may lead to bromoorganic compounds or to organic-halide species (equation **1** in table **4**);
- HOBr/OBr^- reacting with NOM may also lead back to bromide, resulting in a ''catalytic'' destruction of ozone (equations **2** and **3**);
- [Westerhoff *et al.*, 1998a] and [Kim, 2004] have also proposed a combination of the two previous reactions (equation **4**).

Reduction reactions by scavenging of brominated radicals have also been proposed:

- Reduction of •Br to Br^- (equation **5**) essentially has an impact on initial bromate formation, given the importance of •Br during the initial phase of ozonation [Pinkernell & von Gunten, 2001]. Adding this reaction to a chemical pathway for bromate formation has therefore only limited impact: Pinkernell and von Gunten considered this reaction for lowering the bromate concentration by 25% or so;
- Reduction of •OBr to BrOH has also been proposed (equation **6**).

Table 4 Reactions involving NOM within the bromate formation pathway

Reaction		Kinetic constant value ($M^{-1}.s^{-1}$)	Water	Reference
$BrOH + NOM \rightarrow Br - organics$	**(1)**	*No data*	Organic fractions	[Siddiqui and Amy, 1993]; [Huang *et al.*, 2004]
$BrO^- + NOM \rightarrow products + Br^-$	**(2)**	5	NOM free + fraction	[Westerhoff *et al.*, 1998a]
$BrOH + NOM \rightarrow products + Br^-$	**(3)**	5	NOM free + fraction	[Westerhoff *et al.*, 1998a]
$BrOH + NOM \rightarrow \gamma Br^- + (1-\gamma)TOBr$	**(4)**	3.10^5	Sand-filtered Ohio River water	[Kim, 2004]
$^{\bullet}Br + NOM \rightarrow Br^-$	**(5)**	10^9 (fitted with [NOM] = 2.10^{-6} M)	Sand-filtered (Maisons-Laffitte and Zürich)	[Pinkernell & von Gunten, 2001]
$^{\bullet}OBr + NOM \rightarrow BrOH + products$	**(6)**	5.10^3		[Westerhoff *et al.*, 1997]

Very little research is nevertheless available on the reaction of specifically hypobromous acid with model or organic compounds. [Echigo, 2002], studying ten different natural waters at pH comprised between 7 and 8 and at 20°C, observed that the reaction rate constant for the reaction **3** ranged from $2.4.10^5$ $M^{-1}.s^{-1}$ to $1.3.10^6$ $M^{-1}.s^{-1}$. The number of reaction sites in NOM was estimated between 0.2 µmol.mgC^{-1} and 0.7 µmol.mgC^{-1} (as reported by [Kim *et al.*, 2007]), that is between 2.4‰ and 8.4‰ of the TOC. This value was found extremely low by [Kim *et al.*, 2007] when testing these kinetic values: even with the highest values, the bromate formation was still overpredicted. This fact is supported by the outcomes of [Westerhoff *et al.*, 2004]. Working with isolates, Westerhoff found hypobromous acid to be ten times more reactive than hypochlorous acid towards NOM. Besides, hypobromous and hypochlorous acids were found to react differently, respectively substituting into organic structures and cleaving carbon bonds. In the case of hypobromous acid, a small fraction (a few percent) of the halogen adds to NOM [Gallard and von Gunten, 2002]; it is therefore expected that the formation of bromo-organic compounds during ozonation is of intermediate importance.

5.3.4.2. Simple Empirical Approach

A simple empirical approach was proposed. In order to easily control the formation of bromate ions, the kinetics of a key step was chosen to be adjusted, even though NOM may not directly influence this particular reaction. Besides, for simplicity reason, it was decided to limit the number of NOM-dependent parameters that will have to be adjusted when modelling natural water. Therefore, all reactions where NOM appeared and for which an initial concentration has to be fitted were not considered. Instead, the kinetics of the last molecular oxidation – equation **7** – was fitted (frequency factor and energy of activation).

$$BrO_2^- + O_3 \xrightarrow{k_{Brox}} BrO_3^- + O_2 \qquad \textbf{(7)}$$

In addition, this reaction was chosen because its kinetics may differ from author to author: >10^5 $M^{-1}.s^{-1}$ for [von Gunten and Hoigné, 1994]; 10^5 $M^{-1}.s^{-1}$ for [Pinkernell and von Gunten, 2001]. This difference, together with the simplicity of the adjustment, explains the choice of equation **7**. A drastic drop in the kinetics of equation **7** may yield abnormally high concentrations of BrO_2^- in the system. Such accumulation however should not destabilise other kinetics since BrO_2^- only reacts to form bromate ions (directly or indirectly, *via* $^{\bullet}O_2Br$).

[Westerhoff *et al.*, 1998a] have instead considered the first molecular oxidation (equation **8**) and optimised its kinetic reaction rate constant, lowering it from 160 $M^{-1}.s^{-1}$ to 50 $M^{-1}.s^{-1}$.

$$Br^- + O_3 \rightarrow BrO^- + O_2 \quad \textbf{(8)}$$

5.3.4.3. Results

Considering the results of the three water samples together, the values of the frequency factor and the energy of activation of equation **7** were optimised. The results are presented in figure **6**.

Contrasted results are to be seen on figure **6**. A globally satisfying agreement of the simulated concentrations with experimental measurements is observed for low concentrations, while some simulated concentrations are far from the original experimental concentrations, especially for experimental concentrations above 10 $\mu g.L^{-1}$. This observation is of interest for modellers seeking an application of a predictive model for bromate formation, since the crucial zone for experimental concentrations below 20 $\mu g.L^{-1}$ is generally well predicted. Table **5** gathers the measures of the percentages of simulated points located within experimental uncertainty zone.

Table 5 Simulated points within experimental uncertainty, unified model

Concentration range ($\mu g.L^{-1}$)	All waters	Annet-sur-Marne	Vitré	Meulan
[0; 10]	79%	94%	37%	70%
[0; 20]	70%			
All concentrations	68%			

It is worth noting the globally linear answers of the model and the three distinct populations of points, which reinforce the concept of adjusting the kinetics of reaction **7** individually for each water sample. However, the simulated results for Meulan water seem to reach a plateau at higher experimental concentration.

The optimised values are k_{Brox}=1.6.10^3 $M^{-1}.s^{-1}$ at 293K, E_A = 43 $kJ.mol^{-1}$, instead of 1.10^5 $M^{-1}.s^{-1}$ at 293K, E_A = 42 $kJ.mol^{-1}$ for the literature values.

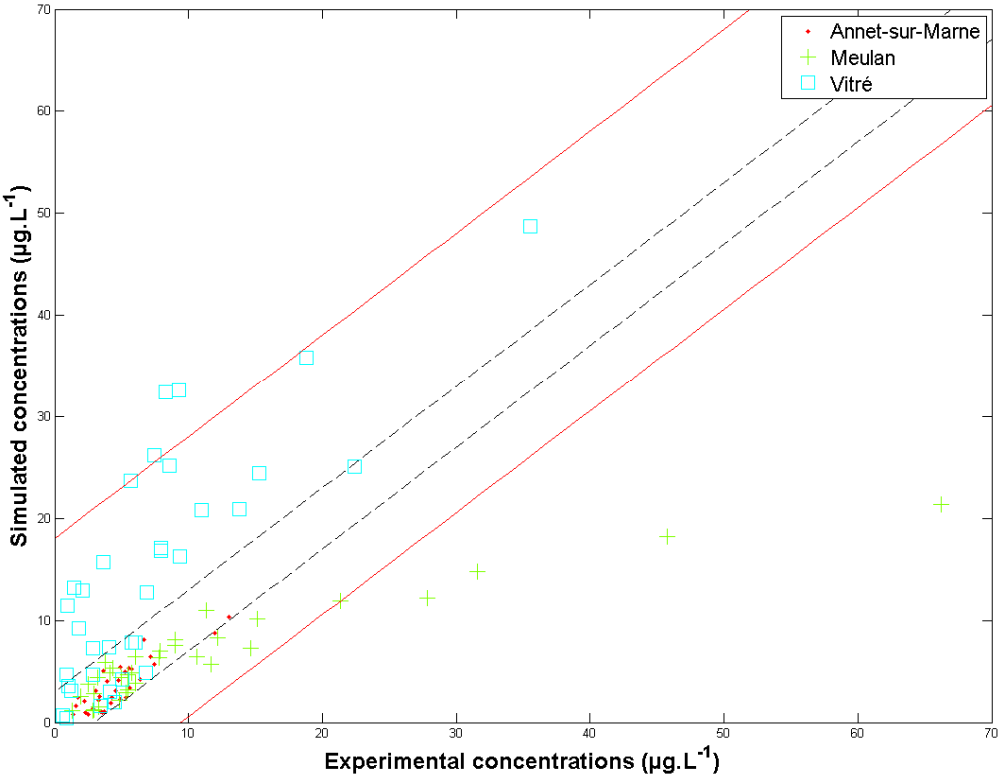

Figure 6 Comparison of simulated and experimental bromate concentrations with a unified model, kinetic values adjusted: k_{Brox}=1.6.10^3 M^{-1}.s^{-1} at 293K, E_A = 43 kJ.mol^{-1}

Considering the average quality of the simulation results obtained with our global model, it was decided not to apply such model to the results of Annet-sur-Marne2 and following water samples. Considering the differences in the quality of the modelling observed among water samples, it is decided to individually optimise the kinetics of reaction **7**. In other words, a global model for bromate formation in natural waters is not adapted to our experimental results.

5.4. An Adaptable Model for the Formation of Bromate in Natural Waters

5.4.1. Principle

The previous model is now adjusted for each water sample using the optimisation code *fminsearchbnd* (see chapter **4**) and tested for all the experiments performed (changes in pH, NOM, temperature, ozone doses etc.)

5.4.2. Annet-sur-Marne

The results of the model simulations are presented on figure **7**. They show an excellent agreement of simulated to experimental concentrations: 94% of the simulated points are located within experimental uncertainty. However, the experimental results did not allow us to explore higher experimental concentrations, as for other water samples. The optimised values are k_{Brox}=2.10^3 M^{-1}.s^{-1} at 293K and E_A = 43 kJ.mol^{-1}.

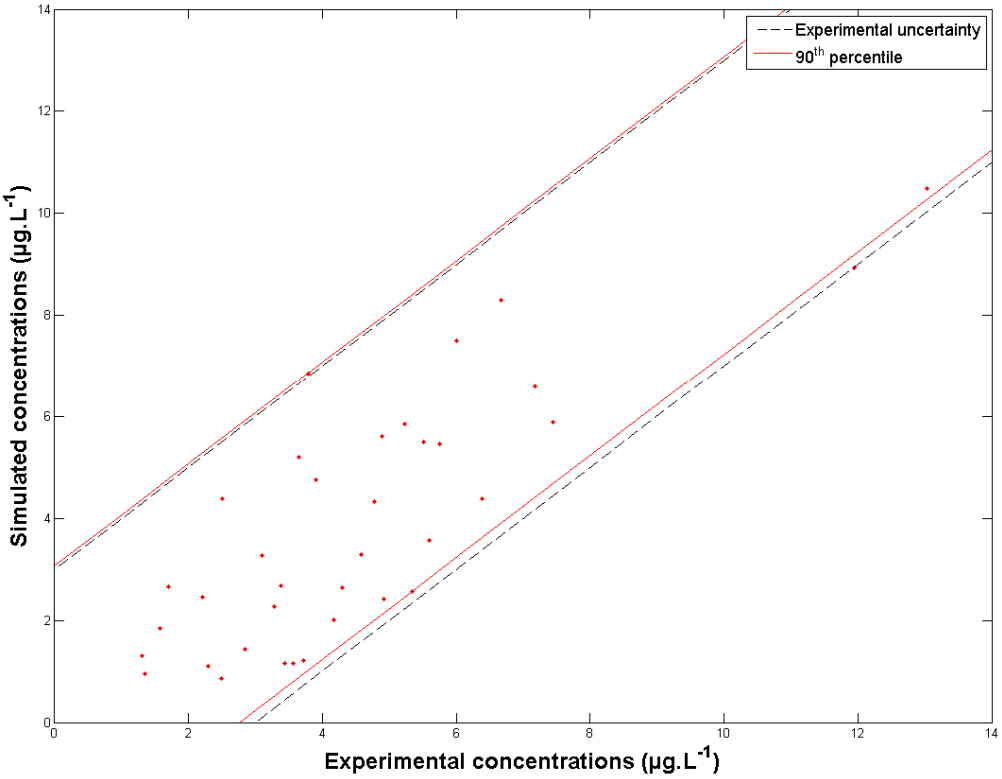

Figure 7 Comparison of simulated and experimental bromate concentrations, Annet-sur-Marne water sample

5.4.3. Vitré

The results of the model simulations are presented on figure **8**. A very good agreement of simulated to experimental concentrations is also to be seen: 73% of the simulated concentrations are located within experimental uncertainty (compared to 37% with an optimisation on all waters). The two outliers (overprediction of the model) correspond to contact times with ozone of 15′ for experiment #6 (see table **1** for the corresponding experimental conditions) and 35′ for experiment #1. The optimised values are k_{Brox}=1.1.10^{2} M^{-1}.s^{-1} at 293K and E_A = 45 kJ.mol^{-1}.

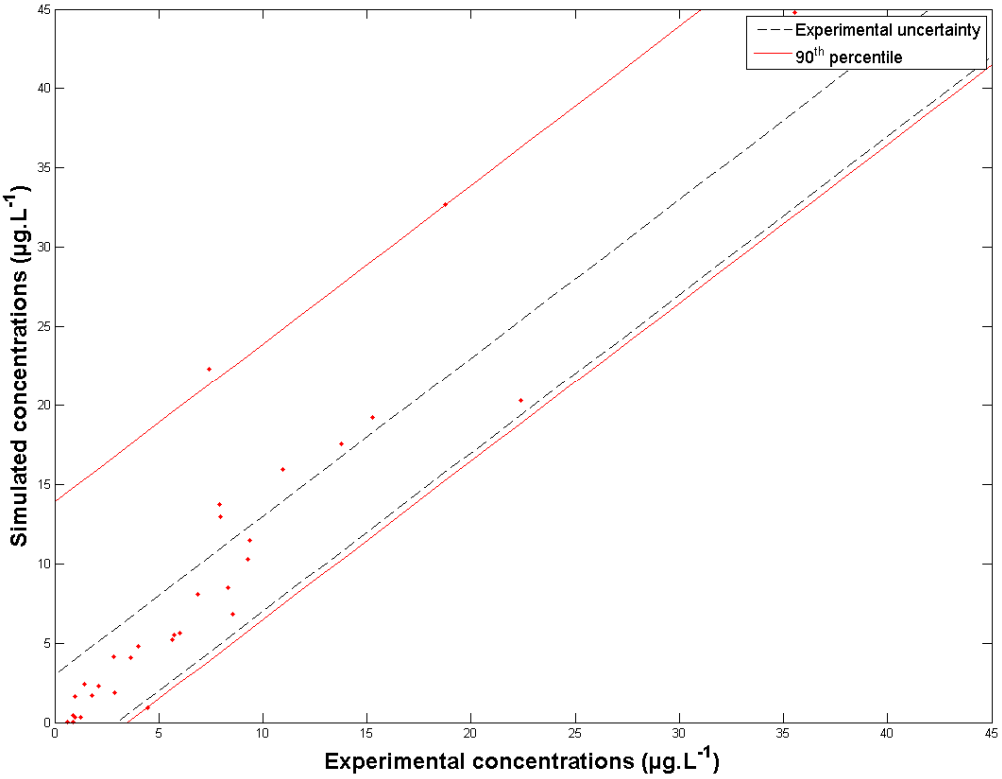

Figure 8 Comparison of simulated and experimental bromate concentrations, Vitré water sample

The concentration profiles of the oxidative species for experiments #1 and #6 are represented in figure **9**. The quality of the simulated profiles may explain the overprediction in bromate concentration only in the case of experiment #6, for which hydroxyl radical concentration is largely overpredicted (underprediction of the *p*CBA concentration).

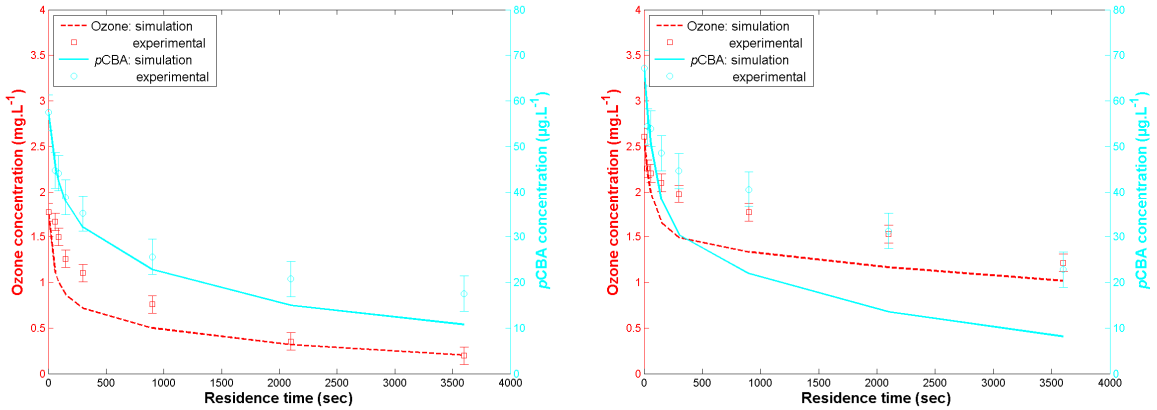

Figure 9 Concentration profiles for ozone and *p*CBA, Vitré water; Experiment #1 (left hand-side), Experiment #6 (right hand-side)

5.4.4. Meulan

The results of the model simulations are presented on figure **11**. A very good agreement of simulated to experimental concentrations is to be seen for concentrations below 20 µg.L-1. For higher experimental concentrations, the simulated concentrations are dramatically low.

Underprediction of the model was observed mainly for the results of experiment #5 (high ozone dose, see table **1**). This could not be explained by important errors in the concentration profiles for the oxidative species: see the relatively good agreement in figure **10**.

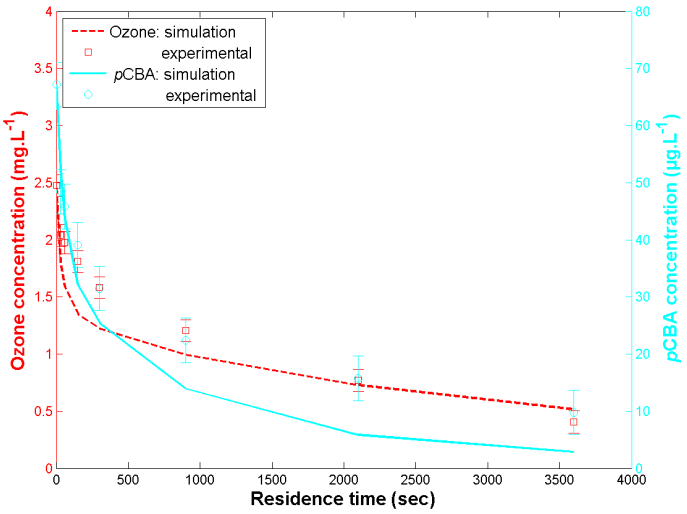

Figure 10 **Concentration profiles for ozone and *p*CBA, experiment #5, Meulan water**

Globally, 53% of the simulated points are located within the experimental uncertainty zone. Considering the crucial concentrations below 20 µg.L^{-1}, 62% of the simulated points are located within experimental uncertainty. The optimised values are k_{Brox}=1.8.10^{3} M^{-1}.s^{-1} at 293K and E_A = 41 kJ.mol^{-1}, which are very close from the values determined for the three water samples together (see **5.3.4.3.**).

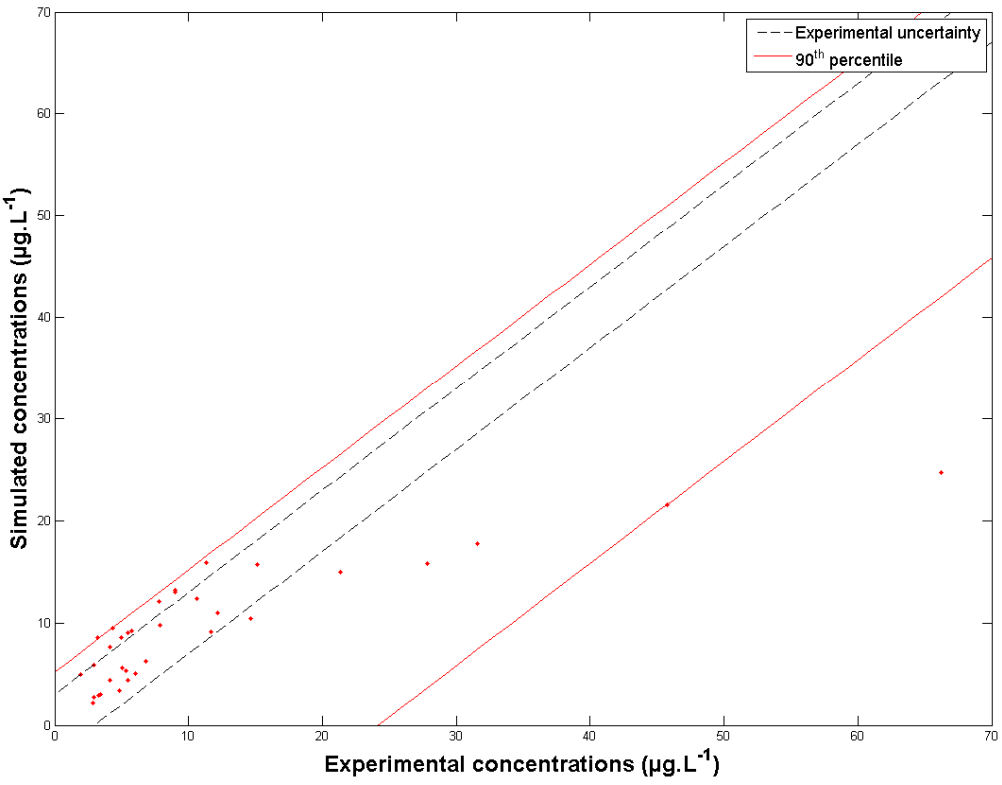

Figure 11 **Comparison of simulated and experimental bromate concentrations, Meulan water sample**

5.4.5. Annet-sur-Marne2

Design of experiments Annet-sur-Marne2 was built up to document two topics: (i) seasonal variation in bromate formation; (ii) robustness of the model to initial bromide concentration. Moreover, three levels in ozone dose were tested in order to test the model with regards to a parameter that had appeared critical with Meulan (Experiment #5) and Vitré (Experiment # 6) waters.

The results of the simulations are presented in figure **12**. One observes a global agreement of the model with experimental measurements: when the ozone dose increases, so the experimental and simulated concentrations; with the same ozone dose, experimental and simulated concentrations increase with initial bromide concentration. However, only average simulation results could be achieved when exploring a large domain combining important variations in ozone dose and initial bromide concentration. In addition, results show that:

- the model overestimates changes in initial bromide concentrations (compare all concentrations at a specific ozone dose);
- the model underestimates changes in ozone dose (compare the lowest concentrations for the three ozone doses etc.)

The optimised values are k_{Brox}=4.5.10^4 M^{-1}.s^{-1} at 293K and E_A = 42 kJ.mol^{-1}. The determined values are the highest among all water samples; they are particularly high compared to those obtained previously with a water sample from Annet-sur-Marne collected in March 2009 (k_{Brox}=2.10^3 M^{-1}.s^{-1} at 293K and E_A = 43 kJ.mol^{-1}). Such spectacular variation corresponds to a seasonal change that is observed every year on the Annet-sur-Marne water works: bromate concentrations rise at the beginning of May, reach their peak at the end of June and decrease afterwards. This evolution is not only due to temperature changes (see chapter **6**, **6.2.4.3.**).

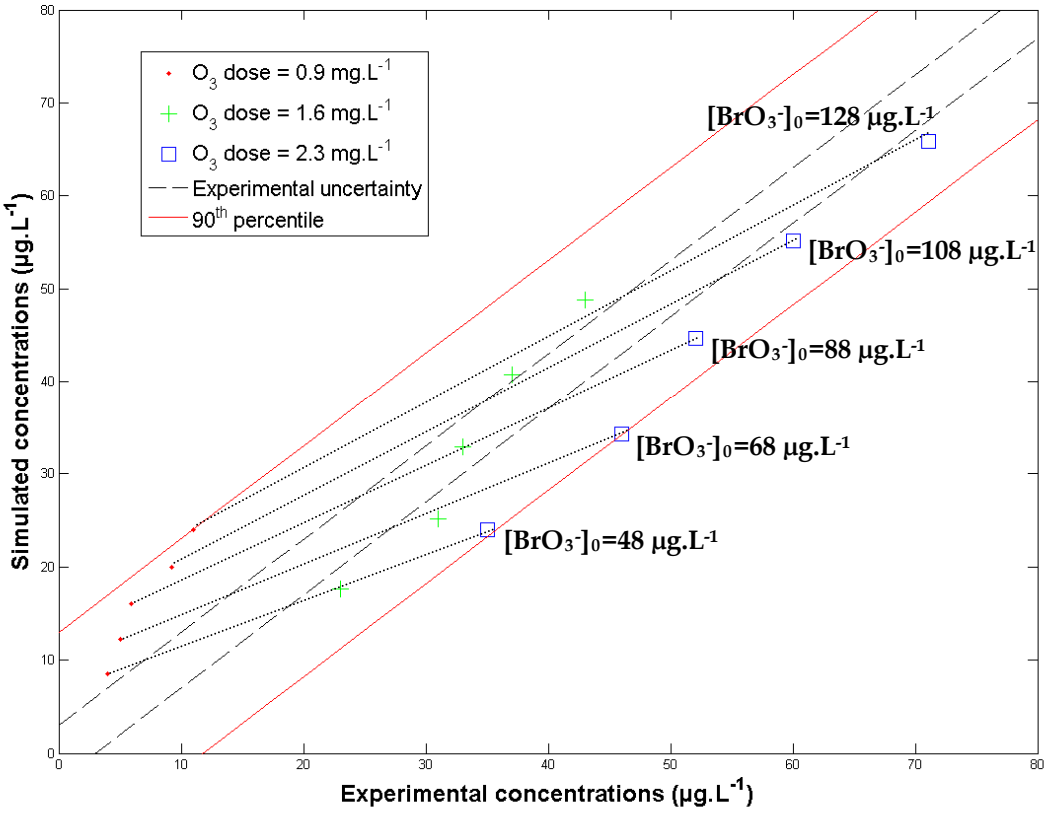

Figure 12 Comparison of simulated and experimental bromate concentrations, Annet-sur-Marne2 water sample

5.4.6. Vitré3

The results of the model simulations are presented on figure **13**. An average agreement is to be seen: two concentrations are highly overpredicted while another is underestimated by 25%. The overpredicted concentrations correspond to an experiment at low temperature and to an experiment where ozone dose was changed (respectively, #4 and #6 in table **2**). However, no relation could be observed between the quality of the simulations for ozone and *p*CBA and the quality of the simulations for bromate.

The comparison of simulated and experimental concentrations for ozone is also given in the small graph. The calibration of the model for the role of NOM had already been performed with dedicated experiments (presented in chapter **4**), so that the results for ozone, which appear in figure **13**, are pure validation. This might also explain the relatively average quality of the results, for ozone and bromate.

The points, the experimental concentration of which is equal to zero, correspond to experiments performed with *tert*-butanol. They have been represented in figure **13**, but their experimental values remain doubtful (see next paragraph).

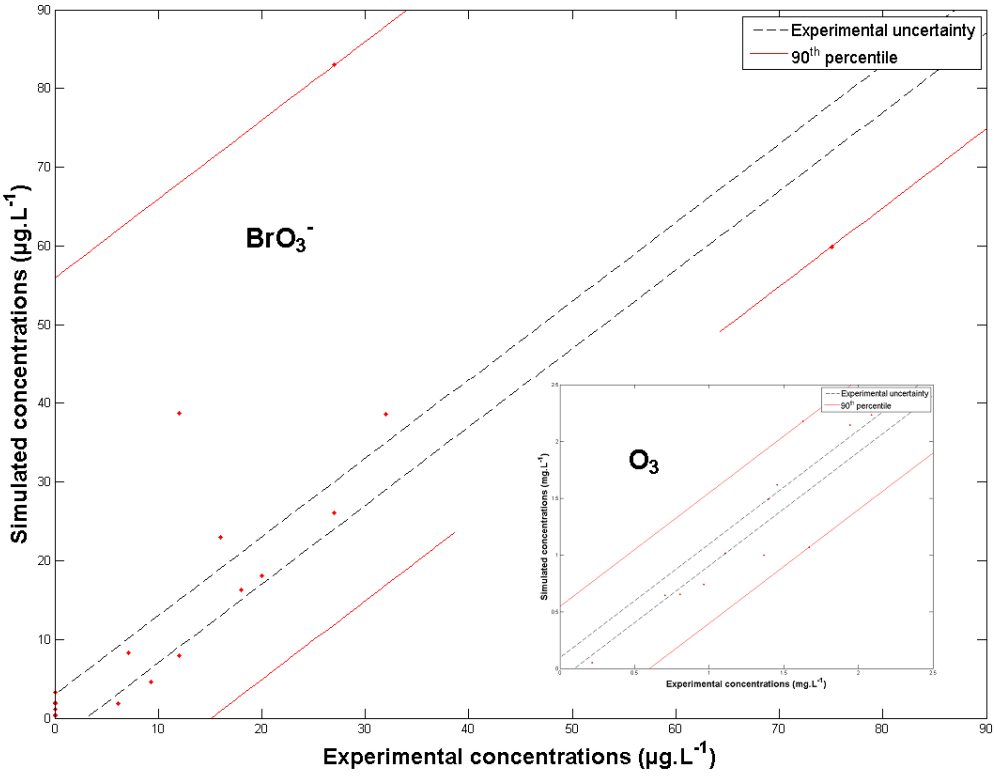

Figure 13 **Comparison of simulated and experimental concentrations, Vitré3 water sample**

5.4.7. Meulan3

The results of the model simulations are presented on figure **14**. The same trends as those observed previously with the Meulan water sample collected in March 2009 are to be observed: some very high experimental concentrations are not predicted as such by the model. These outliers correspond to experiments #1 and #3. Experiment #3 was done with a large ozone dose.

Similarly to the results of Vitré3, the comparison of simulated and experimental concentrations for ozone is also given in the small graph. Poor quality modelling results for

bromate is not necessarily due to poor quality modelling results for ozone. The results of the experiments done with *tert*-butanol adding (experiments #2, #5 and #6, according to table **2**) have not been represented. Experimentally, no bromate was found in those experiments, what appeared contradictory with the results given by the model and the previous results obtained on the same water source, at a different period of the year (Vitré and Meulan). Actually, the analytical technique used at CAE-SM does not allow for measuring bromate concentrations when a large concentration of *tert*-butanol is present in the medium. This was confirmed afterwards.

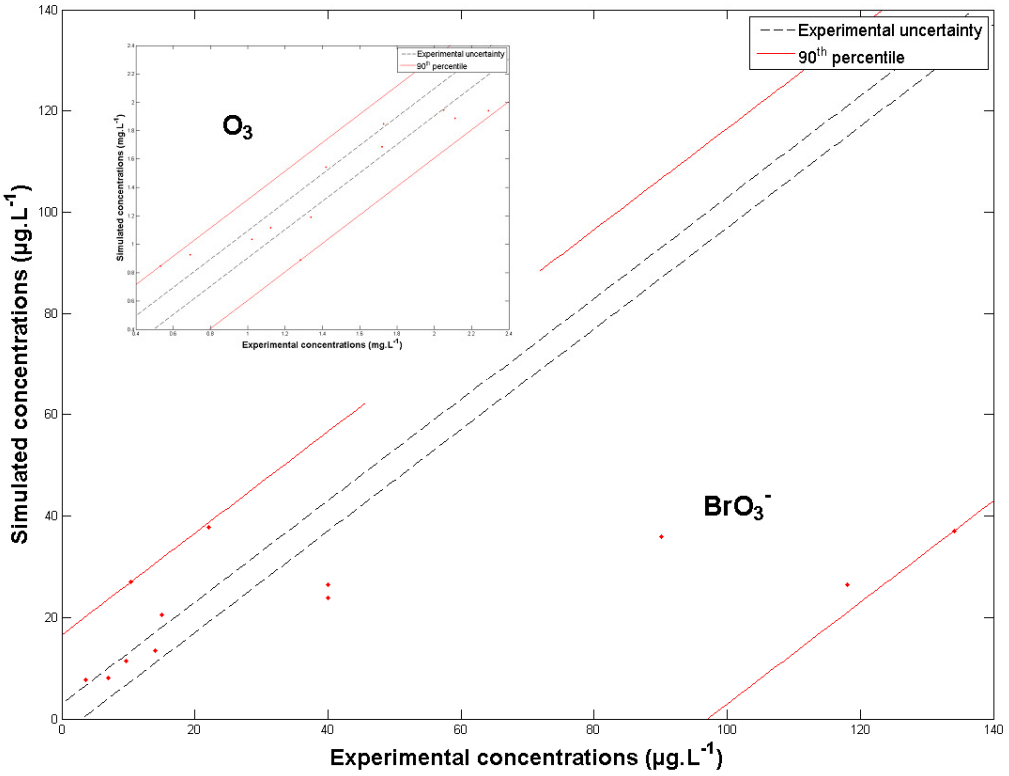

Figure 14 **Comparison of simulated and experimental concentrations, Meulan3 water sample**

5.4.8. Summary

The values determined for the kinetics of the last molecular oxidation step are gathered in table **6**. Whereas the values for the energy of activation are relatively stable, the value of the kinetic rate constant at 293K strongly changes among the water samples studied (from 110 $M^{-1}.s^{-1}$ to 45000 $M^{-1}.s^{-1}$). Seasonal variation is observed mainly for water samples from Annet-sur-Marne and, to a smaller extent, from Meulan. The experiments done with water from Vitré did not give evidence of a seasonal variation in bromate formation.

Globally, the simulation results are satisfactorily when considering the fraction of simulated concentrations located within experimental uncertainty. Other measures of goodness-of-fit or badness-of-fit were not calculated since the number of points is too small for the last three water samples. Note that the model generally gives better results for low experimental concentrations of bromate, that is, below 20 $\mu g.L^{-1}$: globally, 68%of the simulated points were located within uncertainty (all waters). This result is of particular interest for on-site application of the model presented in this chapter.

Table 6 Summary of the kinetics values, adaptable model

Water sample	k(293 K) ($M^{-1}.s^{-1}$)	E_A ($kJ.mol^{-1}$)	Points within uncertainty (%)
Annet-sur-Marne	2.10^3	43	94
Vitré	$1.1.10^2$	45	73
Meulan	$1.8.10^3$	41	62
Annet-sur-Marne 2	$4.5.10^4$	42	7
Vitré 3	$1.8.10^2$	45	56
Meulan 3	$4.3.10^3$	38	25
Literature values	10^5	42[2]	

5.5. Conclusion

Studying the formation of bromate and its modelling in natural waters, six water samples originating from three water resources have been investigated. A single-phase ozonation protocol was used and more than 130 measurements of bromate concentration were performed. The influence of various experimental parameters has been investigated: contact time with ozone, pH, temperature, ozone dose, initial bromide concentration, NOM concentration and NOM content.

A model describing the formation of bromate ions has been built up based on an exhaustive literature review: out of 65 reactions susceptible to occur when bromide-containing water is ozonated, we selected at last 18 reactions. In order to account for the reactivity of NOM, the kinetics of the last molecular oxidation step was optimised. In doing so, only two parameters (frequency factor and energy of activation) were adaptable, while the 34 others remaining set at their original values.

The experimental study and the modelling of the results obtained at lab-scale showed that:

- NOM strongly lowers the amounts of bromate formed. Therefore, predictive models valid in NOM-free waters cannot be applied directly for the simulation of natural water;
- Water samples collected from different water resources are more or less prone to form bromate. Moreover, considering a specific water resource, bromate formation may evolve during the year. Therefore, predictive models have to calibrated regularly;
- The model proposed works well for low bromate levels, typically below 15-20 $\mu g.L^{-1}$: below 20 $\mu g.L^{-1}$, 68% of the simulated concentrations were located within experimental uncertainty. However, divergences can be observed for higher experimental concentrations of bromate, especially when the ozone dose is raised;

This study has also raised some issues that shall be dealt with in future research:

- Domain of validity of the model has not been determined, since the results given are believed to be sufficiently accurate for the targeted concentrations of bromate (<20 $\mu g.L^{-1}$);
- Fundamental studies on how NOM reacts during the formation of bromate shall help to propose new models, which will remain valid in larger experimental domains;

[2] This value has been assumed according to the same assumptions made for all reactions taken from the literature used in this study.

- Calibration strategies should be designed in order to determine which experiments have to be done at lab-scale. Given that the model presented in this study has to be regularly calibrated, on-site calibration may be feasible.

Bibliography

Articles and books

- **Echigo S.**, (2002). Kinetics and speciation of brominated disinfection by-products during ozonation. Ph.D. Thesis, University of Illinois at Urbana-Champaign, U.S.A.
- **Gallard H.** and **von Gunten U.,** (2002). Chlorination of phenols: kinetics and formation of chloroform, *Environmental Science and Technology*, Vol. **36**, pp. 884-890.
- **Huang W.-J., Chen L.-Y., Peng H.-S**., (2004). Effect of NOM characteristics on brominated organics formation by ozonation, *Environment International*, Vol. **29**, pp. 1049-1055.
- **Kim J.-H.,** (2004). Integrated Optimization of Cryptosporidium Inactivation and Bromate formation Control in Ozone Contactors. *Presentation at the Gwangju Institute of Science and Technology*.
- **Kim J.-H., von Gunten U., Mariñas B. J.**, (2004). Simultaneous Predicion of *Cryptosporidium Parvum Oocyst* Inactivation and bromate Formation during Ozonation of Synthetic Waters, *Environmental Science and Technology*, Vol. **38**, pp. 2232-2241.
- **Kim J.-H., Elovitz M. S., von Gunten U., Shukairy H. M., Mariñas B. J.,** (2007). Modeling Cryptosporidium parvum oocyst inactivation and bromate in a flow-through ozone contactor treating natural water, *Water Research*, Vol. **41**, pp. 467-475.
- **Pinkernell U.** and **von Gunten U.**, (2001). Bromate minimization during Ozonation: Mechanistic Considerations, *Environmental Science and Technology*, Vol. **35**, pp. 2525-2531.
- **Reckhow D.A., Singer P.C., Malcolm R.L.,** (1990). Chlorination of humic materials-by-product formation and chemical interpretations, *Environmental Science and Technology*, Vol. **17**, pp. 261-267.
- **Siddiqui M. S**. and **Amy G. L.,** (1993). Factors Affecting DBP Formation during Ozone-Bromide Reactions, *Journal American Water Works Association*, Vol. **85**, pp. 63-72.
- **von Gunten U.** and **Hoigné J.**, (1994). Bromate Formation during Ozonation of Bromide-Containing Waters: Interaction of Ozone and Hydroxyl Radical Reactions, *Environmental Science and Technology*, Vol. **28**, pp. 1234-1242.
- **von Gunten U.,** (2003). Ozonation of drinking water: Part II. Disinfection and by-product formation in presence of bromide, iodide or chlorine, *Water Research*, Vol. **37**, pp. 1469-1487.
- **Wei Q.-S., Feng C.-H., Wang D.-S., Shi B.-Y., Zhang L.-T., Wei Q., Tang H.-X.,** (2008). Seasonal variations of chemical and physical characteristics of dissolved organic matter and trihalomethane precursors in a reservoir: a case study, *Journal of Hazardous Materials*, Vol. **150**, pp. 257-264.
- **Westerhoff P., Chao P., Mash H.,** (2004). Reactivity of natural organic matter with aqueous chlorine and bromine, *Water Research*, Vol. **38**, pp. 1502-1513.
- **Westerhoff P., Song R., Amy G.**, **Minear R.**, (1997). Application of Ozone Decomposition Models, *Ozone: Science and Engineering*, Vol. **19**, pp. 55-73.
- **Westerhoff P., Song R., Amy G., Minear R.**, (1998a). Numerical Kinetic Models for Bromide Oxidation to Bromine and Bromate, *Water Research*, Vol. **32**, pp. 1687-1699.
- **Westerhoff P., Song R., Amy G., Minear R**., (1998b). NOM's role in bromine and bromate formation during ozonation, *Journal of American Water Works Association*, Vol. **90**, pp. 89-94.

6. MODELLING INDUSTRIAL OZONATION UNITS – A CASE-STUDY ON ANNET-SUR-MARNE WATER WORKS

Abstract

Experimental results collected during a full-scale study on an industrial ozonation unit showed that a direct implementation of the chemical models calibrated at lab-scale is possible: modelling results for ozone and bromate are matching experimental measurements. However, slight readjustments of the models should account for seasonal variations in the nature of NOM.

The study investigated an industrial ozonation unit comprising two tanks linked by a pipe, with volumes of 235 m^3 and 252 m^3. Five sampling points were installed along the tank baffles to follow the profiles for ozone and bromate concentrations. Ozone samples were automatically analysed and the concentration values were stored in the Supervisory Control And Data Analysis system of the water works; bromate samples were analysed at laboratory.

The lab-scale calibration results confirmed that the model for the role of NOM is able to account for major changes in pH, temperature, ozone dose, NOM content and NOM nature. Likewise, the lab-scale calibration results showed that the model for the formation of bromate satisfactorily accounts for changes in initial bromide and in ozone doses. Besides, a systematic network was built up to best reproduce hydraulic flow conditions. The systematic network was adjusted in order to fit its Residence Time Distribution to that obtained with a Computational Fluid Dynamics study. Model validation was conducted with experimental results obtained on site, under varying process conditions: liquid flow rate and ozone residual setpoint were allowed to vary, but also ozone gaseous concentration and gaseous flow rate. After the selection of a value for the k_La, simulations were run. The results satisfactorily matched experimental data: 80% of the simulation points for ozone were located within the experimental error of the samples, 94 % for bromate. A slight readjustment of the model for bromate formation showed that seasonal changes in NOM activity may easily be taken into account based on regular concentration measurements.

The results of this full-scale modelling study indicate that the model for bromate formation may be applied to simulate an industrial ozonation unit. However it should periodically be readjusted for accurate predictions of bromate formation, for example with regular control measurements. Regarding ozone decomposition, the model appears to be more stable.

Contents

6.1. Introduction

6.1.1. Annet-sur-Marne Water Works

Originally built in the early 1970's, the water works has been modifying since then to become one of the largest potable water production plant of the Parisian suburban area, delivering in average 105,000 m^3 per day.

It comprises two main units, operating in parallel and merging before chlorination process. A schematic of the plant is given in figure **1**; for simplicity reason, only unit #1 is represented. After being pumped from the Marne River, the water is screened. It then undergoes a preatreatment consisting of a first coagulation stage, associated to a preozonation step. Water next flows into larger tanks for coagulation-flocculation processes to take place. These are performed either with the Actiflo© or Fluorapid© technologies. Water is then filtrated passing through sand and activated carbon layers. Disinfection is achieved by successive ozonation and chlorination. The remaining oxidising agents are quenched by sulphur dioxide dosing. Finally, chlorine is added before water enters the distribution network in order to maintain the bacterial quality along the distribution network.

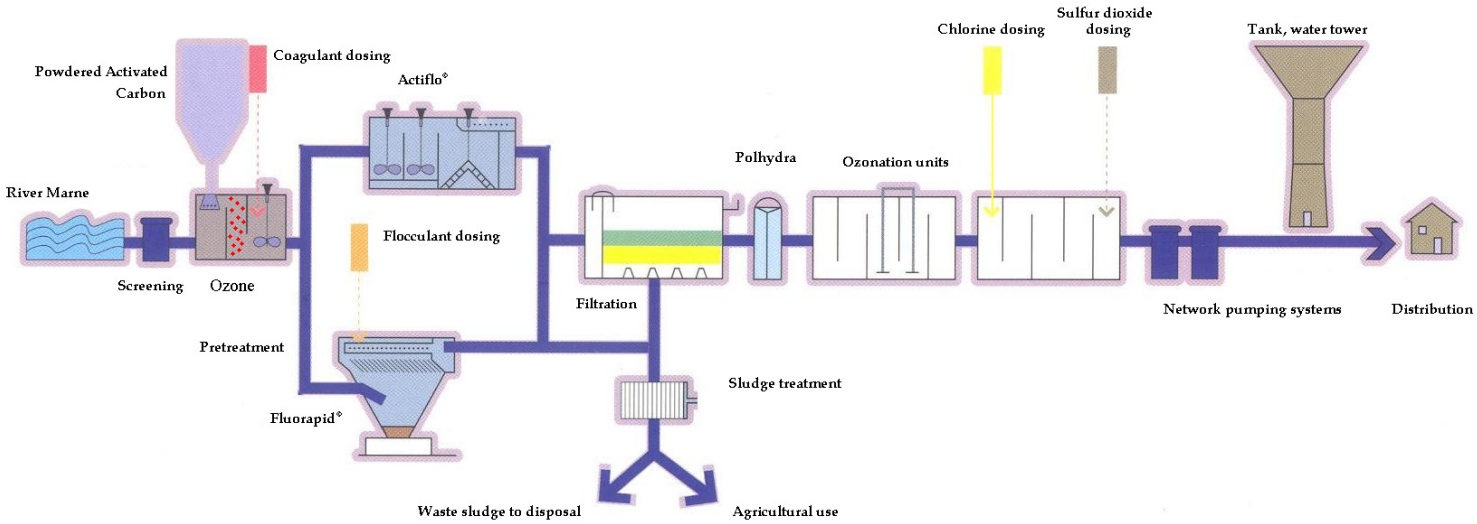

Figure 1 Simplified treatment train of Annet-sur-Marne water works, unit #1

6.1.2. Objectives of the Study

Having assessed the performances of the modelling procedures at lab-scale, this chapter investigates the possibility of up-scaling the approach presented in the previous chapters. Basically, the methodology consists in calibrating at lab-scale and validating on a real industrial unit. Chemical characterisation of the water shall be done at lab-scale with already presented techniques, whereas hydraulic calibration is based on prior studies on the Residence Time Distribution (RTD) of the investigated tank. These steps will be presented in the following and the results will be discussed in regards to a triple objective:

- to test the chemical model;
- to test the calibration procedures;
- to test the software product developed, SimOx.

6.2. Materials and Methods

6.2.1. Ozonation Unit #1

6.2.1.1. Sampling Ports Location

Ozonation unit #1 consists of two tanks of relatively similar volumes (235 m^3 and 252 m^3, respectively for the first and the second tank). These tanks are disposed in series and connected by a tube of diameter 800 mm. A schematic view of the whole unit is proposed in figure **2**. Following the conclusions of a study carried out by the operational centre of Veolia Environnement on the hydrodynamic performances of the unit [Guitard, 2007], baffles and water deflectors were recently added in both tanks; they are also represented on figure **2**.
In addition to the analyses performed on the water entering the unit, five sampling ports were used during the study. Measurements of the residual ozone in the gaseous phase have also been performed. Both types of sampling ports are to be seen on figure **2**. As a reference, the corresponding hydraulic retention times for a water flow rate of 1600 $m^3.h^{-1}$ are given. Considering the experiments presented herein, the water flow rate varied between 1000 $m^3.h^{-1}$ and 1800 $m^3.h^{-1}$, what corresponds to retention times within the unit comprised between 29 min and 16 min, respectively. Sampling ports "Contact 1" and "Contact 4" existed before the study and were adapted, the others were created. In the following, the successive sampling ports will be named "T", "C1", "C2" and "C3" (standing for *Transfer*, *Contact1* etc.)

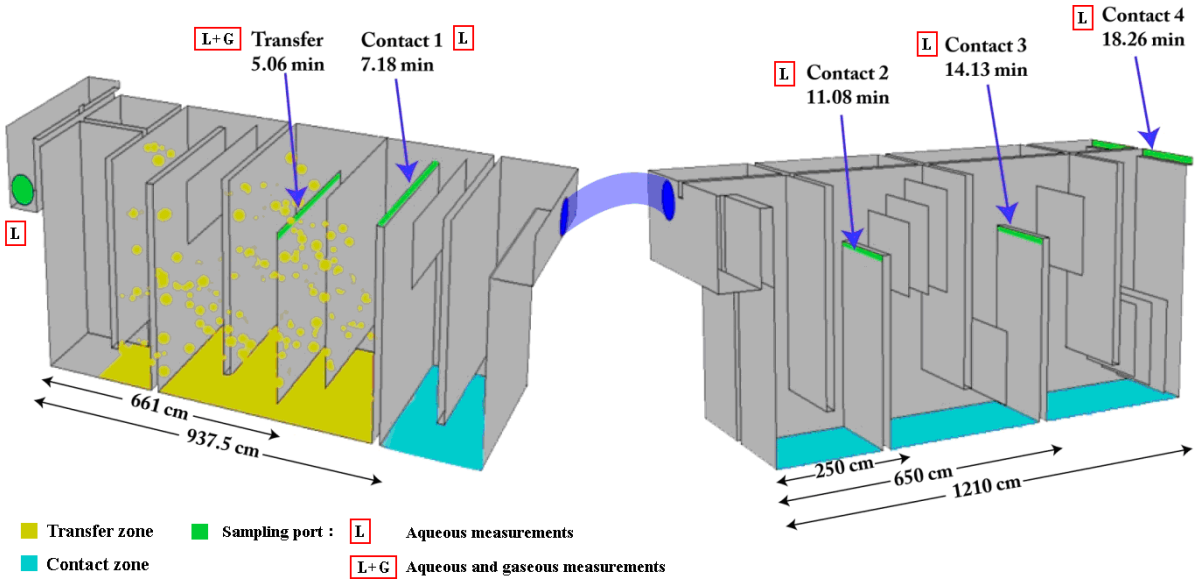

Figure 2 View of ozonation unit #1

Special care has been taken to define the locations of the sampling ports. They are always placed in active zones, in the main stream, thus collecting always "fresh" water. It is indeed important to avoid dead zones and recycling loops, for which the contact time of water with ozone cannot be precisely determined and may be underestimated with use of the corresponding retention time. This is illustrated in figure **3**, where two possible locations for sampling port C3 are compared.

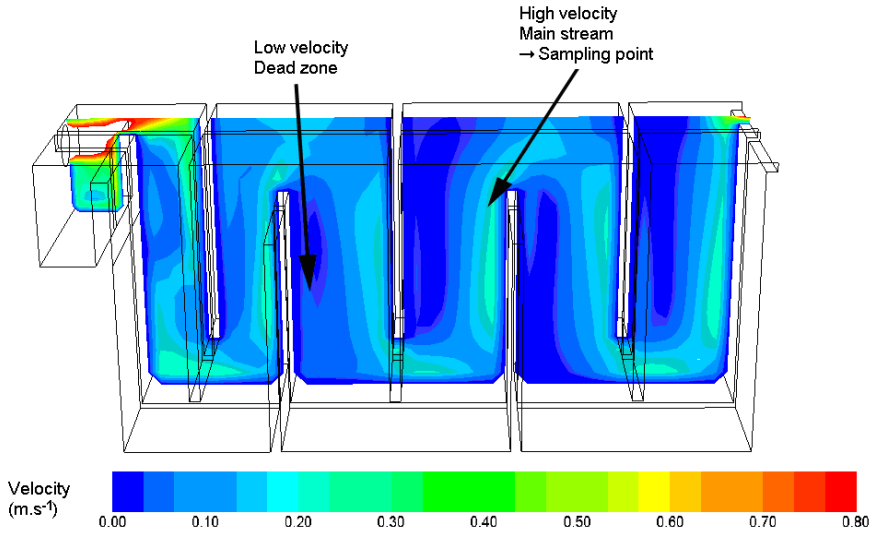

Figure 3 Location of sampling port C3

6.2.1.2. Analysis Apparatus

In order to continuously feed analysers with water, several pumping systems have been installed. Every material in contact with ozone, especially when gaseous, was scrupulously selected. Figure **4** is a photograph of the pump group used to supply the analysers with water.

It is worth mentioning that the distance between the sampling port and the analyser may have varied from one sampling port to another; it was roughly comprised between 15 m and 50 m. Although using high flow rates in the pipes (0.4 $m^3.h^{-1}$) leading to the pumps, this could have caused biased measurements for species like ozone, always depleting and bromate ions, always forming. Therefore, this point has been experimentally studied (see **6.2.4.1.**).

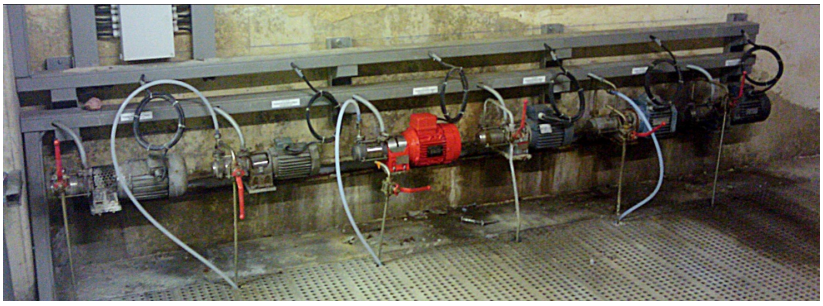

Figure 4 Pump group

Figure 5 Blind flange

Gaseous measurements were performed on the roof of the ozonation unit. A specially conceived blind flange made of PVC was installed (figure **5**) in order to measure ozone concentrations in the exhaust gas.

6.2.2. Data Collected

Water characteristics were measured daily according to the methods presented in table **1**. Important parameters such as alkalinity, UV absorbance at 254 nm and bromide/bromate concentrations were measured twice.

Table 1 Water characteristics measurements

Parameter	First measurement	Second measurement	Method
pH	On site		pH meter
Alkalinity	On site	CAE-SM	Acid-base equilibrium
TOC	CAE-SM		TOC analyser
UV (254 nm)	On site	CAE-SM	Spectrophotometer
Temperature	On site		Thermometric probe
Bromide concentration	CAE-SM	ENSCR	Ionic chromatography

Besides physicochemical parameters characterising water quality, operational process data were recorded consulting the SCADA system of the water works. The principal conditions followed are:

- the setpoint for residual ozone concentration;
- the water flow rate;
- the ozonated air flow rate;
- the ozone concentration in the ozonated air.

6.2.3. Analyses

6.2.3.1. Aqueous Ozone Concentration

Concentrations were measured by means of on-line analysers, which were installed or adapted for this study. Accordingly, two types of analysers were used: already installed Solu Comp II from Rosemount Analytical (Solon, U.S.A.) and Q 45H/64 from ATI (Collegeville, U.S.A.). They are presented in figure **6**, left hand-side and right hand-side photographs respectively.

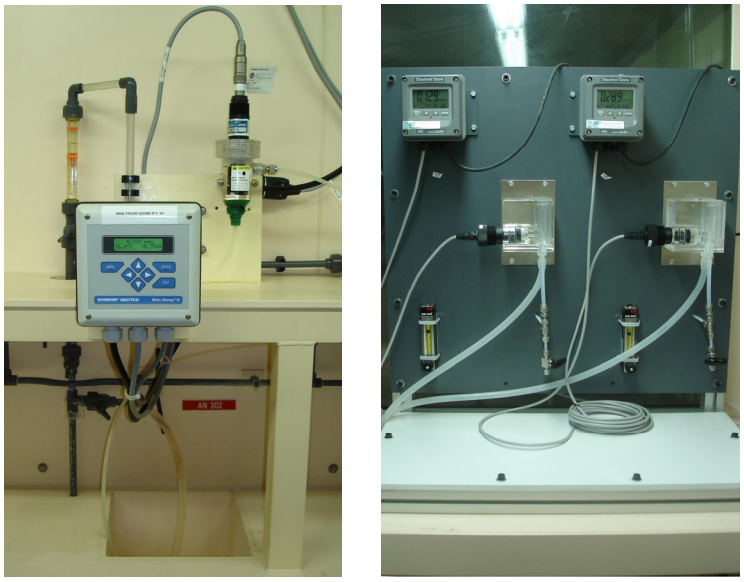

Figure 6 Aqueous ozone analysers used in this study

6.2.3.2. Gaseous Ozone Concentration

Gaseous ozone concentration was measured using the blind flange installed on the roof of ozonation unit. The whole apparatus is reproduced in figure **7**. The photograph shows the small pump supplying the 964 BT analyser (BMT, Berlin, Germany). A laptop continuously recorded the measurements.

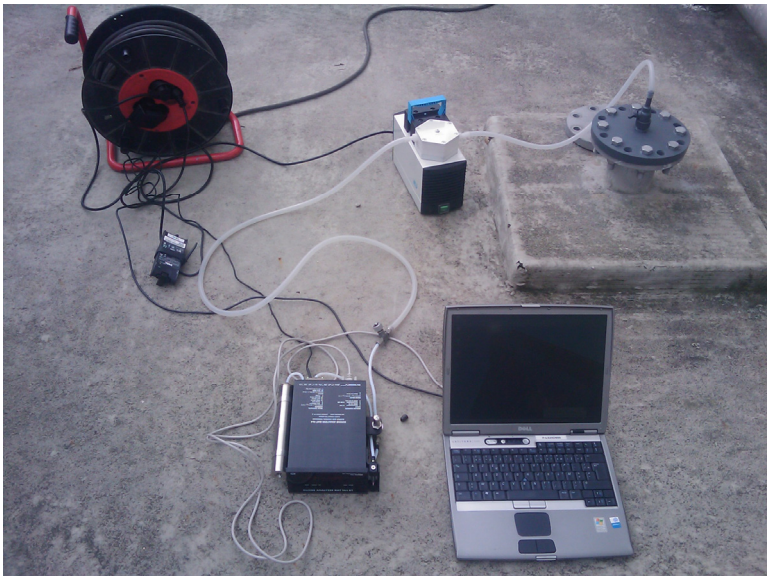

Figure 7 **Apparatus for gaseous ozone concentration measurement**

6.2.3.3. Bromide/Bromate Concentrations

All samples for bromate ion concentration measurements were analysed at ENSCR. Additionally, analyses were carried out at CAE-SM for samples from the unit outlet ("Contact 4"). Analytical methods are as presented in chapter **5**, **5.2.3.1**.

6.2.4. Reliability and Repeatability

6.2.4.1. Aqueous Ozone Concentration

Pipes conducting water from the ozonation tank to the analysers may be 15 m to 50 m. So, ozone might be consumed during the transport of water to the analysers. Transport time is comprised between 30'' and 1'20''. In order to determine precisely the loss of ozone due to the dead time, during which water is transferred, valves were installed at the beginning of the pipes leading to the analysers, almost directly at sampling points. Ozone was then analysed twice: one time automatically, using the analyser; one time, manually sampling water from the valve and using the Indigo-Method [Bader and Hoigné, 1981].

Measurements were performed four times on the three sampling points of the contact tank. The results are presented in figure **8**. For two points out of three, the aqueous ozone concentration is smaller when measured at the valve than read at the analyser. However, the differences between the values remain inferior to the experimental uncertainty. As a consequence, no loss of ozone could be observed in the pipes leading to the analysers.

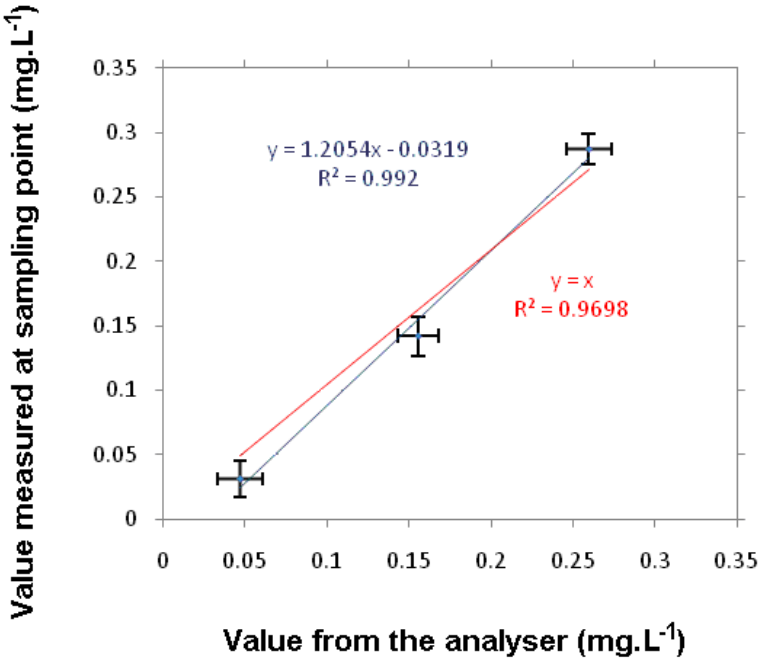

Figure 8 **Evaluation of the loss of ozone in the pipes leading to the analysers**

Calibration of the ATI analysers was first performed with the Indigo method; then, for homogeneity's sake, it was performed with the same method used for the Rosemount analysers (Portable colorimeter II test kit, Hach (Loveland, USA)).
Once calibrated, the values given by the analysers were regularly compared with measurements performed manually with the Indigo method. The comparison of the two measurements is presented in figure **9**. Comparison was carried out during the first experimental period (from July 21st to August 14th). Contrary to the previous comparison, the samples were collected at the same location, that is, at the location of the analysers. The results presented in figure **9** show that the measure given by the analysers is relatively stable (no time drift of the analysers).

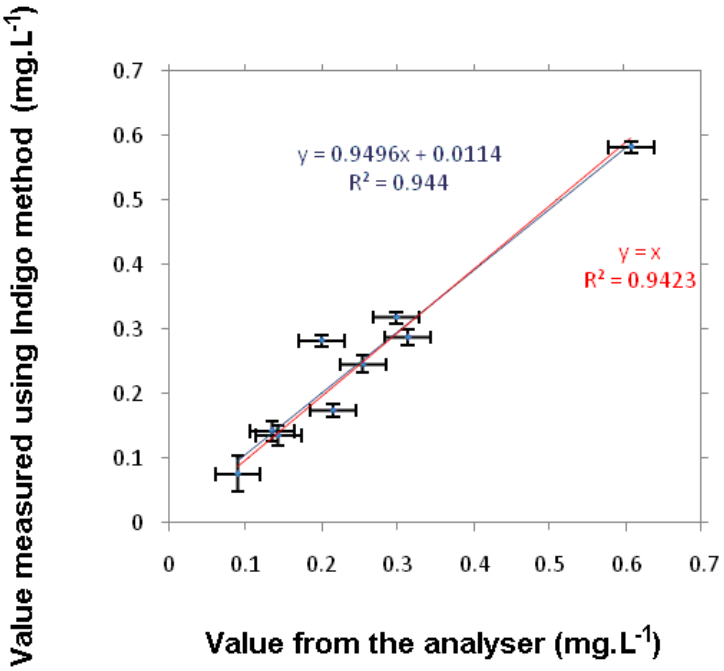

Figure 9 **Evaluation of the time drift of the analysers**

6.2.4.2. Bromate Concentration

Since bromate concentration was measured by two different laboratories, results were constantly compared. 17 samples were analysed twice: one time at ENSCR, one time at CAE-SM. The compared results for bromate concentration are presented in figure **10**; errors bars correspond to experimental uncertainty. Both measurements are in agreement. However, for low concentrations, the values given by the lab at ENSCR were found superior (between 2 $\mu g.L^{-1}$ and 3 $\mu g.L^{-1}$) than that given by the CAE-SM (< 2 $\mu g.L^{-1}$).

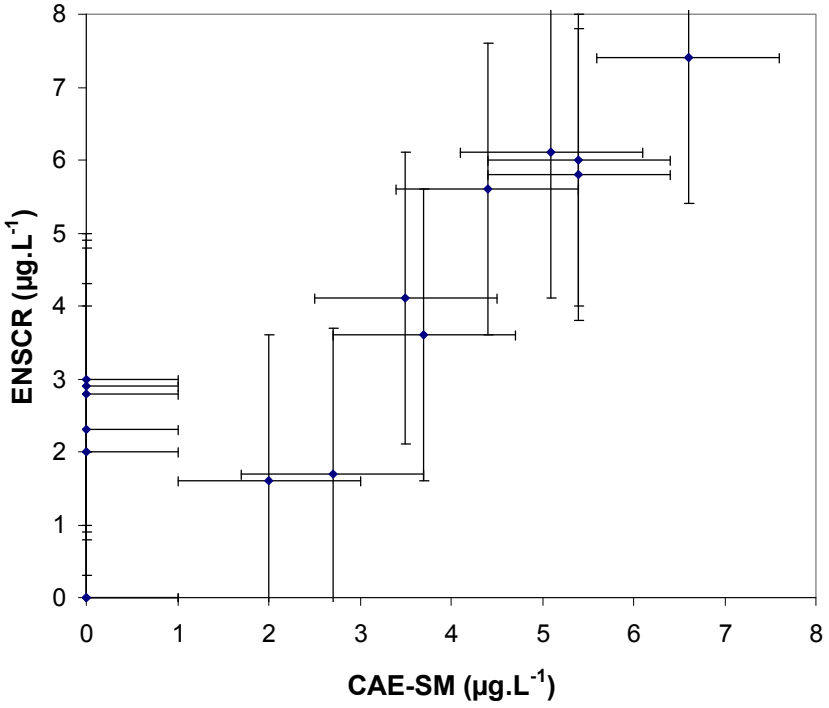

Figure 10 Measurement of the bromate concentration: comparison ENSCR/CAE-SM

6.2.4.3. Experiment Replicates

Two experimental periods were distinguished: July and August on one hand; September and October on the other hand. It appears from historic measurement charts that bromate formation may vary seasonally. In order to determine if such seasonal variations occurred during the study, two experiments were performed during both experimental periods. The results of one of them are reproduced on figure **11**. Whereas ozone profiles do not show significant differences, the level of bromate formed dramatically drops from the first to the second period (the first experiment was done August 8th while the second was done October 9th, see table **2**). As the concentrations for the second period were found equal to zero, the analysis was done three times (twice at CAE-SM, once at ENSCR). The concentration was always lower than the quantification limit. This is all the more interesting, as global indicators of water quality (pH, T, A_T, $[Br^-]$, TOC, UV_{254}) did not vary significantly from the first to the second experimental period. As a consequence, the two periods will be treated separately when comparing or modelling experimental results for bromate concentrations; no distinction will be made for ozone concentrations.

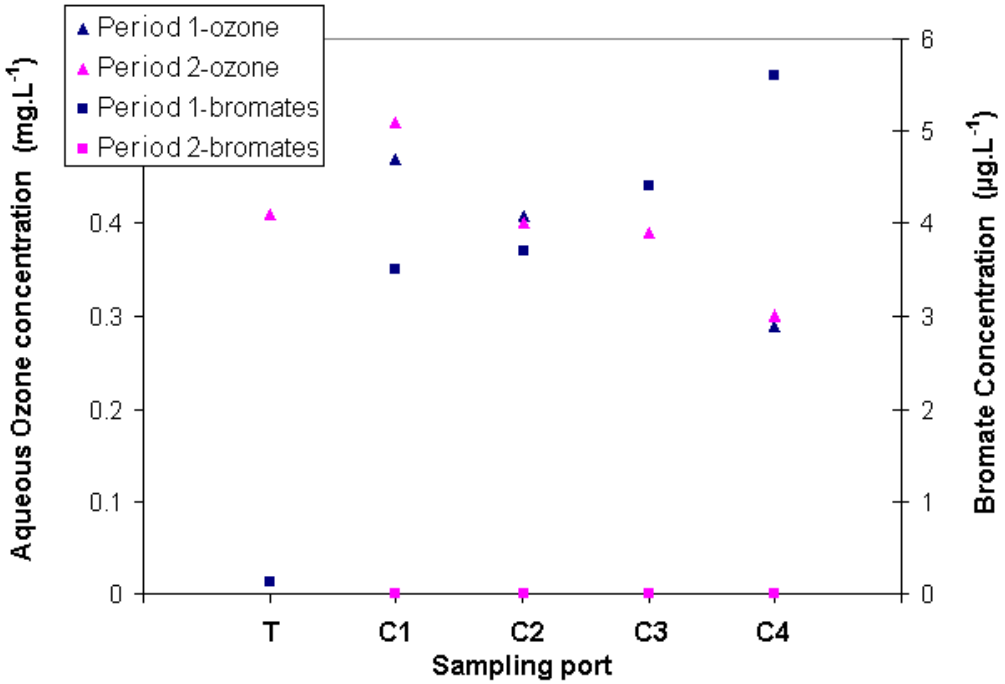

Figure 11 Replicate experiments conducted (Experiments #6 and #16), ozone and bromate concentrations

6.2.5. Experiments Performed

6.2.5.1. Steady-state Conditions

All samplings on the ozonation unit of Annet-sur-Marne water works were performed under steady-state conditions, in order to best control the values of the experimental parameters. Steady-state conditions were typically reached within two or three hours following a change of process conditions. An example is given in figure 12, showing the evolution of ozone concentration after having lowered the water flow rate from 1600 $m^3.h^{-1}$ to 1100 $m^3.h^{-1}$. Therefore, the latest measurements stored in the SCADA system of the water works were systematically consulted before samples were taken to ensure the stability of the unit. Samplings lasted less than 30 minutes.

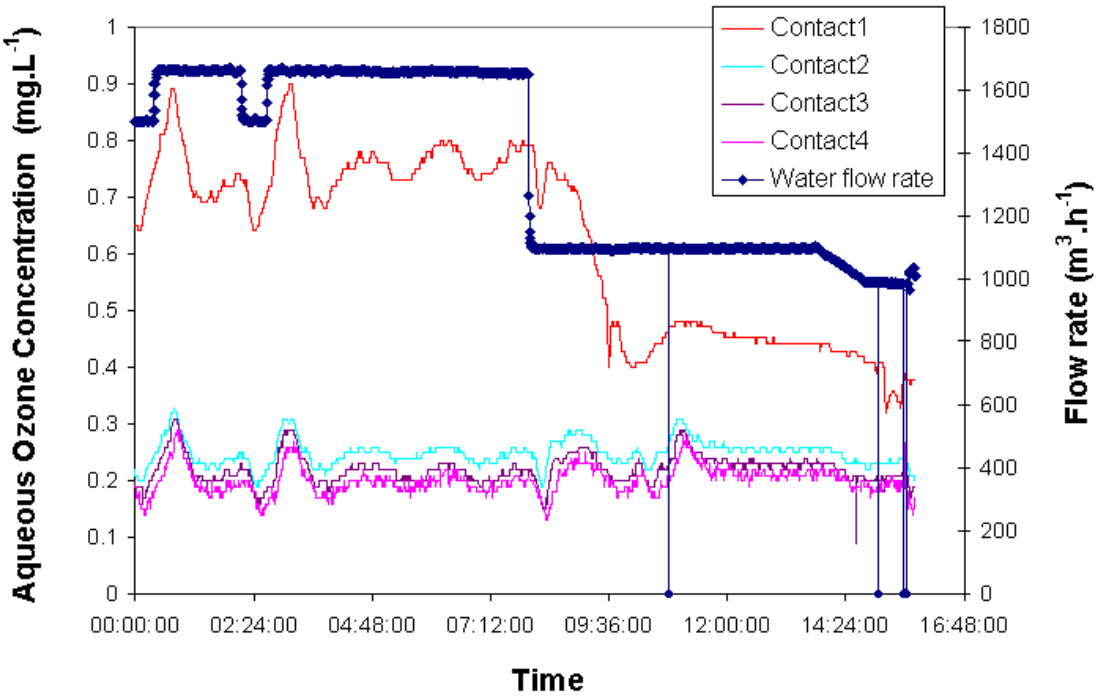

Figure 12 Incidence of a change of water flow rate on aqueous ozone concentration in the ozonation unit with regulated outlet ozone residual (Contact4)

6.2.5.2. Primary and Secondary Process Conditions

Some process conditions may be freely defined by the operators of the water works, while others are exclusively handled by the Programmable Logic Controller. Accordingly, two types of process conditions have been distinguished: primary and secondary conditions. In this study, process conditions, the value of which can be manually set, are termed *primary*, the others *secondary*.

Primary process conditions are:

- The water flow rate passing through the unit;
- The set-point for the residual concentration of ozone (called in the following *set-point*).

Secondary process conditions are:

- The gaseous flow rate of ozonated air;
- The gaseous concentration of ozone.

The analysis of the results will thus focus on the influence of the primary process conditions.

6.2.5.3. Summary

The design of experiments has been developed to determine the effects of the two primary process conditions, the water flow rate and the set-point. It has been divided into two periods:

During the first period, July 21st-August 14th, three set-points at moderate-high water flow rates (from 1480 $m^3.h^{-1}$ to 1850 $m^3.h^{-1}$) were tested. In addition, two replicate experiments were done. In total, 8 experiments were done;

During the second period, September 2nd-October 9th, three set-points at low water flow rate (around 1100 $m^3.h^{-1}$) were tested. In addition, two replicate experiments were done at high water flow rate. In total, 9 experiments were done.

The 17 experiments are summarised in table 2, where physicochemical parameters as pH, temperature, initial bromide concentration, alkalinity etc. are given, as well as the process conditions. A table gathering all experimental results is available in Appendix **J**.

Table 2 Summary of the experiments performed

		Water Characteristics						Operational Process Conditions				
	Parameter	TOC	Br^-	A_T	T	pH	UV 254	$[O_3]_g$	Q_g	Q_l	Setpoint residual	Ozone dose
#	Date	$mg.L^{-1}$	$\mu g.L^{-1}$	$meq.L^{-1}$	°C			$g.Nm^{-3}$	$Nm^3.h^{-1}$	$m^3.h^{-1}$	O_3 in $mg.L^{-1}$	$g.m^{-3}$
1	2009-07-21		40		21.6	7.5		14.6	84	1644	0.2	0.75
2	2009-07-22	1.60	41		21.1	7.5	0.098	13.5	84.4	1481	0.2	0.77
3	2009-07-30	1.80	39	3.70	21.3	7.5	0.109	19.8	84	1756	0.2	0.95
4	2009-08-03	1.80	30	3.70	21.2	7.5	0.105	19.9	63	1504	0.3	0.83
5	2009-08-07	1.70	30		22.4	7.5	0.114	13.9	149	1851	0.4	1.12
6	2009-08-12	1.70	30	3.60	22.7	7.5	0.117	19.9	66.7	1681	0.3	0.79
7	2009-08-14	1.70	33	3.58	22.8	7.5	0.115	19.9	74	1698	0.4	0.87
8	2009-08-14	1.70	33	3.58	22.8	7.5	0.115	19.9	73.1	1704	0.4	0.85
9	2009-09-02			3.64	20.6	7.4	0.108	10.6	81.8	1021	0.2	0.85
10	2009-09-02			3.64	20.6	7.4	0.108	10.2	80.2	990	0.2	0.83
11	2009-09-11	1.50	<30	3.70	19.0	7.4	0.115	13.1	81.6	1100	0.3	0.97
12	2009-09-30	1.50	30	3.76	17.7	7.5	0.107	17.1	61.8	1100	0.4	0.96
13	2009-09-30	1.50	30	3.76	17.7	7.5	0.107	17.6	61.9	1100	0.4	0.99
14	2009-10-06	1.70	34.00	3.58	17.6	7.2	0.109	19.9	64	1690	0.2	0.75
15	2009-10-06	1.70	34.00	3.58	17.6	7.2	0.109	19.9	64	1690	0.2	0.75
16	2009-10-09	1.60	31.00	3.78	16.6	7.4	0.114	19.9	62	1663	0.3	0.74
17	2009-10-09	1.60	31.00	3.78	16.6	7.4	0.114	19.9	61.3	1661	0.3	0.73

6.2.6. Models Used

The model used for predicting ozone and bromate profiles within the tank is similar to that used in the previous chapters **4** and **5** (detailed mechanisms are presented in Appendix **D**). It comprises sets of reactions for the following phenomena:

- Ozone self-decomposition;
- Influence of inorganic carbon;
- NOM influence on ozone decomposition and hydroxyl radical generation;
- Bromate formation.

6.3. Experimental Results

6.3.1. Qualitative Analysis: Major Influences of Process Conditions

We give in the following examples illustrating the main influences of the process conditions on the outlet concentration of bromate. Similarly to the results presented in [Gallard *et al.*, 2003], the outlet bromate concentration can be represented as function of the ozone residual concentration. All outlet bromate concentrations are presented in figure **13**. Periods and flow conditions have been distinguished as they appear to be highly influent. Analysing the results presented in figure **13**, several trends can be noted:

- A good relationship $[BrO_3^-]_{out}$ = f(residual) for experiments done at comparable water flow rates and at the same period of the year. [Gallard *et al*, 2003] found a logarithmic function to best fit experimental data;

- Seasonal character of the formation of bromate: compare the results obtained during period 1 and period 2, at high water flow rates. This phenomenon had already been observed at lab-scale (see chapter **5**);
- Influence of the water flow rate: compare the results of period 2 obtained with high and low water flow rates. Increasing the water flow rate leads to smaller amounts of bromate formed.

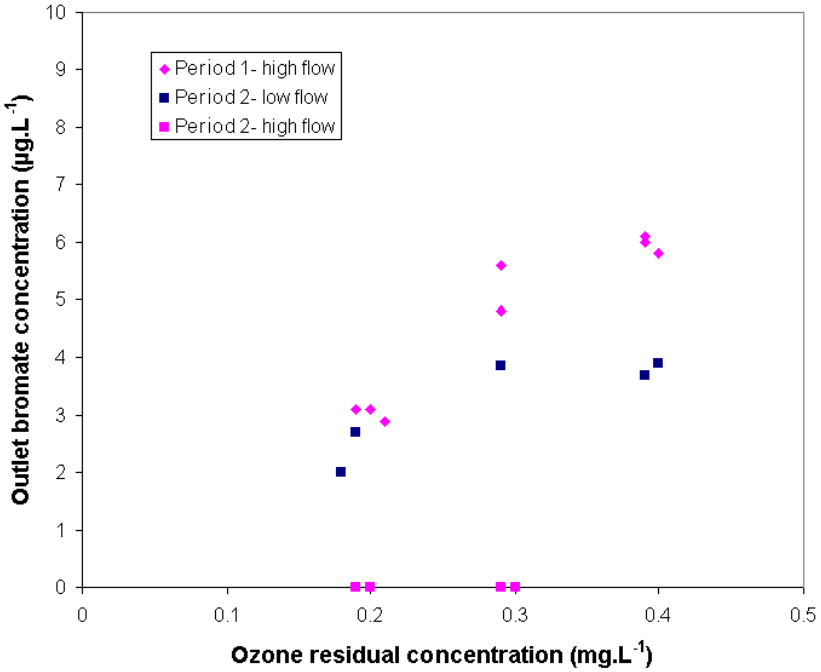

Figure 13 **Influence of ozone residual concentration on bromate formation**

Alternately, [Wert *et al.*, 2007] proposed to represent the outlet concentration of bromate as function of the ozone dose, thus taking in account water and gas flow rates; this has been done in figure **14**. The same seasonal trend can be seen. The relation is here weaker, particularly for the experiments from the first period. On the contrary, the results of the second period appear to be quite homogeneous, despite the change of water flow rate. As it appears from figure **13**, the residual ozone concentration may be a good indicator of the level of bromate formed. However, variations in water flow rate are not taken into account. In addition, the correlation remains valid only in a limited time frame.

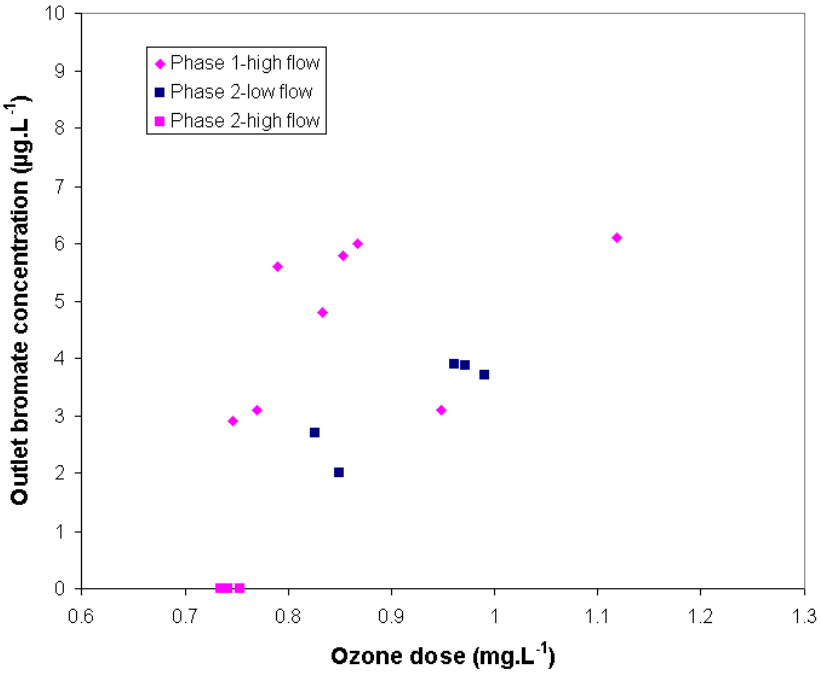

Figure 14 **Influence of ozone dose on bromate formation**

Further, following the example of [von Gunten and Hoigné, 1994], various authors have compared bromate formation with ozone exposure, or Ct (*e.g.* [Legube *et al.*, 2004]). In the present study, we used the Cτ to describe ozone exposure, according to the formula **1** and to the notations defined in figure **15**, τ being the hydraulic retention time, see Appendix **B**. The $C\tau_j$ was calculated for the *j* sampling port according to equation **1**.

$$1 \le j \le 4, C\tau_j = \sum_{i=1}^{j} [O_3]_{Ci} . \tau_{Ci} \qquad \textbf{(1)}$$

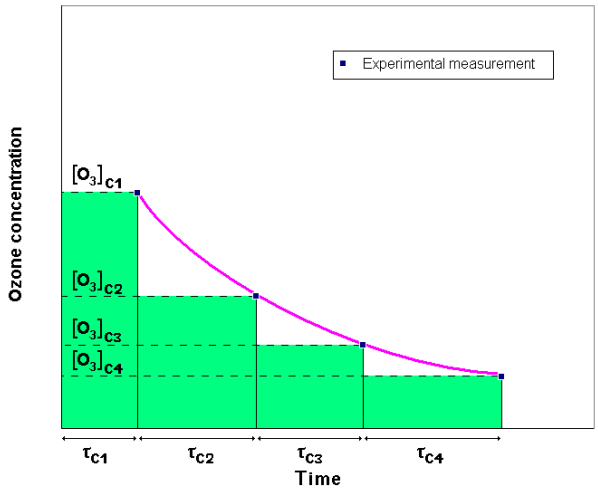

Figure 15 **Definitions of the variables used for calculating the Cτ (corresponding to the green area)**

All the measured bromate concentrations are represented with the corresponding Cτ in figure **16**. Again, the seasonal variation is to be seen by comparing the results obtained at high flow rates for the two periods. The influence of water flow rate is not as sensitive as when considering experiments with the same ozone residual concentration (figure **13**). [Gélinet, 1999] reported that, at pilot-scale, water flow rate had no incidence on the relation

[BrO_3^-] = *f*(Cτ). With exception of outlier points and taking into consideration experimental uncertainty (±2 µg.L^{-1} for bromate measurements), this observation holds.
Considering the results presented in figure **16**, the relation [BrO_3^-] = *f*(Cτ) remains average and should therefore be used with caution when modelling bromate formation. The small insert graph shows the outlet points, similarly to figures **13** and **14** investigating the relation of bromate formation to ozone residual or ozone dose. Note the poor linearity for those points in comparison to the previous graphs **13** and **14**. Studying a pilot-scale with perfectly known flow conditions, [van der Helm *et al.*, 2007] have shown that the relation [BrO_3^-] = *f*(Cτ) may be used as a predictive tool for bromate formation. These results need nevertheless to be extended to a larger experimental domain and up-scaled to on-site units. Previous studies, and notably the work of [von Gunten and Hoigné, 1994], have underlined the variability of the relation between bromate formation and ozone exposure. Numerous experimental factors such as initial bromide concentration, pH, alkaline species alter the relation [BrO_3^-] = *f*(Cτ). Considering the same relation, other studies also showed the influence of temperature and DOC ([Gélinet, 1999]; [Legube *et al.*, 2004]; [Kim Do-Ill and Kim, 2005]), or of the flow conditions [Gillogly *et al.*, 2001].

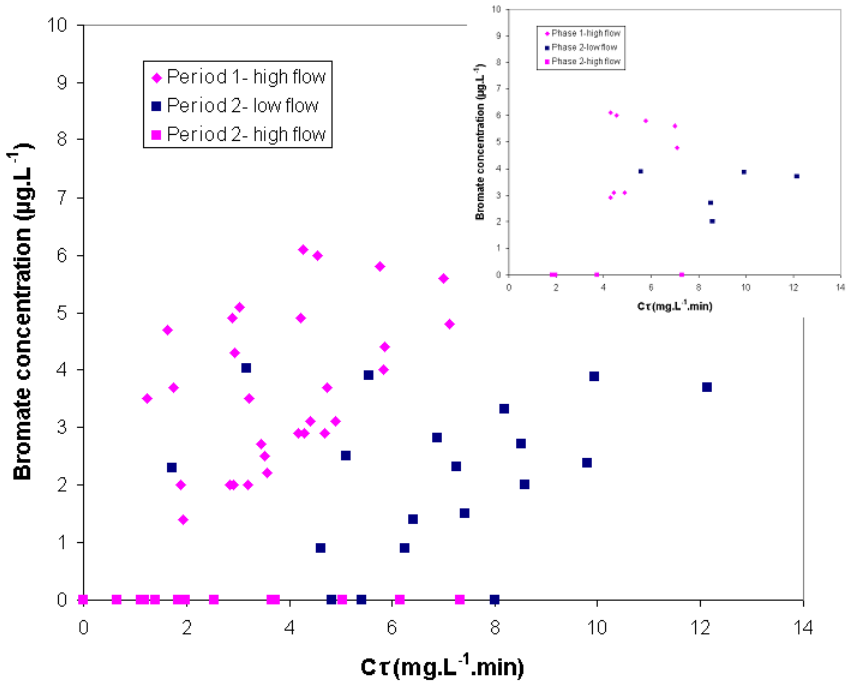

Figure 16 Influence of ozone exposure (Cτ) on bromate formation, all sampling points; insert graph: influence of ozone exposure (Cτ) on bromate formation, sampling point C4

The concentration of ozone measured in the transfer compartment, $[O_3]_T$, has not been taken into account for the calculation of the Cτ value, but it is likely that this would have resulted in a shift of the points of the first period towards lower Cτ values. The values for $[O_3]_T$ presented in Appendix **J** are indeed lower for the experiments of the fist period than for those of the second period. As a result, the gap between the points of the first period and those of the second period would have been slightly larger.

6.3.2. Conclusion

From the analysis of the experimental results harvested during the on-site study, the following conclusions can be drawn:

- Bromate formation is strongly altered by seasonal variations affecting the reactivity of NOM (see also chapter **5**, **5.4.8.**);

- Ozone dose alone or ozone residual alone cannot be considered as good indicators of bromate formation;
- The use of the ozone exposure, Ct or Cτ, as indicator of bromate formation remains uneasy and should be regularly controlled, since the variations of various experimental parameters are not taken into account: pH, temperature, bromide concentration, alkalinity…

Predicting concentration profiles for ozone and bromate remains difficult at full-scale. Simple indicators, based on inlet and/or outlet process parameters are difficult to implement, since their domain of validity are rather limited.

6.4. Modelling Results

6.4.1. Results of the Lab-Scale Calibrations

6.4.1.1. Models for Chemical Kinetics: Role of NOM and Bromate Formation

The chemical reactivity of sand-filtered water from Annet-sur-Marne water works has been characterised several times. Three sets of experiments were used for calibrating the model for the role of NOM on oxidative species; they have been presented in chapter **4** (Annet-sur-Marne, Annet-sur-Marne2 and Annet-sur-Marne3). Two sets of experiments were used for calibrating the model for the formation of bromate ions; they have been presented in chapter **5** (Annet-sur-Marne and Annet-sur-Marne2).

Whereas the influence of NOM on oxidative species is relatively stable over the year (see chapter **4, 4.5.5.**), bromate formation dramatically varies from one season to another (see chapter **5**, **5.4.8.**). Accordingly, two different calibrations for the NOM model could be selected, corresponding to the experimental sets Annet-sur-Marne and Annet-sur-Marne2. These sets were chosen because they brought the best modelling results. Figures **17** (Annet-sur-Marne) and **18** (Annet-sur-Marne 2) show the results of the calibrations for the role of NOM on oxidative species.

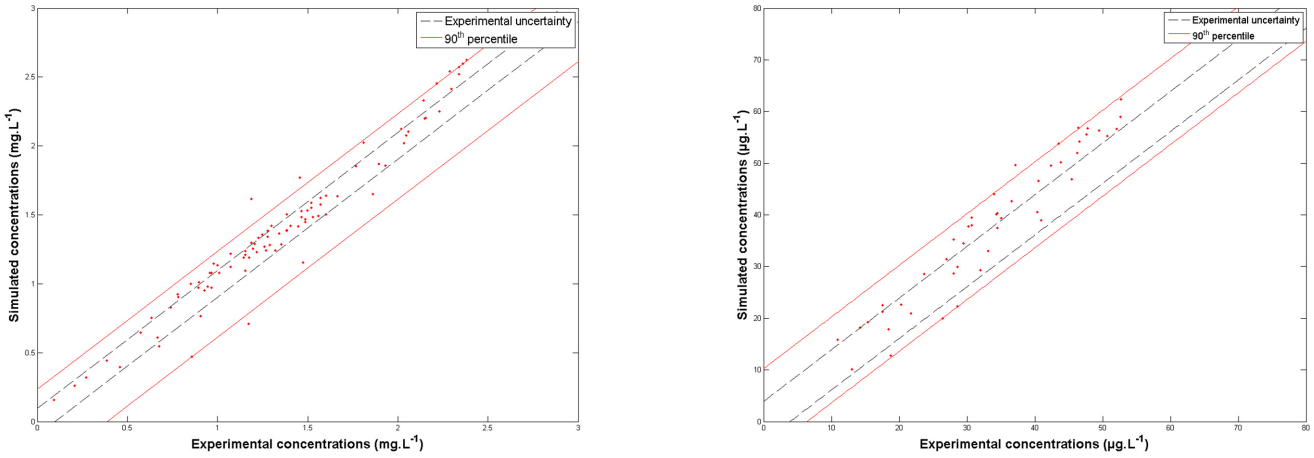

Figure 17 Results of the calibration experiments for oxidative species with Annet-sur-Marne water: ozone concentrations (left hand-side); *p*CBA (right hand-side)

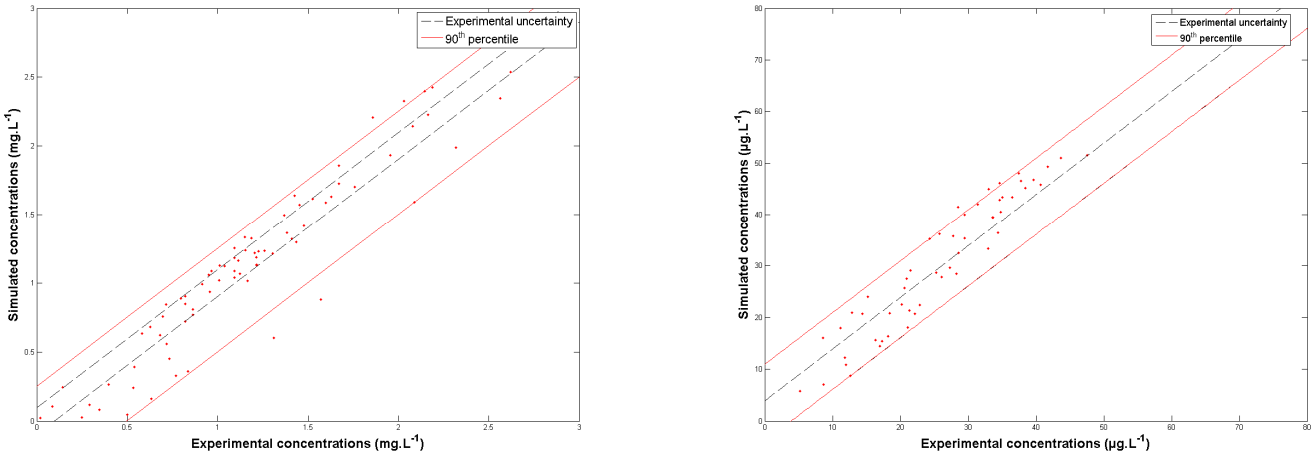

Figure 18 Results of the calibration experiments for oxidative species with Annet-sur-Marne 2 water: ozone concentrations (left hand-side); *p*CBA (right hand-side)

Considering the high variability of bromate formation, it was decided to use the model calibrated with the experiments done in July, that is, just before the on-site experimental study. The results are presented in figure **19** (see chapter **5**, **5.4.5.** for more details).

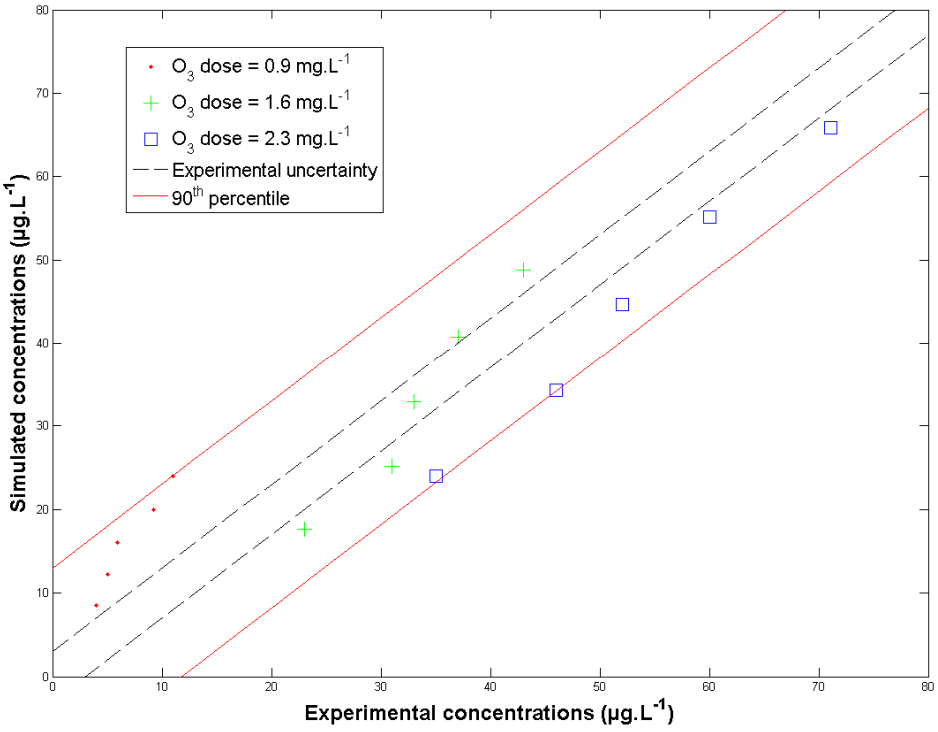

Figure 19 Results of the calibration experiments with Annet-sur-Marne 2 water

6.4.1.2. Hydraulic Modelling

Based on the results of a previous CFD study [Guitard, 2007], a systematic network was proposed to describe the hydraulic flow conditions of the unit. RTDs (Residence Time Distributions) and turbulence analysis by means of CFD were used to calibrate the scheme, according to [de Traversay *et al.*, 2001]. The systematic network was first designed by adjusting its RTD (Residence Time Distribution) to that obtained with the CFD study. The two tanks were treated separately, as the systematic scheme of the first tank was designed

before that of the second tank. Then, CSTRs were placed following the results of the turbulence analysis. Both RTD curves (CFD and systematic) are presented on figure **20**. The associated systematic network is presented in figure **21**. Note the excellent agreement of both RTDs.

The systematic network consists of 46 ideal reactors or groups of ideal reactors (CSTR cascades) placed all along the unit. Generally, two streams were distinguished for the water circulating through the unit, the main stream corresponding to shorter residence times. No recycling loop was used in the systematic network, as the flow conditions appear to be optimal from the results of the CFD study. Considering the geometry of the unit (figures **2** and **21**), optimal hydraulic flow conditions have been reached by adding baffles and deflectors.

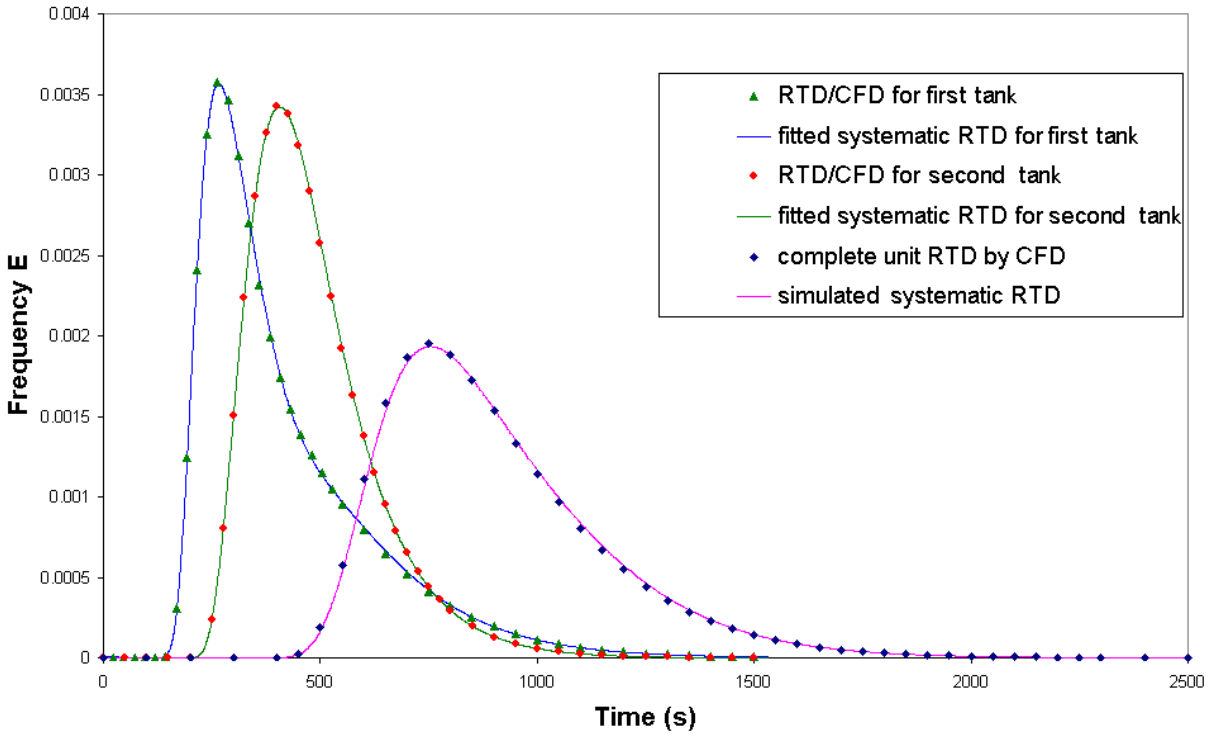

Figure 20 **RTDs obtained with CFD study and systematic network**

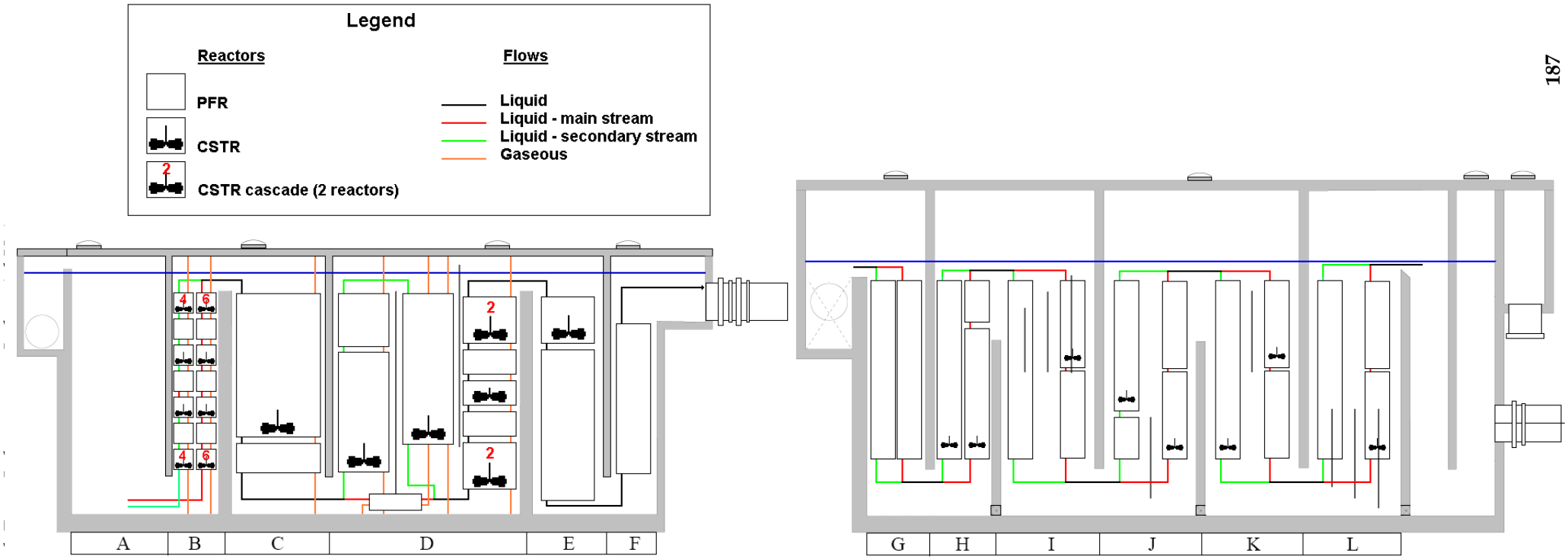

Figure 21 **Systematic scheme proposed for Annet-sur-Marne ozonation unit #1**

6.4.1.3. Transfer Modelling

A classical two-film approach ([Whitman, 1923]) was implemented to model mass transfer. Gas phase resistance was considered negligible, so that the concentration gradient on liquid phase film was assumed to control the ozone mass transfer rate in the bulk fluid. Thus, the interfacial transfer of ozone between gas and water was modelled according to equation **2** (see chapter **2**, **2.3.2.2.**).

$$\Phi^{[O_3]} = k_L \cdot a\left([O_3]_l^* - [O_3]_l\right) \cdot dV \qquad \textbf{(2)}$$

where
- $\Phi^{[O_3]}$: molar flow rate of ozone at the interface (mol.s^{-1})
- k_L : liquid phase mass transfer coefficient (m.s^{-1})
- a : volumetric interfacial area (m^{-1})
- $[O_3]_l$: steady-state liquid phase ozone concentration in the bulk (mol.m^{-3})
- $[O_3]_l^*$: steady-state saturated liquid phase ozone concentration (mol.m^{-3})
- dV : elementary volume considered (m^3)

Values for the mass transfer coefficient k_La generally range from 5.10^{-4} s^{-1} to 0.02 s^{-1} for similar reactors or tanks ([Laplanche *et al.*, 1991]; [Roustan *et al.*, 1996]; [Siddiqui *et al.*, 1998]). Given that ozone dissolution is mostly kinetics-driven, a large value for the k_La was selected: 0.04 s^{-1}. Moreover, the value of k_La was considered constant with temperature. The saturated liquid concentration, $[O_3]_l^*$, was estimated using the modified Henry's law (see chapter **2**, **2.3.2.2.**). A value of Hc = 2.7 was selected, corresponding to the value given by the relation of [Mariñas *et al.*, 1993] at 293K. Given the little variation observed for temperature in the experiments (table **2**), the value was also considered constant throughout the study.
No enhancement factor was considered in the modelling of mass transfer. The water entering the ozonation unit has already been pretreated with granular activated carbon and ozone (see figure **1**). As a consequence, the most reactive sites have already reacted with ozone. We therefore assumed that no transfer acceleration occured due to highly reactive species.

6.4.2. Results of the On-Site Validation: First Approaches

6.4.2.1. Full-scale Validation Results with Annet-sur-Marne 2 Calibration

Full-scale validation results obtained with the models calibrated at lab-scale with Annet-sur-Marne 2 water are presented in figures **22** and **23**, for ozone and bromate concentrations respectively. Only the experimental bromate concentrations of the first period have been taken into account in graph **23**.
Analysing figure **22** and figure **23**, one notes a satisfying agreement of simulation with experiments. Obviously, the results are not as good as for calibration, however the major part of the simulation points are located within the experimental error margins associated to the samples: 75 % of the points for ozone, 60% for bromate (see table **3**). Besides, the simulation results show that the model, calibrated on the basis of the results obtained with Annet-sur-Marne 2 water, may underpredict ozone concentrations and overpredict bromate formation.
Considering the experiments individually, and comparing experimental and simulated data, one can notice two phenomena:

- a progressive worsening of the simulation quality for the ozone concentration prediction: throughout the study, experimental ozone decomposition rates have been falling;

- a systematic overprediction of bromate concentrations; already observed at the beginning of the study, the phenomenon was considerably enhanced in the meantime separating the first from the second period (the results of the second period will be shown in the following).

Both phenomena may, at least partially, be explained by changes in the nature of NOM that would have occurred during the time interval between lab-scale calibrations (first days of July) and on-site experiments, which began July 21 and lasted till October 10.

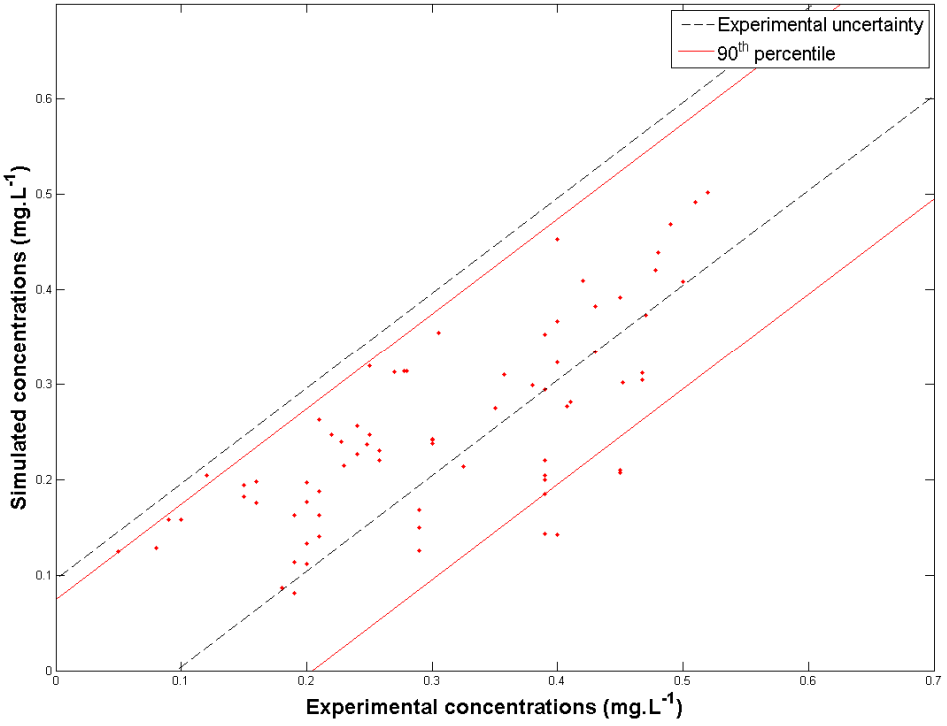

Figure 22 Comparison of simulated and on-site ozone concentrations, Annet-sur-Marne 2 calibration

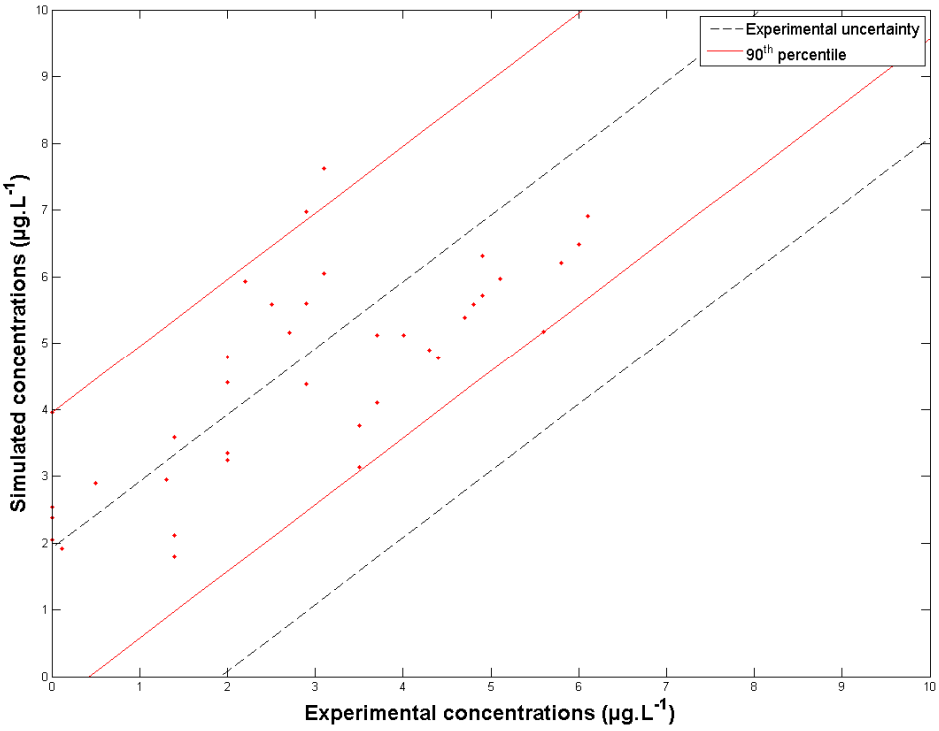

Figure 23 Comparison of simulated and on-site bromate concentrations, Annet-sur-Marne 2 calibration, first period

Given the variability of bromate formation, another set of lab-scale experiments for calibrating the model may have given more accurate results. In agreement with the change observed experimentally in bromate formation (see chapter **5**, **5.4.8.**), it appears from recordings of concentration measurements stored in the SCADA system of the water works, that bromate formation has a seasonal character: bromate formation levels generally increase by the beginning of May; they reach their maximum at the end of June and decrease till November. This variation can be repeatedly observed and is not solely due to changes in temperature, since July and August are generally the two warmest months in Annet-sur-Marne. Moreover, physicochemical properties or process conditions are generally constant (pH, A_T, [Br-], TOC, flows, ozone dose…). If the model for bromate formation would have been calibrated in August, it is therefore likely that it would have given more accurate results.
Modelling results for ozone concentration are more difficult to interpret. Considering the conclusions of chapter **4** and **5**, seasonal variations indeed appear not to play a role as important as on bromate formation. The overconsumption observed on figure **22** may simply be due to the quality of the calibration itself.

6.4.2.2. Validation Results with Annet-sur-Marne Calibration

Though acceptable, the results presented using models calibrated with Annet-sur-Marne 2 water may easily be improved. Considering the relative stability of the reactivity of NOM with ozone, it was decided to implement the model for NOM as calibrated with the experiments with Annet-sur-Marne water sample. These calibration experiments have indeed given the best modelling results, but have been performed in February 2009. The model for bromate formation remains unchanged, calibrated with the experiments done with

Annet-sur-Marne 2 water. The modelling results are presented in figure **24** for ozone and figure **25** for bromate.

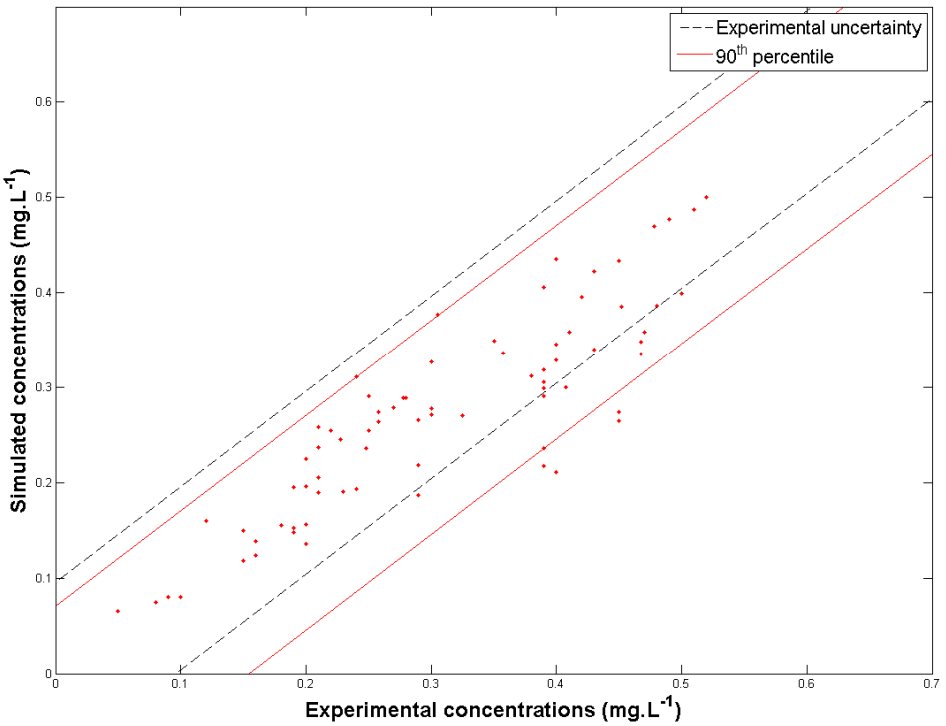

Figure 24 Comparison of simulated and on-site ozone concentrations, Annet-sur-Marne calibration

Using the calibration experiments of Annet-sur-Marne water instead of Annet-sur-Marne 2 water, the predictions for ozone were bettered while predictions for bromate were worsened. As shown by the increase of the fraction of the points comprised within the experimental error margins from 75 % to 84 %, ozone concentrations are better predicted (see figure **24**). Some simulated concentrations remain however quite low compared to experimental concentrations. The general increase in simulated concentrations of ozone has favoured the formation of bromate, as it can be seen by comparing the figures **25** and **23**. The stable percentage of the points comprised within the experimental error margins at 60 % does not truly represent the general increase of simulated concentrations (see table **3**).

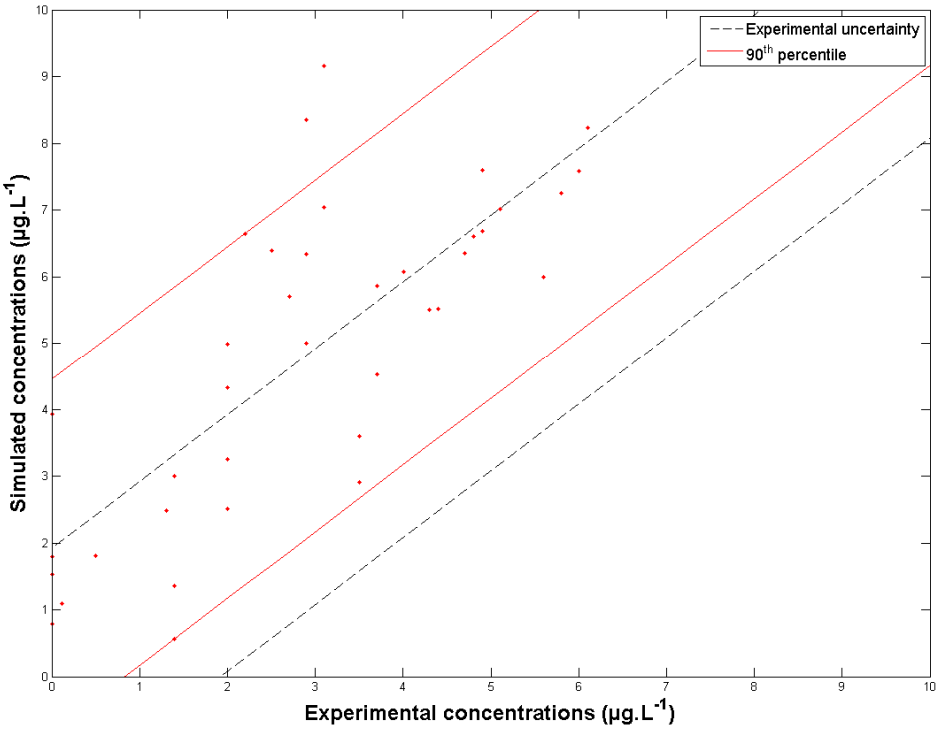

Figure 25 Comparison of simulated and on-site bromate concentrations, ozone : Annet sur Marne calibration, bromate : Annet-sur-Marne 2 calibration, first period

Table 3 Summary of the quality of the validation results, different calibrations

Lab-scale calibration (O_3)	**Lab-scale calibration (BrO_3^-)**	July/October 2009 **O_3 points within uncertainty (%)**	July/August 2009 **BrO_3^- points within uncertainty (%)**
Annet-sur-Marne (February 2009)	Annet-sur-Marne 2 (July 2009)	84	60
Annet-sur-Marne 2 (July 2009)	Annet-sur-Marne 2 (July 2009)	75	60

The results obtained underline the relative stability of the model for ozone decomposition towards seasonal changes of NOM in terms of prediction (the values of the parameters may however change, see Appendix **G**). On the contrary, the model for bromate formation needs to be regularly recalibrated, or readjusted. In the case of bromate concentrations, the percentage of points located within uncertainty did not evolve when changing the lab-scale calibration. However, qualitatively, the results obtained with Annet-sur-Marne2 ozone calibration are slightly better.

6.4.3. Results of the On-Site Validation: Final Approach

6.4.3.1. Taking Into Account Seasonal Variations by Adjusting The Bromate Model

The best modelling results for ozone are obtained using the model calibrated with Annet-sur-Marne experiments, see figure **24**. As a consequence, the model will be kept as it is calibrated for ozone decomposition and radical generation with Annet-sur-Marne experiments. However, the modelling results for bromate concentration are just fair: the model overpredicts concentrations, as shown in figure **25**. In this paragraph, we test the

possibility of a calibration bias for the bromate formation model, readjusting the kinetics (frequency factor) of the last molecular oxidation step.

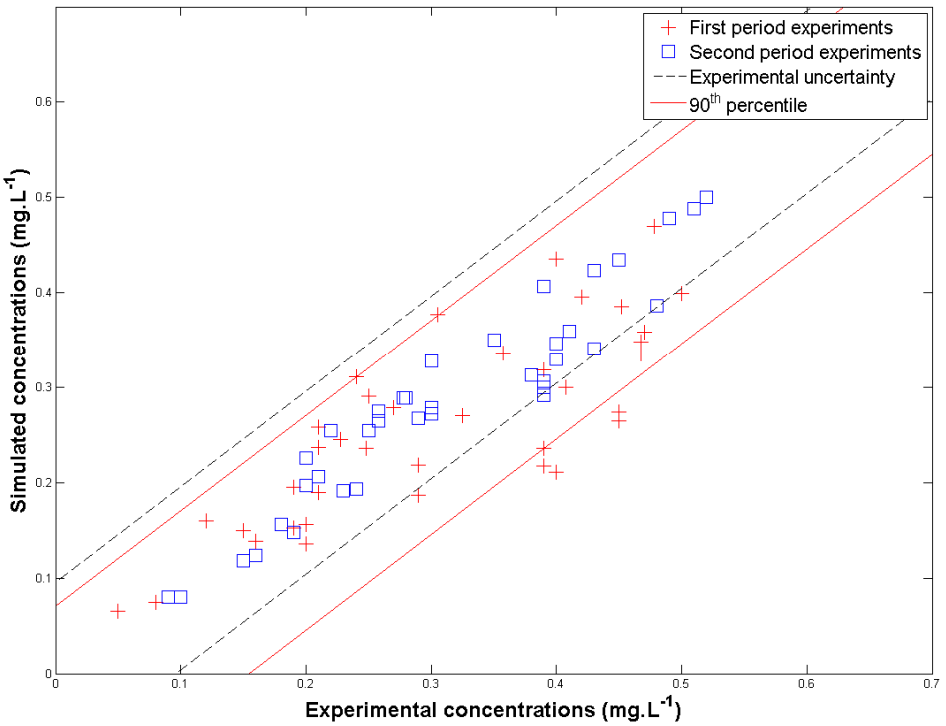

Figure 26 Comparison of simulated and on-site ozone concentrations, Annet-sur-Marne ozone calibration, first and second periods

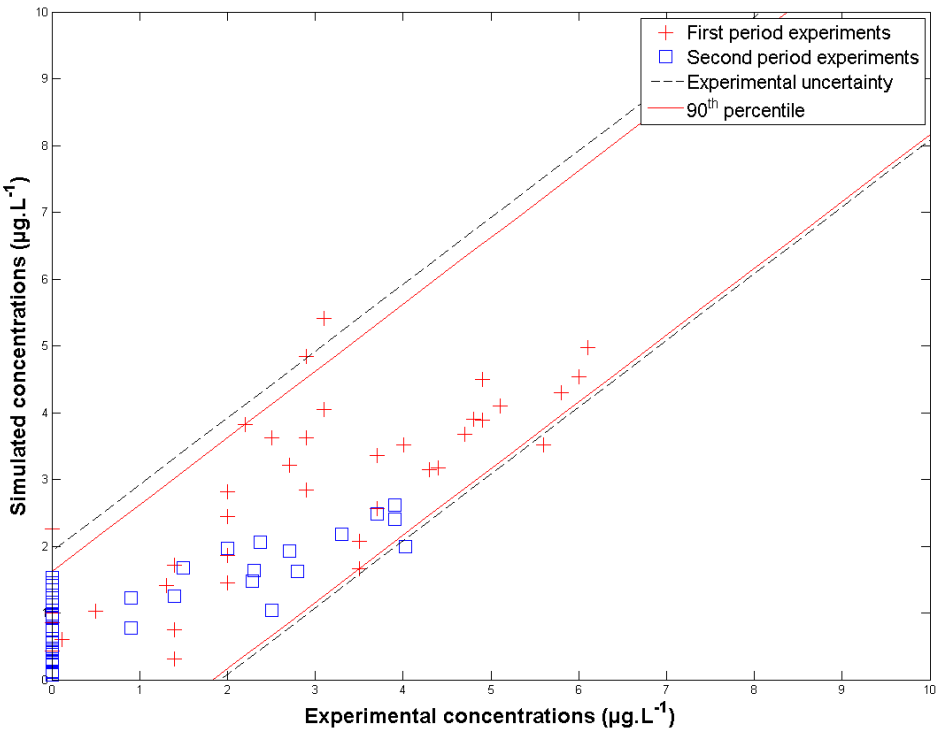

Figure 27 Comparison of simulated and on-site bromate concentrations, ozone: Annet-sur-Marne ozone calibration, bromate: on-site readjustment, first and second periods

The two experimental periods were treated separately. The optimised frequency factors are presented in table **4**. The values were adjusted using the experimental results obtained with the first experiment of each period (experiment #1 for period 1, experiment #9 for period 2); more precisely, all the bromate concentration measurement of experiment #1, only the outlet bromate concentration of experiment #9. All other bromate concentrations were used to validate the model for bromate formation. The modelling results for bromate concentrations are presented in figure **27**, the modelling results for ozone concentrations are presented in figure **26**. In the case of ozone concentrations, the results are the same as in figure **24**, but the two periods appear differently.

Table 4 Summary of the kinetics values for the last molecular oxidation step leading to bromate

Case-study experimental period	k(293 K) ($M^{-1}.s^{-1}$)	E_A ($kJ.mol^{-1}$)	BrO_3^- points within uncertainty (%)	BrO_3^- points used for adjustment (%)
Period 1	$2.1.10^4$	42	92	12.5
Period 2	$5.9.10^3$	42	97	3
Lab-scale calibration (BrO_3^-)				
Annet-sur-Marne	2.10^3	43	94	100
Annet-sur-Marne 2	$4.5.10^4$	42	7	100

The results of lab-scale calibrations with Annet-sur-Marne and Annet-sur-Marne 2 waters are also presented in table **4**. The concentration profiles within the ozonation unit are given for the two experiments used for calibrating the model of bromate formation. They are presented in figure **28** for experiment #1 and in figure **29** for experiment #9. Figures **30** to **32** present some validation results obtained for first period experiments done at high water flow rate; figures **33** to **35** present validation results for second period experiments done at low water flow rate. All modelling results for the full-scale study are presented in Appendix **K**.

6.4.3.2. Adjustment Results

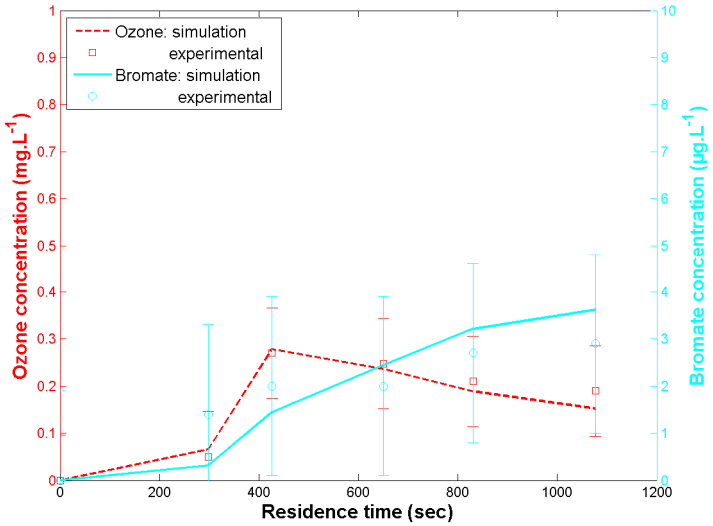

Figure 28 adjustment **Experiment #1 ($[O_3]_g$=14.6 g.Nm^{-3}; Q_g=84 Nm^3.h^{-1}; Q_l=1644 m^3.h^{-1}): first period**

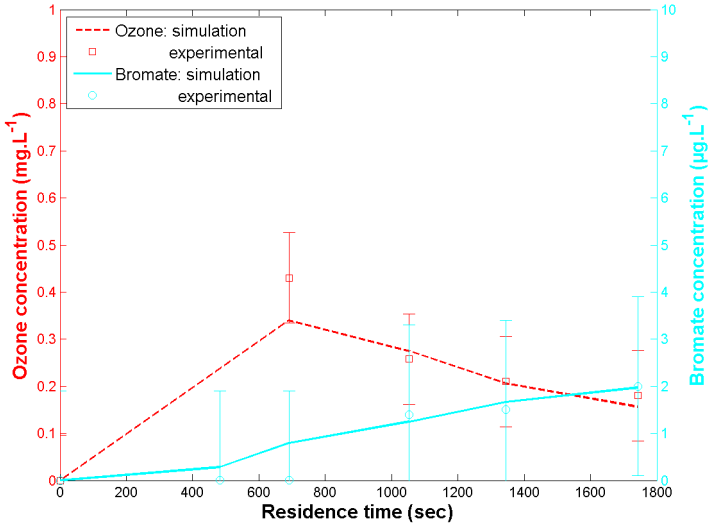

Figure 29 adjustment **Experiment #9 ($[O_3]_g$=10.6 g.Nm^{-3}; Q_g=81.8 Nm^3.h^{-1}; Q_l=1021 m^3.h^{-1}): second period**

6.4.3.3. Validation Results: First Period

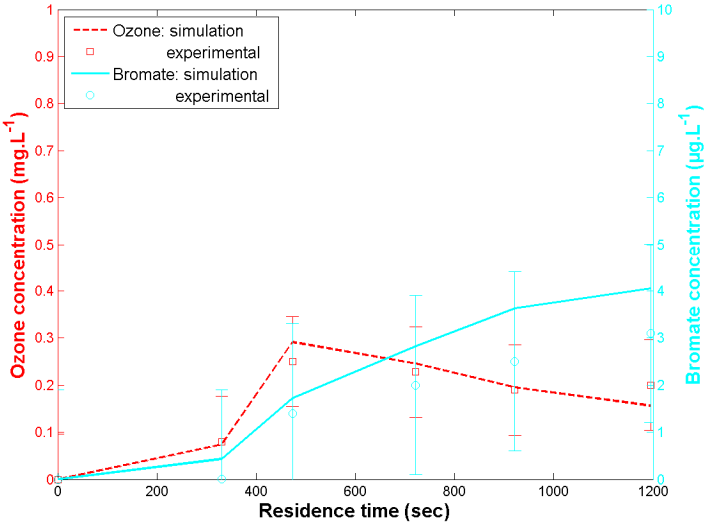

Figure 30 **Experiment #2 ($[O_3]_g$=13.5 g.Nm^{-3}; Q_g=84.4 Nm^3.h^{-1}; Q_l=1481 m^3.h^{-1})**

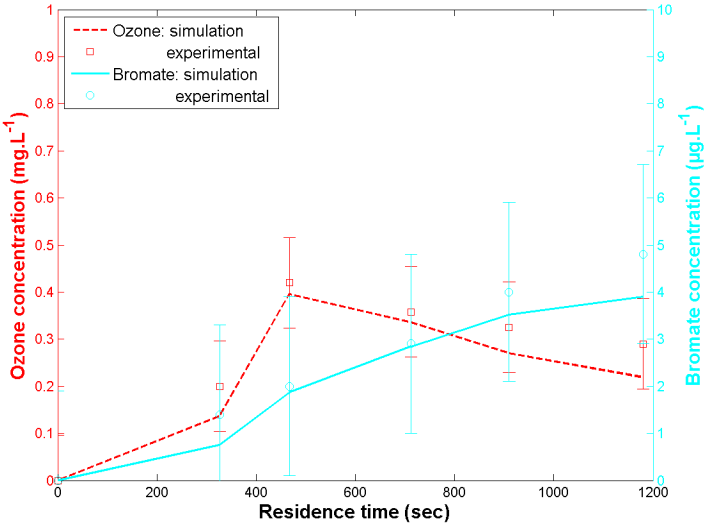

Figure 31 **Experiment #4 ($[O_3]_g$=19.9 g.Nm^{-3}; Q_g=63 Nm^3.h^{-1}; Q_l=1504 m^3.h^{-1})**

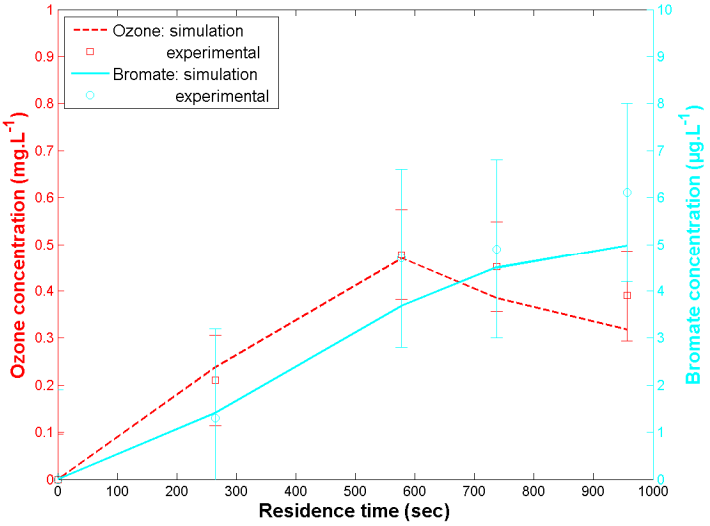

Figure 32 **Experiment #5 ($[O_3]_g$=13.9 g.Nm^{-3}; Q_g=149 Nm^3.h^{-1}; Q_l=1851 m^3.h^{-1})**

6.4.3.4. Validation Results: Second Period

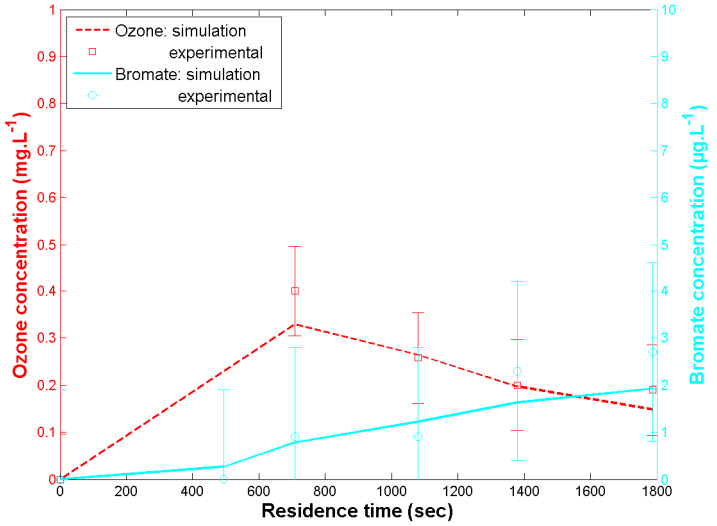

Figure 33 **Experiment #10 ($[O_3]_g$=10.2 g.Nm^{-3}; Q_g=80.2 Nm^3.h^{-1}; Q_l=990 m^3.h^{-1})**

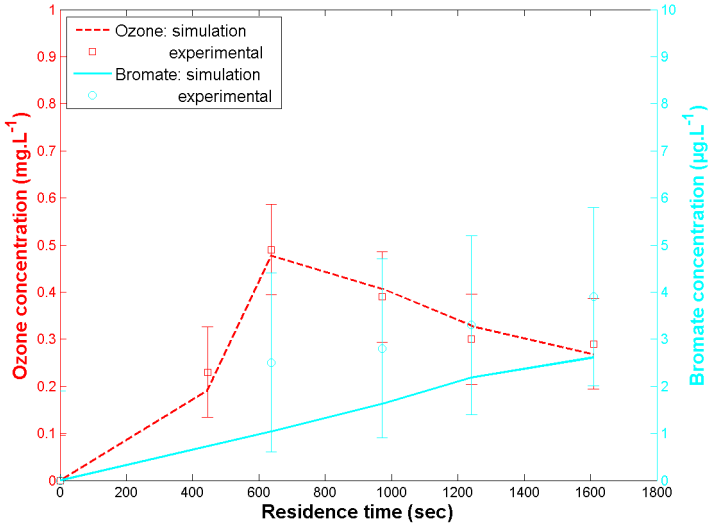

Figure 34 **Experiment #11 ($[O_3]_g$=13.1 g.Nm^{-3}; Q_g=81.6 Nm^3.h^{-1}; Q_l=1100 m^3.h^{-1})**

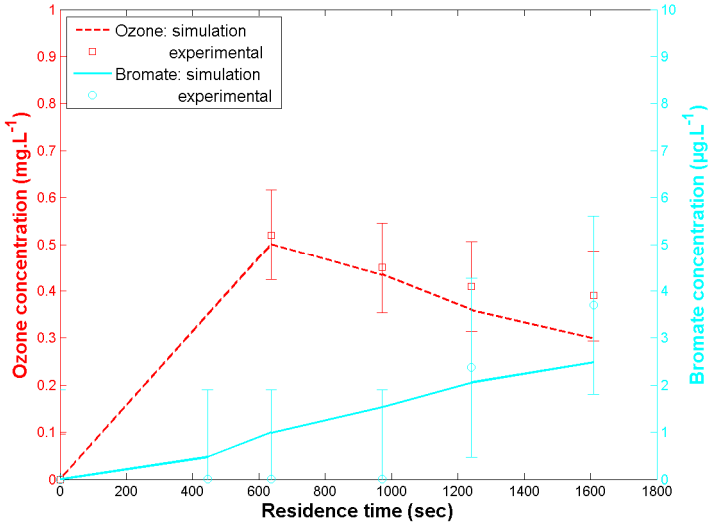

Figure 35 **Experiment #13 ($[O_3]_g$=17.6 g.Nm^{-3}; Q_g=61.9 Nm^3.h^{-1}; Q_l=1100 m^3.h^{-1})**

6.4.4. Discussion

Previous modelling studies of industrial ozonation units have shown the difficulty of predicting accurately bromate formation. Generally, the focus was put on assessment of disinfection efficiency *via* the determination of the concentration of ozone. Different modelling techniques were used and a brief overview is given in Appendix **A**.

As it appears from the comparison of the concentration profiles obtained with lab-scale calibration or with on-site adjustment, the formation of bromate and the decomposition of ozone may be simultaneously predicted. This confirms that the model for bromate formation may be applied to simulate an industrial ozonation unit. However it should periodically be readjusted for accurate predictions of bromate formation (this was done here only considering a single experimental concentration measurement). Regarding ozone decomposition, the model appears to be more stable, but this has to be confirmed over a larger period of testing.

Comparing with studies carried out previously, the following remarks can be made, underlining the originality of this research:

- Coupling simple chemical kinetics with accurate hydraulic description by CFD, [Zhang, 2006] and [Bartand, 2007] have given interesting results on bromate formation. However, their results need to be extended since very few experimental data were used for validation of the model. Moreover, crucial parameters as water flow rate could not be varied due to the difficulty of simulating such changes;
- The one-dimensional axial dispersion reactor model was used to model ozonation units by [Kim *et al.*, 2004] and [Tang *et al.*, 2005]. Kim used more detailed models for chemical kinetics, comparable to those presented in this study. The studies were supported by validation with pilot ([Kim *et al.*, 2004]) or industrial ([Tang *et al.*, 2005]) experimental data. Results were promising in terms of predictions for inactivation of *Cryptosporidium parvum* oocysts and gave interesting insights in bromate formation pathway for NOM-containing water. However, they remain of limited validity in regards to the operating domain explored. Moreover, axial dispersion modelling does not allow for extrapolating to other geometries, see Appendix **A**;
- Systematic networks have also been used, as in this study, to model full-scale ozonation processes. [Siddiqui *et al.*, 1998] defined a systematic network composed of CSTRs and then applied pseudo-first order kinetics for ozone decomposition. Further, a multiple linear correlation for bromate formation was introduced. This study was finally used to explore different scenarios of operating conditions, but the modelling results were not supported by a large amount of experimental measurements. [Gallard *et al.*, 2003] proposed to model inactivation under the same type of assumption, but the experimental data did not allow for modelling bromate formation. More recently, authors combined systematic networks with pseudo-first order ozone decomposition and a single reaction for the formation of bromate ([van der Helm *et al.*, 2007]; [Audenaert *et al.*, 2010]). Moreover, van der Helm introduced UVA as a control parameter, allowing for adapting the model to new process conditions. The results proposed are promising, but still need to be extended.

One possible limitation of this study is the poor quality of the modelling of gaseous ozone concentrations. Experimental gaseous ozone concentration measurements were used to assess the transfer efficiency of the unit. Experimental efficiencies were high: for the four first experiments, a value of 83 % was calculated. The simulations overestimated this parameter:

the calculations gave an efficiency of 97 % due to an overconsumption of ozone in the model. Several explanations can be given to this overconsumption.

- The ozone doses used for calibrating the model for the role of NOM on ozone decomposition are much larger than those used on-site. We know from chapter **4**, that the model has difficulties to extrapolate to other ozone doses, in particular ozone decomposition is generally underpredicted when ozone dose is raised. As a consequence, the ozone decomposition for small on-site ozone doses may have been overestimated;
- The CFD study used to calibrate the systematic network was calculated for a single-phase problem (no gaseous ozone). Gaseous flow may impact on water hydraulics and mass transfer.
- Differences in the behaviour of NOM towards ozone may have caused the model not to be calibrated for the experimental conditions of the case study.

6.5. Conclusion

An integrated modelling procedure, from model calibration at lab-scale to model validation at industrial scale has been presented. Protocols and models have been given.
Calibration results have shown that the models used to predict the decomposition of ozone, the generation of hydroxyl radicals and the formation of bromate were valid for the natural water investigated. A large domain of validity was tested since changes in contact time with ozone, pH, ozone dose, temperature, nature and content of NOM and initial bromide concentration could be modelled adequately. Up-scaling to ozonation unit#1 of Annet-sur-Marne water works was then undertaken. The results have proven the soundness of such approach since the majority of the predicted concentrations were located within the experimental error bars margins of the samples. Moreover, the model does adapt to different process conditions (changes in liquid flow rate, gaseous ozone concentration and gaseous ozone flow rate). However, having performed calibration and validation steps at different periods of the year may have caused the model not to be fully representative of the phenomena observed on site. The validity of the model was confirmed in the case of bromate ions by an *a posteriori* adjustment, which led to a considerable improvement of the validation results.
Therefore, a complementary on-site study shall be planned in the coming months, on a shorter time period, with lab-scale concomitantly perfomed. The possibilities of model parameter readjustments shall also be considered (sensitivity analysis of the model parameters).
Considering the previous studies, this work appears to be original in proposing a modelling approach almost exclusively developed on the base of lab-scale experiments. Further, validation has been done with large amounts of experimental data harvested on-site. The case-study has given evidence that slight modelling readjustments should be performed, yet these have remained very limited (12.5 % and 3 % of the experimental measurements for the first and the second periods, respectively).
The results of this full-scale modelling study indicate that the formation of bromate and the decomposition of ozone may be simultaneously predicted. This confirms that the model for bromate formation may be applied to simulate an industrial ozonation unit. However it should periodically be readjusted for accurate predictions of bromate formation, for example with regular control measurements. Regarding ozone decomposition, the model appears to be more stable.

Bibliography

Articles and books

- **Audenaert W.T.M., Callewaert M., Nopens I., Cromphout J., Vanhoucke R., Dimoulin A., Dejans P., van Hulle S.W.H.**, (2010). Full-scale modelling of an ozone reactor for drinking water treatment, *Chemical Engineering Journal*, Vol. **157**, pp. 551-557.
- **Bader H.** and **Hoigné J**., (1981). Determination of Ozone in Water by the Indigo Method, *Water Research*, Vol. **15**, pp. 449-456.
- **Bartrand T. A.,** (2007). High resolution experimental studies and numerical analysis of fine bubble ozone disinfection contactors, Ph.D. thesis, Drexel University, U.S.A.
- **de Traversay C., Fluck F., Wolbert D., Laplanche A.**, (2001). Hydrodynamics of ozonation tanks: Definition of systemic models from CFD, *Proceedings of the 15th World Ozone Congress,* London, Vol. **3**, pp. 156-164.
- **Gallard H., von Gunten U.**, **Kaiser H. P.**, (2003). Prediction of the disinfection and oxidation efficiency of full-scale ozone reactors, *Journal of Water Supply: Research and Technology – AQUA*, Vol. 52, pp. 277-290.
- **Gélinet K.**, (1999). Importance des caractéristiques physico-chimiques des eaux naturelles sur la formation des ions bromates lors de l'ozonation, Ph.D. thesis, ESIP, France.
- **Gillogly T. *et al.*** (2001). Bromate formation and control during ozonation of low bromide waters, Chapter 7: A Comparison of Bromate Formation within different Scales of Ozone Contactors, *AWWA Research Foundation*, pp. 97-111.
- **Guitard M.,** (2007). Optimisation hydraulique des cuves d'ozonation de l'usine d'Annet-sur-Marne – Rapport final, Veolia Eau – Compagnie Générale des Eaux.
- **Kim J.-H., von Gunten U., Mariñas B. J.**, (2004). Simultaneous predicion of *Cryptosporidium parvum Oocyst* inactivation and bromate formation during ozonation of synthetic waters, *Environmental Science and Technology*, Vol. **38**, pp. 2232-2241.
- **Kim Do-Ill,** (2007). Development and Application of Integrated Ozone Contactor Design and Optimization Tools, Ph.D. thesis, Georgia Institute of Technology, U.S.A.
- **Laplanche A., Le Sauze N., Martin G., Langlais B.**, (1991). Simulation of Ozone Transfer in Water. Comparison With a Pilot Unit, *Ozone: Science and Engineering*, Vol. **13**, pp. 535-558.
- **Legube B., Parinet B., Gélinet K., Berne F., Croué J.-P.,** (2004). Modeling of bromate formation by ozonation of surface waters in drinking water treatment, *Water Research*, Vol. **38**, pp. 2185-2195.
- **Mariñas B. J., Liang S., Aieta E. M.,** (1993). Modeling Hydrodynamics and Ozone Residual Distribution in a Pilot-Scale Ozone Bubble-Diffuser Contactor, *Journal of the American Water Works Association*, Vol. **85**, pp. 90-99.
- **Roustan M., Wang R. Y., Wolbert D.**, (1996). Modeling Hydrodynamics and Mass Transfer Parameters In a Continuous Ozone Bubble Column, *Ozone: Science and Engineering*, Vol. **18**, pp. 99-115.
- **Siddiqui M., Amy G., Ozekin K., Westerhoff P.**, (1998). Modeling Dissolved Ozone and Bromate Ion Formation in Ozone Contactors, *Water, Air and Soil Pollution*, Vol. **108**, pp. 1-32.
- **Tang G., Adu -Sarkodie K., Kim D., Kim J.-H, Teefy S., Shukairy H.**, **Mariñas B. J.**, (2005). Modeling *Cryptosporidium parvum Oocyst* inactivation and bromate formation in a full-scale ozone contactor, *Environmental Science and Technol*ogy, Vol. **39**, pp. 9343-9350.
- **van der Helm A.W.C., Smeets P.W.M.H., Baars E.T., Rietveld L.C., van Dijk J.C.,** (2007). Modeling of Ozonation for Dissolved Ozone Dosing, *Ozone: Science and Engineering*, Vol. **29**, pp. 379-389.
- **von Gunten U.** and **Hoigné J.,** (1994). Bromate Formation during Ozonation of Bromide-Containing Waters: Interaction of Ozone and Hydroxyl Radical Reactions, *Environmental Science and Technology*, Vol. **28**, pp. 1234-1242.
- **Wert E. C.**, **Rosario-Ortiz F. L.**, **Drury D. D.**, **Zinder S. A.,** (2007a). Formation of Oxidation Byproducts from Ozonation of Wastewater, *Water Research*, Vol. **41**, pp. 1481-1490.
- **Whitman W.G.,** (1923), A preliminary experimental confirmation of the two-film theory of gas absorption, *Chemical and Metallurgical Engineering,* Vol. **29, pp.** 146-148.

- **Zhang J.,** (2006). An integrated design approach for improving drinking water ozone disinfection treatment based on computational fluid dynamics, Ph.D. thesis, University of Waterloo, Canada.

Reports, manuals and courses

- **Kim Doo-Ill** and **Kim J.-H.**, (2005). A Computer-Based Design of New Ozone Contactor Treating Paldang Dam Reservoir Water, *Final Report*, available at: http://smartech.gatech.edu/bitstream/1853/9969/1/E-20-K69.pdf, last access: May 2010.

CONCLUSION

This study has investigated the modelling of ozonation processes proposing an integrated modelling procedure, leading from laboratory to an industrial unit. The main objective was to develop a model able to predict concentration profiles for: ozone, bromate and specific micropollutants. The main findings are summarised below:

♦ A semi-empirical model for the role of NOM has been developed. This model is able to adequately reproduce changes in contact time with ozone, pH, temperature, ozone dose, NOM content and NOM concentration. A good agreement of modelling results with experimental data was found for about 75 % of the experiments.
Very good simulation results were obtained for 55 % of the concentration measurements for ozone and for 45 % of the concentrations for *p*CBA. For these concentration measurements, the difference between the model and the experimental observation was found lower than the experimental uncertainty. Consequently, these simulation results cannot be improved from a physical perspective and were hence termed "very good". The good quality of the results for ozone concentrations is of particular interest for assessment of disinfection, given that inactivation mechanisms only consider ozone exposure.
The model was able to adequately reproduce experimental measurements for nine of the eleven water samples studied, covering a wide domain. The more contrasted results for two water samples were characterised by simulations, the quality of which was excellent for ozone and very poor for *p*CBA. The relatively moderate quality of the results obtained with these two waters is probably due to the simultaneous high organic (TOC > 2.4 $mg.L^{-1}$) and low inorganic (A_T < 0.3 $meq.L^{-1}$) contents of the water samples. An explanation can be that scavenger-acting species present in NOM, which have been considered as negligible compared to carbonate species in the proposed model, may be active for the considered waters. The model remains however valid in a large domain: 6.1 ≤pH ≤8.15; 1.02 $meq.L^{-1}$≤ A_T ≤6.02 $meq.L^{-1}$; 0-.0.5 $mg.L^{-1}$≤TOC≤3.1 $mg.L^{-1}$.

♦ A simple calibration procedure of the proposed model for the role of NOM was developed for engineering purpose. This calibration procedure gives modelling results comparable to those obtained with much larger data sets used for calibrating the model: 70% of the experiments were modelled satisfactorily, 48 % of the simulated concentrations for ozone were considered as very good, 47 % for *p*CBA. Only six experiments, done with the developed apparatus at lab-scale, were necessary to fully calibrate the model. This calibration represents two days of experimental work at lab scale and one day of calculation to identify the parameters of the model.

♦ Experiments on the formation of bromate in natural waters brought into light the importance of NOM: Models for the simulation of bromate formation have to be calibrated when dealing with natural water. Natural water samples were always found to be less prone to form bromate than NOM-free waters. Seasonal variations can be taken into account by readjustments of the parameters of the model. Considering the crucial zone below 20 $\mu g.L^{-1}$, 68 % of the simulated concentrations corresponded to experimental concentrations or were located in the experimental uncertainty interval and were thus considered as very good.

♦ Experimental results collected during a full-scale study on an industrial ozonation unit showed that a direct implementation of the chemical models calibrated at lab-scale is possible: modelling results for ozone and bromate are matching experimental measurements. During the four month-lasting study, 80 % and 94 % of the simulated concentrations, respectively for ozone and bromate, were considered as very good. For a longer period of investigation, it is likely that slight readjustments of the models should account for seasonal variations in the nature of NOM, especially for the formation of bromate.

Bearing in mind that the understanding and the modelling of natural water ozonation has only begun thirty years ago with the works of Staehelin and Hoigné, this study aimed at proposing simple solutions for practical predictions of some target compounds (ozone, bromate and, indirectly, hydroxyl radicals). While addressing the research objectives, this study has raised several questions. Some of the future works that can be undertaken to pursue this research are as follows:

♦ Hydroxyl radical scavenging by NOM was not considered in this study and should specifically be studied. For two water samples, with high TOC/A_T ratios, the proposed model (without scavenging by NOM) was unable to simulate experimental observations. The first tries in implementing a simple scavenging scheme were unsuccessful. At present, the question if a simple equation as **1** with C_1=1 truly represents radical-scavenging by NOM remains open. Fundamental research on the number of scavenging sites of specific molecules present in NOM may give interesting insights on the validity and the stoichiometry of reaction **1**.

$$NOM^s + C_1.^{\bullet}OH \rightarrow products \qquad \textbf{(1)}$$

♦ The definition of an optimal group of experiments to be done to calibrate the model for the influence of NOM on ozone decomposition could be of interest in order to get the highest quality in the parameters estimation while reducing the experimental and numerical costs of the primary fitting. So far, a group of six experiments has given good results, but a procedure to systematically minimise the number of experiments without loss in prediction quality may help in reducing further the group, or in improving the validation results.

♦ The domain of validity of the model for bromate formation has to be determined. Important discrepancies between experimental and simulated bromate concentrations were observed for high experimental concentrations (typically above 35 µg.L^{-1}). The model either underpredicted or overpredicted experimental concentrations. It is not likely that considering reactions involved in bromate formation, which were unconsidered in the proposed model would have resulted in a better agreement of experimental and simulated data.

♦ The role played by NOM within bromate formation and its modelling should be studied. This particular aspect was beyond the scope of this study and a simplified model was deliberately chosen. In a first time, classical models involving the couple BrOH/BrO^- could be used to simulate experimental results. In a second time, specific experiments with natural waters and BrOH/BrO^- adding may help understand bromate formation in natural waters.

♦ The results of the case-study can be extended. Firstly, by continuing experimental on-site harvesting and by comparing measured and simulated values (Annet-sur-Marne water works). Secondly, by analysing other industrial units. Annet-sur-Marne was chosen because

(i) of the good simulation results obtained at lab-scale for model calibration; (ii) of the very satisfactory flow conditions (few recirculation or backmixing). In other cases, chemical and hydrodynamic modelling may be more difficult to achieve. It would then be interesting to determine the incidences on full-scale modelling.

♦ A Graphical User Interface-based software product incorporating all the fundamental aspects developed in this work is currently being built up. This tool will greatly assist operators and engineers in their management and expertise of ozonation units. Moreover, such tool could be used in order to gain knowledge on modelling of industrial ozonation processes.

♦ The present work should be extended in considering micropollutant removal and bacterial inactivation. With a good knowledge of the fate of the main oxidative species ozone and hydroxyl radicals, both objectives are easily achievable. However, they need to be experimentally supported since a large amount of micropollutant kinetics is not well documented in the literature.

Appendix A

Complements on Disinfection Modelling

A.1. Introduction

This appendix proposes complements on disinfection modelling as presented in paragraph **1.2.5.** The first section gives more explanations on the Chick and Watson model and also presents the alternative model developed by Hom.
Other techniques used for assessing the disinfection efficiency are presented in the second section of the appendix. They can be seen as complementary methods to the Ct approach already presented. Their relative relevancies are also discussed.

A.2. Models for Microbial Inactivation

Designed primarily to investigate chlorine disinfection, the first studies on the survival of microorganisms after addition of disinfectant in natural environment have been successfully applied to ozone disinfection, and are currently still used. The first models were built for systems that had no chlorine demand. Thus, chlorine concentration was presumed constant throughout the disinfection. The simplest and most famous disinfection model was proposed by Chick and Watson at the beginning of the XXth Century [Chick, 1908]. Chick postulated that the death of microorganisms in a batch reactor within a time interval is caused by a multiplicity of independent phenomena. For a given disinfectant concentration, all the other factors being assumed constant, the mortality remains stable in each time unit. The micro-organism balance including the inactivation kinetics are then as equation **1**.

$$\frac{dN}{dt} = -kC^n N \qquad \textbf{(1)}$$

where

n : disinfectant's reaction order
C : disinfectant concentration
N : microorganism concentration
k : apparent constant rate, sometimes called lethality coefficient

If $n > 1$, disinfectant concentration is the dominant factor in determining the inactivation rate;
If $n < 1$, the contact time is more important than C.

However, the precedent relation is solely valid for a constant disinfectant concentration, what is not the case when one considers a typical disinfection experiment (done with natural water for example). The ozone demand may affect significantly the efficiency of disinfection: qualitatively in oxidizing various organic or inorganic compounds; quantitatively diminishing the residual ozone. To cope with this problem, diverse empirical or semi-empirical approaches were proposed [Gélinet, 1999]. One of them, developed by [Hom, 1972] under constant disinfectant residual concentration in a homogeneous batch system, provides a relationship between disinfectant concentration and contact time, via two empirical constants o_H and n_H (equation **2**). The Hom model successfully describes the disinfection of *Giardia* and *Cryptosporidium* in a batch reactor and converts to the Chick-Watson model when o_H is equal to 1. Under typical disinfection conditions, disinfectant concentration decay is generally assumed to be first order (equation **3**).

$$\frac{dN}{dt} = -k_H o_H C^{n_H} N.t^{o_H - 1} \qquad \textbf{(2)}$$

$$C = C_0 e^{-k't} \quad \textbf{(3)}$$

where

k' : first order decay rate of disinfectant
C_0 : initial disinfectant concentration
k_H, o_H, n_H: empirical constants for Hom model
t : contact time

Variations on these disinfection models are possible but are rarely used. The simple Chick-Watson model is still considered by many as the most appropriate model for comparing *Cryptosporidium* disinfection data from a number of research groups, because of the inherent variation in experimental data (unpublished data, International Cryptosporidium Ct Workshop, Washington, DC, January 12–14, 1998 as cited by [LeChevallier and Au, 2004]).This has led to the formulation of the Ct concept (see **1.2.5.**) promoted by the USEPA and then used in correlation with the SWTR (Surface Water Treatment Rule)[1].

A.3. Methods for Estimating Disinfection

A.3.1. Integrated Disinfection Design Framework (IDDF)

The IDDF has been proposed by [Bellamy *et al.*, 1998] as another approach for designing ozonation processes. It has been based on the segregated flow system, which assumes that molecules are grouped together in aggregates. A similar approach was adopted by [Roustan *et al.*, 1991] in order to evaluate the Ct approach. Contrary to the hypothesis of Roustan, ozone concentration is not assumed constant in IDDF.

IDDF consists of three modules: ozone decomposition *via* a pseudo-first order kinetic rate; pathogen inactivation using Hom law; contactor hydraulics defined by the distribution of normalised residence time function *E*. Once the components of the module selected or set, IDDF calculates inactivation applying the segregated flow model. This approach thus combines kinetics data established in batch reactors (presented in green on figure **1**) and data on the contactor hydraulics (in blue). Results of IDDF are inactivation, and possibly DBP formation levels [Bellamy, 1998], presented in orange on the figure. The notations of figure **1** are the same as presented in **A.2.**, t_m is the mean residence time (see Appendix **B**). Further developments of IDDF have allowed the use of RTD data experimentally determined from tracer tests directly as input to the hydraulics module [Zhang, 2006].

IDDF hydraulics modelling can be compared with an infinite number of parallel plug flow reactors of increasing length. Each reactor corresponds to a residence time, the relative input flow fraction being defined according to the probability density function of the residence times.

The expression for calculating the inactivation kinetics ($\ln\left(\frac{N}{N_0}\right) = -k_H C^{n_H} t^{o_H}$) is valid for a constant oxidant concentration. In fact, the ratio N/N_0 is overestimated for a conservative calculation as $\ln\left(\frac{N}{N_0}\right) \leq -k_H C^{n_H} t^{o_H}$ (this can be shown using integration by parts).

[1] Effective December 31, 1990, the SWTR applies to all US systems that use surface water or groundwater under the direct influence of surface water. The Rule established drinking water treatment techniques in lieu of maximum contaminant levels for *Giardia lamblia*, viruses, heterotrophic plate count bacteria, *Legionella*, and turbidity.

The Rule requires 99.9 percent (3-log) removal and/or inactivation of *Giardia* cysts, and 99.99 percent (4-log) removal and/or inactivation of viruses. To meet these requirements, water systems must disinfect under stringent conditions, filter water until certain source water-quality and site-specific conditions are met, and been operated by qualified personal.

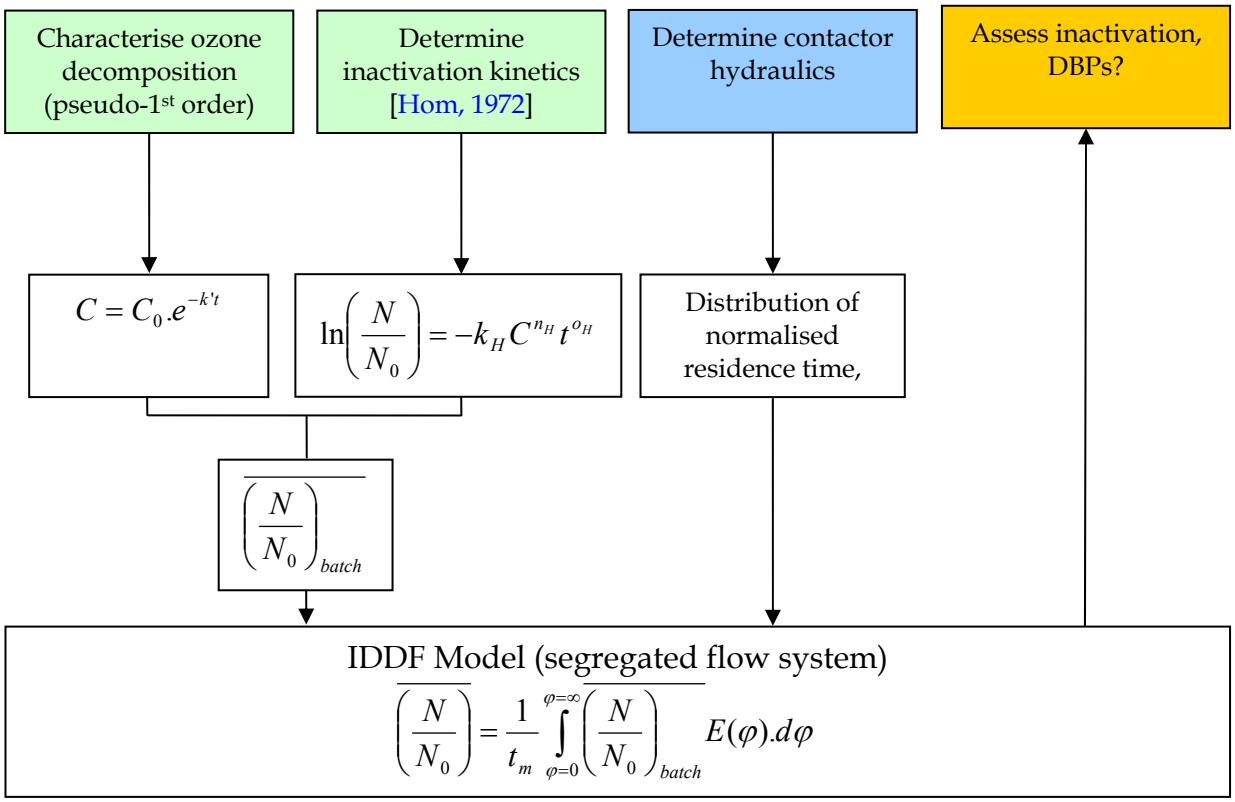

Figure 1 Flowchart for development of mathematical models for Integrated Disinfection Design Framework, adapted from [Bellamy, 1998]

It has been shown that the IDDF method is more accurate than the Ct method in predicting ozone disinfection efficiency [Bellamy *et al.*, 1998]. However, the IDDF model postulates that fluids in the disinfection reactor are completely segregated, what is not true for real fluids [Do-Quang, 1993]. The models used for ozone decomposition also remain of limited validity and exhibit the same weaknesses as with the Ct approach. Under these conditions, accurate predictions for bromate may be obtained only in a very restricted domain. It has been reported that using IDDF may result in an over estimation of ozone disinfection efficiency [Craik, 2005].

A.3.2. Other Approaches

Based on the perfectly micro-mixed model, [Zwietering, 1959] proposed a method for determining conversion terms in continuous flow systems. Using this framework, a mathematical description of a completely micro-mixed reactor was given by [Craik, 2005], integrating live parasite concentration, and the respective rate expressions for ozone decay and inactivation kinetics. According to the modelling results of the study, calculations may tend to underestimate microbial inactivation. Besides, calculations are more resource-consuming for micro-mixed analysis than for segregated flow analysis. This approach has therefore seldom been used by researchers and in engineering design.

ADM (Axial Dispersion flow Model) is a common modelling approach for prediction in bubble column ozone reactors. When modelling two-phase systems, it is often used under the assumption that the liquid phase disperses axially while the gas is considered to have plug flow characteristics [Kim *et al.*, 2002].
Already used by [Mariñas *et al.*, 1993] to predict hydrodynamics and ozone residual profiles in bubble diffuser contactors, ADM was extended in integrating microbial inactivation kinetics models by [Kim *et al.*, 2002]. Further, empirical ozone decomposition and mechanistic bromate formation models were added [Kim *et al.*, 2004]. Both studies of Kim were supported by validation with pilot experimental data. Results were promising in terms of predictions for inactivation of *Cryptosporidium parvum* oocysts and gave interesting insights in bromate formation pathway for NOM-containing water. However, they remain of limited validity in regards to the operating domain explored.

Hydraulics representation is obviously case-dependent and should therefore be calibrated through the optimisation of axial dispersion coefficients for gaseous and liquid phases. The choice to represent hydraulics only with two adjustable parameters allows easy calibration, yet it represents a major obstacle to a wider use of this technique. Using ADM, it is impossible to extrapolate the results to other geometries, scales and operating conditions [Cockx *et al.*, 1997]. Hence, such a model remains valid only for columns with similar geometry ([Kim, 2002]) and may be difficult to apply to on-site ozonation units.

A.3.3. Conclusion

All the presented modelling procedures, except the latest works done by Kim and his co-workers aimed at predicting disinfection efficiency using inactivation kinetics. Very handy, the Ct approach has shown limits of use and could probably advantageously been replaced by an IDDF-like procedure as suggested by [Roustan *et al.*, 1991]. ADM is certainly the best framework to predict concentration profiles; nevertheless it remains of limited use because of its restricted validity regarding hydraulics. Advantages and drawbacks of the reviewed techniques are summarised in table **1**. One should note that the "easiness to solve" criteria is not relevant for ADM, since much more intricate kinetics are considered in this case.

Table 1 Strengths and weaknesses of the reviewed modelling procedures reviewed for disinfection efficiency prediction

Criteria	Ct	IDDF	µ-mixed model	ADM
Inactivation	+	++	+	++
Ozone profiles	-	-	?	+
Bromate profiles	--	--	--	+
Hydraulics	--	+	-	-
Easiness to solve	++	+	-	--

The results gathered from the literature also enlighten the importance of hydraulics and the difficulty inherent to its modelling. However, hydraulics cannot be overlooked, as disinfection, DBP formation and flow conditions are closely linked [Tang *et al.*, 2005]. Accordingly, many researchers have directed their studies towards a better understanding of hydraulics using CFD.

A.4. Bibliography

- **Bellamy W. D., Finch G. R., Haas C. N.,** (1998). Integrated Disinfection Design Framework, *American Water Works Association Research Foundation*, Denver, U.S.A.
- **Chick H.,** (1908). An investigation of the laws of disinfection, *Journal of Hygiene*, Vol. **8**, pp. 92-158.
- **Cockx A., Liné A., Roustan M., DoQuang Z., Lazarova V.,** (1997). Numerical simulation and physical modeling of the hydrodynamics in an air-lift internal loop reactor, *Chemical Engineering Science*, Vol. **52**, pp. 3787-3793.
- **Craik, S. A.,** (2005). Effect of micro-mixing conditions on predictions of *cryptosporidium* inactivation in an ozone contactor, *Ozone: Science and Engineering*, Vol. **27**, pp. 487–494.
- **Do-Quang Z.**, (1993). Etudes expérimentale et numérique des performances des contacteurs de désinfection de l'eau par le chlore, Ph.D. thesis INSA Toulouse, France.
- **Gélinet K.**, (1999). Importance des caractéristiques physico-chimiques des eaux naturelles sur la formation des ions bromates lors de l'ozonation, Ph.D. thesis, ESIP, France.
- **Hom L. W.,** (1972)**.** Kinetics of chlorine disinfection in an ecosystem, *Journal of the Sanitary Engineering Division*, Vol. **98**, pp. 183-194.
- **Kim J. H., Tomiak R. B., Mariñas B. J.**, (2002). Inactivation of Cryptosporidium oocysts in a pilot-scale ozone bubble-diffuser contactor. I: Model development. *Journal of Environmental Engineering-Asce*, Vol. **128**, pp. 514-521.
- **Kim J.-H.,** (2002). Integrated optimization of cryptosporidium inactivation and bromate formation control in ozone contactor, Ph.D. thesis, University of Illinois, U.S.A.

- **Kim J.-H., von Gunten U., Mariñas B. J.**, (2004). Simultaneous predicion of *Cryptosporidium parvum Oocyst* inactivation and bromate formation during ozonation of synthetic waters, *Environmental Science and Technology*, Vol. **38**, pp. 2232-2241.
- **LeChevallier M. W.** and **Au K. K.,** (2004). Water Treatment and Pathogen Control: Process Efficiency in Achieving Safe Drinking Water, World Health Organization, Geneva, Switzerland.
- **Mariñas B. J., Liang S., Aieta E. M.,** (1993). Modeling Hydrodynamics and Ozone Residual Distribution in a Pilot-Scale Ozone Bubble-Diffuser Contactor, *Journal of the American Water Works Association*, Vol. **85**, pp. 90-99.
- **Roustan M., Stambolieva Z., Duguet J. P., Wable O., Mallevialle J.,** (1991). Influence of Hydrodynamics on *Giardia* Cyst Inactivation by Ozone, Study by Kinetics and by "CT" Approach, *Ozone: Science and Engineering*, Vol. **13**, pp. 451-462.
- **Tang G., Adu -Sarkodie K., Kim D., Kim J.-H, Teefy S., Shukairy H.**, **Mariñas B. J.**, (2005). Modeling *Cryptosporidium parvum Oocyst* inactivation and bromate formation in a full-scale ozone contactor, *Environmental Science and Technol*ogy, Vol. **39**, pp. 9343-9350.
- **Zhang J.,** (2006). An integrated design approach for improving drinking water ozone disinfection treatment based on computational fluid dynamics, Ph.D. thesis, University of Waterloo, Canada.
- **Zwietering T. N.,** (1959). The Degree of Mixing in Continuous Flow Systems, *Chemical Engineering Science*, Vol. **11**, pp. 1-15.

Appendix B

Definitions and Properties of RTD

B.1. Definition of the E-function

An exhaustive explanation on tracer studies can be found in [Dumeau de Traversay, 2000] or elsewhere in specialised literature. We shall therefore only say few words on RTD, recalling basic definitions or properties.
The RTD function E is the function defined such as $E(t_0)dt$ is equal to the fraction of fluid exiting the reactor that has spent a time between (t_0) and $(t_0 + dt)$ in the reactor. As it can be graphically seen on figure **1**, this fraction corresponds to the (blue) band under the E curve. Clearly, the normalisation condition implies $\int_0^\infty E(t)dt = 1$. The quantity $\int_{t_1}^\infty E(t)dt$ represents the fraction of fluid having spent a time larger than t_1 in the reactor.

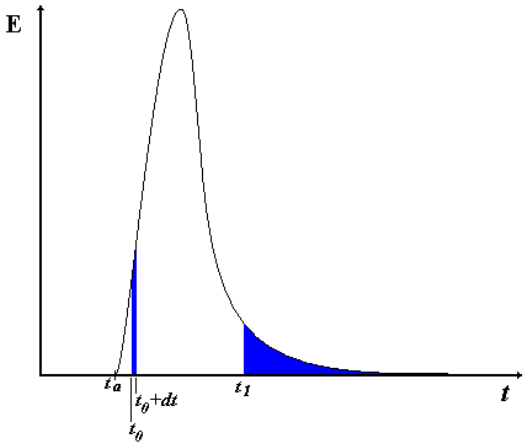

Figure 1 Example of a RTD *E*- curve

B.2. Tracer Tests and Complementary Definitions

The experimental RTD curves are obtained through tracer studies. Roughly speaking, the method consists in injecting the tracer so as to get a Dirac peak or a Heavyside step profile for the tracer inlet concentration, following then the tracer outlet concentration. Injection represents thus a key parameter for this technique as it has to be performed in a manner that do not perturbs nor alters the flow conditions. Various measurements or calculations (see table **1**) can then be done to characterise the hydrodynamic behaviour of a tank

Table 1 **Main parameters associated to RTD**

Formula	Name – description
t_x	Time by which x% of the tracer's mass has transferred
t_a	Time by which the tracer appears
t_{90}/t_{10}	Dispersion indice of Morill
$t_m = \int_0^\infty tE(t)dt$	Mean residence time
$\sigma^2_{hydr} = \int_0^\infty (t - t_m)^2 E(t)dt$	Hydraulic variance (related to dispersion)
$\alpha = \frac{t_{10}}{\tau}$	Hydraulic efficiency
$\tau = \frac{V}{Q_l}$	Hydraulic retention time (equal to mean residence time for a constant density system)

B.3. Bibliography

- **Dumeau de Traversay C.**, (2000). De la mécanique des fluides numérique à l'approche systémique: application aux réacteurs d'oxydation en potabilisation, Ph.D. thesis ENSC-R.

Appendix C

Ozonation Modelling Implemented in Stimela

C.1. Chemical Model for Ozone Decomposition

Ozone decay modelling has been first proposed in [Rietveld, 2005], coded into Stimela environment and slightly modified. We reproduce the model as presented in [Rietveld *et al.*, 2009] in equations **1**, **2** and **3**. The meaning of the symbols used in these equations is given in table **1**.

$$\frac{\partial [O_3]_l}{\partial t} = -\frac{Q_l}{A}\frac{\partial [O_3]_l}{\partial x} + k_L \frac{Q_g}{Q_l}\frac{u_l}{u_g}\frac{6}{d_b}(\kappa K_D [O_3]_g - [O_3]_l) - k_{UV}(UV - UV_{end})\zeta - w[O_3]_l \quad \textbf{(1)}$$

$$\frac{\partial UV}{\partial t} = -\frac{Q_l}{\varepsilon_g A}\frac{\partial UV}{\partial x} - k_{UV}(UV - UV_{end}) \quad \textbf{(2)}$$

$$\frac{\partial [O_3]_g}{\partial t} = -\frac{Q_g}{\varepsilon_g A}\frac{\partial [O_3]_g}{\partial x} - k_L \frac{6}{d_b}(\kappa K_D [O_3]_g - [O_3]_l) \quad \textbf{(3)}$$

The first term for each partial time-derivative expresses the spatial dispersion. For symmetry reason, only one space dimension is considered (x). For both aqueous and gaseous ozone concentrations (equations **1** and **3**, respectively), the second term represents ozone mass transfer, from gas to liquid (see chapter **2, 2.3.2.2.**).

Table 1 Physicochemical symbols used by [Rietveld *et al.*, 2009]

Symbol	Name	Unit	Type	To be calibrated
$[O_3]_l$	Aqueous ozone concentration	mg O_3.L^{-1}	Dynamical	N
$[O_3]_g$	Gazeous ozone concentration	g O_3.Nm^{-3}		
UV	UV absorbance (254 nm)	m^{-1}		
t	Time	s		
UV_{end}	final UV absorbance (254 nm)	m^{-1}	Steady-state	N
x	Space coordinate	m		
k_L	gas transfer coefficient	$m.s^{-1}$	Physicochemical constants	Y
K_D	gas distribution coefficient	(-)		
ζ	yield for ozone consumed per UV decrease	mg O_3.$m.L^{-1}$		
w	first-order ozone decomposition rate	s^{-1}		
k_{UV}	UV (254 nm) decay rate	s^{-1}		
d_b	bubble diameter	m		Y?
A	Reactor surface area	m^2	Process conditions	N
u_l	water velocity	$m.s^{-1}$		
u_g	gas velocity	$m.s^{-1}$		
ε_g	gas hold-up	(-)		
Q_l	Water flow	$m^3.s^{-1}$		
Q_g	Gas flow	$Nm^3.h^{-1}$		
κ	correction factor (T,p)	(-)		

In a classical manner, ozone decay is decomposed in two phases [Hoigné and Bader, 1994]: "instantaneous" and long-term ozone demands. As suggested by precedent works ([Muñoz Ramirez, 1997], [Buffle, 2005]), instantaneous ozone demand can be linked to UV absorbance at 254 nm (third

term in equation **1**; second term in equation **2**). The fourth term in equation **1** represents ozone long-term demand; here a pseudo-first order kinetics has been selected (more details on empirical ozone demand modelling can be found in chapter **1, 1.2.3.**). The model parameters that have to be calibrated are also distinguished in table **1**. This is generally done by comparison to results obtained with batch-scale experiments [van der Helm, 2007].

C.2. Chemical Model for Bromate Formation and Inactivation Kinetics

A regression model, calibrated to specific process conditions (water matrix and flow conditions of the unit), has been proposed and used within the Stimela environment. It has been developed by [van der Helm, 2007], basing on the observation that bromate formation may consist of an initial fast increase followed by a slower increase, linear to the CT value or the ozone treatment dose. This two-step empirical modelling was found to better simulate bromate formation than a classical relationship as those presented in chapter **1**, **1.2.4.** [van der Helm, 2007].

$$[BrO_3^-]_{l,0} = [BrO_3^-]_{l,in} + k_{BrO_3^-,fast}.TD \quad \textbf{(4)}$$

$$\frac{\partial [BrO_3^-]_l}{\partial t} = -\frac{Q_l}{A}\frac{\partial [BrO_3^-]_l}{\partial x} + k_{BrO_3^-,slow}[O_3]_l \quad \textbf{(5)}$$

The first step in bromate formation (related to fast kinetics) is modelled by equation **4**. The bromate concentration hence evolves from $[BrO_3^-]_{l,in}$ (inlet concentration) to $[BrO_3^-]_{l,0}$ (initial concentration for the second phase) proportionally to the treatment dose *TD*. The slower kinetics is represented by equation **5**. Both constants $k_{BrO_3^-,fast}$ and $k_{BrO_3^-,slow}$ shall be calibrated.

In order to describe bacterial inactivation, classical models are used. For example, [van der Helm, 2007] selected the Hom model with $n_H = 1$ and $o_H = 2$ (see Appendix **A**).

C.3. Hydraulics Modelling

Besides, hydraulic modelling is achieved by the definition of hydraulic schemes containing CSTRs (Continuous Stirred-Tank Reactors), possibly including recycles [Dudley *et al.*, 2008]. However, it was not possible to include recycles when modelling online ozonation processes (ozonation process cannot anymore be simulated online, for a brief description of the possibilities that were offered to the user, see [Mandel, 2007]).

C.4. Bibliography

- **Buffle M.-O.**, (2005). Mechanistic Investigation of the Initial Phase of Ozone Decomposition in Drinking Water and Wastewater, Ph. D. thesis, Swiss Federal Institute of Technology Zürich, Switzerland.
- **Dudley J., Dillon G, Rietveld L.,** (2008). Water treatment simulators, *Journal of Water Supply: Research and Technology – AQUA*, Vol. **57**, pp. 13-21.
- **Hoigné J.** and **Bader H.,** (1994). Characterization of water quality criteria for ozonation processes. Part II: Lifetime of added ozone, *Ozone: Science and Engineering,* Vol. **16**, pp. 121-134.
- **Mandel P.**, (2007). Modelling of Micropollutant Removal by Ozonation and Chlorination in potable Water Treatment – Bibliographic Report, *Techneau Deliverable D2.4.2.6*.
- **Muñoz Ramirez G.**, (1997). Approche cinétique de la demande immédiate en ozone, Ph.D. thesis, ENSC-R, France.
- **Rietveld L. C., van der Helm A. W. C., van Schagen K. M., van der Aa L. T. J.,** (2009). Good modelling practice in drinking water treatment, applied to Weesperkarspel plant of Waternet, *Environmental Modelling & Software* , *in press*, doi:10.1016/j.envsoft.2009.05.015.
- **Rietveld L.C.,** (2005). Improving operation of drinking water treatment through modelling, Ph.D. thesis, , Delft University of Technology, The Netherlands.
- **van der Helm, A. W. C.,** (2007). Integrated modeling of ozonation for optimization of drinking water treatment, Ph.D. thesis, Delft University of Technology, The Netherlands.

Appendix D

Chemical Models Used in this Study

D.1. Ozone Decomposition

The mechanism used for ozone self-decomposition derives from the one proposed by [Mizuno *et al.*, 2007c], which can be seen as the latest of the SBH-based models. The mechanism used in this study is presented in table **1**.

Table 1 Self-decomposition mechanism used in this study

Type	Reaction	Kinetic constant value (T=293 K)		Reference
Initiation	$O_3 + HO^- \rightarrow HO_2^- + O_2$	4.10^1 $M^{-1}.s^{-1}$		[Tomiyasu *et al.*, 1985]
	$HO_2^- + O_3 \rightarrow {}^\bullet OH + {}^\bullet O_2^- + O_2$	$2.8.10^6$ $M^{-1}.s^{-1}$		[Staehelin and Hoigné, 1982]
Propagation	$O_3 + {}^\bullet O_2^- \rightarrow {}^\bullet O_3^- + O_2$	$1.6.10^9$ $M^{-1}.s^{-1}$		[Taube and Bray, 1940]
	${}^\bullet HO_3 \rightarrow {}^\bullet OH + O_2$	$1.1.10^5$ s^{-1}		[Bühler *et al.*, 1984]
	${}^\bullet OH + O_3 \rightarrow {}^\bullet HO_2 + O_2$	9.10^5 $M^{-1}.s^{-1}$		[Mizuno *et al.*, 2007c]
	${}^\bullet OH + H_2O_2 \rightarrow {}^\bullet HO_2 + H_2O$	$2.7.10^7$ $M^{-1}.s^{-1}$		[Chelkowska *et al.*, 1992]
	${}^\bullet OH + HO_2^- \rightarrow {}^\bullet O_2^- + H_2O$	$7.5.10^9$ $M^{-1}.s^{-1}$		[Chelkowska *et al.*, 1992]
Termination	$2\,{}^\bullet HO \rightarrow H_2O_2$	5.10^9 $M^{-1}.s^{-1}$		[Farhataziz and Ross, 1977]
	${}^\bullet HO + {}^\bullet O_2^- \rightarrow HO^- + O_2$	10^{10} $M^{-1}.s^{-1}$		[Farhataziz and Ross, 1977]
	${}^\bullet HO + {}^\bullet HO_3 \rightarrow H_2O_2 + O_2$	5.10^9 $M^{-1}.s^{-1}$		[Staehelin *et al.*, 1984]
	${}^\bullet HO_3 + {}^\bullet O_2^- \rightarrow HO^- + 2O_2$	10^{10} $M^{-1}.s^{-1}$		[Staehelin *et al.*, 1984]
	$2\,{}^\bullet HO_3 \rightarrow H_2O_2 + 2O_2$	5.10^9 $M^{-1}.s^{-1}$		[Staehelin *et al.*, 1984]
Acid-base equilibria		**Direct**	**Indirect**	
pK_A = 8.2	${}^\bullet O_3^- + H^+ \leftrightarrow {}^\bullet HO_3$	$5.2.10^{10}$ $M^{-1}.s^{-1}$	$3.3.10^2$ s^{-1}	[Bühler *et al.*, 1984]
pK_A = 4.8	${}^\bullet O_2^- + H^+ \leftrightarrow {}^\bullet HO_2$	2.10^{10} $M^{-1}.s^{-1}$	$3.2.10^5$ s^{-1}	[Buxton *et al.*, 1988]
pK_A = 11.6	$HO_2^- + H^+ \leftrightarrow H_2O_2$	10^{10} $M^{-1}.s^{-1}$	$4.2.10^{-2}$ s^{-1}	[Buxton *et al.*, 1988]

D.2. Influence of Inorganic Carbon

Most reactions used to model the role played by inorganic carbon, that is carbonate species, were taken from the works of [Westerhoff *et al.*, 1997]. Additional reactions were however added; the complete mechanism is presented in table **2**. The kinetics of the deprotonation reactions were calculated basing on the pK_A values and on the kinetics of the protonation.

Table 2 Mechanism for the influence of inorganic carbon

Type	Reaction	Kinetic constant value (293 K)	Reference
Initiation	$CO_3^{2-} + {}^\bullet OH \rightarrow {}^\bullet CO_3^- + HO^-$	$3.9.10^8$ $M^{-1}.s^{-1}$	[Buxton *et al.*, 1988]
	$HCO_3^- + {}^\bullet OH \rightarrow {}^\bullet CO_3^- + H_2O$	5.10^7 $M^{-1}.s^{-1}$	[Farhataziz and Ross, 1977]
Propagation	${}^\bullet CO_3^- + HO_2^- \rightarrow CO_3^{2-} + {}^\bullet HO_2$	$5.6.10^7$ $M^{-1}.s^{-1}$	[Westerhoff *et al.*, 1997]
	${}^\bullet CO_3^- + H_2O_2 \rightarrow HCO_3^- + {}^\bullet HO_2$	8.10^5 $M^{-1}.s^{-1}$	[Farhataziz and Ross, 1977]
Termination	${}^\bullet CO_3^- + {}^\bullet O_2^- \rightarrow CO_3^{2-} + O_2$	4.10^8 $M^{-1}.s^{-1}$	[Westerhoff *et al.*, 1997]
	${}^\bullet CO_3^- + {}^\bullet O_3^- \rightarrow CO_3^{2-} + O_3$	6.10^7 $M^{-1}.s^{-1}$	[Chelkowska *et al.*, 1990]
	${}^\bullet CO_3^- + {}^\bullet HO \rightarrow CO_2 + HO_2^-$	3.10^9 $M^{-1}.s^{-1}$	[Westerhoff *et al.*, 1997]
Acid-base equilibria			
pK_A = 10.3	$CO_3^{2-} + H^+ \rightarrow HCO_3^-$	5.10^{10} $M^{-1}.s^{-1}$	[Westerhoff *et al.*, 1997]
	$HCO_3^- \rightarrow CO_3^{2-} + H^+$	$2.5.10^0$ s^{-1}	Calculated
pK_A = 9.6	${}^\bullet CO_3^- + H^+ \rightarrow {}^\bullet HCO_3$	5.10^{10} $M^{-1}.s^{-1}$	[Westerhoff *et al.*, 1997]
	${}^\bullet HCO_3 \rightarrow {}^\bullet CO_3^- + H^+$	$1.26.10^1$ s^{-1}	Calculated
pK_A = 6.4	$HCO_3^- + H^+ \rightarrow H_2CO_3$ [1]	5.10^{10} $M^{-1}.s^{-1}$	[Westerhoff *et al.*, 1997]
	$H_2CO_3 \rightarrow HCO_3^- + H^+$	2.10^4 s^{-1}	Calculated

[1] The H_2CO_3 formulation is here used for convenience.

D.3. Formation of Bromate

The reactions taken into account to model bromate formation are gathered in tables **3** and **4**, for molecular and radical reactions respectively. The kinetics of the last oxidation step leading to bromate ($BrO_2^- + O_3 \rightarrow BrO_3^- + O_2$) were fitted for each water sample.

Table 3 Molecular reactions within bromate formation pathway

Reaction	Kinetic constant value (293K)	Reference
$Br^- + O_3 \rightarrow BrO^- + O_2$	$1.6.10^2$ $M^{-1}.s^{-1}$	[Haag and Hoigné, 1983]
$BrO^- + O_3 \rightarrow Br^- + 2O_2$	$3.3.10^2$ $M^{-1}.s^{-1}$	[Haag and Hoigné, 1983]
$BrO^- + O_3 \rightarrow BrO_2^- + O_2$	10^2 $M^{-1}.s^{-1}$	[Haag and Hoigné, 1983]
$BrO_2^- + O_3 \rightarrow BrO_3^- + O_2$	$> 10^5$ $M^{-1}.s^{-1}$	[von Gunten and Hoigné, 1994]
	Fitted value	**This study**
$BrO^- + H^+ \rightarrow BrOH$	5.10^{10} $M^{-1}.s^{-1}$	[Westerhoff, 1995]
$BrOH \rightarrow BrO^- + H^+$	$7.9.10^1$ s^{-1}	Calculated with $pK_A = 8.8$ and protonation reaction kinetics

Table 4 Radical reactions within bromate formation pathway

Reaction	Kinetic constant value (293K)	Reference
$BrO^- + {}^\bullet OH \rightarrow {}^\bullet OBr + HO^-$	$4.5.10^9$ $M^{-1}.s^{-1}$	[Buxton and Dainton, 1968]
$BrOH + {}^\bullet OH \rightarrow {}^\bullet OBr + H_2O$	2.10^9 $M^{-1}.s^{-1}$	[Buxton and Dainton, 1968]
$BrO_2^- + {}^\bullet OH \rightarrow {}^\bullet O_2Br + HO^-$	2.10^9 $M^{-1}.s^{-1}$	[Buxton and Dainton, 1968]
$2\,{}^\bullet OBr + H_2O \rightarrow BrO_2^- + BrO^- + 2H^+$	5.10^9 $M^{-1}.s^{-1}$	[Buxton and Dainton, 1968]
${}^\bullet O_2Br + {}^\bullet OH \rightarrow BrO_3^- + H^+$	2.10^9 $M^{-1}.s^{-1}$	[Buxton *et al.*, 1988]
$Br^- + {}^\bullet OH \rightarrow {}^\bullet Br + HO^-$	$1.1.10^9$ $M^{-1}.s^{-1}$	[von Gunten and Hoigné, 1996]
$Br^- + {}^\bullet OH \rightarrow {}^\bullet HOBr^-$	10^{10} $M^{-1}.s^{-1}$	[Zehavi and Rabani, 1972]
${}^\bullet HOBr^- \rightarrow {}^\bullet Br + HO^-$	$4.2.10^6$ s^{-1}	[Zehavi and Rabani, 1972]
${}^\bullet Br + O_3 \rightarrow {}^\bullet OBr + O_2$	$1.5.10^8$ $M^{-1}.s^{-1}$	[von Gunten and Hoigné, 1994]
${}^\bullet Br + BrO^- \rightarrow {}^\bullet OBr + Br^-$	$4.1.10^9$ $M^{-1}.s^{-1}$	[Kläning and Wolff, 1985]
${}^\bullet CO_3^- + BrO^- \rightarrow CO_3^{2-} + {}^\bullet OBr$	$4.3.10^7$ $M^{-1}.s^{-1}$	[Kläning and Wolff, 1985]
${}^\bullet CO_3^- + BrO_2^- \rightarrow CO_3^{2-} + {}^\bullet O_2Br$	$1.1.10^8$ $M^{-1}.s^{-1}$	[Buxton and Dainton, 1968]

D.4. Bibliography

- **Bühler R.E., Staehelin J., Hoigné J.**, (1984). Ozone Decomposition in Water Studied by Pulse Radiolysis. 1. HO_2 / O_2^- and HO_3 / O_3^- as Intermediates, *Journal of Physical Chemistry*, Vol. **88**, pp. 2560-2564.
- **Buxton G. V.** and **Dainton F. S.**, (1968). The Radiolysis of Aqueous Solutions of Oxybromine Compounds; the Spectra and Reactions of BrO and BrO_2, *Proceedings of the Royal Society A.*,304 , pp. 427-439.
- **Buxton G. V., Greenstock C. L., Helman W.P., Ross A. B.,** (1988). Critical Review of Reactions of Hydrated Electrons, *Journal of Physical Chemistry Ref. Data*, Vol. **17**, pp. 513-886.

- **Chelkowska K., Grasso D., Fábián I., Gordon G.,** (1990). Mechanistic Comparison of Residual Ozone Decomposition, *Proceedings of the IOA Conference*, Shreveport, pp. 427-437.
- **Chelkowska K., Grasso D., Fabian I., Gordon G.,** (1992). Numerical Simulations of Aqueous Ozone Decomposition, *Ozone: Science and Technology*, Vol. **14**, pp. 33-49.
- **Farhataziz** and **Ross, A. B.,** (1977). Selective Specific Rates of Reactions of Transients from Water in Aqueous Solutions, National Bureau of Standards: Washington, DC, Natl. Stand. Ref. Data Ser. (U.S., Natl. Bur. Stand.) No. **59**.
- **Haag W. R.** and **Hoigné J.**, (1983). Ozonation of bromide-containing waters: kinetics of formation of hypobromous acid and bromate, *Environmental Science and Technology*, Vol. **17**, pp. 261-267.
- **Kläning U.K.** and **Wolff T.**, (1985). Laser Flash Photolysis of HClO, ClO^-, HBrO, and BrO^- in Aqueous Solution, *Ber. Bunsenges. Physik. Chem.*, Vol. **89**, pp. 243–245.
- **Mizuno T., Tsuno H., Yamada H.,** (2007c). Development of Ozone Self-Decomposition Model for Engineering Design, *Ozone: Science and Engineering*, Vol. **29**, pp. 55-63.
- **Staehelin J.** and **Hoigné J.**, (1982). Decomposition of ozone in water: Rate of Initiation by Hydroxide Ions and Hydrogen Peroxide, *Environmental Science and Technology*, Vol. **16**, pp. 676-681.
- **Staehelin J., Bühler R.E., Hoigné J.**, (1984). Ozone Decomposition in Water Studied by Pulse Radiolysis. 2. OH and HO_4 as Chain Intermediates, *Journal of Physical Chemistry*, Vol. **88**, pp. 5999-6004.
- **Taube, H.** and **Bray, W. C.,** (1940). Chain Reactions in Aqueous Solutions Containing Ozone, Hydrogen Peroxide and Acid, *Journal of the American Chemistry Society*, Vol. **62**, pp. 3357-3373.
- **Tomiyasu H., Fukutomi H., Gordon G.,** (1985). Kinetics and Mechanism of Ozone Decomposition in Basic Aqueous Solution, *Inorganic Chemistry*, Vol. **24**, pp. 2962-2966.
- **von Gunten U.** and **Hoigné J.**, (1994). Bromate Formation during Ozonation of Bromide-Containing Waters: Interaction of Ozone and Hydroxyl Radical Reactions, *Environmental Science and Technology,* Vol. **28**, pp. 1234-1242.
- **von Gunten U.** and **Hoigné J.,** (1996). in *Disinfection By-Products in Water Treatment: The Chemistry of Their Formation and Control*, Edited by Minear R. A., Amy G. L., Chapter 8, CRC Press Inc.: Boca Raton, pp. 187-206.
- **Westerhoff P.,** (1995). Ozone Oxidation of Bromide and Natural Organic Matter, Ph.D. thesis, University of Boulder, USA.
- **Westerhoff P., Song R., Amy G.**, **Minear R.**, (1997). Application of Ozone Decomposition Models, *Ozone: Science and Engineering*, Vol. **19**, pp. 55-73.
- **Zehavi D.** and **Rabani J.**, (1972). The Oxidation of Aqueous Bromide Ions by Hydroxyl Radicals. A Pulse Radiolytic Investigation, *Journal of Physical Chemistry*, Vol. **76**, pp. 312-319.

Appendix E

Complementary Results on the Validity of the Model for NOM

E.1. Méry-sur-Oise Water

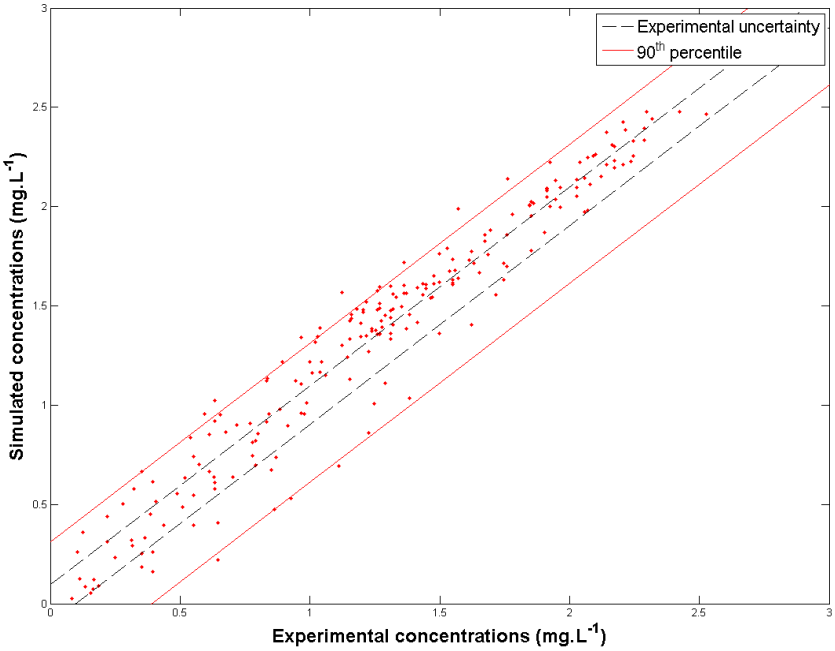

Figure 1 **Comparison of simulated and experimental ozone concentrations, Méry-sur-Oise water**

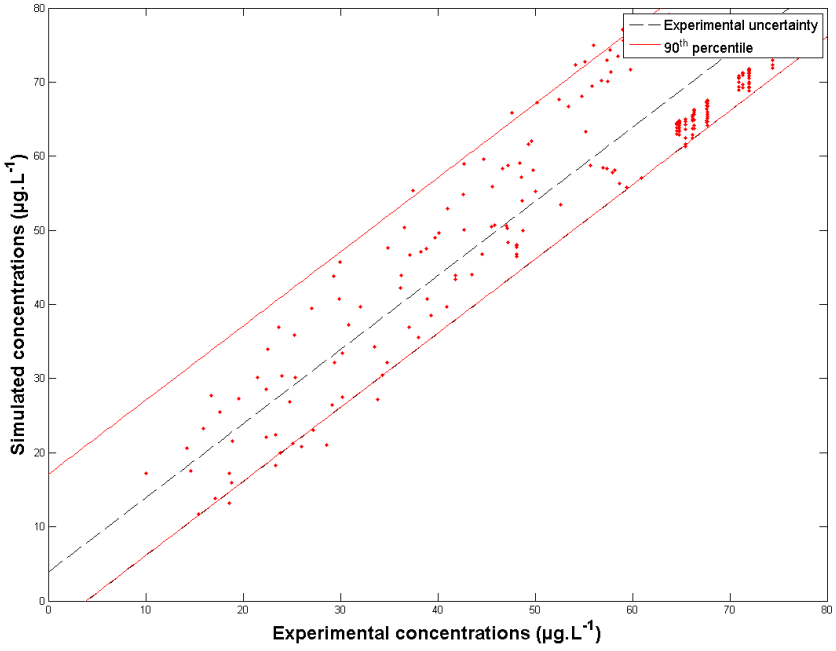

Figure 2 **Comparison of simulated and experimental *p*CBA concentrations, Méry-sur-Oise water**

Table 1 **Statistical results, Méry-sur-Oise water**

Compound	r_P	Pearson test	Offset ($mg.L^{-1}$ or $\mu g.L^{-1}$)	Test	Slope	Test	% points within error
Ozone	0.97	Passed	0.06±0.06	Passed	1.03±0.04	Passed	34.4
*p*CBA	0.93	Passed	8.28±3.06	Failed	0.90±0.06	Passed	64.4

E.2. Maisons-Laffitte water

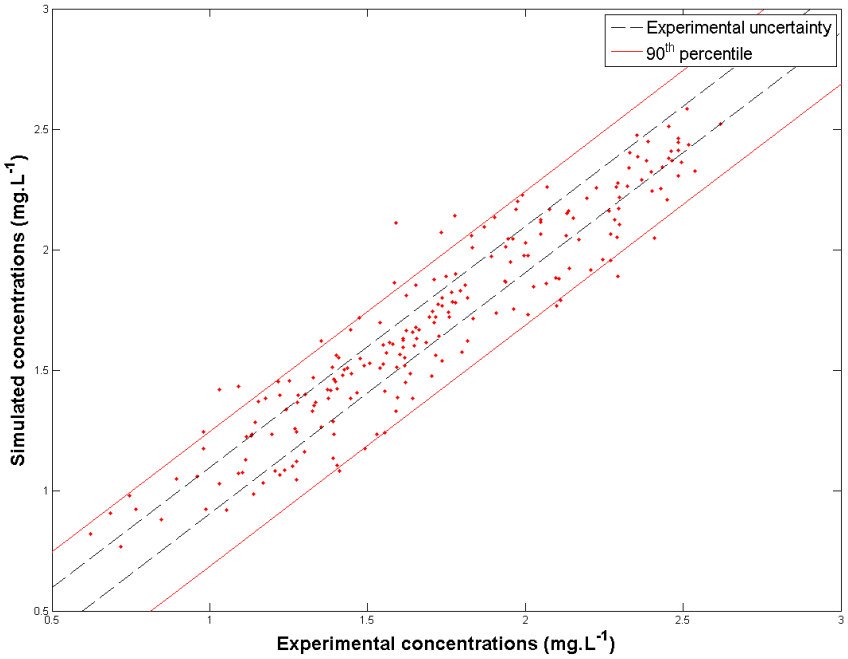

Figure 3 Comparison of simulated and experimental ozone concentrations, Maisons-Laffitte water

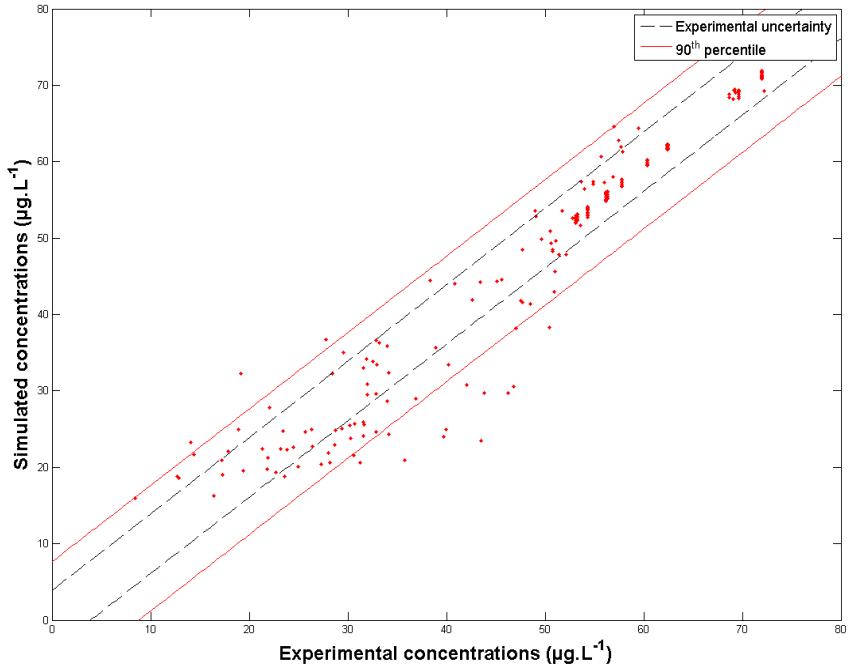

Figure 4 Comparison of simulated and experimental *p*CBA concentrations, Maisons-Laffitte water

Table 2 Statistical results, Maisons-Laffitte water

Compound	r_P	Pearson test	Offset (mg.L^{-1} or µg.L^{-1})	Test	Slope	Test	% points within error
Ozone	0.94	Passed	0.19±0.08	Failed	0.88±0.05	Passed	50.9
*p*CBA	0.96	Passed	-1.43±1.99	Passed	1.00±0.04	Passed	74.8

E.3. Vitré water

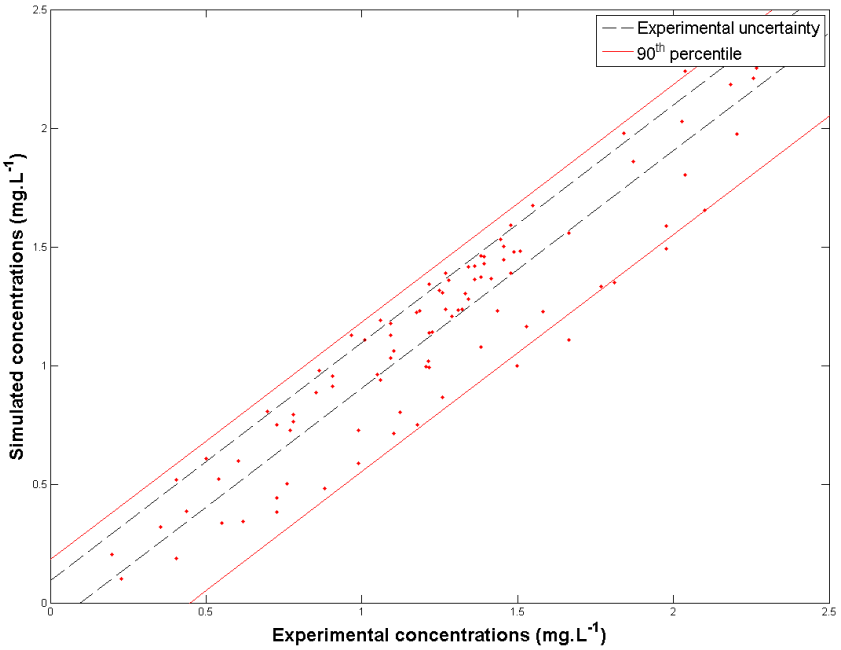

Figure 5 Comparison of simulated and experimental ozone concentrations, Vitré water

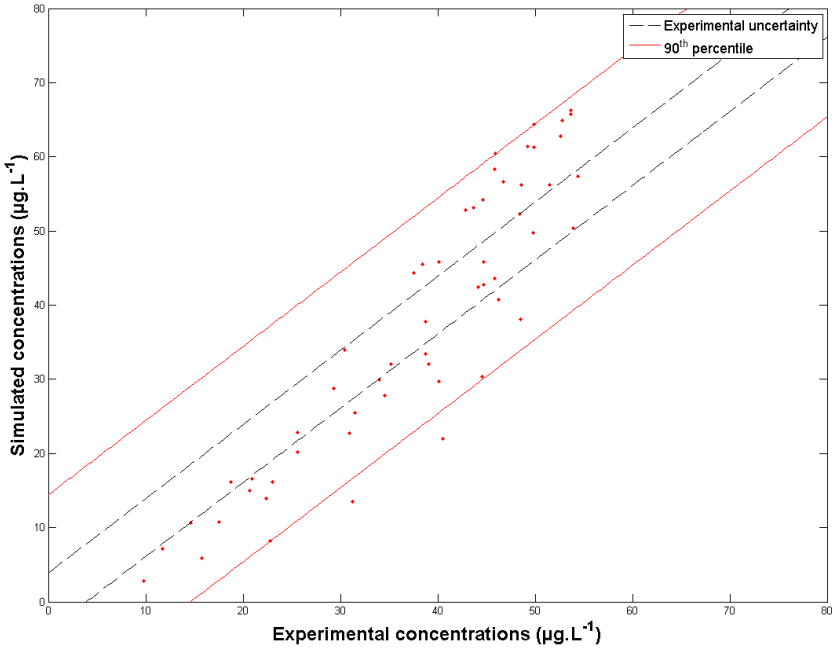

Figure 6 Comparison of simulated and experimental *p*CBA concentrations, Vitré water

Table 3 Statistical results, Vitré water

Compound	r_P	Pearson test	Offset (mg.L^{-1} or µg.L^{-1})	Test	Slope	Test	% points within error
Ozone	0.93	Passed	-0.06±0.12	Passed	0.98±0.09	Passed	50
*p*CBA	0.93	Passed	-13.72±7.15	Failed	1.36±0.18	Failed	25

E.4. Annet-sur-Marne water

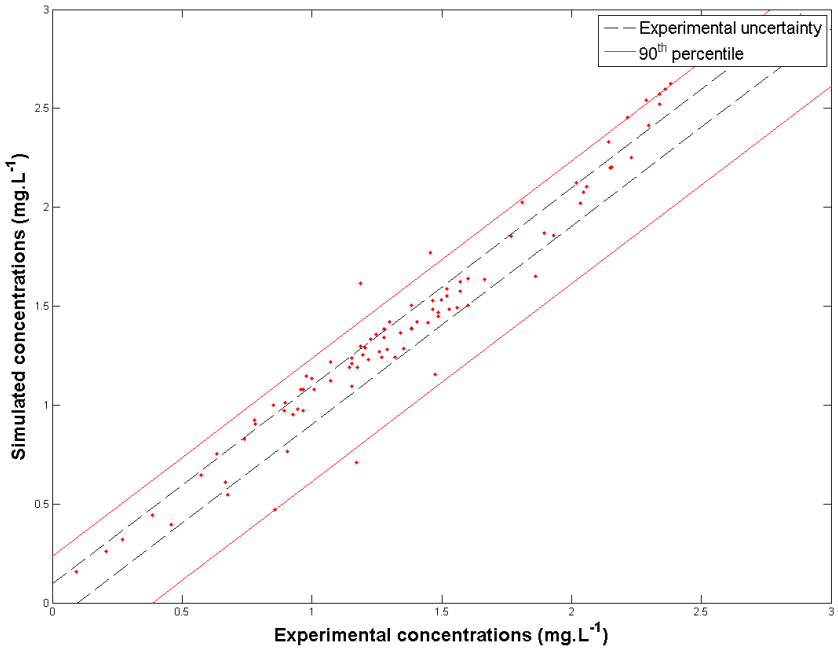

Figure 7 **Comparison of simulated and experimental ozone concentrations, Annet-sur-Marne water**

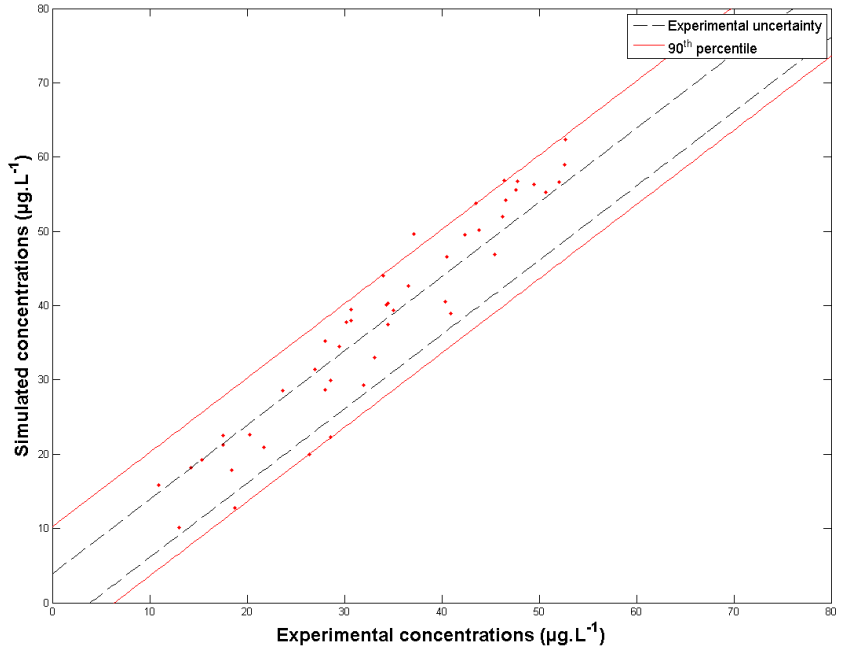

Figure 8 **Comparison of simulated and experimental *p*CBA concentrations, Annet-sur-Marne water**

Table 4 **Statistical results, Annet-sur-Marne water**

Compound	r_P	Pearson test	Offset (mg.L^{-1} or µg.L^{-1})	Test	Slope	Test	% points within error
Ozone	0.97	Passed	-0.01±0.08	Passed	1.04±0.06	Passed	60.4
*p*CBA	0.96	Passed	-0.56±5.25	Passed	1.14±0.15	Passed	29.2

E.5. Meulan water

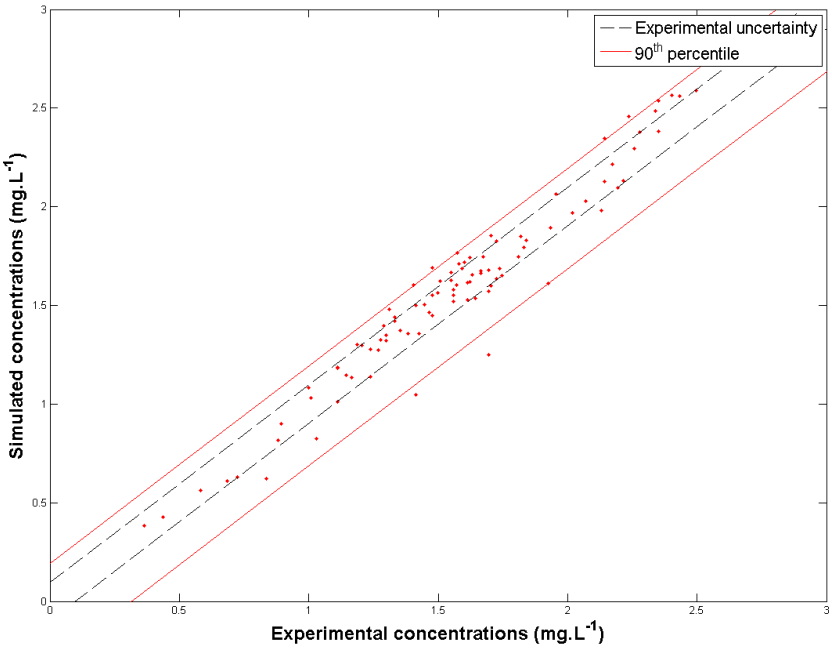

Figure 9 **Comparison of simulated and experimental ozone concentrations, Meulan water**

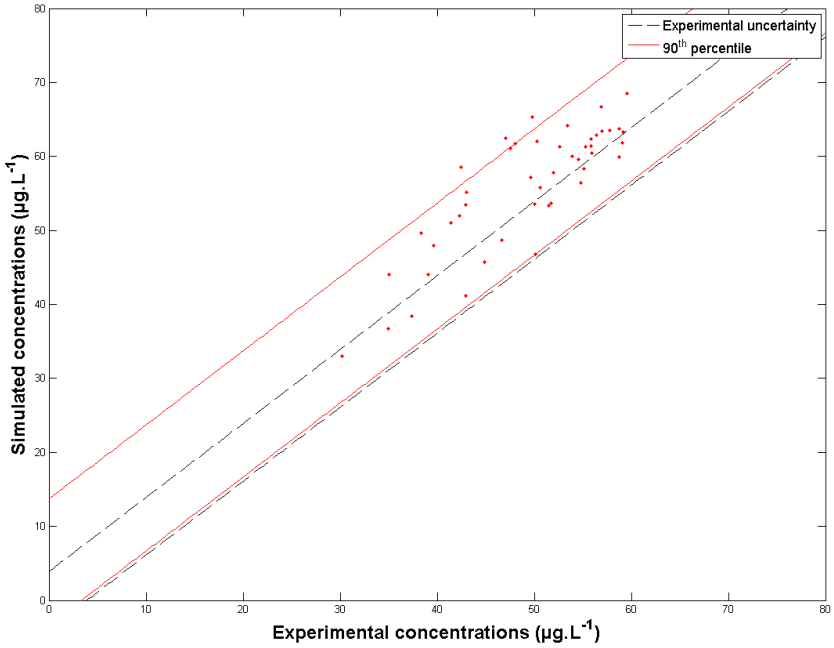

Figure 10 **Comparison of simulated and experimental *p*CBA concentrations, Meulan water**

Table 5 **Statistical results, Meulan water**

Compound	r_P	Pearson test	Offset (mg.L^{-1} or µg.L^{-1})	Test	Slope	Test	% points within error
Ozone	0.97	Passed	-0.04±0.09	Passed	1.04±0.05	Passed	62.1
*p*CBA	0.85	Passed	11.13±15.15	Passed	0.91±0.30	Passed	29.8

E.6. Beaufort water

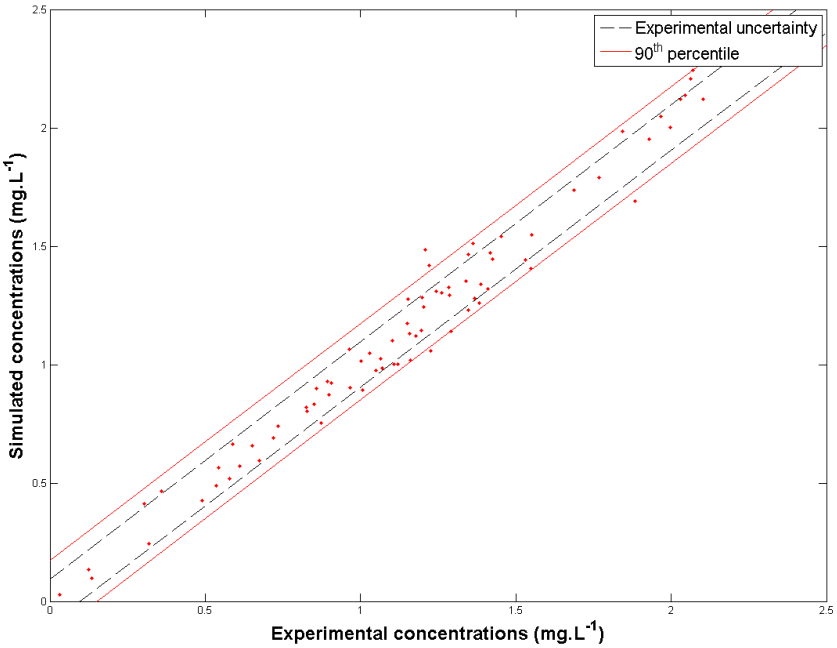

Figure 11 Comparison of simulated and experimental ozone concentrations, Beaufort water

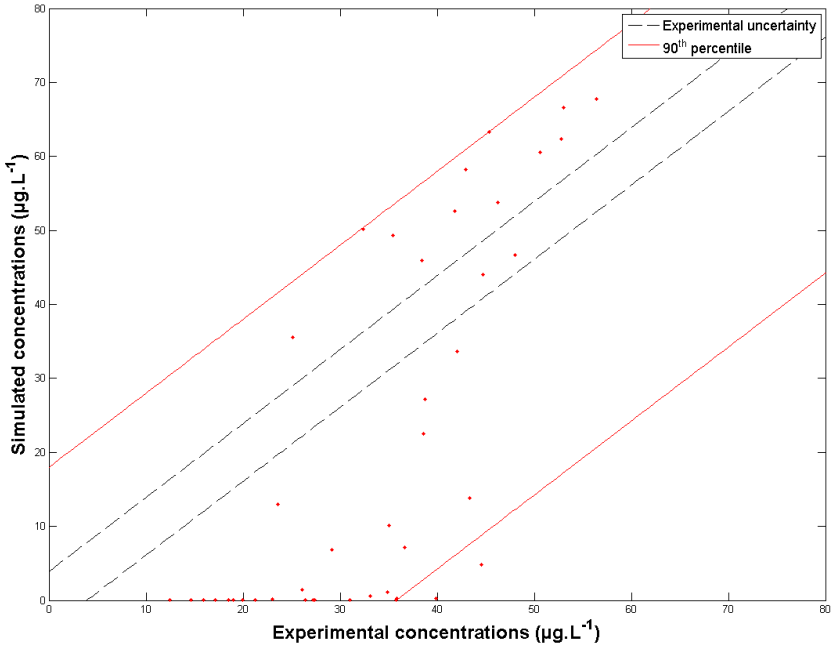

Figure 12 Comparison of simulated and experimental *p*CBA concentrations, Beaufort water

Table 6 Statistical results, Beaufort water

Compound	r_P	Pearson test	Offset (mg.L^{-1} or µg.L^{-1})	Test	Slope	Test	% points within error
Ozone	0.99	Passed	-0.05±0.05	Passed	1.05±0.04	Passed	68.8
*p*CBA	0.75	Passed	-32.10±20.74	Failed	1.59±0.59	Passed	4.7

E.7. Trondheim water

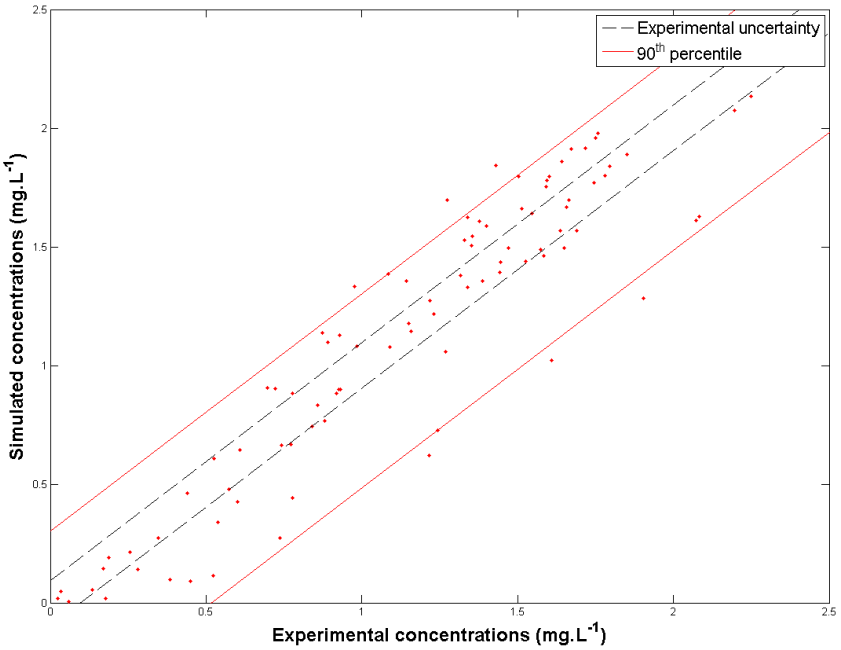

Figure 13 Comparison of simulated and experimental ozone concentrations, Trondheim water

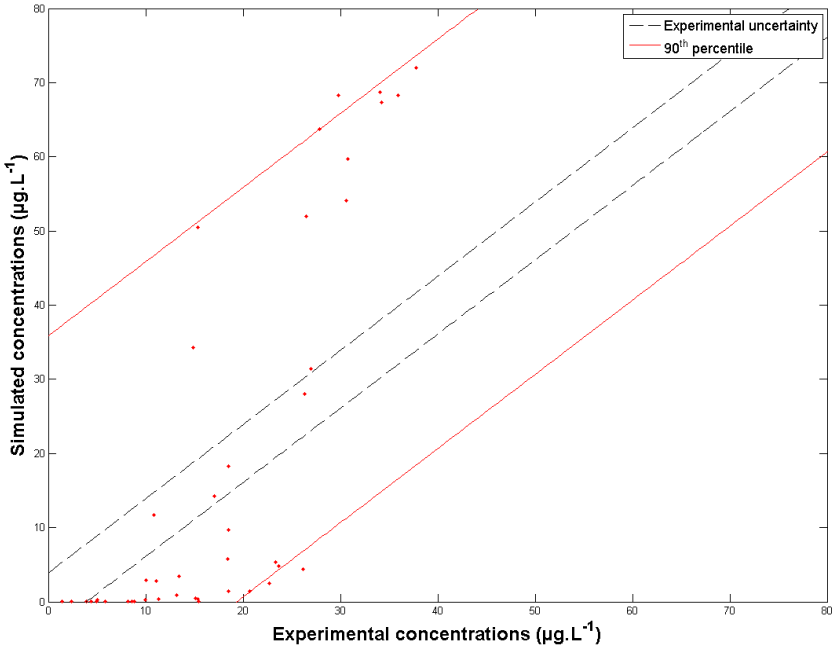

Figure 14 Comparison of simulated and experimental *p*CBA concentrations, Trondheim water

Table 7 Statistical results, Trondheim water

Compound	r_P	Pearson test	Offset (mg.L^{-1} or µg.L^{-1})	Test	Slope	Test	% points within error
Ozone	0.94	Passed	-0.04±0.10	Passed	1.02±0.08	Passed	43.5
*p*CBA	0.80	Passed	-17.47±11.47	Failed	2.05±0.58	Failed	17.8

E.8. Annet-sur-Marne 2 water

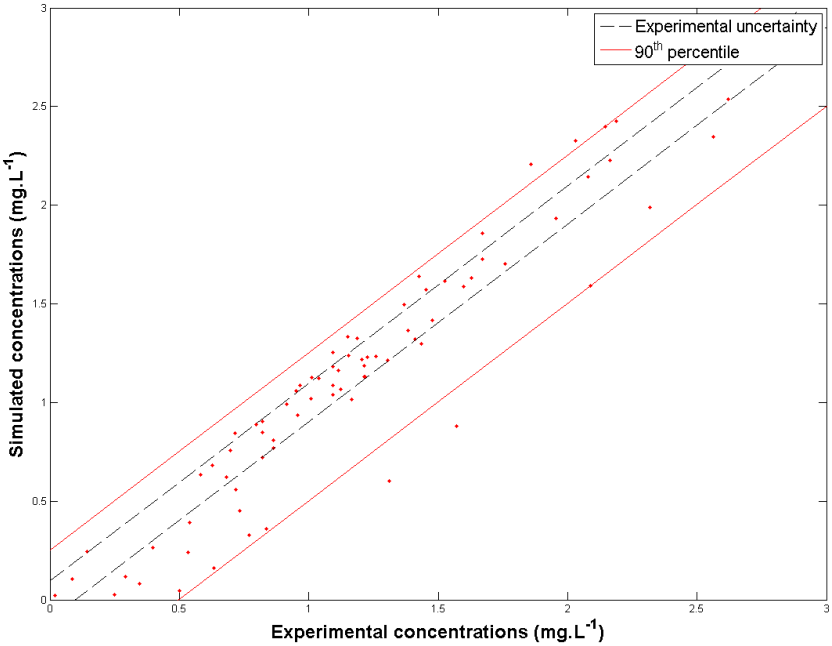

Figure 15 **Comparison of simulated and experimental ozone concentrations, Annet-sur-Marne 2 water**

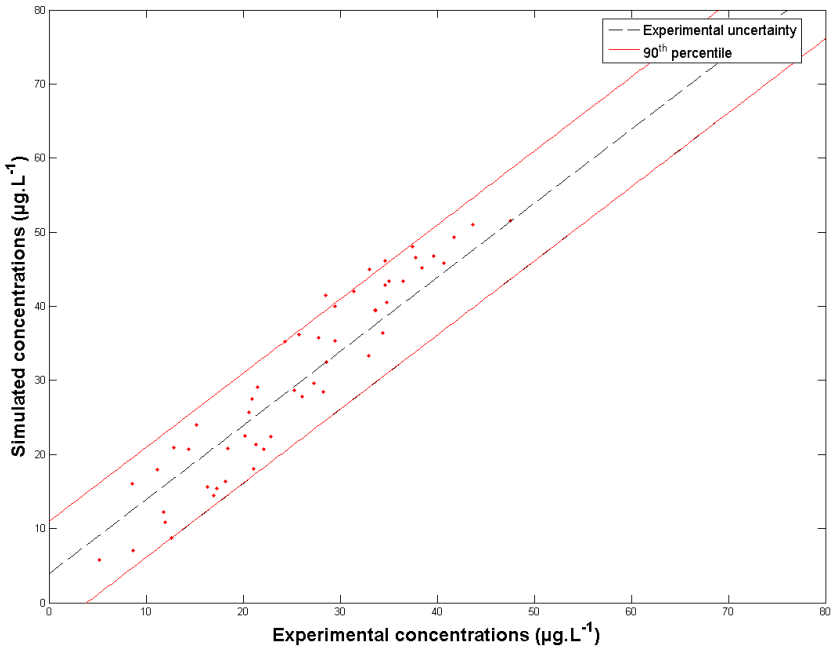

Figure 16 **Comparison of simulated and experimental *p*CBA concentrations, Annet-sur-Marne 2 water**

Table 8 **Statistical results, Annet-sur-Marne 2 water**

Compound	r_P	Pearson test	Offset (mg.L^{-1} or µg.L^{-1})	Test	Slope	Test	% points within error
Ozone	0.95	Passed	-0.10±0.11	Passed	1.05±0.08	Passed	51.9
*p*CBA	0.95	Passed	-0.49±4.97	Passed	1.20±0.18	Passed	42.6

E.9. Annet-sur-Marne 3 water

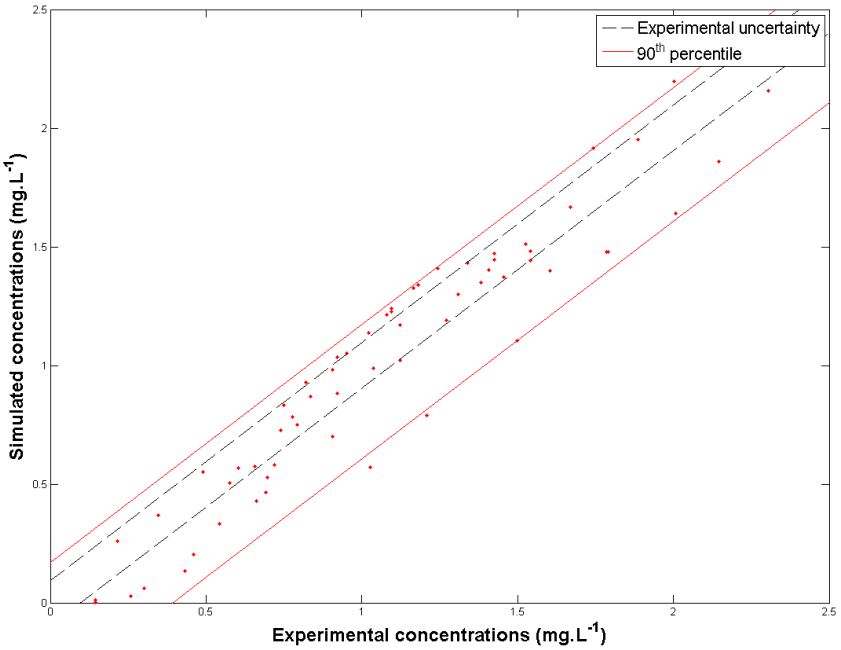

Figure 17 **Comparison of simulated and experimental ozone concentrations, Annet-sur-Marne 3 water**

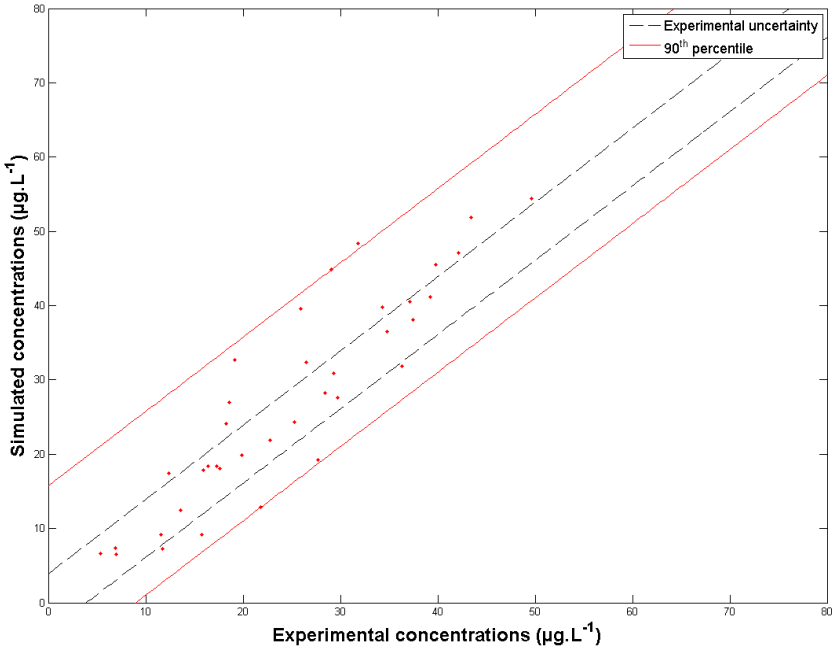

Figure 18 **Comparison of simulated and experimental *p*CBA concentrations, Annet-sur-Marne 3 water**

Table 9 **Statistical results, Annet-sur-Marne 3 water**

Compound	r_P	Pearson test	Offset ($mg.L^{-1}$ or $\mu g.L^{-1}$)	Test	Slope	Test	% points within error
Ozone	0.96	Passed	-0.06±0.10	Passed	1.00±0.08	Passed	42.9
*p*CBA	0.91	Passed	0.48±5.06	Passed	1.09±0.19	Passed	48.7

E.10. Meulan 3 water

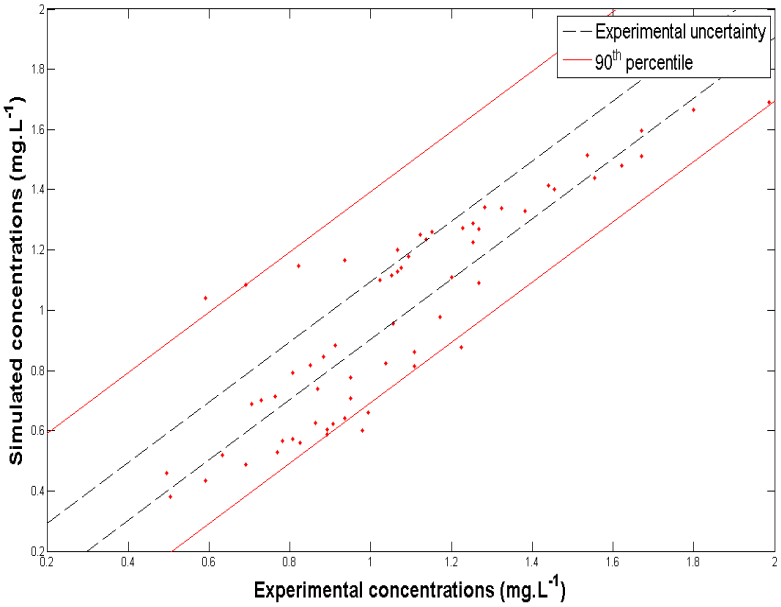

Figure 19 **Comparison of simulated and experimental ozone concentrations, Meulan 3 water**

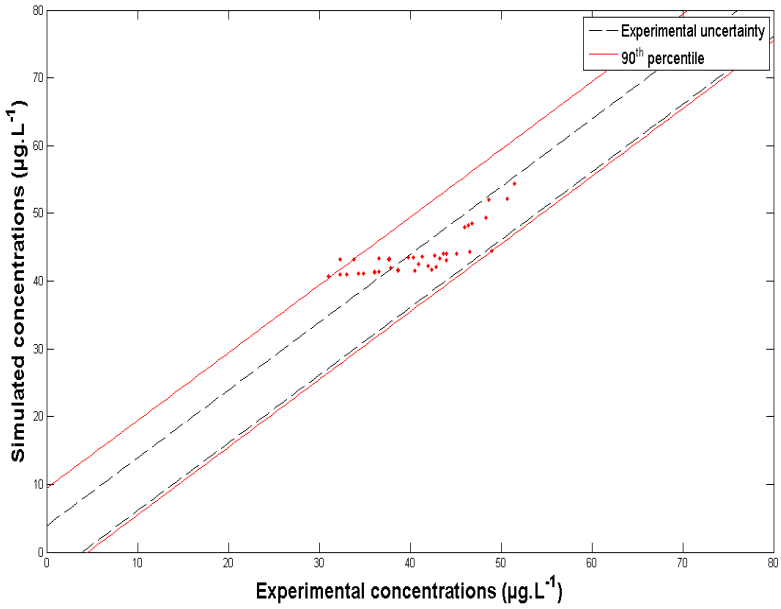

Figure 20 **Comparison of simulated and experimental *p*CBA concentrations, Meulan 3 water**

Table 10 **Statistical results, Meulan 3 water**

Compound	r_P	Pearson test	Offset (mg.L^{-1} or µg.L^{-1})	Test	Slope	Test	% points within error
Ozone	0.87	Passed	-0.02±0.17	Passed	0.95±0.15	Passed	39.7
*p*CBA	0.77	Passed	24.15±11.89	Failed	0.49±0.29	Failed	57.1

E.11. Vitré 3 water

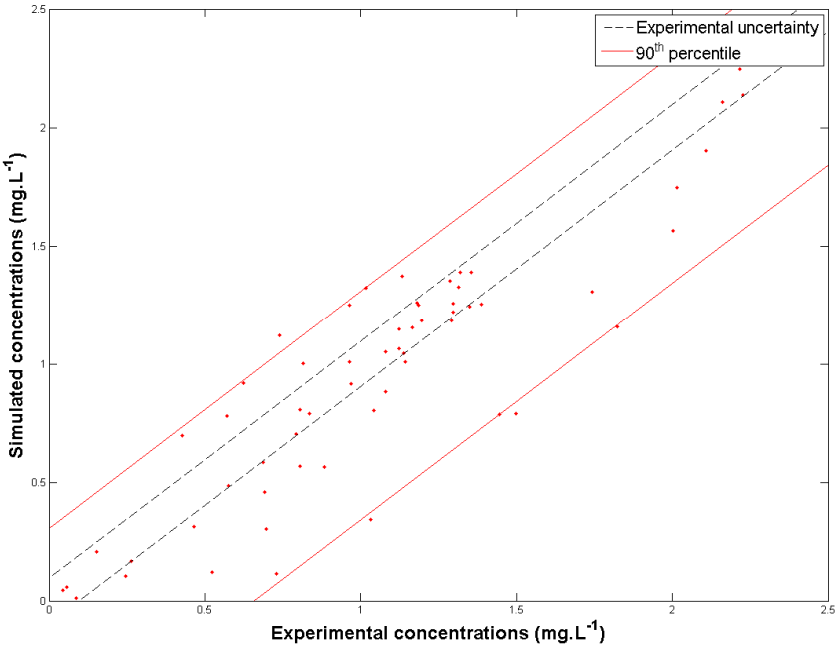

Figure 21 **Comparison of simulated and experimental ozone concentrations, Vitré 3 water**

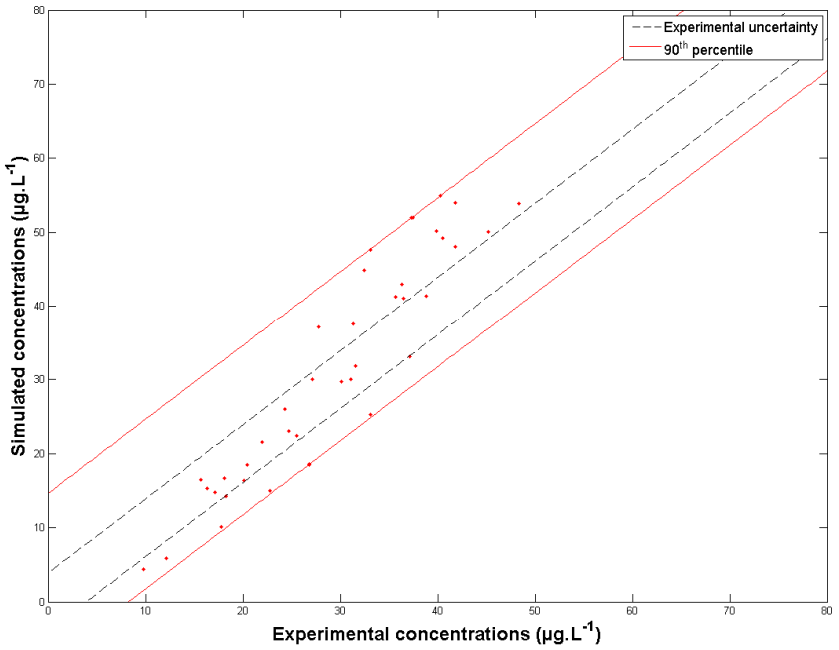

Figure 22 **Comparison of simulated and experimental *p*CBA concentrations, Vitré 3 water**

Table 11 **Statistical results – validation of the model, Vitré 3 water**

Compound	r_P	Pearson test	Offset (mg.L^{-1} or µg.L^{-1})	Test	Slope	Test	% points within error
Ozone	0.91	Passed	0.00±0.14	Passed	0.92±0.12	Passed	47.5
*p*CBA	0.93	Passed	-8.47±6.49	Passed	1.37±0.22	Failed	40.5

Appendix F

Complementary Results on the Validation of a Sequential Reduced Calibration Procedure

F.1. Méry-sur-Oise Water

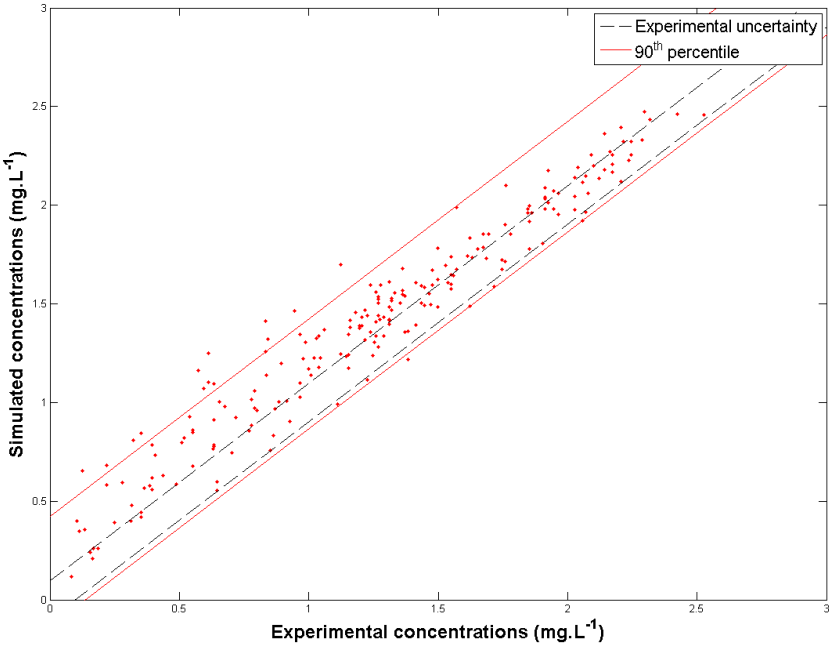

Figure 1 **Comparison of simulated and experimental ozone concentrations, Méry-sur-Oise water**

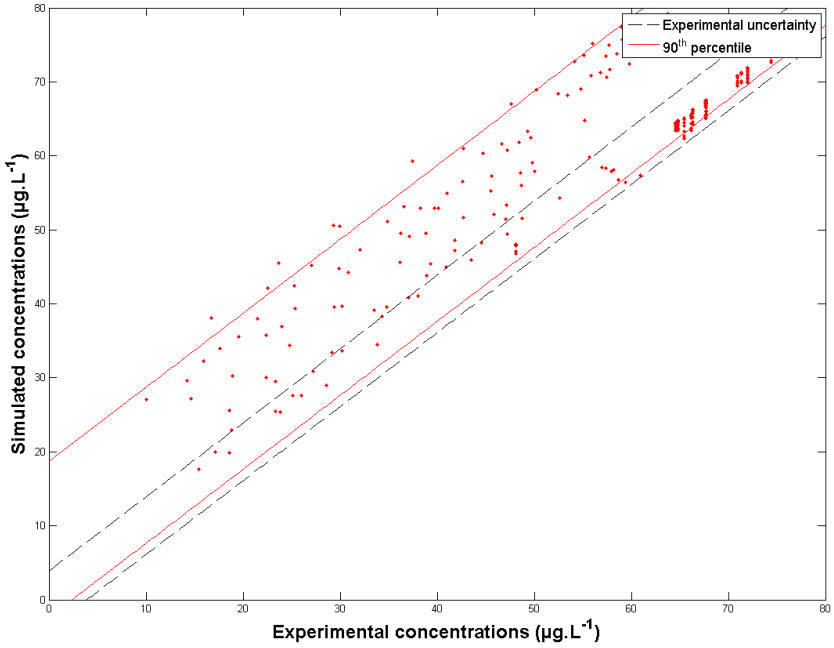

Figure 2 **Comparison of simulated and experimental *p*CBA concentrations, Méry-sur-Oise water**

Table 1 **Statistical results, Méry-sur-Oise water**

Compound	r_P	Pearson test	Offset (mg.L^{-1} or µg.L^{-1})	Test	Slope	Test	% points within error
Ozone	0.97	Passed	0.30±0.07	Failed	0.89±0.05	Passed	31.6
*p*CBA	0.91	Passed	18.38±3.85	Failed	0.75±0.07	Failed	57.9

F.2. Maisons-Laffitte water

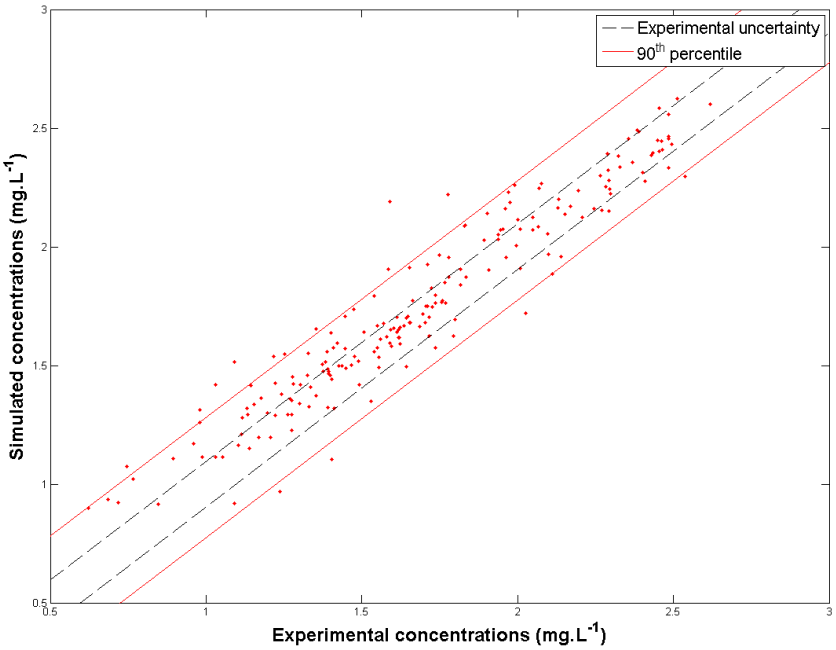

Figure 3 Comparison of simulated and experimental ozone concentrations, Maisons-Laffitte water

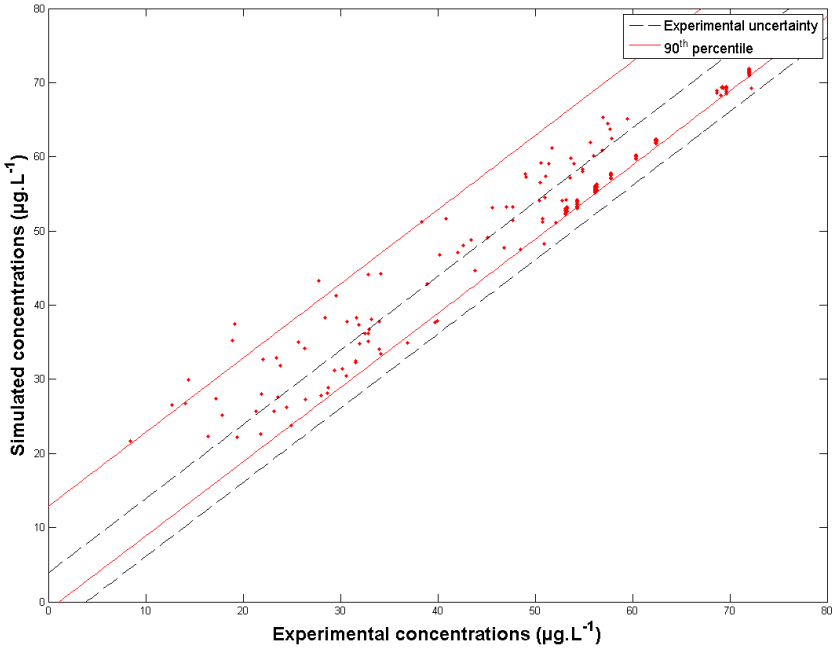

Figure 4 Comparison of simulated and experimental *p*CBA concentrations, Maisons-Laffitte water

Table 2 Statistical results, Maisons-Laffitte water

Compound	r_P	Pearson test	Offset (mg.L^{-1} or µg.L^{-1})	Test	Slope	Test	% points within error
Ozone	0.95	Passed	0.27±0.08	Failed	0.88±0.05	Passed	54.5
*p*CBA	0.97	Passed	10.65±2.21	Failed	0.83±0.04	Passed	74

F.3. Vitré water

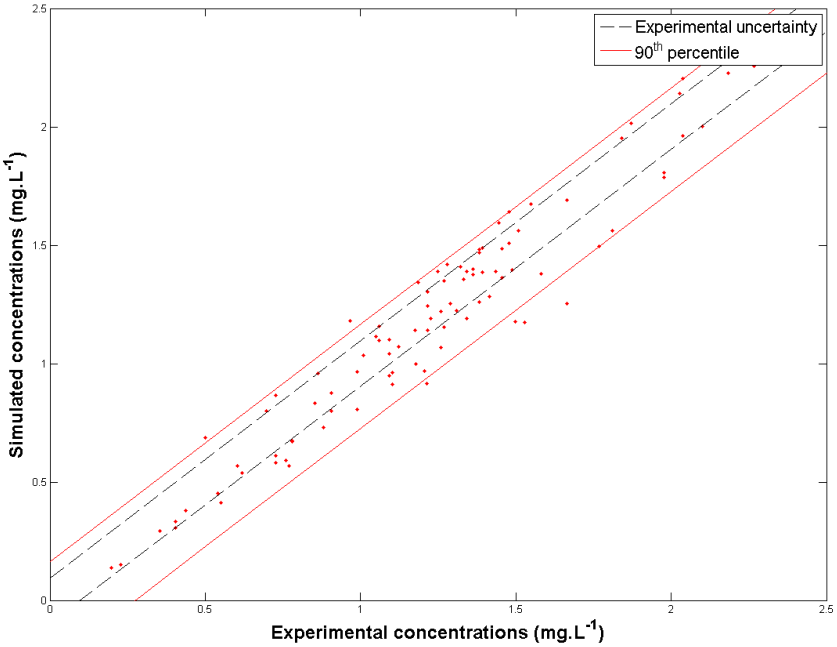

Figure 5 Comparison of simulated and experimental ozone concentrations, Vitré water

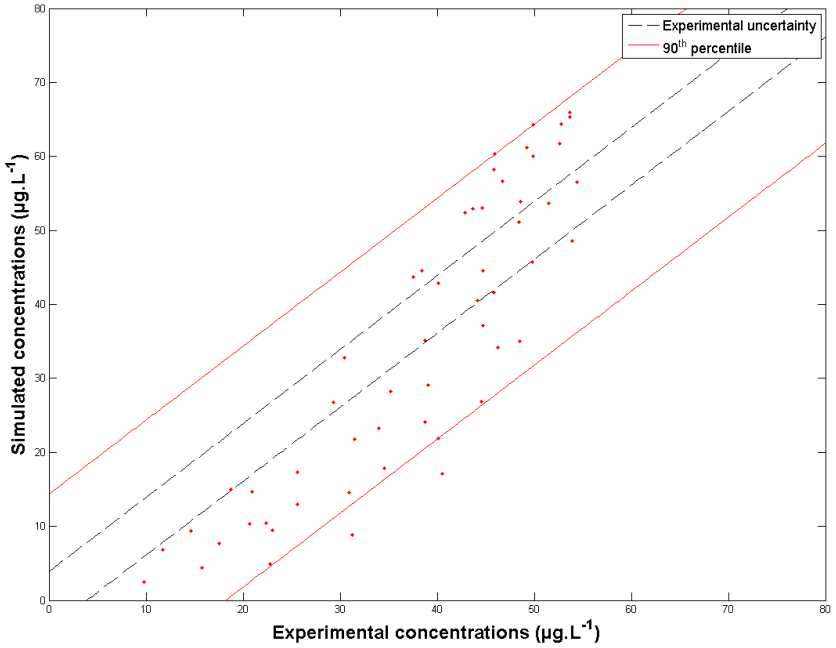

Figure 6 Comparison of simulated and experimental *p*CBA concentrations, Vitré water

Table 3 Statistical results, Vitré water

Compound	r_P	Pearson test	Offset (mg.L^{-1} or µg.L^{-1})	Test	Slope	Test	% points within error
Ozone	0.97	Passed	-0.08±0.08	Passed	1.04±0.06	Passed	46.9
*p*CBA	0.89	Passed	-17.58±9.00	Failed	1.39±0.23	Failed	19.6

F.4. Annet-sur-Marne water

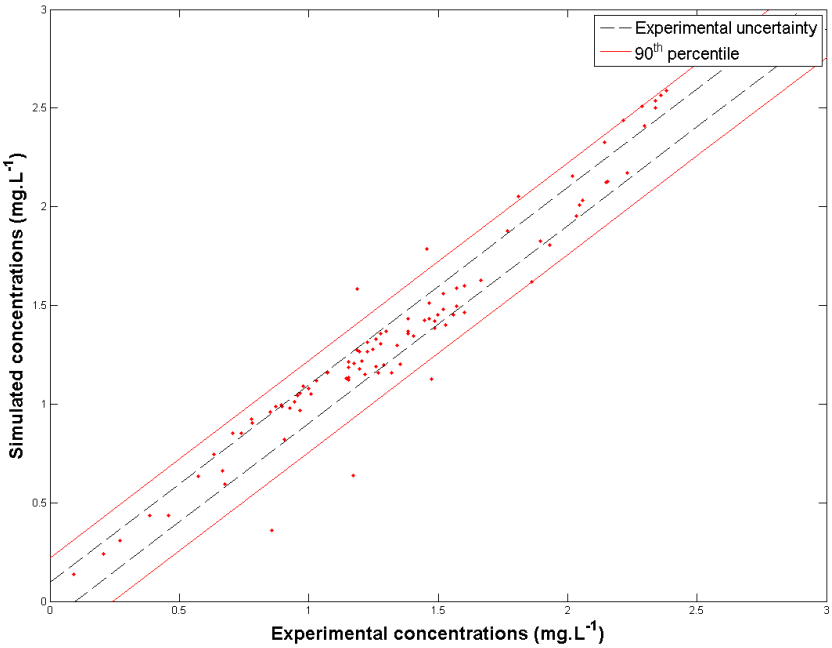

Figure 7 **Comparison of simulated and experimental ozone concentrations, Annet-sur-Marne water**

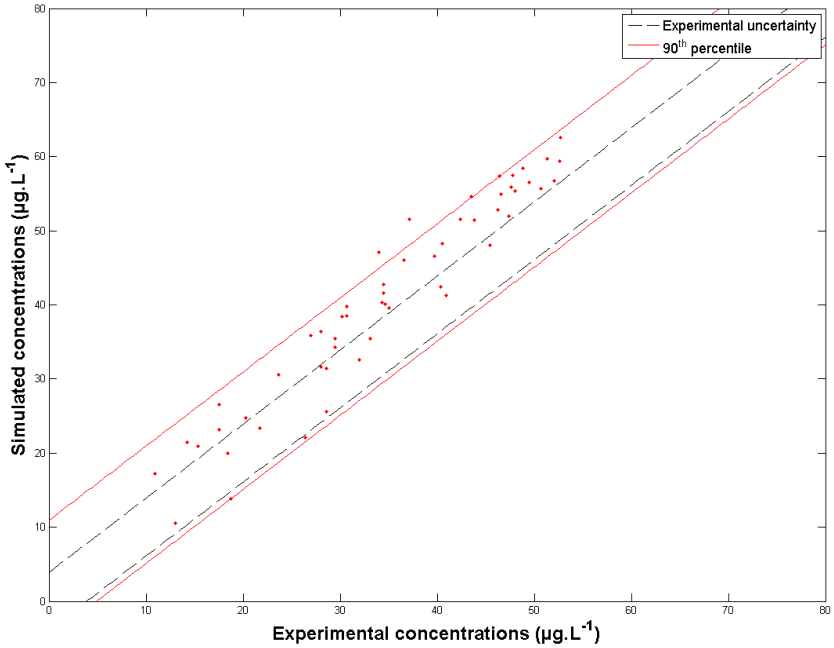

Figure 8 **Comparison of simulated and experimental *p*CBA concentrations, Annet-sur-Marne water**

Table 4 **Statistical results, Annet-sur-Marne water**

Compound	r_P	Pearson test	Offset (mg.L^{-1} or µg.L^{-1})	Test	Slope	Test	% points within error
Ozone	0.97	Passed	0±0.08	Passed	1.02±0.06	Passed	64.3
*p*CBA	0.96	Passed	2.17±5.91	Passed	1.11±0.16	Passed	20

F.5. Meulan water

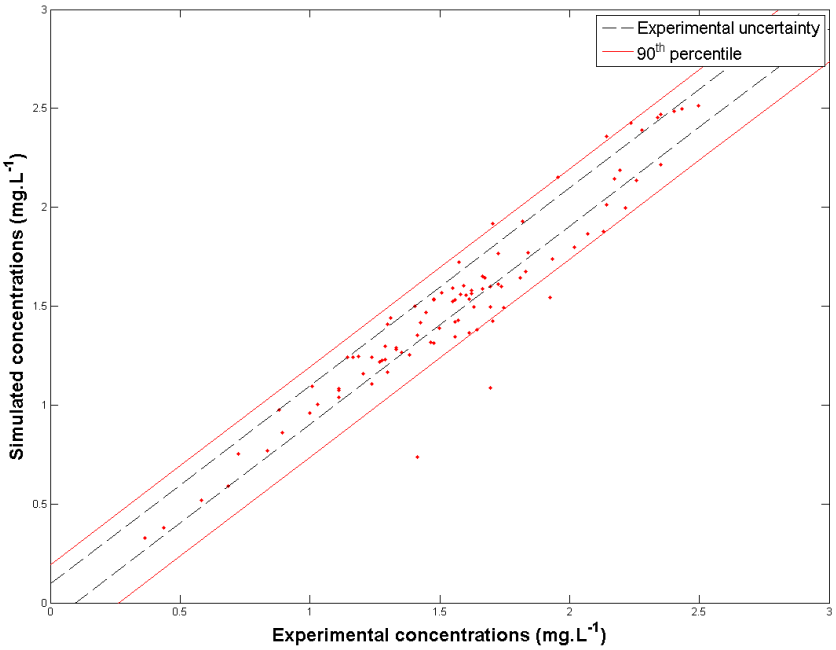

Figure 9 **Comparison of simulated and experimental ozone concentrations, Meulan water**

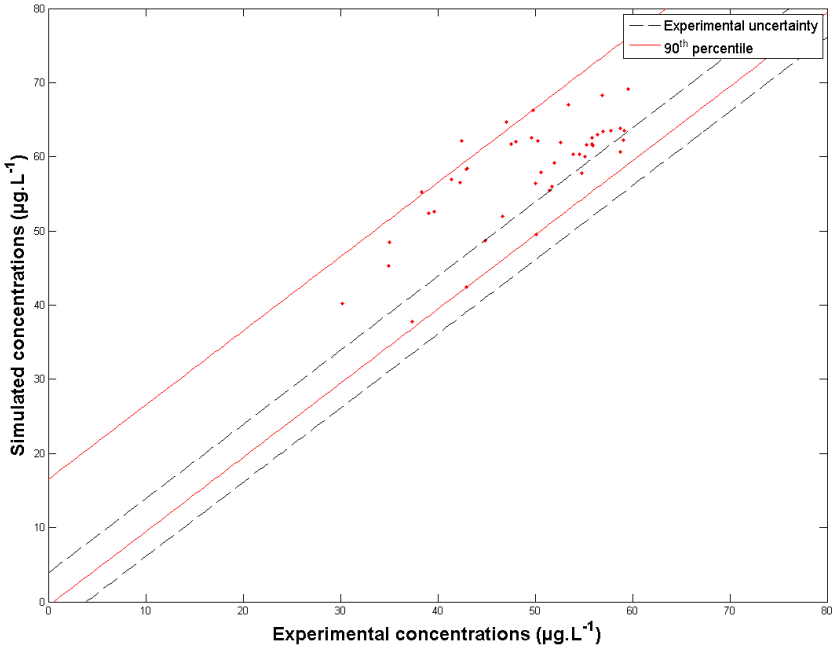

Figure 10 **Comparison of simulated and experimental *p*CBA concentrations, Meulan water**

Table 5 **Statistical results, Meulan water**

Compound	r_P	Pearson test	Offset (mg.L^{-1} or µg.L^{-1})	Test	Slope	Test	% points within error
Ozone	0.95	Passed	-0.04±0.12	Passed	0.99±0.07	Passed	54.7
*p*CBA	0.77	Passed	23.06±19.31	Passed	0.71±0.39	Passed	14.9

Appendix G

Optimised Values of the Parameters of the Model for NOM

G.1. Introduction

Three NOM fractions were distinguished: consumers, initiators and promoters. In order to describe the acid character of the NOM fractions presented, a pK_A was defined for each fraction. Each fraction was thus distributed over two species (acid or base). Because many organic compounds have pH-dependent kinetics in their reactions with ozone, one of the species was considered having a negligible reactivity. The reactions considered are gathered in table **1**.

Table 1 Reactions of NOM considered for ozone decomposition

Type (NOM fraction)	Reaction
Direct consumption (consumers)	$NOM^{d} + O_3 \rightarrow products$
Chain initiation (initiators)	$NOM^{i} + O_3 \rightarrow {}^{\bullet}OH + products$
Chain promotion (promoters)	$NOM^{p} + {}^{\bullet}OH \rightarrow {}^{\bullet}O_2^{-} + products$
Acid-base equilibrium	$NOM_a^{d,i,p} \xleftrightarrow{K_A^{d,i,p}} NOM_b^{d,i,p} + H^+$

The reactive species of each NOM fraction was determined by preliminary optimisations. For a given fraction, only one species was considered and the initial concentration was determined for two different pHs. If the concentration was found to increase with pH, the basic species was selected; otherwise the acid species was selected. The reactive species were assumed to be the same among water samples from the same water resources collected at different times. The initial concentrations presented in the following tables are valid for pH=7.

G.2. Méry-sur-Oise and Maisons-Laffitte Waters

Table 2 Parameter values for Méry-sur-Oise and Maisons-Laffitte waters

Méry-sur-Oise (3.1 $mgC.L^{-1}$)	Active Species (A/B)	Maisons-Laffitte (<0.5 $mgC.L^{-1}$)	Active Species (A/B)	Type of parameter	Fraction
7.07		6.95		pK_A for: $NOM_a \rightarrow NOM_b + H^+$	Initiation
5.76		8.83			Consumption
7.74		8.27			Promotion
$2.53.10^{1}$		$2.99.10^{2}$		Kinetic constant rate at T=293K ($M^{-1}.s^{-1}$)	Initiation
$5.14.10^{3}$		$2.75.10^{3}$			Consumption
$2.02.10^{8}$		$3.62.10^{7}$			Promotion
$3.79.10^{4}$		$5.60.10^{2}$		Energy of activation for initiation, consumption or promotion ($J.mol^{-1}$)	Initiation
$1.41.10^{3}$		$8.55.10^{3}$			Consumption
$5.52.10^{2}$		$2.25.10^{5}$			Promotion
0.4	B	0.1	B	Initial concentration for the considered fraction (mg $C.L^{-1}$) at pH=7	Initiation
0.0	B	0.0	B		Consumption
0.4	B	0.8	B		Promotion

G.3. Annet-sur-Marne Water Samples

Table 3 Parameter values for Annet-sur-Marne water samples

Active Species (A/B)	Annet-sur-Marne (1.3 mgC.L^{-1})	Annet-sur-Marne 2 (1.6 mgC.L^{-1})	Annet-sur-Marne 3 (1.6 mgC.L^{-1})	Type of parameter	Fraction
	6.35	3.34	6.24	pK$_A$ for: $NOM_a \rightarrow NOM_b + H^+$	Initiation
	5.47	3.20	4.48		Consumption
	4.27	2.36	3.60		Promotion
	$2.17.10^1$	$3.09.10^1$	$9.28.10^1$	Kinetic constant rate at T=293K (M^{-1}.s^{-1})	Initiation
	$4.89.10^5$	$1.55.10^7$	$2.07.10^6$		Consumption
	$5.87.10^8$	$1.26.10^6$	$3.43.10^7$		Promotion
	$8.35.10^4$	$8.34.10^4$	$8.20.10^4$	Energy of activation for initiation, consumption or promotion (J.mol^{-1})	Initiation
	$8.54.10^3$	$7.96.10^3$	$1.07.10^4$		Consumption
	$5.73.10^4$	$5.56.10^4$	$6.34.10^4$		Promotion
B	0.4	0.7	0.4	Initial concentration for the considered fraction (mg C.L^{-1}) at pH=7	Initiation
B	0.1	0.1	0.0		Consumption
B	0.8	2.8	1.5		Promotion

G.4. Meulan Water Samples

Table 4 Parameter values for Meulan water samples

Active Species (A/B)	Meulan (0.9 mgC.L^{-1})	Meulan 3 (1.3 mgC.L^{-1})	Type of parameter	Fraction
	3.96	5.19	pK$_A$ for: $NOM_a \rightarrow NOM_b + H^+$	Initiation
	7.33	7.21		Consumption
	6.61	4.05		Promotion
	$1.78.10^1$	$6.99.10^3$	Kinetic constant rate at T=293K (M^{-1}.s^{-1})	Initiation
	$7.31.10^3$	$4.05.10^1$		Consumption
	$7.37.10^5$	$1.01.10^5$		Promotion
	$1.15.10^5$	$1.13.10^5$	Energy of activation for initiation, consumption or promotion (J.mol^{-1})	Initiation
	$8.25.10^4$	$8.77.10^4$		Consumption
	$9.56.10^4$	$9.80.10^4$		Promotion
B	0.4	0.1	Initial concentration for the considered fraction (mg C.L^{-1}) at pH=7	Initiation
A	0.1	0.1		Consumption
B	0.7	1.0		Promotion

G.5. Vitré Water Samples

Table 5 Parameter values for Vitré water samples

Active Species (A/B)	Vitré (2 mgC.L^{-1})	Vitré 3 (2.32 mgC.L^{-1})	Type of parameter	Fraction
	7.96	6.72	pK$_A$ for: $NOM_a \rightarrow NOM_b + H^+$	Initiation
	7.86	5.49		Consumption
	5.51	4.42		Promotion
	$5.80.10^0$	$6.79.10^0$	Kinetic constant rate at T=293K (M^{-1}.s^{-1})	Initiation
	$2.87.10^4$	$4.16.10^7$		Consumption
	$2.04.10^{10}$	$1.47.10^9$		Promotion
	$5.25.10^4$	$4.94.10^4$	Energy of activation for initiation, consumption or promotion (J.mol^{-1})	Initiation
	$1.77.10^5$	$1.69.10^5$		Consumption
	$2.00.10^4$	$2.00.10^4$		Promotion
A	0.7	1.7	Initial concentration for the considered fraction (mg C.L^{-1}) at pH=7	Initiation
A	0.1	0.0		Consumption
B	0.2	0.9		Promotion

G.6. Beaufort and Trondheim Waters

Table 6 Parameter values for Beaufort and Trondheim waters

Beaufort (2.4 mgC.L^{-1})	Active Species (A/B)	Trondheim (3.1 mgC.L^{-1})	Active Species (A/B)	Type of parameter	Fraction
6.34		6.81		pK$_A$ for: $NOM_a \rightarrow NOM_b + H^+$	Initiation
4.72		8.31			Consumption
6.50		7.39			Promotion
$2.31.10^1$		$2.07.10^1$		Kinetic constant rate at T=293K (M^{-1}.s^{-1})	Initiation
$1.10.10^3$		$3.85.10^3$			Consumption
$5.56.10^7$		$8.01.10^8$			Promotion
$7.00.10^4$		$6.25.10^4$		Energy of activation for initiation, consumption or promotion (J.mol^{-1})	Initiation
$7.55.10^2$		$4.14.10^4$			Consumption
$2.29.10^4$		$1.60.10^4$			Promotion
0.1	A	0.8	B	Initial concentration for the considered fraction (mg C.L^{-1}) at pH=7	Initiation
0.2	B	0.2	A		Consumption
0.5	A	0.6	A		Promotion

Appendix H

Optimised Values of the Parameters of the Model for NOM Sequential Reduced Calibration Procedure

H.1. Waters from the First Design of Experiments

Table 1 Parameter values for Méry-sur-Oise and Maisons-Laffitte waters, sequential reduced calibration

Méry-sur-Oise (3.1 mgC.L^{-1})	Active Species (A/B)	Maisons-Laffitte (<0.5 mgC.L^{-1})	Active Species (A/B)	Type of parameter	Fraction
6.84		6.81		pK$_A$ for: $NOM_a \rightarrow NOM_b + H^+$	Initiation
6.54		8.57			Consumption
7.38		7.52			Promotion
$3.45.10^1$		$1.00.10^2$		Kinetic constant rate at T=293K (M^{-1}.s^{-1})	Initiation
$6.70.10^2$		$6.93.10^3$			Consumption
$3.96.10^8$		$2.93.10^9$			Promotion
$3.78.10^4$		$2.96.10^3$		Energy of activation for initiation, consumption or promotion (J.mol^{-1})	Initiation
$1.14.10^3$		$4.67.10^3$			Consumption
0		$2.21.10^5$			Promotion
0.2	B	0.0	B	Initial concentration for the considered fraction (mg C.L^{-1}) at pH=7	Initiation
0.1	B	0.0	B		Consumption
0.6	B	0.5	B		Promotion

H.2. Waters from the Second Design of Experiments

Table 2 Parameter values for Vitré and Annet-sur-Marne waters, sequential reduced calibration

Vitré (2 mgC.L^{-1})	Active Species (A/B)	Annet-sur-Marne (1.3 mgC.L^{-1})	Active Species (A/B)	Type of parameter	Fraction
8.74		6.52		pK$_A$ for: $NOM_a \rightarrow NOM_b + H^+$	Initiation
8.00		5.67			Consumption
6.22		4.41			Promotion
$7.69.10^0$		$1.41.10^1$		Kinetic constant rate at T=293K (M^{-1}.s^{-1})	Initiation
$8.45.10^3$		$6.32.10^4$			Consumption
$4.05.10^9$		$4.08.10^8$			Promotion
$4.84.10^4$		$8.61.10^4$		Energy of activation for initiation, consumption or promotion (J.mol^{-1})	Initiation
$1.78.10^5$		$1.06.10^4$			Consumption
$2.68.10^4$		$5.78.10^4$			Promotion
0.6	A	0.4	B	Initial concentration for the considered fraction (mg C.L^{-1}) at pH=7	Initiation
0.1	A	0.1	B		Consumption
0.3	B	1.4	B		Promotion

Table 3 Parameter values for Meulan and Trondheim waters, sequential reduced calibration

Meulan ($0.9\ mgC.L^{-1}$)	Active Species (A/B)	Trondheim ($3.1\ mgC.L^{-1}$)	Active Species (A/B)	Type of parameter	Fraction
6.21		6.81		pK_A for: $NOM_a \rightarrow NOM_b + H^+$	Initiation
8.01		8.31			Consumption
6.14		7.39			Promotion
$4.28.10^0$		$2.07.10^1$		Kinetic constant rate at T=293K ($M^{-1}.s^{-1}$)	Initiation
$3.80.10^3$		$3.85.10^3$			Consumption
$2.83.10^8$		$8.01.10^8$			Promotion
$1.17.10^5$		$6.25.10^4$		Energy of activation for initiation, consumption or promotion ($J.mol^{-1}$)	Initiation
$8.35.10^4$		$4.14.10^4$			Consumption
$9.11.10^4$		$1.60.10^4$			Promotion
0.9	B	0.8	B	Initial concentration for the considered fraction (mg $C.L^{-1}$) at pH=7	Initiation
0.1	A	0.2	A		Consumption
0.7	B	0.6	A		Promotion

Appendix I

Modelling Results of Two Models For Bromate Formation

I.1. The Two Compared Models

In order to assess if intermediate species $^{\bullet}Br_2^-$, Br_3^-, Br_2, Br_2OH^- could be neglected in the bromate formation pathway, the model used in this study, called in the following "Simplified model", was compared to a model including the species $^{\bullet}Br_2^-$, Br_3^-, Br_2, Br_2OH^- ("Complete model").
The simplified model is presented in chapter **5**, **5.3.2**. The complete model is schematically presented in figure **1**. The values of the reaction rate constants can be found in chapter **1**, **1.6**.The results given by the two models were compared on the basis of real experimental conditions, namely the results obtained with the following water samples: Vitré, Annet-sur-Marne and Meulan. The results are presented in the following.

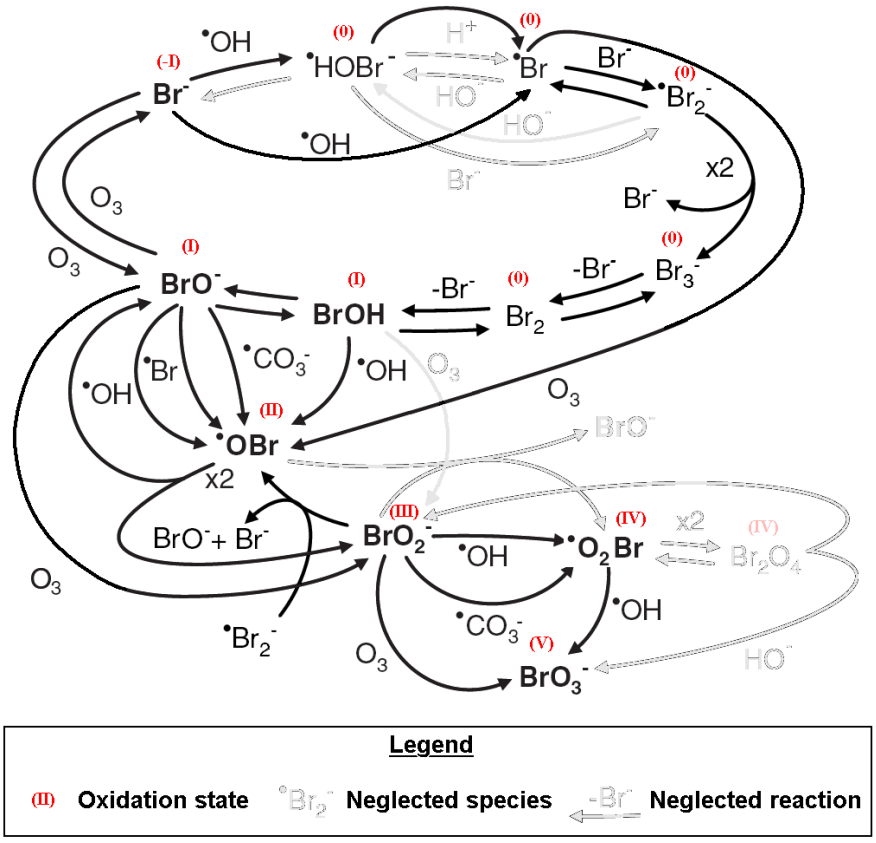

Figure 1 **Schematic overview of the complete model for bromate formation**

I.2. Vitré Water Sample

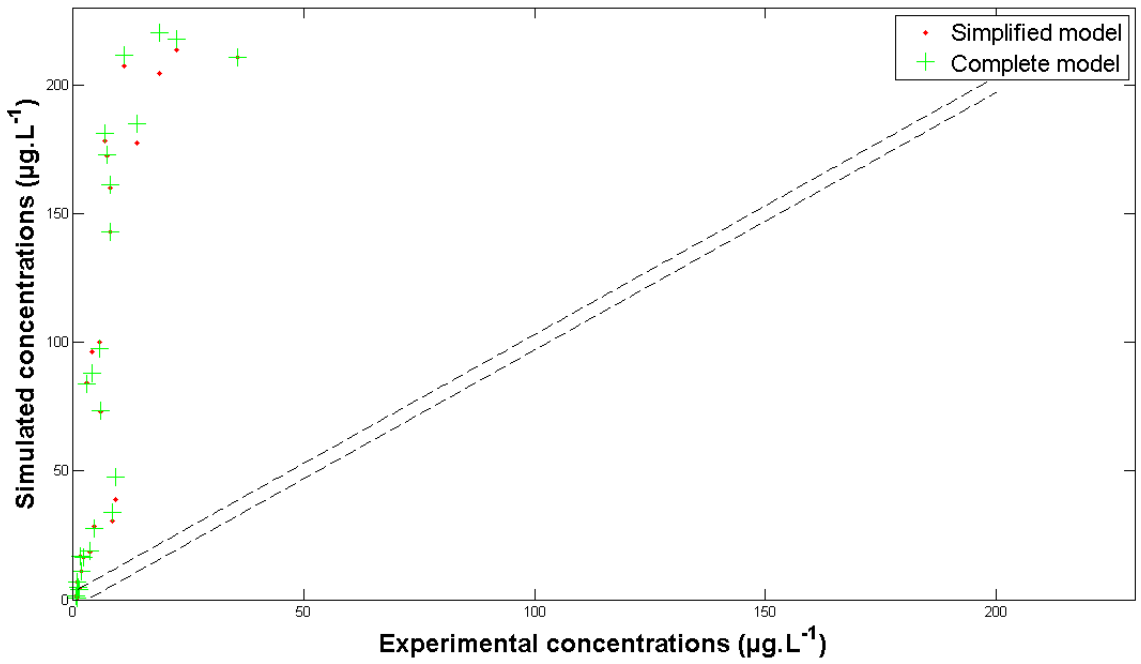

Figure 2 Comparison of modelling results given by the complete and the simplified models, Vitré water sample

I.3. Annet-sur-Marne Water Sample

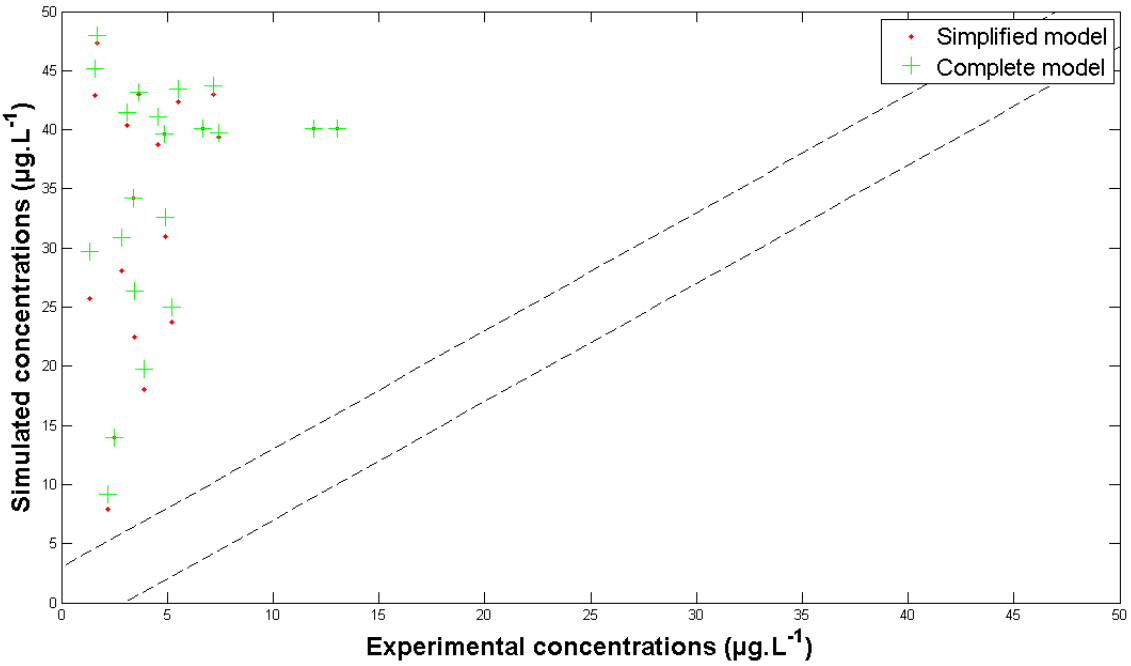

Figure 3 Comparison of modelling results given by the complete and the simplified models, Annet-sur-Marne water sample

I.4. Meulan Water Sample

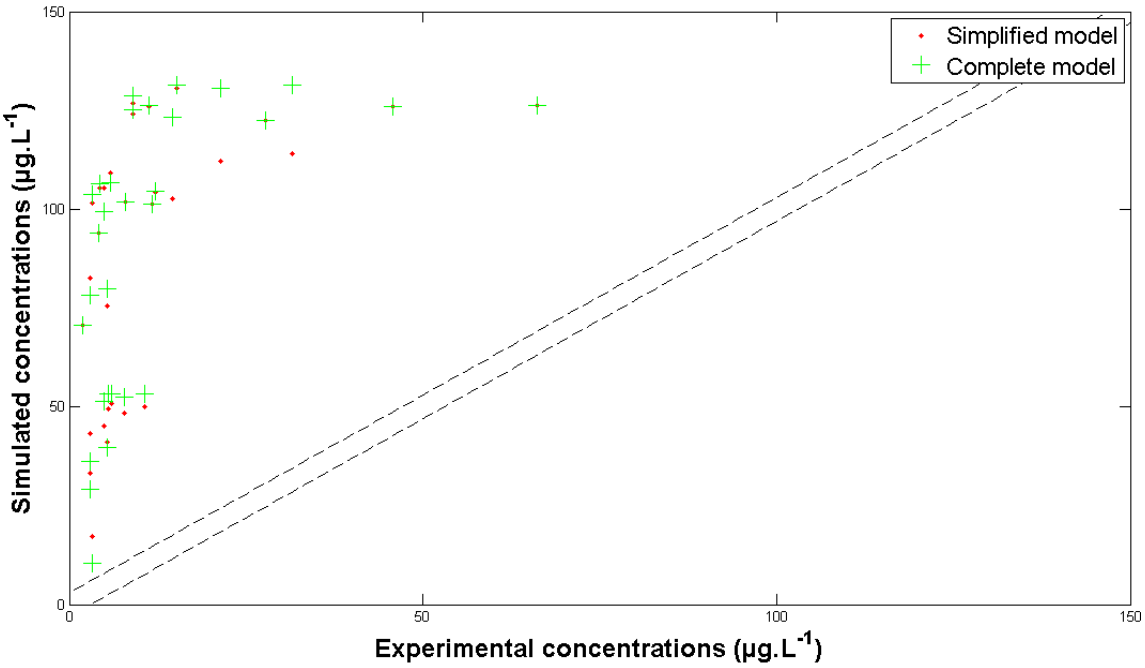

Figure 4 Comparison of modelling results given by the complete and the simplified models, Meulan water sample

I.4. Conclusion

As it appears from the comparison of the modelling results given by the two models on the three water samples investigated, the modelling results of the two models are very much comparable. The complete model seems to give slightly higher values, although this is not systematic (see low experimental concentrations with Meulan for instance). The species $^{\bullet}Br_2^-$, Br_3^-, Br_2, Br_2OH^- will therefore be neglected in this study.

Appendix J

Experimental Results of the On-Site Study

		Water Characteristics						Operational Process Conditions					Ozone						Bromate				
	Parameter	TOC	Br^-	A_T	T	pH	UV 254	$[O_3]_g$	Q_g	Q_l	Setpoint residual	Ozone dose	T	C1	C2	C3	C4	E	T	C1	C2	C3	C4
#	Date	$mg.L^{-1}$	$\mu g.L^{-1}$	$meq.L^{-1}$	°C			$g.Nm^{-3}$	$Nm^3.h^{-1}$	$m^3.h^{-1}$	O_3 in $mg.L^{-1}$	$g.m^{-3}$	$g.m^{-3}$						$\mu g.L^{-1}$				
1	2009-07-21		40		21.6	7.5		14.6	84	1644	0.2	0.75	0.05	0.27	0.25	0.21	0.21	2.35	1.4	2	2	2.7	2.9
2	2009-07-22	1.60	41		21.1	7.5	0.098	13.5	84.4	1481	0.2	0.77	0.08	0.25	0.23	0.19	0.2	2.35		1.4	2	2.5	3.1
3	2009-07-30	1.80	39	3.70	21.3	7.5	0.109	19.8	84	1756	0.2	0.95	0.08	0.4	0.27	0.22	0.19	3.5	0.5		2.2	2.9	3.1
4	2009-08-03	1.80	30	3.70	21.2	7.5	0.105	19.9	63	1504	0.3	0.83	0.2	0.42	0.36	0.35	0.29	3.75	1.4	2	2.9	4	4.8
5	2009-08-07	1.70	30		22.4	7.5	0.114	13.9	149	1851	0.4	1.12	0.1		0.48	0.48	0.39	3.5	1.3		4.7	4.9	6.1
6	2009-08-12	1.70	30	3.60	22.7	7.5	0.117	19.9	66.7	1681	0.3	0.79		0.47	0.41	0.39	0.29	5	0.12	3.5	3.7	4.4	5.6
7	2009-08-14	1.70	33	3.58	22.8	7.5	0.115	19.9	74	1698	0.4	0.87	0.04		0.47	0.45	0.39	5	0		3.7	5.1	6
8	2009-08-14	1.70	33	3.58	22.8	7.5	0.115	19.9	73.1	1704	0.4	0.85	0.16	0.5	0.47	0.45	0.4	4.75		3.5	4.3	4.9	5.8
9	2009-09-02			3.64	20.6	7.4	0.108	10.6	81.8	1021	0.2	0.85		0.43	0.26	0.21	0.18	2.25		0	1.4	1.5	2
10	2009-09-02			3.64	20.6	7.4	0.108	10.2	80.2	990	0.2	0.83		0.4	0.26	0.2	0.19	2.2		0.9	0.9	2.3	2.7
11	2009-09-11	1.50	<30	3.70	19.0	7.4	0.115	13.1	81.6	1100	0.3	0.97	0.4	0.49	0.31	0.3	0.29	3.2		2.5	2.8	3.3	3.9
12	2009-09-30	1.50	30	3.76	17.7	7.5	0.107	17.1	61.8	1100	0.4	0.96	0.41	0.51	0.30	0.33	0.4	3.6	0		2.3	4.02	3.9
13	2009-09-30	1.50	30	3.76	17.7	7.5	0.107	17.6	61.9	1100	0.4	0.99	0.4	0.52	0.45	0.41	0.39	3.6		0	0	2.4	3.7
14	2009-10-06	1.70	34.00	3.58	17.6	7.2	0.109	19.9	64	1690	0.2	0.75	0.31		0.18	0.15	0.19	3.2		0	0	0	0
15	2009-10-06	1.70	34.00	3.58	17.6	7.2	0.109	19.9	64	1690	0.2	0.75	0.3		0.18	0.18	0.2	3.3	0		0	0	0
16	2009-10-09	1.60	31.00	3.78	16.6	7.4	0.114	19.9	62	1663	0.3	0.74	0.41	0.51	0.4	0.39	0.3	3.2	0		0	0	0
17	2009-10-09	1.60	31.00	3.78	16.6	7.4	0.114	19.9	61.3	1661	0.3	0.73	0.41	0.53		0.38	0.29	3.3		0	0	0	0

Appendix K

Modelling Results of the Case-Study on Annet-sur-Marne Water Works

K.1. First Experimental Period

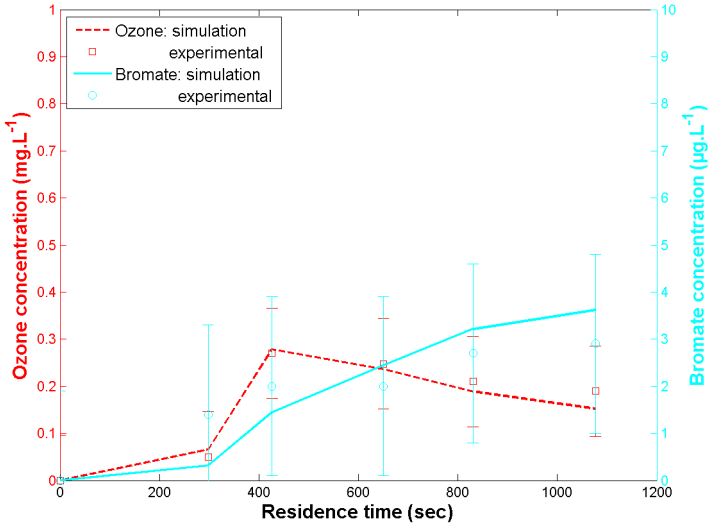

Figure 1 **Experiment #1 ($[O_3]_g$=14.6 g.Nm^{-3}; Q_g=84 Nm^3.h^{-1}; Q_l=1644 m^3.h^{-1})**

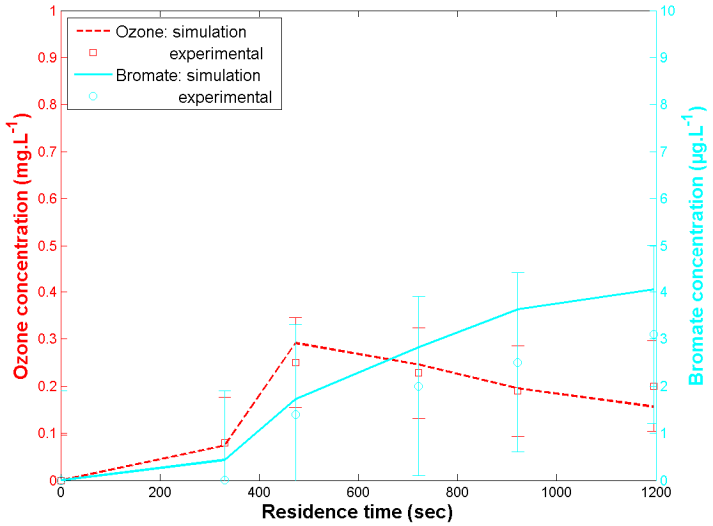

Figure 2 **Experiment #2 ($[O_3]_g$=13.5 g.Nm^{-3}; Q_g=84.4 Nm^3.h^{-1}; Q_l=1481 m^3.h^{-1})**

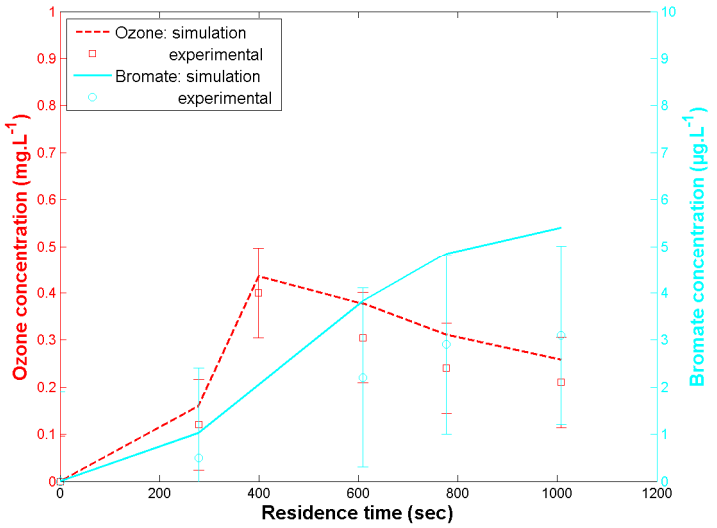

Figure 3 **Experiment #3 ($[O_3]_g$=19.8 g.Nm^{-3}; Q_g=84 Nm^3.h^{-1}; Q_l=1756 m^3.h^{-1})**

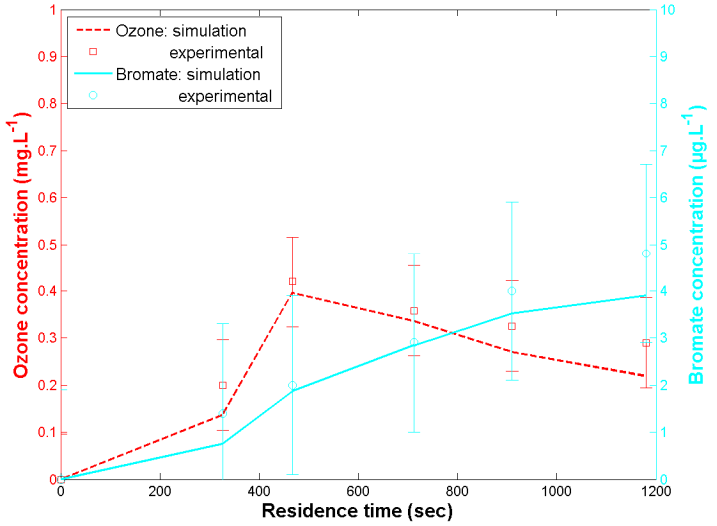

Figure 4 **Experiment #4 ($[O_3]_g$=19.9 g.Nm^{-3}; Q_g=63 Nm^3.h^{-1}; Q_l=1504 m^3.h^{-1})**

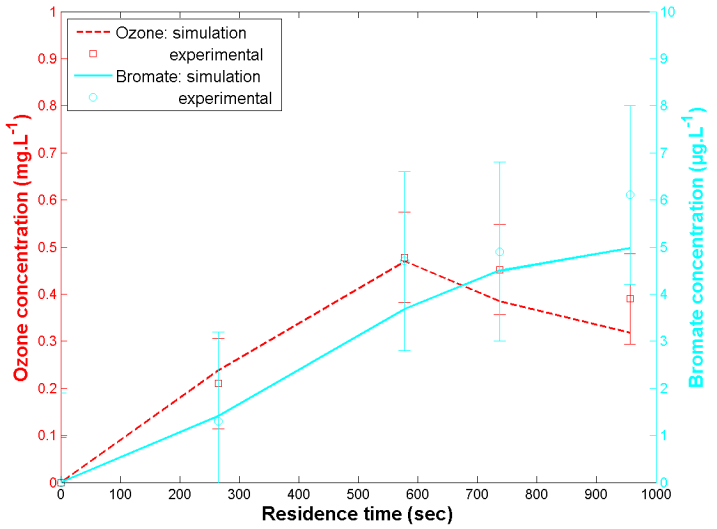

Figure 5 **Experiment #5 ($[O_3]_g$=13.9 g.Nm^{-3}; Q_g=149 Nm^3.h^{-1}; Q_l=1851 m^3.h^{-1})**

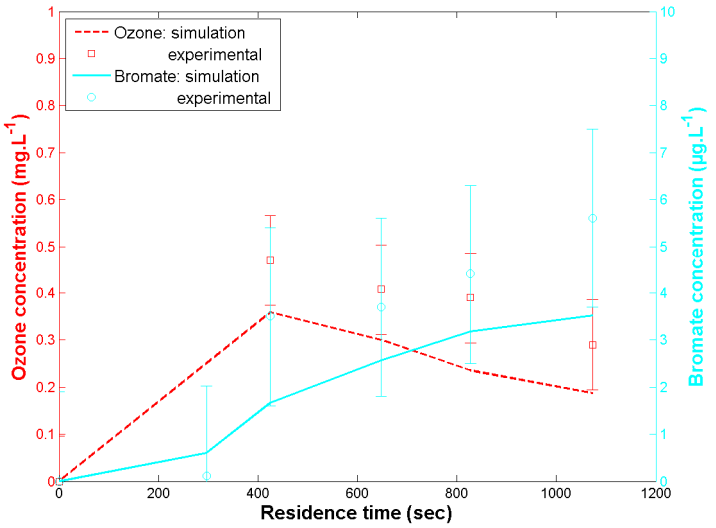

Figure 6 **Experiment #6 ($[O_3]_g$=19.9 g.Nm^{-3}; Q_g=66.7 Nm^3.h^{-1}; Q_l=1681 m^3.h^{-1})**

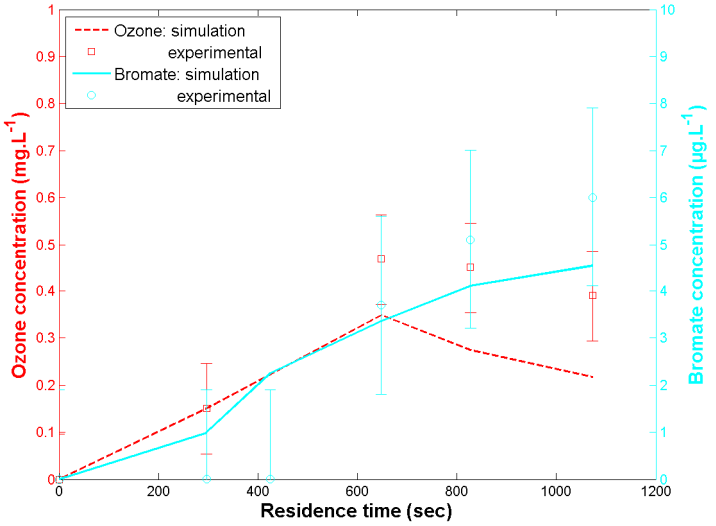

Figure 7 **Experiment #7 ($[O_3]_g$=19.9 g.Nm^{-3}; Q_g=74 Nm^3.h^{-1}; Q_l=1698 m^3.h^{-1})**

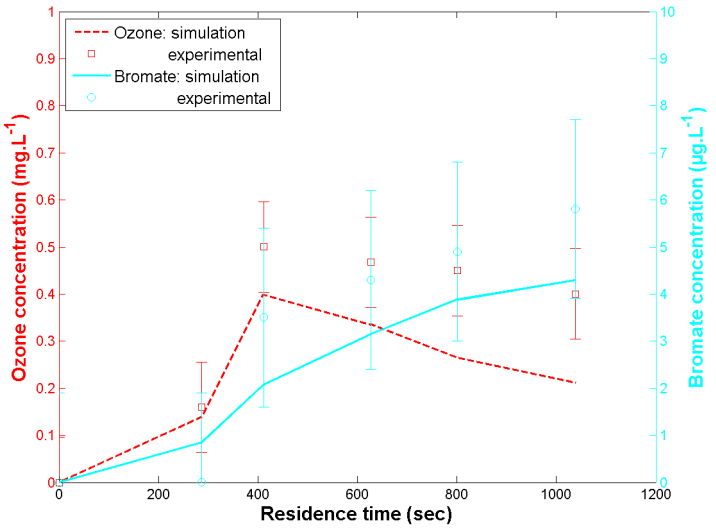

Figure 8 **Experiment #8 ($[O_3]_g$=19.9 g.Nm^{-3}; Q_g=73.1 Nm^3.h^{-1}; Q_l=1704 m^3.h^{-1})**

K.2. Second Experimental Period

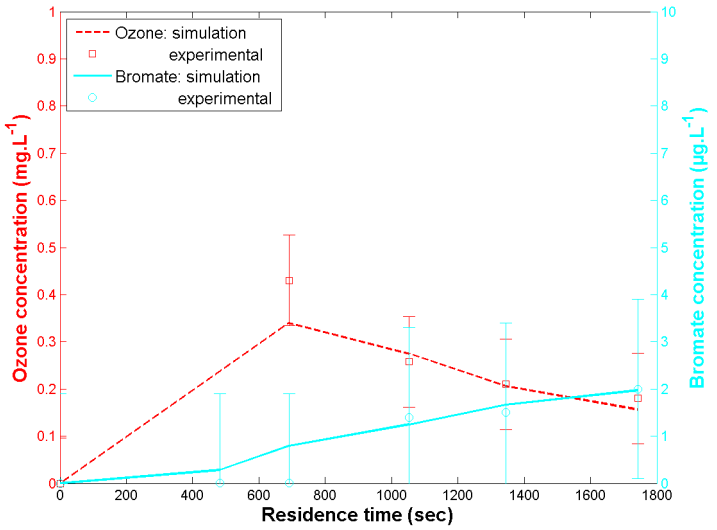

Figure 9 **Experiment #9 ($[O_3]_g$=10.6 g.Nm^{-3}; Q_g=81.8 Nm^3.h^{-1}; Q_l=1021 m^3.h^{-1})**

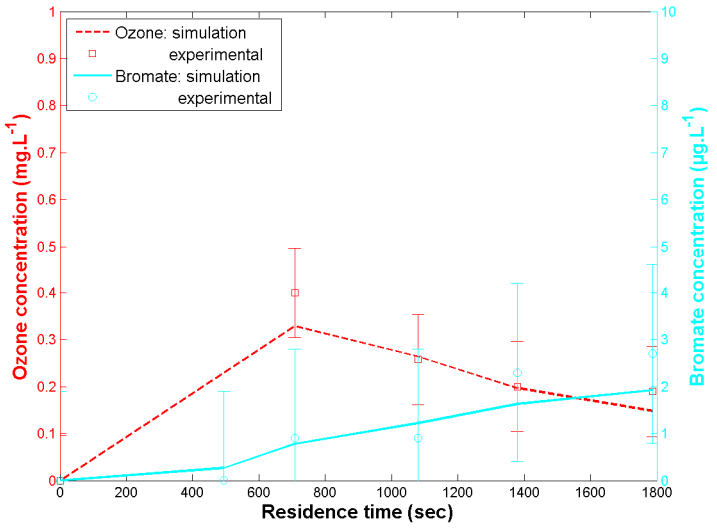

Figure 10 **Experiment #10 ($[O_3]_g$=10.2 g.Nm^{-3}; Q_g=80.2 Nm^3.h^{-1}; Q_l=990 m^3.h^{-1})**

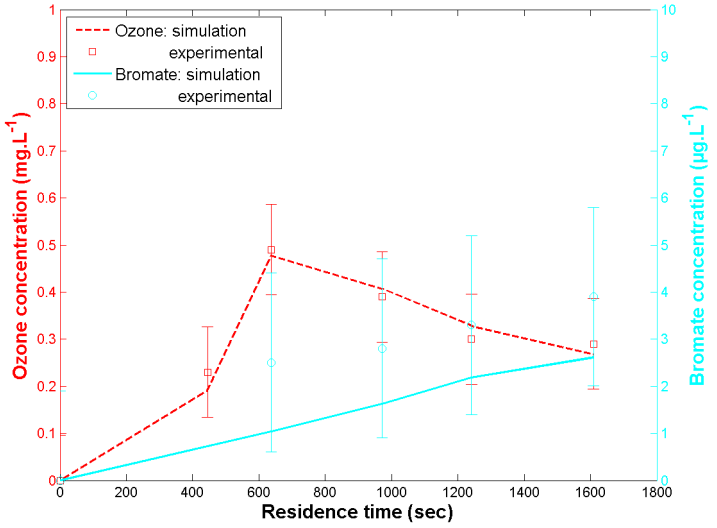

Figure 11 **Experiment #11 ($[O_3]_g$=13.1 g.Nm^{-3}; Q_g=81.6 Nm^3.h^{-1}; Q_l=1100 m^3.h^{-1})**

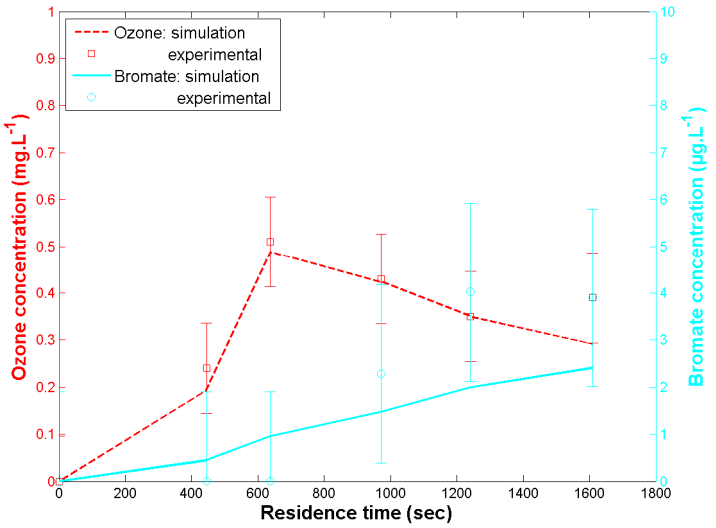

Figure 12 **Experiment #12 ($[O_3]_g$=17.1 g.Nm^{-3}; Q_g=61.8 Nm^3.h^{-1}; Q_l=1100 m^3.h^{-1})**

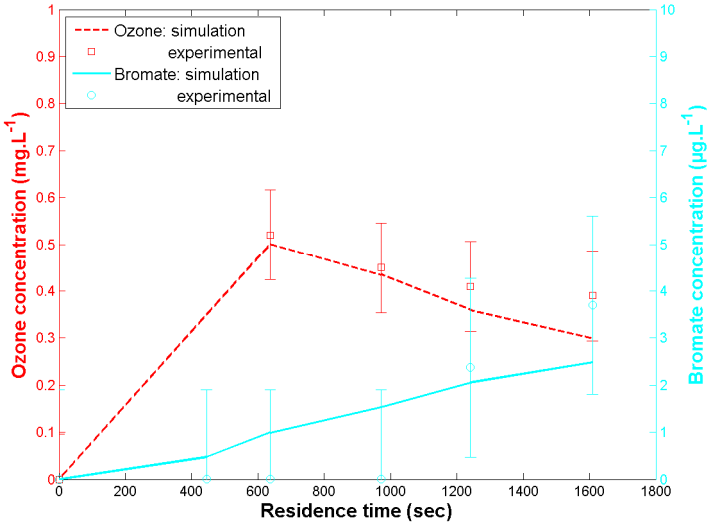

Figure 13 **Experiment #13 ($[O_3]_g$=17.6 g.Nm^{-3}; Q_g=61.9 Nm^3.h^{-1}; Q_l=1100 m^3.h^{-1})**

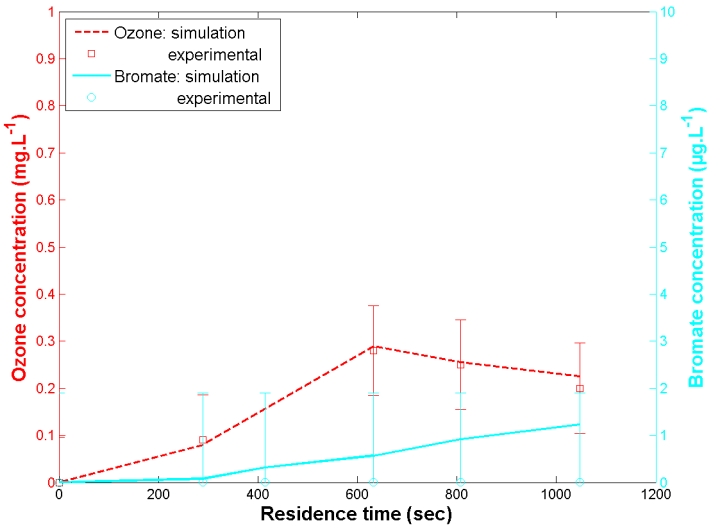

Figure 14 **Experiment #14 ($[O_3]_g$=19.9 g.Nm^{-3}; Q_g=64 Nm^3.h^{-1}; Q_l=1690 m^3.h^{-1})**

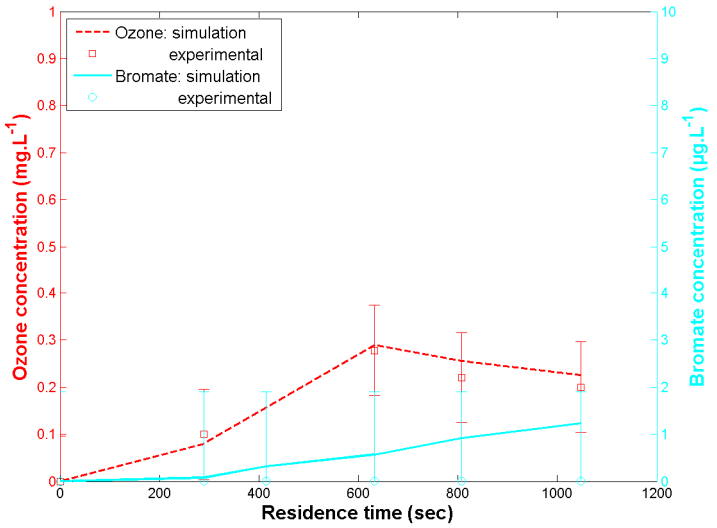

Figure 15 **Experiment #15 ($[O_3]_g$=19.9 g.Nm^{-3}; Q_g=62 Nm^3.h^{-1}; Q_l=1690 m^3.h^{-1})**

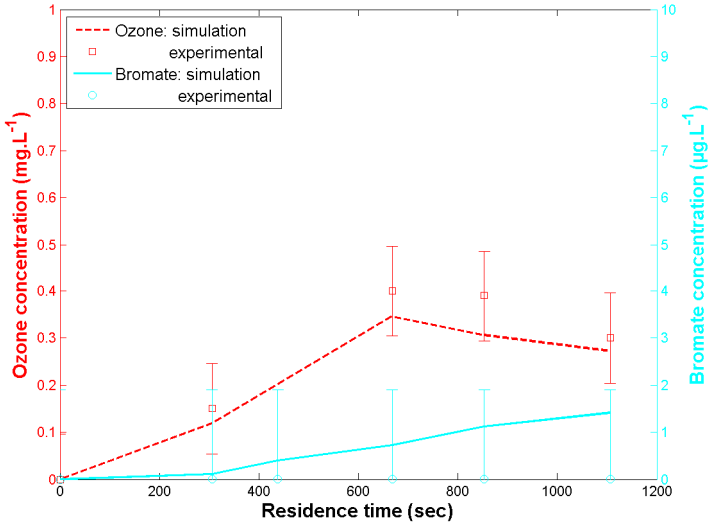

Figure 16 **Experiment #16 ($[O_3]_g$=19.9 g.Nm^{-3}; Q_g=62 Nm^3.h^{-1}; Q_l=1663 m^3.h^{-1})**

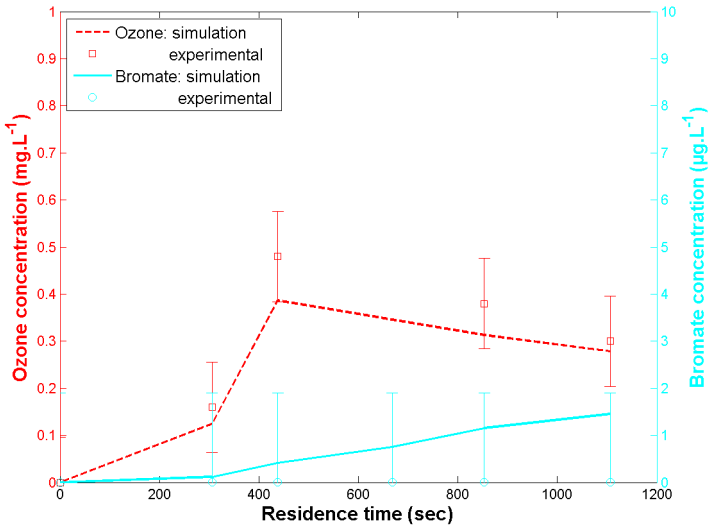

Figure 17 **Experiment #17 ($[O_3]_g$=19.9 g.Nm^{-3}; Q_g=61.3 Nm^3.h^{-1}; Q_l=1661 m^3.h^{-1})**

Appendix L

Extended Abstract in French
Résumé étendu en français

MODELISATION DU PROCEDE D'OZONATION LORS DE LA POTABILISATION DES EAUX APPLICATION AU CONTROLE DES SOUS-PRODUITS DE DESINFECTION : DU LABORATOIRE A L'UNITE INDUSTRIELLE

INTRODUCTION

De nouveaux outils de modélisation pour un contexte changeant

Au cours des dernières décennies, les contextes légal, environnemental et technologique du procédé d'ozonation ont profondément changé. Partant, les traiteurs d'eau se sont tournés de plus en plus vers les technologies de l'information pour la conduite d'unités industrielles d'ozonation.

En raison du probable effet cancérigène de l'ion bromate - le principal sous-produit de l'ozonation – la norme sur la concentration en bromates dans les eaux d'alimentation s'est durcie. Dans la communauté Européenne, la limite est passée de 50 $\mu g.L^{-1}$ à 25 $\mu g.L^{-1}$ (décembre 2003) et enfin à 10 $\mu g.L^{-1}$ (décembre 2008). Plus loin, une baisse supplémentaire à 5 $\mu g.L^{-1}$ est envisageable [Bonacquisti, 2006].

L'émergence des micropolluants dans la ressource est également un élément à prendre en compte. Reconnus comme une classe importante de polluants organiques, les micropolluants sont détectés de plus en plus fréquemment dans les eaux de surface, comme dans les réserves souterraines, à des concentrations allant du $ng.L^{-1}$ au $\mu g.L^{-1}$ (*e.g.* [Serensen *et al.*, 2006]). Par exemple, une très large gamme de résidus pharmaceutiques a été détectée dans l'environnement : antibiotiques, antiépileptiques, analgésiques, antinéoplasiques, contraceptifs, substances agissant comme perturbateurs endocriniens… [von Gunten *et al.*, 2005].

Avec l'avènement de l'informatique, les résultats d'études fondamentales en cinétique chimique ont pu être appliqués pour modéliser le procédé d'ozonation. Diverses approches ont été testées et parfois appliquées sur site. Aujourd'hui, confrontés à un contexte de plus en plus contraignant, les traiteurs d'eau sont à la recherche d'une description encore plus fine des phénomènes mis en jeu dans les procédés de traitement de l'eau. La modélisation apparaît de fait comme une solution de plus en plus viable.

Des modèles adaptables

Les modèles pour la description d'unités d'ozonation doivent être adaptables. D'une part, la concentration et la nature des espèces composant la MON (Matière Organique Naturelle) sont extrêmement variables d'une ressource à une autre ou d'une saison à une autre : par conséquent, l'eau naturelle peut réagir de manière très différente avec l'ozone. D'autre part, les conditions hydrauliques d'écoulement de l'eau sont spécifiques à chaque unité d'ozonation car la géométrie des installations est différente d'un site à l'autre : par conséquent, les temps de séjour (et donc les doses d'ozone) peuvent être très différents.

La MON est généralement décrite comme un mélange de substances organiques avec des propriétés variables en termes d'acidité, de poids et de structure moléculaires [Goslan *et al.*, 2002]. La concentration de MON, sa composition et sa chimie sont donc très variables et dépendent de la source

de matière organique (allochtone/autochtone), de la température, de la force ionique, du pH… De plus, la MON varie également de manière saisonnière, par exemple à travers les apports en carbone particulaire dus aux blooms algaux [Leenheer et Croué, 2003]. La difficulté à quantifier les concentrations des divers sites de la MON susceptibles de réagir avec l'ozone explique en grande partie la quasi impossibilité de relier les caractéristiques physico-chimiques à une modélisation cinétique [Bezbarua, 1997].
Les conditions d'écoulement hydraulique influencent notablement l'efficacité de la désinfection et la formation des ions bromates en affectant l'avancement des réactions biologiques et chimiques [Roustan *et al.*, 1996]. Par conséquent, la distribution de temps de séjour est un élément majeur dont il faut tenir compte.
Considérant qu'une modélisation à l'échelle industrielle ne peut disposer que de peu de données opérationnelles, de nombreux chercheurs ont utilisés des méthodes statistiques (régressions multilinéaires, réseaux artificiels de neurones…). Ces méthodes sont cependant limitées par leur faible capacité d'extrapolation en dehors du domaine de calibration des modèles. De plus, il est généralement difficile de relier ces modèles à des notions de physique ou de chimie.

Objectifs et contraintes
L'objectif premier du présent travail est de développer et d'évaluer une procédure intégrée de modélisation pour les unités industrielles d'ozonation qui permette de prédire les profils de concentration suivants : ozone (en particulier pour évaluer la désinfection), bromates et certains micropolluants. Cet objectif peut être divisé en les sous-objectifs suivants :

- Sélectionner ou développer des modèles pour les phénomènes mis en jeu lors de l'ozonation des eaux naturelles,
- Définir un cadre de modélisation permettant de considérer la chimie et l'hydraulique des installations,
- Sélectionner des méthodes numériques pour calibrer et valider les modèles,
- Déterminer les domaines de validité des modèles,
- Proposer une stratégie pour calibrer au mieux les paramètres des modèles, *i.e.* s'adapter au mieux aux observations expérimentales,
- Tester et discuter l'application sur site,
- Proposer une procédure de modélisation pour les unités industrielles.

En regard de ces objectifs, les contraintes suivantes devront être respectées :

- Simplicité et rapidité de la procédure de calibration,
- Le modèle doit pouvoir s'adapter à la majorité des installations industrielles,
- Les estimations en termes de concentration de bromates doivent être suffisamment justes pour être utilisées comme prédictions,
- Temps de calcul court et facilité d'utilisation pour l'utilisateur final.

Présentation des différents chapitres
Les trois premiers chapitres présentent l'état de l'art ainsi que les choix qui ont été faits en matière de modélisation chimique (chapitre **1**), modélisation hydraulique (chapitre **2**), techniques numériques (chapitre **3**). Le chapitre **4** présente les résultats de modélisation de données de laboratoire et concernant la décomposition de l'ozone et la génération de radicaux hydroxyles dans des eaux naturelles. Le chapitre **5** présente les résultats de modélisation de données de laboratoire et concernant la génération d'ions bromates dans des eaux naturelles. Le chapitre **6** présente les résultats de modélisation de données industrielles de site (étude de cas).

1. CHIMIE DE L'OZONE

1.1. Introduction

L'ozone est un gaz faiblement soluble dans l'eau qui doit être dissous pour attaquer les microorganismes. Une fois dissous, l'ozone est impliqué dans de nombreuses réactions chimiques, ceci de deux manières : directement par réactions moléculaires ; indirectement par réactions radicalaires impliquant les radicaux formés lors de la décomposition de l'ozone. En raison de sa grande réactivité, l'ozone aqueux est instable : à pH neutre, son temps de demi-vie est généralement en dessous des 60 minutes.
De nombreux facteurs expérimentaux influencent la décomposition : le pH, la température, l'alcalinité, la matière organique… Si on s'intéresse à la formation des bromates, il faut également tenir compte de l'ammoniaque et de la concentration en bromures. Les influences des principaux facteurs expérimentaux sont résumées dans le tableau **1**.

Tableau 1 Effets de différents facteurs expérimentaux (adapté de [Westerhoff, 2002])

Hausse du facteur	Efficacité de la désinfection	Vitesse de décomposition de l'ozone	Vitesse de formation des bromates
pH	-	+	+
Température	+	+	+
Bromures	*inchangé*	*inchangé*	+
Alcalinité	+	-	*+à haut pH, -sinon*
MON	-	+	-
Ammoniaque	*inchangé*	*inchangé*	-

Pendant longtemps, les mécanismes régissant la chimie de l'ozone sont restés méconnus. La manière la plus simple de modéliser la désinfection, la décomposition de l'ozone ou la formation des bromates était de construire des lois empiriques. Ces lois prennent souvent la forme de régressions multilinéaires et s'appuient sur une exploration exhaustive des conditions opératoires susceptibles d'être rencontrées. La modélisation par lois empiriques présente l'avantage de ne pas nécessiter d'outil de calcul perfectionné, mais demande de nombreuses données expérimentales. De plus, les résultats de ce type de modèle sont très rarement extrapolables. On trouvera plus de détails dans les travaux de [Gurol et Singer, 1982] et [Jarvis *et al.*, 2007].
On choisit par la suite de présenter plus en détail les modèles mécanistiques ou quasi-mécanistiques développés pour chacun des phénomènes susceptibles de se produire lors de l'ozonation d'eaux naturelles.

1.2. Auto-décomposition de l'ozone

Les modèles mécanistiques utilisés pour décrire l'auto-décomposition de l'ozone dérivent des travaux de deux équipes de chercheurs. D'un côté, Staehelin, Bühler et Hoigné (SBH) ont proposé dans trois articles ([Staehelin et Hoigné, 1982] ; [Bühler *et al.*, 1984] ; [Staehelin *et al.*, 1984]) un modèle développé à pH légèrement acide ; de l'autre côté, Tomiyasu, Fukutomi et Gordon (TFG) ont proposé un modèle développé dans des solutions basiques (pH~12) [Tomiyasu *et al.*, 1985]. Les deux modèles ont par la suite été largement repris par d'autres chercheurs qui les ont souvent réadaptés. Nous présentons dans les points suivants les principales différences des approches SBH et TFG :

- Initiation radicalaire : Dans les deux modèles, cette réaction fait intervenir les ions hydroxyles HO^-. L'initiation a lieu en deux étapes pour SBH, en une étape pour TFG.
- Radicaux intermédiaires : les radicaux $^{\bullet}HO_3$ et $^{\bullet}HO_4$ du modèle SBH n'ont jamais été observés expérimentalement.
- Profils de concentration : des différences significatives ont été mises en évidence pour le couple H_2O_2/HO_2^-, et dans une moindre mesure pour le radical superoxyde $^{\bullet}O_2^-$ par [Gordon, 1995].

Pour cette étude, un modèle de type SBH a été choisi ; il repose sur les travaux de [Mizuno *et al.*, 2007c]. Les différences les plus significatives proposées par Mizuno par rapport au modèle SBH sont

la suppression du radical $^{\bullet}HO_4$ et la réduction du coefficient de vitesse d'une des réactions de propagation radicalaire de 3.10^9 à 9.10^5 $M^{-1}.s^{-1}$.

1.3. Influence de l'alcalinité

Le rôle joué par le carbone inorganique a été étudié par de nombreux auteurs ([Hoigné et Bader, 1976] ; [Yurteri et Gurol, 1988] ; [Morioka *et al.*, 1993] ; [von Gunten et Hoigné, 1994] ; [Acero et von Gunten, 2000] ; [Mizuno *et al.*, 2007b]).
La caractéristique principale des espèces carbonatées est leur faculté à réagir avec les radicaux hydroxyles, créant ainsi des radicaux carbonates, moins actifs dans la décomposition de l'ozone. On considère de fait les ions carbonates et hydrogénocarbonates comme des inhibiteurs de la décomposition de l'ozone. Les espèces carbonatées jouent également un rôle important lors de la formation des ions bromates [von Gunten et Hoigné, 1994].
De manière générale, il existe un certain consensus sur les réactions à considérer et sur leurs cinétiques. Nous choisirons pour cette étude de nous appuyer sur le modèle proposé par [Westerhoff *et al.*, 1997].

1.4. Influence de la MON

La MON reste le facteur chimique le moins bien connu et caractérisé des eaux naturelles. Par conséquent, il n'existe pas encore de modèle mécanistique qui rende compte de l'effet de la fraction organique des eaux naturelles avec l'ozone. En revanche, [Staehelin et Hoigné, 1985] ont proposé un modèle quasi-mécanistique qui repose sur une division de la MON en quatre fractions : *consommatrice*, *initiatrice*, *promotrice* et *inhibitrice*. Le modèle est présenté dans le tableau **2**. Ce type de modèle nécessite de calibrer la réactivité de chacune des fractions.

Tableau 2 **Modèle quasi-mécanistique pour le rôle de la MON, [Staehelin et Hoigné, 1985]**

Fraction	Réaction
Consommatrice	$O_3 + NOM^{d} \rightarrow products$
Initiatrice	$O_3 + NOM^{i} \rightarrow {}^{\bullet}OH + products$
Promotrice	${}^{\bullet}OH + NOM^{p} \rightarrow {}^{\bullet}O_2^{-} + products$
Inhibitrice	${}^{\bullet}OH + NOM^{s} \rightarrow products$

D'autres modèles ont été proposés, mais ils reposent généralement toujours sur la distinction de la MON en quatre fractions. On retiendra de la bibliographie qu'il est difficile de comparer les résultats provenant des différentes études : d'une part car les modèles mécanistiques ne sont jamais exactement les mêmes, d'autre part car les données cinétiques sont rarement spécifiées (concentration initiale de chaque fraction et coefficients de vitesse respectifs). De plus, le comportement chimique de l'eau change avec la ressource (comparer les conclusions de [Cho *et al.*, 2003] et [Park *et al.*, 2001]).

1.5. Formation des bromates en eau synthétique

Les bromates sont formés par oxydations successives des ions bromures. Les ions bromures sont présents dans les eaux naturelles à des concentrations allant de 10 à 1000 $\mu g.L^{-1}$. De manière générale, les eaux avec moins de 20 $\mu g.L^{-1}$ ne posent pas de problème quant à la génération de bromates. La situation est plus problématique pour des concentrations de l'ordre de 50-100 $\mu g.L^{-1}$. Au-delà de 100 $\mu g.L^{-1}$, le risque associé aux bromates est fort [von Gunten, 2003b].
La figure **1** présente schématiquement les diverses réactions qui peuvent être prises en compte pour simuler la formation des ions bromates. Les nombres entre parenthèses y représentent les degrés d'oxydation. On s'aperçoit de la complexité du phénomène et de la répartition des réactions moléculaires et radicalaires (*grosso modo* 1/3 : 2/3).

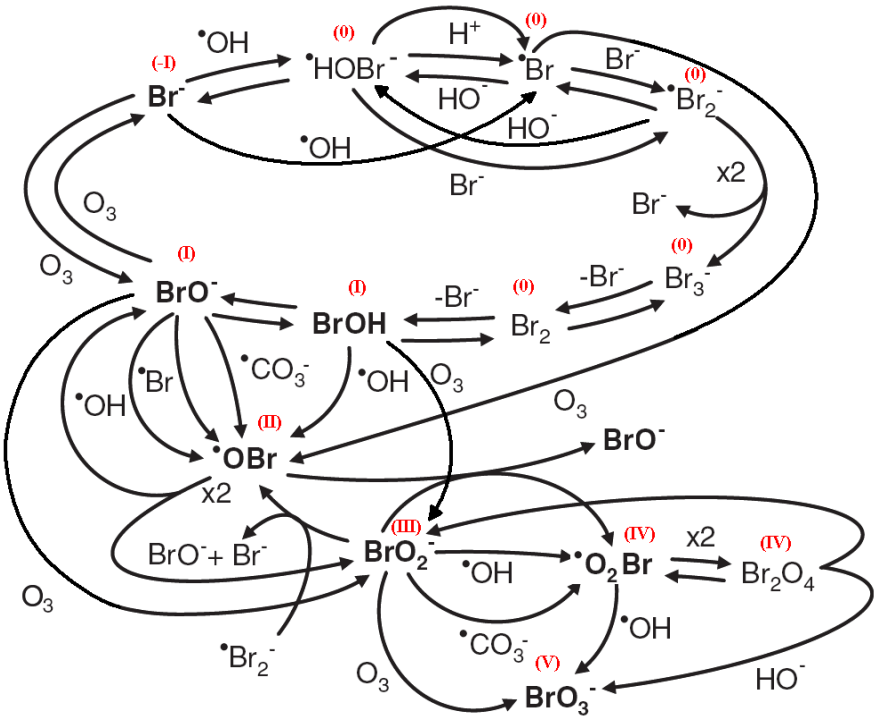

Figure 1 **Mécanisme de formation des bromates (adapté de [Kim *et al.*, 2007])**

1.6. Conclusion

L'ozone réagit avec de nombreuses molécules présentes dans l'eau et sa chimie demeure en partie à découvrir. L'étude bibliographique a permis de sélectionner les types de modèles qui seront utilisés pour cette étude :

- Auto-décomposition de l'ozone : nous nous appuierons sur le modèle de [Mizuno *et al.*, 2007c] ,
- Influence de l'alcalinité : nous nous appuierons sur le modèle de [Westerhoff *et al.*, 1997],
- Formation des bromates : toutes les réactions présentes dans la littérature ne seront pas prises en compte, mais une sélection sera effectuée de manière à « couper les branches mortes » du chemin réactionnel,
- Influence de la MON : Nous choisirons de distinguer quatre fractions dans la MON (*consommatrice*, *initiatrice*, *promotrice* et *inhibitrice*). Leur réactivité chimique devra être déterminée (calibration du modèle). On retiendra qu'il faut calibrer entre 10 et 20 paramètres.

2. CONDITIONS HYDRAULIQUES

2.1. Introduction

Les conditions hydrauliques ont un impact important sur l'avancement chimique de nombreuses réactions. En effet, la géométrie des installations industrielles influe directement sur le temps de séjour des molécules d'eau dans la cuve d'ozonation. Il est donc primordial de pouvoir tout à la fois prendre en compte les cinétiques chimiques et l'hydraulique des installations.
L'approche la plus courante pour modéliser les conditions hydrauliques consiste aujourd'hui à utiliser la CFD (mécanique numérique des fluides). Cette technique a pour principe la résolution des équations de Navier-Stockes décrivant l'écoulement en tous les points d'un maillage permettant de recréer la géométrie de l'installation à étudier. La description qui en résulte est particulièrement détaillée et permet de connaître parfaitement les conditions d'écoulement de l'eau. En revanche, il se révèle très difficile de coupler la résolution hydraulique avec une description détaillée des phénomènes chimiques susceptibles de se produire. Les études qui ont été menées jusqu'à présent n'ont pu considérer que quelques réactions chimiques (moins de 10) alors qu'il faudrait en inclure plus de 60 (*e.g.* [Do-Quang *et al.*, 1999] ; [Zhang, 2006] ; [Bartrand, 2007] ; [Wols *et al.*, 2010]). De plus, la prise en compte d'un écoulement réellement diphasique est encore balbutiante en CFD.
Nous présentons dans la suite de ce chapitre l'approche retenue pour modéliser et les conditions hydrauliques et les cinétiques chimiques.

2.2. L'approche systémique

L'approche systémique est classiquement utilisée en génie des procédés. Elle consiste à représenter les conditions hydrauliques par un assemblage de réacteurs idéaux dont les caractéristiques sont parfaitement connues. En particulier, les équations bilans ont des formes analytiques (équations différentielles ou algébriques). On diminue ainsi la complexité du problème.

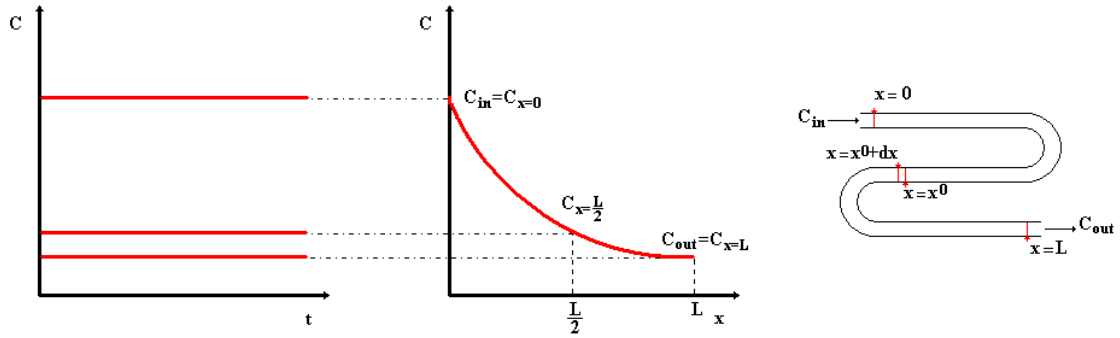

Figure 2 Profils caractéristiques de concentration pour un réacteur piston; schéma d'un réacteur piston

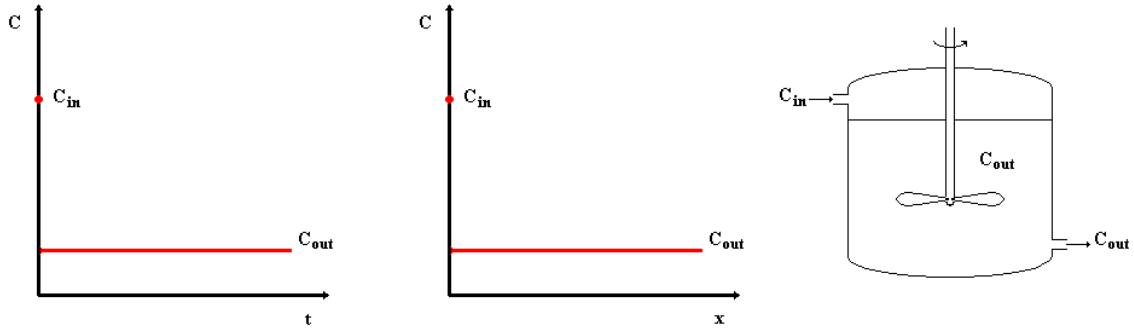

Figure 3 Profils caractéristiques de concentration pour un réacteur parfaitement agité; schéma d'un réacteur parfaitement agité

Dans l'approche systémique, on s'intéresse donc aux entrées et sorties de chacun des réacteurs. Nous considérerons deux types de réacteurs idéaux : les réacteurs piston et les réacteurs parfaitement agités

(cf. figures **2** et **3**, pour des réacteurs monophasiques). L'agencement des réacteurs idéaux peut inclure des boucles de recyclage ou des courts-circuits.
Les réacteurs sont considérés en régime permanent. La différence entre les deux types de réacteurs idéaux est que la concentration des espèces dépend de l'espace dans le cas du réacteur piston. Les bilans de masse sont donc effectués sur un volume élémentaire pour les réacteurs piston et sur l'ensemble du réacteur pour un réacteur parfaitement agité. De nombreux auteurs ont utilisé l'approche systémique pour modéliser des procédés d'ozonation ([Smith et Zhou, 1994] ; [Roustan *et al.*, 1998] ; [Dumeau de Traversay, 2000] ; [Mizuno *et al.*, 2004]).

2.3. Equations

La cinétique des réactions chimiques est modélisée selon la théorie des collisions et toutes les réactions sont considérées comme élémentaires du point de vue de la cinétique. En d'autres termes, les molécularités sont considérées égales aux coefficients stœchiométriques. L'activation thermique des réactions est modélisée par la loi d'Arrhenius.
Le transfert gaz-liquide est modélisé par la théorie du double-film de Lewis et Whitman [Whitman, 1923]. L'ozone étant faiblement soluble dans l'eau, la résistance au transfert dans la phase gazeuse est négligée. Par conséquent, c'est le gradient de concentration dans la phase liquide qui contrôle le transfert de masse [Langlais *et al.*, 1991]. On exprime alors le transfert interfacial en introduisant le coefficient de transfert de masse du côté liquide k_L et l'aire volumique interfaciale a.
Différentes lois permettent d'exprimer le k_La en fonction de données expérimentales ou de données de procédé, comme la vitesse superficielle de gaz [Hikita *et al.*, 1981] ou la section de la colonne à bulles et le flux gazeux [Langlais *et al.*, 1991]. La concentration d'ozone aqueux à l'interface s'exprime grâce à la loi de Henry en fonction de la concentration gazeuse. Différentes lois donnent la dépendance de la constante de Henry en fonction de la température. Nous présentons dans la suite les équations bilans pour les deux types de réacteurs idéaux considérés dans l'étude.

2.3.1. Réacteur parfaitement agité

La caractéristique principale des réacteurs parfaitement agités est que les concentrations des espèces présentes y sont constantes. La figure **5** présente un réacteur parfaitement agité diphasique ainsi que ses paramètres, en ne considérant qu'une seule espèce chimique appelée A.

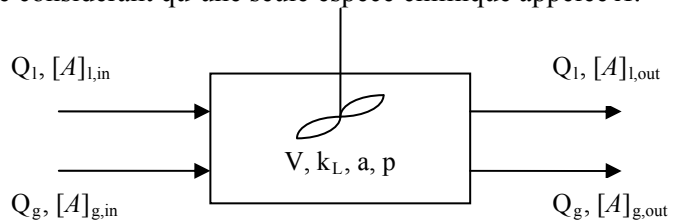

Légende: Respectivement,
Q représente un flux volumique
Les indices g et l pour les phases gaz et liquide
in et out pour les entrées et sorties
p: pression au sein du réacteur
V: volume du réacteur

Figure 4 **Schéma d'un réacteur parfaitement agité diphasique**

Les bilans de masse pour le réacteur parfaitement agité sont exprimés dans les équations **1** et **2**, respectivement pour le liquide et le gaz (il n'y a pas de réaction en phase gazeuse).

$$Q_l\left([A]_{l,in} - [A]_{l,out}\right) + Vk_La \cdot \left(\frac{[A]_{g,out}}{H_c^A} - [A]_{l,out}\right) + Vr^A = 0 \quad \textbf{(1)}$$

$$Q_g\left([A]_{g,in} - [A]_{g,out}\right) - Vk_La \cdot \left(\frac{[A]_{g,out}}{H_c^A} - [A]_{l,out}\right) = 0 \quad \textbf{(2)}$$

avec H_c^A : constante de Henry pour le composé *A*

2.3.2. Réacteur piston monophasique

La figure **5** présente un réacteur piston monophasique. Ici, l'homogénéité des concentrations des espèces chimiques n'est garantie que pour un volume élémentaire, par exemple entre x_0 et x_0+dx. Le bilan de masse est effectué sur un volume élémentaire, résultant dans un système d'équations différentielles ordinaires pour l'espèce *A* (équations **3** et **4**).

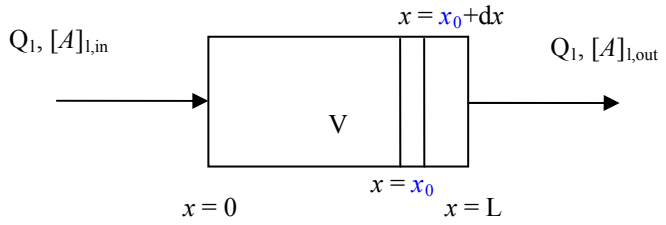

Légende: Respectivement,
Q représente un flux volumique
Les indices g et l pour les phases gaz et liquide
in et out pour les entrées et sorties
L: Longueur du réacteur piston

Figure 5 Schéma d'un réacteur piston monophasique

$$\frac{\partial [A]_l}{\partial x} = r^A \qquad \text{pour } 0 < x \leq L \qquad \textbf{(3)}$$

$$[A]_l = [A]_{l,in} \qquad \text{pour } x = 0 \qquad \textbf{(4)}$$

On peut modéliser des réacteurs piston diphasiques (ce qui est rarement utile dans le cas de l'hydraulique des cuves d'ozonation) par une cascade de réacteurs parfaitement agités. En pratique, on prend un nombre assez important de petits réacteurs parfaitement agités (de 50 à 100), cf. e.g. [Smeets *et al.*, 2006].

2.4. Conclusion

La modélisation du couplage chimie/hydraulique se fera en utilisant des schémas systémiques. La résolution des bilans de masse n'est pas toujours chose aisée, et trois difficultés sont à surmonter : la non-linéarité des équations (cinétique chimique), la taille des systèmes (boucles de recirculation), la *raideur* du problème (coexistence de cinétiques lentes et très rapides).

Il est important de souligner que la calibration d'un modèle systémique doit s'appuyer sur des données soit numériques, soit expérimentales. La distribution des temps de séjour sert généralement de référence pour sélectionner et dimensionner les réacteurs idéaux composant le schéma systémique.

3. APPROCHE NUMERIQUE

3.1. Introduction

Les objectifs de la modélisation ont été définis en introduction de cette étude. L'étude bibliographique des phénomènes chimiques et hydraulique a ensuite permis de définir le cadre de la modélisation (couplage de modèles chimiques mécanistiques avec des schémas systémiques). La formulation mathématique a découlé des choix faits en termes de modèles cinétiques, de transfert, et par rapport aux réacteurs idéaux considérés.
On a vu par ailleurs qu'un modèle universel permettant de représenter le comportement chimique de la MON en présence d'ozone n'existe pas. Nous nous appuierons par conséquent dans cette étude sur un modèle MON quasi-mécanistique dont les cinétiques sont à calibrer. Partant, nous nous intéresserons dans cette partie à sélectionner et décrire les méthodes utilisées pour calibrer et valider les modèles.
La calibration consiste, à supposer que le modèle adopté est le bon, à déterminer les valeurs optimales des paramètres qui permettent au modèle de reproduire au mieux les observations. Si le modèle ne donne pas satisfaction, on peut le changer et choisir un autre modèle ou reformuler la description mathématique du modèle. La validation consiste, une fois le modèle calibré, à vérifier que le modèle reproduit bien des observations n'ayant pas servi lors de la calibration. C'est généralement lors de cette étape qu'une décision est prise sur la validité du modèle.

3.2. Etude du modèle

Avant de mettre en œuvre des techniques d'optimisation pour déterminer les valeurs optimales des paramètres, il est indispensable d'étudier le modèle. Nous nous sommes intéressés dans le cadre de cette étude à savoir si tous les paramètres étaient « identifiables », c'est-à-dire si leur valeur optimale peut être déterminée à coup sûr. D'autres méthodes, non utilisées pour cette étude, peuvent également être appliquées de manière à déterminer le caractère *bien posé* du problème, c'est-à-dire si la formulation mathématique du problème d'optimisation est adaptée à la recherche des valeurs optimales des paramètres.

3.2.1. Identifiabilité

L'identifiabilité a pour but de déterminer si un paramètre est :

- *Uniquement* ou *globalement identifiable* ; la solution pour ce paramètre est alors unique,
- *Localement identifiable ;* il existe alors un nombre fini de solutions pour ce paramètre,
- *Non-identifiable ;* il y a alors une infinité de solutions pour lesquelles le modèle reproduit (exactement) les observations.

On distingue généralement deux types de méthodes pour étudier l'identifiabilité des paramètres : les méthodes théoriques et les méthodes pratiques. Les méthodes théoriques ne traitent que des problèmes linéaires. On a donc recours à des linéarisations pour pouvoir les appliquer à des problèmes non-linéaires [van den Bos, 2007], par exemple en s'appuyant sur des développements en série de Taylor [Pohjanpalo, 1978]. Cependant, l'utilisation de ces techniques théoriques reste très peu aisée, en raison du bruit des observations expérimentales, de la taille des problèmes non-linéaires… [Jeppsson, 1996].
Les méthodes pratiques reposent pour l'essentiel sur l'emploi d'analyses de sensibilité et sur l'estimation de la covariance des paramètres. La sensibilité des sorties du modèle (par exemple en s'appuyant sur la valeur de la fonction objectif, cf. plus bas) par rapport aux paramètres permet de déterminer leur importance relative. La covariance permet de déterminer si les paramètres sont corrélés.
Compte-tenu du nombre de paramètres à déterminer (entre 10 et 20) et du peu de données disponibles dans la littérature quant à leurs possibles valeurs, les espaces de recherche sont certainement très vastes. Il est donc judicieux dans ce cas d'étudier la sensibilité globale (et non locale) des paramètres. Les techniques à appliquer s'appuient généralement sur un échantillonnage et sur une analyse de la variance. Nous nous ne présenterons pas le principe de ces méthodes, mais on retiendra que notre choix s'est porté sur la technique *e*FAST (*extended* Fourier Amplitude Sensitivity Test) qui est une technique d'analyse de sensibilité globale basée sur l'analyse de la variance [Saltelli *et al.*,

2000]. Nous n'estimerons pas la covariance des paramètres (voir les arguments avancés par [Hill et Osterby, 2003] notamment).

3.2.2. Reparamétrisation

La formulation classique des modèles de cinétique chimique peut poser des problèmes lors de la calibration en raison de la corrélation des paramètres et des différences d'ordre de grandeur. Nous effectuons donc pour les constantes de vitesse les changements de variables suivants (équations **5** à **7**, où θ_1' et θ_2' désignent les nouveaux paramètres à identifier). On trouvera d'autres exemples de changements de variables dans [Kittrell *et al.*, 1966] et [Hawthorn, 1974], par exemple.

$$k = k_0 e^{\frac{-E_A}{RT}} = \exp\left[\theta_1' - \frac{1}{T}.\theta_2'\right] \quad \textbf{(5)}$$

$$\theta_1' = \ln(k_0) \quad \textbf{(6)} \qquad \theta_2' = \frac{E_A}{R} \quad \textbf{(7)}$$

3.3. Estimation paramétrique

L'estimation paramétrique s'appuie sur l'évaluation de la qualité des sorties du modèle par rapport aux observations expérimentales servant de référence. Différentes techniques peuvent être utilisées à cette fin :

- l'estimation Bayesienne,
- l'estimation du maximum de vraisemblance,
- l'estimation des moindres carrés pondérés,
- l'estimation des moindres carrés.

Ces approches sont classées par ordre décroissant de connaissance des paramètres et de leur distribution. Les deux premières approches sont probabilistes, la première considérant les paramètres comme des variables aléatoires. L'estimation par moindres carrés présuppose l'idéalité du modèle considéré ; en d'autres termes, le modèle est réputé exact le temps de la procédure de calibration. Si les résultats de validation ne donnent pas satisfaction, on change alors le modèle. Il existe par ailleurs des méthodes d'estimation dites *robustes* qui permettent de gérer les données expérimentales avec beaucoup de bruit [Fieller, 2004].

Dans notre cas, nous avons supposé un modèle parfait et pris en compte (i) l'incertitude expérimentale de mesure au travers de la variance et (i) le fait que les concentrations expérimentales peuvent avoir des ordres de grandeur différents. Nous avons donc défini en équation **8** la fonction objectif suivante (moindres carrés pondérés relatifs) :

$$O(\theta) = \sum_{i=1}^{n} \left(\frac{Y_{\exp,i} - Y_{sim,i}(\theta)}{Y_{\exp,i}.\sigma_{\exp,i}} \right)^2 \quad \textbf{(8)}$$

3.4. Optimisation

Le caractère non-linéaire des équations à résoudre nous a conduits à considérer des méthodes d'optimisation ne reposant pas sur l'évaluation du Jacobien. Ce choix a également été motivé par la mauvaise connaissance des solutions *a priori*, ces méthodes étant performantes au voisinage des solutions. En outre, compte-tenu de la taille de l'espace des paramètres à explorer lors de l'optimisation, il est pratiquement certain que l'unicité de la solution ne peut être garantie, tout comme pour de nombreux problèmes biologiques ou chimiques [Jeppsson, 1996]. Néanmoins, nous avons essayé de trouver des solutions les plus globales possibles.

Tenant compte des spécificités du modèle et des objectifs de l'optimisation, nous avons décidé de procéder en deux étapes :

- exploration du domaine des paramètres à l'aide d'une technique souvent employée pour les études de sensibilité ou les plans d'expériences, LHS (Latin Hypercube Sampling) [McCay *et al.*, 1979],

- optimisation à l'aide d'une version améliorée de la méthode originellement proposée par [Nelder et Mead, 1965] et implémentée dans le logiciel Matlab™ [Lagarias *et al.*, 1998].

3.5. Validation

On a distingué deux types de mesures statistiques pour valider les résultats du modèle : les mesures de qualité de l'ajustement (*goodness-of-fit*) et d'inadéquation de l'ajustement (*badness-of-fit*).

3.5.1. Goodness-of-fit

Suivant les conclusions de [Schunn et Wallach, 2005], nous avons utilisé à la fois la valeur de la fonction objectif et la mesure du coefficient de corrélation R^2. Sachant que les concentrations expérimentales (ozone et *p*CBA, cf. chapitre **4**) ont des ordres de grandeur différents, nous avons procédé au changement de variables **9** avant de calculer le coefficient de détermination selon **10**.

$$Y_{\exp,sim}^{pCBA} = y_{\exp,sim}^{pCBA} \cdot \frac{\overline{Y}_{\exp}^{O_3}}{\overline{y}_{\exp}^{pCBA}} \quad \textbf{(9)}$$

$$R^2 = 1 - \frac{\sum_i \left(Y_{\exp,i} - Y_{sim,i}\right)^2}{\sum_i \left(Y_{\exp,i} - \overline{Y}_{\exp}\right)} \quad \textbf{(10)}$$

3.5.2. Badness-of-fit

Pour mesurer le degré de liaison linéaire entre les observations expérimentales et les sorties du modèle, nous utilisons le test de corrélation paramétrique de Pearson. Les intervalles de confiance pour la pente et l'ordonnée à l'origine de l'ajustement seront comparés avec les incertitudes expérimentales. On trouvera plus de détails dans [Legendre, 2009].

3.6. Conclusion

On étudiera l'identifiabilité pratique des paramètres à l'aide d'une étude de sensibilité avec la méthode *e*FAST. L'estimation paramétrique s'appuiera sur une fonction objectif définie comme un moindre carré relatif pondéré. L'optimisation se fera en deux temps : exploration et sélection des meilleurs candidats à optimiser, optimisation par la méthode de Nelder-Mead.

4. MODELISATION DE LA DECOMPOSITION DE L'OZONE DANS L'EAU NATURELLE

4.1. Introduction

On s'intéresse dans ce chapitre à la modélisation, pour des eaux naturelles, des concentrations en ozone et en radicaux hydroxyles. En effet, ces deux espèces étant les principaux oxydants impliqués dans le procédé, la connaissance de leur concentration est fondamentale pour la prédiction des ions bromates ou des micropolluants. Ainsi, de nombreuses études de modélisation se sont d'abord intéressées à l'ozone et aux radicaux hydroxyles (*e.g.* [Bezbarua, 1997] ; [Westerhoff *et al.*, 1997] ; [Kim *et al.*, 2007]).

On s'est particulièrement intéressé à remplir les sous-objectifs suivants : développer un protocole pour caractériser la réactivité de l'eau naturelle par rapport à l'ozone, justesse des prédictions, domaine de validité du modèle (caractéristiques physico-chimiques des eaux et conditions expérimentales), procédure de calibration (quelles expériences sont à mener en laboratoire pour calibrer le modèle ?), variations saisonnières de la réactivité des eaux naturelles vis-à-vis de l'ozone.

4.2. Matériels et méthodes

4.2.1. Protocole expérimental

Afin de se concentrer sur le devenir de l'ozone dissous et des radicaux hydroxyles dans l'eau naturelle, nous avons séparé la dissolution de l'ozone de sa réaction dans l'eau à étudier. La figure **6** présente un schéma du protocole expérimental. La dissolution d'ozone a lieu dans un flacon de 2L (partie gauche de la figure **6**) alors que la réaction a lieu dans une seringue de 100 mL hermétique au gaz (partie droite de la figure **6**). L'ozone gazeux entre par un tube coudé (a), est dispersé par un poreux (b) ; les évents sortent *via* le tube coudé (c) directement vers le destructeur. Une seringue de 10 mL est utilisée pour prélever de l'ozone aqueux (d), puis cette quantité est injectée dans le réacteur préalablement rempli avec l'eau à étudier (e). Cette méthode permet de prélever plusieurs fois sans générer d'espace de tête (l'ozone passant facilement en phase gazeuse). Des protocoles similaires ont été utilisés, *e.g.* [Kim *et al.*, 2004].

Les prélèvements ont permis de suivre, pour chaque expérience, les profils temporels des concentrations en ozone et en *p*CBA (acide *para*-chlorobenzoïque), ce dernier utilisé comme marqueur de radicaux hydroxyles en raison de sa réactivité ([Elovitz et von Gunten, 1999] ; [Beltrán, 2004]). Les temps de prélèvements étaient 30'' ; 1' ; 2'30'' ; 5' ; 15' ; 35' et 60'. Tous les matériaux en contact avec l'ozone ont été choisis en vertu de leur compatibilité (verre, téflon et acier inoxydable). Les conditions d'agitation ont été optimisées [Mandel, 2008].

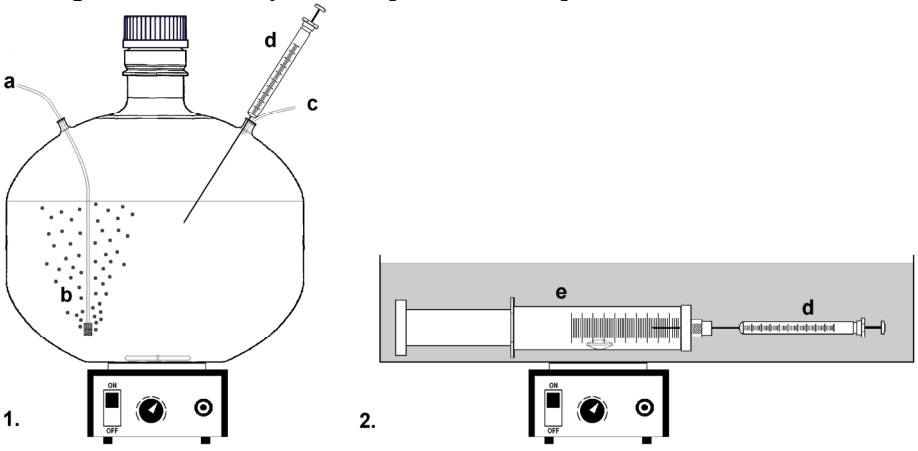

Figure 6 **Schéma du protocole expérimental**

Le protocole a permis de faire varier de nombreux paramètres physico-chimiques. Ces conditions expérimentales ont été choisies en fonction de leur influence sur les profils de concentration en ozone ou en radicaux hydroxyles. D'après la littérature, les paramètres les plus influents sont : l'inhibition radicalaire, le pH, la température, la dose d'ozone, la concentration en MON. Les valeurs de chacun des paramètres sont données dans le tableau **3**. Différents plans d'expériences ont été bâtis à partir des valeurs présentées dans le tableau **3**.

Tableau 3 Valeurs des conditions expérimentales

Paramètre	Moyen/méthode	Niveau 1	Niveau 2
Inhibition radicalaire	Ajout de *tert*-butanol	Pas d'ajout	Excès de 10 mM
pH	Ajout d'acide nitrique	pH naturel	pH naturel - 1
Température	Bain thermostaté	20 °C / 19 °C	5 °C / 13,5 °C
Dose d'ozone	Volume d'ozone aqueux injecté	~1,7 $mg.L^{-1}$	~2,4 $mg.L^{-1}$
Concentration de MON	Dilution de l'eau naturelle avec de l'eau ultra pure ozonée puis déozonée	Pas de dilution	Dilution au 1:2

4.2.2. Caractéristiques des eaux

Différents types d'eau ont été étudiés : des eaux de puits (Maisons-Laffitte), des eaux de trois différentes rivières (l'Oise, la Seine et la Marne) et des eaux de retenue (barrages de Vitré et Beaufort, lac de Trondheim). De plus les eaux d'Annet-sur-Marne, Meulan et Vitré ont été prélevées au moins deux fois (à deux saisons différentes) de manière à appréhender des changements saisonniers. Les caractéristiques des eaux sont récapitulées dans le tableau **4**.

Tableau 4 Principales caractéristiques des eaux étudiées

Eau	Origine de l'eau	pH	A_T $meq.L^{-1}$	Bromures $\mu g.L^{-1}$	COT $mg\ C.L^{-1}$	UV 254 nm 5 cm
Méry-sur-Oise	(Novembre 2008) Eau de surface filtrée sable	7,85	4,55	51	3,1	0,164
Maisons-Laffitte	(Décembre 2008) Puits artésien	8,15	2,4	34	<0,5	0,119
Vitré	(Février 2009) Eau de retenue filtrée sable	7,4	1,02	155,6	2	0,130
Annet-sur-Marne	(Février 2009) Eau de surface filtrée sable	7,4	2,82	29	1,3	0,093
Meulan	(Mars 2009) Eau de surface filtrée sable	7,25	6,24	88,4	0,9	0,091
Beaufort	(Mars 2009) Eau de retenue filtrée sable	6,05	0,12	111	2,4	0,142
Trondheim	(Mars 2009) Eau du lac Jontsvatnet	7,35	0,32	140,5[1]	3,1	0,102
Annet-sur-Marne 2	(Juillet 2009)	8,05	4,24	48	1,6	0,082
Annet-sur-Marne 3	(Octobre 2009)	7,7	3,08	30	1,6	0,098
Meulan 3	(Novembre 2009)	7,3	6,02	94[2]	1,3	0,088
Vitré 3	(Novembre 2009)	7,1	1,24	200[2]	2,3	0,118

[1] Trondheim a été dopée avec du bromure de potassium. Concentration originelle : 20.5 $\mu g.L^{-1}$

[2] Vitré 3 et Meulan 3 ont été dopées avec du bromure de potassium. Concentrations originelles : 180 and 74 $\mu g.L^{-1}$, respectivement.

4.2.3. Analyses

L'ozone aqueux a été analysé avec la méthode spectrophotométrique du Carmin-Indigo [Bader et Hoigné, 1981]. L'analyse du *p*CBA a été effectuée par UPLC (Ultra Performance Liquid

Chromatography). Le COT (Carbone Organique Total), le pH, l'alcalinité, l'absorbance UV à 254 nm ont été mesurés suivant les procédures classiques.

4.2.4. Modèles

Le modèle mécanistique pour l'auto-décomposition de l'ozone s'appuie sur celui de [Mizuno *et al.*, 2007c], pour lequel une des deux réactions d'initiation a été modifiée. Finalement, l'étape d'initiation du modèle retenu se compose des réactions **11** et **12**.

$$O_3 + HO^- \rightarrow HO_2^- + O_2 \quad \textbf{(11)}$$

$$HO_2^- + O_3 \rightarrow {}^{\bullet}OH + {}^{\bullet}O_2^- + O_2 \quad \textbf{(12)}$$

Le modèle pour l'influence de l'alcalinité s'appuie sur celui de [Westerhoff *et al.*, 1997].
Le modèle pour l'influence de la MON reprend la distinction classique en fractions proposée par [Staehelin et Hoigné, 1985]. Pour les eaux étudiées, nous avons considéré que l'effet inhibiteur de la MON était négligeable devant celui des ions carbonates, suivant les conclusions de [Savary, 2002]. A cette typologie (*consommateurs*, *initiateurs*, *promoteurs*) s'ajoute une spéciation de chaque fraction en espèce acide ou basique. Concrètement, un pK_A a été défini (calibré) pour chaque fraction et une seule espèce par fraction a été supposée réactive. Le modèle est présenté dans le tableau **5**. Pour l'utiliser, il est donc nécessaire de calibrer 12 paramètres : les 3 concentrations initiales des fractions ; les 3 facteurs de fréquence des réactions de consommation, d'initiation, de promotion ; les 3 énergies d'activation associées; les 3 facteurs de fréquence des réactions acide → base [Mandel *et al.*, 2009].

Tableau 5 Réactions avec la MON

Type (fraction de MON)	Réaction
Consommation (consommateurs)	$NOM^{\,d} + O_3 \rightarrow products$
Initiation de chaîne (initiateurs)	$NOM^{\,i} + O_3 \rightarrow {}^{\bullet}OH + products$
Promotion de chaîne (promoteurs)	$NOM^{\,p} + {}^{\bullet}OH \rightarrow {}^{\bullet}O_2^- + products$
Equilibres acido-basiques	$NOM_a^{d,i,p} \xleftrightarrow{K_A^{d,i,p}} NOM_b^{d,i,p} + H^+$

La spéciation acide/base des fractions de MON s'appuie sur le fait qu'une grande partie de la MON est constituée par des acides (humiques, taniques, fulviques…) et que la réactivité des formes acides et basiques n'est pas la même. On peut prendre l'exemple des acides formique ou glycolique [Staehelin et Hoigné, 1985] ; [Poznyak and Araiza, 2005].
Tous les modèles utilisés dans cette étude peuvent être trouvés en Annexe **D**.

4.3. Tests numériques

4.3.1. Identifiabilité

Afin de déterminer la pertinence de la procédure d'identification des paramètres, nous avons étudié la sensibilité de la fonction de la fonction objectif par rapport aux paramètres du modèle. Des problèmes réels (*i.e.* avec de vraies concentrations expérimentales et une solution inconnue) et des problèmes pseudo-théoriques (pour lesquels nous avons choisi les valeurs des paramètres à déterminer et pour lesquels les concentrations de référence ont été générées) ont été étudiés. Il ressort de cette étude que :

- les réactions d'initiation et de consommation jouent un rôle important vis-à-vis des profils d'ozone et de *p*CBA,
- la réaction de promotion joue un rôle moins important,
- les constantes d'acidité ont moins d'importance que les concentrations initiales des différentes fractions.

4.3.2. Test de la procédure d'identification

De manière à tester la procédure d'identification, un problème pseudo-théorique a été généré et les valeurs des paramètres (connues) ont été re-déterminées par la procédure d'identification. Nous avons

également comparé la procédure d'identification à une optimisation par algorithmes génétiques. Il résulte de ces tests que :

- De très bons résultats ont été obtenus en termes d'ajustement modèle-observations expérimentales dans les deux cas,
- Les deux procédures sont comparables au niveau du nombre d'itérations,
- Les valeurs de certains paramètres sont très loin de la valeur optimale (en particulier pour les paramètres de la fraction promotrice, ce qui est cohérent avec les résultats de l'étude d'identifiabilité).

On retiendra donc qu'il n'y a probablement pas unicité de la solution pour les valeurs des paramètres, et qu'en tous les cas, les solutions trouvées ont toutes les chances d'être des minima locaux malgré les efforts d'exploration.

4.4. Résultats

4.4.1. Résultats pour un échantillon d'eau : Annet 2

A titre illustratif, nous reprenons ici les résultats du modèle obtenus avec l'échantillon d'eau Annet 2. Les résultats de 10 expériences différentes sont présentés dans les figures Error! Not a valid link. et Error! Not a valid link., pour lesquelles les conditions expérimentales ont toutes été changées suivant un plan d'expériences.

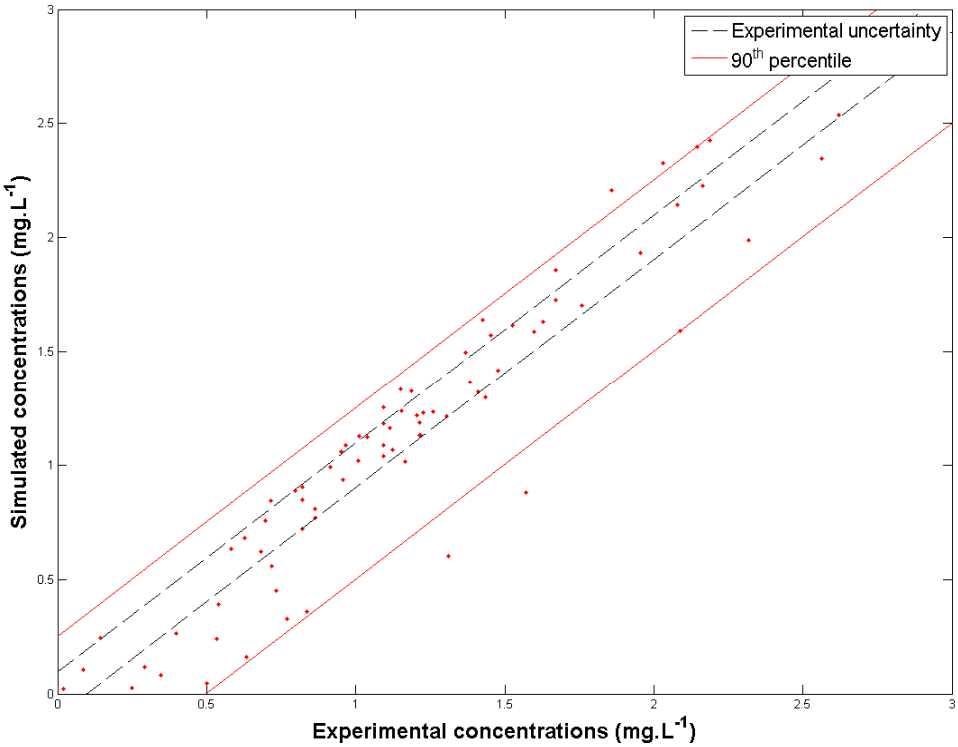

Figure 7 Comparaison des concentrations simulées et expérimentales pour l'ozone, Annet 2

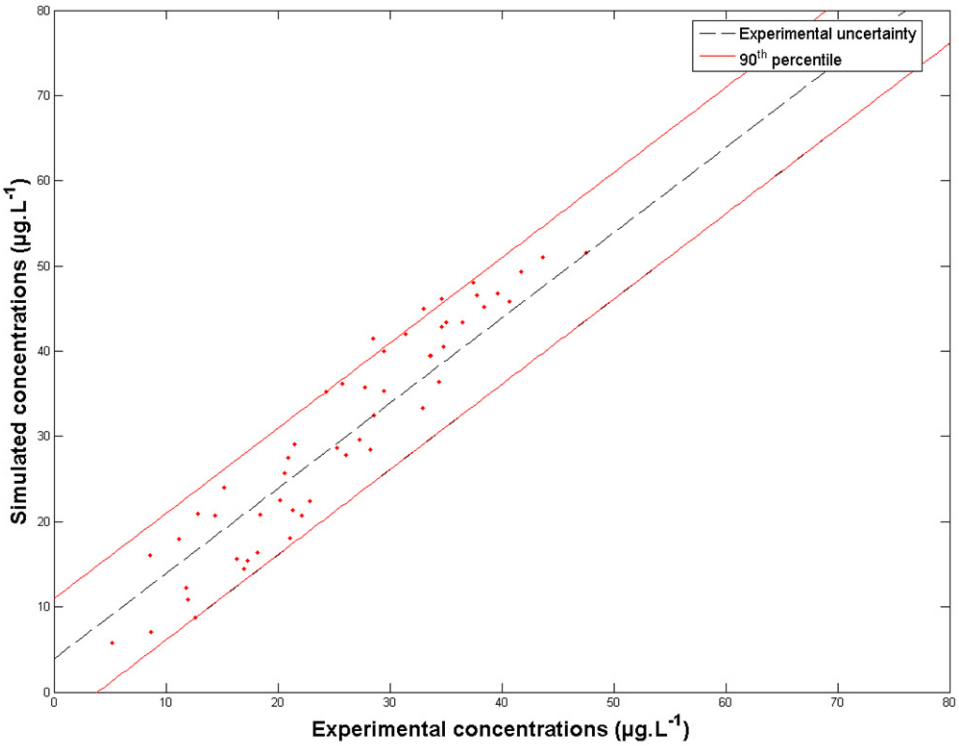

Figure 8 Comparaison des concentrations simulées et expérimentales pour le *p*CBA, Annet 2

On observe généralement une bonne adéquation entre résultats de simulation et observations expérimentales. De manière générale, de tels ajustements ont été observés pour pratiquement tous les échantillons d'eau. La qualité de l'ajustement pour les concentrations de *p*CBA est souvent moins bonne que celle pour l'ozone. Tous les résultats d'ajustement sont disponibles en Annexe **E**. Ils sont également accompagnés des résultats des tests statistiques *badness-of-fit*.

4.4.2. Résumé des résultats

S'appuyant sur des mesures statistiques de qualité de l'ajustement (*goodness-of-fit*), nous avons défini trois qualités d'ajustement : *très bon*, *bon* et *médiocre ou mauvais*. Les expériences (c'est-à-dire les séries temporelles correspondant aux mêmes conditions expérimentales) ont ensuite été classées dans une des trois catégories. Les résultats sont présentés dans leur ensemble en figure **Error! Not a valid link.**.

Si l'on excepte les échantillons d'eau de Beaufort et de Trondheim, (i) pour 78% des eaux nous avons plus des deux tiers des expériences *bien* ou *très bien* modélisées ; (ii) seulement 22% des eaux ont plus d'un tiers de leurs expériences qualifiées de *médiocre ou mauvaises*. Par ailleurs, on a une idée de la qualité de l'ajustement en confrontant les figures **Error! Not a valid link.** et **Error! Not a valid link.** avec la répartition sur le diagramme **Error! Not a valid link.**. Deux échantillons ne donnent en revanche pas satisfaction : Beaufort et Trondheim. On peut noter que la fraction d'expériences *très bien* modélisées reste cependant élevée car nous avons remarqué pour ces eaux que les profils d'ozone restaient très bien modélisés, mais que la prédiction pour le *p*CBA était mauvaise.

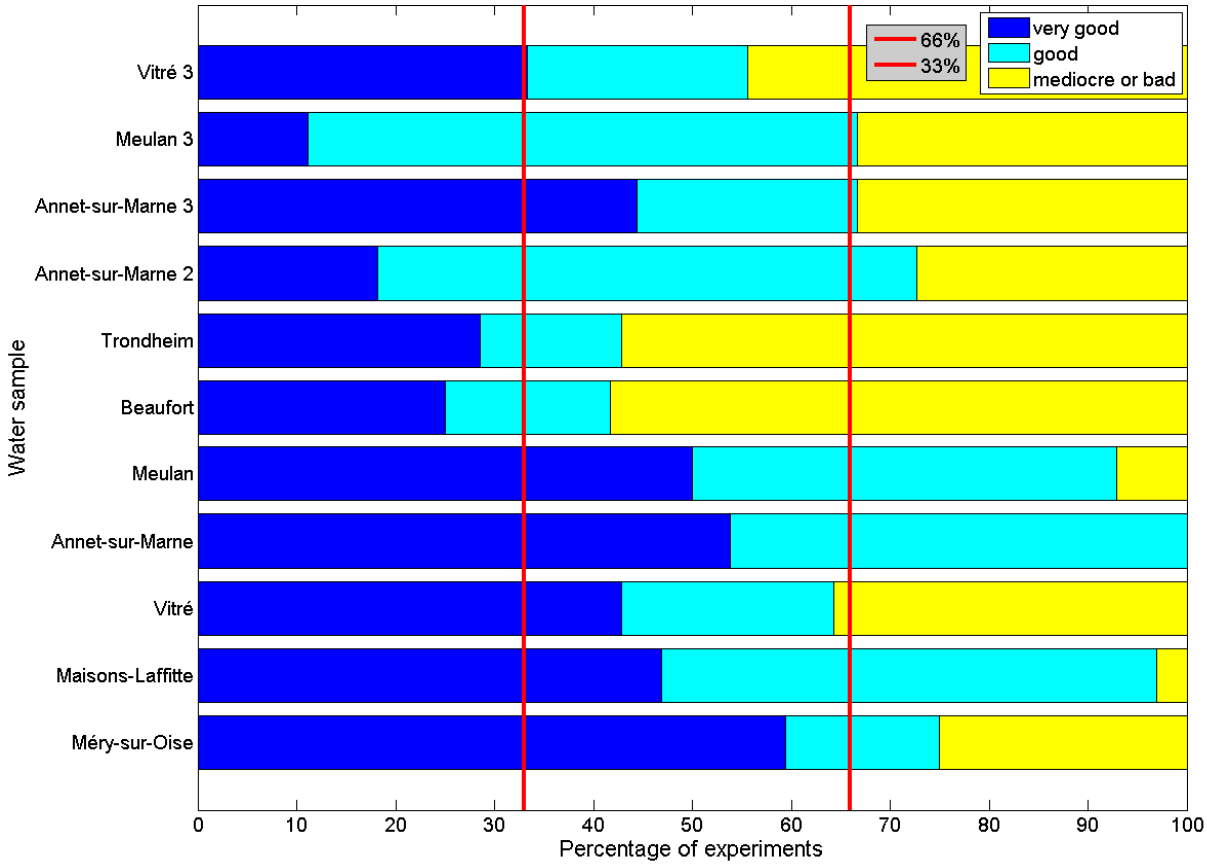

Figure 9 Distribution de la qualité des simulations, toutes les eaux

4.4.3. Domaine de validité du modèle

Les résultats expérimentaux ayant servi à tester le modèle proposé ont permis de déterminer le domaine de validité du modèle, tant du point de vue des caractéristiques des eaux que pour les conditions expérimentales.

De nombreuses combinaisons (pH, A_T, COT) ont été testées, grâce notamment aux baisses de pH et aux dilutions de MON. Dans la très grande majorité des cas, le modèle est capable de donner des résultats acceptables. On retiendra néanmoins que la combinaison {faible alcalinité et fort contenu organique} ne peut pas être modélisée correctement, comme avec les eaux de Beaufort et Trondheim. Une explication pour ce défaut du modèle vient peut-être du fait que sous ces conditions, l'effet inhibiteur de la MON n'est désormais plus négligeable devant celui des ions alcalins. En effet, pour les deux eaux, on avait de très bons profils d'ozone avec des profils de *p*CBA mauvais. Cependant, des essais de simulation avec un modèle intégrant l'effet inhibiteur de la MON n'ont pas donné satisfaction. Peut-être faut-il modifier la stœchiométrie de la réaction, ou bien considérer d'autres espèces inhibitrices (phosphates ?)

Certaines conditions expérimentales ont par ailleurs été moins bien modélisées. On retiendra que le modèle prédit moins bien les expériences pour lesquelles on a :

- grande dose d'ozone
- baisses simultanées de température et de pH
- dilution de la MON et baisse de pH.

4.4.4. Réduction du groupe de calibration et validation du modèle

Jusqu'à présent, pour les résultats de simulation d'une eau, nous avions considéré tous les points pour calibrer le modèle. Ceci nous a permis de déterminer le domaine de validité du modèle, mais il n'y a pas eu de calibration au sens propre. Dans ce paragraphe, on présente des résultats de validation, c'est-à-dire qu'on a considéré uniquement un groupe restreint d'expériences pour calibrer le modèle et qu'on l'a ensuite validé avec les expériences restantes.

Le choix des expériences à considérer pour calibrer le modèle s'est fait à l'aide d'une régression multilinéaire, de manière à déterminer les paramètres expérimentaux dont l'influence est la plus sensible sur les profils d'ozone et de *p*CBA. Nous avons donc choisi de calibrer le modèle « aux bornes » et de le valider « au centre ». Les expériences considérées pour calibrer le modèle sont les suivantes [Mandel *et al.*, 2009]:

- Expérience de référence (eau naturelle à température ambiante, petite dose d'ozone)
- Expérience de référence avec ajout de *tert*-butanol
- Expérience de référence à pH naturel – 1
- Expérience de référence avec ajout de *tert*-butanol et à pH naturel - 1
- Expérience de référence à température basse (5 ou 13°C)
- Expérience de référence à température basse avec ajout de *tert*-butanol.

De plus, la calibration est séquencée, c'est-à-dire que tous les paramètres du modèle ne sont pas déterminés en même temps. L'emploi d'expériences avec du *tert*-butanol permet de ne pas considérer la fraction promotrice de la MON par exemple.

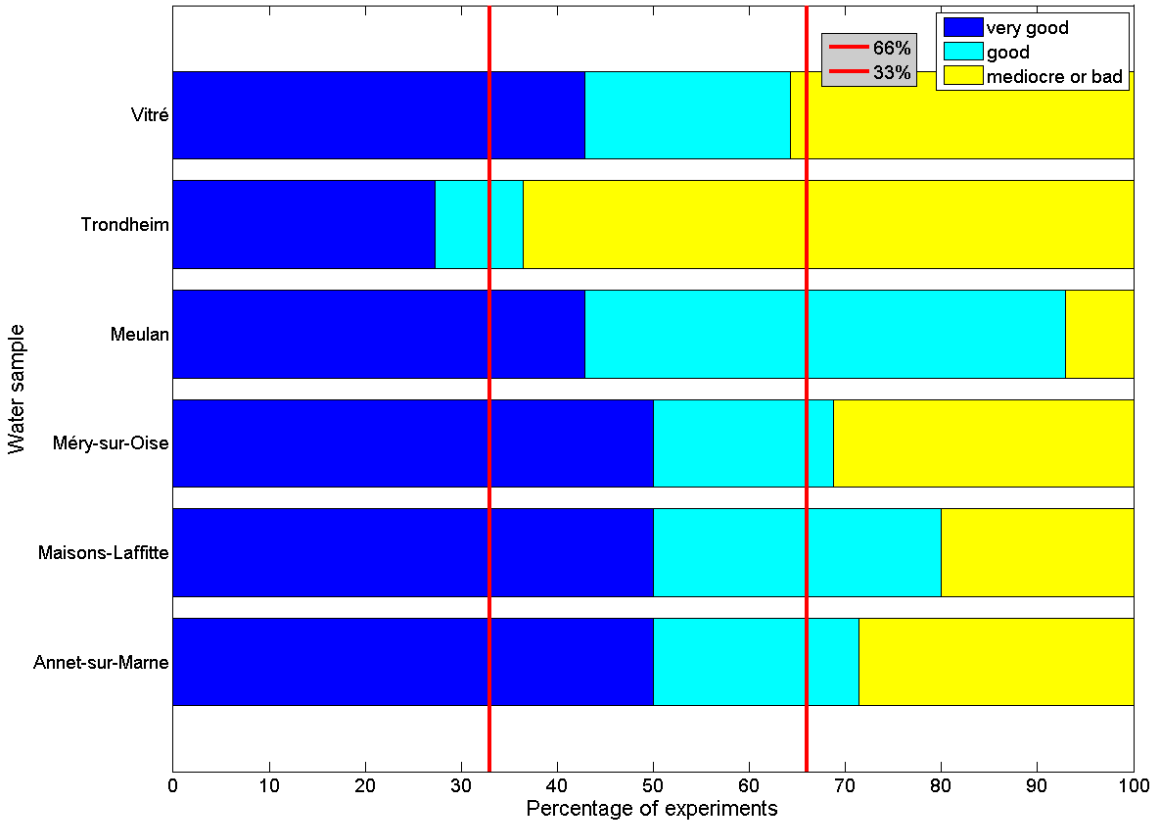

Figure 10 Distribution de la qualité des simulations, calibration réduite séquencée

Cette procédure de calibration réduite et séquencée a été appliquée à cinq échantillons d'eau dont les résultats sont présentés en figure Error! Not a valid link.. Globalement, les résultats obtenus avec cette calibration sont presque aussi bons que ceux obtenus précédemment en considérant toutes les expériences pour calibrer le modèle. Ces résultats sont donc particulièrement intéressants dans la mesure où ils montrent qu'on peut ne mener que quelques expériences ciblées en laboratoire pour calibrer le modèle. Le modèle est par là même validé. Les résultats détaillés de cette procédure de calibration restreinte et séquencée sont présentés en Annexe **F**.

4.5. Conclusion

On s'est intéressé dans ce chapitre à proposer un modèle quasi-mécanistique pour le rôle de la MON, à le calibrer et à le valider. Nous avons développé un protocole expérimental pour pouvoir s'appuyer sur

un jeu de données expérimentales conséquent : 11 échantillons d'eau, 1200 concentrations d'ozone, 900 concentrations de *p*CBA.
Les résultats de cette étude ont montré que :

- Le modèle est valide sur un large domaine
  - $6 \leq pH \leq 8$
  - $1\ meq.L^{-1} \leq A_T \leq 6\ meq.L^{-1}$
  - $0\text{-}0.5\ mgC.L^{-1} \leq COT \leq 3.5\ mgC.L^{-1}$
- Dans ce domaine, 75 % des expériences sont *très bien* ou *bien* simulées,
- Le modèle peut être calibré en une semaine,
- Pour les eaux peu alcalines ($A_T \approx 0.3\ meq.L^{-1}$) et fort contenu organique ($COT \approx 2.5\ mgC.L^{-1}$), le modèle ne peut prédire les concentrations en *p*CBA.

5. MODELISATION DE LA FORMATION DES IONS BROMATES DANS L'EAU NATURELLE

5.1. Introduction

Il est indispensable de modéliser correctement les profils de concentration des espèces oxydantes (ozone et radicaux hydroxyles) si l'on souhaite déterminer le devenir de nombreuses molécules présentes dans l'eau. En particulier, si l'on souhaite modéliser la formation d'ions bromates dans les eaux naturelles.

La formation des ions bromates a été étudiée depuis un certain nombre d'années et les premiers modèles mécanistiques datent des années 1980. Cependant, la modélisation pour les eaux naturelles demeure difficile, principalement en raison de la complexité des modèles disponibles (quelles réactions choisir ?) et du rôle encore méconnu de la MON. Pour ces raisons, il n'existe pas de modèle unifié pour la formation des bromates dans les eaux naturelles. Il est également intéressant d'observer que si certaines études ont montré que les variations saisonnières de qualité de MON ont une influence sur la formation de trihalométhanes [Wei *et al.*, 2008] ou d'espèces organiques bromées [Huang *et al.*, 2004], il n'existe, à notre connaissance, pas d'étude similaire pour les bromates.

L'objectif de ce chapitre est de proposer et de valider un modèle pour la formation des ions bromates dans les eaux naturelles. Nous nous appuierons sur de nombreux résultats expérimentaux, avec différents types d'eau, collectés à différentes périodes de l'année.

5.2. Matériels et méthodes

Deux protocoles ont été appliqués pour étudier la formation des bromates : celui présenté dans le chapitre **4** et un protocole dont nous avons montré qu'il lui était équivalent. Nous avons étudié 6 échantillons d'eau : Annet-sur-Marne, Vitré, Meulan, Annet-sur-Marne 2, Vitré 3 et Meulan 3 (cf. caractéristiques dans le tableau **4**). Les analyses bromates ont été effectuées avec un chromatographe ionique DIONEX. Les autres analyses sont similaires à celles présentées dans le chapitre **4**.

5.3. Un modèle unique ?

Dans ce paragraphe, nous nous intéressons à modéliser la formation des bromates dans différentes eaux naturelles avec le même modèle. En effet, l'influence de la MON lors de la formation des ions bromates reste en grande partie inexpliquée. Si les auteurs s'accordent généralement sur le fait que la formation de bromates est moins importante dans les eaux naturelles que dans les eaux synthétiques, toutes conditions expérimentales étant égales par ailleurs - *e.g.* [Westerhoff *et al.*, 1998b] ; [Pinkernell et von Gunten, 2001] – les voies d'action et les cinétiques de la MON dans le mécanisme de formation des bromates demeurent peu connus.

Afin de simplifier le modèle de formation des bromates, nous avons considéré que certaines espèces (Br_2O_2, Br_2O_4, $^{\bullet}Br_2^-$, $Br_3^{\bullet}$…) pouvaient être négligées, ainsi que certaines réactions ($^{\bullet}OH + BrO_3^- \rightarrow {}^{\bullet}OBr + HO^- + O_2 << BrO_2^- + {}^{\bullet}OH \rightarrow {}^{\bullet}O_2Br + HO^-$ par exemple). Ces simplifications ont d'abord été proposées en comparant les réactivités des réactions de formation, de disparition, les équilibres acido-basiques… puis validées par simulations numériques. Sur les 51 réactions majeures trouvées dans la littérature, seules 18 ont été gardées finalement. Les résultats des tests numériques sont présentés en Annexe **I**. Le mécanisme simplifié est représenté schématiquement en figure **11**. Les résultats obtenus avec ce modèle pour les eaux d'Annet-sur-Marne, Vitré et Meulan sont représentés en figure **12**.

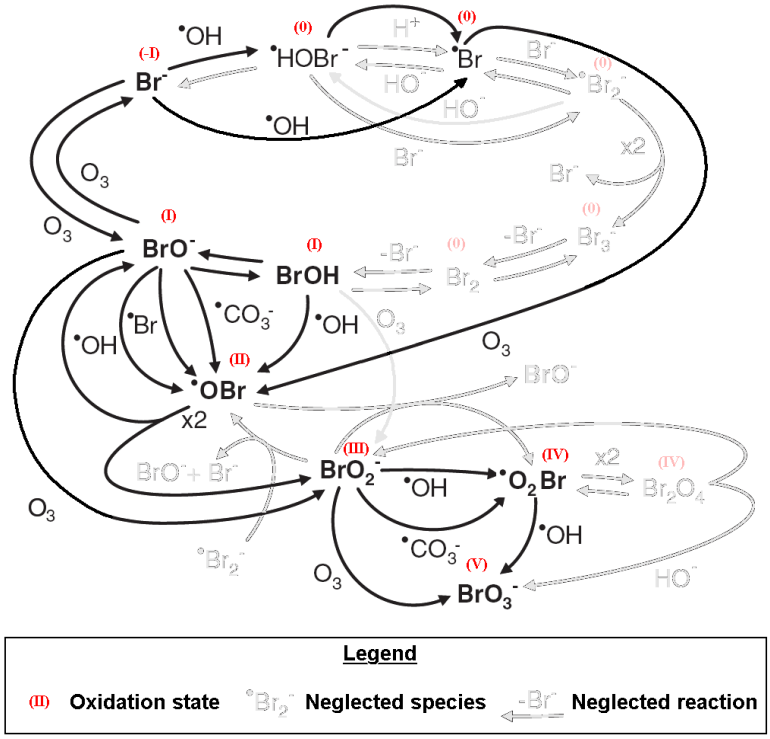

Figure 11 **Représentation schématique du mécanisme de formation des ions bromates**

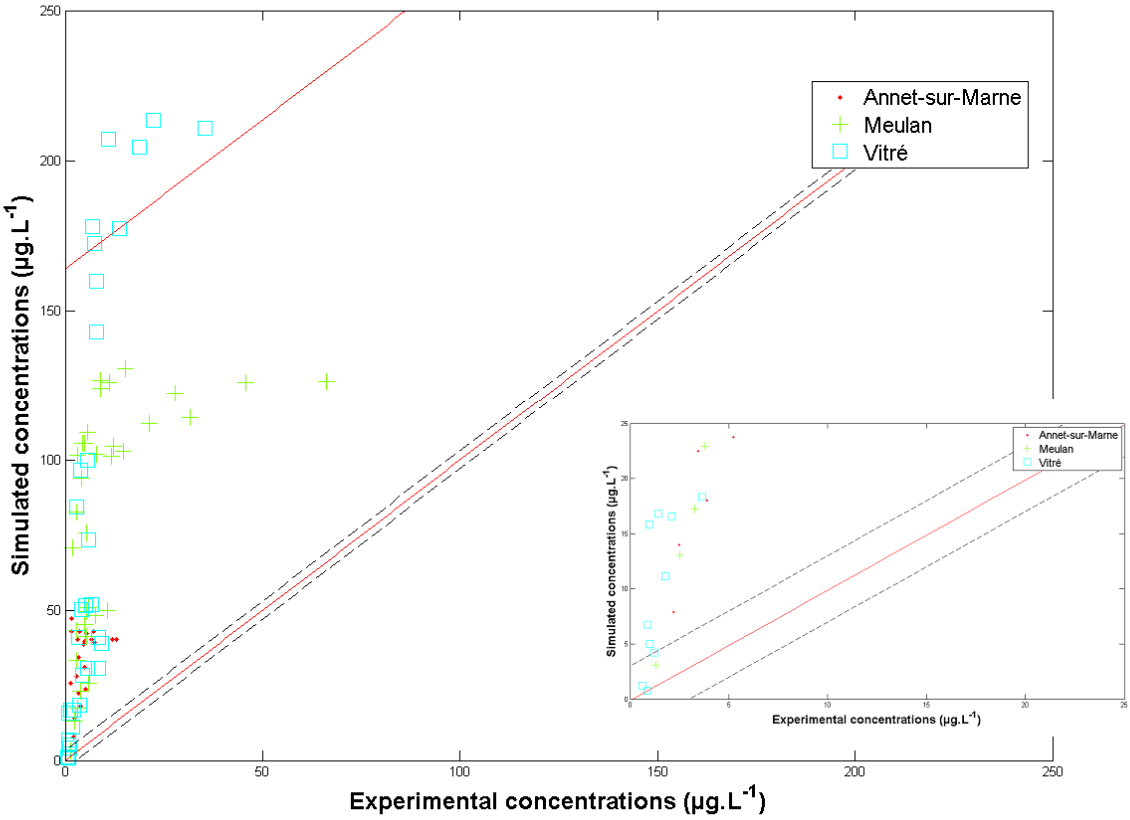

Figure 12 **Comparaison des concentrations simulées et expérimentales de bromates avec un modèle unique, valeurs cinétiques de la littérature; zoom sur les concentrations inférieures à 25 µg.L^{-1}.**

Les résultats présentés en figure **12** montrent que le modèle surestime grandement la formation des bromates, à des degrés divers selon l'eau considérée. Le ratio entre les valeurs simulées et les valeurs expérimentales varie ainsi entre 3 (eau de Meulan) et 10 (eau de Vitré). Ces valeurs sont comparables avec celles obtenues dans de précédentes études ([Westerhoff *et al.*, 1998a] ;[Kim *et al.*, 2007]). Il apparaît donc essentiel d'inclure la MON dans le mécanisme de formation des bromates. En d'autres termes, on ne peut appliquer un modèle chimique unique pour prédire la formation des bromates dans les eaux naturelles.

5.4. Prise en compte de la MON dans la formation des bromates

5.4.1. Approches précédentes

Différents auteurs ont proposé des solutions pour tenir compte de l'effet de la MON. Ils ont généralement ajouté des réactions faisant intervenir l'acide hypobromeux ou sa base conjuguée (réactions **13** à **16**). D'autres approches ont consisté à inhiber certains radicaux bromés du mécanisme de formation des bromates (réactions **17** et **18**). Ces approches sont récapitulées dans le tableau **6**.

Tableau 6 Réactions impliquant la MON dans la formation des bromates

Réaction		Valeur de la constante cinétique ($M^{-1}.s^{-1}$)	Eau	Référence
$BrOH + NOM \rightarrow Br - organics$	**(13)**	*Pas de données*	Fractions organiques	[Siddiqui et Amy, 1993] ; [Huang *et al.*, 2004]
$BrO^- + NOM \rightarrow products + Br^-$	**(14)**	5	Eau synthétique avec fractions	[Westerhoff *et al.*, 1998a]
$BrOH + NOM \rightarrow products + Br^-$	**(15)**	5	Eau synthétique avec fractions	[Westerhoff *et al.*, 1998a]
$BrOH + NOM \rightarrow \gamma Br^- + (1-\gamma)TOBr$	**(16)**	3.10^5	Eau filtrée sable de la rivière Ohio	[Kim, 2004]
$^{\bullet}Br + NOM \rightarrow Br^-$	**(17)**	10^9 (ajusté pour [NOM] = 2.10^{-6} M)	Eau filtrée sable (Maisons-Laffitte et Zürich)	[Pinkernell et von Gunten, 2001]
$^{\bullet}OBr + NOM \rightarrow BrOH + products$	**(18)**	5.10^3		[Westerhoff *et al.*, 1997]

Outre les réactions faisant intervenir la MON (ou une fraction de la MON définie comme fraction du COT), [Westerhoff *et al.*, 1998a] ont également ajusté la cinétique de la première oxydation moléculaire des ions bromures (réaction **19**), faisant passer la valeur de la constante cinétique de 160 à 50 $M^{-1}.s^{-1}$.

$$Br^- + O_3 \rightarrow BrO^- + O_2 \qquad \textbf{(19)}$$

5.4.2. Approche proposée

Contrairement à la démarche qui a été adoptée lors de l'étude de l'influence de la MON sur la décomposition de l'ozone (chapitre **4**), le but était ici de proposer un modèle simple à calibrer, sans viser à représenter exactement le comportement chimique des espèces en présence. Par conséquent, s'appuyant sur l'idée déjà développée par [Westerhoff *et al.*, 1998a], nous avons décidé d'ajuster la cinétique d'une étape d'oxydation moléculaire (réaction **20**). Ce choix a pour avantage de ne pas nécessiter la détermination d'une concentration initiale de MON réductrice. Au total, seuls deux paramètres ont été optimisés (facteur de fréquence et énergie d'activation).

$$BrO_2^- + O_3 \xrightarrow{k_{Brox}} BrO_3^- + O_2 \qquad \textbf{(20)}$$

Notre choix s'est porté sur la dernière oxydation moléculaire car on s'aperçoit que les bromates sont essentiellement formés par voie moléculaire lors du passage Br(III) → Br(V) – résultats non montrés – et que le contrôle de la formation des bromates est très aisé via la cinétique de la réaction **20**. Par ailleurs, le choix d'une réaction terminale permet de limiter l'impact d'une modification de vitesse de réaction sur l'ensemble du mécanisme. Une accumulation anormale de BrO_2^- ne devrait pas déstabiliser le mécanisme sachant que BrO_2^- ne peut qu'être oxydé pour former des bromates, par voie moléculaire ou radicalaire.

5.4.3. Résultats

A titre illustratif, nous donnons dans ce paragraphe les résultats du modèle de prédiction pour la formation des bromates avec deux échantillons d'eau : Annet-sur-Marne et Vitré, respectivement présentés en figures **13** et **14**. On constate que les prédictions du modèle pour l'eau d'Annet-sur-Marne sont excellentes, puisque toujours situées dans l'erreur expérimentale (±3 µg.L^{-1}). On pourra regretter toutefois que le spectre de concentrations ne soit pas plus étendu. Les résultats de Vitré sont également intéressants car ils montrent que le modèle ne peut être valide sur toute une gamme de concentration (de 0 à 35 µg.L^{-1}) : le modèle surévalue la formation de bromates pour les hautes concentrations expérimentales. Avec l'eau de Meulan, le modèle sous-évalue les hautes concentrations expérimentales. Ce phénomène se répète avec les échantillons prélevés à une autre saison.

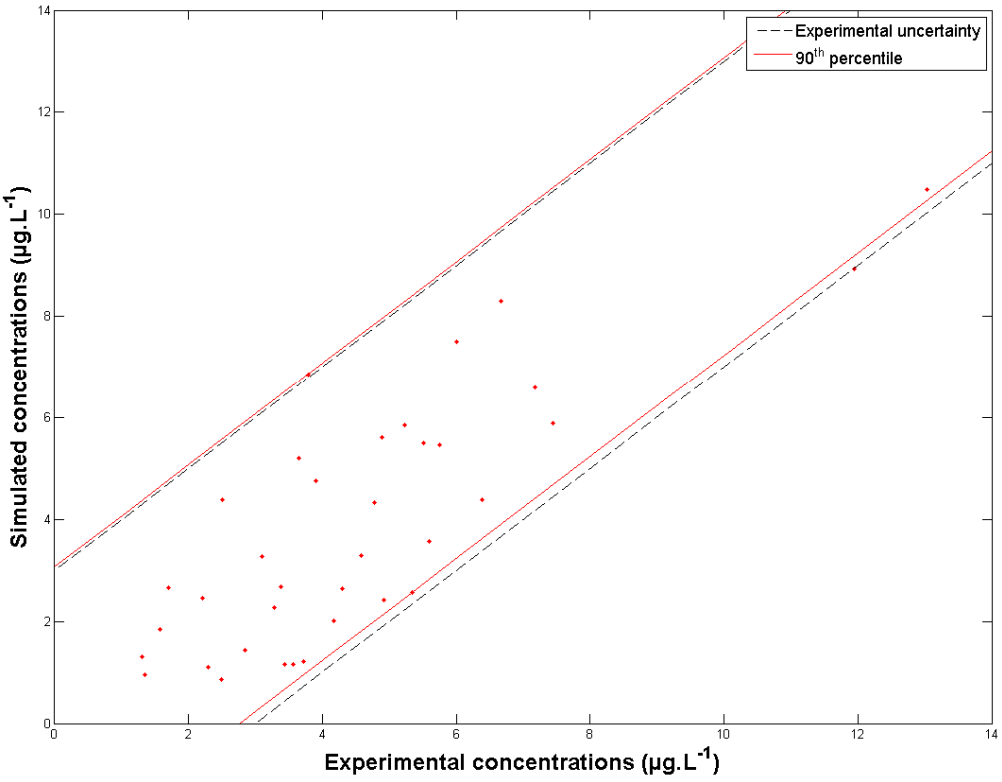

Figure 13 Comparaison des concentrations simulées et expérimentales en bromates, eau d'Annet-sur-Marne

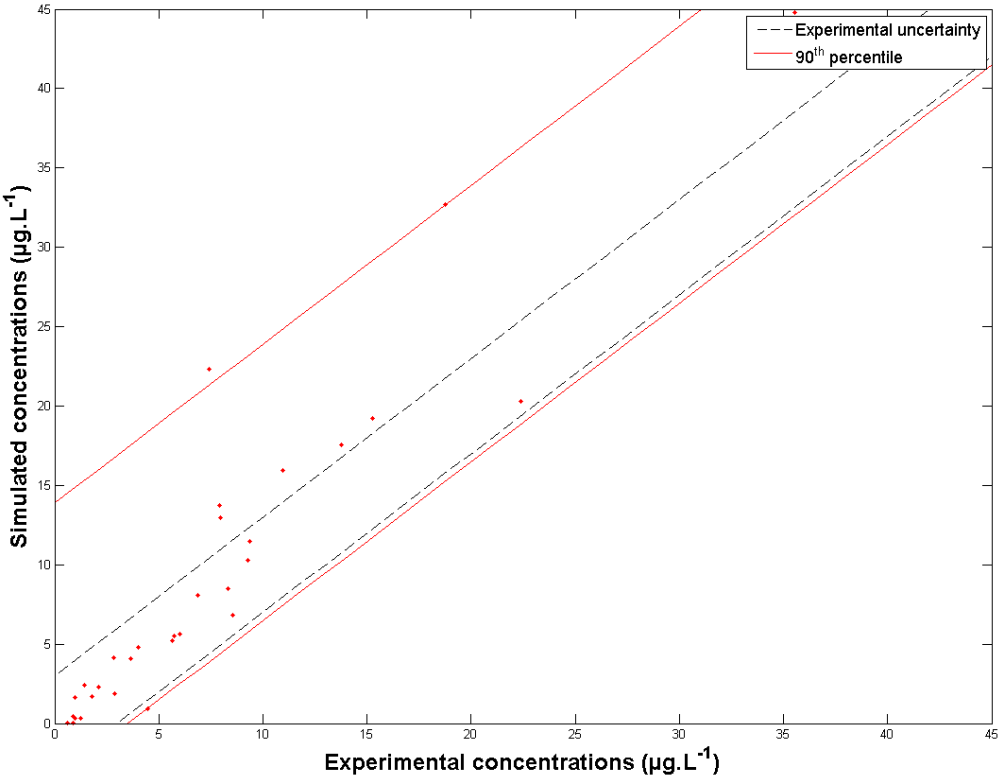

Figure 14 Comparaison des concentrations simulées et expérimentales en bromates, eau de Vitré

5.5. Conclusion

Sur la base d'un modèle validé pour les concentrations en espèce oxydantes, nous nous sommes intéressés dans ce chapitre à proposer un modèle mécanistique prédictif pour la formation des ions bromates. Nous nous sommes appuyés sur un jeu de données assez conséquent : environ 300 concentrations mesurées sur six échantillons d'eau provenant de trois ressources à deux saisons.
Les résultats de cette étude ont montré que :

- Les modèles mécanistiques pour la formation de bromates doivent inclure la MON et doivent être calibrés pour chaque échantillon d'eau,
- Nous avons simplifié le modèle de formation des bromates et proposé une manière simple de le calibrer pour prendre en compte l'influence de la MON,
- Le modèle donne des résultats précis pour des concentrations inférieures à 20 $\mu g.L^{-1}$ (68% des points simulés se situent dans l'incertitude expérimentale).

6. MODELISATION D'UNE UNITE INDUSTRIELLE D'OZONATION – ETUDE DE CAS A ANNET-SUR-MARNE

6.1. Introduction

Après avoir déterminé les performances des modèles prédictifs (O_3, $^{\bullet}OH$ et BrO_3^-) sur la base de résultats de laboratoire, ce chapitre s'intéresse à l'application des modèles à l'échelle industrielle. L'idée est ici de calibrer à l'échelle du laboratoire et de valider ensuite à l'échelle industrielle. L'avantage de cette démarche est qu'elle ne requiert pas d'expériences de calibration sur site. Par ailleurs, les études de modélisation à échelle industrielle s'appuient généralement sur des modèles empiriques ou semi-empiriques ([Audenaert *et al.*, 2010] ; [Zhang *et al.*, 2007] ; [Rietveld *et al.*, 2008]). Par conséquent, il n'existe pas de données sur l'application d'un modèle cinétique mécanistique à une cuve industrielle, ce qui est présenté dans ce chapitre.

La calibration des modèles chimiques se fait comme précédemment en s'appuyant sur des manipulations de paillasse. La calibration du schéma systémique décrivant l'hydraulique de la cuve s'appuie sur les courbes de DTS (Distribution de Temps de Séjour). Les DTS ont été calculées par CFD lors d'études hydrauliques précédentes. Nous présenterons ces étapes et nous discuterons les résultats en examinant particulièrement la validation des résultats à l'échelle de la cuve industrielle.

6.2. Matériels et méthodes

L'unité d'ozonation étudiée se compose de deux cuves de volumes à peu près égaux (235 et 252 m^3 pour la première et la seconde cuve). Une vue d'ensemble est proposée figure **15**. Des points de piquage ont été installés tout au long du trajet de l'eau de manière à caractériser la décomposition de l'ozone et la formation des bromates au sein de l'unité. Les analyses en routine de l'eau sortant et entrant dans l'unité ont également été enregistrées via la supervision. L'ozone gazeux a également été mesuré (cf. figure **15**). Pour tous les points de prélèvements, le temps de rétention hydraulique pour un débit de 1600 $m^3.h^{-1}$ est donné sur la figure **15**. Les points de piquage ont été placés de manière optimale pour collecter de l'eau issue du flux principal, s'assurant ainsi de la « fraîcheur » de l'eau.

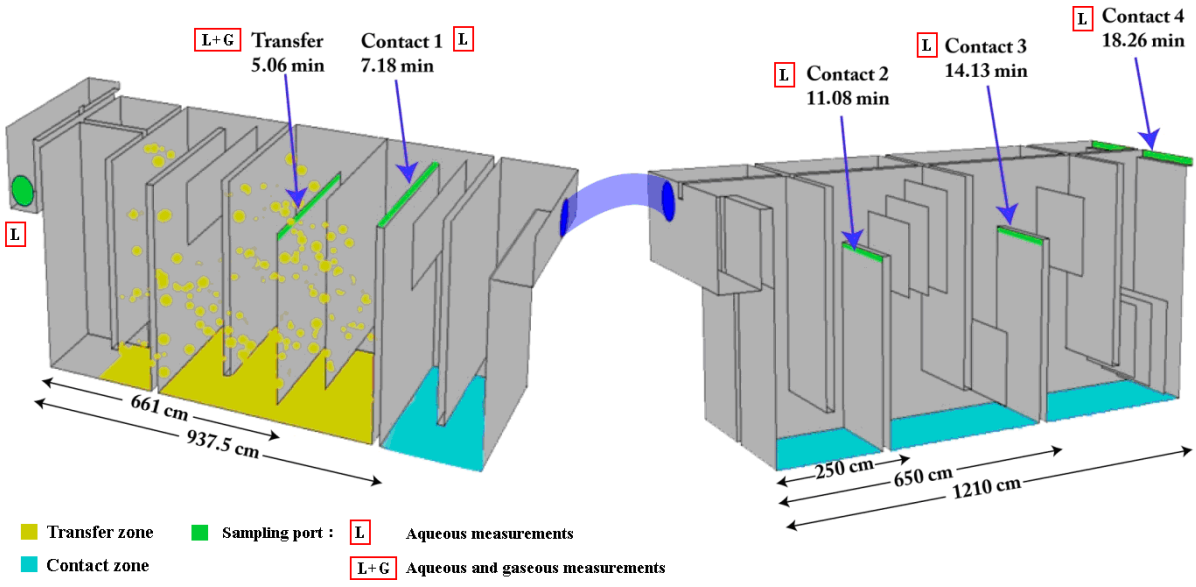

Figure 15 Vue de l'unité d'ozonation

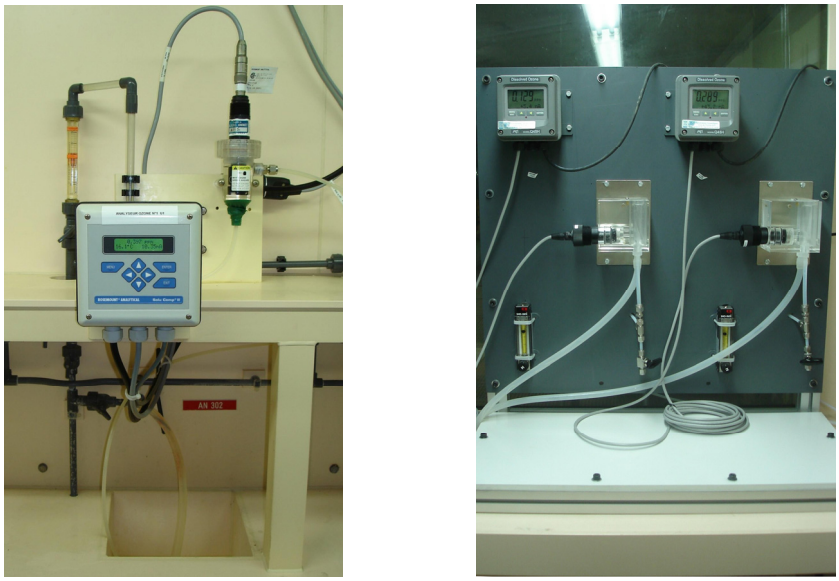

Figure 16 Les deux types d'analyseurs d'ozone utilisés dans cette étude ; Solu Comp II (Rosemount Analytical) à gauche, Q 45H/64 (ATI) à droite

Un appareillage conséquent comprenant des pompes, des analyseurs d'ozone aqueux et une bride pour les prélèvements gazeux a été installé. Nous donnons en figure **16** les photographies des deux types d'analyseurs en ligne d'ozone aqueux utilisés. Les mesures étaient automatiquement enregistrées dans le logiciel de supervision de l'usine. En outre, de nombreux essais de répétabilité et de comparaison de mesures ont été effectués de manière à s'assurer de la validité des mesures. En particulier, nous avons montré qu'il n'y avait pratiquement pas de consommation d'ozone dans les tuyaux d'amenée d'eau jusqu'aux analyseurs en ligne. Les concentrations en bromates étant mesurées dans deux laboratoires différents, nous avvons constaté la cohérence des mesures.

Tableau 7 Résumé des conditions expérimentales pendant l'étude sur site

Caractéristiques de l'eau

	COT ($mg.L^{-1}$)	$[Br^-]$ ($\mu g.L^{-1}$)	A_T ($meq.L^{-1}$)	T (°C)	pH
Minimum	1,50	30,00	3,58	16,60	7,20
Médian	1,70	32,00	3,67	20,60	7,50
Maximum	1,80	41,00	3,78	22,80	7,50

Conditions de process

	Contrôlées directement		*Définies par la supervision*		
	Q_l ($m^3.h^{-1}$)	Consigne résiduel ($mg.L^{-1}$)	$[O_3]_g$ ($g.Nm^{-3}$)	Q_g ($Nm^3.h^{-1}$)	Dose O_3($mg.L^{-1}$)
Minimum	990	0,20	10,20	61,30	0,73
Médian	1661	0,30	19,80	73,10	0,83
Maximum	1851	0,40	19,90	149,00	1,12

Les conditions expérimentales (qualité d'eau et conditions de process) des quatre mois d'expérimentations sur site sont compilées dans le tableau **7**. Deux périodes expérimentales ont été observées : juillet-août 2009, puis septembre-octobre 2009. Pendant la première période, nous avons travaillé à débit d'eau élevé (entre 1480 et 1850 $m^3.h^{-1}$) et nous avons testé trois consignes pour le résiduel d'ozone : 0,2 ; 0,3 et 0,4 $mg.L^{-1}$. Les trois mêmes consignes ont été testées à débit d'eau faible (entre 990 et 1100 $m^3.h^{-1}$) lors de la deuxième période expérimentale. On trouvera les conditions expérimentales détaillées en Annexe **J**.

Par ailleurs, des expériences réplicats de la première période ont été menées lors de la deuxième période. Les résultats ont montré que si les profils d'ozone étaient comparables, la formation de bromates avait en revanche fortement diminué entre les deux périodes.

6.3. Résultats

6.3.1. Résultats de calibration

La calibration a lieu en laboratoire : des expériences de paillasse sont menées et le modèle de cinétique chimique est optimisé selon la procédure décrite dans le chapitre **4** ; à partir des courbes DTS obtenues à l'aide d'une étude CFD [Guitard, 2007], nous calibrons un schéma systémique. Dans ce paragraphe, nous ne présenterons pas les résultats de calibration du modèle de cinétique chimique (influence de la MON) qui sont similaires à ce qui a été présenté précédemment. En revanche, nous présentons en figure **17** les courbes de DTS obtenues par l'étude CFD et par le schéma systémique proposé. L'ajustement s'est fait cuve après cuve à l'aide de DTS intermédiaires. On notera le très bon ajustement des courbes.

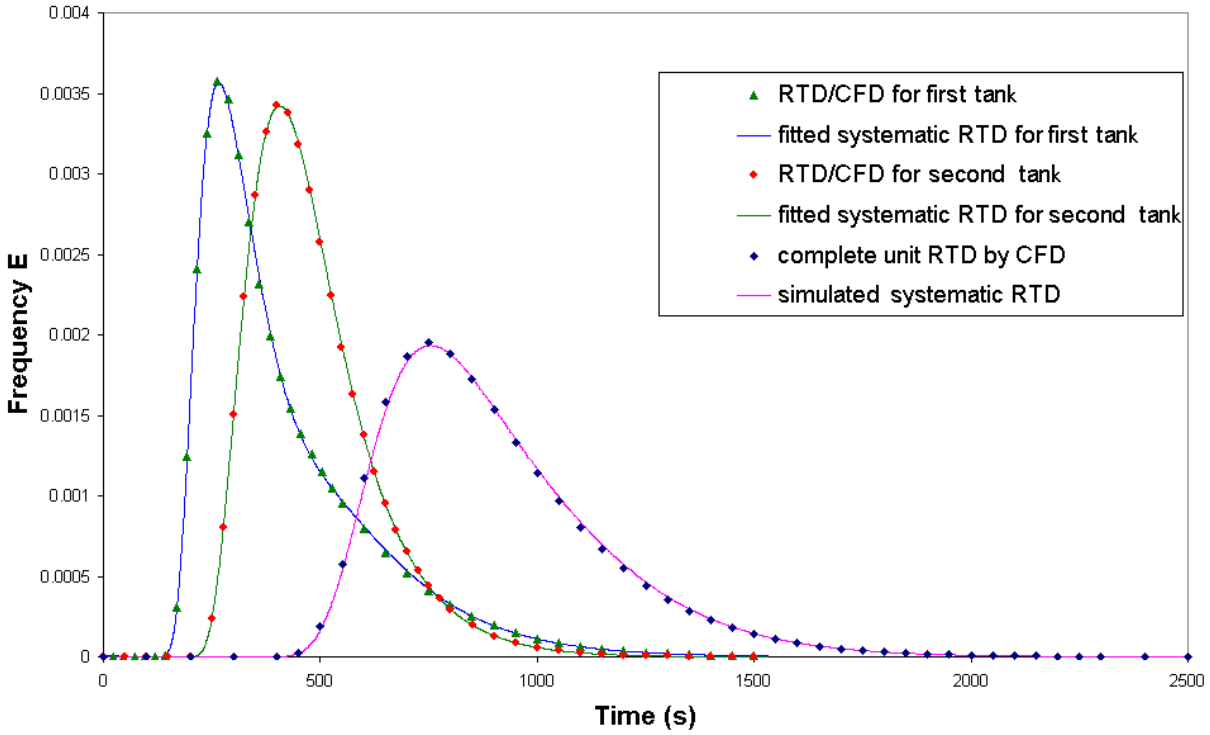

Figure 17 Courbes de DTS (RTD) obtenues avec la CFD et avec le schéma systémique

6.3.2. Résultats de validation

Nous présentons dans les figures **18** et **19** les résultats de validation obtenus avec les concentrations expérimentales de l'étude de terrain. Pour les concentrations en bromates (figure **19**), seuls les relevés expérimentaux de la première période ont été considérés car une forte diminution de la formation de bromates avait été observée expérimentalement, ce qui ne permettait pas à un même modèle d'être applicable pour les deux périodes. On notera la bonne correspondance des concentrations simulées et expérimentales pour l'ozone, malgré une tendance à sous-évaluer les hautes concentrations expérimentales. Pour les bromates en revanche, si la tendance est bonne, de nombreuses concentrations ont été surestimées.

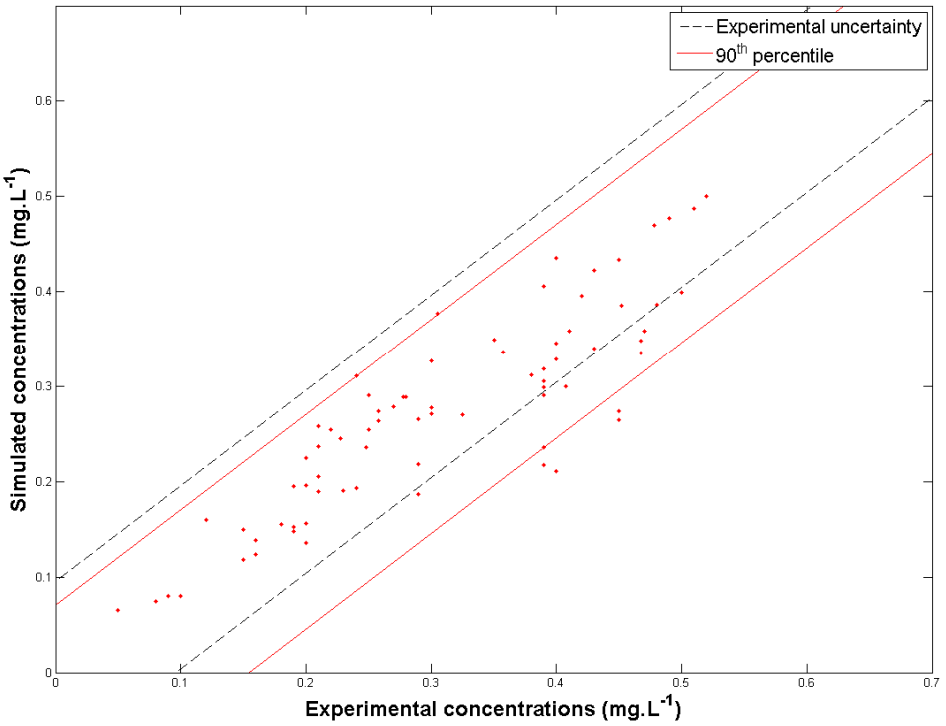

Figure 18 Comparaison des concentrations simulées et expérimentales en ozone, unité industrielle, calibration en labo

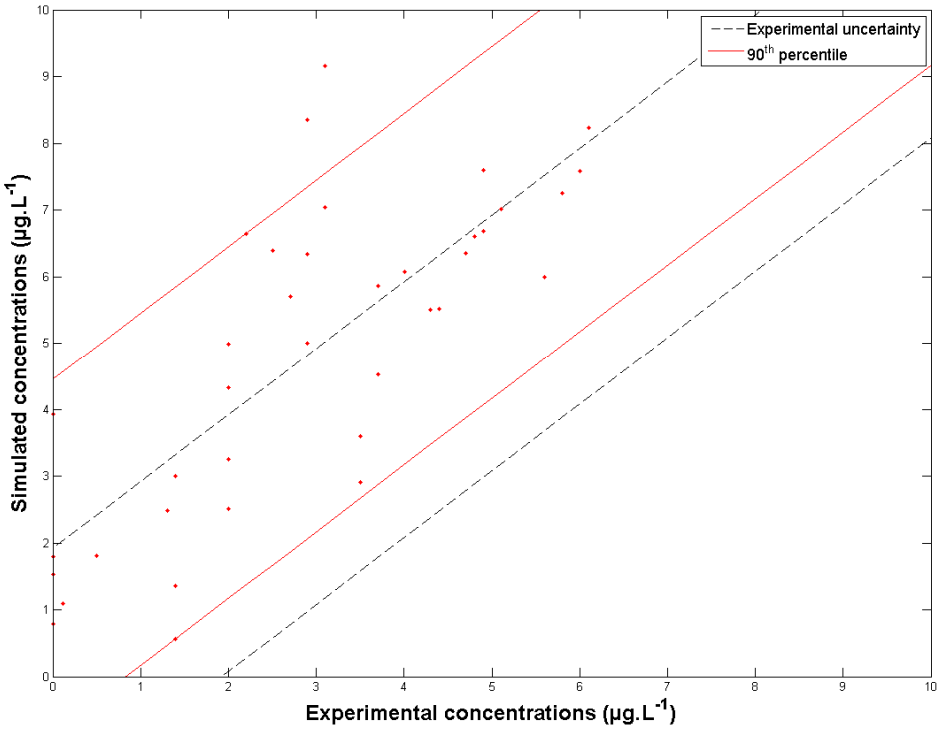

Figure 19 Comparaison des concentrations simulées et expérimentales en bromate, première période expérimentale, unité industrielle, calibration en labo

De manière à pouvoir modéliser les concentrations de bromates de la deuxième période, nous décidons de réajuster le modèle de formation des bromates directement à partir de concentrations expérimentales obtenues sur l'unité industrielle d'ozonation. La simplicité d'ajustement du modèle permet ainsi de ne considérer qu'un profil de concentration (5 points) pour ajuster au mieux la cinétique de la réaction $BrO_2^- + O_3 \xrightarrow{k_{Brox}} BrO_3^- + O_2$ pour les expériences de la première période expérimentale. Pour la deuxième période expérimentale, un seul point a suffi pour réajuster le modèle valablement pour les 34 points restants. Cette opération est extrêmement simple à réaliser et n'a duré que 15 minutes pour tous les calculs de simulation.

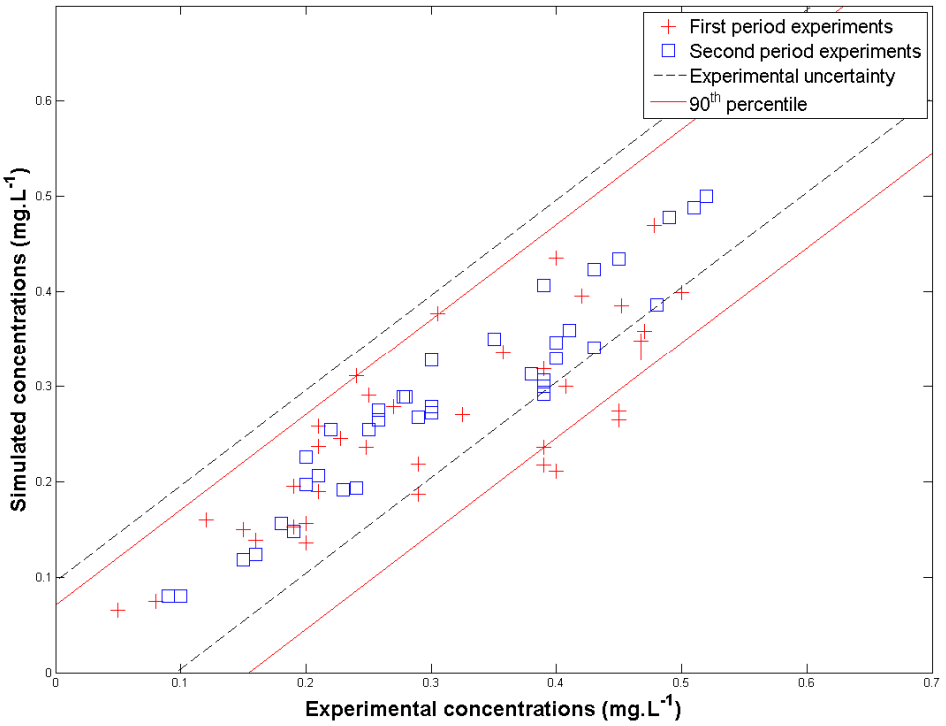

Figure 20 Comparaison des concentrations simulées et expérimentales en ozone, unité industrielle, calibration en labo

La figure **20** reprend les résultats de simulations pour l'ozone présentés en figure **18**, mais en faisant apparaître la distinction entre première et seconde périodes. En regard, nous présentons en figure **21** les résultats de simulation pour la formation des ions bromates. Nous avons considéré à peu près 7% des points expérimentaux pour réajuster le modèle. On notera la différence de niveau de production en ions bromates entre les deux périodes. Tous les résultats expérimentaux sont présentés en Annexe **K**.

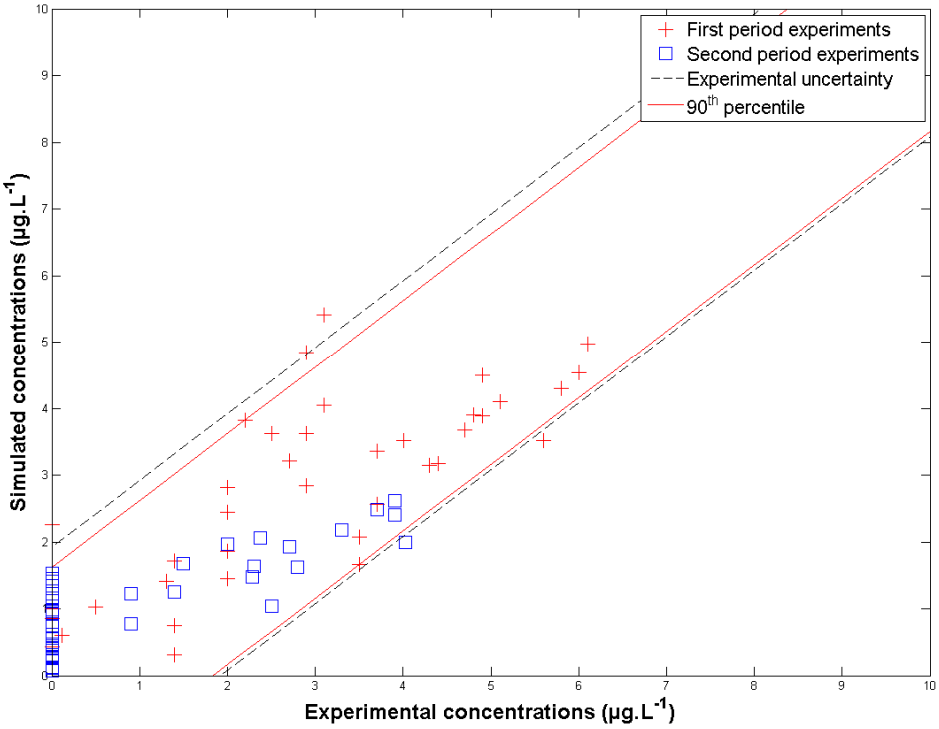

Figure 21 Comparaison des concentrations simulées et expérimentales en bromate, première période expérimentale, unité industrielle, réajustement avec des données de site

6.4. Conclusion

Une étude de cas sur l'unité industrielle d'ozonation de l'usine d'Annet-sur-Marne a été menée. La cuve a été complètement équipée en appareils d'analyse et de nombreuses variations de conditions de process ont été testées. Nous nous sommes plus particulièrement intéressés à faire varier le débit d'eau entrant et la consigne en ozone résiduel. La procédure de modélisation est particulièrement intéressante et ambitieuse dans la mesure où la calibration des modèles, tant chimique qu'hydraulique, s'appuie sur des résultats obtenus en laboratoire, et que le modèle est ensuite validé à partir de mesures de site.

On retiendra les résultats suivants :

- La procédure de modélisation (calibration en labo et validation sur site) marche tout à fait avec l'ozone (75% des points simulés situés dans l'erreur expérimentale) et donne de bonnes indications sur le niveau de bromates formés,
- Il est souhaitable de réajuster périodiquement le modèle de formation des ions bromates avec des mesures de site. En ajustant deux fois le modèle sur quatre mois, plus de 90% des prédictions du modèle se sont situées dans l'erreur expérimentale,
- Le modèle a été testé pour de nombreuses conditions de process et est robuste vis-à-vis d'un changement de celles-ci,
- La modélisation du transfert n'a pas donné totale satisfaction et devra être perfectionnée.

CONCLUSION

Cette étude propose une démarche complète de modélisation, depuis les résultats de paillasse jusqu'à l'application sur unité industrielle. Une attention particulière a été accordée à documenter et vérifier chaque étape du développement. Nous avons ainsi proposé des méthodes expérimentales, des techniques numériques et ensuite interprété les résultats à l'aune de ce qui avait été fait par ailleurs. Résumons les principales conclusions de ce travail :

- Un modèle quasi-mécanistique pour le rôle de la MON dans la décomposition de l'ozone et la génération des radicaux hydroxyles a été proposé. Le modèle est capable de reproduire les concentrations expérimentales observées, même lors de changements de temps de contact, de pH, de température, de dose d'ozone, de concentration de MON et de nature de MON (présence d'un inhibiteur). Une bonne correspondance des résultats simulés et expérimentaux a été notée pour 75% des expériences. Le modèle est valide pour de nombreuses eaux. Seules les eaux peu alcalines ($A_T < 0,3$ meq.L^{-1}) et fortement chargées en matière organiques ont des profils radicalaires qui ne peuvent être modélisés correctement.
- Une procédure simplifiée de calibration pour le modèle décrivant le rôle de la MON a été proposée. Cette procédure donne de très bons résultats (*i.e.* comparables avec ceux obtenus quand beaucoup plus d'expériences sont utilisées pour calibrer) et ne nécessite que 6 expériences de laboratoire. Au total (avec les calculs d'optimisation), le modèle peut être calibré en une semaine.
- Les expériences sur la formation des ions bromates en eaux naturelles ont montré que la MON joue un rôle crucial dans le mécanisme et doit à ce titre figurer, de manière implicite ou explicite, dans le modèle de formation des bromates. Nous avons proposé dans cette étude un modèle simple à calibrer et qui donne de bons résultats pour des concentrations inférieures à 20 µg.L^{-1} : 68% des concentrations simulées correspondent aux observations (à l'incertitude de mesure près).
- Les résultats collectés sur une unité industrielle d'ozonation lors d'une étude terrain ont montré que les modèles utilisés peuvent être calibrés à partir de résultats obtenus en labo ou avec une étude CFD et ensuite utilisés en validation sur une unité industrielle. La démarche fonctionne parfaitement bien pour l'ozone. Si l'on souhaite modéliser la formation des ions bromates, il est préférable de réajuster régulièrement le mécanisme de formation. Cette opération est simple à réaliser et donne de bons résultats.

Les perspectives de ce travail sont les suivantes :

- L'inhibition radicalaire par la MON doit encore être étudiée. C'est probablement ce point qui a empêché le modèle d'être valide pour les eaux peu alcalines et fortement organiques.
- Le rôle de la MON dans la formation des bromates peut être certainement pris en compte de manière plus juste au niveau chimique. Il serait intéressant de comparer notre modèle avec des modèles faisant intervenir l'acide hypobromeux.
- Les résultats de l'étude de cas devront être étendus, en durée, ou en considérant une autre usine.
- L'application aux micropolluants permettra de valider encore un peu plus la démarche sur la modélisation des profils d'ozone et de radicaux hydroxyles.

Bibliographie

- **Acero J. L.** et **von Gunten U.**, (2000). Influence of Carbonate on the Ozone/Hydrogen Peroxide Based Advanced Oxidation Process for Drinking Water Treatment, *Ozone: Science and Engineering*, Vol. **22**, pp. 305-328.
- **Audenaert W.T.M., Callewaert M., Nopens I., Cromphout J., Vanhoucke R., Dimoulin A., Dejans P., van Hulle S.W.H.**, (2010). Full-scale modelling of an ozone reactor for drinking water treatment, *Chemical Engineering Journal*, Vol. **157**, pp. 551-557.
- **Bader H.** et **Hoigné J**., (1981). Determination of Ozone in Water by the Indigo Method, *Water Research*, Vol. **15**, pp. 449-456.
- **Bartrand T. A.,** (2007). High resolution experimental studies and numerical analysis of fine bubble ozone disinfection contactors, Ph.D. thesis, Drexel University, U.S.A.
- **Beltrán F. J.,** (2004). Ozone Reaction Kinetics for Water and Wastewater Systems, *LEWIS Publishers*, Washington D.C., U.S.A.
- **Bezbarua B. K.,** (1997). Modeling Reactions of Ozone with NOM, Ph.D. thesis, University of Massachusetts Amherst, USA.
- **Bonacquisti T. P**., (2006). A drinking water utility's perspective on bromide, bromate, and ozonation, *Toxicology*, Vol. **221**, pp. 145-148.
- **Bühler R.E., Staehelin J., Hoigné J.**, (1984). Ozone Decomposition in Water Studied by Pulse Radiolysis. 1. HO_2 / O_2^- and HO_3 / O_3^- as Intermediates, *Journal of Physical Chemistry*, Vol. **88**, pp. 2560-2564.
- **Cho M., Kim H., Cho S. H., Yoon J.**, (2003). Investigation of Ozone Reaction in River Waters causing Instantaneous Ozone Demand, *Ozone: Science and Engineering*, Vol. **25**, pp. 251-259.
- **Do-Quang, Z., Cockx, A., Liné, A., Roustan, M.,** (1999). Computational fluid dynamics applied to water and wastewater treatment facility modeling, *Environmental Engineering and policy*, Vol. **1**, pp. 137-147.
- **Dumeau de Traversay C.**, (2000). De la mécanique des fluides numérique à l'approche systémique: application aux réacteurs d'oxydation en potabilisation, Ph.D. thesis ENSC-R, France.
- **Elovitz M. S.** et **von Gunten U.**, (1999). Hydroxyl Radical/Ozone Ratios during Ozonation Processes. I. The R_{ct} Concept, *Ozone: Science and Engineering*, Vol. **21**, pp. 239-260.
- **Fieller N.**, (2004). Statistical Modelling and Computing, *Course of the University of Sheffield, Department of Probability and Statistics*, Available at: http://www.nickfieller.staff.shef.ac.uk/sheff-only/StatModall05.pdf
- **Gordon G.**, (1995). The Chemical Aspects of Bromate Control in Ozonated Drinking Water Containing Bromide Ion, *Water Supply*, Vol. **13**, pp. 35-43.
- **Goslan E. H., Fearing D. A., Banks J., Wilson D., Hills P., Campbell A. T., Parsons S. A.,** (2002). Seasonal variations in the disinfection by-product precursor profile of a reservoir water, *Journal of Water Supply: Research and Technology – AQUA*, Vol. **51**, pp. 475– 482.
- **Guitard M.,** (2007). Optimisation hydraulique des cuves d'ozonation de l'usine d'Annet-sur-Marne – Rapport final, Veolia Eau – Compagnie Générale des Eaux.
- **Gurol M. D.** et **Singer P. C.,** (1982). Kinetics of Ozone decomposition: A Dynamic Approach, *Environmental Science and Technology*, Vol. **16**, pp. 377-383.
- **Hawthorn R. D.,** (1974). Afterburner Catalysts-effects of Heat and Mass Transfer Between Gas and Catalytic Surface, *AIChE Symposium Series*, Vol. **70**, pp. 428-438.
- **Hikita H., Asai S., Tanigawa K., Segawa K., Kitao M**., (1981). The volumetric liquid-phase mass transfer coefficient in bubble columns, *Chemical Engineering Journal*, Vol. **22**, pp. 61-69.
- **Hill M. C.** et **Osterby O.,** (2003). Determining extreme parameter correlation in ground water models, *Ground Water*, Vol. **41**, pp. 420-430.
- **Hoigné J.** et **Bader H.,** (1976). The Role of Hydroxyl Radical Reactions in Ozonation Processes in Aqueous Solutions, *Water Research*, Vol. **10**, pp. 377-386.
- **Huang W.-J., Chen L.-Y., Peng H.-S**., (2004). Effect of NOM characteristics on brominated organics formation by ozonation, *Environment International*, Vol. **29**, pp. 1049-1055.
- **Jarvis P., Parsons S. A., Smith R.,** (2007). Modeling Bromate Formation During Ozonation, *Ozone: Science and Engineering*, Vol. **29**, pp. 429-442.
- **Jeppsson U.,** (1996). Modelling Aspects of Wastewater Treatment Processes, Ph.D. thesis, Lund University, Sweden. Available at: http://www.iea.lth.se/~ielulf/publications/phd-thesis/PhD-thesis.pdf
- **Kim J.-H.,** (2004). Integrated Optimization of Cryptosporidium Inactivation and Bromate formation Control in Ozone Contactors. *Presentation at the Gwangju Institute of Science and Technology*.
- **Kim J.-H., Elovitz M. S., von Gunten U., Shukairy H. M., Mariñas B. J.,** (2007). Modeling Cryptosporidium parvum oocyst inactivation and bromate in a flow-through ozone contactor treating natural water, *Water Research*, Vol. **41**, pp. 467-475.
- **Kim J.-H., von Gunten U., Mariñas B. J.**, (2004). Simultaneous Predicion of *Cryptosporidium Parvum Oocyst* Inactivation and bromate Formation during Ozonation of Synthetic Waters, *Environmental Science and Technology*, Vol. **38**, pp. 2232-2241.
- **Kittrell J. R., Hunter W. G., Watson C. C.,** (1966). Obtaining precise Parameter Estimates for nonlinear catalytic rate models, AIChE Journal, Vol. **12**, pp. 5-10.

- **Lagarias J. C., Reeds J. A., Wright M. H., Wright P. E.**, (1998). Convergence Properties of the Nelder-Mead Simplex Method in Low Dimensions, *SIAM Journal of Optimization*, Vol. **9**, pp. 112-147.
- **Langlais B., Reckhow D. A., Brink D.R.,** (1991). Ozone in Water Treatment: Application and Engineering, *LEWIS Publishers*, Washington D.C., U.S.A.
- **Leenheer J. A.** et **Croué J.-P.**, (2003). Characterizing Aquatic Dissolved Organic Matter, *Environmental Science and Technology*, Vol. **37**, pp. 19A-26A.
- **Legendre P.,** (2009). Cours de Biostatistique I, Université de Montréal, available at: http://www.bio.umontreal.ca/legendre/BIO2041/index.html.
- **Mandel P.,** (2008). Modelling Micropollutant Removal by Ozonation and Chlorination in potable Water Treatment—Experimental Report, *TECHNEAU Technical Deliverable D.2.4.2.5.*
- **Mandel P., Wolbert D., Roche P., Pham H.-H., Bréant P.,** (2009). A modelling procedure for on-site ozonation steps in potable water treatment, *Water Science and Technology: Water Supply*, Vol. **9**, pp. 459-467.
- **McCay M. D., Beckman R. J., Conover W. J.,** (1979). A Comparison of Three Methods for Selecting Values of Input Variables in the Analysis of Output from a Computer Code, *Technometrics*, Vol. **21**, pp. 239-245.
- **Mizuno T., Park N.-S., Tsuno H., Hidaka T.,** (2004). Development of the Simulation Model to Predict Dissolved Ozone Concentration for a Real Water Treatment Plant, *Environmental Engineering Research*, Vol. **41**, pp. 237-246.
- **Mizuno T., Tsuno H., Yamada H.,** (2007b). Effect of Inorganic Carbon on Ozone Self-Decomposition, *Ozone: Science and Engineering*, Vol. **29**, pp. 31-40.
- **Mizuno T., Tsuno H., Yamada H.,** (2007c). Development of Ozone Self-Decomposition Model for Engineering Design, *Ozone: Science and Engineering*, Vol. **29**, pp. 55-63.
- **Morioka T., Motoyama B., Hoshikawa H., Murakami A., Okada M. Moniwa T.,** (1993). Kinetic Analysis on the Effects of Dissolved Inorganic and Organic Substances in Raw Water on the Ozonation of Geosmin and 2-MIB, *Ozone: Science and Engineering*, Vol. **15**, pp. 1-18.
- **Nelder J. A.** et **Mead R.,** (1965). A Simplex Method for Function Minimization, *The Computer Journal*, Vol. **7**, pp. 308-313.
- **Park H.-S., Hwang T.-M., Kang J. W., Choi H., Oh H.-J.,** (2001).Characterization of raw water for the ozone application measuring ozone consumption rate, *Water Research*, Vol. **35**, pp. 2607-2614.
- **Pinkernell U.** et **von Gunten U.**, (2001). Bromate minimization during Ozonation: Mechanistic Considerations, *Environmental Science and Technology*, Vol. **35**, pp. 2525-2531.
- **Pohjanpalo H.,** (1978). System Identifiability Based on Power Series Expansion of the Solution, *Mathematical Biosciences*, Vol. **41**, pp. 21-33.
- **Poznyak T.** et **Araiza B.,** (2005). Ozonation of Non-Biodegradable Mixtures of Phenol and Naphtalene Derivatives in Tanning Wastewaters, *Ozone: Science and Engineering*, Vol. **27**, pp. 351-357.
- **Rietveld L.C., van der Helm A.W.C., van Schagen K.M., van der Aa L.T.J., van Dijk J.C.,** (2008). Integrated simulation of drinking water treatment, *J. Wat. Supp.: Res. & Technol.-AQUA*, Vol. **57**, pp. 133-141.
- **Roustan M., Debellefontaine H., Do-Quang Z., Duguet J.-P.,** (1998). Development of a Method for the Determination of Ozone Demand of a Water, *Ozone: Science and Engineering*, Vol. **20**, pp. 513-520.
- **Roustan M., Duguet J.-P., Lainé J.-M., Do-Quang Z., Mallevialle J.,** (1996). Bromate ion formation: impact of ozone contactor hydraulics and operating conditions, *Ozone: Science and Engineering*, Vol. **18**, pp. 87-97.
- **Saltelli A., Tarantola S., Chan K. P. S.,** (1999). A quantitative Model-independent method for global sensitivity analysis of model output, *Technometrics*, Vol. **41**, pp. 39-56.
- **Savary B.**, (2002). Influence des caractéristiques d'une eau naturelle sur la formation des ions bromates au cours de l'ozonation: Observations-Prévisions-Simulations dans un réacteur diphasique du type colonne à bulles, Ph.D. thesis ENSC-R, France.
- **Schunn C. D.** et **Wallach D.,** (2005). Evaluating goodness-of-fit in comparison of models to data, in W. Tack (Ed.), *Psychologie der Kognition: Reden and Vorträge anlässlich der Emeritierung von Werner Tack*. Saarbrüken, Germany: University of Saarland Press, pp. 115-154.
- **Serensen B. H., Nielsen S. N., Lanzky P. F., Ingerslev F., Holten Lutzhoft H. C., Jorgensen S. E.,** (1998). Occurrence, Fate and Effects of Pharmaceutical Substances in the Environment, A Review, *Chemosphere*, Vol. **36**, pp. 357-393.
- **Siddiqui M. S**. et **Amy G. L.,** (1993). Factors Affecting DBP Formation during Ozone-Bromide Reactions, *Journal American Water Works Association*, Vol. **85**, pp. 63-70.
- **Smeets P. W. M. H., van der Helm A. W. C., Dullemont Y. J., Rietveld L. C., van Dijk J. C., Medema G. J.,** (2006). Inactivation of *Escherichia coli* by ozone under bench-scale plug flow and full-scale hydraulic conditions, *Water Research*, Vol. **40**, pp. 3239-3248.
- **Smith D. W.** et **Zhou H.,** (1994). Theoretical Analysis Of Ozone Disinfection Performance In A Bubble Column, *Ozone: Science and Engineering*, Vol. **16**, pp. 429-441.
- **Staehelin J.** et **Hoigné J.**, (1982). Decomposition of ozone in water: Rate of Initiation by Hydroxide Ions and Hydrogen Peroxide, *Environmental Science and Technology*, Vol. **16**, pp. 676-681.
- **Staehelin J., Bühler R.E., Hoigné J.**, (1984). Ozone Decomposition in Water Studied by Pulse Radiolysis. 2. OH and HO_4 as Chain Intermediates, *Journal of Physical Chemistry*, Vol. **88**, pp. 5999-6004.
- **Staehelin, J.** et **Hoigné, J.,** (1985). Decomposition of Ozone in Water in the Presence of Organic Solutes Acting as Promoters and Inhibitors of Radical Chain Reactions, *Environmental Science and Technology*, Vol. **19**, pp. 1206-1213.
- **Tomiyasu H., Fukutomi H., Gordon G.,** (1985). Kinetics and Mechanism of Ozone Decomposition in Basic Aqueous Solution, *Inorganic Chemistry*, Vol. **24**, pp. 2962-2966.
- **van den Bos, A.,** (2007). Parameter Estimation for Scientists and Engineers, *Wiley-Interscience*, Hoboken, U.S.A.

- **von Gunten U.** et **Hoigné J.,** (1994). Bromate Formation during Ozonation of Bromide-Containing Waters: Interaction of Ozone and Hydroxyl Radical Reactions, *Environmental Science and Technology*, Vol. **28**, pp. 1234-1242.
- **von Gunten U.,** (2003b). Ozonation of drinking water: Part II. Disinfection and by-product formation in presence of bromide, iodide or chlorine, *Water Research*, Vol. **37**, pp. 1469-1487.
- **von Gunten U., Huber M. M., Göbel A., Joss A., Hermann N., Löffler D., McArdell C. S., Ried A., Siegrist H., Ternes T. A.,** (2005). Oxidation of Pharmaceuticals during Ozonation of municipal Wastewater Effluents: A pilot Study, *Proceedings of the IOA 17th World Ozone Congress,* Strasbourg.
- **Wei Q.-S., Feng C.-H., Wang D.-S., Shi B.-Y., Zhang L.-T., Wei Q., Tang H.-X.,** (2008). Seasonal variations of chemical and physical characteristics of dissolved organic matter and trihalomethane precursors in a reservoir: a case study, *Journal of Hazardous Materials*, Vol. **150**, pp. 257-264.
- **Westerhoff P.**, (2002). Kinetic-based models for bromate formation in natural waters, EPA final report.
- **Westerhoff P., Song R., Amy G.**, **Minear R.**, (1997). Application of Ozone Decomposition Models, *Ozone: Science and Engineering*, Vol. **19**, pp. 55-73.
- **Westerhoff P., Song R., Amy G., Minear R.**, (1998a). Numerical Kinetic Models for Bromide Oxidation to Bromine and Bromate, *Water Research*, Vol. **32**, pp. 1687-1699.
- **Westerhoff P., Song R., Amy G., Minear R**., (1998b). NOM's role in bromine and bromate formation during ozonation, *Journal of American Water Works Association*, Vol. **90**, pp. 89-94.
- **Whitman W.G.,** (1923), A preliminary experimental confirmation of the two-film theory of gas absorption, *Chemical and Metallurgical Engineering,* Vol. **29, pp.** 146-148.
- **Wols B. A., Hofman J. A. M. H., UIjttewaal W.S. J., Rietveld L. C., van Dijk J. C.,** (2010). Evaluation of different disinfection calculation methods using CFD, *Environmental Modelling and Software*, Vol. **25**, pp. 573-582.
- **Yurteri C.** et **Gurol M. D.**, (1988). Ozone consumption in natural waters: effects of background organic matter, pH and carbonate species. *Ozone: Science and Engineering*, Vol. **10**, pp. 277-290.
- **Zhang J.,** (2006). An integrated design approach for improving drinking water ozone disinfection treatment based on computational fluid dynamics, Ph.D. thesis, University of Waterloo, Canada.
- **Zhang J., Huck P. M., Anderson W. B., Stubley G. D.,** (2007). A Computational Fluid Dynamics Based Integrated Disinfection Design Approach for Improvement of Full-scale Ozone Contactor Performance, *Ozone: Science and Engineering*, Vol. **29**, pp. 451-460.

SUMMARY

Facing major challenges, management of ozonation process will increasingly need prediction tools based on modelling. Dealing with different types of waters (chemistry) and different types of tanks (hydraulics), modelling of ozonation units has to adapt to site-specific conditions. The main objective of this work was to develop an integrated modelling procedure for industrial ozonation processes for predicting concentration profiles of: ozone, bromate and specific micropollutants. Two types of chemical models were considered: semi-empirical models with adjustable kinetics (for the role of Natural Organic Matter, NOM) and mechanistic models with predetermined kinetics (for other phenomena related to ozonation). Hydraulic flow conditions were modelled by systematic networks (patterns of ideal reactors). Ozone decomposition, hydroxyl radical generation and bromate formation were studied at lab-scale with a specially developed apparatus. Various experimental conditions were tested: pH, temperature, ozone doses, initial bromide concentrations, concentration of NOM and nature of NOM. The model was able to adequately reproduce experimental measurements for nine of the eleven water samples studied, covering a wide domain: $6.1 \leq pH \leq 8.15$; $1.02\ meq.L^{-1} \leq A_T \leq 6.02\ meq.L^{-1}$; $0\text{-}.0.5\ mg.L^{-1} \leq TOC \leq 3.1\ mg.L^{-1}$. For bromate, considering the crucial zone between the quantification limit and 20 $\mu g.L^{-1}$, a large majority of the simulated concentrations corresponded to experimental concentrations or were located in the experimental uncertainty interval. A full-scale study showed that models calibrated at lab-scale may be used directly on-site to predict the formation of bromate and ozone profiles. Readjustments of the model for bromate formation should however account for seasonal changes.

Keywords: Ozonation; Modelling; Drinking Water; Natural Organic Matter; Bromate; Parameter identification; Process Simulation.

RÉSUMÉ

Afin de gérer au mieux le pilotage des unités d'ozonation lors de la potabilisation des eaux, un modèle prédictif a été développé. L'objectif du modèle était de pouvoir prédire, sur une installation industrielle, les concentrations en ozone, en bromates et en différents micropolluants. Le modèle chimique proposé est mécanistique et peut être subdivisé en plusieurs parties : auto-décomposition de l'ozone, influence de l'alcalinité, formation de bromates, influence de la MON (Matière Organique Naturelle). Le modèle d'influence de la MON comporte 12 paramètres ajustables, le modèle pour la formation des bromates comporte un paramètre ajustable, les valeurs des autres paramètres sont fixées d'après la littérature. Le modèle hydraulique est de type systémique et comprend des réacteurs idéaux (parfaitement agités et piston). L'identifiabilité du jeu de paramètres a été conduite par une analyse de sensibilité (eFAST). La procédure d'optimisation par méthode de Nelder-Mead a été testée. Le modèle proposé permet de rendre bien compte des variations de temps de contact avec l'ozone, de pH, de température, de concentration de MON, de doses d'ozone sur la décomposition de l'ozone et la génération de radicaux. Les essais sur la formation de bromates ont montré que le modèle donne de bons résultats pour des concentrations inférieures à 20 $\mu g.L^{-1}$, ce qui est particulièrement intéressant dans le cas d'une application industrielle. Enfin, une étude sur une unité industrielle a montré que des modèles calibrés en laboratoire (chimie, hydraulique) peuvent être appliqués directement sur site. Le modèle de formation des bromates est néanmoins instable dans le temps et doit être périodiquement réajusté.

Mots-clés: Ozonation; Modélisation; Eau potable; Matière Organique Naturelle; Bromate; Identification paramétrique; Simulation de procédé.